U.S. DEPARTMENT OF ENERGY

Office of ENERGY EFFICIENCY & RENEWABLE ENERGY

Decarbonization of Off-Road, Rail, Marine, and Aviation (DORMA) Program

2022 Annual Progress Report

Vehicle Technologies Office

(This page intentionally left blank)

Disclaimer

This report was prepared as an account of work sponsored by an agency of the United States government. Neither the United States government nor any agency thereof, nor any of their employees, makes any warranty, expressed or implied or assumes any legal liability or responsibility for the accuracy, completeness, or usefulness of any information, apparatus, product, or process disclosed or represents that its use would not infringe privately owned rights. Reference herein to any specific commercial product, process, or service by trade name, trademark, manufacturer, or otherwise does not necessarily constitute or imply its endorsement, recommendation, or favoring by the Unites States government or any agency thereof. The views and opinions of authors expressed herein do not necessarily state or reflect those of the United States government or any agency thereof.

Acknowledgements

We would like to express our sincere appreciation to Energetics, A Division of VSE Corporation and Oak Ridge National Laboratory for their technical and artistic contributions in preparing and publishing this report. In addition, we would like to thank all the participants for their contributions to the programs and all the authors who prepared the project abstracts that comprise this report.

Acronyms

0D, 0-D	zero-dimensional
1D, 1-D	one-dimensional
2D	two-dimensional
3D, 3-D	three-dimensional
6AT	6-speed automatic transmission
8AT	8-speed automatic transmission
AC	alternating current
ACI	advanced compression ignition
ADT	articulated dump truck
AFIDA	Advanced Fuel Ignition Delay Analyzer
AFR	air-to-fuel ratio, air–fuel ratio
AFRL	Air Force Research Laboratory
AHRR	apparent heat release rate
AJT	alcohol to jet
Al	aluminum
AM	additive manufacturing
AMR	adaptive mesh refinement
AMReX	publicly available software framework designed for building massively parallel block-structured adaptive mesh refinement (AMR) applications
ANL	Argonne National Laboratory
ANN	artificial neural network
APC	active pre-chamber
APP	accelerator pedal position
APS LABS	Advanced Power Systems Research Center at Michigan Technological University
Ar	argon
ARC-M1	Army Research Combustor
ARCP	auxiliary resonant commutated pole
ASC	ammonia slip catalyst
ASME	American Society of Mechanical Engineers
ASOI, aSoI	after the start of injection
ASTM	ASTM International, formerly American Society for Testing and Materials
AT	aftertreatment
atdc, aTDC, ATDC	after top dead center
aTDCf	after firing top dead center
atm	atmosphere(s)
atSAC	thermally durable single-atom catalyst
a.u.	arbitrary units
BD1090	burn duration from 10 mass fraction burned to 90 mass fraction burned
BEV	battery electric vehicle
bhp	brake horsepower
BMEP	brake mean effective pressure
BP	budget period

BPF	bandpass filter
BPP	brake pedal position
BSFC	brake specific fuel consumption
BSI	boosted spark ignition
BSNOx	brake specific oxides of nitrogen
BTDC, bTDC	before top dead center
BTE	brake thermal efficiency
C	carbon
C	Celsius
Ca	calcium
CA	California
CA	crank angle
CA50	crank angle at 50% mass fraction burned
CAC	charge air cooler
CAD	crank angle degree(s)
CAD	computer-aided design
CAE	computer-aided engineering
CAH	charge air heater
CAN	controller area network
CARB	California Air Resources Board
CCD	charge-coupled device
CDA	cylinder deactivation
C_{dc}	direct current (DC) bus capacitor
CDC	conventional diesel combustion
Ce	cerium
CE	combustion engine
C-EGAI	controlled end-gas autoignition
CET	columnar to equiaxed transition
CFD	computational fluid dynamics
CFR	Cooperative Fuel Research
CH_4	methane
C_3H_6	propene
C_3H_8	propane
CHA	chabazite
CI	compression ignition
cm	centimeter(s)
CMOS	complementary metal-oxide sensor
CMPC	center mount prechamber
CN	cetane number
CO	Colorado
CO	carbon monoxide
CO_2	carbon dioxide
CONVERGE	computational fluid dynamics software package
Co-Optima	Co-Optimization of Fuels and Engines
COTS	commercial off-the-shelf

COV, CoV	coefficient of variation
COVID-19	coronavirus disease 2019
CPT	cyclopentane
CPU	central processing unit
Cr	resonant circuit capacitor
CR, cr	compression ratio
CRADA	cooperative research and development agreement
CRC	Coordinating Research Council
CRZ	central recirculation zone
CS	cooled spray
CSA	cross sectional area
CSI	Convergent Science Inc.
CSLA	constant speed load acceptance
CSU	Colorado State University
CT	Connecticut
CT	computed tomography
CTL	compact track loader
Cu	copper
CV	continuously variable
CVT	continuously variable transmission
CVVD	continuously variable valve duration
CVVT	continuously variable valve timing
cyl	cylinder
d	day
DAR	diluent–air ratio
DBI-EI	diffuse back-illumination extinction imaging
DC	District of Columbia
DC	direct current
DCCO	deceleration cylinder cut off
DCN	derived cetane number
DEF	diesel exhaust fluid
deg	degree(s)
DFI	ducted fuel injection
DFT	density functional theory
DG	degreened
DI	direct injection
DIB	disobutylene
DIJ	direct injection
DISI	direct injection spark ignition
DME	dimethyl ether
DMF	dimethylfuran
DNS	direct numerical simulation
DOC	diesel oxidation catalyst
DOCF	diesel oxidation catalyst loaded onto a diesel particulate filter
DOE	U.S. Department of Energy

DORMA	Decarbonization of Off-Road, Rail, Marine, and Aviation
DOT	U.S. Department of Transportation
DPF	diesel particulate filter
DRIFTS	diffuse reflectance infrared Fourier transform spectroscopy
DSD	droplet size distribution
DSF®	Dynamic Skip Fire
DSL	dimpled stepped-lip
DSM	dynamic system modeling
DTNA	Daimler Trucks North America
E10	10% ethanol, 90% gasoline blend
E30	30% ethanol, 70% gasoline blend
E85	85% ethanol, 15% gasoline blend
E100	neat ethanol
eADT	electrified articulated dump truck
EB	embedded boundary
ECM	electric control module
ECN	Engine Combustion Network
ECU	engine control unit
E-EGR	enhanced exhaust gas recirculation
EERE	U.S. Department of Energy Office of Energy Efficiency and Renewable Energy
e.g.	exempli gratia, “for example”
EGR	exhaust gas recirculation
EGT	exhaust gas temperature
e-HVAC	electronic heating, ventilation, and air conditioning
EID	electronic injector definition
EIVC	early intake valve closing
eIVT	electric infinitely variable transmission
eLS	electronic load sensing
E/N	reduced electric field, the ratio of electric field to concentration of neutral particles
ENWM	enrichment wall model
EOCP	electronic open circuit pump
EPA	U.S. Environmental Protection Agency
EPR	electron paramagnetic resonance
EREV	extended-range electric vehicle
et al.	et alii (Latin, meaning and others)
etc.	et cetera (Latin, meaning and the rest)
ETMS	electrification thermal management system
eV	electron volt
EVC	exhaust valve closing
EVO	exhaust valve opening
EXAFS	X-ray absorption fine structure
EXP, Exp	experiment; experimental
FACE	Fuels for Advanced Combustion
FAF	fresh air flow
Fe	iron

FE	fuel economy
FE	freight efficiency
FEA	finite element analysis
FF	feedforward
FID	flame ionization detector
FIS	fuel injection system
FL	focal length
FLIR	forward-looking infrared
FOA	funding opportunity announcement
FP	fluid power
FSN	filter smoke number
FT	Fischer–Tropsch
ft^3	cubic feet
FTE	freight ton efficiency
FTIR	Fourier-transform infrared spectroscopy
FTP	Federal Test Procedure
FUP	fuel injection pressure
FWHM	full width at half maximum
FY	Fiscal Year
g	gram(s)
gal	gallon(s)
GCI	gasoline compression ignition
GDI	gasoline direct injection; gasoline direct injector
GEM	Greenhouse Gas Emissions Model
Gen	generation
GHG	greenhouse gas
GHRR	gross heat release rate
GHSV	gas hourly space velocity
g/kWh	gram(s) per kilowatt-hour
GM	General Motors
GPS	global pathway selection
GREET	Greenhouse gases, Regulated Emissions, and Energy use in Technologies model
GT	Gamma Technologies
GTE	gross thermal efficiency
h	hour(s)
H	hydrogen
H_2	diatomic hydrogen
H2D2	heavy-duty hybrid diesel
H_2-ICE	hydrogen internal combustion engine
H_2-TPR	hydrogen temperature programmed reduction
HATCI	Hyundai America Technical Center, Inc.
HC	hydrocarbon
H/C	hydrogen-to-carbon ratio
HCCI	homogeneous charge compression ignition
HCF	high cycle fatigue

HD	heavy-duty
HDV	heavy-duty vehicle
He	helium
HECM	hydraulic–electric control module
HEFA	hydroprocessed esters and fatty acids
HER	electro-hydraulic remote
HEV	hybrid electric vehicle
HEX	hydraulic excavator
HFCH	high-flow cylinder head
HHDDT	heavy heavy-duty diesel truck driving cycle
HHEA	hybrid hydraulic–electric architecture
HIL	hardware-in-the-loop
HO_2	hydroperoxyl radical, hydrogen peroxide
H_2O	water
HOV, HoV	heat of vaporization
hp	horsepower
HP	high pressure
HPFP	high-pressure fuel pump
HPSC	high-pressure spray chamber
hr	hour(s)
HRR	heat release rate
HSFW	high-speed flywheel
HSS	hybrid with stop-start
HSSL	high-speed serial link
HT	hydrothermal
HTA	hydrothermally aged, hydrothermal aging
HT-LT	high temperature–low temperature
HV	high volatility
HV	high voltage
HVAC	heating, ventilation, and air conditioning
HVO	hydrotreated vegetable oil
HW	hardware
Hz	Hertz
IAT	intake air throttle
ICE	internal combustion engine
ICEF	Internal Combustion Engine Fall Technical Conference
ICME	integrated computational materials engineering
ICN	indicated cetane number
ICP	inductively coupled plasma
ICP-AES	inductively coupled plasma atomic emission spectroscopy
IDT	ignition delay time
i.e.	id est, “that is”
IL	Illinois
I_{LA}, I_{LB}, I_{LC}	Phase A, B, and C output current from ARCP inverter
IMAP	intake manifold air pressure

IMEP	indicated mean effective pressure
IMEPg, $IMEP_g$	gross indicated mean effective pressure
IMEPn	net indicated mean effective pressure
in	inch(es)
IN	Indiana
Inc.	Incorporated
I/O	input/output
IQT	Ignition Quality Tester apparatus at National Renewable Energy Laboratory
IR	infrared
ISCO	indicated specific carbon monoxide emissions
ISFC	indicated specific fuel combustion
$ISFC_n$	net indicated specific fuel consumption
ISHC	indicated specific unburned hydrocarbon emissions
$ISNO_x$	indicated specific oxides of nitrogen
ISO	International Organization for Standardization
ISPM	indicated specific particulate matter (soot) emissions
ITE	indicated thermal efficiency
IVC	intake valve closing
IWI	incipient wetness impregnation
J	joule(s)
K	Kelvin
k-ε	turbulence
kg	kilogram(s)
kHz	kilohertz
kJ	kilojoule(s)
KL	soot optical thickness
km	kilometer(s)
kV	kilovolt(s)
kW	kilowatt(s)
kWh, kW-hr	kilowatt-hour(s)
L, l	liter(s)
LBNL	Lawrence Berkeley National Laboratory
LBO	lean blow off
lbs.	pounds
LCA	life cycle analysis
LD	light-duty
LDRD	Laboratory Directed Research and Development office at Sandia National Laboratories
LE	Lagrangian–Eulerian
LECM	large engine control module
LED	light-emitting diode
LES	large eddy simulation
LEV III	low-emission vehicle III
LEVO	late exhaust valve opening
LHV	lower heating value
Li	lithium

LiDAR	light-detection and ranging
LIVC	late intake valve closing
LLC	Limited Liability Company
LLCF	low life-cycle carbon fuels
LLNL	Lawrence Livermore National Laboratory
LNG	liquefied natural gas
LOL	lift-off length
LO-SCR	light-off selective catalytic reduction
LP	low pressure
LPG	liquefied petroleum gas
LPPSC	low-pressure precision sand casting
L_r	resonant circuit inductor
LS	load sensing
LTC	low-temperature combustion
LTC-D	low-temperature combustion (diesel)
LTGC	low-temperature gasoline combustion
LTHR	low-temperature heat release
LTP	low-temperature plasma
LV	low volatility
LWL	large wheel loader
m	meter(s)
m^2	square meter(s)
m^3	cubic meter(s)
MARAD	U.S. Department of Transportation Maritime Administration
max	maximum
MC	main chamber
MCC	mixing-controlled combustion
MCCI	mixing-controlled compression ignition
MCE	multi-cylinder engine
MCTE	multi-cylinder test engine
MD	medium-duty
MERRA-2	Modern-Era Retrospective Analysis for Research and Applications, Version 2
MFB	mass fraction burned
mg	milligram(s)
M/G	motor/generator
MGU	motor-generator unit
mi	mile(s)
MI	Michigan
min	minimum
min	minute(s)
MJ	megajoule(s)
MJI	MAHLE pre-chamber turbulent jet ignition
mm	millimeter(s)
MM	multimode
MN	Minnesota

mol	mole(s), molar
mol%	mole fraction
MON	motor octane number
MOSFET	metal oxide semiconductor field effect transistor
MP	multi-pressure
MPa	megapascal(s)
MPC	model predictive control
mpg, MPG	mile(s) per gallon
MPH, mph	mile(s) per hour
MPR	multi-pressure rail
MPRR	max pressure rise rate
ms	millisecond(s)
MS	mass spectrometer, mass spectroscopy
MTU	Michigan Technological University
MZ-WSR	well-stirred reactor model with multi-zone
N	Newton(s) (unit of force)
N	nitrogen
NARAC	National Atmospheric Release Advisory Center
NASA	National Aeronautics and Space Administration
NC	North Carolina
ND	North Dakota
n.d.	no date
Nd:YAG	neodymium-doped yttrium aluminum garnet
NETL	National Energy Technology Laboratory
NG	natural gas
NH_3	ammonia
NHV	noise, vibration, and harshness
NI	National Instruments
NJFCP	National Jet Fuels Combustion Program
nm	nanometer(s)
N-m, Nm	Newton-meter(s)
NM	non-methane
NMEP	net mean effective pressure
NMOG	non-methane organic gases
NMR	nuclear magnetic resonance
NNSPM	neural-network species prediction model
NO	nitric oxide
NO_2	nitrogen dioxide
N_2O	nitrous oxide
N_2O_2	dinitrogen dioxide
NO_x	oxides of nitrogen
NREL	National Renewable Energy Laboratory
ns	nanosecond(s)
NSFC	net specific fuel consumption
NVO	negative valve overlap

O	atomic oxygen
O1, O2, O3	Objective 1, Objective 2, Objective 3
O_2	diatomic (molecular) oxygen
O_3	ozone
OC	oxidation catalyst
OEM	original equipment manufacturer
OHC	oxidation half cycle
OME	oxymethylene ethers
OP	opposed piston
Opt GRs	optimum gear ratios
ORC	organic Rankine cycle
ORNL	Oak Ridge National Laboratory
ORZ	outer recirculation zone
OSC	oxygen storage capacity, oxygen storage components
OSU	Ohio State University
P	pressure
Pa	Pascal(s)
Pa	paladium
PAH	polycyclic aromatic hydrocarbon
PC	pre-chamber
PC	personal computer
PC-MCC	prechamber-enabled mixing-controlled combustion
PCP	peak cylinder pressure
Pd	palladium
PD	photodiode
PDF	probability density function
P-DRGEP	plasma specific extension to the directed relation graph method with error propagation
PFI	port fuel injection
PFI-DI	port fuel injection/in-cylinder direct injection
PF-PLIF	photo-fragmentation planar laser-induced fluorescence
PFR	plasma flow reactor
PGM	platinum group metal
PHC	polyhedral ceria
PI	principal investigator
PISO	Pressure-Implicit with Splitting of Operators algorithm
PLIF	planar laser-induced fluorescence
PM	particulate matter
PM	permanent magnet
PMAC	permanent magnet alternating current
PNNL	Pacific Northwest National Laboratory
P.O.	Post Office
POLA	Port of Los Angeles
POME	polyoxymethylene ether
P2P	pin to pin
PPC	passive pre-chamber

PPCI	partially premixed compression ignition
ppm	part(s) per million
PRF	primary reference fuel
PRF	Powertrain Research Facility at Argonne National Laboratory
Pro-E	Pro-Engineer model created using Creo Software
PSM	Particle Size Mimic
Pt	platinum
PTO	power take-off
PWM	pulse width modulation
PXIe	peripheral component interconnect extensions
Q1	first quarter (Q2 second quarter, Q3.... etc.)
RANS	Reynolds-averaged Navier–Stokes
R80B20	a low-net-carbon blend of 80 vol% renewable diesel with 20 vol% biodiesel
RCM	rapid compression machine
R&D	research and development
RDD&D	research, development, demonstration, and deployment
Rh	rhodium
RHC	reduction half cycle
RMCSET	Ramped Modal Cycle Supplemental Emissions Testing
ROI	rate of injection
ROI	region of interest
RON	research octane number
rpm, RPM	revolution(s) per minute
RR	Rosin–Rammler
RSM	Reynolds Stress Model
RTD	resistance temperature detector
rtp	real-time transport protocol
RVP	Reid vapor pressure
s	second(s)
S	sulfur
SA	spark-assisted
SAC	single-atom catalyst
SAE	SAE International, formerly the Society of Automotive Engineers
SAF	sustainable aviation fuel
SATF	synthetic aviation turbine fuel
SB	stroke brake
SC2	SuperComm 2 Database
SCE	single-cylinder engine
SCR	selective catalytic reduction
SD	spray dried
SEM	spectral element method
SET	supplemental engine test
SG	Scapegoat hardware
SHA	single-hole atomizer
Si	silicon

SI	spark ignition, spark ignited
SIMPLE	Semi-Implicit Method for Pressure-Linked Equations algorithm
SISO	single input single output
SL	stepped-lip
SMD	Sauter mean diameter
SMPC	side mount prechamber
S-N	stress–life
SNL	Sandia National Laboratories
SOC	state of charge
SoI, SOI	start of injection
SO_x	sulfur oxides
Spaci-MS	spatially variable mass spectroscopy analysis
SPK	synthetic paraffinic kerosene
SRM	stochastic reactor model
SSWM	shear stress wall model
SSZ-13	aluminosilicate zeolite
ST1	SuperTruck 1
ST2	SuperTruck 2
Std	standard
SULEV	super ultra-low emissions vehicle
SV	space velocity
SVF	soot volume fraction
T	temperature
T	silicon carbide MOSFET in ARCP inverter power circuit
TBC	thermal barrier coating
TBD	to be determined
TC	turbocharger
TCO	total cost of ownership
Td	Townsend
TDC	top dead center
TGDI	turbocharged gasoline direct injection
THC	total hydrocarbons
TJI	turbulent jet ignition
TKE	turbulence kinetic energy
TN	Tennessee
TOR	turnover rate
tPDF	transported probability density function
TPR	temperature-programmed reduction
TQ	torque
Tr	silicon carbide MOSFET in resonant circuit
TWC	three-way catalyst
UCF	University of Central Florida
UDDS	Urban Dynamometer Driving Schedule
UDP/IP	user data protocol/internet protocol
UHC	unburned hydrocarbon

UHP	ultra-high pressure
UIUC	University of Illinois at Urbana-Champaign
ULEV	ultra-low-emission vehicle
U.S.	United States
US06	U.S. Environmental Protection Agency high-acceleration aggressive drive cycle
U.S. DRIVE	United States Driving Research and Innovation for Vehicle efficiency and Energy sustainability
U.S. Std. Atm.	U.S. Standard Atmosphere
UT	Austin University of Texas at Austin
UV	ultraviolet
UVA	University of Virginia
V	volt(s)
V6	six-cylinder piston engine in which the cylinders share a common crankshaft and are arranged in a V configuration
V8	eight-cylinder piston engine in which the cylinders share a common crankshaft and are arranged in a V configuration
VCF	velocity–composition–frequency
V_{dc}	direct current (DC) bus voltage
VNT	variable nozzle turbine
VoF	volume of fluid
vs.	versus
VTO	U.S. Department of Energy Vehicle Technologies Office
W	watt(s)
WA	Washington
WG	wastegate
WHR	waste heat recovery
WI	Wisconsin
WLTP	Worldwide Harmonised Light Vehicle Test Procedure
WSR	well-stirred reactor
WSRMZ	well-stirred reactor model with multi-zone
wt%	weight of the component divided by total sample weight, multiplied by 100
WV	West Virginia
WVU	West Virginia University
XPS	X-ray photoelectron spectroscopy
XRD	X-ray diffraction
Z	zeolite
Zero-RK	Zero-Order Reaction Kinetics combustion software package

List of Symbols

°	degree(s)
°ATC	degrees above top center
°ATDC	degree(s) after top dead center
°bTDC	degree(s) before top dead center
°C	degree(s) Celsius
°CA	crank angle degree(s)
°F	degree(s) Fahrenheit
>	greater than
φ	angular position
<	less than
µg	microgram(s)
µJ	microjoule(s)
µm	micrometer(s)
µs	microsecond(s)
%	percent
ϕ	fuel/air equivalence ratio
ηc	combustion efficiency (= chemical energy released / chemical energy injected)
ηf	fuel-conversion efficiency (= work per cycle / chemical energy injected)
χξ	scalar dissipation rate

Executive Summary

On behalf of the Vehicle Technologies Office (VTO) of the U.S. Department of Energy, we are pleased to introduce the Fiscal Year 2022 Annual Progress Report for the Decarbonization of Off-Road, Rail, Marine, and Aviation Program. In support of VTO's goal of economy-wide decarbonization by 2050, the Office will play a leading role in decarbonizing the transportation sector and addressing the climate crisis by driving innovation and deploying clean transportation technologies, all while maintaining transportation service quality and safety. The Program supports research, development, and demonstration of new propulsion and vehicle technologies in applications that will reduce greenhouse gas (GHG) emissions and achieve a net-zero-GHG economy by 2050. These technologies include optimization of high-efficiency engines and emission control systems that can use low-GHG, renewable fuels such as advanced biofuels, hydrogen, and e-fuels, and the integration of electrified and hybrid powertrains into vehicles to further reduce GHG emissions.

The Program supports a multi-laboratory initiative, in close collaboration with industry and academia, to achieve goals for decarbonization of the non-road sector. The Program will apply the unique facilities and research capabilities at the national laboratories to develop innovations and data that industry can use to improve non-road powertrains, providing efficiency improvements and GHG and criteria emission reductions. The Program coordinates with and uses expertise from other agencies, DOE offices, and VTO subprograms as needed.

This report highlights progress achieved by the Decarbonization of Off-Road, Rail, Marine, and Aviation Program during Fiscal Year 2022. The nature, current focus, and recent progress of the Program are described in this report, and summaries of current national laboratory, industry, and university projects provide an overview of the exciting work being conducted to address critical technical barriers and challenges to decarbonizing the non-road sector.

While the Program, formerly known as the Advanced Engine and Fuel Technologies Program, had traditionally focused research and development (R&D) on on-road vehicles and engines, in Fiscal Year 2022, it transitioned to support R&D focused on reducing GHG and criteria emissions from non-road vehicles and engines, including engines used for off-road, rail, marine, and aviation applications, while improving their ability to utilize renewable fuels. Since these difficult-to-electrify transportation sectors will continue to use internal combustion engines for several decades, reducing their contribution to greenhouse gas emissions is increasingly important.

Gurpreet Singh, Program Manager, Decarbonization of Off-Road, Rail, Marine, and Aviation Program
Vehicle Technologies Office

Siddiq Khan
Vehicle Technologies Office

Kevin Stork
Vehicle Technologies Office

Table of Contents

List of Figures

List of Tables

(This page intentionally left blank)

Vehicle Technologies Office Overview

Vehicles move our national economy. Annually, vehicles transport 18 billion tons of freight—about $55 billion worth of goods each day[1]—and move people more than 3 trillion vehicle-miles.[2] Growing our economy requires transportation, and transportation requires energy. The transportation sector accounts for approximately 30% of total U.S. energy needs[3] and the average U.S. household spends over 15% of its total family expenditures on transportation,[4] making it, as a percentage of spending, the most costly personal expenditure after housing. Transportation is critical to the overall economy, from the movement of goods to providing access to jobs, education, and healthcare.

The transportation sector has historically relied heavily on petroleum, which supports over 90% of the sector's energy needs today,[5] and, as a result, surpassed electricity generation to become the largest source of CO_2 emissions in the country.[6] The Vehicle Technologies Office (VTO) will play a leading role to decarbonize the transportation sector and address the climate crisis by driving innovation within and deployment of clean transportation technologies.

VTO funds research, development, demonstration, and deployment (RDD&D) of new, efficient, and clean mobility options that are affordable for all Americans. VTO leverages the unique capabilities and world-class expertise of the National Laboratory system to develop new innovations in vehicle technologies, including: advanced battery technologies; advanced materials for lighter-weight vehicle structures and better powertrains; energy-efficient mobility technologies and systems (including automated and connected vehicles as well as innovations in connected infrastructure for significant systems-level energy efficiency improvement); combustion engines to reduce greenhouse gas and criteria emissions; and technology integration that helps demonstrate and deploy new technology at the community level. Across these technology areas and in partnership with industry, VTO has established aggressive technology targets to focus RDD&D efforts and ensure there are pathways for technology transfer of federally supported innovations into commercial applications.

VTO is uniquely positioned to accelerate sustainable transportation technologies due to strategic public–private research partnerships with industry (e.g., U.S. DRIVE, 21st Century Truck Partnership) that leverage relevant expertise. These partnerships prevent duplication of effort, focus DOE research on critical RDD&D barriers, and accelerate progress. VTO advances technologies that assure affordable, reliable mobility solutions for people and goods across all economic and social groups; enable and support competitiveness for industry and the economy/workforce; and address local air quality and use of water, land, and domestic resources.

Annual Progress Report

As shown in the organization chart (below), VTO is organized by technology area: Batteries R&D; Electrification R&D; Materials Technology R&D; Decarbonization of Offroad, Rail, Marine, and Aviation; Energy Efficient Mobility Systems; and Technology Integration. Each year, VTO's technology areas prepare an Annual Progress Report (APR) that details progress and accomplishments during the fiscal year. VTO is pleased to submit this APR for Fiscal Year (FY) 2022. The APR presents descriptions of each active project in FY 2022, including funding, objectives, approach, results, and conclusions.

---

[1] Bureau of Transportation Statistics, DOT, Transportation Statistics Annual Report 2020, Table 4-1, https://www.bts.gov/tsar.
[2] Davis, Stacy C., and Robert G. Boundy. Transportation Energy Data Book: Edition 39. Oak Ridge National Laboratory, 2021, https://doi.org/10.2172/1767864. Table 3.8 Shares of Highway Vehicle-Miles Traveled by Vehicle Type, 1970-2018.
[3] Ibid. Table 2.2 U.S. Consumption of Total Energy by End-use Sector, 1950-2018.
[4] Ibid. Table 11.1 Average Annual Expenditures of Households by Income, 2019.
[5] Ibid. Table 2.3 Distribution of Energy Consumption by Source and Sector, 1973 and 2019.
[6] Environmental Protection Agency, Draft U.S. Inventory of Greenhouse Gas Emissions and Sinks, 1990-2019, Table 2-11. Electric Power-Related Greenhouse Gas Emissions and Table 2-13. Transportation-Related Greenhouse Gas Emissions.

Organization Chart

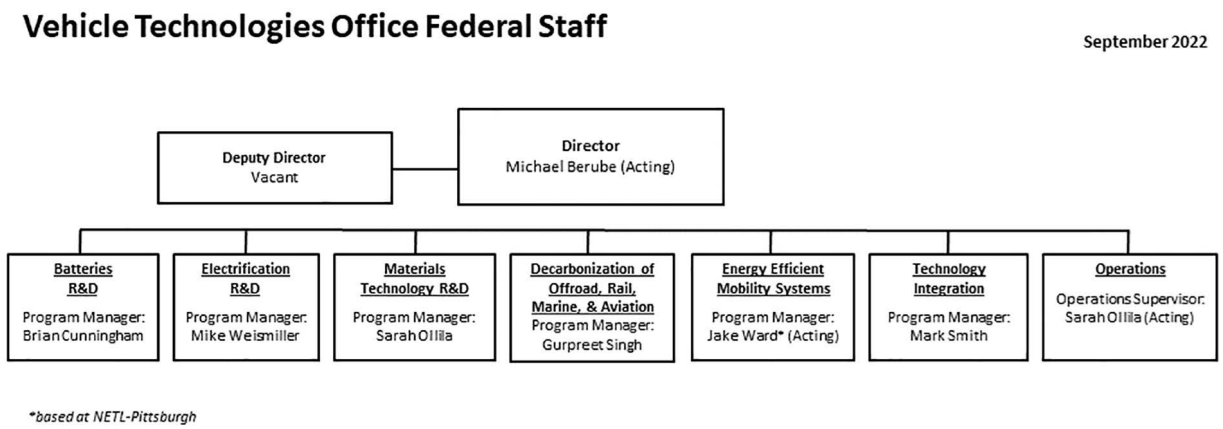

Decarbonization of Off-Road, Rail, Marine, and Aviation (DORMA) Program Overview

Introduction

The Decarbonization of Off-Road, Rail, Marine, and Aviation (DORMA) Program supports the U.S. Department of Energy (DOE) Vehicle Technologies Office's goals of transportation decarbonization, increasing domestic energy security through fuel diversification, improving internal combustion engine efficiency, reducing greenhouse gas and air pollutant emissions, and reducing vehicle initial and operating costs for consumers and businesses. The Program supports research, development, and demonstration of new propulsion and vehicle technologies that will reduce greenhouse gas (GHG) emissions in difficult-to-decarbonize transportation applications and enable achievement of a net-zero-GHG economy by 2050. These technologies include optimization of high-efficiency engines and emission control systems that can use low-GHG, renewable fuels such as advanced biofuels, hydrogen, and e-fuels (aka electro-fuels, i.e., fuels synthesized from zero-carbon feedstocks, typically facilitated with renewable electricity), and the integration of electrified and hybrid powertrains into vehicles to further reduce GHG emissions.

The Program utilizes unique capabilities and expertise at the national laboratories and collaborates closely with academia and industry to strengthen the knowledge base for the next generation of higher-efficiency, ultra-low-emissions combustion engines for non-road vehicles. In addition, a science-based understanding of how renewable fuels affect engine efficiency and emissions and how engines can be modified to take advantage of desirable fuel properties could enable further efficiency improvements.

The DORMA Program focused on the following research areas in Fiscal Year 2022: off-road, rail, marine, and aviation technologies along with legacy on-road projects (Figure 1). Projects competitively selected and awarded through funding opportunity announcements are fully funded through the duration of the project in the year the funding is awarded. Directly funded work at the national laboratories is subject to change based on annual appropriations.

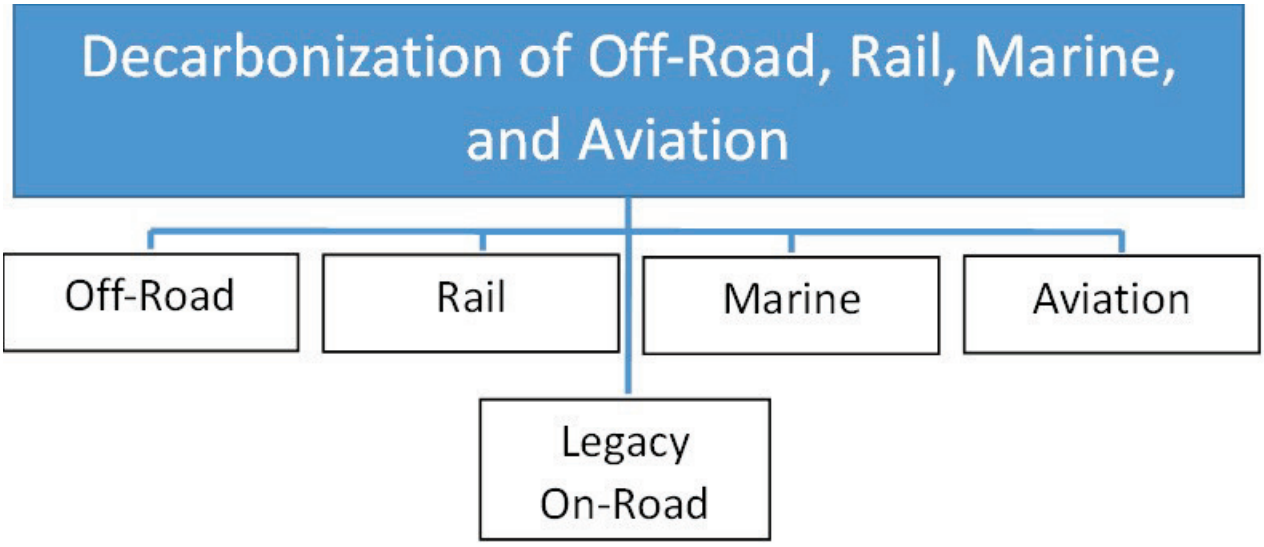

Figure 1 Fiscal Year 2022 research areas within the DORMA Program

Goals

The off-road, rail, marine, and aviation sectors, the focus areas of this program, contribute 26% of U.S. transportation GHG emissions, as shown in Figure 2. As passenger and commercial vehicles become electrified, the goal of this Program will be to support research and development (R&D) focused on reducing GHG and criteria emissions from non-road heavy-duty vehicles, including engines used for off-road, rail, marine, and aviation applications, while improving their ability to utilize renewable and low-carbon fuels. Since these difficult-to-electrify transportation sectors will continue to use internal combustion engines for several decades, reducing their contribution to GHG emissions is increasingly important.

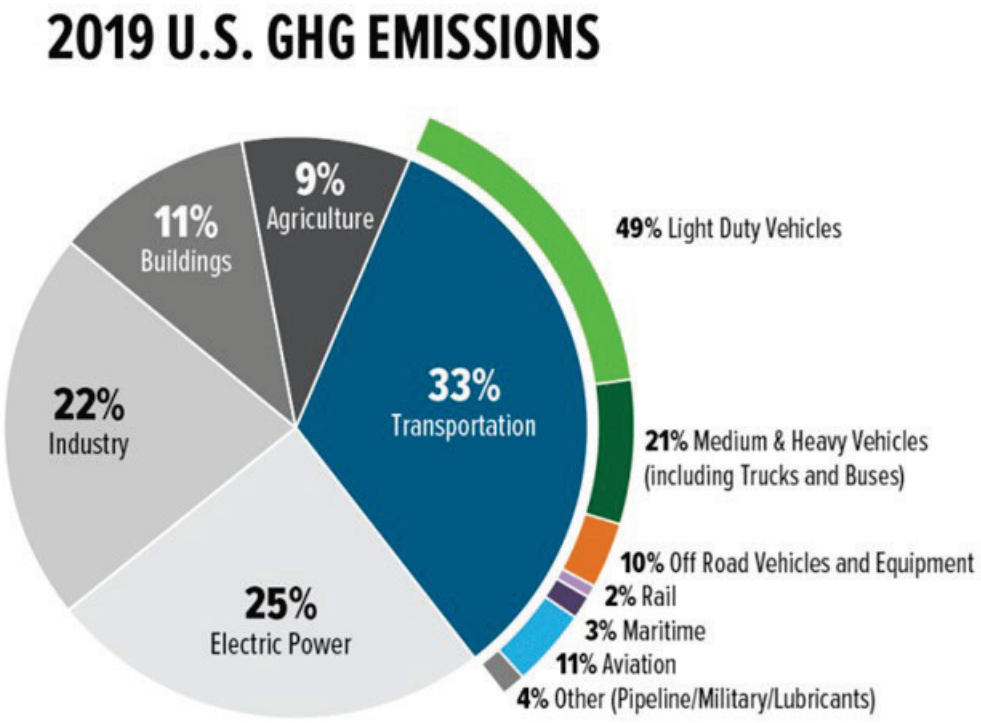

Figure 2 Sources of U.S. GHG emissions in 2019. Total 2019 U.S. GHG emissions with transportation and mobile sources breakdown. Data derived from the U.S. Environmental Protection Agency's *Inventory of U.S. Greenhouse Gas Emissions and Sinks* [1] (mapping mobile sources of emissions to off-road transportation vehicles). Aviation and maritime include emissions from international aviation and maritime transport. Fractions may not add up to 100% due to rounding.

Status of Current Technology

While on-road transportation is making the transition to electrification, technologies for electrifying non-road transportation are available for limited applications and the infrastructure to support those technologies is not yet in place. However, GHG and criteria emissions reductions can be achieved in the near term by using renewable fuels in internal combustion engines in these applications owing to recent significant advances in engine efficiency, exhaust emission reduction, and cost reduction for these technologies. Integrated with hybrid and plug-in hybrid electric vehicle powertrains, internal combustion engines can be operated at fuel-efficient speed–load conditions. Next-generation hybrid engine–electric drivetrains for non-road applications could offer cost-competitive and fuel-efficient options as the U.S. transportation sector transitions to full electrification.

Off-Road

Off-road vehicles account for approximately 10% of the total transportation energy use in the United States. There are a wide range of engine sizes, duty cycles, and vehicle applications within this sector. Unlike most highway vehicles, off-road vehicles typically provide the conveyance function of mobile equipment, with the engine's power used both to propel the vehicle and to perform auxiliary work, such as digging or harvesting. Different applications in the off-road sector have specific and primary requirements for ruggedness, durability, and operational factors, and the priorities for features can differ between applications.

One common attribute of off-road vehicles is the use of compression-ignition diesel engines because of their durability, low-speed torque, and fuel efficiency. Engine efficiency can be increased through combustion system improvements, integration with advanced powertrains (including electrification), waste heat recovery, efficient air handling and accessories, and improved idle efficiency. Many of these technology areas have been commercialized for engines used in on-road vehicles and can also be applied to common off-road engines, particularly to engines with less than 15 L displacement. However, experts state it is critical that engine design and specification be performed with knowledge of the expected operational conditions.

Off-road equipment is often reliant on hydraulic fluid power systems for actuation of implements due to the high load operation and challenging and harsh environments. Hydraulic systems have inherently low efficiency since they use throttling for control, but there is potential for further improvements.

Vehicle efficiency should be viewed from the whole-system level, rather than at the level of the individual components. A deeper understanding of real-world operation is needed to further optimize not only the engine and fluid power components but also the overall system. At the system level, there are opportunities for improved energy efficiency through automation and electrification. Electro-hydraulic architectures combine the benefits of electric motors and hydraulics, improving energy efficiency by eliminating throttling losses, while maintaining the power density of hydraulic actuation and managing the system cost of motors and batteries. For vehicles that make many repetitive movements, there are opportunities for energy recovery. Onboard energy storage and hybridization can help smooth transients in engine operation and allow for engine downsizing, both of which increase the vehicle efficiency. Depending on vehicle usage and availability of charging infrastructure, full battery electric vehicles may be an appropriate solution to increase efficiency.

Rail

The vision for rail decarbonization laid out in the U.S. National Blueprint for Transportation Decarbonization [2] includes battery electrification, hydrogen fuel cells, hydrogen-fueled internal combustion engines, and sustainable fuels for locomotives. While the rail industry is open to embracing any technologies that would lead them to decarbonization, they have highlighted major underlying challenges for both battery electric and hydrogen fuel cell technologies for locomotive applications. The industry, however, is eager to use sustainable or renewable fuels in their locomotives. This will help them reduce the emissions from their existing locomotives while next-generation decarbonization technologies are developed and readied for deployment. This strategy has been widely supported by most stakeholders with whom the Program has consulted while developing the research needs for rail decarbonization, including the Federal Railroad Administration (FRA).

While rail transportation carries 40% of U.S. shipments, much more than any other developed country, it is a relatively small source of GHG emissions, accounting for only about 2% of U.S. transportation energy use and GHG emissions [3], as shown in Figure 2. Freight rail overwhelmingly dominates rail energy use, consuming more than 90% of U.S. rail energy, while passenger and commuter rail consume a fraction of the energy [4], as shown in Figure 3.

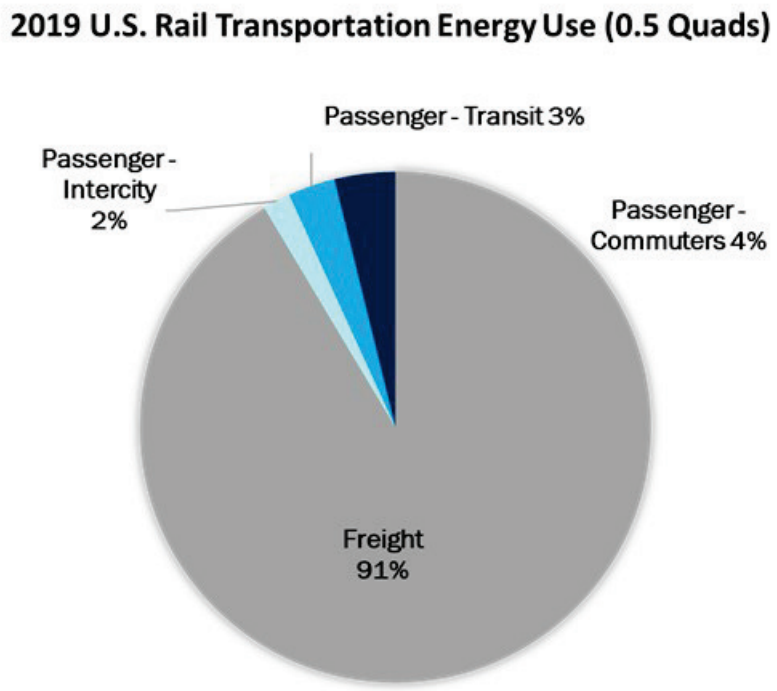

Figure 3 Rail energy consumption in the United States in 2019 [4]

Rail transportation consumes around 3.5 billion gallons of diesel per year in North America, which could result in about 90 billion pounds of CO_2 emissions [5]. In the U.S, 52% of all rail freight consists of agriculture and energy products, and the other 48% consists of consumer goods and other miscellaneous products. Rail freight carries the most non-containerized cargo (coal) and liquid bulk, notably oil deliveries, and the share of box cargo is also increasing [6]. Intermodal cargo will likely see high growth, further increasing its share of rail shipments [7]. A 2018 report from the Center for Climate and Energy Solutions (C2ES) estimated that ton-miles for freight transportation via rail were projected to increase 27% from 2017 to 2050, as industrial output increases [8]. As high fuel prices have greater cost impacts on road trucks than rail, rail's share of freight shipments is also likely to increase with increases in fuel prices.

Freight trains are, on average, 3–4 times more efficient at moving freight than trucks [9]. The energy intensity of Class I (defined as railroads with revenues exceeding $900 million per year) freight transportation has slowly but steadily improved from 350 Btu per ton-mile in 2000 to under 300 Btu per ton- mile in 2019 [10], as shown in Figure 4. When freight switchers and passenger trains are included, the resulting figure drops as low as 270 Btu per ton-mile, based on 2015 data. As freight trucks continue to increase their efficiency and reduce GHG impact through electrification, freight rails need to further their efficiency and reduce carbon footprint to maintain their competitive advantage over trucks.

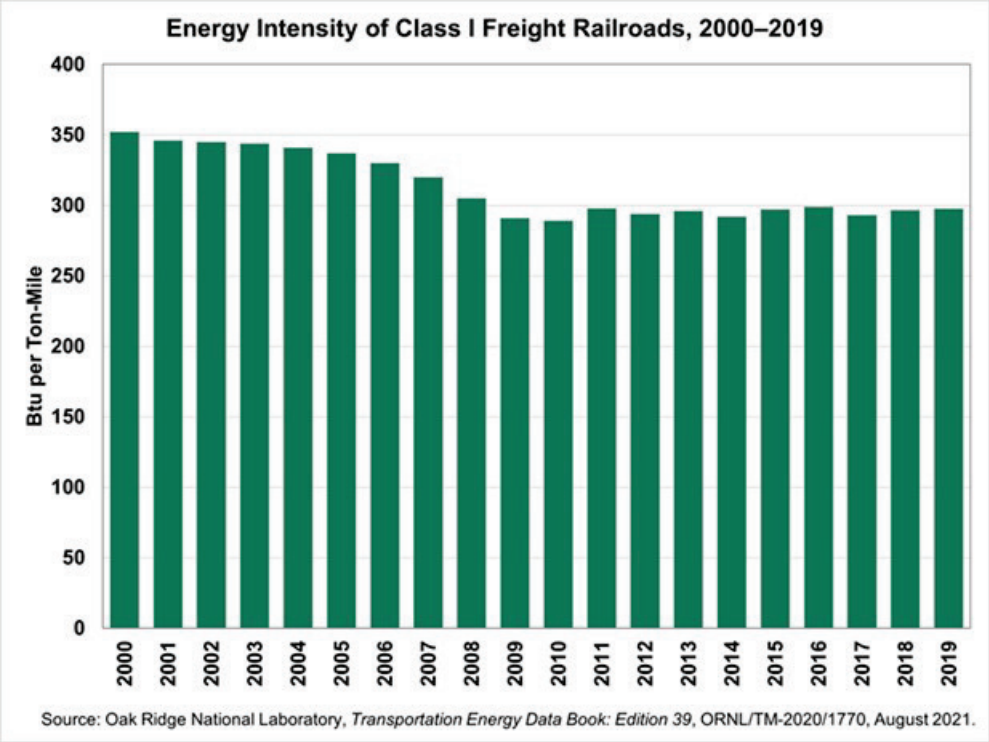

Figure 4 Energy intensity of Class 1 freight railroads [10]

Marine

The marine sector emits approximately 3% of U.S. transportation-affiliated GHG emissions[1]. Almost all marine vessels currently use fossil fuels, but there are significant opportunities to diversify energy sources used to power marine vessels, including widespread hybridization, use of alternative liquid fuels (such as methanol and ammonia), judicious use of hydrogen fuel cell powertrains, and battery-electrification of select applications. Large, ocean-going vessels are typically powered by enormous low-speed, two-stroke, cross-head compression ignition engines running on low-sulfur fuel, either distillate or heavier marine fuel oils. As these vessels are long-lived, major capital assets, it is generally impractical to re-power existing vessels of the largest size (such as tankers and container ships), so the realistic options for decarbonization by 2050 are limited to ultra-low-carbon fuels. Commercial harbor craft and inland vessels are primarily driven by medium-speed, four-stroke compression ignition engines running on diesel fuel. Recreational vessels are typically powered by four-stroke spark-ignited engines fueled with gasoline.

Diversity of vessel types and a dearth of quality data on operations and fuel use are typical of the marine sector. While this considerably complicates a comprehensive strategic approach to decarbonizing the sector, there are some likely opportunities to decarbonize some high-profile and high-exposure applications, such as electrification of passenger ferries and use of renewable fuels on U.S. cruise ships and inland marine vessels.

By far, the greatest marine source of energy use and GHG emissions is represented by international shipping. Moreover, projections of growth in global shipping emissions between now and 2050 run as high as 50%. As such, a critical aspect to decarbonizing the marine sector in the United States involves making low-carbon fuels available to visiting container and other cargo ships. These ships are almost entirely owned and flagged outside of the United States. The United States does not have a commercial large-ship construction industry,

[1] This figure includes international marine transport.

which limits opportunities for U.S. companies to directly benefit from technology breakthroughs applicable to these ships.

The DORMA Program is, therefore, focused on fuels issues for the largest ships. For medium-sized vessels, such as fishing vessels, ferries, tugboats, tow boats, service boats of various kinds, and so on, the Program considers engines operating on low-carbon fuels, fuel cells, hybrid systems, and battery electrification. In considering data on fuels, emissions, and technologies applicable to recreational boats, the DORMA Program follows U.S. Environmental Protection Agency emissions inventory classifications and groups these vessels with off-road vehicles.

Aviation

The principal strategy for decarbonization of aviation, at least through 2050, is likely to be increased use of sustainable aviation fuel (SAF). Commercial jets are long-lived technologies with unique requirements, chief of which is the ability to refuel internationally with compatible fuel. Thus, the international standards for aviation fuel (Jet A and Jet A-1) have tight specifications, and any SAF fuel blends must retain backwards compatibility with flying stock. The SAF Grand Challenge, the roadmap for which was published in the fall of 2022, seeks to develop 35 billion gallons of drop-in SAF by 2050, with an intermediate target of 3 billion gallons by 2030. While this drop-in fuel will be backwards compatible for use in current aircraft, there remain significant end use research opportunities to which the DORMA Program can contribute. For example, a significant amount of the global warming forcing function appears to be related to contrails formed in jet exhaust. DOE research can help improve understanding of factors contributing to the formation of contrails and other pollutant emissions (which can have a significant impact on air quality near airports). Federal Aviation Administration certifications for jet turbine engines, which prioritize aircraft safety, are organized around ASTM standards, and the resultant certifications are valid only for the fuel specified. For all commercial jet engines, the fuel used for certification is Jet A/A-1, as defined in ASTM D1655. While this standard was originally developed for petroleum-derived fuel, there is an allowance for synthetic fuels (e.g., not petroleum-derived fuels) to be treated as Jet A/A-1, meaning that they are a drop-in fuel.

Currently, ASTM D7566 lists seven drop-in SAFs that are approved for use, and all are primarily hydrocarbons with only trace levels of oxygenates or heteroatoms permitted. These SAFs can differ from petroleum-derived Jet A/A-1 in relative content of n-paraffins, iso-paraffins, cyclo-paraffins, and aromatics as well as the individual constituents. The drop-in terminology applies to the blended fuel (SAF blended with Jet A/A-1), as nearly all currently available SAFs are non-drop-in as neat fuels. An ASTM task force was formed in 2021 with an effort to modify the ASTM D7566 drop-in standard to allow 100% SAF.

Developing a better understanding of the relationship between fuel composition and engine performance and predictive modeling capability, along with an understanding of infrastructure impacts, is a key objective of the nascent DOE SAF end use R&D effort. This can be seen as, in part, an extension and continuation of the National Jet Fuels Combustion Program initiated in 2014, and complementary to research already supported by the Federal Aviation Administration, NASA, and others. Specific areas to which the DORMA Program anticipates making contributions include:

1. Small-volume screening of candidate SAF blendstocks.
2. Transferability of laboratory results to full-scale and next-generation combustors.
3. Blending impacts of multiple different SAFs, and criteria pollutant impacts of using SAF blends.
4. Improving understanding of fuel injection and mixing under sub-critical, trans-critical, and supercritical conditions.

5. Understanding effects of SAF properties on different figures of merit, including lean blowout, high-altitude relight, etc.

6. Developing data, knowledge, and computational tools and transferring them to industry.

Fiscal Year 2022 Technical Focus Areas and Objectives

The DORMA Program supports R&D to improve the understanding of the combustion and emissions control processes of off-road, rail, marine, and aviation applications and their optimization with renewable fuels. The Program also explores the potential for electrification and hybridization to further reduce GHG and criteria emissions. Leveraging the unique facilities and capabilities at the national laboratories and collaborating closely with academia and industry, the Program conducts cutting-edge research to strengthen the knowledge base and technical expertise in high-efficiency, advanced combustion engines and fuels, generating the insights needed by non-road vehicle manufacturers to improve the efficiency of engines and reduce emissions.

The Program's objectives in 2022 were as follows:

- Develop science-based understanding of how engine efficiency and emissions are impacted by renewable fuel properties and, conversely, how engines and emissions controls can be modified to take advantage of desirable fuel properties to meet future emissions regulations.

- Reduce the fuel use penalty and improve the effectiveness and durability of emissions control (exhaust aftertreatment) devices used with renewable fuels.

- Further advance engine technologies such as turbomachinery, flexible valve systems, advanced combustion, and fuel system components for renewable fuels.

- Develop a hardware-in-the-loop engine research facility for system-level and drive-cycle technology development to enable net-zero-carbon fuel efficient designs for hydrogen (H_2) internal combustion engines and fuel cells for off-road and marine applications. Optimize hybrid powertrains for off-road vehicles.

- Explore trans-critical phenomena of SAFs through high-fidelity simulations at relevant conditions.

- Develop predictive computational fluid dynamics capabilities for the analysis of ignition performance of SAFs at high altitude.

The Program maintained close collaboration with industry through several working groups and teams to utilize these networks in identifying and addressing critical issues, setting goals, adjusting research priorities, and tracking progress. These working groups include a broad range of stakeholders representing vehicle and engine manufacturers, energy companies, biofuel producers, manufacturers of catalysts and emissions control systems, fuel distributors and retailers, national laboratories, and universities.

Technical Highlights

Off-Road

University of Minnesota is conducting research to develop a systematic method and tools to optimize and evaluate energy savings for connected and autonomous off-road vehicles. The project will develop systematic optimization and control strategies for connected and autonomous off-road vehicles to achieve significant energy savings (20%–40%) with improved productivity, as well as develop a hardware-in-the-loop (HIL) testbed to evaluate the energy savings of connected and autonomous off-road vehicles in a time-efficient, safe, and cost-effective fashion. In Fiscal Year (FY) 2022, the project developed the communication system,

determined a solution of optimization for both transport and digging phases, and constructed an HIL testbed. (Sun I.1)

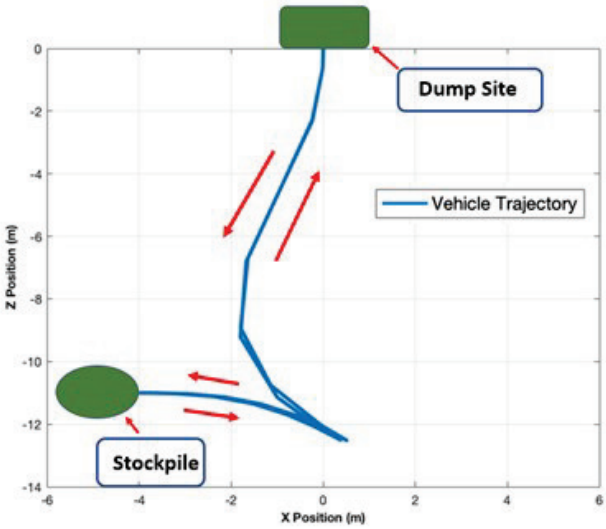

Figure 5 Optimal vehicle trajectory during the transport phase (Sun, I.1)

Purdue University is demonstrating the advantages of its proposed multi-pressure rail (MPR) system when applied to agricultural tractors and their implements. In FY 2022, the project team (1) formulated and implemented a supervisory controller suitable for operating the hydraulic functions through the MPR system, (2) validated the simulation model of the MPR system and its supervisory controller based on the results of the standalone test rig built during the previous fiscal year, (3) formulated and simulated layouts for compatible MPR solutions for an MPR tractor coupled with a non-MPR implement and vice versa, (4) procured components and a data acquisition system to implement the MPR solution on the reference vehicles, (5) modified the reference vehicles to implement the MPR prototypes, (6) performed field tests on significant duty cycles with the MPR prototypes and measured system performance parameters, (7) and confirmed the model prediction for the MPR system on the reference vehicles based on the field test. (Vacca I.2)

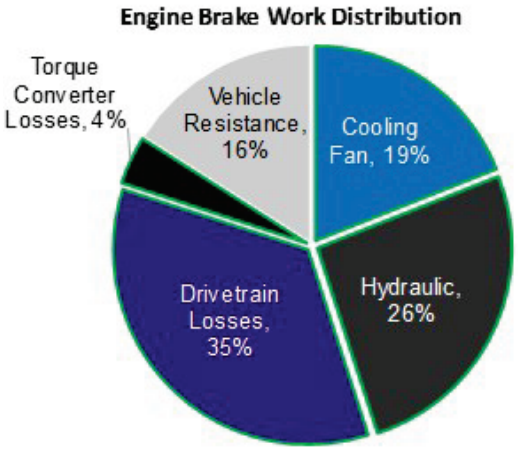

Figure 6 Engine brake work distribution (composite cycle) (Worm I.3)

Michigan Technological University is electrifying the propulsion and fluid power systems of a Pettibone 204i off-road material handler to demonstrate at least 20% reduction in real-world fuel consumption without negatively impacting emissions, performance, operability, noise, vibration, harshness, etc. In FY 2022, the project partners created a design palette of viable commercial off-the-shelf electrification components and defined a short list of electrification architectures with the highest probability of meeting the project goals using reduced-order, first-principles analysis techniques. The team conducted a full-cycle simulation of the identified potential electrification architectures using the detailed Simcenter Amesim model, completed an engineering decision analysis of the simulation results with the intent of selecting an architecture and specific components, and completed the engineering and design effort required to integrate the electrification components. (Worm I.3)

University of Wisconsin–Madison is conducting research with the goal to enable a greater than 10% increase in efficiency of off-road vehicles by integrating electric machines and advanced internal combustion engines through systematic assessment of the benefits and drawbacks of electrification for the off-road sector, developing a hybrid powertrain capable of improving efficiency by over 10% in a wheel loader application, and using electrification to enable downsizing. In FY 2022, it performed system-level experiments to test the engine with an electrified powertrain, designed components for vehicle-level testing, and performed system-level analysis to compare multiple architectures for hybrid off-highway vehicles. (Kokjohn I.4)

Figure 7 Compact track loader to be electrified (Li, I.5)

University of Minnesota is developing and demonstrating a fully electric compact track loader (CTL) with high efficiency using a system architecture that leverages hydraulic actuation to reduce the size and cost of the electric components. The target is to reduce electricity (and battery) usage by 40%, as compared to the standard strategy of replacing the current machine's diesel engine with an electric motor. In FY 2022, the team designed and optimized the system architecture to be prototyped, designed and developed hardware-in-the-loop laboratory testbeds for the work and propel circuits, and generated potential soft-switching valve concepts to minimize throttling loss during pressure-rail transitions. (Li I.5)

John Deere Intelligent Solutions Group is conducting research, development, and validation of a hybrid-powertrain-enabled articulated dump truck (ADT) testbed potentially capable of ≥25% fuel savings and ≥25% greenhouse gas (GHG) and criteria pollutant reductions when compared to a conventional ADT vehicle with a 9 L engine. In FY 2022, the project conducted dynamic system modeling (DSM, described further below) of the following major components needed for fabrication of the diesel–electric hybrid powertrain to be integrated in the 310E model of the eADT: 6.8 L engine; 250 kW, 700 V dual inverter; 700 V battery pack; 15 kW, 700 V/48 V direct current (DC)-to-DC converter. (Singh I.6)

University of Minnesota is developing a methodology for improving the efficiency of high-power, off-road mobile machines that takes advantage of electrification without the need for very high power or costly electric components. It will develop a system architecture that marries the comparative advantages of hydraulic actuation and electrical actuation. In FY 2022, the team experimentally validated the motion control strategy on a high-pressure hardware-in-the-loop testbed, prototyped the proposed integrated hydraulic–electric power conversion machine, and characterized the power conversion machine's performance. (Li I.7)

Caterpillar Inc. is designing and demonstrating a high-efficiency power system with a heavy-duty hybrid diesel engine system for use in off-road machine applications. In FY 2022, the project validated the complete power system in a transient cell in the Phase 2 hybrid engine system and performed technoeconomic analysis to address cost barriers and provide total-cost-of-ownership value assessment. (McDavid I.8)

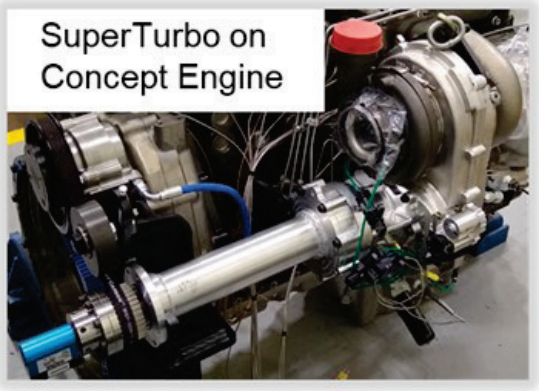

Figure 8 Phase 2 concept engine with SuperTurbo assembled (McDavid, I.8)

Eaton Corporation is researching, developing, and validating engine and aftertreatment (AT) system technologies for significantly reducing nitrogen oxides (NO_x) and greenhouse gas (GHG) emissions for off-road powertrains over multiple duty cycles spanning the segment's diverse applications, while maintaining affordability and robustness to ensure economic viability. In FY 2022, the project determined system definition and performance metrics, built a baseline and aged the AT system using hydrothermal aging, designed and built the base future engine, designed the modular AT system, and assessed the baseline GHG correction compared to the modular AT system architecture. (McCarthy I.9)

Marquette University will demonstrate a heavy-duty engine that can use any blend of gasoline and ethanol and develop the prechamber-enabled mixing-controlled combustion (PC-MCC) concept for gasoline/ethanol blends for heavy-duty engines. In FY 2022, chemical-reacting computational fluid dynamics (CFD) simulations of a

1.6 L single-cylinder, heavy-duty engine were conducted to determine the minimum required prechamber (PC) volume for robust ignition and an acceptable range for passageway size to ensure proper PC breathing and PC jet flame penetration. Detailed packaging studies were conducted to determine appropriate mounting locations for the PC igniter and direct injector in both single-cylinder and multi-cylinder heavy-duty engines. (Dempsey I.10)

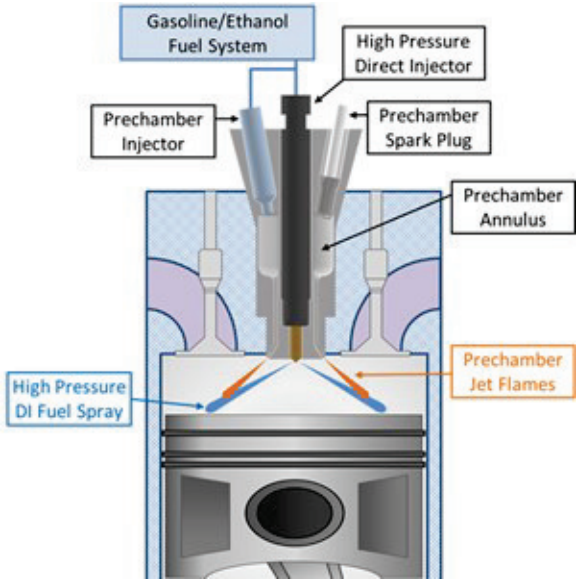

Figure 9 Prechamber enabled mixing-controlled combustion (Dempsey, I.10)

In FY 2022, Pacific Northwest National Laboratory is applying advanced imaging techniques to a diesel particulate filter (DOCF) to characterize washcoat effects on the physical characteristics of the filter and the resulting impact on flow uniformity (or lack thereof) and catalyst usage. Researchers completed and commissioned SpaciMS (spatially resolved capillary inlet mass spectroscopy) capability for testing DOCF structures under various conditions, and preliminary data sets have been generated for modeling calibration. The engine testing capability is nearing completion with instrumentation to support chemical and thermal DOCF assessment under different exhaust environments. In addition, the DOCF modeling capability was completed and is ready for calibration with the laboratory's kinetic calibration efforts and SpaciMS data. (Rappe I.11)

Sandia National Laboratories is working to establish a comprehensive understanding of the in-cylinder processes associated with in-cylinder mixture formation and its impact on engine performance, emissions, wall heat loss, and coupling with advanced ignition systems. In FY 2022, the research team applied laser and imaging diagnostics in an optical, heavy-duty engine equipped with a medium-pressure hydrogen direct injector to assess the impact of injection timing and injection pressure on in-cylinder mixture formation and associated engine performance. The team also established a framework to study hydrogen pre-ignition mechanisms decoupled from each other under controlled conditions and validated the framework by characterizing the hot-spot pre-ignition mechanism. (Srna I.12)

Sandia National Laboratories is providing the scientific understanding needed to design, optimize, and calibrate the next generations of off-road compression-ignition engines that comply with increasingly stringent pollutant emissions regulations while achieving thermal efficiencies exceeding 50%. In FY 2022, researchers (1) quantified the fuel efficiency and pollutant emissions benefits of a second-generation DSL piston, (2) characterized the sources of unburned hydrocarbons (UHCs) during catalyst-heating operation, quantifying the contribution of each injection event to the total tailpipe UHC emissions, (3) applied a laser-based extinction technique in an optically accessible exhaust runner to investigate the spatiotemporal origins of formaldehyde in catalyst-heating operation, (4) explored new strategies to mitigate pollutant formation and maximize exhaust enthalpy for optimum catalyst-heating operation, (5) assessed the effects of fuel's autoignition reactivity (cetane number) and distillation characteristics (boiling range) on engine cold-start performance, and (6) demonstrated an advanced wireless telemetry system for on-board engine data acquisition and a novel heat-flux micro-sensor to provide time-resolved heat-flux data. (Lopez-Pintor I.13)

Sandia National Laboratories is working to glean a fundamental understanding of the impacts of SAFs on flame stabilization combustion dynamics using high-fidelity simulations and performing statistical analysis of the data to evaluate, develop, and improve combustion models. In FY 2022, they performed high-fidelity simulations of spray flames under gas turbine operating conditions, verified spray injection modeling strategies using experimental data, identified chemical mechanisms capable of predicting flame stabilization at high

pressures and moderate temperatures, and identified mixing and mixture reactivity effects on flame stabilization dynamics. (Chen I.14)

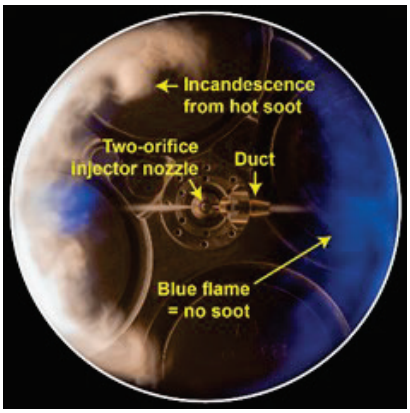

Figure 10 Image acquired through a window in the piston of an optical engine, showing a conventional diesel combustion spray on the left, producing a cloud of incandescent soot particles, and ducted fuel injection on the right, producing no soot. (Mueller, I.15)

Sandia National Laboratories will enhance the fundamental and practical understanding of ducted fuel injection (DFI) to facilitate its successful and rapid commercial implementation to reduce net-carbon and criteria pollutant emissions from difficult-to-decarbonize, heavy-duty applications. In FY 2022, they determined whether DFI can be used to curtail soot emissions at full-load conditions with a low-net-carbon fuel, continued advancing the fundamental understanding of key physical processes governing DFI performance, and assembled a consortium of industry stakeholders to assist in further developing DFI for successful commercial application. (Mueller I.15)

Sandia National Laboratories utilized a research diesel injector of special design to understand the interaction between separate fuel spray plumes, with diagnostics performed within optically accessible spray chambers. In FY 2022, researchers characterized the spray, combustion, and sooting behavior of a four-hole Engine Combustion Network diesel injector and measured the limits of soot-free diesel combustion using oxymethylene ethers, including detailed mixture fraction, upstream formaldehyde, and high-temperature combustion. They also assessed liquid penetration, ignition, and combustion for methanol diesel sprays and led a multi-institution, international research effort on engine spray combustion called the Engine Combustion Network. (Pickett I.16)

Lawrence Livermore National Laboratory identified a need to develop accurate fuel chemistry models for use by industry designers in difficult-to-decarbonize markets such as off-road, rail, marine, and aviation. In FY 2022, researchers worked to develop predictive kinetic models for the combustion of low-life-cycle carbon fuel components and mixtures that span near-term to long-term decarbonization goals, as well as predictive kinetic models for emissions, such as soot and NO_x, from the combustion of low-life-cycle carbon fuels. (Wagnon I.17)

Pacific Northwest National Laboratory (PNNL) is advancing aftertreatment catalyst technology with high durability and low-temperature activity applicable to internal combustion engine exhaust systems. Researchers are focused on developing the fundamental information that clarifies current barriers to aftertreatment materials and enables the pursuit of pathways to mitigate or circumvent those barriers through materials design. In FY 2022, PNNL developed new classes of thermally stable single-atom catalysts to reduce the use of platinum group metals for low-temperature oxidation and improved the performance and stability of next-generation oxidation catalysts so that engines with dramatically enhanced fuel efficiencies can be implemented while still meeting future U.S. Environmental Protection Agency emissions regulations. (Wang I.18)

Pacific Northwest National Laboratory is working to understand the function of aftertreatment devices at the atomic-, nano-, and micro-scales and to predict the integrated performance of system designs considered. In FY 2022, the team demonstrated and established the structure-function relation of next generation selective catalytic reduction (SCR) catalyst technologies with superior SCR performance and hydrothermal stability and developed the necessary fundamental and applied understanding of barriers faced by current-generation SCR materials so that their function can be accurately predicted through full useful life. (Wang I.19)

Pacific Northwest National Laboratory (PNNL) is working to characterize high-mileage field-aged catalysts from Cummins to provide guidance in developing complex aging protocols, develop characterization tools to monitor the dynamic changes upon progressive aging, identify the cause of degradation, and develop procedures to simulate real-world aging of selective catalytic reduction (SCR) catalysts. In FY 2022, PNNL (1) revealed gaps between real-world and laboratory-accelerated aging via detailed kinetics studies, (2) used in situ

X-ray photoelectron and electron paramagnetic resonance (EPR) spectroscopies to reveal the nature of sulfur poisoning and elucidate possible mechanisms, (3) used operando EPR spectroscopy to elucidate transformations of SCR active Cu during real-world and laboratory-accelerated aging, and (4) developed real-world sulfur aging models that accurately describe the aging behavior of catalysts. (Gao I.20)

Oak Ridge National Laboratory is addressing emissions control challenges associated with running rail, marine, and off-road engines on low lifecycle carbon fuels (LLCFs) through measurement of the fuel chemistry effects of LLCFs on a commercial emissions control catalyst and evaluation of potential alternative emissions control solutions to handle the unique emissions from promising LLCFs. In FY 2022, researchers measured the catalytic reactivity of alcohol LLCFs and their aldehyde partial oxidation products over a commercially relevant, aged diesel oxidation catalyst and published results from prior investigations of Co-Optima blendstock fuel reactivity on emissions control catalysts. (Sinha Majumdar I.21)

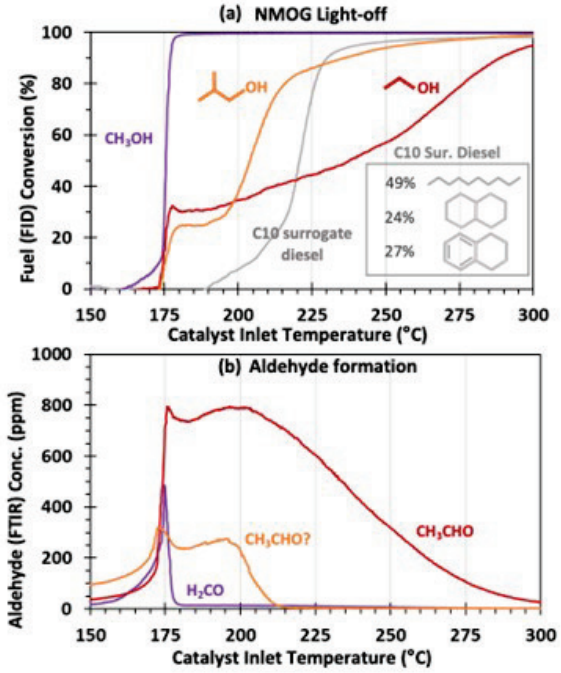

Figure 11 (a) Non-methane organic gases (NMOG) conversion of a C10 diesel surrogate and LLCF alcohols such as methanol (purple), ethanol (red), and isobutanol (orange) with (b) corresponding Fourier transform infrared (FTIR) aldehyde traces over an aged commercial diesel oxidation catalyst under lean conditions. (Sinha Majumdar, I.21)

Argonne National Laboratory (ANL) is enabling net-zero-carbon, fuel-efficient design for hydrogen internal combustion engines (ICEs) for off-road and marine applications using hardware-in-the-loop (HIL) simulation for system-level and drive-cycle-appropriate technology development. In FY 2022, ANL commissioned a new Vieletech test cell control system, commissioned an HIL powertrain test cell control system, and developed a LabVIEW interface with Autonomie/RoadRunner. (Biruduganti I.22)

Rail

Westinghouse Air Brake Technologies Corporation (Wabtec) is providing critical dimensional scaling guidance for ducted fuel injection (DFI) and cooled spray (CS) technologies and demonstrating more than 75% particulate matter reduction over a range of operating conditions using CS technology. In FY 2022, researchers evaluated at least three CS configurations in a Wabtec metal engine, quantified the performance impacts of CS components over the engine operating map, demonstrated at least 50% soot reduction for some operating conditions using CS, and compared conventional diesel combustion to DFI in the optical engine at higher loads with larger injector orifices than previously demonstrated. (Klingbeil II.1)

Argonne National Laboratory is developing and evaluating the performance of a dual-fuel technology in the Progress Rail 1010J single-cylinder, four-stroke locomotive engine (1010J-SCE) using methanol and dimethyl ether (DME) fuels. In FY 2022, the team recommissioned the Progress Rail 1010J-SCE four-stroke locomotive engine, prepared the facility and recommissioned all the 1010J-SCE subsystems, and performed engine shakedown tests to assess the engine's condition. (Elhannouny II.2)

Argonne National Laboratory (ANL) is developing and validating computational tools for combustion of low-carbon fuels, with a focus on hydrogen, in heavy-duty rail engines for use in evaluating different technologies and fuel injection options to enable up to 100% operation on hydrogen and low-carbon fuels for rail engines. In FY 2022, ANL developed an accurate tool for modeling dual-fuel combustion in locomotive engines,

quantified accuracy of the tool through comprehensive validation studies, and evaluated the effect of turbulence and combustion models on model accuracy. (Ameen II.3)

Argonne National Laboratory (ANL) is enabling efficient engine operation in rail applications via the use of low lifecycle carbon fuels such as biodiesel and renewable diesel and identifying the necessary modifications to the 1010J-SCE engine and injection system to allow use of these fuels while meeting Tier 4 emission regulations. In FY 2022, ANL recommissioned the 1010J-SCE engine test facility and developed baseline models for high-fidelity nozzle flow simulations. (Xu II.4)

Figure 12 Wabtec single-cylinder locomotive research engine and dynamometer at the ORNL National Transportation Research Center (Edwards, II.5)

Oak Ridge National Laboratory (ORNL) is developing solutions for the use of low lifecycle carbon fuels and low-emissions technologies for locomotive engines, including port-fuel-injection retrofit hardware configurations and operating strategies for dual-fuel operation, as well as direct injection hardware configurations and operating strategies for near-complete fuel substitution while maintaining engine performance and emissions compliance. In FY 2022, the team executed an agreement between ORNL and Wabtec and began installation of the Wabtec single-cylinder research engine, subsystems, and low lifecycle carbon fuels infrastructure. (Edwards II.5)

Marine

Argonne National Laboratory is developing predictive computational capabilities for the analysis and design of advanced internal combustion engines for off-road applications through development of predictive models for the simulation of low-carbon-fuel off-road internal combustion engines, as well as through modeling best practices to efficiently design off-road engines using low-carbon fuels. In FY 2022, researchers finalized the scope of work to address DOE/industry priorities for off-road sector decarbonization and defined the technical scope and legal terms of the cooperative research and development agreement (CRADA) before submitting the CRADA documents for approval. (Scarcelli III.1)

Oak Ridge National Laboratory is developing engine technologies to displace the maximum amount of diesel fuel with methanol (up to 100%), in collaboration with a major marine engine manufacturer, while maintaining or improving engine performance, efficiency, durability, and emissions relative to the current diesel baseline. In FY 2022, the team established support for a multi-year CRADA with a major marine engine original equipment manufacturer to pursue marine engine decarbonization with methanol, develop a scope of work, and submit the CRADA document for approvals. Additionally, the team solicited project input and support from the U.S. Department of Transportation Maritime Administration for the CRADA project. (Szybist III.2)

Aviation

Argonne National Laboratory is assessing fuel behavior through a validated two-phase flow model based on X-ray data and appropriate combustion, turbulence, chemical kinetics models, and best practices. In coordination with the U.S. Department of Energy's Bioenergy Technologies Office, the fuels and fuel properties will be determined and evaluated both experimentally and computationally for use by industry. Research will be performed under four major tasks: (1) X-ray measurement for model development, (2) computational fluid dynamics simulations and validation to model the behavior of sustainable aviation fuels in a combustor, (3) rapid compression machine adaptation for fuels and operating conditions modeling, and (4) high-fidelity simulations of a combustor toward direct numerical simulation capability to capture flow and flame dynamics. (Som IV.1)

Sandia National Laboratories is investigating the characteristics of spray combustion at conditions relevant to modern aero-engines across the main, yet challenging operating points. In FY 2022, the custom injection system based on the single-hole atomizer was used to inject different types of liquid jet fuels, including sustainable aviation fuels, in a constant-volume pre-burn chamber where ambient conditions were set to mimic representative thermodynamic conditions that can be found in real aero-engine combustors. Flame stabilization and associated fundamental mechanisms under conditions relevant to aero-engine combustion were investigated, using formaldehyde planar laser-induced fluorescence and excited hydroxyl radical chemiluminescence. The data acquired with these two diagnostic techniques were combined with diffuse back-illumination extinction imaging measurements to investigate differences in soot formation between the fuels. (Manin IV.2)

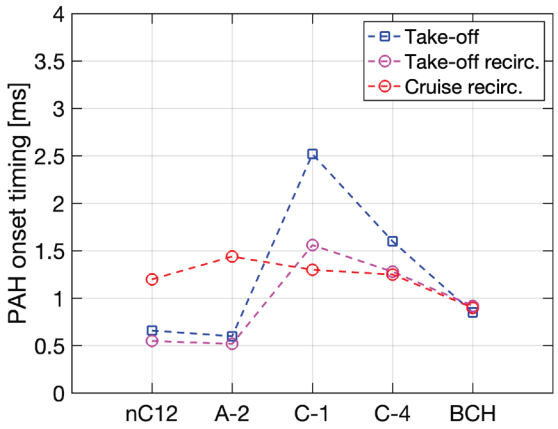

Figure 13 Measured peak soot mass for all conditions and fuels: a nominal reference Jet A fuel (A-2), an alcohol-to-jet fuel containing highly branched dodecane and hexadecane type components (C-1), a blend made of 40% C-1 and 60% iso-paraffins ranging from 9 to 12 carbon atoms (C-4), and an advanced bio-derived cyclo-alkane fuel (BCH) (Manin, IV.2)

Lawrence Livermore National Laboratory is developing a chemistry model that captures significant trends in particle size and number of the formation and destruction of water–ice particles, creating a method to couple soot and ice formation models with existing cloud microphysics models to predict the initial evolution of sustainable aviation fuel contrails. The captured trends and predictions will be used to release updates onto the combustion solver software library Zero-RK for the stakeholders to access combustion and contrail modeling tools. In FY 2022, the team established access to atmospheric thermodynamic data at flight conditions relevant to the contrail formation and evolution processes, verified that the current fuel chemistry and soot formation models will produce stable simulations, and identified additions to expand the fuel combustion model to include atmospheric chemistry, ice nucleation, and other cloud microphysics models. (Wagnon IV.3)

Crosscutting

Lawrence Livermore National Laboratory is advancing the state of the art in low lifecycle carbon fuels (LLCF) combustion simulation through the development of fast and accurate models, as well as collaboration with industry partners to prove capability and impact of combustion software. In FY 2022, the team created fuel surrogate and reduced kinetic models for LLCF combustion research and developed neural-network species prediction models that accelerate computational fluid dynamics simulations containing detailed reaction models by reducing the number of kinetic species that need to be resolved. (Whitesides V.1)

National Renewable Energy Laboratory (NREL) is creating unique experimental capabilities for measuring critical properties of conventional jet fuel and synthetic aviation turbine fuel (SATF) over the full range of turbine engine operating conditions, developing an improved ignition delay metric for jet fuels, utilizing NREL's existing flow reactor and constant volume combustion chamber capability to inform development of reduced kinetic models for current and future forms of sustainable aviation fuel, and simulating and investigating the impacts of fuel properties on the performance of a single-nozzle flame tube and uncertainty in fuel property measurements on the simulation results. In FY 2022, researchers identified and acquired instruments to measure density and viscosity over the full temperature and pressure range, identified an instrument to measure surface tension over the full temperature and pressure range, and demonstrated that the Advanced Fuel Ignition Delay Analyzer can measure cetane numbers for jet fuels and SATF that are identical to those measured by other methods. (McCormick V.2)

Legacy On-Road

Combustion

Auburn University is advancing the predictive capabilities of low-temperature plasma (LTP) ignition submodels for the optimization of fuels and multimode engines to support the development of LTP ignition technologies to enable multimode engine concepts and to contribute to the overarching goal of developing more efficient engines with sustainable future fuels. In FY 2022, researchers (1) developed a plasma-specific kinetic mechanism for ethanol oxidation and pyrolysis, (2) simulated LTP ignition of ethylene–air mixtures using the AMReX library1 and newly developed high-fidelity models, and (3) integrated circuit dependence in a discharge model to estimate discharge efficiency and implement fuel dissociation via electron impact in VizGlow. (Tsolas VI.A.1)

Purdue University is radically improving the predictive accuracy and efficiency of turbulent combustion submodels for turbulent jet ignition (TJI) through the development of a hierarchically informed engineering model for turbulent combustion in TJI. The hierarchically reduced model will ensure predictive accuracycomparable to that produced by high-order models but with a significantly reduced computational cost. In FY 2022, the team developed a high-fidelity predictive large-eddy simulation (LES) solver for the entire cycle of TJI combustion, validated the high-fidelity LES combustion solver by using a model TJI rig, and simulated the Argonne National Laboratory engine with conventional combustion models to verify the model validation framework. (Wang VI.A.2)

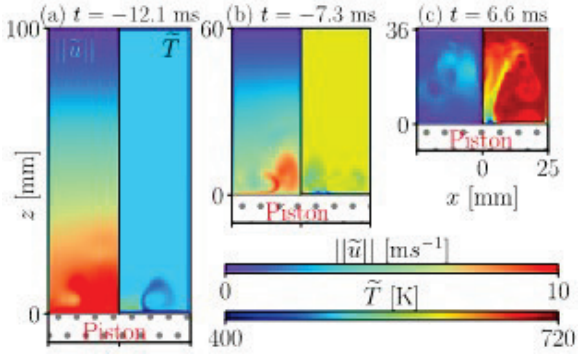

Figure 14 Velocity (left, mirrored) and temperature (right) fields on the deforming rapid compression machine quarter domain of the short ignition case at three time instances (Ihme, VI.A.3)

Stanford University is developing improved physical submodels and examining multimode combustion regimes to support the Office of Energy Efficiency and Renewable Energy Co-Optima program through (1) development of accurate submodels for predicting multimode combustion regimes, wall-heat transfer, non-equilibrium plasma ignition, and combustion-mode transition; (2) validation of the computational submodels against experiments and direct numerical simulation data in conjunction with sensitivity analysis; (3) support of the direct transition of the resulting submodels into other engine simulation tools through the development of self-contained modules; and (4) examination of complex combustion regimes in multistage ignition and high-pressure spray combustion. (Ihme VI.A.3)

Hyundai America Technical Center, Inc., is co-optimizing a multimode-capable engine with fuel formulation to improve vehicle fuel economy by 15% over the baseline, attain a power target of at least 150 hp, meet or exceed LEV III emission targets, demonstrate multimode combustion control, validate computational fluid dynamics (CFD) models, populate a spray and combustion database, and produce a CFD mesh and models for spray and engine data. In FY 2022, the research team (1) refined a multimode rapid prototyping controller for the multimode engine control, (2) developed a combustion strategy for low temperature combustion mode, (3) evaluated strategies for rated engine operating conditions, (4) confirmed the overall combustion strategy for the multimode engine through engine testing, (5) demonstrated combustion mode switching, (6) completed engine testing for fuel formulation effects and fuel optimization for the multimode engine, (7) validated a CFD model for multimode engine and different fuels, and (8) confirmed fuel economy improvement with the proposed multimode engine. (Zhu VI.A.4)

Oak Ridge National Laboratory is co-optimizing the combustion chamber geometry, injector geometry, and fuel physical properties for two diesel fuel chemistries, conventional diesel and hydrotreated vegetable oil (HVO), subject to emissions and mechanical limit constraints for improved engine thermal efficiency. In FY 2022, researchers defined significant fuel property ranges for conventional diesel and HVO, coupled and tested

an optimizer with CAESES and CONVERGE computational fluid dynamics engine models to establish workflow, defined operating conditions of interest for optimization, and discretized piston bowl shape geometry for automatic geometry generation. (Chuahy VI.A.5)

Argonne National Laboratory is quantifying the effects of fuel volatility as an independent fuel property on low-temperature heat release (LTHR), both experimentally and numerically, and proving or disproving the hypothesis that preferential evaporation of volatile components in direct ignition engines produces reactivity stratification such that the less reactive volatile components govern the overall reactivity. In FY 2022, the team developed and blended a set of fuels designed to test the hypothesis that preferential evaporation of volatile fuel components in direct ignition engines produces reactivity stratification such that the less reactive volatile components govern the overall reactivity and conducted a series of a priori computational fluid dynamics simulations to test the differences between single- and multi-component evaporation models on LTHR. (Som VI.A.6)

Alternative Fuel Engines

Cummins Inc., is developing and demonstrating a Dynamic Skip Fire® (DSF)-enabled, heavy-duty (HD) natural gas (NG) engine capable of diesel-like performance and efficiency while maintaining the capability to meet emissions standards. In FY 2022, the project team developed the engine overhead layout; designed overhead and cylinder deactivation components; and designed, analyzed, and simulated engine models to define control system requirements and drive cycle simulation. The focus was on hardware design of the overhead components, development of the control system requirements and interfaces, and engine model development for simulation. The engine model was used to simulate engine operation with DSF to assess the impact of DSF on base engine controls, as well as to develop algorithms. Baseline engine data for the HD NG engine was used to develop the initial DSF firing frequency map. (Shah VI.B.1)

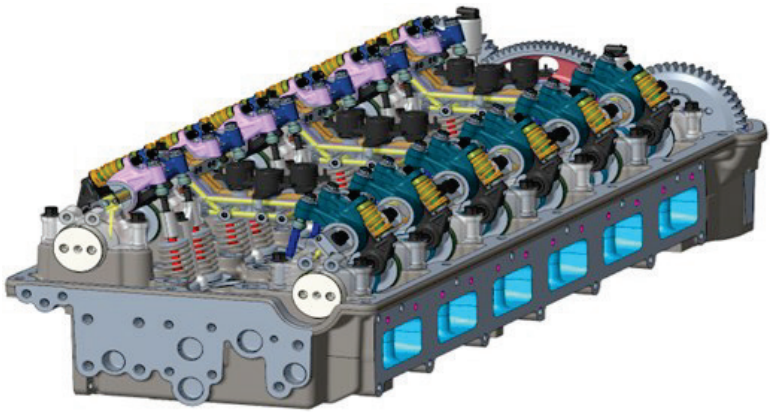

Figure 15 Head and overhead assembly (Shah, VI.B.1)

Colorado State University is addressing fundamental limitations to achieving near-diesel efficiencies in heavy-duty on-road liquefied petroleum gas (LPG) engines. The focus is on the Cummins 15-L heavy-dutyengine platform. The main project goal is to increase the peak torque efficiency of a 15-L LPG engine to 44%. FY 2022 efforts included fabrication and delivery of a Cummins X15 custom cylinder head for LPG direct injection, production and spray imaging of prototype LPG direct injectors, incorporation of the LPG spray model into a CONVERGE computational fluid dynamics model and generation of initial simulation results, and LPG port fuel injection baseline testing on the Cummins X15 single cylinder engine. (Olsen VI.B.2)

Oak Ridge National Laboratory is developing and demonstrating direct-injected liquified petroleum gas (LPG) stoichiometric spark-ignition engine technologies to achieve fuel efficiency and torque parity with current medium-duty diesel engines. The objective is to provide experimental data that demonstrates technologies and approaches to achieve a cycle efficiency of 41% in the supplemental emissions test steady-state cycle while meeting all applicable 2027 criteria emissions regulations. In FY 2022, the team optimized a long-stroke stoichiometric propane spark-ignition engine platform using advanced simulation tools and developed a fundamental understanding of the particular fuel properties of LPG that promote its stability under exhaust dilution using direct numerical simulations and high-fidelity engine simulations. (Splitter VI.B.3)

WM International Engineering LLC is developing a state-of-the-art fuel system that operates with mixtures of propane and DME to improve the efficiency of a light-duty engine while providing significant emission reductions. In FY 2022, researchers completed fuel system modeling of the electro-hydraulic fuel system and developed calibration maps of the first interim design for operation with diesel and the propane–dimethyl ether (DME) mixture. Fuel bench testing was designed and built for (1) performance, validated with diesel and propane–DME, and (2) durability, tested with propane–DME for spray visualization experiments with the base hardware. The team completed the advanced fuel system design and issued manufacturing drawings for machining and also completed engine performance modeling to demonstrate that the use of a propane–DME mixture supports the efficiency and CO_2 targets of the project. (de Ojeda VI.B.4)

University of Wisconsin–Madison is enabling a 15% reduction in CO_2 emissions compared to current diesel engines by developing an MCCI combustion strategy capable of operating on blends of propane and dimethyl ether (DME). To achieve this goal, researchers will develop and demonstrate a high-efficiency mixing-controlled combustion engine suitable for operation on propane and propane–DME blends. In FY 2022, the team designed and adapted a propane–DME fuel system to the target medium-duty test engine, set up a test cell to enable combustion system development, and evaluated predictive ability of propane–DME reaction mechanisms. (Kokjohn VI.B.5)

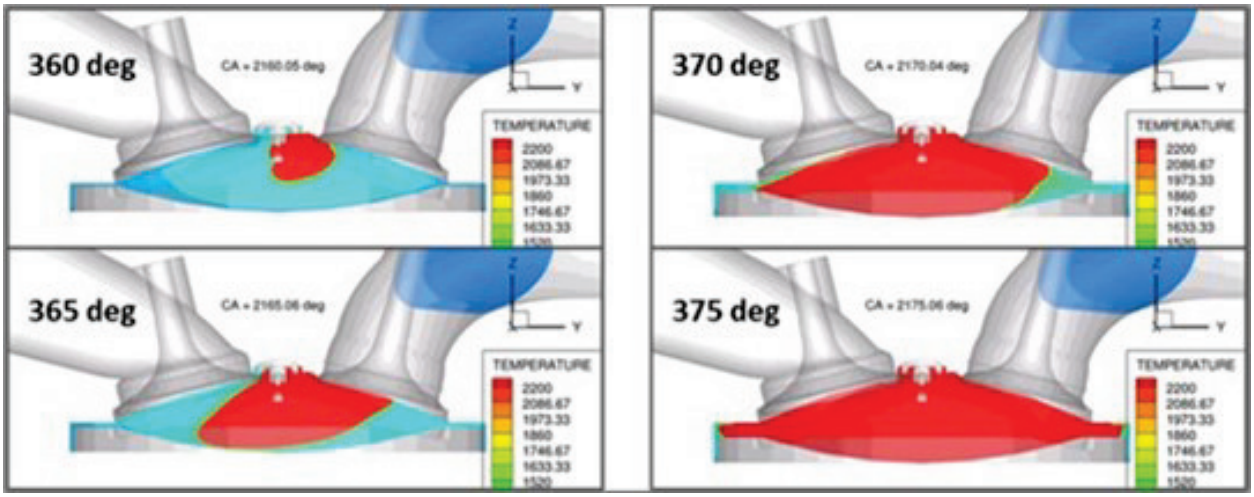

Figure 16 Combustion at rated power (Lutz, VI.B.6)

Cummins Inc., is researching, developing, and validating a next-generation, combustion-system-equipped, heavy-duty natural gas engine that utilizes high tumble charge motion, building upon a proven high-cylinder-pressure-capable heavy-duty base engine platform in the 10-L displacement range. In FY 2022, researchers (1) created simulation models to predict engine performance based on other models developed for spark-ignition engines; (2) used these models to determine the engine architecture and path to reach program efficiency targets; (3) began the design of a new cylinder head with pent roof, tumble intake port geometry, and optimized combustion deck cooling; (4) began design of the port-injected fuel system, including injector installation, fuel rail, fuel filter, fuel regulator, and sensors; and (5) began optimization of the combustion system using computational fluid dynamics simulation. (Lutz VI.B.6)

Emission Control

Washington State University is demonstrating vehicle federal test procedure, US06 test performance, and highway fuel economy test performance comparable to a baseline system with a reduction in platinum group metal (PGM) content by a factor of 2–4. The FY 2022 objective focused on technology transfer and validation by incorporating the powder formulation into a slurry-based washcoat and applying it to a suitable ceramic catalyst support. Researchers conducted simulated engine tests and baseline with current BASF three-way

catalysts, with the specific goal of meeting or exceeding the BASF baseline catalyst performance (SULEV30) with a factor of 2–4 reduction in PGM content. (Wang VI.C.1)

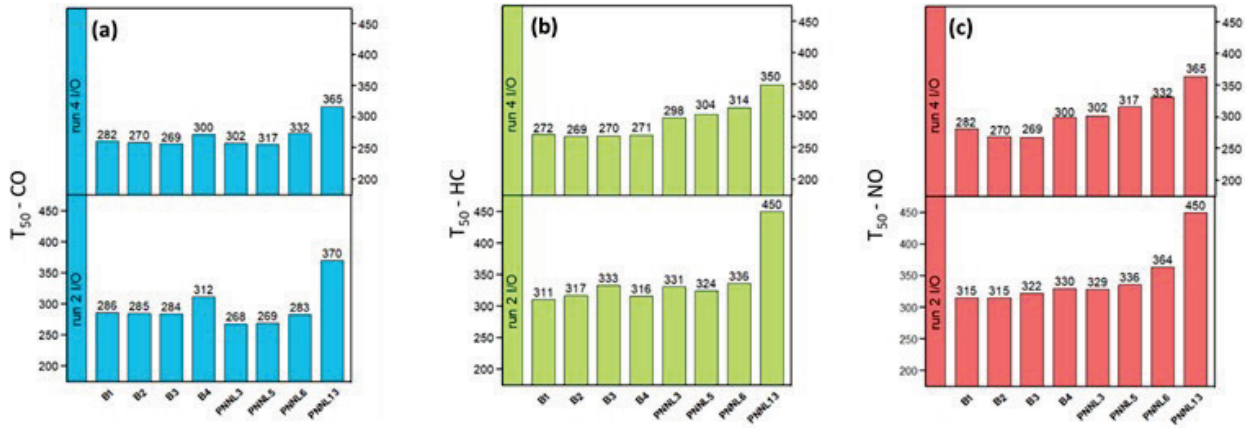

Figure 17 Temperatures required to reach 50% conversion for (a) CO, (b) hydrocarbon (HC), and (c) NO. Upper panels (Run 4 l/O) were generated after sweeping to rich conditions, lower panels (Run 2 l/O) were generated before sweeping to the rich conditions. Catalyst testing conditions: gas hourly space velocity = 70,000 hr^{-1}, oscillating feed (1 s lean – 1 s rich), feed contains CO, H_2, O_2, HC (C_3, $C_3^=$), NO, CO_2, H_2O. (Wang, VI.C.1)

General Motors LLC is enabling new technologies to reduce platinum group metal (PGM) use in the U.S. gasoline vehicle fleet by 50% while meeting future emission regulations, thereby reducing three-way catalyst (TWC) cost by 50% with no loss of performance or reliability over the baseline TWC system and enhancing the competitiveness of the U.S. automotive industry. In FY 2022, the team optimized Pd and Rh catalyst formulations at the powder level for equivalent performance and improved aging resistance at 60% less PGM loading, optimized Pd and Rh catalyst synthesis techniques at the core-sample level for equivalent performance and simplicity for large-scale production, and performed advanced characterization and a reaction kinetics study to gain insights into the deactivation mechanism. (Li VI.C.2)

West Virginia University is developing and validating the simulation tools that enable virtual coupling of engine combustion with aftertreatment systems so that original equipment manufacturers and the research community can use the simulation tools to simulate the real driving emissions from heavy-duty diesel trucks, further optimizing heavy-duty diesel engines and aftertreatment systems for near-zero exhaust emissions. In FY 2022, the team (1) examined engine combustion, emissions, and aftertreatment system performance under steady-state operating conditions; (2) developed a computational fluid dynamics model capable of simulating heavy-duty diesel engine combustion and emissions; (3) developed aftertreatment system component models; (4) developed a one-dimensional engine simulation model; and (5) developed a urea injection model. (Li VI.C.3)

University of Wisconsin–Madison is developing an integrated simulation of combustion and aftertreatment systems to enable control optimization, thermal management optimization, insulation strategies, etc., while ensuring that conversion efficiencies of the components are improved. In FY 2022, researchers (1) developed the Zero-D Velocity–Composition–Frequency transported Probability Density Function (0DVCF-tPDF) combustion model and validated it against computational fluid dynamics simulations; (2) built and calibrated the baseline engine model, a digital twin of a heavy-duty diesel engine; (3) developed the baseline aftertreatment models for each component device; (4) experimentally evaluated the baseline engine and aftertreatment system for model validation with engine experiments; (5) performed laboratory aging of catalyst samples, and measured properties of the diesel oxidation catalyst and selective catalyst reduction (SCR) materials using a synthetic exhaust flow reactor; and (6) recalibrated the Oak Ridge National Laboratory SCR model to predict the performance of the SCR material. (Strzelec VI.C.4)

Advanced Engine Technologies

Volvo Group North America is refining its SuperTruck 2 model to demonstrate greater than 100% improvement in vehicle ton-miles per gallon compared with a best-in-class 2009 truck, 55% brake thermal efficiency (BTE), and technologies that are commercially cost-effective in terms of a simple payback. In FY 2022, the project team finalized the fuel-efficient engine installation, completed the vehicle demonstrator build and commissioning, demonstrated 55% BTE on an engine dynamometer, and field tested the demonstrator. (Bond VI.D.1)

Cummins Inc., is working to design, develop, and demonstrate a very high-efficiency engine optimized around the drive cycle that will strongly increase vehicle freight efficiency and maintain compliance with the current heavy-duty-diesel emissions regulation for line haul vehicles, while the vehicle system will remain compliant with the current greenhouse gas regulatory requirements. In FY 2022, the project team achieved freight efficiency of the demonstration truck in excess of 125% improvement over the 2009 baseline from the original SuperTruck project, demonstrated 55% brake thermal efficiency, installed and calibrated the Cummins powertrain and completed assembly of the demonstrator vehicle, including the interior cabin improvements, and the trailer was prepared for installation of solar panels and fairings. (Dickson VI.D.2)

Figure 18 Cummins / Peterbilt SuperTruck II freight efficiency demonstrator vehicle (Dickson, VI.D.2)

Navistar, Inc., is working under the SuperTruck 2 project to research, develop, and demonstrate a heavy-duty engine that can meet 2010 federal emission standards and achieve 55% BTE demonstrated in an operational engine at a 65 mph cruise point on a dynamometer and contribute to greater than 100% improvement in vehicle freight efficiency relative to a 2009 baseline. Navistar is also working toward development of engine technologies that are commercially cost-effective. In FY 2022, researchers evaluated a newly designed high-flow cylinder head for BTE improvement, optimized an organic Rankine cycle waste heat recovery system that contributes to achieving 55% BTE, and completed technologies assessments for their respective commercial viability. (Zukouski VI.D.3)

Daimler Truck North America SuperTruck 2 research focuses on development and demonstration of a Class 8 long-haul truck that can meet prevailing federal emissions standards, satisfy applicable safety and regulatory requirements, and achieve 115% improvement in vehicle fuel economy relative to a 2009 baseline, exceed 55% BTE, and be cost-effective. In FY 2022, the project team finished building the final demonstrator, optimized the final vehicle feature integration into the demonstrator, performed dyno testing of the engine, and completed vehicle tests to demonstrate 115% improvement in fuel economy. (Villeneuve VI.D.4)

PACCAR Inc., is conducting research, development, and demonstration of a Class 8 long-haul tractor–trailer combination that meets prevailing federal emission standards and applicable safety and regulatory requirements while achieving greater than 100% freight efficiency relative to a 2009 baseline, 55% BTE, and cost-effectiveness. In FY 2022, the team demonstrated waste heat recovery of 4% BTE, engine build and testing at 51% BTE, mild hybrid powertrain validation and integration, and vehicle design freeze. (Meijer VI.D.5)

General Motors is a partner in a collaborative project with Oak Ridge National Laboratory (ORNL), The Ohio State University (OSU), Michigan Technological University, and ECK Industries Inc., to develop an advanced medium-duty truck engine. This engine is to be equipped with advanced materials and combustion

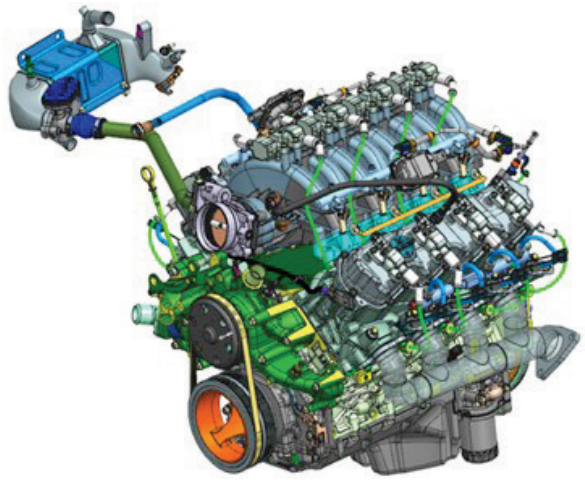

Figure 19 Complete Phase 2 engine system (Wang, VI.D.6)

technologies capable of achieving ≥10% fuel efficiency improvement and ≥15% engine weight reduction when compared to the Model Year 2015 GM L96 VORTEC 6.0 L V8 engine, compliant with applicable U.S. Environmental Protection Agency emission standards, with performance demonstrated via simulation coupled with engine dynamometer testing. In FY 2022, the Phase 2 engine design was completed with incorporation of the advanced combustion and materials technologies developed in Phase 1 for the proposed medium-duty truck engine capable of meeting efficiency requirements. (Wang VI.D.6)

Ford Motor Company is combining advanced combustion system technologies, thermal management strategies, and advanced materials to demonstrate a turbocharged gasoline engine with peak efficiency exceeding the best of today's hybrid electric vehicle engines to develop engine-efficiency and weight-saving technologies that enable competitive, profitable internal combustion engines, targeting the highest production-volume powertrains. In FY 2022, researchers continued single-cylinder engine dynamometer studies supporting calibration optimization; completed fabrication, assembly, and test prep of the first multi-cylinder engine; and completed evaluation of the weight savings in addition to studying additional weight-reduction actions. (Shelby VI.D.7)

Achates Power, Inc., is advancing the cost-effectiveness of high-efficiency, low-emissions engines by experimentally validating simulation models of a three-cylinder, six-piston and a novel two-cylinder, four-piston opposed-piston engine with electrified air handling components, as well as simulating the performance of a four-cylinder, eight-piston engine. In FY 2022, the project team simulated and optimized two-cylinder opposed-piston performance in baseline vehicle drive-cycles to verify >10% miles per gallon improvement; developed baseline three-cylinder, opposed-piston engine datasets for model predictive control optimization; performed build, shakedown, and baseline of a novel two-cylinder opposed-piston engine; and validated novel 1D and 3D air-handling optimization models and a 3D computational fluid dynamics combustion bowl geometry optimization model on a two-cylinder engine with experimental results. (Redon VI.D.8)

Achates Power, Inc., is demonstrating advanced opposed-piston (OP) two-stroke technology for heavy-duty commercial vehicles with hybridization that significantly improves energy efficiency and reduces emissions over conventional engines in the 2025–2030 timeframe. This heavy-duty hybrid powertrain project is demonstrating the ability to beat the California Air Resources Board's Clean Truck criteria emissions standards for NO_x and particulate matter while also reducing CO_2 emissions by 13%–20% compared to a non-hybrid OP baseline, which is already 7% lower CO_2 compared to Model Year 2021 conventional engines. In addition, zero- or near-zero-emissions capability of the OP engine will be investigated through the use of hydrogen fuel. In FY 2022, research focused on engine performance, engine-out, and tailpipe-out emissions for hybrid powertrain model development; hydrogen combustion computational fluid dynamics simulation; and single-cylinder OP engine adaptation for hydrogen combustion. (Redon VI.D.9)

Patents and Invention Disclosures

1. Song, X., and A. Paramasivan. 2022. "Systems and Methods for Autonomously Optimizing the Management of Worksite Machinery." U.S. provisional patent application filed, February 2022. (Sun, I.1)

2. Song, X., S. Yu, and Z. Sun. 2022. "Systems and Methods for Predicting Resistive Forces Encountered by Industrial Machines." U.S. provisional patent application filed, July 2022. (Sun, I.1)

3. Sun, Z., C. Edson, G. Zhao, and J. Yao. 2022. "Control System for Automated Wheel Loader." Invention disclosure filed. (Sun, I.1)

4. Li, P.Y. 2021. "Device having hybrid hydraulic-electric architecture." U.S. Patent 11,060,539. (Li, I.7)

5. Sandia Invention Disclosure SD-16000: Mueller, C. J. and C.W. Nilsen. 2021. "Techniques for Further Mixing Enhancement with Ducted Fuel Injection." Sandia National Laboratories. (Mueller, I.15)

References

1. United States Environmental Protection Agency. 2023. "Inventory of U.S. Greenhouse Gas Emissions and Sinks." https://www.epa.gov/ghgemissions/inventory-us-greenhouse-gas-emissions-and-sinks.

2. Department of Energy: Office of Energy Efficiency and Renewable Energy. 2023. *The U.S. National Blueprint for Transportation Decarbonization: A Join Strategy to Transform Transportation*. https://www.energy.gov/eere/us-national-blueprint-transportation-decarbonization-joint-strategy-transform-transportation.

3. Greene, David L.; Schafer, Andreas. 2003. *Reducing Greenhouse Gas Emissions from U.S. Transportation*. Pew Center on Global Climate Change. http://web.mit.edu/globalchange/www/PewCtr_MIT_Rpt_Schafer.pdf.

4. U.S. Energy Information Administration. 2020. "Annual Energy Outlook 2020: *Table: Table 35. Transportation Sector Energy Use by Mode and Type*." https://www.eia.gov/outlooks/aeo/data/browser/#/?id=45-AEO2020&sourcekey=0.

5. Association of American Railroads. 2021. "Freight Rail Facts & Figures."

6. Container-Xchange. 2023. "Rail freight: Complete guide." https://www.container-xchange.com/blog/rail-freight-overview/.

7. The Expresswire. 2023. "Intermodal Freight Transportation Market Outlook and Forecast till 2030." May 23. https://www.marketwatch.com/press-release/intermodal-freight-transportation-market-outlook-and-forecast-till-2030-2023-05-05.

8. Ahmad, Fatima Maria; Lawson, Ashley. 2018. *Decarbonizing U.S. Transportation.* Center for Climate and Energy Solutions.

9. Association of American Railroads. 2023. "Freight Railroads and Climate Change." https://www.aar.org/wp-content/uploads/2023/06/AAR-Climate-Change-2023-Report.pdf.

10. Davis, Stacy C., and Robert G. Boundy. 2021. *Transportation Energy Data Book: Edition 39.* Oak Ridge National Laboratory, Oak Ridge, Tennessee.

I Off-Road

I.1 Optimization and Evaluation of Energy Savings for Connected and Autonomous Off-Road Vehicles (University of Minnesota)

Zongxuan Sun, Principal Investigator
Mechanical Engineering, University of Minnesota, Twin Cities
111 Church Street SE
Minneapolis, MN 55455
Email: zsun@umn.edu

Gurpreet Singh, DOE Program Manager
U.S. Department of Energy
Email: Gurpreet.Singh@ee.doe.gov

Start Date: September 24, 2020 End Date: December 31, 2023
Project Funding: $1,738,118 DOE share: $1,670,000 Non-DOE share: $68,118

Project Introduction

This project is to develop a systematic method and tools to optimize and evaluate energy savings for connected and autonomous off-road vehicles. Unlike on-road vehicles, off-road vehicles work in a controlled environment (worksite) and are operated by professional drivers. This offers distinct advantages to bring connectivity and automation to off-road vehicles to save energy and improve productivity. However, there are two unique challenges for connected and autonomous off-road vehicles. One is the diversity of off-road vehicles and applications. There are many different types of construction and agriculture vehicles used in different applications. Without a systematic and cost-effective method, optimizing and evaluating their energy savings is time-consuming and costly. The second is the complex fluid-power-based powertrain architecture, which includes both work and drive circuits. Co-optimization of the vehicle dynamics (vehicle and work-tool motion trajectories) and the powertrain operation (engine and hydraulic circuits) in real time is challenging.

Existing studies on energy-efficient operation of off-road vehicles using connectivity and automation are limited. First, the majority [1], [2], [3], [4] focused on enabling autonomous function rather than improving energy efficiency; second, some work investigated the variations among different drivers and revealed the potential for energy savings, but without optimal control strategies; third, some studies were mainly for offline analysis without real-time optimization, did not consider the interactions with other on-site vehicles using connectivity and did not extend the control to both driving and working functions. In general, there was no systematic method to co-optimize the vehicle dynamics and powertrain operation in real-time to achieve significant energy savings and productivity improvement for connected and autonomous off-road vehicles, which is the major contribution of this project.

Objectives

The objective of this project is to develop a systematic method and tools to optimize and evaluate energy savings for connected and autonomous off-road vehicles. The outcome includes a real-time optimization and control system that can intelligently operate the connected and autonomous off-road vehicles to achieve 20%–40% energy savings with improved productivity, a reconfigurable hardware-in-the-loop (HIL) testbed that can precisely measure the fuel consumption and emissions for various types of off-road vehicles in different operation scenarios, and HIL-based testing to evaluate the energy savings of the developed optimization and control system.

Overall Objective

- Develop systematic optimization and control strategies for connected and autonomous off-road vehicles to achieve significant energy savings (20%–40%) with improved productivity.
- Develop an HIL testbed to evaluate the energy savings of connected and autonomous off-road vehicles in a time-efficient, safe, and cost-effective fashion.

Fiscal Year 2022 Objectives

- Development of communication system
- Solution of optimization for both transport and digging phases
- Construction of an HIL testbed.

Approach

University of Minnesota will lead the project with two partners, Texas A&M University and CNH Industrial. University of Minnesota will develop and validate the full vehicle model for a wheel loader (including the fluid power system), build the HIL testbed, implement the co-optimization control, and evaluate energy savings using the HIL testbed. Texas A&M University will develop and validate the reduced order model, construct the worksite simulation, and develop the co-optimization of vehicle dynamics and powertrain operation. CNH Industrial will define the representative off-road vehicle applications, coordinate actual vehicle testing at CNH, and provide industrial feedback on the testing and optimization results.

For the task of optimization and control of off-road vehicles, the control system will perform co-optimization of vehicle speed and tool motion, the fluid power system, and the engine through automation. To formulate the model-based optimization problem, the target off-road vehicle model will be developed. Efficient numerical methods will be applied to solve the optimization. For the task of HIL testbed development, an HIL testbed will be developed to evaluate energy savings of the control and co-optimization system. The HIL testbed has an actual engine loaded by a hydrostatic dynamometer (dyno) based on real-time simulation of work and drive circuits of the target off-road vehicle. For the final task, the HIL testbed will be used to evaluate the fuel economy and emissions benefits of the optimization and control with laboratory instruments and will benchmark with baseline field data. The performance of the optimal control system will be evaluated at different levels of automation for the selected off-road application.

Results

All the objectives for Fiscal Year 2022 have been achieved. The main achievements include development of the communication system, solution of optimization for both transport and digging phases, and HIL testbed construction. Detailed technical results are presented in this section.

I. Development of Communication System

- Review of communication systems for off-road vehicles.
- Setup and evaluation of communication system in the lab.

Based on the laboratory testing, the communication system is capable of transmitting messages at various time intervals (<1 s) across different distances (1 m to 22 m).

II. Solution of Optimization for Both Transport and Digging Phases

- A joint optimization that seamlessly integrates the transport phase and the digging phase has been formulated.
- A systematic approach has been set up to numerically solve the joint optimization in real time.

A model-based optimization that includes both the transport phase and the digging phase has been formulated. In this optimization, the transition between the transport phase and the digging phase has been explicitly modeled to improve the overall system efficiency. The optimization allows the user to set different tradeoffs between energy efficiency and productivity. The solution of the optimization shows 36% improvement in energy efficiency relative to human drivers. The computational time for the optimization is about 72% of the cycle time of the wheel loader, which enables its application in real-time operation. Figure I.1.1 and Figure I.1.2 show the optimal vehicle trajectory during the transport phase and the optimal bucket trajectory during the digging phase, respectively.

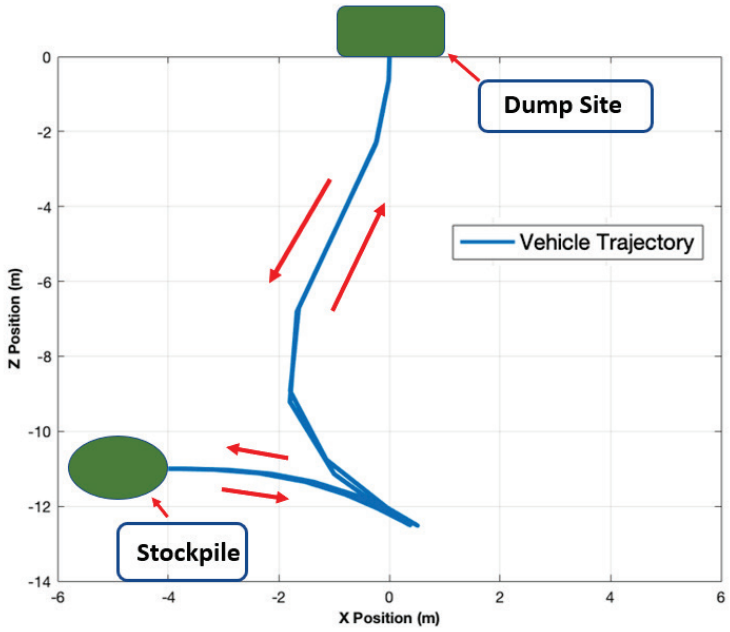

Figure I.1.1 Optimal vehicle trajectory during the transport phase

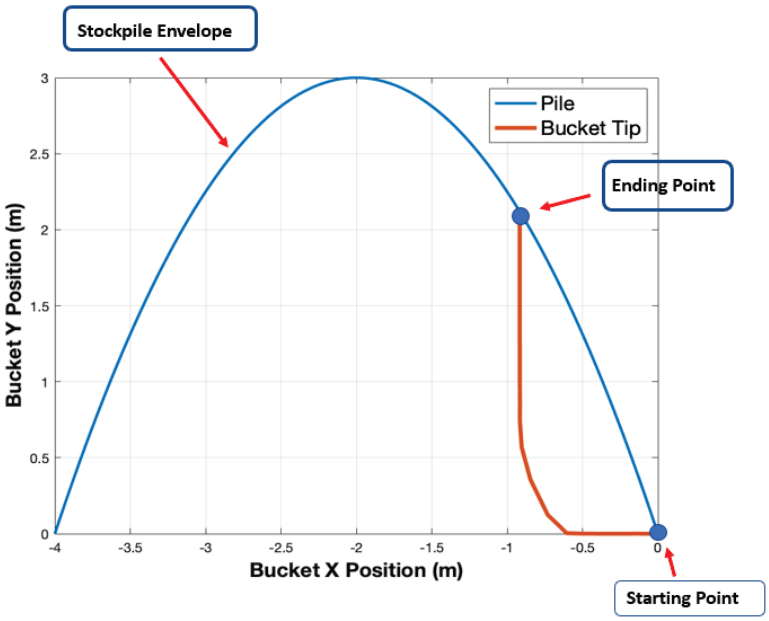

Figure I.1.2 Optimal bucket trajectory during the digging phase

III. HIL Testbed Construction

- An HIL testbed to evaluate connected and autonomous off-road vehicles has been designed.
- The HIL testbed has been constructed and integrated in the lab.

The HIL testbed uses a hydrostatic dynamometer to motor or load an engine as if the engine is driving an off-road vehicle. The speed and load of the engine are calculated using the well-calibrated model including both the driving and working circuits. The hydrostatic dynamometer is then controlled to ensure the engine is operating at the appropriate conditions in real time. The architecture of the overall HIL testbed is shown in Figure I.1.3. The system includes three parts: the hydraulic system and accessories, the test engine and accessories, and the control system. Based on the design, the HIL testbed has been constructed in the lab. The picture of the HIL testbed is shown in Figure I.1.4. The testbed uses a production engine from a commercial wheel loader. Laboratory instruments can be used to measure the fuel consumption and emissions.

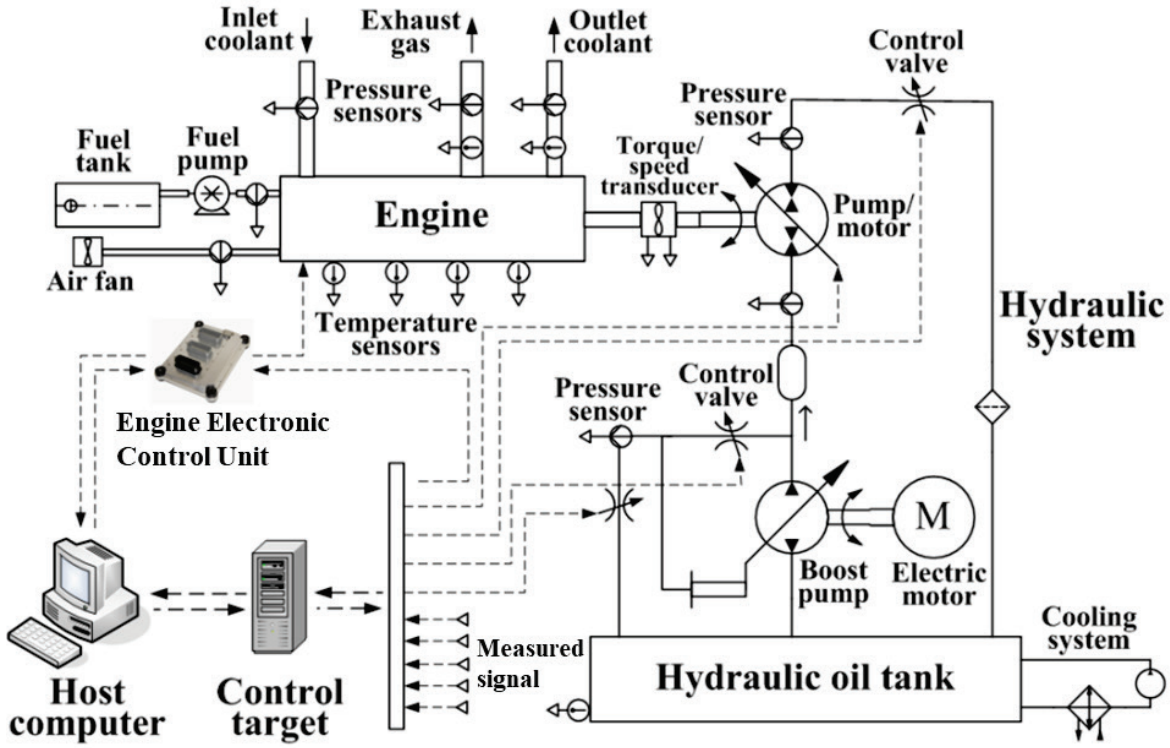

Figure I.1.3 Architecture of the HIL testbed

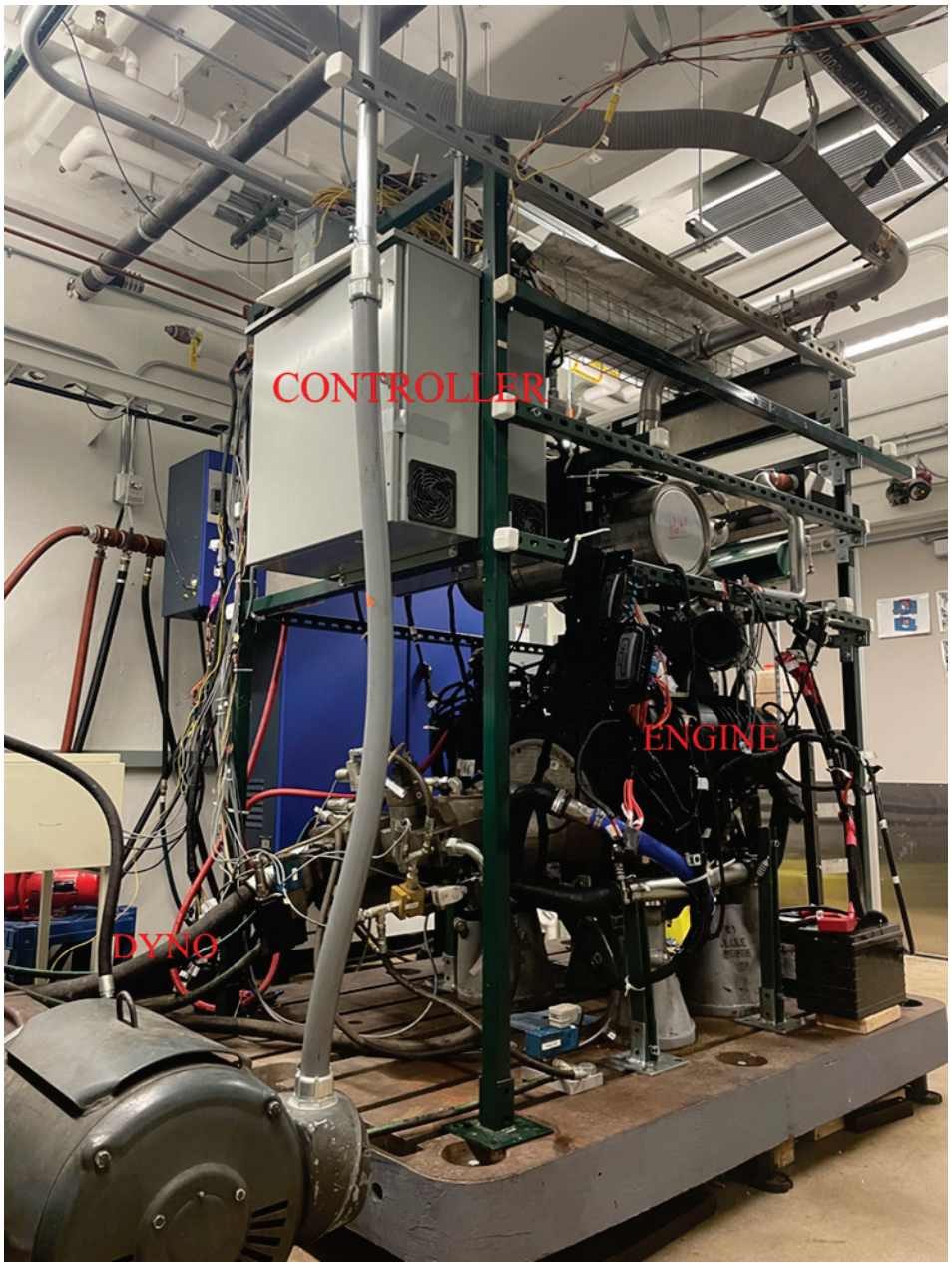

Figure I.1.4 Picture of the HIL testbed

Conclusions

This is the second year of the three-year project. All major objectives for the fiscal year have been achieved.

- A communication system has been developed and evaluated.
- Real-time solution for the joint optimization that includes both the transport and digging phases has been developed. The optimal solution shows 36% improvement in energy efficiency by automation relative to human drivers.

- An HIL testbed for evaluating connected and autonomous off-road vehicles has been designed and constructed. The HIL testbed can be used to evaluate different automation levels as well as their impact on energy efficiency and productivity of off-road vehicles.

Patent and Invention Disclosures

1. Song, X., and A. Paramasivan. 2022. "Systems and Methods for Autonomously Optimizing the Management of Worksite Machinery." U.S. provisional patent application filed, February 2022.

2. Song, X., S. Yu, and Z. Sun. 2022. "Systems and Methods for Predicting Resistive Forces Encountered by Industrial Machines." U.S. provisional patent application filed, July 2022.

3. Sun, Z., C. Edson, G. Zhao, and J. Yao. 2022. "Control System for Automated Wheel Loader." Invention disclosure filed.

References

1. Sarata, S., H. Osumi, Y. Kawai, and F. Tomita. 2004. "Trajectory Arrangement Based on Resistance Force and Shape of Pile at Scooping Motion." IEEE International Conference on Robotics and Automation, 2004. Proceedings: 3488–3493. https://doi.org/10.1109/ROBOT.2004.1308793.

2. Ghabcheloo, R., M. Hyvonen, J. Uusisalo, O. Karhu, J. Jara, and K. Huhtala. 2009. "Autonomous Motion Control of a Wheel Loader." Proceedings of the ASME 2009 Dynamic Systems and Control Conference: 427–434. https://doi.org/10.1115/DSCC2009-2653.

3. Dobson, A.A., J.A. Marshall, and J. Larsson. 2017. "Admittance Control for Robotic Loading: Design and Experiments with a 1-Tonne Loader and a 14-Tonne Load-Haul-Dump Machine." *Journal of Field Robotics* 34 (1): 123–150. https://doi.org/10.1002/rob.21654.

4. Dadhich, S., F. Sandin, U. Bodin, U. Andersson, and T. Martinsson. 2019. "Field Test of Neural-Network Based Automatic Bucket-Filling Algorithm for Wheel-Loaders." *Automation in Construction* 97: 1–12. https://doi.org/10.1016/j.autcon.2018.10.013.

Acknowledgements

The U.S. Department of Energy Project Officer for this project is John Terneus. The co-Principal Investigators for the project are Dr. Kim Stelson (University of Minnesota), Dr. Xingyong Song (Texas A&M University), and Gary Kassen (CNH Industrial). The Project Manager is Michael Gust (University of Minnesota).

I.2 A New Approach for Increasing Efficiency of Agricultural Tractors and Implements (Purdue University)

Andrea Vacca, Principal Investigator
Purdue University
Maha Fluid Power Research Center
1500 Kepner Drive
Lafayette, IN 47905
Email: avacca@purdue.edu

Gurpreet Singh, DOE Program Manager
U.S. Department of Energy
Email: Gurpreet.Singh@ee.doe.gov

Start Date: January 1, 2022 End Date: December 31, 2023
Project Funding: $991,652 DOE share: $798,780 Non-DOE share: $192,872

Project Introduction

Agricultural vehicles are a major contributor to diesel consumption and greenhouse gas emissions. Tractors and their implements (planters, seeders, bailers, etc.) strongly rely on fluid power (FP) technology to achieve their main functions, as FP offers advantages in terms of cost, flexibility, power-to-weight ratio, and durability in harsh conditions. Today's tractors use highly efficient FP technology, such as hydromechanical power splits for the propulsion system and load sensing systems for functions including hitches, steering, and suspension. These functions can be actuated with an energy efficiency well above 50%. However, for most of the high-power implements that a tractor can operate, the combined energy efficiency of the tractor-implement system drops dramatically to values well below 25%. This occurs due to excessive energy losses caused by regulation conflicts between the control valves present in the circuits of both the tractor and the implement. *The goal of this project is to develop and demonstrate a new highly efficient design concept for the hydraulic control system of both agricultural tractors and their implements. This design concept is based on a solution referred to as **Multi-Pressure Rail (MPR)***. Compared to the state-of-the-art technology, the proposed MPR solution can provide the following benefits:

- **Double the existing energy efficiency** for the overall hydraulic control system of the tractor and implement. For planters, this will increase the efficiency from about 25% to about 50%.
- Reduce heat generation and therefore **the cooling power requirement of the tractor FP system**. This is expected to lower the need of the FP system 15%–20% when powering implements.
- Meet and exceed the control accuracy requirements of current agricultural implements.
- **Reduce complexity,** and cost, of the overall system by eliminating redundancy of the hydraulic control valves, which are currently present in both the tractor and the implement.
- Maximize commercial success by formulating a solution that preserves **compatibility** across different brands and technology levels. An MPR tractor must operate a non-MPR implement and vice versa.
- Lower the energy consumption of the in-tractor FP functions (such as suspensions, hitches, and steering) by 15% or more, by extending the MPR concept to the whole tractor circuit.

With tasks that include both simulation and experimental activities, the project demonstrates the benefits outlined above by using a cash crop high tractor (of a power greater than 300 hp) and a 16-row planter as a reference. These machines represent a substantial portion of the domestic farm equipment market; therefore, proof of concepts on such vehicles can easily impact the U.S. market of vehicles most strongly affecting fuel

consumption and greenhouse gas emissions in agriculture. The project team is composed of Purdue University (A. Vacca); Bosch Rexroth, a leader in the fluid power components and systems industry (E. Busquets); Case New Holland, a leading original equipment manufacturer in the off-road vehicle market (G. Kassen); and the National Renewable Energy Laboratory (K. Kelly).

Objectives

Overall Objectives

To accomplish the main project goal of demonstrating the advantages of the proposed MPR system applied to agricultural tractors and their implements, the following three main project objectives have been identified.

- Objective 1 (O1): MPR Configuration. Determine the best configuration of the proposed MPR system in terms of ease of implementation, cost, and maximization of energy efficiency. O1 includes formulating the layout architecture, identifying the electro-hydraulic components, and determining the control strategies that optimize energy efficiency.

- Objective 2 (O2): MPR Compatibility. Determine the MPR configuration and the control strategy that allow compatibility between MPR machines and non-MPR machines. O2 also quantifies the fuel savings in all possible configurations: MPR tractor–MPR implement, MPR tractor–standard implement, and standard tractor–MPR implement.

- Objective 3 (O3): Technology Demonstration. Demonstrate the advantages of the proposed technology through actual experiments. This experimental activity includes (i) the development of a standalone test rig to test the MPR components and related control strategies and (ii) test on a cash crop high tractor (>300 hp) and a 16-row planter, which are chosen as a representative high-power agricultural tractor implement combination.

Fiscal Year (FY) 2022 Objectives

Related to the main project objectives O1, O2, and O3 above, the following objectives were reached during FY 2022.

- Formulate and implement a supervisory controller suitable to operating the hydraulic functions through the MPR system. (O1)

- Validate the simulation model of the MPR system and its supervisory controller based on the results of the standalone test rig built during the previous fiscal year. (O1)

- Formulate and simulate layouts for compatible MPR solutions for both the cases of an MPR tractor coupled with a non-MPR implement and vice versa. (O2)

- Procure components and a data acquisition system to implement the MPR solution on the reference vehicles (tractor and planter). (O3)

- Modify the reference vehicles to implement the MPR prototypes. (O3)

- Perform field tests on significant duty cycles with the MPR prototypes and measure system performance parameters, including velocity tracking of each hydraulic function and overall system efficiency. (O3)

- Confirm the model prediction for the MPR system on the reference vehicles based on the field test, demonstrating the claimed energy-efficiency performance. (O3)

Approach

The team accomplished the above objectives through a research approach that included analytical design studies, numerical simulations, and intensive experimentation.

The simulation models for the reference vehicles in their stock configuration (which were developed in the previous budget period) were used as a reference to estimate the behavior of the MPR system. As a result, simulation models for the MPR tractor and the MPR planter were created in Simcenter Amesim to identify the best specifications for the hydraulic components, including the supply pumps and the hydraulic control valves.

Such models were also used to estimate the energy-efficiency performance and the dynamic behavior of different formulations of the MPR controller. The MPR controller consists of a supervisory controller (which determines the instantaneous configurations of the whole system, in terms of connections of each function with the pressure rails) and low-level controllers (which regulate the supply pumps and the hydraulic control valves). This controller has been implemented in Simulink and used in co-simulation with the above Amesim models to replicate the behavior of the vehicles during the reference drive cycles.

The most time-consuming tasks of FY 2022 were dedicated to the preparation and testing of the MPR vehicle prototypes. The same vehicles used for collecting the baseline measurements, a New Holland T8 tractor and a Case IH Early Riser 16-row planter, were modified to accommodate the electro-hydraulic components that implement the MPR solution. For this purpose, the team used electronic-controlled pumps (a version not yet commercially available) specifically configured for this application, and customized hydraulic control valves. A data acquisition and control system was installed to both vehicles to control the new hydraulic actuation system and measure the most important parameters to evaluate energy consumption and dynamic behavior of the controlled functions. Field tests were executed using the prototype vehicles on the same Purdue University farm that was used for the baseline tests in the previous fiscal year. The field tests followed the same drive cycles identified during 2021.

The team also put effort into simulating the in-tractor functions (steering priority and hitch) with the vision of estimating the opportunities of extending the MPR system to these functions. Additional tasks were dedicated to the formulation and the simulation of a solution that can guarantee compatibility across vehicles of different technologies (MPR tractor connected to a non-MPR implement and vice versa).

Finally, tasks were also dedicated to evaluating the return on investment cost for the proposed technology.

Most of these tasks were performed at the Maha Fluid Power Research Center of Purdue University (Maha), which has led all the conceptual and simulation activities related to the MPR technology. The Purdue team also implemented all the prototype vehicles at Maha and performed the field tests at a Purdue-owned farm. The contribution of both industry partners was essential to the FY 2022 project outcomes. Engineers at Bosch Rexroth put effort into providing the electro-hydraulic pumps modified for this application, as well as sensors and control valves to implement the prototype vehicles. Case New Holland worked intensively with the Purdue team to properly modify the vehicle, identify a proper metric to assess the dynamic performance of the system, and perform the field tests. Case New Holland also assisted in the formulation of the compatibility solutions and in the cost analysis task.

National Renewable Energy Laboratory's contribution during FY 2022 was limited due to staff change. National Renewable Energy Laboratory worked on the MPR system models to evaluate the applicability of data-driven approaches that can ease application of the MPR technology to different types of implements.

Results

The project made significant progress during FY 2022 toward meeting the project objectives O1, O2, and O3 stated above. The following paragraphs detail the major accomplishments.

Accomplishments Related to O1 – MPR Configuration

- A control logic for hydraulic control systems using MPR technology was formulated and implemented in Simulink. The logic for the reference vehicles is schematically represented in Figure I.2.1.

- The proposed control logic for the MPR system was tested and simulated on the standalone test rig developed at Maha to verify its performance before implementation on actual vehicles. This allowed validation of the simulation approach used to model the MPR system and its control (Figure I.2.2).

Accomplishments Related to O2 – MPR Compatibility

- The team deeply investigated solutions that enable compatibility across different technologies. It was concluded that an MPR tractor can power a traditional implement without modifications to the system. In this case, energy-efficiency gains can be achieved by controlling the pressure levels of the rails. The team estimated efficiency improvements in the range of 40% for this configuration.

  The case of a traditional tractor connected to an MPR implement is more delicate. In this case, compatibility can still be guaranteed with no modifications by using the power-beyond connection usually present in tractors. Depending on the tractor technology (electronic load sensing or conventional), energy-efficiency improvements can be achieved. A conventional tractor can ensure the same performance as the baseline, while an eLS tractor can achieve performance closer to that of the full MPR solution.

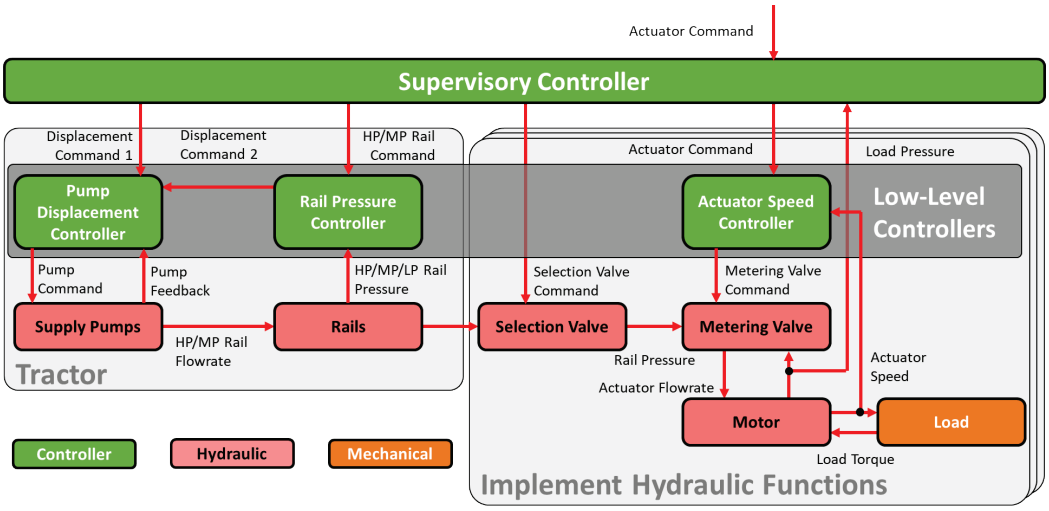

HP – high pressure; MP – multi-pressure

Figure I.2.1 Overall structure of the MPR controller

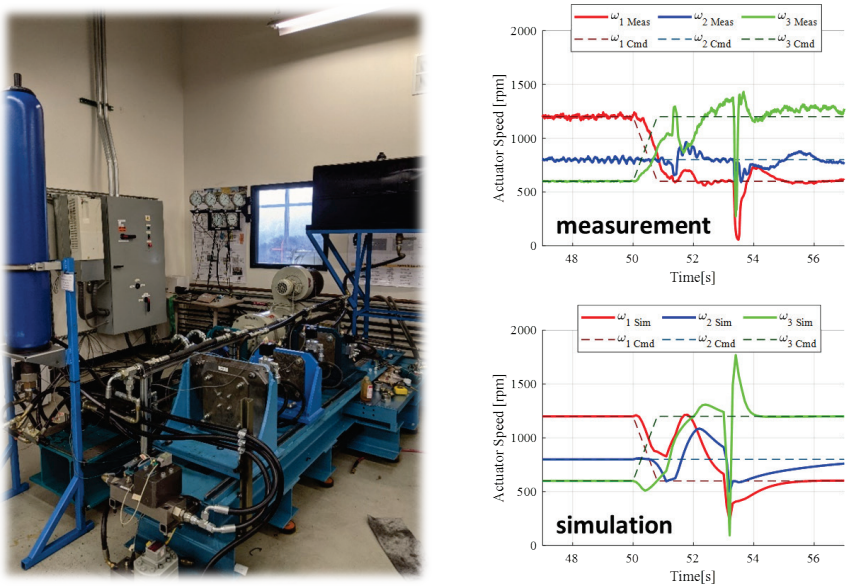

Figure I.2.2 Left: Standalone test rig for MPR testing. Right: Example of simulation vs. measurement during a harsh transient (i.e., change in command and load) on the system with three hydraulic functions.

- Simulation models and International Organization for Standardization (ISO) schematics for compatible solutions that will be tested on the reference vehicles in 2023 were developed.

Accomplishments Related to O3 – Technology Demonstration

- The reference vehicles (a New Holland T8 tractor and a 16-row Case IH planter), previously used for baseline measurements of energy consumption in 2021, were modified in 2022 by installing electro-hydraulic components that can implement the MPR technology. Several of these components were custom made for the application. Figure I.2.3 shows the simplified schematic of the tractor configuration, along with a significant picture of the experimental setup. The data acquisition and control system implemented in the vehicles permits running the vehicles in typical in-field operation while also measuring the main performance parameters.

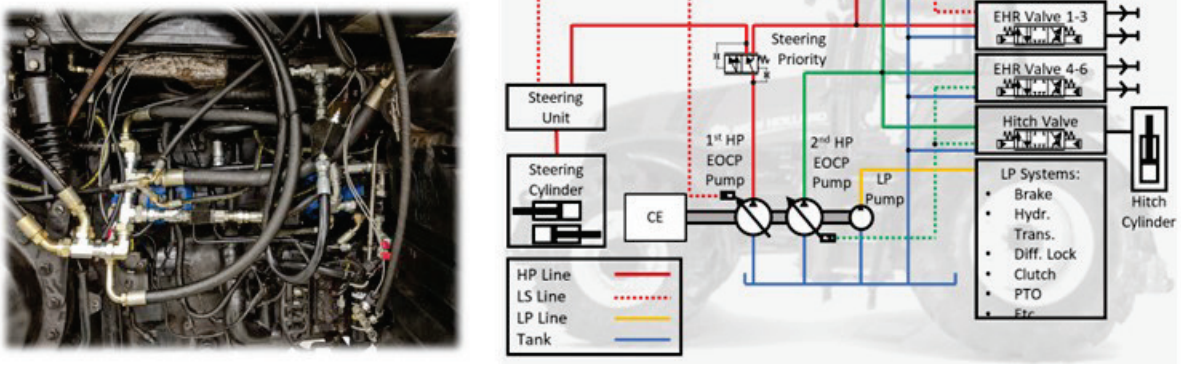

CE – combustion engine; LS – load sensing; LP – low pressure; EOCP – electronic open circuit pump; HER – electro-hydraulic remote; PTO – power take off

Figure I.2.3 Left: Reference vehicle modifications, installation of ePumps. Right: Simplified ISO schematic of the MPR tractor prototype.

- A test campaign was performed at a Purdue University-owned farm (Figure I.2.4) to verify the performance of the MPR solution with different settings of the control system. Thirty-five different tests were considered to reflect all typical operating conditions of the tractor-planter system as well as two different settings of the MPR controller (fixed and variable high pressure [HP]). Results for power savings are above expectations, as summarized in Table I.2.1. Measurements demonstrate more than doubled energy efficiency of the HP system of the tractor (from measurements of power taken at the pump supply) for the most typical operating conditions (velocity <6 mph). The test campaign also permitted demonstration of control tracking of the function velocity in line with the baseline technology.

Figure I.2.4 Picture taken during the test campaign of the prototype vehicles with MPR technology

Table I.2.1 Measured Power Reduction and System Efficiency of the MPR Solution vs. Baseline

Operating Condition	Pump Power Reduction (%)		System Efficiency - Pump Outlet (%)		Percent System Efficiency Increase (%):	
Solution:	**Fixed hp**	**Var. hp**	**Fixed hp**	**Var. hp**	**Fixed hp**	**Var. hp**
1,500 RPM, 6 MPH	50.91	52.14	39.36	39.26	**114.66**	**114.11**
1,800 RPM, 6 MPH	50.33	54.18	38.62	39.13	**122.56**	**125.55**
2,100 RPM, 6 MPH	48.50	53.38	35.60	38.54	**113.93**	**131.60**
1,800 RPM, 10 MPH	38.92	47.38	33.46	36.76	**78.63**	**98.28**
2,100 RPM, 10 MPH	35.32	45.49	29.04	33.86	**56.14**	**82.06**

hp – horsepower; RPM – revolutions per minute; MPH – miles per hour

Conclusions

- The project has formulated and demonstrated a technology that doubles the energy efficiency of the tractor-implement hydraulic control system. The technology is referred to as the MPR system, and it reduces throttling losses by using a pressure-based control method suitable for multi-actuator systems powered by hydraulic remotes.

- A cash crop high tractor (>300 hp) and a 16-row planter were used both for baseline measurements (FY 2021) as well as for measurements of MPR prototypes.

- The team formulated a control methodology for controlling MPR systems while guaranteeing proper velocity tracking of the controlled functions (as in conventional systems). This control methodology was validated on standalone tests before actual vehicle implementation.
- Tests on the MPR vehicle prototypes demonstrated relative incremental improvements in energy efficiency always above 80%. A doubled efficiency (or more) is found in most of the tested operating conditions.
- Solutions for compatible technology have been formulated and modeled. Tests on compatible technology will be performed in FY 2023. A compatible technology is key for commercialization in the agriculture sector.

Key Publications

1. Guo, X., R. Madau, J. Lengacher, A. Vacca, R. Cardoso, and E. Busquets. 2022. "Multi-Pressure Rail System Design with Variable Pressure Control Strategy." Presented at the 13th International Fluid Power Conference (13 IFK), Aachen, Germany, June 13–15.
2. Guo, X., J. Lengacher, and A. Vacca. 2022. "A Variable Multi-Pressure Rail System Design for Agricultural Applications." *Energies* 15 (17): 6173. https://doi.org/10.3390/en15176173.
3. Guo, X., and A. Vacca. 2022. "A New Approach for Increasing Efficiency of Agricultural Tractors and Implements." Presented at the Center for Compact and Efficient Fluid Power Summit, Minneapolis, MN, June 8.
4. Guo, X., and A. Vacca. 2022. "A Multi-Pressure Rail Approach to Increase Efficiency of Agricultural Tractors and their Implements." Presented at the 2022 Maha Fluid Power Conference, West Lafayette, IN, May 18.

Acknowledgements

The team would like to acknowledge John Terneus, Michael R. Weismiller, and Gurpreet Singh at the Vehicle Technologies Office for help with the project management and for the technical feedback provided.

I.3 Improved Efficiency of Off-Road Material Handling Equipment through Electrification (Michigan Technological University)

Jeremy Worm, Principal Investigator
Michigan Technological University
1400 Townsend Drive
Houghton, MI 49931
Email: jjworm@mtu.edu

Gurpreet Singh, DOE Program Manager
U.S. Department of Energy
Email: Gurpreet.Singh@ee.doe.gov

Start Date: October 1, 2019 End Date: March 31, 2024
Project Funding: $3,606,393 DOE share: $2,498,209 Non-DOE share: $1,108,184

Project Introduction

Historically, product development criteria for off-highway equipment have focused on intended task execution, reliability, longevity, operator ergonomics, and cost. Factors such as energy efficiency were secondary to these functional factors. However, a significant amount of diesel fuel is consumed in off-highway equipment, such that a significant savings opportunity exists. A distinct subset of off-highway fuel utilization is in material handling (loading and unloading rail cars and trucks and moving materials around processing facilities). Off-road material handling machines spend a significant portion of operating time at zero or very low load (e.g., tactical movements of the machine or material engagement apparatus), making them a prime candidate for electrification. Furthermore, some of the usage scenarios for this category of machine include moving heavy material from an elevated to a ground height (unloading material from rail cars, for example), thus providing opportunity for gravimetric potential energy recovery.

Through this project, Michigan Technological University's Advanced Power Systems Research Center (APS LABS), in partnership with Pettibone (original equipment manufacturer of off-road material handling machines) and relying upon established Tier 1 suppliers, will electrify the propulsion and fluid power system of a Pettibone 204i off-road material handler.

The overarching goal of this project is to apply electrification and demonstrate a real-world fuel consumption reduction of at least 20% in a Pettibone Cary-Lift 204i off-road material handler while maintaining compliance to Tier 4 final emissions regulations. Performance in all other areas—lift and carry operation; controllability; and noise, vibration, and harshness (including engine restart)—will not deteriorate. This goal directly supports the U.S. DOE Energy Efficiency and Renewable Energy mission to achieve net-zero greenhouse gas emissions by 2050.

To date, 1.5 budget periods of the project have been completed. Standard operating cycles have been developed, a high-fidelity model of the machine has been developed and validated, a detailed analysis of the energy flow of the baseline machine is complete, and the electrification architecture has been determined.

Objectives

The project goal to demonstrate at least 20% reduction in real world fuel consumption without negatively impacting emissions, performance, operability, noise, vibration, harshness, etc., will be achieved through several objectives.

Overall Objectives

The overall project objectives are the following:

- Develop an instrumentation package and integrate it on the production machine to support baseline testing (test course and in-field).
- Quantify baseline machine performance, including fuel consumption, acceleration, top speed, actuator speeds, lift capacity, noise, vibration, harshness, etc.
- Synthesize the baseline data (test course and in-field) into standard operating cycles that can be used throughout the remainder of this project and into the future for original equipment manufacturers, researchers, etc.
- Develop a configurable vehicle model (representing both the propulsion and fluid power systems) in Simcenter Amesim where the electrification architectures can be evaluated.
- Create a design palette of viable commercial off-the-shelf electrification components and define a short list of electrification architectures with the highest probability of meeting the project goals using reduced-order, first-principles analysis techniques.
- Conduct a full-cycle simulation of the identified potential electrification architectures using the detailed Simcenter Amesim model.
- Complete an engineering decision analysis of the simulation results with the intent of selecting an architecture and specific components based on fuel consumption, performance, cost, risk, etc.
- Complete the engineering and design effort required to integrate the electrification components (mounting, coupling, cabling, etc.).
- Fabricate new hardware as needed and assemble the prototype electrified machine.
- Develop the supervisory and component-level controls as needed.
- Calibrate the control system.
- Demonstrate the project goals have been achieved through both the test course and in-field testing.

Fiscal Year 2022 Objectives

As a subset of the overall project objectives listed above, the subset of objectives that have been worked on during Fiscal Year 2022 are the following:

- Create a design palette of viable commercial off-the-shelf electrification components and define a short list of electrification architectures with the highest probability of meeting the project goals using reduced-order, first-principles analysis techniques.
- Conduct a full-cycle simulation of the identified potential electrification architectures using the detailed Simcenter Amesim model.
- Complete an engineering decision analysis of the simulation results with the intent of selecting an architecture and specific components based on fuel consumption, performance, cost, risk, etc.
- Complete the engineering and design effort required to integrate the electrification components (mounting, coupling, cabling, etc.).

Approach

This project was envisioned to occur over a three-year period. However, the project had significant COVID-19-related delays to some elements on the critical path, including manufacture and subsequent access to the production machine. As such, the project timing has been pushed back by 18 months through no cost

time extension. That said, the project will consist of two technical phases encompassing three budget periods. Phase 1 will focus on analysis, design, component evaluation, and subsystem laboratory testing. Phase 2 will focus on vehicle integration, controls development and calibration, systems-level testing, validation, and demonstration.

High-level workflow through Phase 1 includes both an experimental and analytical parallel path. The experimental path is to instrument the machine, establish baseline performance using a test course developed at APS LABS and through field testing at customer locations, develop standardized operating cycles, and produce measurements as needed to support modeling efforts (model parameterization, calibration, and validation). The analytical path through Phase 1 involves developing a detailed model incorporating both propulsion and fluid power systems and applying the model as part of an engineering decision analysis to identify the most appropriate architecture and hardware set based on project objectives, risk, etc. Phase 2 will include the engineering (both hardware and software) required to fully integrate the electrification system, associated fabrication and physical integration, calibration of the control system, and finally demonstration through real-world testing that the project goals have been achieved.

Successful completion of this body of work will require close collaboration between the prime (Michigan Tech APS LABS) and the sub (Pettibone, the machine manufacturer). Although Michigan Tech will take the lead in all tasks and activities, Pettibone's support will be absolutely critical and cannot be overstated. This is especially true in the engineering and design aspects of electrification system integration, which is on the critical path in Phase 2. Additionally, Pettibone is crucial in providing the overall voice of the customer, program constraints and requirements, and otherwise-hard-to-obtain parameters.

Results

Fiscal Year 2022 has produced several results in this project. The most significant results are summarized here:

- All baseline experiments are complete, including on the test course that was constructed at APS LABS as well as two end-user facilities (see Figure I.3.1).

Figure I.3.1 Baseline testing at an end-user facility

- The high-fidelity model of the baseline machine has been fully validated through experimental data independent of the data used to calibrate the model. The cumulative fuel consumption over a time-weighted standardized operating cycle matches within 2% between experimental and simulated results, with only a 0.4% difference for the load cycle in particular (Figure I.3.2). This time-weighted composite cycle is made up of sub-cycles including material load, material unload, machine transport, and idle. The time weighting was determined through field testing at multiple end-user facilities.

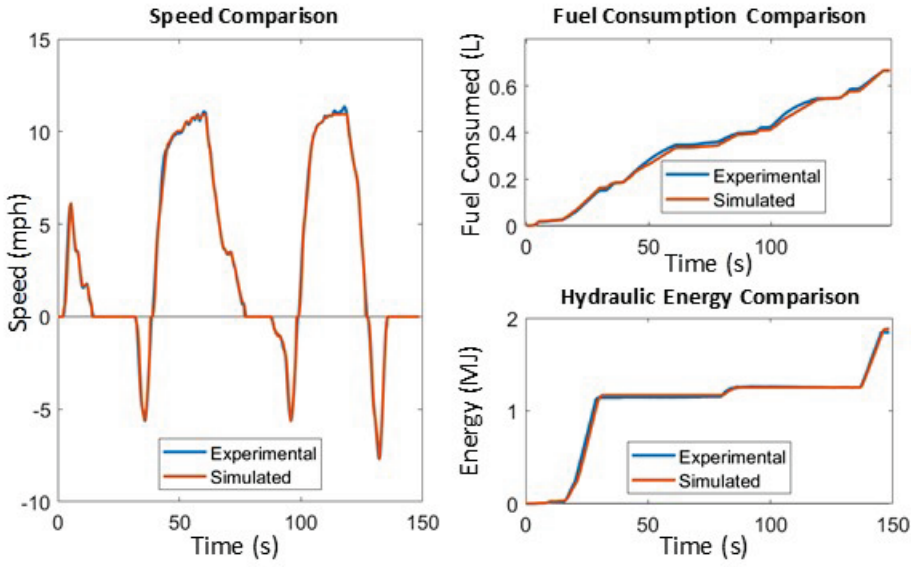

Figure I.3.2 Comparison between experimental and simulated results

- The validated model was used to analyze the distribution of engine brake work in the baseline machine during the individual and composite drive cycles. This is shown in Figure I.3.3 for the composite drive cycle. Here, it can be seen that 19% of engine brake work goes into the cooling fan (the fan is always coupled to the engine and sized for 57°C ambient temperature) while a total of 39% goes into drivetrain and torque converter losses (even when the machine is stationary, there are losses in the torque converter and transmission when it is shifted to neutral).

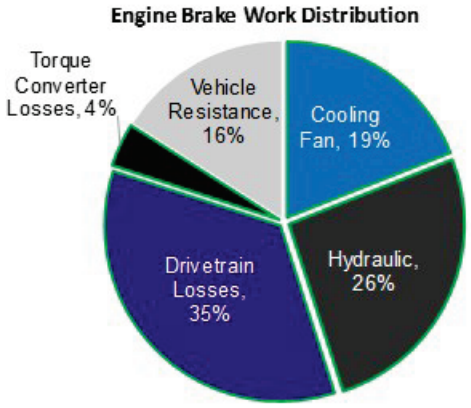

Figure I.3.3 Engine brake work distribution (composite cycle)

- A Pugh-style engineering decision analysis was completed to determine the electrification architecture to implement in the prototype demonstration machine. The Pugh analysis incorporated 27 weighted performance attributes (e.g., fuel consumption, material lift speed, machine top speed, and production cost) and examined 59 architecture permutations. The architecture permutations were intended to cover a wide range of options, from a simple stop–start function to a full battery electric vehicle (BEV).

- The third round of the analysis revealed two architectures as optimal: a relatively simple system utilizing low-voltage stop–start and an electric cooling fan, and a more sophisticated extended-range electric vehicle (EREV) with a downsized engine and electrified hydraulics.

- The simple electrification architecture employing low-voltage stop–start functions was shown (using the validated model) to provide a 9.8% reduction in fuel consumption over the weighted composite cycle. The absolute difference in energy for an eight-hour shift is shown in Figure I.3.4. The addition of an electric fan was estimated to bring the total fuel-consumption reduction to over 20%.

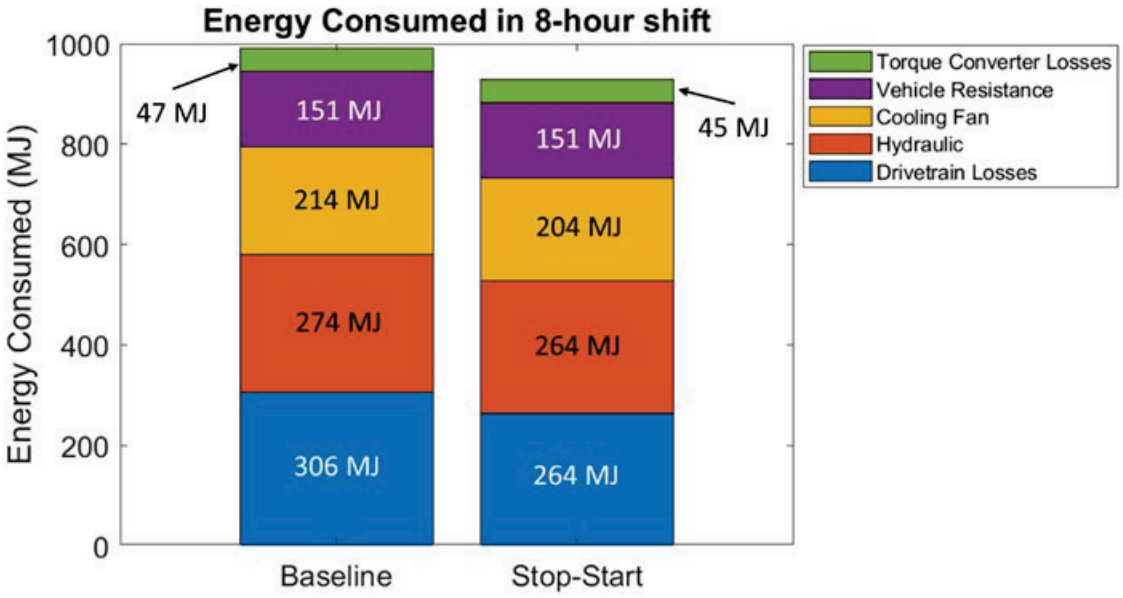

Figure I.3.4 Energy consumption difference due to low-voltage stop-start over the weighted composite cycle

- Figure I.3.5 shows the lifetime CO_2 emissions for several architectures of interest compared to the baseline machine. These are not necessarily the highest-ranked architectures (in fact, BEV scored rather low overall for various reasons) but do provide an interesting comparison. Here, it is shown that the EREV resulted in the lowest CO_2 emissions with a 42% reduction from baseline.

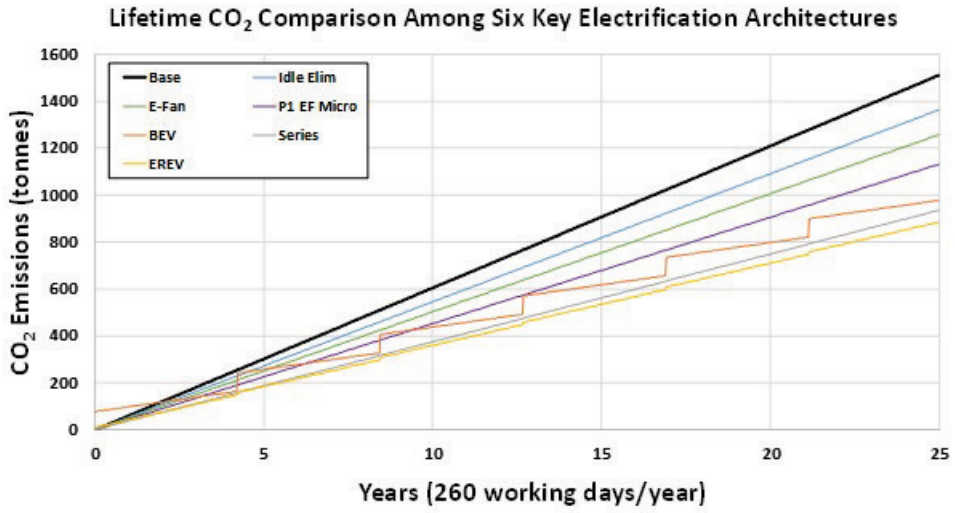

Figure I.3.5 Lifetime CO_2 emissions comparison for six architectures of interest from the second round Pugh analysis

- Once all analysis was complete, the team felt that although the stop–start scenario with an electric fan was the most practical choice (it met the project's fuel-consumption targets while being low-risk and low-cost), the EREV architecture was more in line with the spirit of the project, as it will push the bounds of innovation and provide even greater energy and CO_2 reductions.

Conclusions

The following conclusions can be drawn from the work conducted in Fiscal Year 2022.

- All baseline experimentation is complete.
- A high-fidelity model has been developed, calibrated, and validated.
- An electrification architecture has been identified (namely, EREV) that will exceed project targets and provide a 42% reduction in lifetime CO_2 emissions compared to the baseline.

Key Publications

1. Goodenough, B. 2022. "Off-Road Fuel Savings Greater than 20%." Presented at SAE International COMVEC 2022, Indianapolis, IN, September 22.
2. Goodenough, B., D. Robinette, J. Worm, and A. Czarnecki. Forthcoming. "Reducing Fuel Consumption on a Heavy-Duty Nonroad Vehicle: Conventional Powertrain Modifications." Submitted to SAE International World Congress Experience 2023.

Acknowledgements

The project team wishes to sincerely thank the DOE Project Manager John Terneus and DOE Program Manager Dr. Gurpreet Singh and Technology Manager Dr. Michael Weismiller for their guidance and insight throughout the project thus far. The team also wishes to thank key suppliers including Dana, Parker, Terzo, BorgWarner/Cascadia, eMatrix, and EMP for their willingness to support the project thus far and as the electrified solution is being developed. Finally, the team thanks their colleagues and leadership at Michigan Tech and Pettibone for their continued support of this work.

I.4 Improving Efficiency of Off-Road Vehicles by Novel Integration of Electric Machines and Advanced Combustion Engines (University of Wisconsin–Madison)

Sage Kokjohn, Principal Investigator
University of Wisconsin System
21 North Park Street Suite 6401
Madison, WI 53715
Email: Kokjohn@wisc.edu

Gurpreet Singh, DOE Program Manager
U.S. Department of Energy
Email: Gurpreet.Singh@ee.doe.gov

Start Date: October 1, 2019 End Date: June 30, 2023
Project Funding: $3,956,523 DOE share: $2,695,296 Non-DOE share: $1,261,227

Project Introduction

Modern off-road equipment will increasingly rely on electrified implements that will deliver precision control with a smaller footprint than hydraulics. The primary energy converter, however, will be an onboard reciprocating internal combustion engine because of the power density of hydrocarbon fuels in comparison to electrical energy storage and the remote locations where much of this equipment is deployed. Adding energy storage and electric machines creates opportunities to improve efficiency while reducing emissions. The goal of this work is to evaluate how the extra flexibility that an enhanced electrical system provides can be best used to enable high-efficiency, low-emissions combustion technologies. The proposed system includes consideration of hybridization of both the torque application and air-handling systems to maximize efficiency while minimizing cost.

Objectives

The overall goal of this project is to enable a greater than 10% increase in efficiency of off-road vehicles by integrating electric machines and advanced internal combustion engines. The powertrain system to be developed in this work will include an advanced internal combustion engine, a high-voltage (700 V) traction motor, and an electrified air-handling and thermal-energy-recovery system. The system development effort will combine multi-fidelity simulations of the engine and electric machines, control system development, system (vehicle) testing, and techno-economic analysis to evaluate the merits of hybridization as a pathway to improve efficiency, reduce engine-out emissions, and reduce aftertreatment cost and complexity of off-road vehicles. The primary objective of the current budget period was to develop the tools necessary to analyze and compare relevant architectures.

Overall Objectives

- Systematically assess the benefits and drawbacks of electrification for the off-road sector.
- Develop a hybrid powertrain capable of improving efficiency by over 10% in a wheel loader application.
- Utilize electrification to enable downsizing.

Fiscal Year 2022 Objectives

- Perform system-level experiments to test the engine with an electrified powertrain.
- Design components for vehicle-level testing.

- Perform system-level analysis to compare multiple architectures for hybrid off-highway vehicles.

Approach

The outcome of the project will be a detailed understanding of the potential emissions and efficiency benefits of coupling electric machines and internal combustion engines for off-road vehicle applications. The effort will include implementation and testing of the developed engine system in a wheel loader application. The target efficiency improvement of greater than 10% will be achieved through a combination of extreme downsizing enabled through the addition of a high-voltage traction motor that allows for regeneration and electrical energy storage, an optimized combustion process, advanced supervisory control, and electrified air handling. Key efforts include:

- Computational analysis to develop and optimize an engine system that takes advantage of electrification for off-highway vehicle applications
- Supervisory control system development for hybrid electric powertrain systems in off-highway vehicles
- System testing of transient operation using electrically assisted intake boosting and hybridization on-engine and in-vehicle
- A comparative assessment of the potential for mild and heavy hybridization in the off-road sector
- Techno-economic analysis of the cost–emissions–efficiency tradeoffs.

Results

The following key technical achievements were made in Fiscal Year (FY) 2022:

- Demonstrated functionality of hybrid air system operation over transient operating conditions, including implementation of a single-input–single-output (SISO) controller.
- Completed design of a hybrid vehicle, including an electrified air system and high-voltage energy storage and traction motors.
- Performed a system-level analysis of hybrid architecture to assess performance and emissions, and developed optimized engine calibration that takes advantage of hybrid architecture to reduce fuel consumption and emissions.

Figure I.4.1 shows the baseline and electrified systems. The baseline configuration is a 6.8 L engine in a series-hybrid arrangement without energy storage. System-level modeling has shown that the engine can be downsized to a 4.5 L configuration using a BorgWarner eBooster® to enable low-speed torque, along with a high-voltage battery to enable torque shaving and energy recovery.

Testing of the SISO controller was performed to evaluate its effectiveness at controlling the air–fuel ratio (AFR) and exhaust gas recirculation (EGR). Experiments were conducted by applying a ramped load to the engine and allowing the SISO controller to respond to the load change with the eBooster control. The load profile used begins with steady engine operation at 100 Nm; a ramped 800 Nm/s load increase is then applied until the engine load reaches 500 Nm. Figure I.4.2 shows sample data acquired with and without the SISO eBooster control.

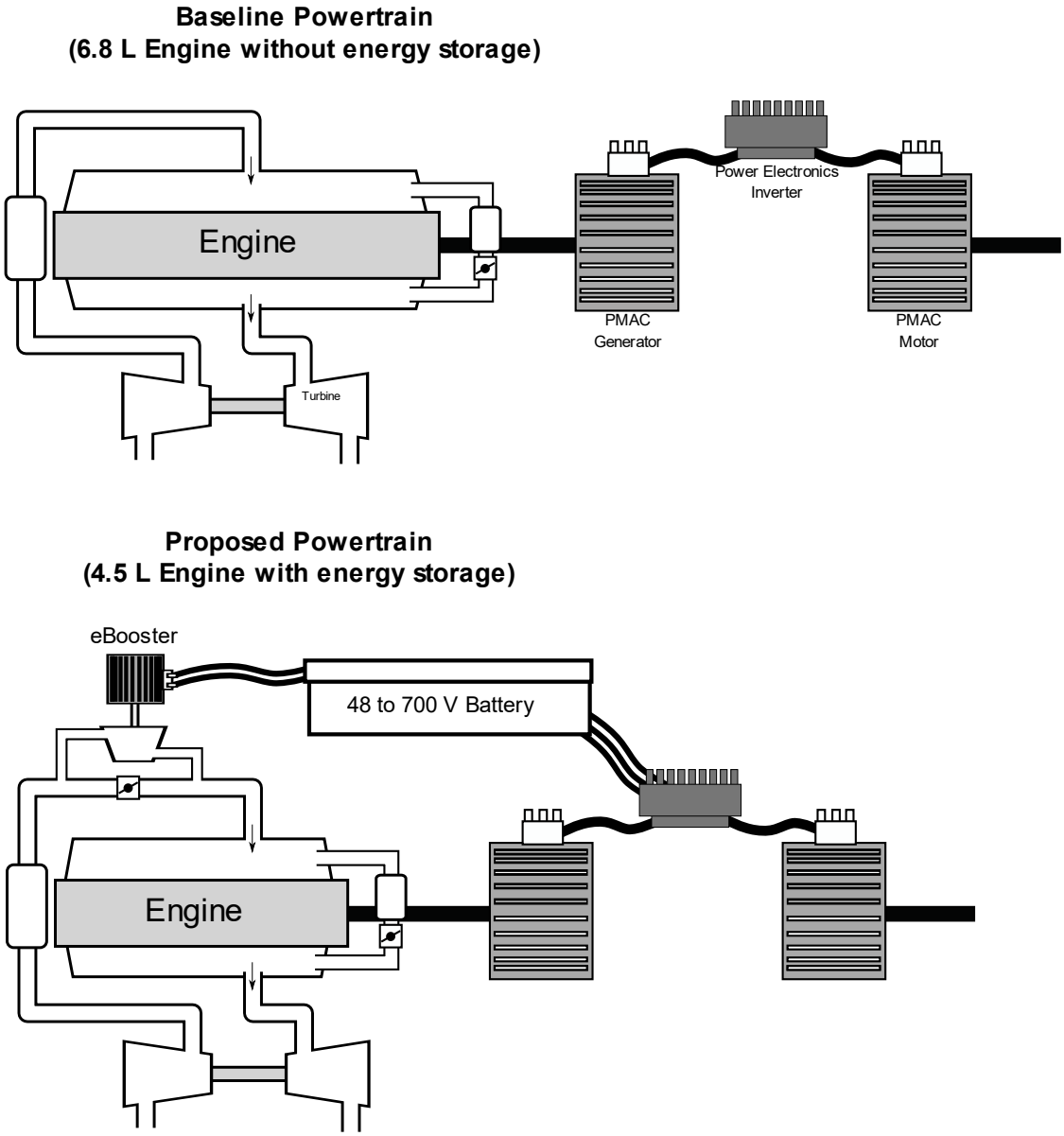

PMAC – permanent magnet alternating current

Figure I.4.1 (top) Baseline powertrain used in the John Deere 644K wheel loader and (bottom) powertrain evaluated in the present project

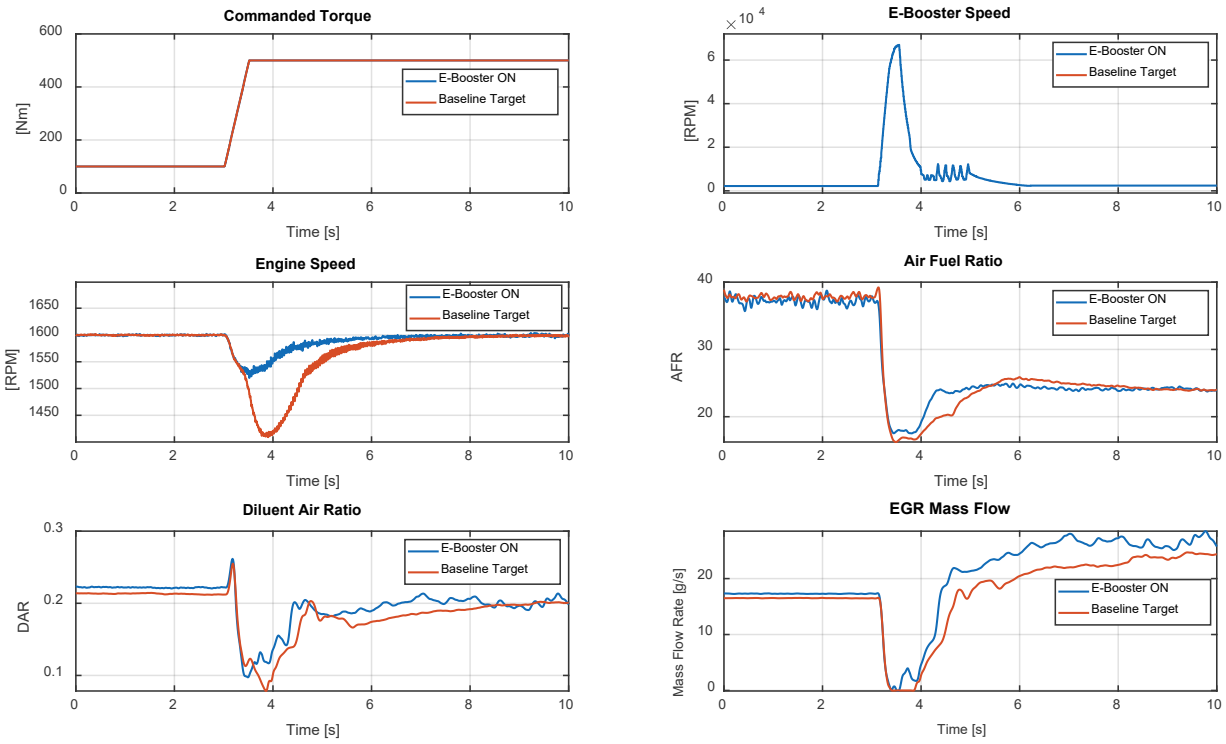

Figure I.4.2 Comparison of engine response with and without eBooster at 1,600 rpm with an 800 Nm/s slew rate

For the baseline case, the engine speed droops as the engine attempts to meet the air and fuel requirements for the applied load. The EGR mass flow drops as the EGR valve is closed to divert more enthalpy to the turbocharger. As a result, the diluent–air ratio (DAR) also falls from the reduced EGR flow. DAR is defined as the ratio of total diluent mass present to the total intake charge mass present. The AFR decreases because of a significant increase in fueling to meet the load requirement then steadily climbs as the air requirements are met by the spooling turbocharger. At 6.0 s, it is also notable that the AFR peaks locally after the load application, then slowly settles to its setpoint, indicating the engine control unit may have overcompensated with airflow during the transient period. With the eBooster enabled, the engine response is similar; however, the magnitude and recovery time of the dips are reduced. Recovery time is defined as the time required from the start of the load application to when the measurement recovers to within 5% of the target steady-state setpoint. Engine speed droop is reduced by 7.9% and is recovered 67.7% faster; the DAR dip is reduced by 35.3%, and EGR and DAR recovery times are decreased by 47.9% and 12.3%, respectively. The dip in AFR is reduced by 7.9%, and the recovery time is improved by 35.4%. The overcompensation of airflow causing a post-transient AFR peak is also highly reduced with eBoosting. Throughout active eBoosting, the AFR remains above the target AFR.

System-level analysis was performed to assess model predictability and perform optimization to take advantage of the electrified powertrain. A machine-learning-based emissions model was developed using supplied test data for the architecture. The model was then embedded into GT-POWER engine simulation software to enable accurate predictions of nitrogen oxides (NO_x) and soot over a wide range of operating conditions. The validated model was exercised to recalibrate the engine to minimize brake-specific fuel consumption (BSFC) while staying under emissions constraints. From the comparison of the optimized EGR and start of injection (SOI) results to the corresponding base calibration targets shown in Figure 3 (left), one can notice the substantial increase in EGR targets. The increase is on the order of 10%–15% for the optimized calibration and is most substantial at low-load conditions. Using the derived maps for EGR, SOI, and exhaust throttle position, the simulated comparison of BSFC and peak cylinder pressure (PCP) to the base calibration values is illustrated in Figure I.4.3 (right). It is seen that up to a 16% reduction in BSFC results from the use of

the optimized calibration at low load across all engine speed conditions, and up to a 6% reduction carries through into medium–high load conditions at high-speed conditions. However, at these peak power conditions where the most advanced injection timings take place, the BSFC benefit comes with a tradeoff of increased PCP. Up to a 20% increase in PCP is observed in this high-power operating region, with increases also seen at low-load high-speed conditions in which SOI and EGR were significantly modified.

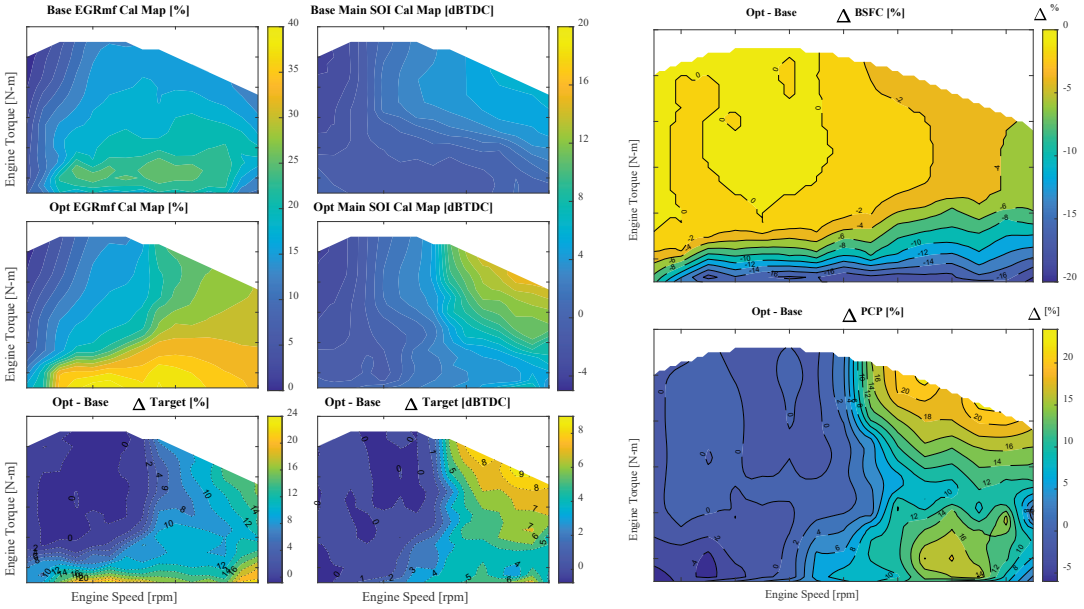

Figure I.4.3 (left) Comparison of base engine EGR and SOI calibration to the optimized calibration maps enabled by utility of the eBooster. (right) BSFC and PCP map comparison between optimized calibration and base calibration shows significant BSFC reduction at low load conditions and increased PCP at peak power conditions.

The optimized calibration allows substantial reductions in fuel consumption due to the higher EGR levels and advanced SOI timings enabled by the eBooster. One concern with using higher EGR levels is transient response; accordingly, to ensure transient response was suitable, constant speed load acceptance (CSLA) simulations were performed. Figure 4 shows CSLA results at two engine speeds. Addition of the eBooster to the optimized calibration allows the transient response of the optimized configuration to be better than the baseline (non-eBooster) engine. It can be seen that both NO_x and soot are also controllable over the load step, with the optimized eBooster configuration typically showing improved performance compared to the baseline configuration. Furthermore, Figure I.4.4 shows the importance of the eBooster when additional EGR is used. That is, without the eBooster, the transient response is much slower than the baseline case, and transient soot emissions increase substantially.

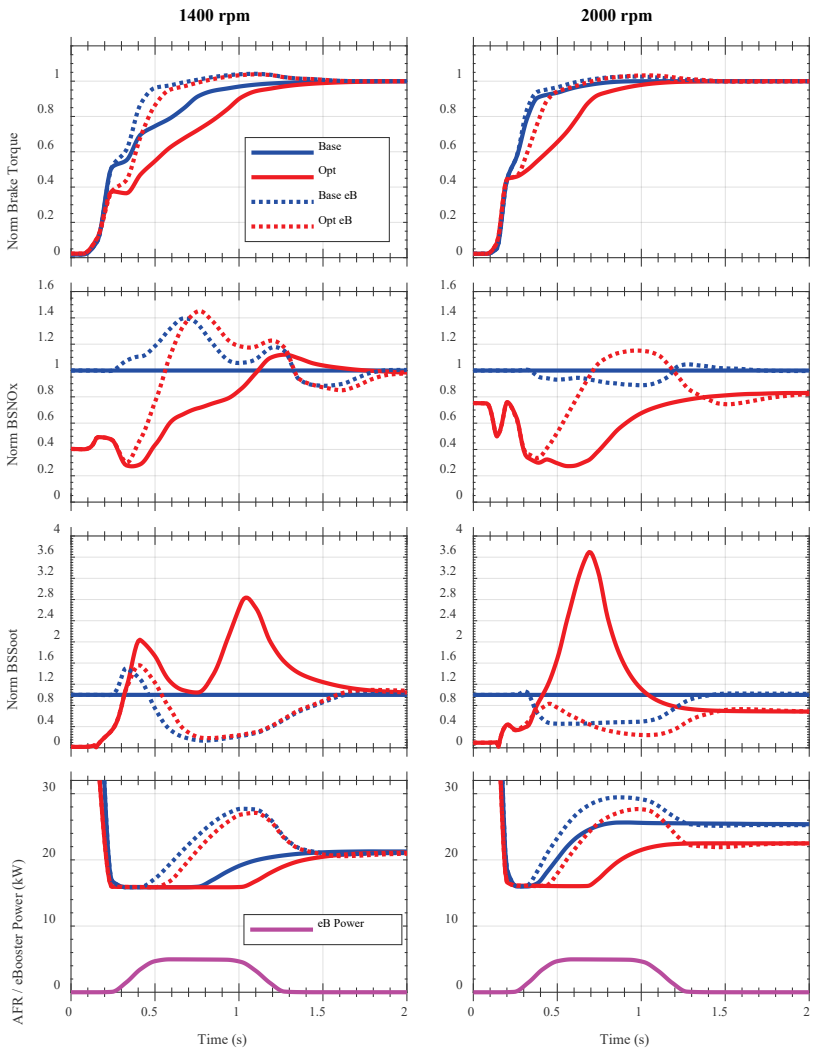

Figure I.4.4 CSLA results comparison for engine speeds of 1,400 rpm and 2,000 rpm. Two different engine calibrations for EGR and SOI are simulated with and without eBooster power delivery.

Test vehicle design and fabrication was undertaken in FY 2022. Component placement design has been completed for the prototype vehicle. High-voltage batteries and power electronics are on either side of the vehicle behind and below the cab. Low-voltage power electronics are distributed in and under the cab. Figure I.4.5(a) shows the final system-level design for the test vehicle. Fabrication and installation of components were completed. Figure I.4.5(b) shows the vehicle build nearing completion. Preliminary proof-of-concept testing began late in FY 2022. Figure 5(c) shows the vehicle operating during shakedown testing at John Deere testing facilities. The vehicle is currently functional, and supervisory control implementation and proof-of-concept testing experiments are planned for FY 2023.

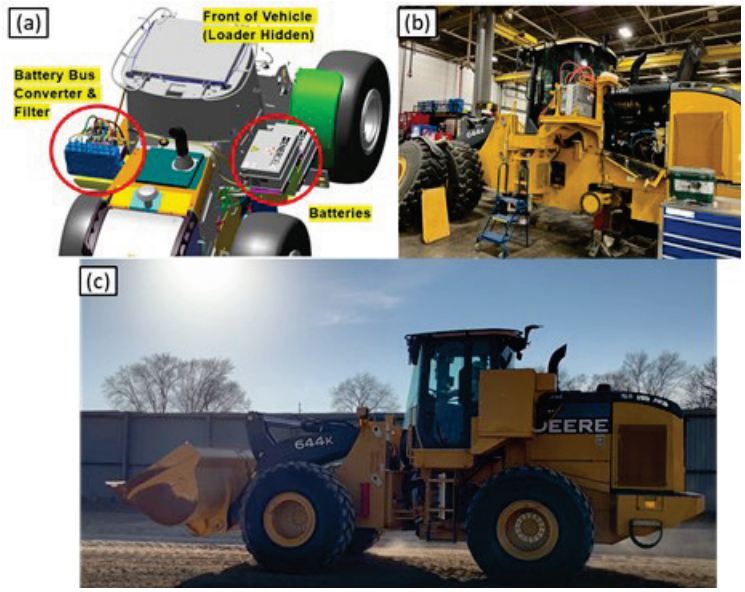

Figure I.4.5 (a) Location of electrical components on test vehicle. (b) Test vehicle build. (c) Test vehicle operating at testing facility.

Conclusions

- Electrification of air handling enables the engine to be reoptimized, thanks to the improved control over airflow, resulting in a BSFC reduction of up to 16% with improved transient emissions.
- Engine testing with the electrified air-handling system showed 8% less speed droop over a load transient compared to the baseline, non-electrified air system.
- Vehicle-level design and fabrication are complete, and preliminary vehicle-level testing is under way.

Key Publications

1. Mazanec, J., and S.L. Kokjohn. Forthcoming. “Enabling Off-Highway Diesel Engine Downsizing and Performance Improvement Using Powertrain Hybridization and Electrically Assisted Turbocharging.” *International Journal of Engine Research*.
2. Babu, A., R.M. Hanson, and S.L. Kokjohn. Forthcoming. “Comparison of Intake Boosting and Cylinder Deactivation as Enabling Strategies for Gasoline Compression Ignition.” SAE 23PFL-0232, Paper submitted to 2023 SAE World Congress.

I.5 Fully Electric-Powered, Hydraulic-Assisted Compact Track Loader (University of Minnesota)

Perry Y. Li, Principal Investigator
University of Minnesota
111 Church Street SE
Minneapolis, MN 55455
Email: Lixxx099@umn.edu

Michael Weismiller, DOE Technology Manager
U.S. Department of Energy
Email: Michael.Weismiller@ee.doe.gov

Start Date: February 1, 2022 End Date: April 30, 2025
Project Funding: $2,991,289 DOE share: $2,365,364 Non-DOE share: $625,925

Project Introduction

Commercial off-road vehicles such as excavators and loaders are typically powered by a diesel engine and actuated using hydraulics. In general, they are not very fuel-efficient, with only about 20% of the engine work making it to the useful output work. To reduce the greenhouse gas (GHG) footprint of such vehicles, these machines need to be significantly more efficient. Moreover, many municipalities (especially in Europe) are beginning to restrict and regulate the use of diesel engines within their cities. It would be useful to make the machines fully electric-powered. As the electric grid relies less on fossil fuel and more on renewable energy sources, electrification is a path towards lowering these machines' GHG footprint.

With the inefficient existing actuation system, simply replacing the diesel engine with an electric motor and battery would be prohibitive in terms of cost and space. Moreover, the high-power nature of off-road machines can also make electrification challenging because direct electrification requires that each degree of freedom be powered by an electric machine capable of the full power of that degree of freedom. As electric actuation is much less power-dense than hydraulic actuation, this increases the cost and size of the machine.

A previous project (DE-EE0008384) studied a novel system architecture that combines hydraulic actuation and electric actuation in a complementary fashion. The hybrid hydraulic–electric architecture (HHEA) was found capable of saving 50%–80% of the energy input for the work circuit of a variety of off-road vehicles performing representative duty cycles [1], [2], [3]. Moreover, the electric machines are significantly smaller if the electro–hydrostatic actuator approach is used. The goal of this project is to demonstrate the feasibility of using the HHEA as the basis for a high-efficiency, fully electric-powered compact track loader (CTL).

Objectives

The goal of the proposed project is to demonstrate the feasibility, performance, and potential cost of a fully electric-powered, functional, and highly efficient CTL. The target performance is the machine's requiring 40% less battery power than if the stock machine were electrified by simply replacing the diesel engine with an electric motor and battery. It is expected that with such a machine, the GHG footprint would be reduced by 80%, even if only 50% of the electricity is generated from non-fossil-fuel resources.

The HHEA will be applied to both the CTL's work circuit and propel circuit (which is new) to reduce energy use, downsize the electrical components, and reduce the cost of electrification. Figure I.5.1 shows the stock CTL to be modified.

Figure I.5.1 CTL to be electrified

Overall Objectives

- Develop and demonstrate a fully electric-powered CTL with high efficiency using a system architecture that leverages hydraulic actuation to reduce the size and cost of the electric components. The target is to reduce electricity (and battery) usage by 40%, as compared to the standard strategy of replacing the current machine's diesel engine with an electric motor.
- Compare the life cycle GHG emissions of the fully electric-powered CTL and one with a downsized internal combustion engine.
- Evaluate the feasibility of a high-speed soft-switching valve for pressure-rail-switching applications to reduce switching losses by 50%.

Fiscal Year 2022 Objectives

- Design and optimize the system architecture to be prototyped.
- Design and develop hardware-in-the-loop laboratory testbeds for the work and propel circuits.
- Generate potential soft-switching valve concepts to minimize throttling loss during pressure-rail transitions.

Approach

The proposed HHEA is illustrated in Figure I.5.2, both for the linear actuators used for lifting and tilting the arm and bucket and for the two rotary actuators used for propulsion. A set of multiple common pressure rails is used to provide the majority of power, and small electric motors are used to modulate that power to meet the demand of the duty cycle. For each degree of freedom, there are n^2 combinations of pressure rails (n being the number of common pressure rails; n=3 in Figure I.5.2) to connect to either side of the linear or rotary actuators. They represent n^2 discrete options of force or torque that can be provided by the common pressure rails. By using the electric motors to buck/boost the pressure on one side of the linear actuator or to directly add or subtract torque to the rotary actuator, the exact desired force and torque can be achieved with a combination of the hydraulic and electric actuations. Since the electric motors are used to modulate the force/torque between the force/torque levels provided by the pressure rails, their torque/power requirements can be quite modest. Efficiency of the HHEA is high because (1) energy can be regenerated either electrically or hydraulically, (2) all hydraulic machines operate at fixed displacement (making them efficient), and (3) on/off valves are

used (instead of metering valves) so that throttling can be avoided except when the on/off valves are partially open during transitions.

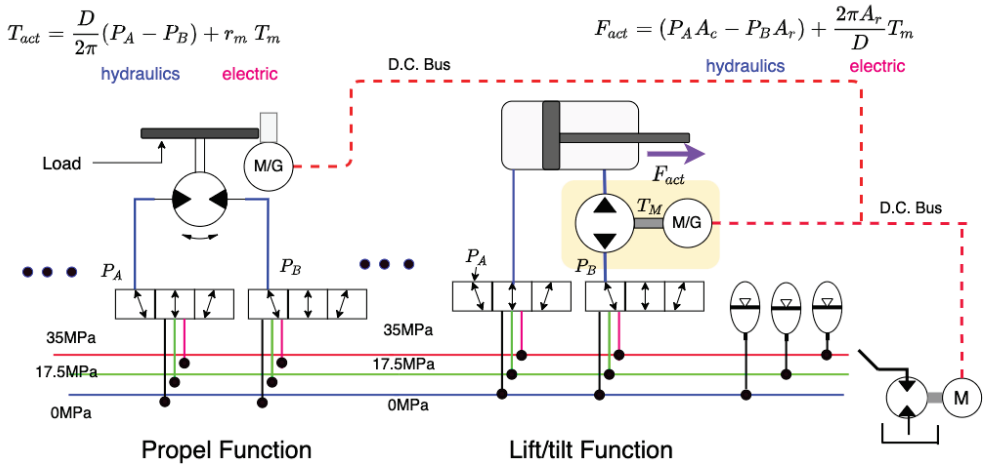

Figure I.5.2 HHEA for linear and rotary degrees of freedom

The research team consists of the University of Minnesota (with expertise in fluid power and control), the University of Wisconsin (with expertise in electric motors and drives), Case New Holland (a leading original equipment manufacturer [OEM] in CTLs), and Danfoss Power Solutions and Parker Hannifin (both Tier 1 suppliers of hydraulic and electric machines). The team will optimize the HHEA system architecture to be implemented on the CTL in Figure I.5.1 and develop real-time control strategies for both optimizing energy use and ensuring smooth and precise motion as demanded by the operator. Finally, since the HHEA relies on the rapid and efficient transition between common pressure rails, a soft-switching concept will be studied to reduce the energy loss during pressure rail transitions.

Results

- An optimal-energy-savings analysis tool has been adapted for the CTL to evaluate the different design options. The tool uses a dynamic programming method to compute the optimal selection of common pressure rails and to determine the energy-savings potential of each design for each representative duty cycle.

- A static system model of the stock machine has been created to evaluate the required energy consumption and fuel input to understand the performance of the stock machine. The model utilizes manufacturers' provided performance maps of the existing components.

- Preliminary analysis of the HHEA's potential to save energy has been performed. Representative drive cycles provided by the OEM partner have been analyzed using both the optimal-energy-savings analysis tool and the stock machine's static model. Results for one typical mission duty cycle are shown in Figure I.5.3, indicating 37% energy savings in engine work if the HHEA is adopted compared to the stock machine architecture. The percentage of energy savings for the work circuit is 86%, while that for the propel circuit is 10.4%. This level of energy savings is in line with the target of 40%, especially since additional energy savings are expected when the prime mover's operation is considered.

- Throttling losses in the switching valves have been analyzed. It was found that, with conventional switching valves, throttling losses account for about 15% of the total losses in a system that utilizes the HHEA. Simulation studies also suggest that, while decreasing the switching valves' transition time can decrease throttling, a portion of the losses cannot be removed by increasing the speed of the

switching valves. This residual loss is due to the compressibility of the fluid. Soft-switching strategies are currently being devised to minimize these compressibility-related losses.

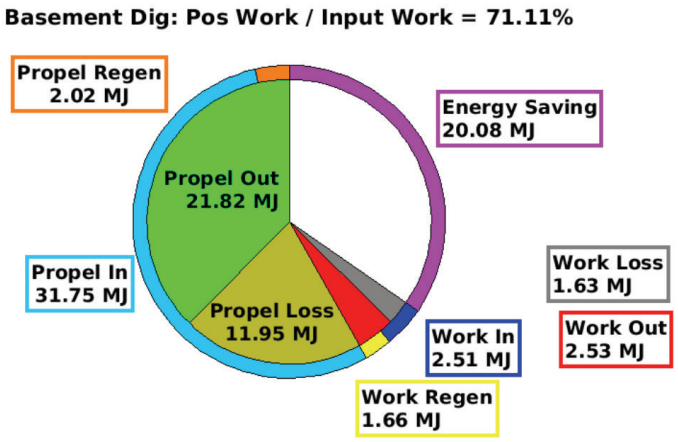

Figure I.5.3 Energy distribution chart of a CTL utilizing the proposed HHEA

Conclusions

- Preliminary analysis has confirmed the feasibility of the 40% target efficiency improvement with the use of the proposed HHEA for both the propel and work circuits of a compact track loader.
- Analysis of the throttling losses in the switching valves for pressure rail switching have confirmed the potential usefulness of the "soft-switch" concept to minimize the portion of the switching losses that is due to fluid compressibility.

References

1. Li, P.Y., J. Siefert, and D. Bigelow. 2019. "A Hybrid Hydraulic-Electric Architecture for High Power Off-Road Mobile Machines." *Proceedings of the ASME/BATH 2019 Symposium on Fluid Power and Motion Control*, Sarasota, FL, October 7–9. http://dx.doi.org/10.1115/FPMC2019-1628.

2. Siefert, J., and P. Y. Li. 2022. "Optimal Control of the Energy-Saving Hybrid Hydraulic-Electric Architecture (HHEA) for Off-Highway Mobile Machines." *IEEE Transactions on Control Systems Technology* 30, no. 5: 2018–2029. https://doi.org/10.1109/TCST.2021.3131435.

3. Khandekar, A., J. Wills, M. Wang, and P. Y. Li. 2021. "Incorporating Valve Switching Losses Into a Static Optimal Control Algorithm for the Hybrid Hydraulic-Electric Architecture (HHEA)." *Proceedings of the ASME/BATH 2021 Symposium on Fluid Power and Motion Control*, virtual/online, October 19–21. https://doi.org/10.1115/FPMC2021-69045.

Acknowledgements

The U.S. Department of Energy project officer for this project is John Terneus. The co-principal investigator is Dr. Eric Severson from the University of Wisconsin–Madison. Industry partners include CNH Industrial, Danfoss, and Parker Hannifin.

I.6 Articulated Dump Truck Electrification – Greenhouse Gas Reductions and Commercialization of New Technology in Construction Vehicles Fleet (John Deere Intelligent Solutions Group)

Brij Singh, Principal Investigator
John Deere Intelligent Solutions Group
4101 19th Avenue North
Fargo, ND 61265-8010
Email: SinghBrijN@JohnDeere.com

Michael Weismiller, DOE Technology Manager
U.S. Department of Energy
Email: Michael.Weismiller@ee.doe.gov

Start Date: July 15, 2022 End Date: November 14, 2025
Project Funding: $3,814,669 DOE share: $2,756,732 Non-DOE share: $1,057,937

Project Introduction

An articulated dump truck (ADT) handles the construction material and works alongside an excavator and/or wheel loader. This equipment (the excavator and/or wheel loader) fills the dump body on the ADT, and then the ADT transports the construction material to the worksite. This is a cyclic process, and most of the time the engine in the ADT idles, resulting in significant fuel burns and unnecessary greenhouse gas (GHG) emissions.

This project brings together expertise in wide-bandgap power electronics systems, 700 V lithium-ion battery packs, and vehicle power management to develop an integrated diesel–electric hybrid powertrain for ADTs. This hybrid powertrain will be integrated in the 310E model of a John Deere ADT. This prototype vehicle will be called an electrified ADT (eADT). Compared to a conventional 310E model of the ADT (a non-electrified vehicle with a hydrostatic powertrain), the prototype 310E model of the eADT will provide significant fuel savings and a reduction in GHG and criteria pollutants.

Objectives

The objective of this project is to research, develop, and validate a hybrid-powertrain-enabled ADT testbed potentially capable of ≥25% fuel savings and ≥25% GHG and criteria pollutant reductions when compared to a conventional ADT vehicle with a 9 L engine.

Overall Objectives

- Demonstrate >25% fuel savings by eADT compared to a conventional ADT.
- Downsize the engine from 9 L (330 kW) in a 310E conventional ADT to 6.8 L (224 kW) in the 310E eADT. The dual path of power flow from engine to vehicle traction system will optimize eADT performance and productivity compared to a conventional model with a similar payload.
- Use an optimum size of Li-ion battery pack rated ~80 kWh or less and 700 V pack voltage.
- Demonstrate improved performance and productivity.
- Demonstrate better shift quality and a smoother driving experience for the vehicle operator.

Fiscal Year 2022 Objectives

- The project team conducted dynamic system modeling (DSM, described further below) of the following major components needed for fabrication of the diesel–electric hybrid powertrain to be integrated in the 310E model of the eADT:
  - 6.8 L engine
  - 250 kW, 700 V dual inverter
  - 700 V battery pack
  - 15 kW, 700 V/48 V direct current (DC)-to-DC converter
- The project developed specifications of all major components of the hybrid powertrain (partially completed).

Approach

Learning from recent past successes [1], [2], [3], [4], [5], this project is driven by customers' needs and feedback from construction-vehicle fleet owners (Figure I.6.1), who have been asking Deere & Company for electrified vehicles. Deere has introduced a diesel-series-electric powertrain in the JD 644K and 944K hybrid loaders, and customer requests are about hybrid and electric versions of an ADT. Therefore, the project approach is driven by technology needs in Deere & Company and enterprise aspirations to reduce the overall carbon footprint in construction and mining companies. The proposed diesel–electric hybrid powertrain that will be developed through this project will result in ≥25% fuel savings and engine downsizing from 9 L (330 kW) to 6.8 L (224 kW).

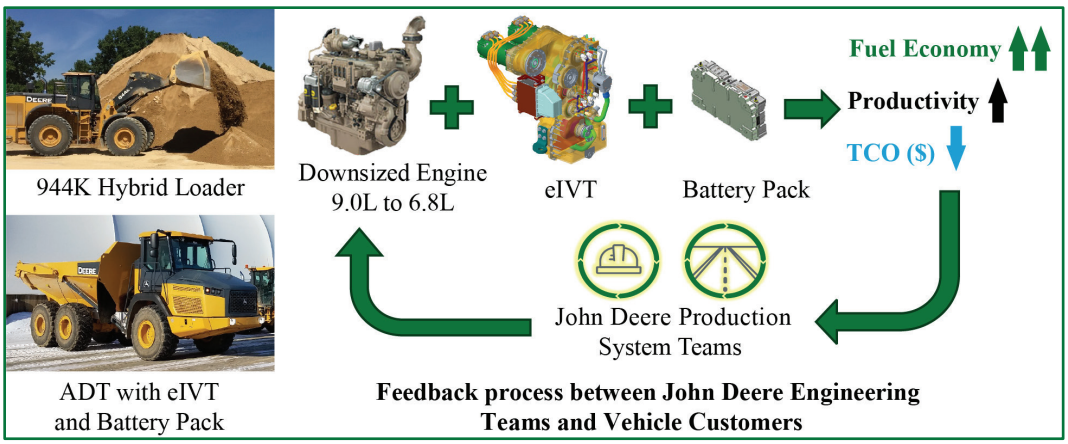

TCO – total cost of ownership

Figure I.6.1 Proposed eADT with a novel electric infinitely variable transmission (eIVT)-based powertrain

Project activities spread over three budget periods (BPs), BP1 to BP3. In BP1, the project will develop specifications for components needed to fabricate the hybrid powertrain, followed by component design. These tasks will use John Deere's DSM simulation platform. BP1 elements of research include development of power-conversion technologies such as a soft-switched SiC inverter carried out by the University of Arkansas; the aspiration would be a scaled-up power rating of the SiC inverter to 250 kW. This inverter will be applicable to the direct interface and integration of the 700 V Li-ion battery pack. Additionally, the 15 kW, 700 V/48 V DC-to-DC converter also has elements of research and development led by North Carolina State University, such as a power-dense magnetic circuit and efficiency enhancement.

In BP2, components designed in BP1 will be thoroughly tested for operating conditions associated with the 310E model of the eADT. Component testing will include both benchtop testing and back-to-back motor dynamometer-based characterization of the diesel–electric hybrid powertrain.

In BP3, the developed and prototype version of the hybrid powertrain will be integrated into the 310E model of the ADT, and the vehicle will be tested for fuel-economy gains and an assessment of GHG reductions.

Led by the principal investigator at John Deere Intelligent Solutions Group in Fargo, North Dakota, the project team will design and select diesel–electric hybrid powertrain components, and test verification will occur in the power electronics research and development building (also at the Fargo site). The powertrain will be test-verified in the power lab at John Deere Coffeyville Works. Vehicle system integration of the powertrain will occur at John Deere Dubuque Works, followed by demonstration at that location's vehicle proving ground.

Results

Accomplishments include the following:

- DSM of the eIVT-based diesel–electric hybrid powertrain of the eADT developed [6].
- Down-selection of the auxiliary resonant commutated pole (ARCP) inverter topology.
- PLECS® simulation resulting in DC-to-DC converter specifications.
- Estimate of >25% fuel economy improvements through eliminating idling.
- Projected engine downsizing, due to fuel savings, from 9 L (330 kW) to 6.8 L (224 kW).
- Estimate of over 10,000 metric tons of GHG reductions due to the fuel savings from powertrain deployment and engine downsizing.

Figure I.6.2 through Figure I.6.6 illustrate the outcomes of BP1 Quarter 1 results and findings.

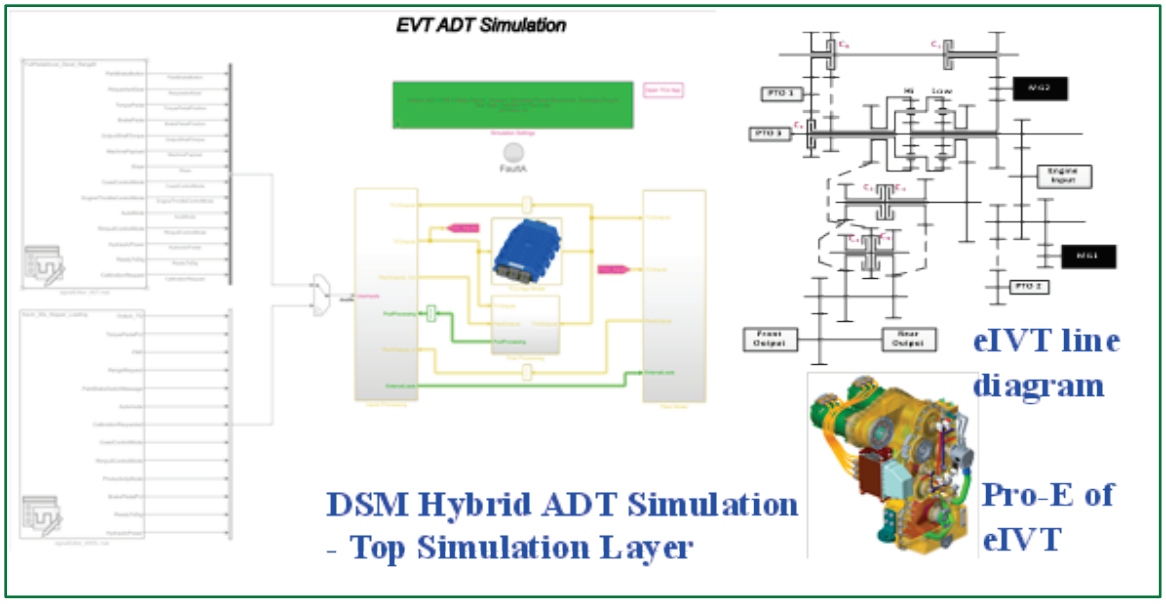

Pro-E – Pro-Engineer model created using Creo Software

Figure I.6.2 DSM simulation at the top layer of an eIVT-based 310E model of eADT

DSM work is complete, including entering a model of the eADT with engine, eIVT powertrain, and Li-ion battery. DSM blocks are illustrated in Figure I.6.2.

Project activities led by the University of Arkansas resulted in down-selection of the ARCP topology of the soft-switched inverter. The ARCP inverter will be simulated in BP1 design of the resonant circuit. Simulation work will be followed by prototype design and fabrication of the 10 kW 700 V DC bus ARCP inverter. The ARCP inverter is shown in Figure I.6.3.

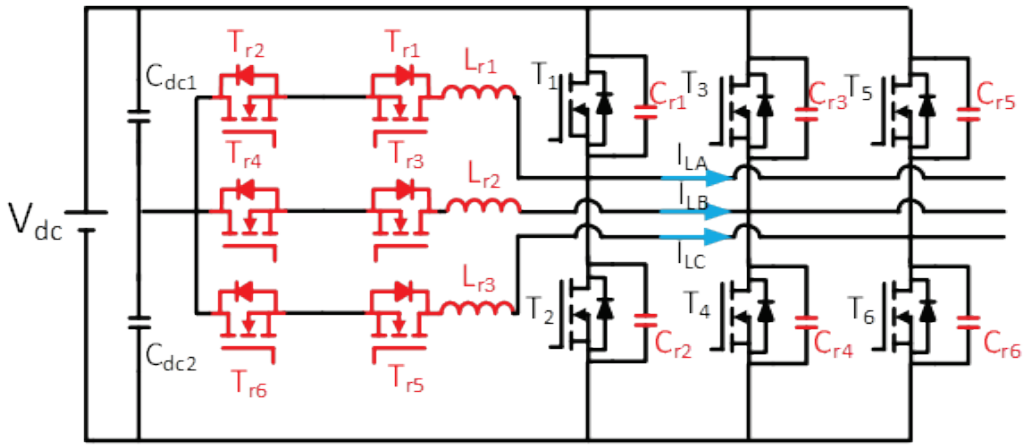

Key:
V_{dc}: DC bus voltage
C_{dc}: DC bus capacitor
T_r: silicon carbide MOSFET in resonant circuit
L_r: resonant circuit inductor
T: silicon carbide MOSFET in ARCP inverter power circuit
C_r: resonant circuit capacitor
I_{LA}, I_{LB}, and I_{LC}: Phase A, B, and C output current from ARCP inverter

Figure I.6.3 ARCP topology of soft-switched inverter

The task/activities related to the SiC/Si DC-to-DC converter (based on a metal–oxide–semiconductor field-effect transistor, or MOSFET) are led by North Carolina State University. The North Carolina State University team has produced preliminary specifications of the DC-to-DC power converter, as indicated in Figure I.6.4.

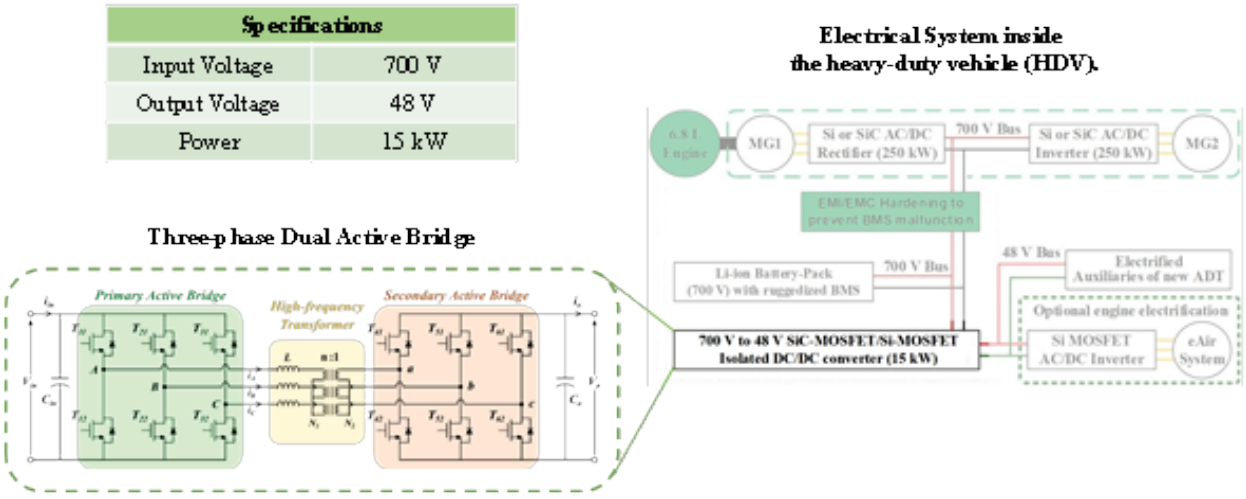

Figure I.6.4 PLECS®/MATLAB®/Simulink® simulation of the SiC/Si DC-to-DC converter

The John Deere team has collected field data from a conventional (mechanical drive) 310E ADT model. As shown in Figure I.6.5, the ADT operates under idling conditions for a significant time, leading to unnecessary fuel consumption. These data will be used to size the Li-ion battery pack.

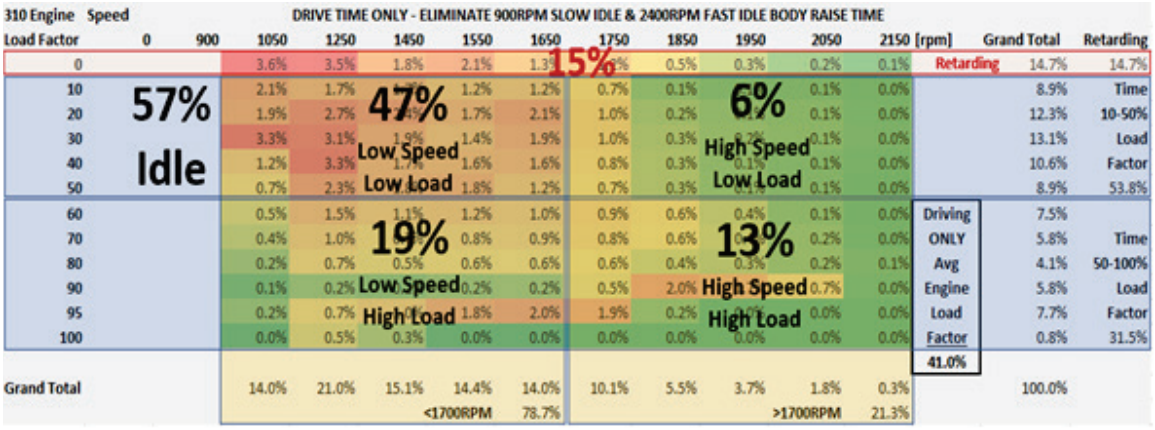

Figure I.6.5 JDLink™ [7] data indicating that the non-electrified 310E model spends nearly 15% of its drive cycle in braking (retardation) mode. With electrification using a diesel–electric hybrid powertrain, significant energy can be captured, resulting in fuel savings and GHG reductions.

The project has worked on the eADT. Figure I.6.6 illustrates the 310E ADT model purposed for early prototyping.

Figure I.6.6 310E ADT model of an early eADT prototype, purposed for data collection

Conclusions

Field data collected from a fleet of 310E model ADTs indicate that idle fuel consumption is excessively high, as high as 10 liters of diesel per hour while the vehicle is doing no work. Therefore, deployment of the diesel–electric hybrid powertrain will enable the engine-off condition, resulting in over 10,000 metric tons of GHG emissions avoided over the fleet's lifetime using the 310E model of eADTs.

References

1. Roth, Michael. 2020. "John Deere 944K Hybrid Wheel Loader Reaches 1 Million Field Operating Hours." *Rental Equipment Register*. October 24, 2020. https://www.rermag.com/earthmoving/article/21145781/john-deere-944k-hybrid-wheel-loader-reaches-1-million-field-operating-hours.

2. Morey, Bruce. 2016. “Off-Highway Hybrids: Opportunities and challenges.” *SAE Off-Highway Engineering*, February 2016, 16–18. Available on p. 14: https://www.nxtbook.com/nxtbooks/sae/16OFHP02/index.php?startid=2#/p/14.

3. John Deere. 2021. “John Deere Joint Tests Its First Electric-Powered Backhoe with National Grid.” January 6. https://www.deere.com/en/news/all-news/2021jan06-electric-powered-backhoe/.

4. Golf Course Industry. 2010. “Deere mowers honored with engineering award.” February 15. https://www.golfcourseindustry.com/article/gci-020510-john-deere-ae50-award/.

5. Lambert, Fred. 2016. “John Deere unveils latest all-electric tractor prototype for zero-emission agriculture.” *Electrek*. December 5, 2016. https://electrek.co/2016/12/05/john-deere-electric-tractor-prototype/.

6. Wikipedia. 2022. “Simcenter Amesim.” Last edited September 22, 2022. https://en.wikipedia.org/wiki/Simcenter_Amesim. Vehicle powertrains modeled by virtual design and simulation using DSM in the John Deere Coffeeville Works.

7. John Deere. 2022. “JDLink™ Connectivity.” https://www.deere.com/en/technology-products/precision-ag-technology/data-management/jdlink/.

Acknowledgements

The project’s principal investigator and the John Deere team acknowledge Professor S. Bhattacharya and Mr. Sagar Rastogi from North Carolina State University and Dr. Yue Zhao and Mr. Nan Lin from the University of Arkansas for their contribution of tasks completed in BP1 Quarter 1. The principal investigator and John Deere team also acknowledge John Terneus, Michael Weismiller, and Gurpreet Singh for their time and effort during project review meetings.

I.7 Hybrid Hydraulic–Electric Architecture of Mobile Machines (University of Minnesota)

Perry Y. Li, Principal Investigator
University of Minnesota
111 Church Street SE
Minneapolis, MN 55455
Email: lixxx099@umn.edu

Gurpreet Singh, DOE Program Manager
U.S. Department of Energy
Email: Gurpreet.Singh@ee.doe.gov

Start Date: September 1, 2018 End Date: April 30, 2022
Project Funding: $1,890,769 DOE share: $1,504,680 Non-DOE share: $386,089

Project Introduction

Most off-road mobile machines, such as excavators, wheel loaders, agricultural combines, etc., are hydraulically actuated because of hydraulics' unsurpassed power density. However, due to the use of throttling control, the inability to reuse energy from overrunning loads, and the hydraulic components being inefficient at partial load, the average efficiency from the engine output to the useful work performed is only 21% [1]. Yet, mobile hydraulic machines consume a significant portion (0.4%–1.3%) of the total energy consumed in the United States. Thus, improving energy efficiency of such machines is important.

As in the on-road automotive sector, there is also a trend for mobile hydraulic machines to be electrified to take advantage of the potential benefits of better efficiency and faster and more precise control. A common approach is for the work circuits (e.g., the arm of the wheel loader instead of the propulsion function) to be controlled using electric motors and drives via the electro-hydraulic actuators. While this is quite feasible for lower-power machines, the cost, size, and weight of the electric motors, drives, and batteries can be prohibitive for high-power machines. This is because the electric components need to provide the full power required by the machine.

The goal of this project is to develop a methodology for improving the efficiency of high-power, off-road mobile machines that takes advantage of electrification without the need for very high power or costly electric components. Our general idea is to develop a system architecture that marries the comparative advantages of hydraulic actuation and electrical actuation. In particular, the majority of power would be delivered by the power-dense hydraulic, which would then be modulated by small but highly controllable electrical actuation.

Objectives

Overall Objectives

- Develop an actuation system architecture that combines the benefits of hydraulic and electric actuations and that is applicable to a wide range of multi-degree-of-freedom mobile machines.
- Develop a tightly integrated, efficient, powerful, and compact hydraulic–electric power conversion machine for use with the system architecture.
- Demonstrate that the proposed system architecture can achieve a target efficiency of greater than 65% or an energy savings of greater than 40% over the baseline system in a typical off-road machine platform while maintaining or surpassing the control performance expected of current machines.

Fiscal Year 2022 Objectives

- Experimentally validate the motion control strategy on a high-pressure (300 bar) hardware-in-the-loop (HIL) testbed.
- Prototype the proposed integrated hydraulic–electric power conversion machine and characterize its performance.

Approach

The proposed hybrid hydraulic–electric architecture (HHEA) is shown in Figure I.7.1. It makes use of a set of common pressure rails at different pressure levels that serve all degrees of freedom of the system. Each degree of freedom is controlled by a hydraulic–electric control module (HECM), which combines hydraulic power from the common pressure rails and electric power from the direct-current (DC) bus or battery. The HECM consists of a set of on/off valves that select which pressure rails are to be used for a given time and a tightly integrated electric motor and hydraulic pump/motor that serve to modulate the hydraulic power. This architecture is envisioned for efficiency since it does not use throttling for control and can regenerate energy from overrunning loads. Moreover, electric components are only needed to modulate the total power for each degree of freedom so they do not need to be capable of very high power, thus keeping them reasonably small and cost-effective.

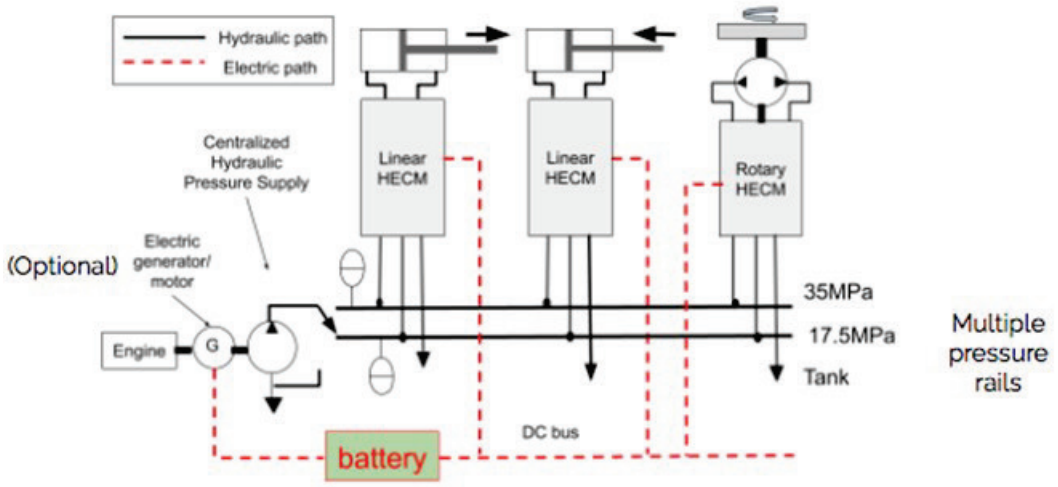

Figure I.7.1 Hybrid Hydraulic–Electric Architecture

In Fiscal Year (FY) 2019, FY 2020, and FY 2021, the energy-savings potential of the HHEA has been analyzed for a 20-ton wheel loader, a 22-ton medium-sized excavator, and a 5-ton mini-excavator using original-equipment-manufacturer-supplied representative duty cycles. The analysis in FY 2021 has included switching losses that were neglected in earlier years. The architecture was found to save 50%–80% of input energy compared to baseline load-sensing systems. It was also found that the torque requirements for the electric machines can be downsized to 10%–20% of the sizes if directly electrified using an electro-hydraulic actuator approach. A motion control algorithm that mitigates the pressure-rail switching effect and provides precise motion was experimentally validated on a medium-pressure-capable (20 MPa) HIL testbed. A high-pressure (30 MPa) HIL testbed was designed but not yet constructed. An optimized high-efficiency, high-power-density hydraulic–electric conversion machine has been designed. A prototype of the machine was manufactured and tested. Along with the prototype being very compact, it was estimated that the more efficient hydraulic–electric conversion would save an additional 10% of energy.

In FY 2022, the motion control strategy was further validated in the high-pressure setting. To this end, the 30-MPa-capable HIL testbed was constructed and the control performance was evaluated on the testbed. Furthermore, the prototype of the proposed power-dense hydraulic–electric conversion machine was also

completed, and performance characterizations were carried out experimentally, first as individual hydraulic and electric machines before testing them as an integrated unit.

Results

- The 30 MPa HIL testbed was completed and commissioned (see Figure I.7.2). The system is capable of mimicking the controlled external load of representative duty cycles.
- The nonlinear backstepping nominal control and the least-norm transition control algorithms were successfully validated on the 30 MPa HIL testbed.
    - In the absence of pressure-rail switching, the backstepping controller can maintain a trajectory tracking error of less than 5 mm with or without load variation. Figure I.7.3 shows a sample result where the external load is varying.
    - With the use of the least-norm transition controller (together with the nominal backstepping controller), the same tracking error of less than 5 mm is achieved even with pressure-rail switches. Figure I.7.4 illustrates a case where pressure-rail switches occur at 35 s and 60 s but the transition controller is able to mitigate the effects of the switches so that the tracking error is not affected.

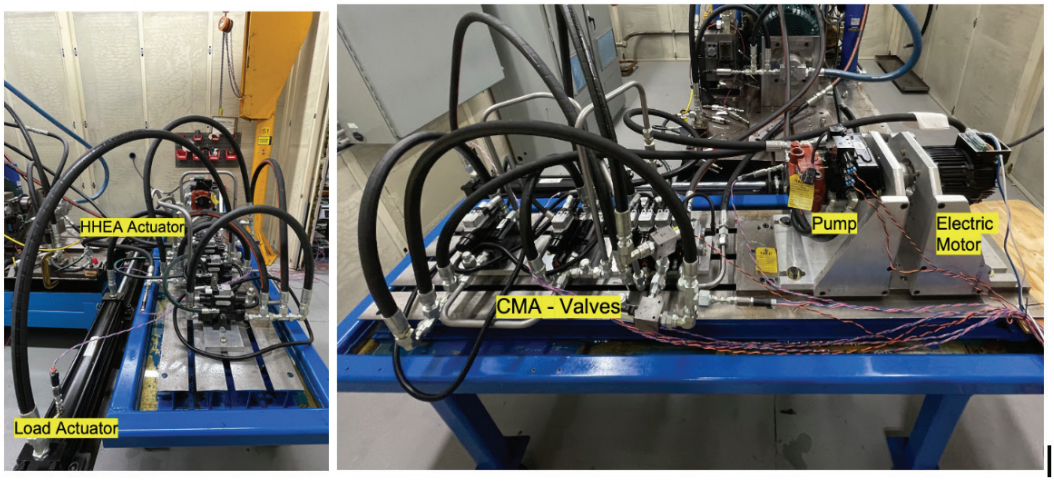

Figure I.7.2 High-pressure (30 MPa) hardware-in-the-loop test bed

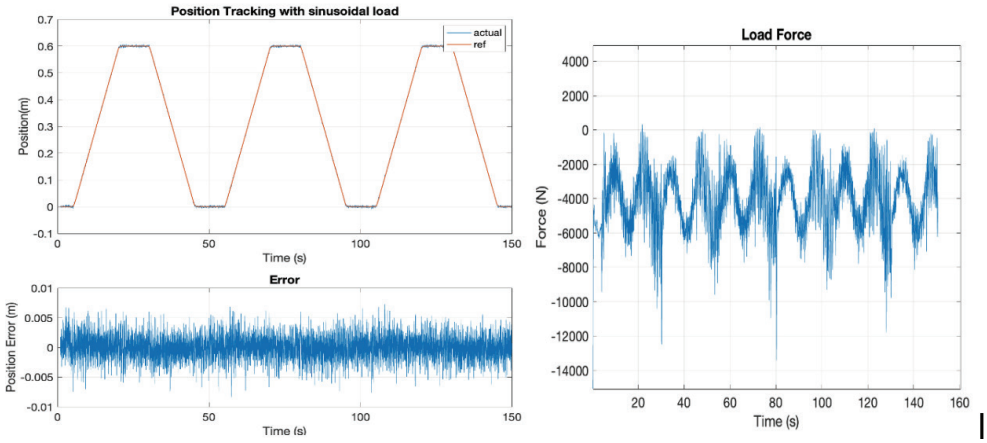

Figure I.7.3 Tracking control performance with load force variation

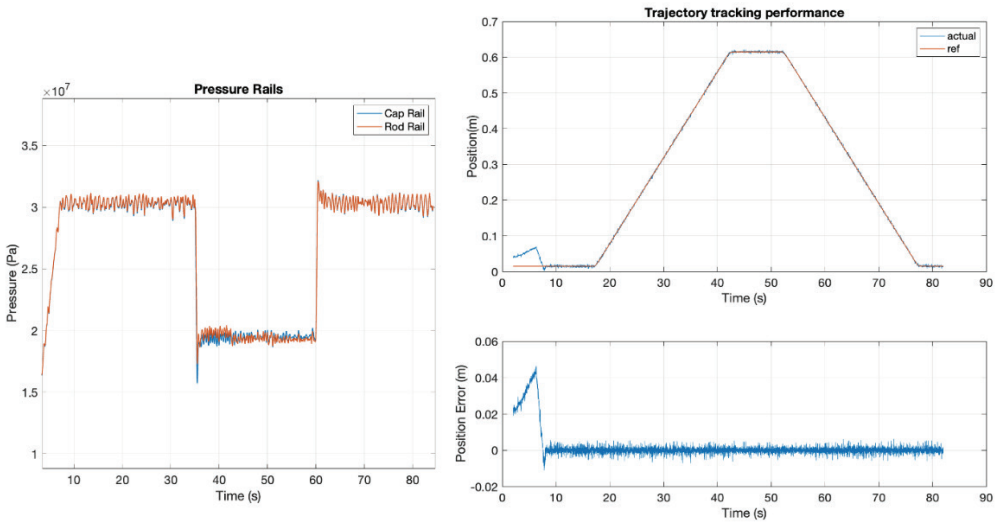

Figure I.7.4 Tracking control with transition control in the presence of pressure-rail switching at 35 s and 60 s

- Manufacture of a high-power-density hydraulic–electric power conversion machine was completed, consisting of a radial hydrostatic piston hydraulic pump/motor and an axial-flux electric motor. Figure I.7.5 and Figure I.7.6 show the assembled unit.
- The ratings of the machine are a peak power of 20 kW, maximum speed of 12,500 rpm, maximum torque of 15.8 Nm, peak efficiency of 88%, and an active mass power density of 6.8 kW/kg. The machine is among the highest power density machines utilizing conventional materials.
- When testing the radial hydrostatic piston hydraulic machine, the pistons were damaged due to charge pump failure. The pistons had to be redesigned several times to improve their robustness and manufacturability.
- Experimental testing of the hydraulic machine alone revealed larger than expected volumetric losses due to an out of specification pintle-cylinder gap. A mechanical efficiency map was also obtained.
- Experimental testing of the electric machine on a dynamometer (capable of a max speed of 6,000 rpm and max power of 5.6 kW) shows that various electric system characteristics such as peak torque, torque constant, inductances, and resistances are close to the calculated values. Efficiencies were measured, modeled, and extrapolated to the full range of operating conditions.
- Controllability of the machine was tested by demonstrating the electric machine's ability to control torque. It was shown that the electric machine running as a generator can faithfully track the desired torque profile determined from representative duty cycles (see Figure I.7.7 for an example).
- Running the integrated machine as a generator (with the hydraulic machine working as a pump and the electric machine working as a generator) successfully produces the expected three-phase back-electromotive-force profile.
- Further testing on the integrated machine was halted due to an accident caused by loss of charge pressure, leading to the machine being damaged. The machine must be disassembled and repaired before testing can continue.
- Although the integrated machine cannot be fully tested, individual characterizations of the electric and hydraulic machines can be combined to predict the integrated machine's performance. The integrated

machine would have a power density of 6.1 kW/kg (active material mass), exceeding the project target of 5 kW/kg. The analytical models of the integrated machine predicted an efficiency of 85%. The predicted efficiency based on hardware measurement is 63%. The difference is due to an excessive leakage gap between the cylinder block and pintle as well as slightly larger than expected stator resistance, iron losses, and air-gap viscous losses.

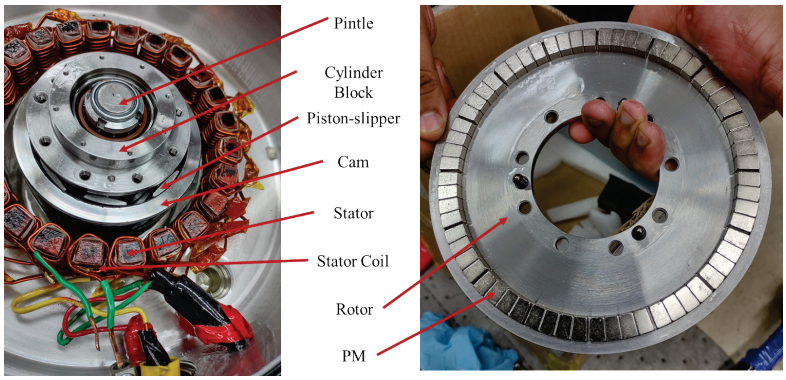

PM – permanent magnet

Figure I.7.5 Integrated hydraulic–electric machine with an axial flux motor and a radial piston pump

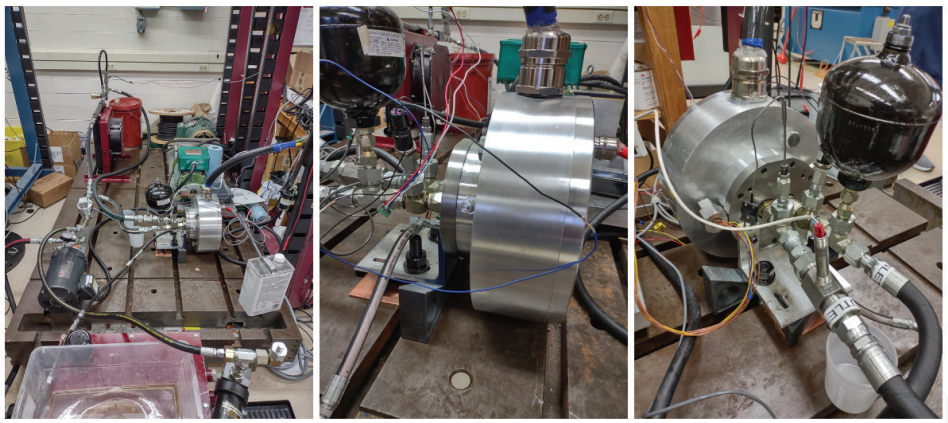

Figure I.7.6 Integrated hydraulic–electric conversion machine on the test stand

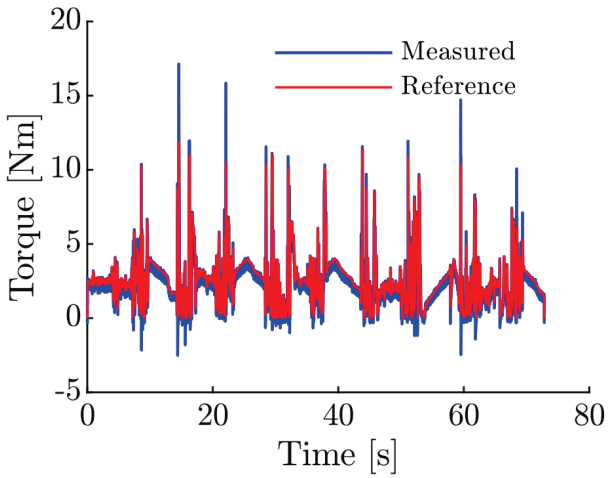

Figure I.7.7 Tracking of the desired torque profile

Conclusions

- The proposed HHEA approach can provide 50%–80% energy savings compared to the baseline load-sensing system for a variety of off-road machines and duty cycles. By using hydraulics to transmit the majority of power, the architecture's required electric motor sizes can be 85% smaller than if an electro-hydraulic actuator approach is used.

- The performance of a control algorithm, consisting of a backstepping nominal control and a least-norm transition control, has been experimentally demonstrated on a high-pressure (30 MPa) HIL testbed to be able to precisely control the motion of the machine. These tests show the controller can successfully mitigate the potentially harmful effect of pressure-rail switching, which is fundamental to the system architecture.

- A high-power-density, high-efficiency integrated hydraulic–electric power conversion machine has been designed, prototyped, and characterized. It has the potential to be one of the most power-dense machines.

Patent and Invention Disclosures

1. Li, P.Y. 2021. "Device having hybrid hydraulic-electric architecture." U.S. Patent 11,060,539.

Key Publications

1. Wills, J., A. Keester, and P.Y. Li. 2021. "A Power Take-Off (PTO) for Wave Energy Converters Based on the Hybrid Hydraulic–Electric Architecture (HHEA)." *Proceedings of the ASME/BATH 2021 Symposium on Fluid Power and Motion Control*, virtual/online, October 19–21. https://doi.org/10.1115/FPMC2021-68871.

2. Khandekar, A., J. Wills, M. Wang, and P. Y. Li. 2021. "Incorporating Valve Switching Losses into a Static Optimal Control Algorithm for the Hybrid Hydraulic–Electric Architecture (HHEA)." *Proceedings of the ASME/BATH 2021 Symposium on Fluid Power and Motion Control*, virtual/online, October 19–21. https://doi.org/10.1115/FPMC2021-69045.

3. Chatterjee, A., and P.Y. Li. 2021. "HIL Testbed and Motion Control Strategy for the Hybrid Hydraulic–Electric Architecture (HHEA)." *Proceedings of the ASME/BATH 2021 Symposium on Fluid Power and Motion Control*, virtual/online, October 19–21. https://doi.org/10.1115/FPMC2021-68888.

4. Nahin, M., G. Bohach, F.N.U. Nishanth, E.L. Severson, and J. Van de Ven. 2021. "Dynamic Modeling and Design of a Radial Hydrostatic Piston Pump for Integrated Pump-Motor." *Proceedings of the ASME/BATH 2021 Symposium on Fluid Power and Motion Control*, virtual/online, October 19–21. https://doi.org/10.1115/FPMC2021-68788.

5. Nishanth, F.N.U., J. Van Verdeghem, and E.L. Severson. 2021. "Recent Advances in Analysis and Design of Axial Flux Permanent Magnet Electric Machines." *2021 IEEE Energy Conversion Congress and Exposition (ECCE),* Vancouver, BC, Canada, October 10–14. https://doi.org/10.1109/ECCE47101.2021.9595085.

6. Nishanth, F.N.U., G. Bohach, M.M. Nahin, J. Van de Ven, and E.L. Severson. 2022. "Development of an Integrated Electro-Hydraulic Machine to Electrify Off-Highway Vehicles." *IEEE Transactions on Industry Applications* 58 (5): 6163–6174. https://doi.org/10.1109/TIA.2022.3189609.

7. Nishanth, F.N.U., and E.L. Severson. 2022. "A Review of Torque-Dense Electric Drive Systems with Potential to Bridge the Gap with Hydraulics for Off-Highway Vehicle Electrification." *2022 IEEE Transportation Electrification Conference & Expo (ITEC),* Anaheim, CA, June 14–17: 397–402. https://doi.org/10.1109/ITEC53557.2022.9813839.

8. Wills, J., and P.Y. Li. 2022. "Accumulator Sizing for the Hybrid Hydraulic Electric Architecture (HHEA) Using Dynamic Programming." *Proceedings of the BATH/ASME 2022 Symposium on Fluid Power and Motion Control*, Bath, United Kingdom, September 14–16. https://doi.org/10.1115/FPMC2022-90184.

9. Nishanth, F.N.U., G. Bohach, M.M. Nahin, J. Van de Ven, and E.L. Severson. 2022. "Development of an Integrated Electro-Hydraulic Machine to Electrify Off-Highway Vehicles." *IEEE Transactions on Industry Applications* 58 (5): 6163–6174. https://doi.org/10.1109/TIA.2022.3189609.

References

1. Love, Lonnie, Eric Lanke, and Pete Alles. 2012. *Estimating the Impact (Energy, Emissions and Economics) of the US Fluid Power Industry*. Oak Ridge, TN: Oak Ridge National Laboratory. https://doi.org/10.2172/1061537.

Acknowledgements

The U.S. Department of Energy Project Officer for this project is John Terneus. The co-principal investigators are Dr. James Van de Ven from the University of Minnesota, Dr. Eric Severson from the University of Wisconsin–Madison, and Dr. Rachel Wang from Eaton Corporation. Industry partners include Danfoss, CNH Industrial, JCB, and Toro.

I.8 Heavy-Duty Hybrid Diesel Engine with Front-End Accessory Drive-Integrated Energy Storage (Caterpillar Inc.)

Robert McDavid, Principal Investigator
Caterpillar Inc.
Technical Center – Building F
14009 Old Galena Road
Mossville, IL 61552
Email: McDavid_Robert_M@cat.com

Gurpreet Singh, DOE Program Manager
U.S. Department of Energy
Email: Gurpreet.Singh@ee.doe.gov

Start Date: October 1, 2018 End Date: September 30, 2022
Project Funding: $7,374,000 DOE share: $3,441,000 Non-DOE share: $3,933,000

Project Introduction

This project aims to design and demonstrate a high-efficiency power system with a 13-L concept engine (downsized from 18 L) for use in off-road machine applications. Hybrid power and energy systems will be added to enable transient load assist to maintain machine productivity, energy recovery, and start/stop (or anti-idle). The power system will have a hybrid front-end accessory drive that incorporates a high-speed flywheel (HSFW), a mechanical-drive turbocharger (SuperTurbo), and a motor-generator unit (MGU).

Objectives

- Research, develop, and demonstrate a heavy-duty hybrid diesel (H2D2) engine system for off-road applications (see Figure I.8.1).
- Demonstrate the following performance targets:
  - 17% (+/-2) more fuel efficient than current Tier 4 diesel engine.
  - Equivalent transient response versus baseline diesel engine.
  - Tier 4 Final exhaust emissions levels.

Figure I.8.1 Three target off-road machine applications

Approach

- Phased Approach:
  - Concept design and simulation completed in 2020.
    - Systems-level modeling of hybrid power system concept.
    - Defined concept trade-offs and provided performance predictions.

- Major subsystem analysis and specification completed in 2021.
  - 1D and 3D thermofluid, structural, and dynamic simulations.
  - Addressed durability, performance, and modularity.
- Phase 1 concept demonstrator engine completed in 2021 to validate engine-only performance predictions.
- Phase 2 hybrid engine system validation of the complete power system in a transient cell to be completed in late 2022.
- Technoeconomic analysis to address cost barriers and provide total-cost-of-ownership value assessment to be completed in late 2022.

Results

System Simulation

- Final Concept 2a selected (see Figure I.8.2).
  - The "a" denotes the electric drive for the HSFW.
  - Concept 2a preferred for the best transient response, complete HSFW-to-engine decoupling, and flexible packaging.
- System simulation (engine + hybrid systems) continued to be refined in 2022.
  - The transient hybrid strategy evolved with system maturity.
  - Ranges in brake specific fuel consumption (BSFC)/efficiency improvement stem from application and cycle variation (see Figure I.8.3).

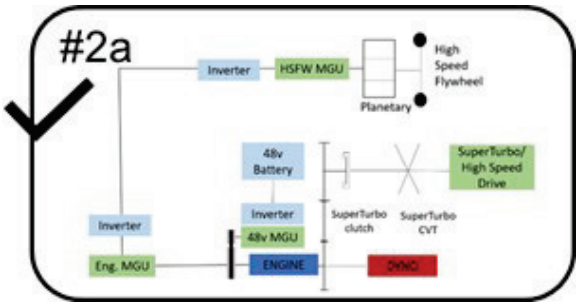

CVT – continuously variable transmission

Figure I.8.2 Schematic of finalized hybrid

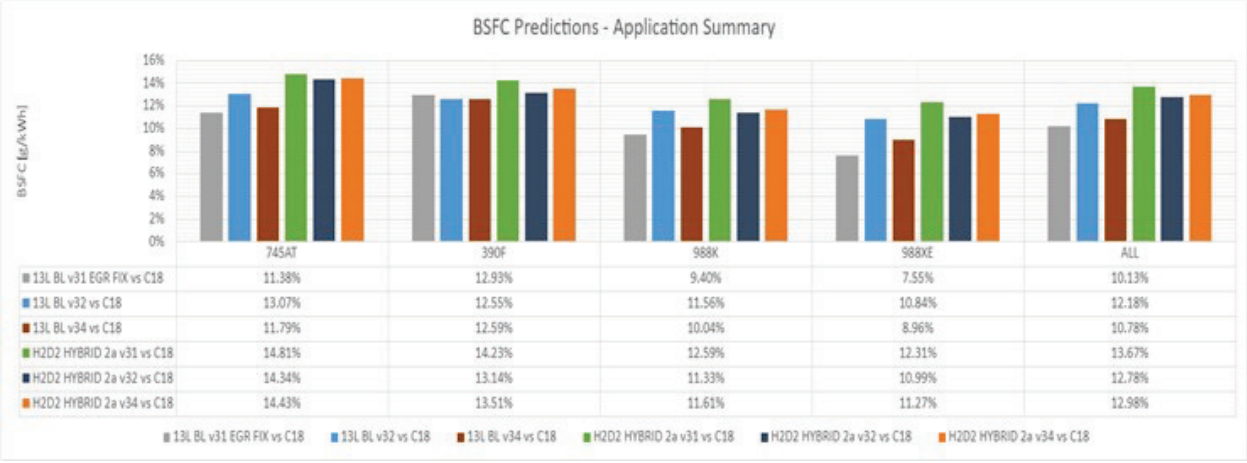

EGR – exhaust gas recirculation

Figure I.8.3 Summary of predicted BSFC improvement (versus the baseline 18-L engine) as a function of hybrid configuration and machine application

Concept Engine and Aftertreatment

- Test-to-simulation (pre-hardware predictions) efficiency ranges were confirmed (Figure I.8.4a).
- Phase 2 build and test cell installation was completed (Figure I.8.4b).

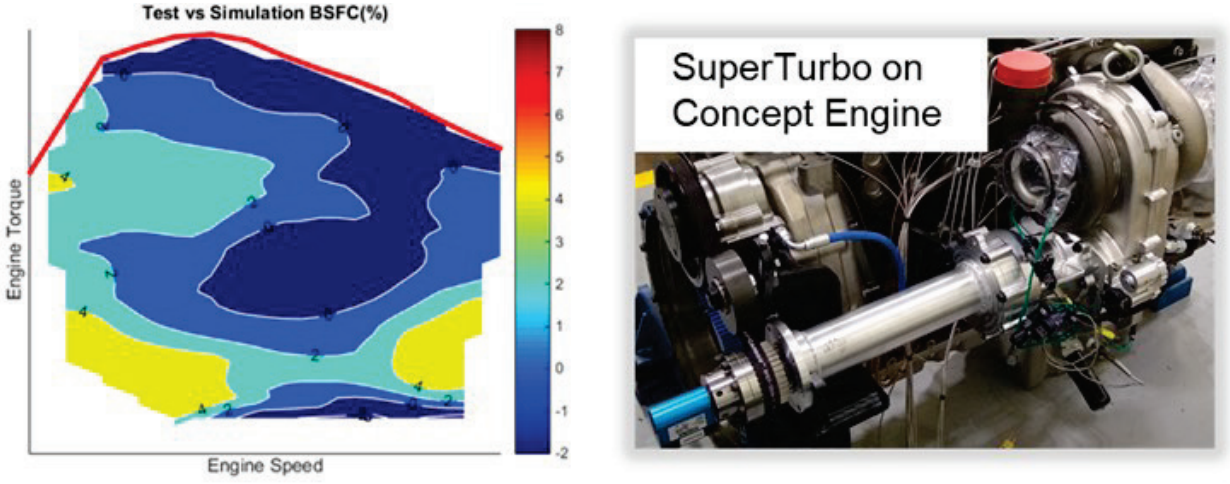

(a) (b)

Figure I.8.4 (a) Core engine test versus simulation BSFC prediction error and (b) Phase 2 concept engine with SuperTurbo assembled

- Validation testing is underway.
- Initial thermal barrier coating (TBC) test data obtained (Figure I.8.5).

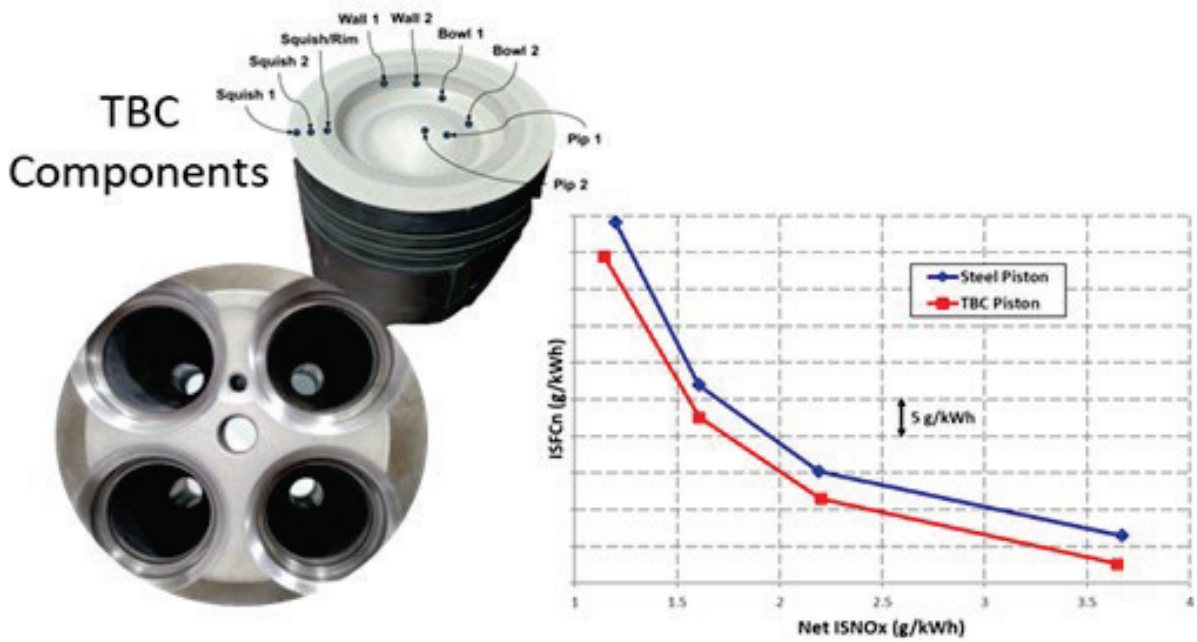

ISFCn – net indicated specific fuel consumption; $ISNO_x$ – indicated specific oxides of nitrogen

Figure I.8.5 Thermal barrier coating efficiency results

- Cooling package benefits derive from more efficient core engine (Figure I.8.6).

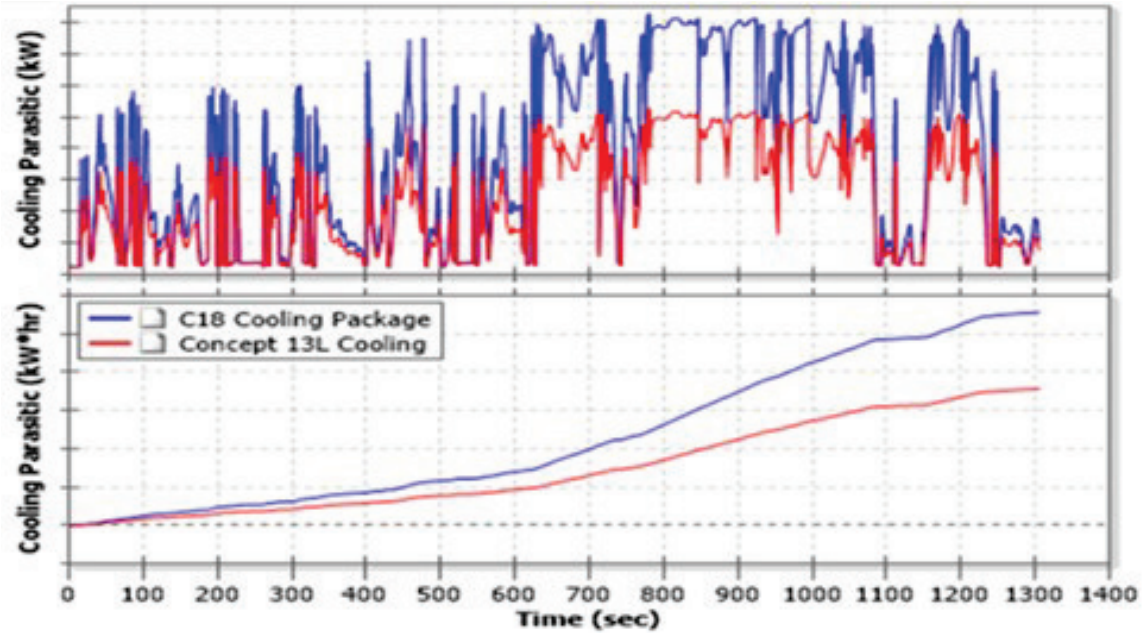

Figure I.8.6 Predicted reduction in cooling system parasitic loading derived from more efficient engine

SuperTurbo Device

- Turbocompound performance was simulated.
- Calibration was optimized.
- Flow and sizing selection were completed. The prototype turbine and housing were completed with five nozzle rings for flow adjustment (Figure I.8.7).

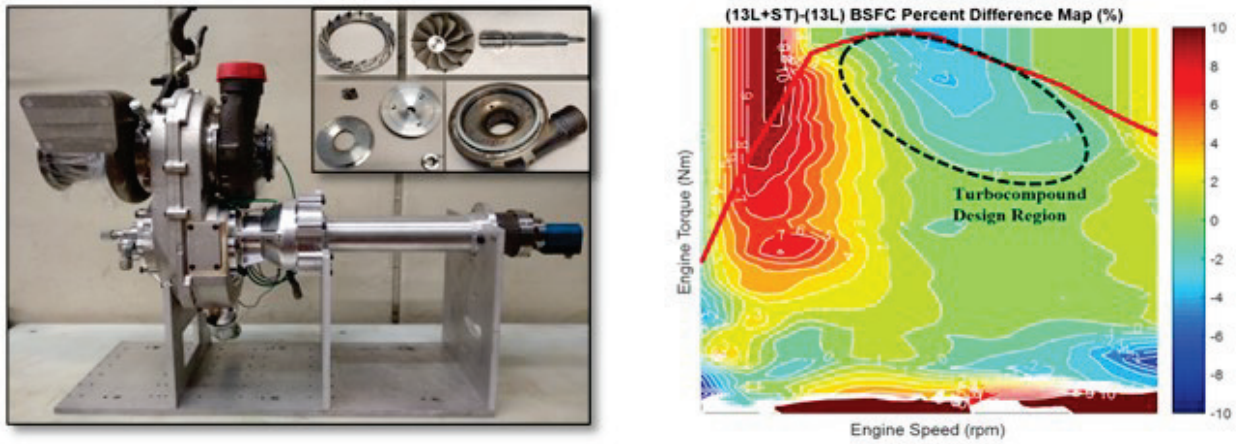

(a) (b)

Figure I.8.7 (a) Delivered SuperTurbo device and (b) predicted BSFC changes with SuperTurbo

- Preliminary transient engine response and SuperTurbo tuning were completed (Figure I.8.8).

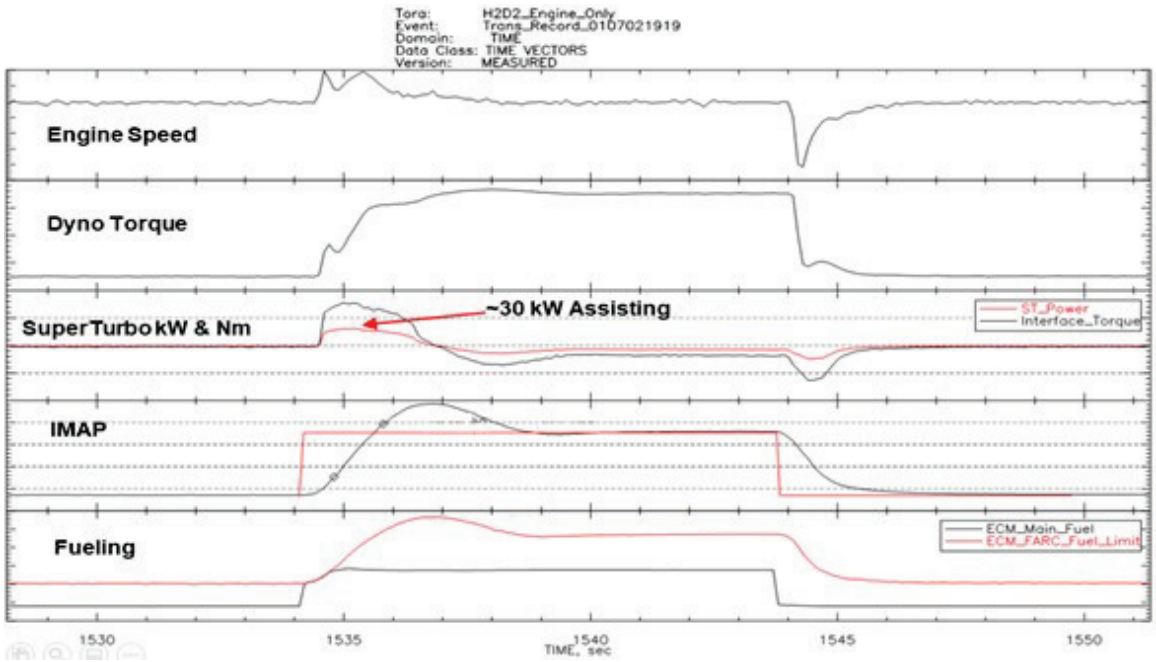

IMAP – intake manifold air pressure; ECM – electronic control module; FARC – fuel–air ratio control; ST – SuperTurbo

Figure I.8.8 Preliminary SuperTurbo testing demonstrated acceptable performance to begin the validation testing campaign.

- 1,200 rpm
- 20%–80% load

Hybrid System - Controls and Systems Integration

- Hybrid device and driveline losses were mapped.
- HSFW and electric drive capability were confirmed.
  - +110 kW discharging and -130 kW charging power.
  - +12,000 Nm/s discharging at engine input.
- 48 V MGU capability was confirmed (Figure I.8.9).
  - +20 kW discharging and -25 kW charging power.
  - 1,366 Nm/s discharging at engine input.

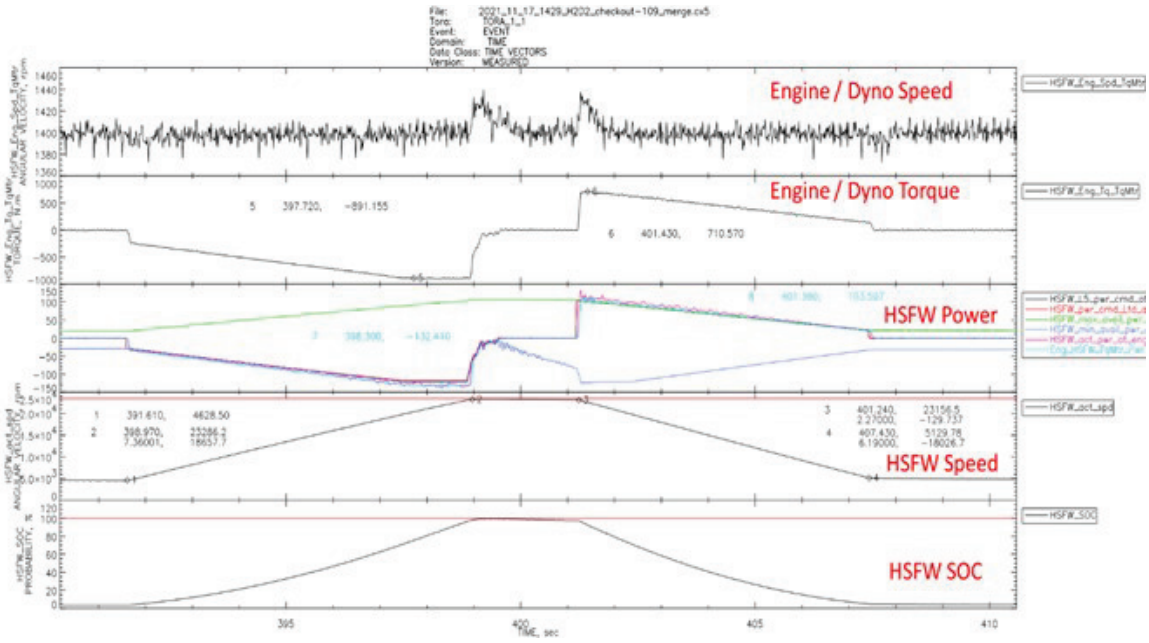

Figure I.8.9 Torque, speed, and power measurements confirming HSFW and electric drive capability

- Start/Stop Analysis
  - Completed key machine analysis.
  - Hundreds to thousands of hours of data with 10%–35% machine idle time.
  - Fuel savings model was generated with deterioration factors for debounce and recharge efficiency.
  - Fuel Saving Factor (FSF) model was developed and applied to machine applications (assuming 10 second debounce, 300 second max idle off, 4 kW hotel load) (Figure I.8.10).
    - 745AT (Articulated Truck): 0.6%–2.6% fuel savings
    - 988K (Wheel Loader): 0.8%–3.5% fuel savings
    - 390F (Hydraulic Excavator): 0.6%–2.8% fuel savings.

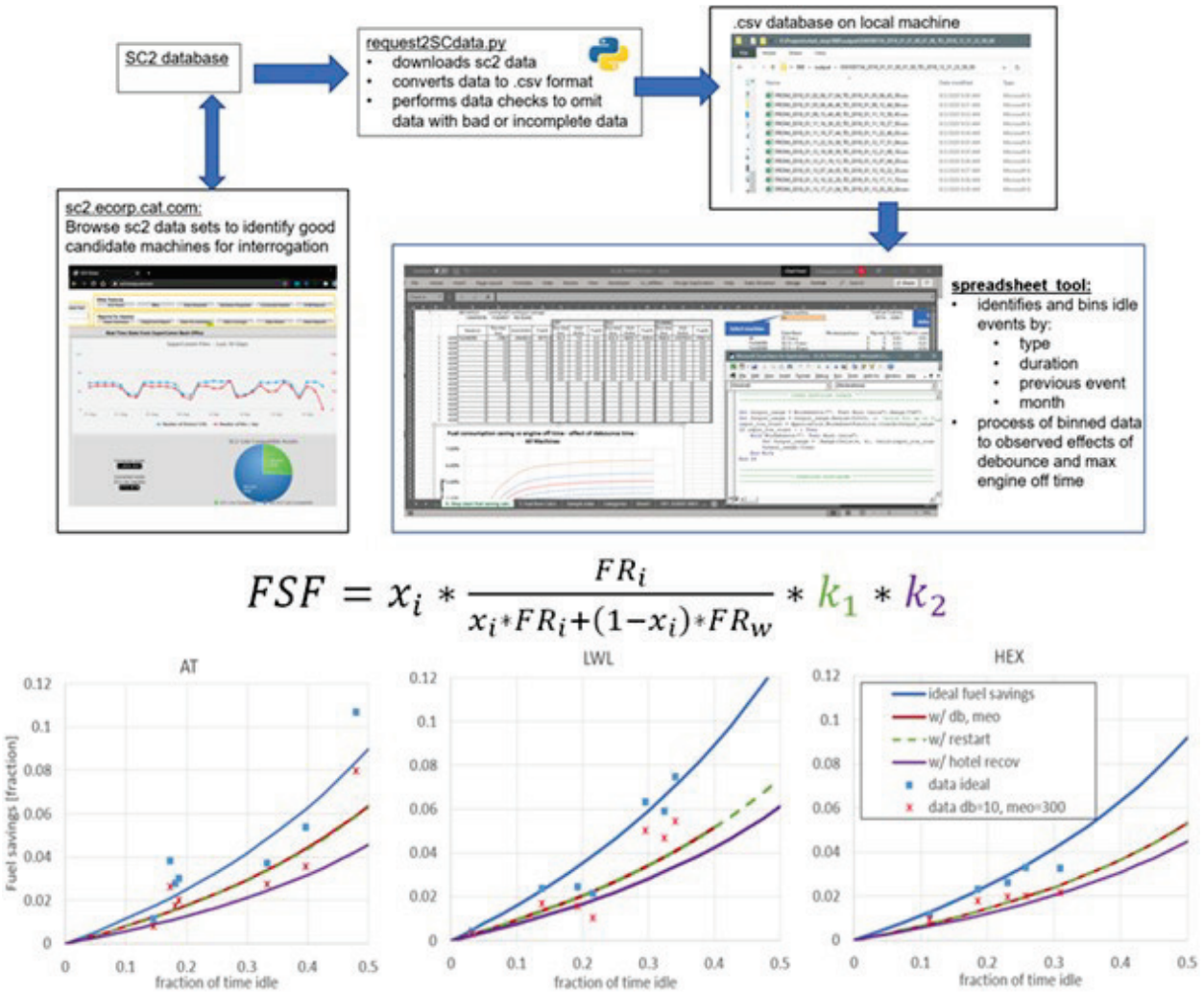

SC2 – SuperComm 2 Database; LWL – large wheel loader; HEX – hydraulic excavator

Figure I.8.10 Start/stop analysis process summary and results

Conclusions

2022 Summary

- Engine
  - The smaller concept engine was built, is on track to deliver the predicted efficiency improvements, and accounts for the majority of the system efficiency gains.
  - Significant engine downsizing and efficiency improvements are partially enabled by the transient response assist capabilities of the hybrid devices.
- Hybrid Aspects
  - The HSFW and MGU performance was validated.
  - The SuperTurbo was completed with successful integration and preliminary performance assessment.

Based on the concept down-selection simulations, the Phase 1 single- and multi-cylinder engine testing, and the hybrid-only system physical validation performed so far, Table I.8.1 has been updated to show the current predictions of the efficiency gains from the various elements of the hybrid power system over the three target off-road machine applications (shown in Figure I.8.1). A clear line of sight toward the program goal of 17% ± 2 efficiency improvement still remains.

Table I.8.1 Current predictions of high-level efficiency contributions over the baseline 18-L engine power system

~~7.6%–12.9%~~ 9.0%–12.6%	13-L concept engine
~~1.5%–2.5%~~ 0.3%–1.1%	SuperTurbo turbo-compounding
~~1.5%–2.0%~~ 0.5%–1.9%	HSFW and 48-V MGU
0.5%–2.0%	TBC
0.6%–3.5%	Start/stop implementation
TBD	Advanced engine controls (real-time optimizer)
2.0%–3.0%	Reduced cooling parasitic
13.5%–24.1%	**Current Total**

The project successfully passed Go/No-Go Milestones 1 and 2 as reported in the 2021 annual project report.

Future Work

- Finalize the engine-only and full-system hybrid validation testing. The hybrid-only testing was completed and now the engine-only testing is in progress. The combined hybrid system will be brought together and tested.
- Document steady-state and transient performance, emissions, and efficiency.
    - Steady-state engine and system performance will be mapped. Tailpipe emissions, efficiency, and heat rejection and typical durability measurements will be completed.
    - Transient operation will include machine work cycles, load response tests, and non-road transient cycle and rapid compression machine certification cycles for Tier 4 Final emissions compliance.
- Complete the technoeconomic analysis leveraging the validation data. A total-cost-of-ownership analysis will be completed based on the bill of materials and the measured performance.

Acknowledgements

We would like to acknowledge the support and guidance of David Ollett, National Energy Technology Laboratory Program Manager, and Chad Koci, Project Lead (Caterpillar Inc.), for the day-to-day execution and leadership of the project.

I.9 Simultaneous Greenhouse Gas and Criteria Pollutants Emissions Reduction for Off-Road Powertrains (Eaton Corporation)

Dr. James E. McCarthy, Jr., Principal Investigator
Eaton Corporation
26201 Northwestern Highway
Southfield, MI 48076-3925
Email: JimMcCarthy@Eaton.com

Siddiq Khan, DOE Technology Manager
U.S. Department of Energy
Email: Siddiq.Khan@ee.doe.gov

Start Date: February 1, 2022 End Date: November 30, 2025
Project Funding: $2,978,523 DOE share: $2,377,904 Non-DOE share: $600,619

Project Introduction

The objective of this project is to research, develop, and validate engine and aftertreatment (AT) system technologies for significantly reducing nitrogen oxides (NO_x) and greenhouse gas (GHG) emissions for off-road powertrains. The system will be tested over the regulatory cycles and select field cycles.

A future off-highway 13 L engine is being developed in combination with an advanced modular AT system to meet the NO_x and GHG targets. The advanced engine has reduced parasitic loads in combination with cylinder deactivation and an exhaust gas recirculation (EGR) pump. The advanced AT system has provisions for a light-off selective catalytic reduction (SCR) followed by a primary AT system (similar to the production system today with the addition of a diesel particulate filter [DPF]). Electric heaters upstream of all SCRs in combination with a fuel burner upstream of the primary AT are options that will be investigated.

Objectives

The project objective is to research, develop, and validate AT system-level strategies capable of ≥10% GHG reduction and ≥90% NO_x reduction for off-road powertrains over multiple duty cycles spanning the segment's diverse applications, while maintaining affordability and robustness to ensure economic viability.

Overall Objectives

Budget Period 1

- Determine system definition and performance metrics.
- Establish baseline NO_x and GHG emissions based on the Tier 4 final architecture.
- Design, build, and commission future engines.
- Design, fabricate, and commission a modular AT system.
- Adjust baseline GHGs to be comparable with the modular AT system architecture.

Budget Period 2

- Evaluate a future engine with multiple AT architectures for meeting NO_x and GHG targets.
- Define optimal configuration for final testing.

- Demonstrate progress to the NO_x and GHG targets by reducing emissions above a straight line from point A (>90% NO_x and >3.5% GHG reductions) to point B (>50% NO_x and >7% GHG reductions).

Budget Period 3

- Build and commission optimized testbed.
- Quantify performance achieved.
- Provide final assessment.

Fiscal Year 2022 Objectives

- Determine system definition and performance metrics.
- Build baseline and age the AT system using hydrothermal aging prior to testing.
- Design and build the base future engine.
- Design a modular AT system.
- Assess baseline GHG correction compared to the modular AT system architecture.

Approach

The program approach is to optimize a 13 L off-road engine for better efficiency using multiple engine technologies and couple this with a modular AT system that involves multiple catalysts and exhaust heating devices for the purpose of NO_x and GHG reduction. The engine is a Fiat Powertrain 13 L that will be equipped with Eaton cylinder deactivation and EGR pump systems. The AT system catalyst design was specified by Fiat Powertrain and Johnson Matthey. The exhaust heating devices include a fuel burner designed by Tenneco and Eaton along with electric heaters designed by Corning and Vitesco. The modular AT system is designed with project partners along with Tenneco for design, layout, and future fabrication. The AT systems will be aged using the hydrothermal protocol at Southwest Research Institute. Engine testing will start at Fiat Powertrain in Burr Ridge, Illinois, while the engine and AT testing will be optimized at Oak Ridge National Laboratory.

Results

Key accomplishments for Fiscal Year 2022 include:

- Developed a complete program management plan for Budget Period 1.
- Defined the engine as the 13 L model rated at 407 kW at 2,100 rpm for use in a Case IH Steiger four-wheel drive tractor application.
- Procured baseline Tier 4 final engine and AT system. The AT system is at Southwest Research Institute ready for aging using a hydrothermal profile.
- Assessed GHG impact for comparing the baseline system to the modular AT system. Results show that fuel consumption increases by 1% for every 100 mbar of added backpressure. These results will be applied to the three regulatory cycles and five field cycles in the next reporting period.
- Designed the modular AT system in a flexible architecture capable of evaluating a variety of AT and exhaust thermal management alternatives. Specific catalyst formulations and sizes have been defined. The AT “canning” details have been established. Figure I.9.1 shows the modular AT system.

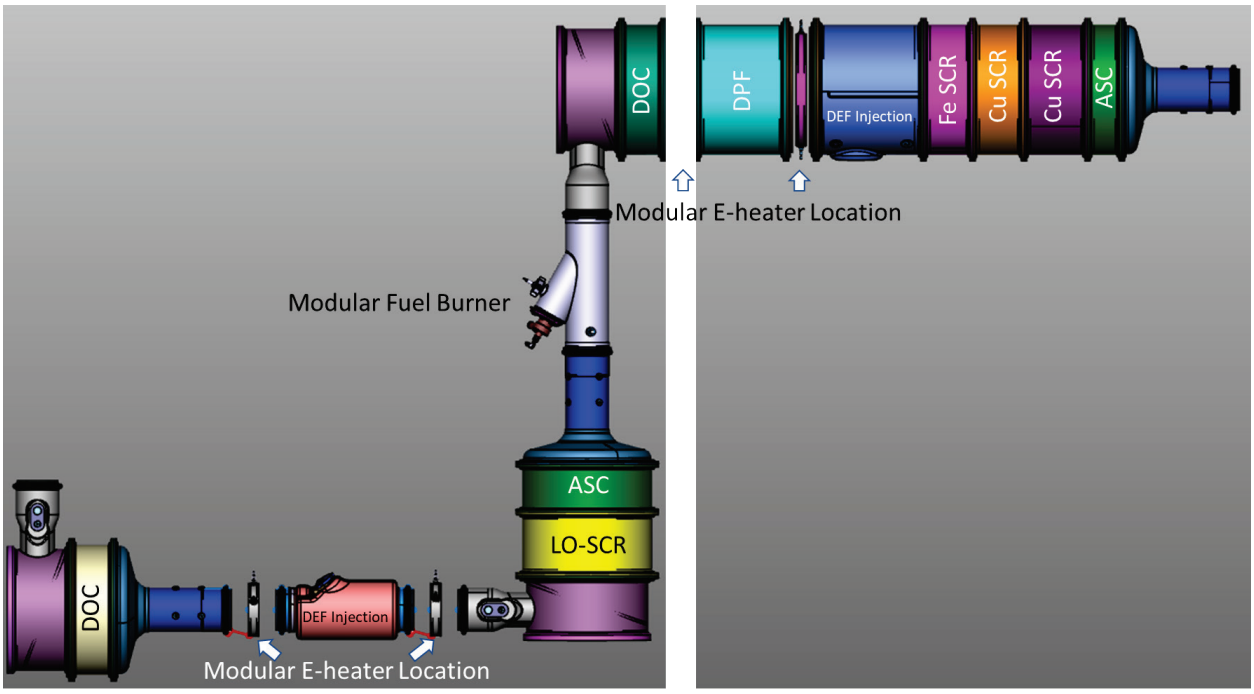

DOC – diesel oxidation catalyst; DEF – diesel exhaust fluid; ASC – ammonia slip catalyst; LO-SCR - light-off selective catalytic reduction

Figure I.9.1 Modular AT system layout

- Commissioned the fuel burner system to be added to the modular AT system.
- Built and received two of the six electric heaters to be added to the modular AT system.
- Expanded the program scope, remaining budget neutral, to include two different sizes of SCR monoliths, both for the LO-SCR and main downstream SCR. This setup will provide evidence for understanding trade-offs such as necessary catalyst size (i.e., catalyst cost) relative to performance metrics.
- Defined speed/torque versus time for the three regulatory cycles (including the new low-load cycle) and five field cycles (heavy tillage, planting, air seeder, scraper, and trailer grain cart).
- Readied the base portion of the future engine to add the systems below:
  - 48 V and 24 V EGR pumps
  - Cylinder deactivation system.

Conclusions

- Designed the modular AT system in a flexible architecture capable of evaluating a variety of AT and exhaust thermal management alternatives.
- Defined and built the base future engine.
- Building associated engine systems including the EGR pump and cylinder deactivation systems.

Acknowledgements

- The contributions of Ivan Tate and Ryan Bradley from Fiat Powertrain on engine development and program leadership are greatly appreciated.
- The contributions of Vitaly Prikhodko and Josh Pihl from Oak Ridge National Laboratory for test planning and program leadership are greatly appreciated.
- The contributions of the Eaton team—including Mike Coates for the EGR pump, Eric Hughes and Ryan Krieger for the cylinder deactivation system, Laura Schilling for program management, Nelson Laret for government compliance, Jen Yakiwchuk for finance compliance, and Mihai Dorobantu for government leadership—are greatly appreciated.
- The contributions of Tom Harris and Ed Pavicich from Tenneco for modular AT system design are greatly appreciated.

I.10 Development of a Flex-Fuel Mixing Controlled Combustion System for Gasoline/Ethanol Blends Enabled by Prechamber Ignition (Marquette University)

Adam Dempsey, Principal Investigator
Marquette University
P.O. Box 1881
Milwaukee, WI 53201-1881
Email: adam.dempsey@marquette.edu

Gurpreet Singh, DOE Program Manager
U.S. Department of Energy
Email: Gurpreet.Singh@ee.doe.gov

Start Date: April 1, 2022 End Date: June 30, 2025
Project Funding: $481,000 DOE share: $385,000 Non-DOE share: $96,000

Project Introduction

The proposed project will demonstrate a heavy-duty engine converted from using diesel fuel to a flex-fuel engine that can use any blend of gasoline and ethanol. The combustion system is an innovative concept that allows very low cetane fuels to be used in a conventional mixing-controlled combustion (MCC) strategy without auxiliary heating, changes to the basic engine structure, or advanced controls. This allows the engine to maintain the operational characteristics of a diesel engine, such as excellent snap torque response, high torque at low speed, high efficiency, knock-free operation, and combustion robustness.

As shown in Figure I.10.1, this concept uses an actively fueled prechamber (PC) and high-pressure direct injector, both utilizing the same fuel. The PC is fueled during the compression stroke. The PC charge is ignited by a spark plug near top dead center, ejecting hot jet flames into the main chamber in the vicinity of the direct injector. The high-pressure direct injector delivers most of the fuel (>90%) shortly after the PC has been ignited. The direct-injection (DI) fuel sprays interact with the PC jet flames and ignite readily, regardless of fuel cetane number. Thus, this combustion strategy can be fuel agnostic while achieving MCC [1].

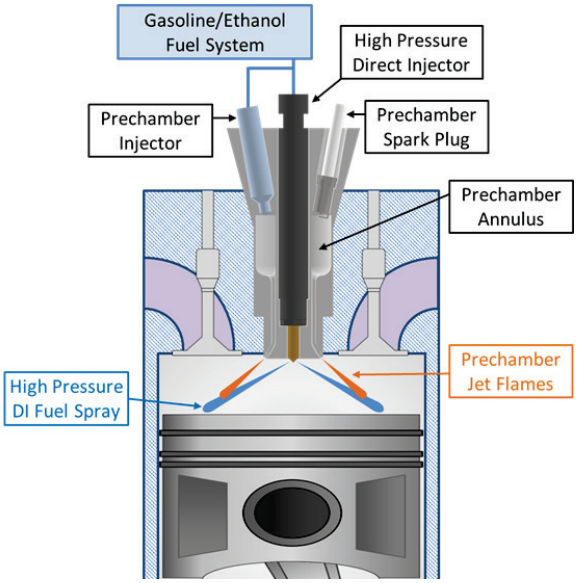

Figure I.10.1 Prechamber enabled mixing-controlled combustion

In this project, the engine will use gasoline/ethanol blends—up to and including pure ethanol, with no change in engine hardware or calibration—and deliver diesel-engine performance. This is attractive to engine original equipment manufacturers, as the use of renewable fuels is increased via increased ethanol blending ratios, with little to no change to the engine. Ethanol is an extremely successful, domestic renewable fuel that is widely available as gasoline/ethanol blends. Ethanol has been unable to be used in heavy-duty engines due to its low cetane number and the fact that heavy-duty applications struggle to be converted to spark-ignition engines.

Objectives

The objective of this project is to develop the prechamber enabled mixing-controlled combustion (PC-MCC) concept for gasoline/ethanol blends for heavy-duty engines. The goal is to use simulations and experiments to design the hardware, operating strategy, and control strategy.

Overall Objective

- The proposed PC-MCC concept is expected to deliver a 10% to 50% reduction in life-cycle CO_2 emissions compared to diesel fuel when operating on E15 (15% ethanol/85% gasoline blend) and E100 (100% ethanol), respectively.
- The high-level goal of the project is to optimize the PC igniter and the DI mixing-controlled combustion system for gasoline/ethanol blends in heavy-duty engines. Actively fueled prechambers have historically not been used in this manner, and thus the system design parameters and global operating strategy must be determined.
- The final project demonstration will be a multi-cylinder John Deere 9 L engine running in a laboratory environment as a flex-fuel engine. It will be shown that the engine can cover the entire baseline diesel engine operating space when running on gasoline/ethanol blends from E10 to E100, while maintaining mixing-controlled combustion and diesel-like performance characteristics.

Fiscal Year (FY) 2022 Objectives

The first two quarters of the project took place in FY 2022, and the following summarize the goals of the project during this time.

- Chemical-reacting computational fluid dynamics (CFD) simulations of a 1.6 L single-cylinder, heavy-duty engine were conducted to determine the minimum required PC volume for robust ignition and an acceptable range for passageway size to ensure proper PC breathing and PC jet flame penetration. It is critical the PC igniter's geometric properties be determined before manufacturing a prototype for testing.
- Detailed packaging studies were conducted to determine appropriate mounting locations for the PC igniter and direct injector in both single-cylinder and multi-cylinder heavy-duty engines. It was shown that the PC igniter's geometric characteristics can be modified to accommodate various mounting locations in the cylinder head.
- Optical rapid compression machine (RCM) experiments were conducted to measure the sooting tendency of gasoline/ethanol blends as a function of equivalence ratio. In turn, reacting CFD modeling was conducted to validate chemical kinetic and soot formation models used in the CFD simulations.

Approach

This technology development project includes a combination of fundamental combustion experiments, applied CFD modeling, prototype design and fabrication, engine experiments, and a technology assessment for various off-road vehicle applications. Figure I.10.2 illustrates a high-level development plan for flex-fuel PC-MCC.

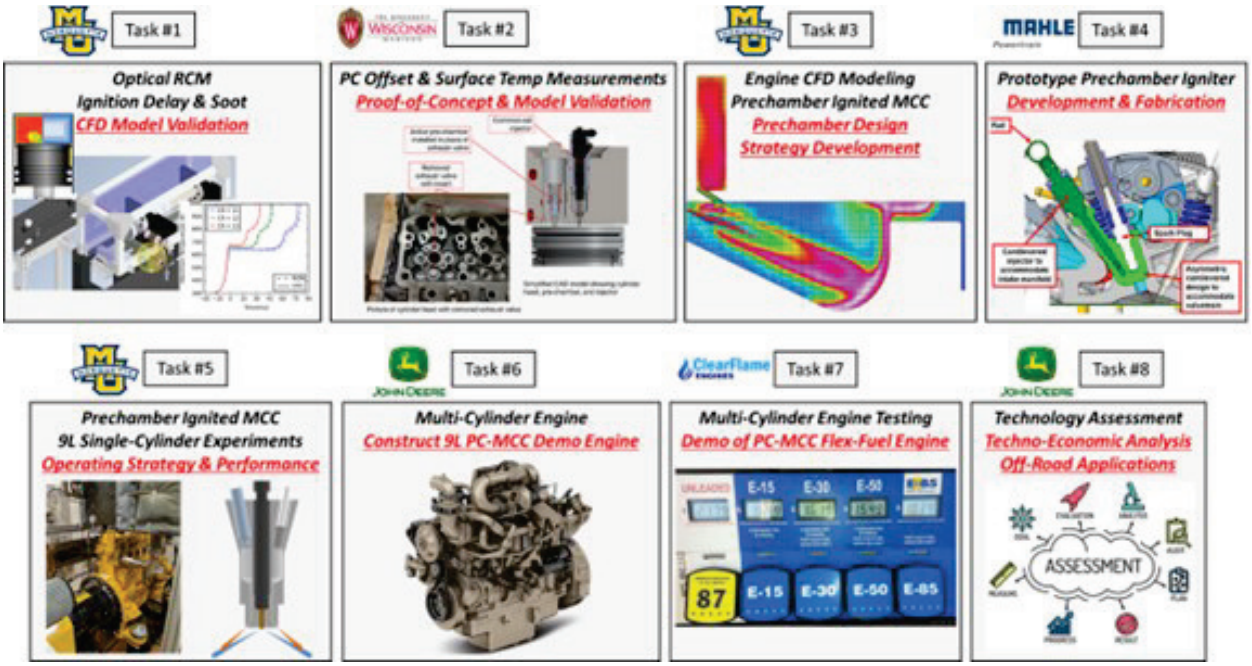

Figure I.10.2 Overall project approach and high-level tasks completed by each project partner

Results

The key accomplishments for this project in FY 2022 are summarized below.

- Completed optical RCM experimental characterization of the sooting tendency of E10, E30, E85, and E100 fuels under homogenous fuel-rich conditions. The critical equivalence ratio for forming soot increases with ethanol content.
- RCM CFD modeling results show that the empirical Hiroyasu two-step soot model and the detailed Particle Size Mimic (PSM) soot model both underpredict the soot formed during the RCM experiments. The current focus is to understand how these models can be tuned and altered to more accurately predict the sooting tendency of gasoline/ethanol blends.
- Engine CFD modeling with pure ethanol fuel (E100) has demonstrated that the mounting location of the PC igniter is of very little consequence. Essentially, designing a location into the cylinder head where the PC igniter can fit is the priority. Then the PC igniters' geometric characteristics can be determined to ensure sufficient ignition assistance.
- Design studies have shown that packaging the actively fueled PC igniter into the cylinder head of a Caterpillar C9.3B diesel engine and a John Deere 9 L diesel engine is plausible with redesign of the casting to eliminate port breaches and challenging sealing surfaces. The details of this work will not be shown here due to confidentiality but will hopefully be shared in a future annual report.

The optical RCM experiments use a single-pass laser extinction diagnostic to measure the soot formed in the homogeneous, fuel-rich autoignition event that takes place in the RCM. The experimental setup and example data are shown Figure I.10.3a. The RCM combustion chamber is created with a creviced piston, which is shown from the CFD model in Figure I.10.3b; this figure also shows the predicted temperature distribution in the RCM combustion chamber shortly after ignition. Figure I.10.3c shows results comparing the experiments to the CFD predictions for soot formed as a function of the equivalence ratio of the mixture. The default settings for the Hiroyasu and PSM soot models underpredict the amount of soot formed at a given equivalence ratio. Both models can be "tuned"—more so for Hiroyasu than PSM. For Hiroyasu, the pre-exponential

constant and the activation energy on the soot formation rate can be tuned, and for PSM the pre-cursor species can be altered to tune its behavior. Figure I.10.3c shows that the agreement can be improved considerably when the models are tuned for E30 fuel, but the amount of soot formed with E100 is still dramatically underpredicted. Future work will continue to refine the approach to predict soot formation of gasoline/ethanol blends more accurately, such that computational tools can be used to design mixing-controlled combustion engines using these blends.

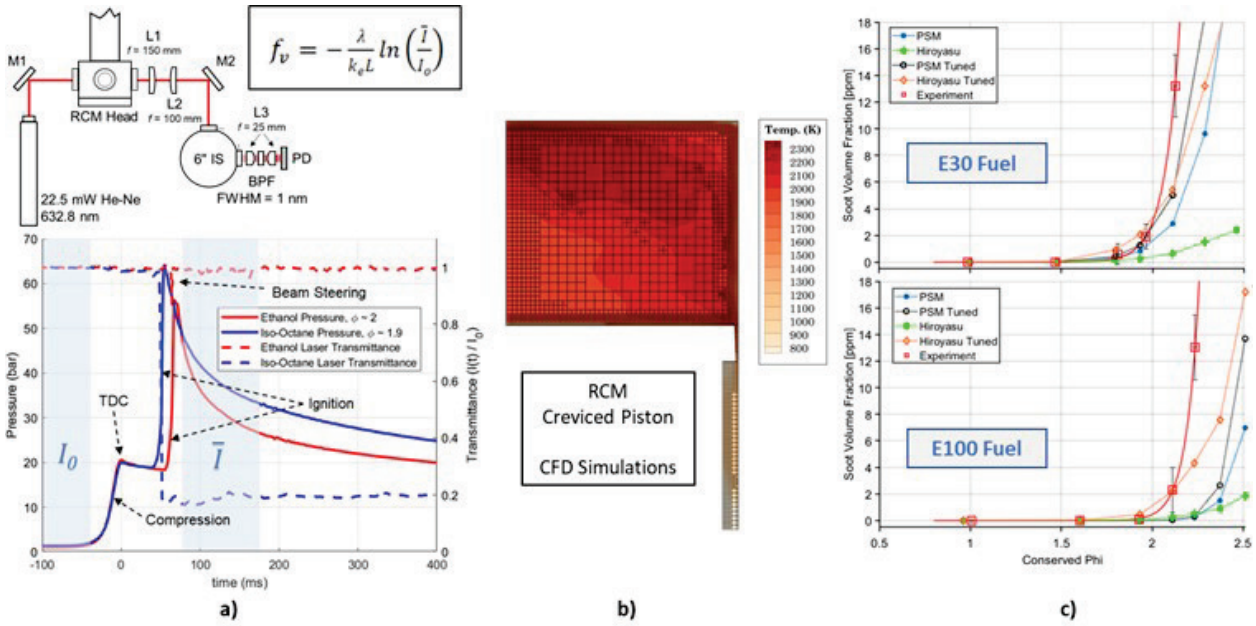

BPF – bandpass filter; PD – photodiode; FWHM – full width at half maximum; TDC – top dead center

Figure I.10.3 (a) Optical RCM laser extinction experimental setup and example results, (b) RCM CFD modeling of the creviced piston geometry, and (c) results comparing the experiments and CFD modeling

CFD modeling of a single-cylinder Caterpillar C9.3B engine has been conducted to design the appropriate mounting location for the PC igniter that provides sufficient ignition assistance of the direct-injected fuel while meeting packaging constraints in the cylinder head. Figure I.10.4a shows the operating condition that was studied, which was a high-speed, low-load condition where ignition assistance is needed the most. Two different PC mounting locations were investigated: a center mount prechamber (Figure I.10.4b) and a side mount prechamber (Figure I.10.4c). Both of these configurations have shown to be plausible in terms of packaging in the engine cylinder head, with the side mount being the most practical packaging arrangement.

a)

	Parameter	Value
Engine	Displacement [L]	1.55
	Bore/Stroke [mm]	115/149
	Compression Ratio [-]	16
Operation	Engine Speed [rpm]	1800
	Load (gross) [bar]	~4
	Rail Pressure [MPa]	70
	DI Injection Timing [°ATDC]	-7.5
	EGR % [-]	0
BCs	Intake/Exhaust Pressure [bar]	1.2/1.3
	Intake/Exhaust Temp. [°C]	40/300

b)

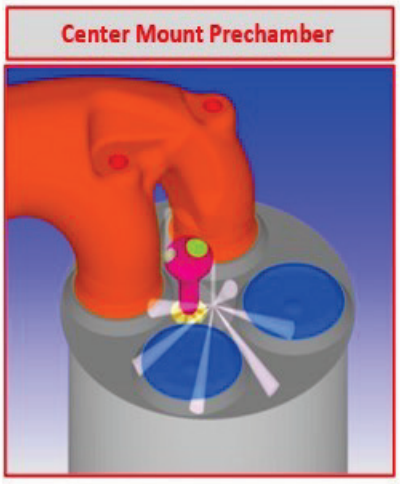

c)

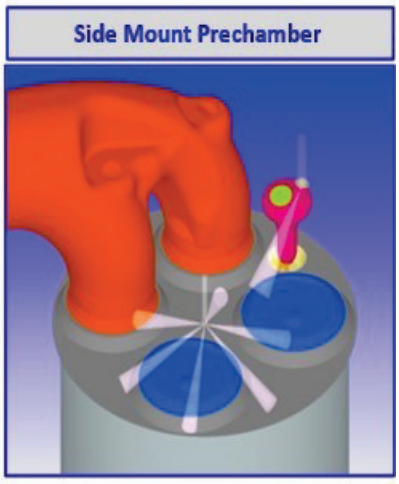

ATDC – after top dead center

Figure I.10.4 (a) Operating condition studied in CFD simulations, (b) center mount prechamber (CMPC) configuration, and (c) side mount prechamber (SMPC) configuration

Figure I.10.5 shows the interior details of the PC igniter used in these CFD simulations and the PC geometric parameters that were varied. The CMPC igniters always used six nozzle holes and varied the PC orifice diameter and the PC volume. The SMPC utilized two, three, and four nozzle holes, and varied the PC orifice diameter and PC volume.

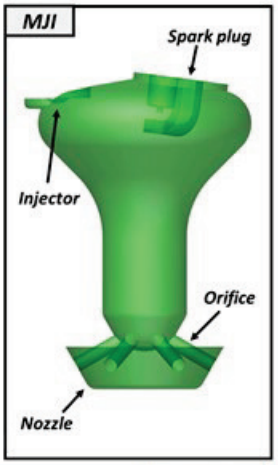

	CMPC	SMPC
PC Orifices [#]	6	2, 3, 4
PC Volume [cc]	2, 3, 4	2, 3, 4
PC Orifice Dia. [mm]	0.98-1.38	1.4-2.08
PC Orifice Area (CSA) [mm^2]	4.5, 6.8, 9.1	4.5, 6.8, 9.1
PC Orifice Angle [deg]	145	145

MJI – Mahle jet ignition; CSA – cross sectional area

Figure I.10.5 Details of simulated PC igniter. and PC geometric parameters investigated

Figure I.10.6 shows the general operating strategy for PC-MCC and how it differs from conventional diesel combustion. During the compression stroke, the PC is fueled with 3–6 mg of fuel, depending on the operating strategy and intake pressure. The goal is to create an ignitable mixture in the PC at spark timing. Approximately 10–15 crank angle degrees (CAD) before direct fuel injection, the PC is sparked, which ejects PC jet flames into the main combustion chamber to serve as the ignition source for the direct-injected ethanol fuel. Without the ignition assistance from the PC jet flames, the directed-injected ethanol fuel would completely misfire.

Figure I.10.7 shows CFD simulation results from varying the PC orifice size for the SMPC and CMPC configurations. As the orifice size is varied for the CMPC configuration, the main chamber ignition delay and combustion process is essentially unaffected. This is due to the proximity of the PC and the DI injector, and thus PC jet flame penetration plays very little role in the ignition assistance process. However, for the SMPC, as the PC orifice size is increased the PC jet flame penetration increases and the main chamber ignition delay is reduced. For the SMPC configuration, the largest PC orifice size is required to have ignition delays that are like conventional diesel combustion.

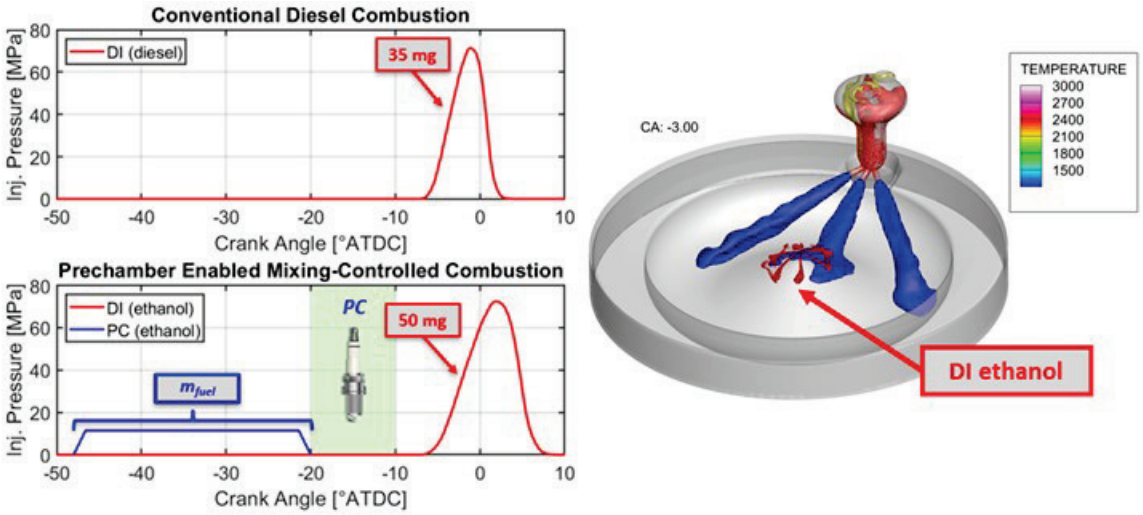

Figure I.10.6 Fuel injection strategy for a conventional diesel engine and the PC-MCC concept with pure ethanol fuel (left). In-cylinder temperature visualization (in Kelvin) of three-hole SMPC with pure ethanol fuel (right).

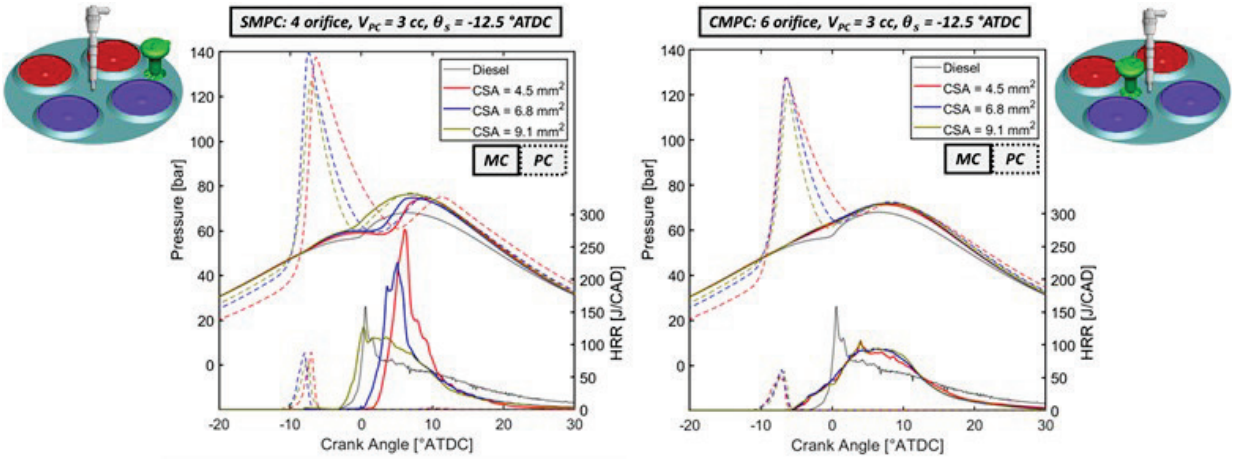

HRR – heat release rate

Figure I.10.7 Comparison of CFD combustion simulations varying the PC orifice size for (left) SMPC and (right) CMPC, both with pure ethanol fuel

As can be seen from the engine CFD simulations, the PC-MCC strategy with a CMPC igniter results in ignition delays for ethanol fuel that are even shorter than for diesel fuel. This is excellent, and, although not shown here, the ignition can be controlled with the PC spark timing and PC fueling. The SMPC can be designed to be a good ignition assistance device if the PC orifices are large enough to ensure adequate PC jet flame penetration towards the direct injector. With large PC orifices, the SMPC can achieve ignition delays that are similar to diesel fuel and achieve mixing-controlled combustion, which is the objective with this low cetane fuel.

Conclusions

- The CFD soot models were shown to underpredict the soot formation as compared to the RCM experiments. The goal is to ultimately tune and validate the soot models to accurately predict soot formation in the RCM for gasoline/ethanol fuel blends, such that, when the engine is modeled under mixing-controlled combustion conditions, accurate predictions of the soot emissions can be expected. Thus, the project team needs to focus on improving the CFD soot models to capture the RCM experiments more accurately for gasoline/ethanol blends.

- Although not shown in this report due to confidentiality, it has become clear that the side mount prechambers are the most appealing from a packaging perspective. The center mount prechambers may be packageable in larger engine bores, but in the ~9 L engine platforms targeted in this study, the side mount prechambers will be the likely path for testing and demonstration in hardware.

- As outlined here, the side mount PC igniters provide sufficient ignition assistance if designed correctly with large enough PC orifices to ensure adequate PC jet flame penetration.

- The primary focus of this project in FY 2023 is to fabricate a prototype side mount prechamber for single-cylinder testing with gasoline/ethanol fuel blends in the single-cylinder Caterpillar C9.3B engine.

Key Publications

This project only completed two quarters in FY 2022. Thus, there were no publications associated with this project funding in FY 2022. Several publications have been submitted and are under review. These publications will be reported in future DOE annual reports.

References

1. Dempsey, A., M. Chowdhury, S. Kokjohn, and J. Zeman. 2022. "Prechamber Enabled Mixing Controlled Combustion - A Fuel Agnostic Technology for Future Low Carbon Heavy-Duty Engines." SAE Technical Paper 2022-01-0449. https://doi.org/10.4271/2022-01-0449.

Acknowledgements

This material is based upon work supported by the DOE's Office of Energy Efficiency and Renewable Energy under the Award Number DE-0009872.

The Principal Investigator would also like to thank the project contributors from the following institutions:

- Marquette University: Dr. Casey Allen, Jard Zeman, Musharrat Chowdhury, Joe Gross, and John Kempf
- Mahle Powertrain: Dr. Mike Bunce, Dr. Ziming Yan, and Devanshu Singla
- University of Wisconsin–Madison: Dr. Sage Kokjohn, Mike Andrie, Aravindh Viswanathan, Reed Hanson, and Jacob Mazanec
- John Deere: Dr. Danan Dou and Craig Lohmann
- ClearFlame Engine Technologies: Dr. Julie Blumreiter and Pete Woon
- Missouri Corn Merchandising Council: Lane Howard and Bradley Schad

I.11 Reducing the Cost and Complexity of Off-Road Aftertreatment (Pacific Northwest National Laboratory)

Kenneth G. Rappé, Principal Investigator
Pacific Northwest National Laboratory
P.O. Box 999
Richland, WA 99354
Email: Ken.Rappe@pnnl.gov

Siddiq Khan, DOE Technology Manager
U.S. Department of Energy
Email: Siddiq.Khan@ee.doe.gov

Start Date: October 1, 2020 End Date: December 31, 2023
Project Funding: $3,193,000 DOE share: $2,500,000 Non-DOE share: $693,000

Project Introduction

Aftertreatment systems supporting advanced engines have several unit operations in series, each of which is a complex system requiring dedicated sensor and diagnostic infrastructure to monitor performance. A diesel oxidation catalyst loaded onto a diesel particulate filter (DOCF) can significantly benefit advanced aftertreatment systems without the side effects observed in other multifunctional aftertreatment embodiments [1]. DOCF technology will be advanced in this project to enable a more thermally responsive aftertreatment system with reduced complexity and decreased platinum group metal (PGM) usage compared to current final Tier 4 emission configurations. This promising technology offers the potential to provide a more compact and thermally responsive aftertreatment solution and the potential to be core architecture in upcoming systems with low nitrogen oxides (NO_x).

The integration of diesel oxidation catalyst and diesel particulate filter components into a single DOCF device offers significant potential benefits in terms of cost, efficiency, and system size. However, there are barriers to the successful widespread deployment of this technology. Regarding efficient management of soot, questions remain that require a more thorough understanding through advanced modeling. Additionally, a lack of information exists regarding the impacts of typical poisons (ash and fuel-born, e.g., sulfur) that need to be better understood. Therefore, an in-depth inquiry into DOCF performance capability is warranted, and significant opportunities exist to further improve its function and utility while reducing PGM requirements.

In Fiscal Year (FY) 2022, advanced imaging techniques were applied to the DOCF to characterize washcoat effects on the physical characteristics of the filter and the resulting impact on flow uniformity (or lack thereof) and catalyst usage. Pacific Northwest National Laboratory researchers completed and commissioned SpaciMS (spatially resolved capillary inlet mass spectroscopy) capability for testing DOCF structures under various conditions, and preliminary data sets have been generated for modeling calibration. The engine testing capability is nearing completion with instrumentation to support chemical and thermal DOCF assessment under different exhaust environments. In addition, the DOCF modeling capability was completed and is ready for calibration with the laboratory's kinetic calibration efforts and SpaciMS data.

Objectives

Overall Objectives

- Develop DOCF technology for combined carbon monoxide (CO), hydrocarbon, and particulate matter (PM) emissions control to enable a single device capable of meeting regulatory compliance targets in a more compact and thermally responsive aftertreatment configuration that employs 40% less PGM when compared to current systems compliant with the Tier 4 Stage V off-road emissions standard.

- Identify an advanced DOCF washcoat design that enables fast CO and hydrocarbon light-off for efficient pollutant conversion and active regeneration efficiency and necessary nitrogen dioxide (NO_2) production, with broad coverage axially to manage soot via passive oxidation.
- Identify a front-zone washcoat design that enables fast CO and hydrocarbon light-off with minimum PGM usage and that capitalizes on the wall-flow device configuration.
- Identify a DOCF design that facilitates reduced cold-start CO, hydrocarbon, and NO_x emissions; enable cost-effective PM management (i.e., filtration and oxidation) with reduced fuel penalty; and predict and mitigate the adverse impact of ash deposits on device performance.

Fiscal Year 2022 Objectives

- Develop modeling capabilities with high accuracy for predicting DOCF performance in various configurations and conditions.
- Complete development and commission spatially resolved intra-channel gaseous analysis (i.e., SpaciMS) to enable high predictive model accuracy.
- Complete development of engine testing capability for validating DOCF modeling results.
- Support predictive model accuracy with advanced device catalyst, aging, and ash characterization.

Approach

This project will develop and implement highly accurate advanced modeling strategies for DOCF simulation based on realistic conditions. A two-dimensional (2D) modeling approach will be used for modeling the DOCF. Multiple bench- and engine-scale test capabilities will be utilized to support the modeling activity by measuring DOCF performance across the array of relevant test conditions. This includes engine-scale accelerated ash-aging employed to optimize DOCF designs against ash-related excessive pressure drop and catalytic activity loss. This project will also advance the SpaciMS analytical technique developed for flow-through catalysts and apply it to wall-flow devices. The result will be an analytical tool and technique enabling unprecedented efficiency and accuracy of modeling and accelerated development of complex multifunctional aftertreatment devices. The resulting tool will have the potential for impacts on technologies far past DOCF.

This project will also pursue the integration of advanced mixed metal oxide materials in washcoat design with the goal of reduced PGM usage or improved PGM utilization as a means of enabling a more sustainable and versatile DOCF washcoat design. Researchers will study mixed metal oxide design structures that enable greater nitric oxide (NO) oxidation—not subject to CO or hydrocarbon self-limitation—during CO and hydrocarbon light-off.

Results

Advanced DOCF Imaging and Characterization

In FY 2022, the project analyzed and characterized a degreened John Deere DOCF device and an ash-aged commercial DOCF to inform on the digital microstructure of the device and to enable flow simulations within the device microstructure. These efforts provide information about the microstructural characteristics of the device filter wall to be captured in the modeling efforts. Results also enable flow simulation within the wall to inform on flow uniformity and effective catalyst usage. Accomplishments are as follows:

- The degreened John Deere developmental DOCF device was characterized with ultra-high-resolution X-ray computed tomography (CT) and a numerical approach whereby the catalyst washcoat was observed from the entire part scale (~50 µm resolution) and specific structural/washcoat information was obtained from single wall scans (~1 µm resolution). This multiscale analysis technique provided 3D datasets, which were analyzed via VGStudioMax™ and Avizo software platforms. These efforts

yielded porosity, pore size distribution, and pore geometry information that will support accuracy of the device-scale modeling efforts.

- High-resolution CT scans were made at several axial and radial locations from within the sample to characterize the washcoat variations in Zones 1 and 2 of the DOCF device. By way of advanced segmentation algorithms, the catalyst washcoat was spatially characterized in the high-resolution CT data. An Avizo software program was used to run a computational fluid dynamics (CFD) simulation within the digital microstructure whereby pressure and fluid flow were resolved within the complex microstructure. In addition, the system permeability was calculated.

- Figure I.11.1 shows the pressure magnitude from CFD simulation in a 2D cross-section view through the substrate thickness in Zone 1 with thicker washcoat. This figure shows pressure gradients throughout the substrate and demonstrates less uniform flow versus Zone 2.

- Figure I.11.2 shows the results of CFD modeling in the DOCF Zone 1 with the thicker washcoat and is presented with color-coded velocity magnitudes. This cross-section, taken from Zone 1 of the device, shows flow constrictions, likely due to narrowing of pore throats as a result of the thicker washcoat.

Figure I.11.1 Pressure magnitude from CFD simulation through DOCF washcoat Zone 1 showing pressure gradients throughout thickness of substrate.

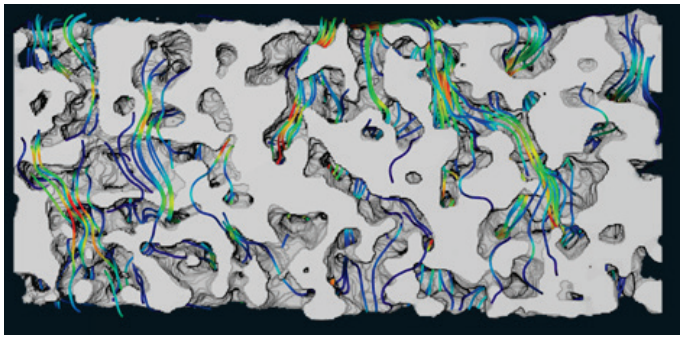

Figure I.11.2 Flow field with color-coded velocity magnitudes in DOCF cross-section taken from DOCF Zone 1 with thicker washcoat; red areas show flow constrictions, likely due to narrow pore throats from the thicker washcoat.

Bench-Scale Performance of Advanced DOCF

SpaciMS testing (spatial chemical and temperature measurement) of a John Deere DOCF device was conducted in FY 2022, following commissioning of the capability, and continues into FY 2023. Preliminary spatial performance information, generated via SpaciMS in FY 2022, shows the temperature and species concentrations and concentration gradients in the inlet and outlet channels of the DOCF device as a function of axial position. Figure I.11.3 below shows an example of a data set collected at 35,000 gas hourly space

velocity (GHSV) (hr^{-1}) and 180°C inlet temperature, with the top figure showing the inlet channel and the bottom figure showing the outlet channel.

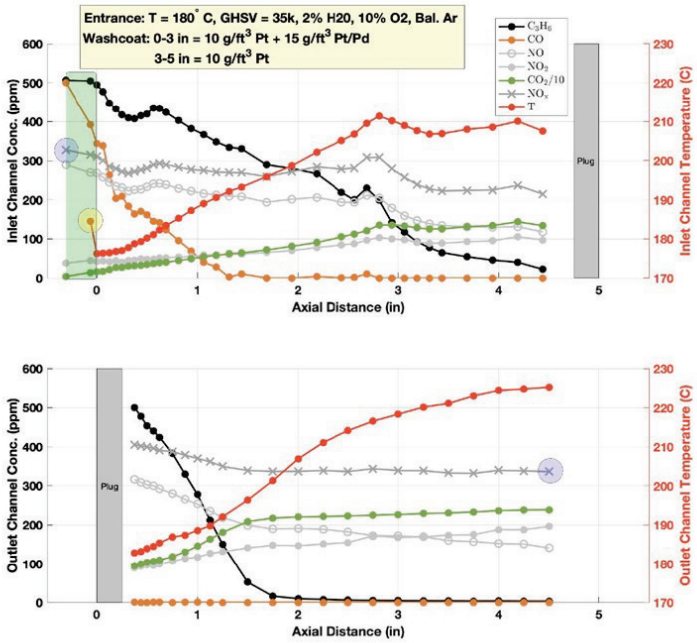

Figure I.11.3 SpaciMS characterization of degreened DOCF; the top figure shows the inlet channel, and the bottom figure shows the outlet channel. Test conditions: 180°C feed, 35,000 GHSV, 10% O_2, 2% H_2O, 500 ppm CO, 500 ppm C_3H_6, 350 ppm NO in feed.

The SpaciMS data provides detailed insight into DOCF performance and behavior and will help to enable device-scale modeling capability with high accuracy. Below are some key observations from the SpaciMS testing that will contribute to accurate modeling of the DOCF device:

- CO oxidation occurs comparatively fast at the front of the DOCF device.
- C_3H_6 oxidation contributes a significant exotherm axially across the DOCF device and dictates the thermal characteristics observed at the DOCF outlet. C_3H_6 oxidation is accelerated in the latter zone of the DOCF device.
- The transition between washcoat zones (and thus the location of this transition) is a key parameter in the global performance observed in the DOCF device and dictates both the chemical and thermal characteristics observed axially across the DOCF.

Engine Dynamometer Setup, Configuration, and Calibration

The John Deere engine setup for testing is complete, and a prototype canned DOCF has been received for engine testing. Figure I.11.4 shows a picture of the installed engine testbed on a rolling cart. Installation is complete for temperature measurements of the DOCF. The measurements will be performed by wire thermocouples at four radii and six axial positions. Three thermocouples in each washcoat at varying radii allow for thermal gradients to be observed over each, and each thermocouple measures the temperature of an equal substrate volume in each of the two DOCF washcoat sections.

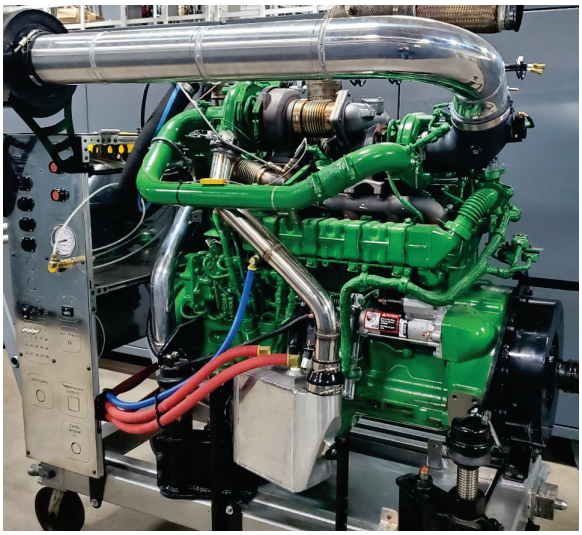

Figure I.11.4 A 6.8 L John Deere engine testbed.

Additional accomplishments and progress with the on-engine DOCF testing capability are as follows:

- The project team has added test cell instrumentation for recording thermocouples for temperature distribution in the DOCF. Equipment for exhaust gas chemical speciation is complete, including:
    - A Horiba 5 gas bench to measure CO, CO_2, O_2, total hydrocarbon, NO, and NO_2.
    - A mass spectrometer to provide secondary NO and NO_x measurement.
    - An AVL smoke meter for PM measurements and hot stack gas sampling.

Exhaust gas temperature and pressure, PM concentration, and species concentrations CO_2, O_2, NO, NO_2, CO, and hydrocarbon will be measured at the inlet and exit of the DOCF. Exhaust gas mass flow rate and H_2O and N_2 species concentrations will be subsequently calculated.

- Equipment is complete for making mass measurements of the DOCF and measurements of PM exhaust concentration. Also, a 25 kW electric heater has been implemented in line with the DOCF for improved temperature control testing repeatability. The project team has developed a DOCF-plus-electric-heater structure to hold and enable removal of the DOCF, allowing researchers to weigh the DOCF and determine PM mass accumulation at set intervals during testing.
- The project team has configured a capability for exhaust bypass for improved control, stability, and characterization of the exhaust and DOCF performance. This capability will enable the engine to be operated and warmed up without the exhaust passing through the DOCF; then, when the engine is at steady state, it can be switched to allow exhaust to flow through the DOCF.

Advanced DOCF Device Modeling

The four primary sub-models of the DOCF model—Gas State, Reaction Kinetics, Particulate Matter, and Thermal—have been implemented in both axial and radial spatial domains, thus making the DOCF model 2D. Key accomplishments made this fiscal year are as follows:

- The Reaction Kinetics sub-model was completed this fiscal year and implemented with both the Thermal and Particulate Matter sub-models. This work will facilitate one of the leading project objectives: determining the effect of washcoat spatial distribution and formulation. This sub-model includes both PM accumulation (i.e., filtration) and PM oxidation, thus making the DOCF model

applicable to both SpaciMS and engine calibration. This sub-model predicts species concentrations axially in both channels and radially through the soot cake and wall, with spatially varying kinetics.

- The project team merged the Thermal and Particulate Matter routines into the DOCF model, including mapping the data structures. This work leveraged existing 2D selective catalytic reduction filter sub-models previously developed. The Thermal and Particulate Matter sub-models contain time-integrated temperatures of the wall, inlet channel, outlet channel, and PM in the cake and wall. This contrasts with the gas state and wall reaction sub-models, which are steady-state boundary value problem solutions.

- A technique was developed to allow critical first approximations of wall species solutions to be made from previous solutions to find future solutions. Until now, dynamic modeling sensitivity and accuracy has depended on initial approximations. This technique addresses that challenge and will improve model execution time.

- The DOCF model has been calibrated to the first round of SpaciMS data using Exothermia reaction coefficients. In addition, the filtration and pressure drop sub-model implementation was completed, which marks the final major component of the DOCF.

Conclusions

A John Deere DOCF device was analyzed via X-ray CT, and results were used for characterization spatial washcoat variation and filter microstructural and flow information, both of which will be used to improve modeling accuracy. SpaciMS analysis capability has been commissioned and is currently being used to map performance of the John Deere DOCF device over a range of conditions. Similarly, the project has nearly completed engine testing capability for DOCF structures under realistic exhaust conditions and under controlled conditions in the presence of soot. Both capabilities will be used to support accurate and realistic model development. The DOCF modeling capability development is complete, including the four primary sub-models: Gas State, Reaction Kinetics, Particulate Matter, and Thermal. Strategies have also been incorporated to allow for good critical first approximations of wall species. The model is now ready for calibration data from SpaciMS testing, kinetics calibration efforts, and engine testing.

References

1. Hruby, E., S. Huang, R. Duddukuri, and D. Dou. 2019. "NO_x Performance Degradation of Aftertreatment Architectures Containing DOC with SCR on Filter or Uncatalyzed DPF Downstream of DEF Injection." SAE Technical Paper 2019-01-0740.

I.12 Heavy-Duty Hydrogen Combustion (Sandia National Laboratories)

Aleš Srna, Principal Investigator
Sandia National Laboratories
P.O. Box 969, MS 9053
Livermore, CA 94551-0969
Email: ASrna@sandia.gov

Gurpreet Singh, DOE Program Manager
U.S. Department of Energy
Email: Gurpreet.Singh@ee.doe.gov

Start Date: October 1, 2021 End Date: September 30, 2022
Project Funding: $400,000 DOE share: $400,000 Non-DOE share: $0

Project Introduction

Hydrogen internal combustion engines (H_2-ICE) in off-road, marine, rail, and power-generation sectors represent a robust and affordable technology with an existing domestic supply chain that is not limited by requirements for rare earths and precious metals. As such, these engines present a viable alternative to direct conversion of hydrogen to electricity using fuel cells. Hence, H_2-ICE technology should be developed in parallel with fuel cell technology to support faster decarbonization in hard-to-electrify sectors. Advantageous properties of hydrogen, such as higher flame speed and resistance to auto-ignition, allow for highly efficient operation. However, there are challenges to H_2-ICE development:

- The low volumetric energy content of hydrogen, which requires the use of direct injection to maintain engine power density but can potentially increase nitrogen oxides (NO_x) formation associated with sub-optimal fuel stratification.
- Susceptibility to pre-ignition from external sources due to hydrogen's low minimum ignition energy, which can lead to uncontrolled combustion events.

The lack of understanding of in-cylinder processes associated with both these challenges may result in sub-optimal hardware configurations and engine operating strategies that can erode the efficiency and emission advantages of hydrogen, thereby reducing the attractiveness of this technology.

This project seeks to establish comprehensive understanding by establishing validation data required by industry. Industry can use these data to develop competitive and highly efficient engine hardware and control strategies that can fully exploit the high-efficiency and low-emissions potential of hydrogen as a carbon-free fuel, thereby advancing the decarbonization of difficult-to-electrify sectors.

In Fiscal Year (FY) 2022, the in-cylinder mixing was characterized to evaluate the impacts of injection pressure and injection timing on mixture homogeneity and NO_x formation. Results are being used to develop a database for validation and optimization of hydrogen direct-injection computational fluid dynamics (CFD) simulations (industry frequently uses CFD for hardware optimization). Furthermore, a framework was developed to characterize and understand various potential pre-ignition sources under controlled conditions, with each source evaluated independently. This framework was utilized in FY 2022 to study hot-spot pre-ignition.

Objectives

Overall Objectives

- Develop a comprehensive understanding of the in-cylinder processes associated with in-cylinder mixture formation and its impact on engine performance, emissions, wall heat loss, and coupling with advanced ignition systems.
- Develop a detailed understanding of the in-cylinder processes responsible for pre-ignition under various H2-ICE operating conditions and propose efficient mitigation strategies.
- Perform optical engine experiments to sufficiently address the incomplete science base.
- Establish an experimental database required for validation of CFD codes used for H_2-ICE hardware optimization. This database will include information on in-cylinder flows, in-cylinder mixture formation, early flame kernel evolution, engine thermodynamic efficiency, engine-out emissions, wall heat loss, and performance characterization of various advanced ignition systems.

Fiscal Year 2022 Objectives

- Apply laser and imaging diagnostics in an optical, heavy-duty engine equipped with a medium-pressure hydrogen direct injector to assess the impact of injection timing and injection pressure on in-cylinder mixture formation and associated engine performance.
- Establish a framework to study hydrogen pre-ignition mechanisms decoupled from each other under controlled conditions. Validate the framework by characterizing the hot-spot pre-ignition mechanism.

Approach

This project uses an optically accessible, heavy-duty hydrogen-fueled engine with a displacement of 2.34 L, low-swirl flat cylinder head, and a cylindrical piston bowl. Details about this test rig can be found in previous literature [1], [2]. The engine's fuel system was adapted to supply compressed hydrogen seeded with an evaporated "fuel tracer" to enable tracer planar laser-induced fluorescence (tracer PLIF) diagnostic, and a prototype medium-pressure, outward-opening, hollow-cone hydrogen injector (BorgWarner, DI-CHG10, 10 g/s flow rate) was centrally mounted in the cylinder head. Figure I.12.1 shows the schematic layout of the engine and fueling system, along with details of the optical setup used to characterize in-cylinder mixing.

The project team selected tracer PLIF as the optical diagnostic technique to measure in-cylinder fuel concentration in various imaging planes, as illustrated in Figure I.12.1, following the approach from Salazar and Kaiser [3], [4]. Researchers used 1,4,-difluorobenzene as a fluorescent tracer, which was first seeded into hydrogen at a concentration of 0.1% by volume or roughly 5% in terms of fuel mass, then excited in the plane of the light sheet formed from the beam of a frequency-quadrupled Nd:YAG (neodymium-doped yttrium aluminum garnet) laser. A non-intensified, charge-coupled device equipped with a UV lens and a 300±25 nm band-pass filter detected the tracer fluorescence. The fuel equivalence ratio in the light-sheet plane was calculated from the acquired PLIF images after correcting for laser pulse energy, white-field, dark-field, laser-light absorption, and fluorescence yield sensitivity to temperature, assuming that the tracer closely follows the concentration of hydrogen—a reasonable hypothesis, considering the in-cylinder turbulence and flow timescales [4]. Different imaging planes with horizontal and vertical light-sheet locations were used to provide mixing information representative of the entire combustion chamber (Figure I.12.1). Researchers acquired 60 images for each injection setting and horizontal light-sheet location (10 images for a vertical light sheet) to ensure statistical convergence of data; the imaging timings were clustered around the spark timing typical for spark-ignition engines, with additional timings during the fuel injection. Mixing experiments were conducted in an inert nitrogen atmosphere, and in the second stage, experiments were conducted in an ambient of air using a laser spark to ignite the fuel–air mixture in addition to the tracer PLIF imaging technique. The tracer PLIF diagnostic provided semi-quantitative mixing information in the horizontal plane of the spark about 1 µs before the spark timing, and the ensuing flame kernel evolution was tracked with a high-speed intensified complementary metal–oxide sensor (CMOS) camera.

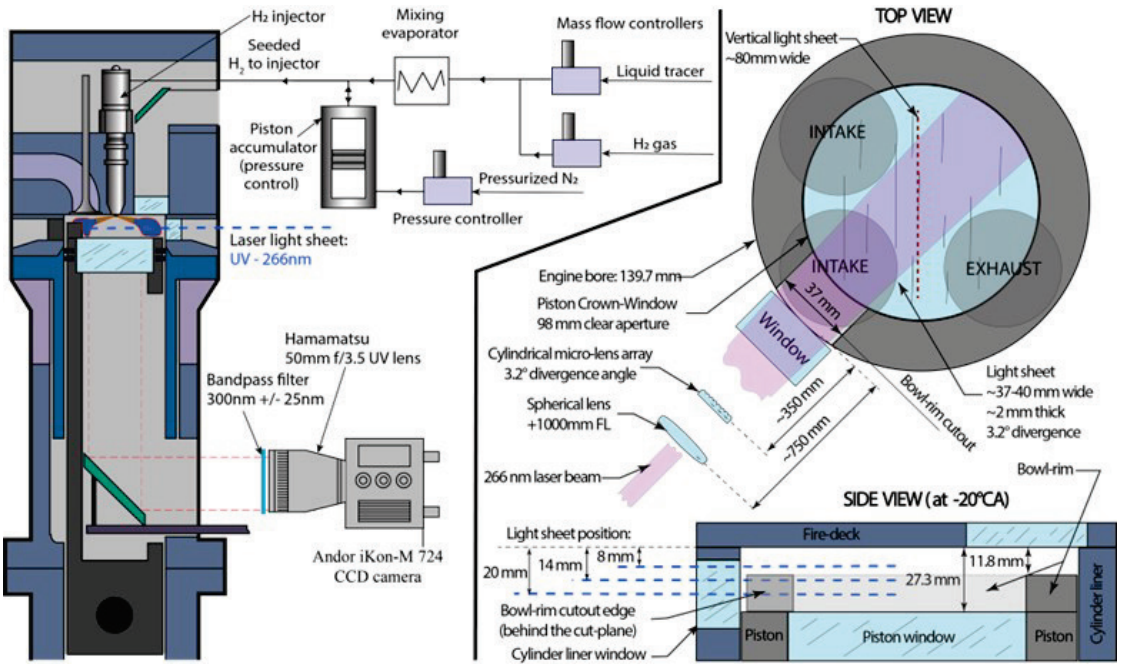

CA – crank angle; UV – ultraviolet; FL – focal length

Figure I.12.1 Schematic of the optical engine and illustration of the optical setup and arrangement for tracer PLIF characterization of in-cylinder mixture

The project carried out characterization of hot-spot pre-ignition by mounting an electrically heated diesel-engine glow plug to serve as a hot spot (Figure I.12.2). This hot-spot tip protruded about 13 mm into the engine combustion chamber and 16 mm below the cylinder head. The hot-spot temperature was characterized during engine operation at 600 and 1,200 rpm using an infrared camera calibrated using a thin-wire thermocouple wrapped around the glow plug. The temperature was varied by adjusting the supply voltage, and the pre-ignition timing and frequency were determined from the pressure traces and by using high-speed imaging of OH* chemiluminescence.

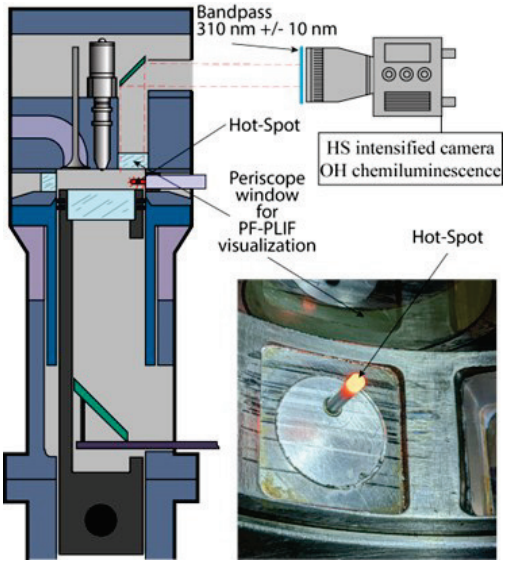

HS – high speed; PF-PLIF – photo-fragmentation planar laser-induced fluorescence

Figure I.12.2 Schematic and photograph of the engine configuration used for hot-spot pre-ignition characterization featuring a glow-plug as the in-cylinder hot spot

Results

The results related to in-cylinder mixture formation presented in this section encompass the jet evolution during injection, a sample visualization of in-cylinder mixture distribution, a statistical presentation of in-cylinder mixture at spark timing, and the measured engine-out nitric oxide (NO) emission. Figure I.12.3 presents the early jet evolution for injection starting at 180°CA at a high injection pressure. Both the macroscopic and finely resolved flow patterns are visible, first macroscopically, as two lobes from the dissected annular jet are visible. However, this hollow cone then collapses into a single jet within 1°CA from the needle opening, and the entire internal volume of the jet is filled with hydrogen. The collapsed jet penetrates along the injector axis until it impinges onto the piston and starts to recirculate. On a smaller scale, an alternating bright and dark pattern becomes visible on the outer lobes of the jet near the nozzle from 183.5°CA onward and becomes more coarsely granular at later timings, which is associated with the shock pattern of under-expanded flow created as a result of the high pressure ratio across the injector. The pattern becomes coarser as the needle continues to lift after the start of injection and as the pressure across the nozzle builds up. These data are useful for understanding of global in-cylinder flow patterns as well as for validation of detailed CFD simulations of hydrogen injection and for development of simplified jet models.

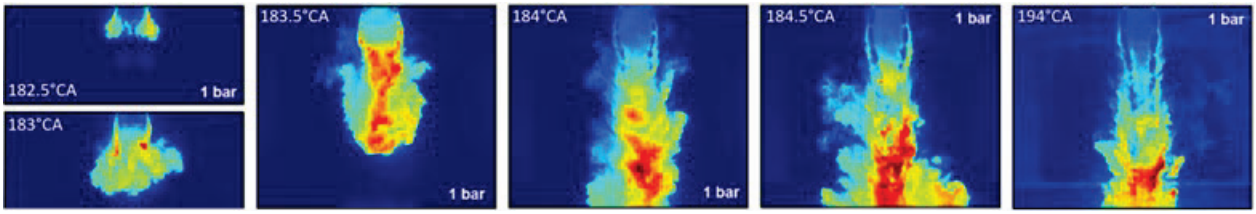

Figure I.12.3 Visualization of early jet evolution by tracer PLIF for injection with high injection pressure starting at 180°CA. The injector axis in this visualization is vertical with the injector nozzle outlet aligned with the top edge of the image frame. The laser light sheet dissected the jet along the injector axis.

Figure I.12.4 showcases the wealth of available information on mixture distribution in various horizontal planes and in the vertical plane, including single-shot images, ensemble-average data, and the standard deviation representing cyclic variability. These data were acquired for a range of injection conditions and used to form a database that can be used to validate CFD simulations—engineering tools frequently used for design and optimization of engine components. The high cyclic variability of the mixture at certain locations within the combustion chamber stands out and was attributed to the in-cylinder flow pattern induced by the jet. Such cyclic variability is undesired and may lead to increased nitrogen oxides (NO_x) formation and combustion variability. Based on the understanding gained, this can potentially be improved by modifying engine swirl and the injector flow pattern; this approach is scheduled for future testing. The three-dimensional mixture information was evaluated further to provide probability density of equivalence ratio across the entire combustion chamber at spark timing (340°CA) for all tested operating conditions (Figure I.12.5). The mixture becomes progressively stratified as the injection is delayed and injection pressure decreased, which may lead to undesired NO_x emissions, as demonstrated by emissions measurements in fired engine operation (Figure I.12.5, right). Combined, these mixture and engine-out NO emissions can be used to develop guidelines on the maximum permissible mixture stratification to comply with emission legislation and to inform future engine operating strategies. As demonstrated, a sub-ppm engine-out NO emission can be achieved in sufficiently lean operation, and a wide window of injection timing allows for a sub-10 ppm emissions level. These findings are encouraging since a delayed injection enhances the in-cylinder turbulence, leading to a faster flame evolution and potentially improved efficiency while mitigating pre-ignition concerns.

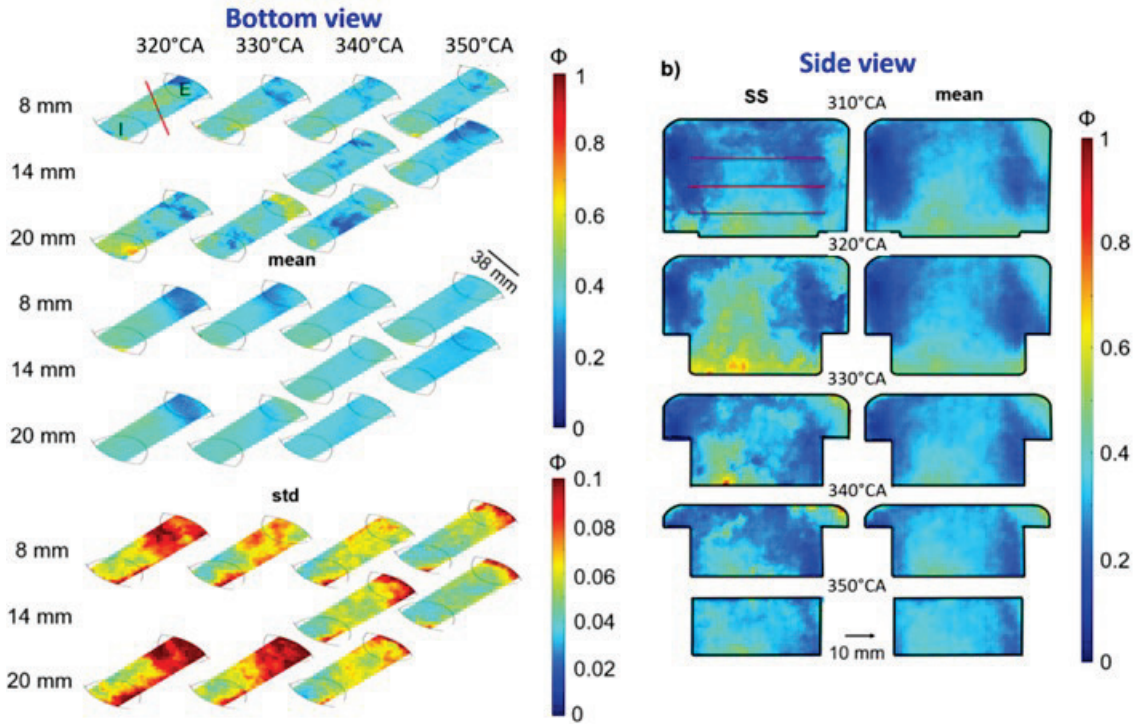

Figure I.12.4 (left) A visualization of quantified in-cylinder mixture distribution in horizontal planes at various distances from the cylinder head, shown as single-shot images (top), average (middle), and cyclic standard deviation (std) of mixture (bottom); (right) the single-shot and ensemble average mixture in the vertical plane. The timing labels refer to the imaging time. Injection started at 240 °CA using a high-injection-pressure setting.

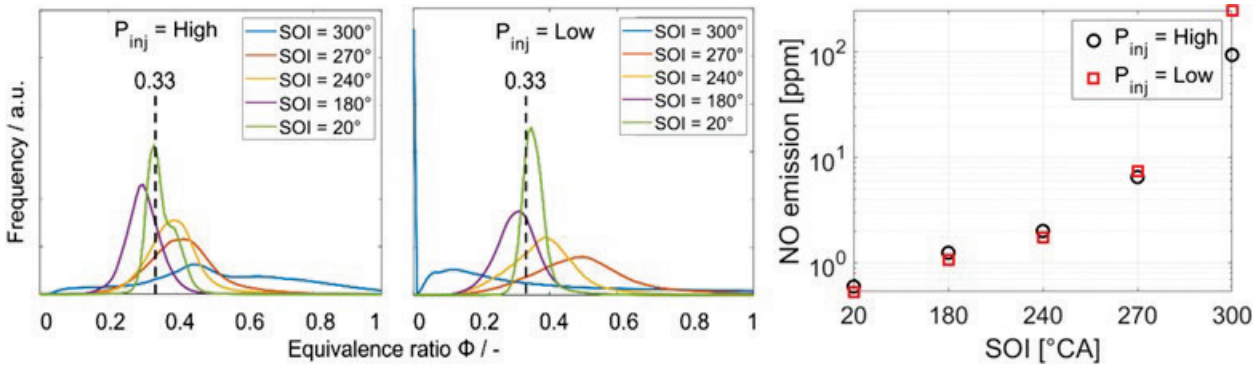

SOI – start of injection

Figure I.12.5 Volume-averaged mixture equivalence ratio probability density function for different injection timings at high (left) and low (right) injection pressure, and the associated engine-out NO concentration measured in fired-engine operation

Finally, the results of hot-spot pre-ignition characterization are presented in Figure I.12.6. Experimental testing varied the start of hydrogen injection timing and the hot-spot temperature to measure pre-ignition frequency and characterize the pre-ignition timing, thereby yielding an understanding of the hot-spot pre-ignition phenomenon. It was shown that the earliest pre-ignition timing is limited by the timing of fuel reaching the surface of the hot spot. At the same time, pre-ignition rarely occurred late in the compression stroke, and the hot-spot temperature affected only the pre-ignition frequency and did not change the pre-ignition timing. This finding is contrary to the experience gained working with hydrocarbon fuels, which indicates that a reduced hot-spot temperature delays the pre-ignition timing toward the end of the compression stroke when in-cylinder pressure and temperature are the highest [6]. To explain this finding, the research team conducted

homogeneous reaction calculations of ignition delay of hydrogen–air mixtures. This revealed interesting chemical kinetic properties of hydrogen with ignition delay sharply increasing after a certain pressure threshold has been reached, regardless of temperature, which is contrary to hydrocarbon fuels; for the latter, the ignition delay reduces with pressure increase. This explains the trends of pre-ignition not occurring late in the compression stage and the low control authority of hot-spot temperature over the pre-ignition timing. This finding also highlights a potential pre-ignition mitigation approach using delayed ignition timing and jet patterns that avoid fuel coming into direct contact with the hot spots until late in the compression stroke. Also, the high temperature of the hot spot needed to trigger pre-ignition suggests that other pre-ignition mechanisms may be dominant under most engine operating conditions, prompting the need for further research.

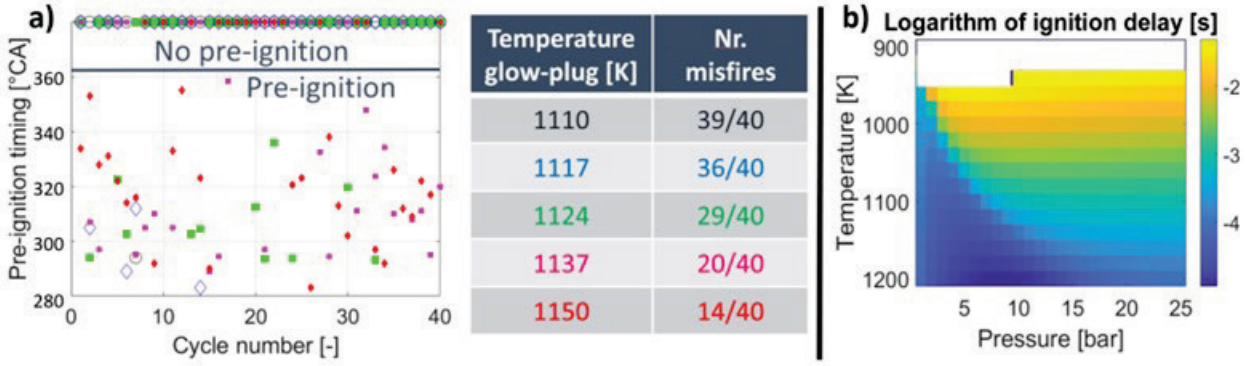

Temperature glow-plug [K]	Nr. misfires
1110	39/40
1117	36/40
1124	29/40
1137	20/40
1150	14/40

Figure I.12.6 (a) A scatter plot (left) showing the timing of pre-ignition depending on the hot-spot temperature (refer to table for color-coding and pre-ignition frequency) for 40 acquired cycles; (b) a false-color plot showing the hydrogen mixture ignition delay depending on pressure and temperature (homogeneous reactor simulation at equivalence ratio of 0.3, using kinetic mechanism from [5])

Conclusions

The conclusions for FY 2022 are as follows:

- Flow from a medium-pressure, outward-opening, hollow-cone injector used in this study rapidly collapses, and the ensuing hydrogen jet propagates along the injector axis until it impinges on the piston and recirculates backwards along the cylinder walls. This large-scale flow pattern was found to dominate the resulting in-cylinder mixture distribution.
- Quantitative measurements of in-cylinder equivalence ratio evolution revealed a strong dependence of charge stratification at spark timing on the injection timing and injection pressure, with later and low injection pressures creating more stratified mixture with local zones at significantly higher equivalence ratio than the global mean. High cyclic variability of mixture was observed in certain zones associated with the jet recirculation following the impingement on the piston. In these zones, local equivalence ratio significantly exceeded the ensemble average, which has important implications for NO_x formation. None of the injection parameters created a highly desirable mixture distribution that would avoid fuel near walls and provide enriched mixture near a potential spark location. Injectors with deflection attachment and stronger in-cylinder swirl are suggested as potential solutions to optimize the in-cylinder mixture distribution.
- Direct injection of hydrogen during the intake or early-compression stroke creates few-to-no zones sufficiently rich for NO_x formation, which results in sub-ppm engine-out NO concentration—a highly promising outcome.
- The framework of pre-ignition induced by using an electrically heated hot spot was proven to yield valuable insight into the hot-spot pre-ignition, which is primarily influenced by the hot-spot temperature, flow field around the hot spot, in-cylinder mixture distribution, and most relevant, the

chemical kinetic properties of hydrogen, which show delayed ignition at elevated pressure. Therefore, the pre-ignition timing is limited to the timeframe between the fuel reaching the hot spot and in-cylinder pressure exceeding the threshold of 2–5 bar.

Key Publications

1. Laichter, J., S.A. Kaiser, R. Rajasegar, and A. Srna. n.d. "Optical Investigation of Mixture Preparation in a Hydrogen-Fueled Heavy-Duty Engine with Direct-Injection." Submitted to SAE Technical Papers (under review).

2. Yip, H.L., A. Srna, A. Wehfritz, S. Kook, E.R. Hawkes, and Q.N. Chan. 2022. "A Parametric Study of Autoigniting Hydrogen Jets under Compression-Ignition Engine Conditions." *International Journal of Hydrogen Energy* 47, no. 49 (June 8): 21307–21322. https://doi.org/10.1016/j.ijhydene.2022.04.253.

3. Rorimpandey, P., H.L. Yip, A. Srna, G. Zhai, A. Wehrfritz, S. Kook, E.R. Hawkes, and Q.N. Chan. 2023. "Hydrogen-Diesel Dual-Fuel Direct-Injection (H2DDI) Combustion under Compression-Ignition Engine Conditions." *International Journal of Hydrogen Energy* 48, no. 2 (January 5): 766–783. https://doi.org/10.1016/j.ijhydene.2022.09.241.

4. Yip, H.L., A. Srna, G. Zhai, A. Wehrfritz, S. Kook, E.R. Hawkes, and Q.N. Chan. 2022. "Laser-Induced Plasma-Ignited Hydrogen Jet Combustion in Engine-Relevant Conditions." *International Journal of Hydrogen Energy* 48, no. 4 (January 12): 1568–1581. https://doi.org/10.1016/j.ijhydene.2022.09.296.

5. Srna, A., R. Rajasegar, and J. Laichter. 2022. "Updates on Sandia Heavy-Duty Hydrogen DI Engine Research and Preliminary H2 In Cylinder Mixing Results." Presented at the 2022 Fall Advanced Engine Combustion program review meeting.

References

1. Dec, J.E. 1997. "A Conceptual Model of DI Diesel Combustion Based on Laser-Sheet Imaging." SAE Technical Paper 970873.

2. Espey, C., and J.E. Dec. 1993. "Diesel Engine Combustion Studies in a Newly Designed Optical-Access Engine Using High-Speed Visualization and 2-D Laser Imaging." SAE Technical Paper 930971.

3. Salazar, V.M., and S.A. Kaiser. 2009. "An Optical Study of Mixture Preparation in a Hydrogen-Fueled Engine with Direct Injection Using Different Nozzle Designs." *SAE International Journal of Engines* 2, no. 2: 119–131.

4. Salazar, V.M., and S.A. Kaiser. 2009. "Optimizing Precision and Accuracy of Quantitative PLIF of Acetone as a Tracer for Hydrogen Fuel." *SAE International Journal of Fuels and Lubricants* 2, no. 1: 737–761.

5. O'Connaire, M., H.J. Curran, J.M. Simmie, W.J. Pitz, and C.K. Westbrook. 2004. "A Comprehensive Modeling Study of Hydrogen Oxidation." *International Journal of Chemical Kinetics* 36: 603–622.

6. Yu, X., et al. 2017. "A Robust Preignition Rating Methodology: Evaluating the Propensity to Establish Propagating Flames under Real Engine Conditions." SAE Technical Paper 2017-01-2241.

Acknowledgements

Rajavasanth Rajasegar of Sandia National Laboratories, Judith Laichter and Sebastian A. Kaiser of the University of Duisburg-Essen, and Ibrahim I. Barbery Avila of the Technical University of Valencia are recognized for their significant technical contributions to the project. Paul C. Miles of Sandia National

Laboratories is recognized for the fruitful discussions and managerial leadership of the project. Kyra N. Schmidt of Sandia National Laboratories is recognized for her technical support of the optical engine. Junmei Shi of BorgWarner is recognized for the fruitful discussions and for supplying the prototype hydrogen injector.

Sandia National Laboratories is a multi-mission laboratory managed and operated by National Technology and Engineering Solutions of Sandia, LLC, a wholly owned subsidiary of Honeywell International, Inc., for the U.S. Department of Energy's National Nuclear Security Administration under contract DE-NA-0003525.

I.13 Off-Road Liquid Fuel Combustion (Sandia National Laboratories)

Dario Lopez Pintor, Principal Investigator
Sandia National Laboratories
P.O. Box 969, MS 9053
Livermore, CA 94551-0969
Email: DLopezP@sandia.gov

Stephen Busch, Principal Investigator (until December 2021)
Sandia National Laboratories
P.O. Box 969, MS 9053
Livermore, CA 94551-0969
Email: SBusch@sandia.gov

Gurpreet Singh, DOE Program Manager
U.S. Department of Energy
Email: Gurpreet.Singh@ee.doe.gov

Start Date: October 1, 2021 End Date: September 30, 2022
Project Funding: $400,000 DOE share: $400,000 Non-DOE share: $0

Project Introduction

Liquid fuels are the dominant energy vector for transportation, and they are expected to remain one of the largest energy sources for hard-to-electrify applications such as off-road, rail, marine, and aviation for decades. Some of the advantages of liquid fuels over other propulsion technologies include very high energy densities, easy on-vehicle storage, existing infrastructure, and generally competitive cost. Moreover, renewable low-life-cycle-carbon liquid fuels can be rapidly deployed and have an immediate impact on net greenhouse gas emissions of off-road machinery.

The Off-Road Liquid Fuel Combustion project focuses on understanding and improving liquid fuel utilization in mixing-controlled compression-ignition (diesel-like) engines. Note that compression-ignition engines are preferred for off-road applications over other propulsion technologies because of their reliability, durability, robustness, transient response, and very high efficiency. For compression-ignition engines, rapid fuel–air mixing can reduce fuel consumption and pollutant emissions, and it has been demonstrated that dimpled stepped-lip (DSL) pistons developed at Sandia National Laboratories (Sandia) promote the formation of vortices that are correlated with faster, more efficient combustion [1]. In this fiscal year, an improved DSL piston has been fabricated and tested in engine experiments to quantify its effects on engine performance and emissions. Operation during the first minutes after a cold start is another important aspect of compression-ignition engines. The goal during catalyst-heating operation is to quickly reach exhaust aftertreatment light-off temperatures while minimizing tailpipe pollutants [2]. This fiscal year, the project team performed experiments to understand pollutant formation during catalyst heating operation; based on this new understanding, an engine operation strategy was proposed that improves virtually all the aspects of catalyst-heating operation. Finally, thermal management to improve engine efficiency and reduce heat rejection remains one of the final frontiers of engine research, but activities are constrained by the limitations of existing commercial heat-flux sensors, and improved experimental capabilities are needed for better heat-transfer characterization and modeling [3]. During this fiscal year, researchers fabricated and tested a novel heat-flux micro-sensor with sub-millisecond time response, together with an advanced wireless telemetry system for on-board engine data acquisition.

Objectives

Overall Objective

The project aims to provide the scientific understanding needed to design, optimize, and calibrate the next generations of off-road compression-ignition engines that comply with increasingly stringent pollutant emissions regulations while achieving thermal efficiencies exceeding 50%.

Fiscal Year 2022 Objectives

- Quantify the fuel efficiency and pollutant emissions benefits of a second-generation DSL piston.
- Characterize the sources of unburned hydrocarbons (UHCs) during catalyst-heating operation, quantifying the contribution of each injection event to the total tailpipe UHC emissions.
- Apply a laser-based extinction technique in an optically accessible exhaust runner to investigate the spatio-temporal origins of formaldehyde in catalyst-heating operation.
- Explore new strategies to mitigate pollutant formation and maximize exhaust enthalpy for optimum catalyst-heating operation.
- Assess the effects of fuel's autoignition reactivity (cetane number) and distillation characteristics (boiling range) on engine cold-start performance.
- Demonstrate an advanced wireless telemetry system for on-board engine data acquisition and a novel heat-flux micro-sensor to provide time-resolved heat-flux data.

Approach

Experimental studies were conducted in the Sandia off-road mixing-controlled research engine facility using an all-metal, single-cylinder research engine [4]. This facility allows operation over a wide range of conditions and has been designed to provide precise control of virtually all operating parameters, allowing well-characterized experiments. An improved DSL piston was machined from aluminum piston blanks provided by Ford Motor Company and tested to evaluate its effects on engine performance through thermodynamic and energy analyses. An optically accessible exhaust runner developed at Sandia in collaboration with Caterpillar Inc. [5] was used to perform high-speed mid-infrared laser extinction measurements of formaldehyde emissions, which were combined with high-speed UHC measurements from a fast flame ionization detector for a detailed analysis of pollutant emissions under catalyst-heating operation. Novel heat-flux micro-sensors were fabricated with the support of Stratio Inc. (a Stanford University spin-off). Custom steel-made pistons were fabricated to allocate the wireless telemetry system and heat-flux sensors inside the engine, with the support of Tenneco Inc.

Results

The project achieved the following key accomplishments for Fiscal Year 2022:

- Because of enhanced in-cylinder air utilization, the improved DSL piston reduces soot emissions by 45% at early injection timings, compared to a state-of-the-art production diesel piston.
- A novel operation strategy for catalyst-heating operation provides 3.5% higher efficiency, 4.0% higher exhaust enthalpy, 32.1% less UHCs, 14.8% less CO, and 17.3% less nitrogen oxides (NO_x) than an optimized five-injection strategy (two pilot, one main, two post) representative of those used in modern diesel engines.
- An advanced wireless telemetry system for on-board data acquisition demonstrated good operation in an engine with acquisition frequencies up to 50 kHz. A novel heat-flux micro-sensor demonstrated reliable response for temperatures up to 200°C.

To evaluate the benefits of the baseline DSL piston, the engine is operated at low load at 1,200 rpm and at part load at 1,600 rpm. These points represent a significant portion of engine operation for line haul, dump truck, and other off-road applications [6], and they are included in the International Organization for Standardization (ISO) 8178 emission certification cycles for off-road vehicles, locomotives, and marine engines. A sweep of main injection timing with a production stepped-lip (SL) piston serves as the reference case against which the benefits of the DSL piston are measured. Figure I.13.1 shows the relative variation in thermal efficiency, smoke emissions, and NO_x emissions between the improved DSL piston and the production SL piston. Results correspond to an early injection with a commanded start of main injection equal to 5.1 crank angle degrees (CAD) after top dead center (aTDC). This early injection timing was selected because it corresponds to engine peak efficiency operation.

The DSL piston was designed to promote the formation of vortices at early injection conditions in which the SL piston fails to promote vorticity [1]. Thanks to this enhanced vorticity, the DSL piston reduces smoke emissions by 45% at both loads, with virtually no impact on thermal efficiency and a marginal effect on NO_x emissions. Smoke reduction is achieved by better air utilization in the squish region and improved soot oxidation. The enhanced vorticity of the DSL piston also leads to faster late-cycle burn rate than the SL piston, which speeds up the mixing-controlled heat release rate and acts to increase the efficiency. However, heat losses increase with DSL, likely due to higher convection in the squish region and cylinder head. The opposite effects of faster burn rate and higher heat losses with the DSL piston result in virtually no impact on efficiency.

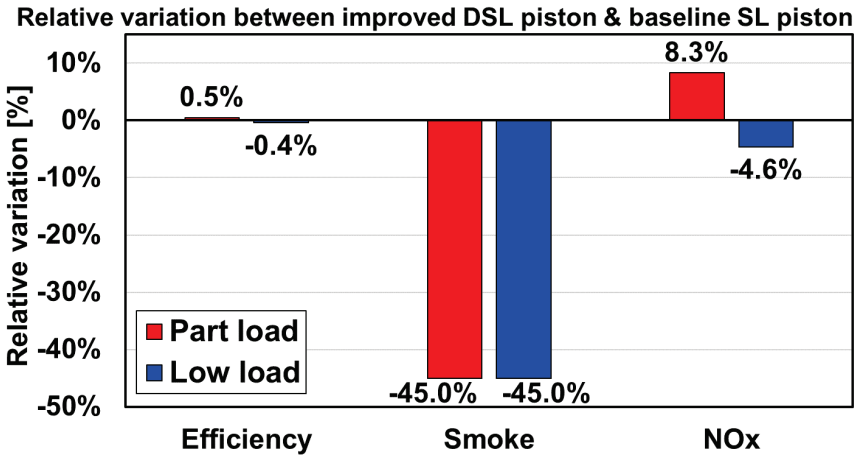

Figure I.13.1 Relative variation in thermal efficiency, smoke, and NO_x emissions between the improved DSL piston and the SL piston for commanded start of main injection of 5.1 CAD aTDC and for low and part loads

Time-resolved formaldehyde emission measurements were performed with a novel high-speed laser extinction diagnostic technique implemented in an optically accessible exhaust runner and demonstrated for the first time at catalyst-heating operating conditions in a compression-ignition engine. Figure I.13.2 shows (a) the in-cylinder pressure signal, (b) time-resolved cyclic UHC emissions obtained with a fast flame ionization detector, and (c) the formaldehyde absorbance obtained by laser extinction. Starting from a five-injection strategy (two pilot, one main, two post) that has been optimized for catalyst-heating operation (black line), the injection events were systematically deactivated to quantify the contribution of each injection to the total UHC and formaldehyde emissions. Thus, Figure I.13.2 includes results with only the first pilot injection (red); both pilot injections (yellow); both pilots and main (green); and both pilots, main, and first post injection (blue).

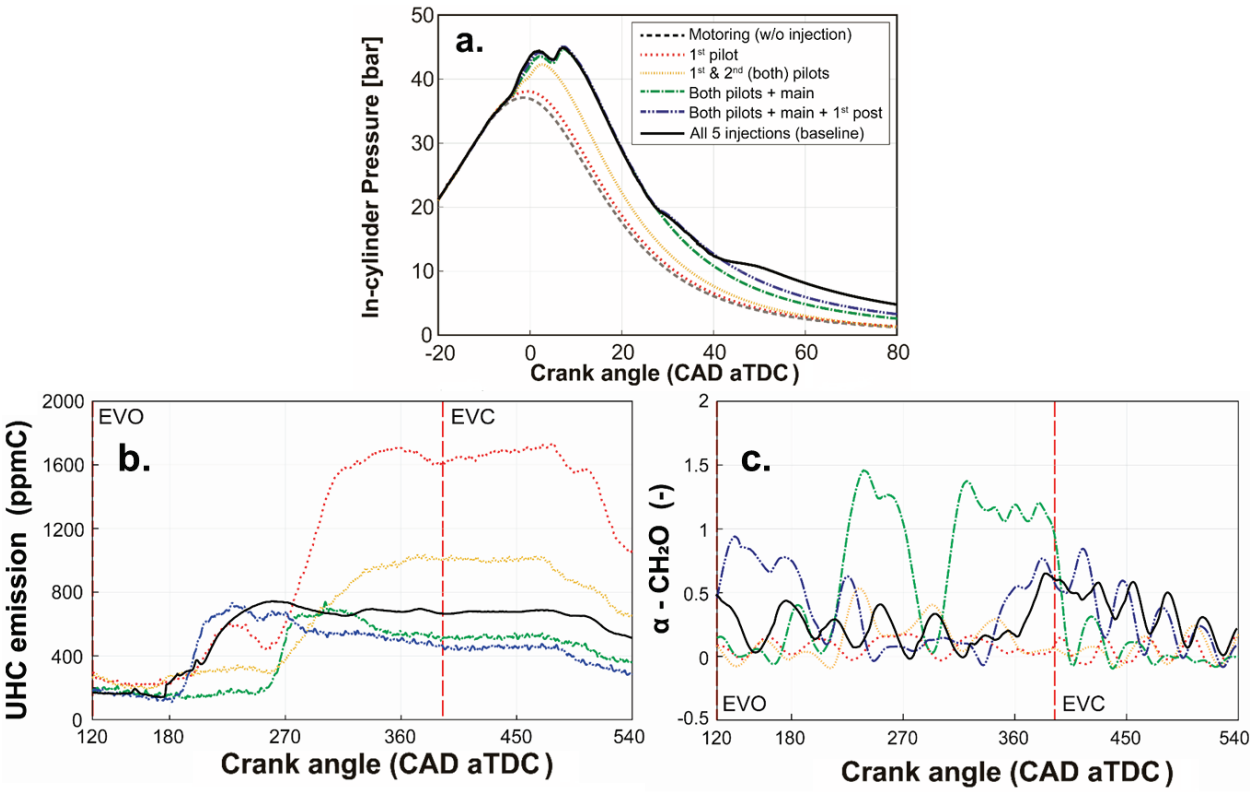

ppmC – parts per million of carbon ions; EVO – exhaust valve opening; EVC – exhaust valve closing

Figure I.13.2 (a) In-cylinder pressure, (b) time-resolved cyclic UHC emissions, and (c) time-resolved formaldehyde absorbance for individual injection strategies under catalyst-heating operation

Results show that UHC and formaldehyde emissions under catalyst-heating operation are formed by two main sources. First, a comparison between the cases with post injections (blue and black series) and the case with no post injections (green series) shows that pollutants released during the first part of the exhaust stroke (from exhaust valve opening to 250 CAD aTDC) are formed mainly by the post injections, likely as a result of overly mixed regions promoted by the very long ignition delay times of these post injections that do not burn completely. Second, a comparison between the case with only pilot injections (red and yellow series) and the case with pilots and main (green series) shows that UHCs and formaldehyde released during the latter part of the exhaust stroke (from 250 CAD aTDC to EVC) are likely formed by the interactions between partially oxidized hydrocarbons from the pilot injections and the main injection. A detailed analysis of the effects of injection timing on emissions (not shown here for brevity's sake) indicates that emissions from the pilot injections are controlled by the ability of the main injection to burn the partially oxidized species from the pilots, and therefore, UHC and formaldehyde emissions cannot be improved by acting only on the pilot injections. Furthermore, pertinent timing of first post injection is key for effective combustion of the second post injection.

Based on the new understanding discussed above, the project team developed a science-driven injection strategy aimed to improve engine performance under catalyst-heating operation. Conceptually, the new strategy consists of one main combustion event near top dead center that increases the in-cylinder temperature, followed by a series of pilot-like short injections that counteract the effect of the expansion process on the in-cylinder thermodynamic conditions, keeping the temperature relatively constant during expansion for better ignitability of post injections, which is the key to reaching high exhaust enthalpies and low UHC and formaldehyde emissions. Finally, a single post injection is used to increase the exhaust enthalpy. The number

of intermediate pilot-like injections depends on the timing of the post injection: the later the post-injection timing, the greater the number of pilot-like injections required to counteract the expansion effects.

Figure I.13.3 shows the engine performance for a non-optimized example of this new strategy that consists of two injection events before top dead center, followed by three pilot-like injections during the expansion stroke and a late post injection (six injections in total for this specific example). Results obtained with the optimized five-injection strategy are also included in the figure for comparison. More specifically, experimental measurements of (a) exhaust enthalpy, (b) thermal efficiency, (c) indicated specific hydrocarbon emissions (ISHC), (d) indicated specific CO emissions (ISCO), (e) indicated specific NO_x emissions ($ISNO_x$), and (f) indicated specific soot emissions (ISPM) are included in the figure. The six-injection example improves virtually all the engine parameters except soot. Both the exhaust enthalpy and the thermal efficiency significantly increase by 4.0% and 3.5%, respectively, whereas UHC, CO, and NO_x emissions decrease by 32.1%, 14.8%, and 17.3%, respectively. Soot increases, but the efficacy of the diesel particulate filter is not deteriorated by cold catalyst-heating conditions, so the penalty is relatively acceptable. It is worth noting that the six-injection example presented in Figure I.13.3 is not the result of any optimization process, so better results can likely be obtained in future studies.

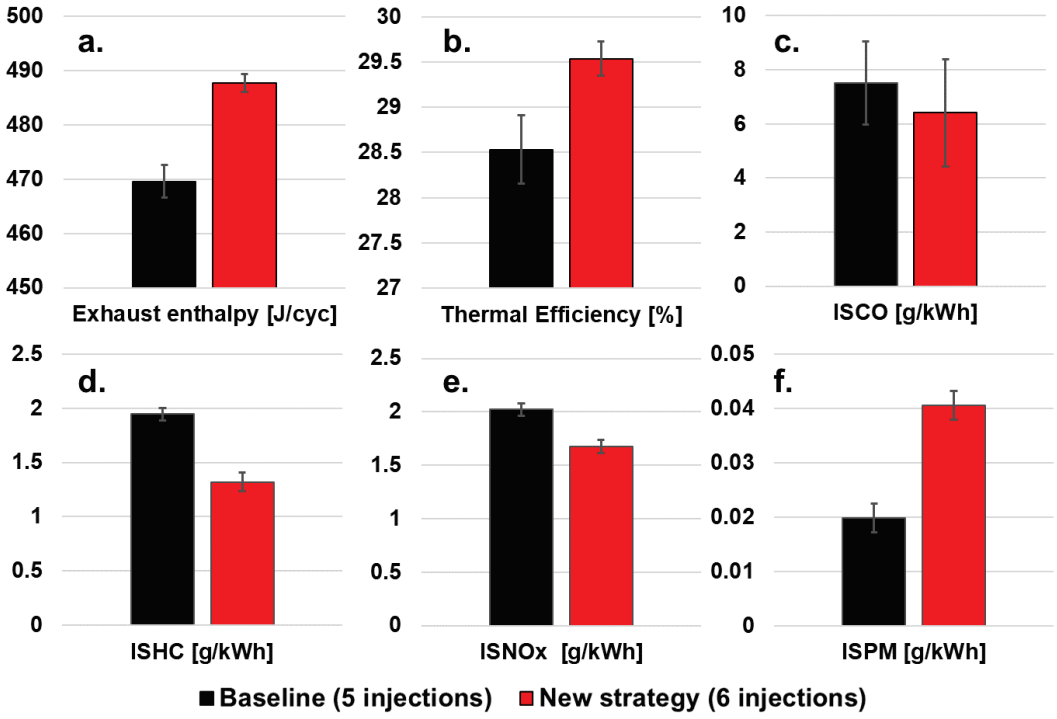

Figure I.13.3 (a) Exhaust enthalpy, (b) thermal efficiency, (c) ISHC, (d) ISCO, (e) $ISNO_x$, (f) and ISPM for both the baseline five-injection strategy (black) and the new catalyst-heating strategy (red)

The effects of fuel's autoignition reactivity (cetane number) and distillation characteristics (boiling range) on engine performance under catalyst-heating operation were also studied using five different diesel-like fuels. Results show that fuels with a higher cetane number and/or lower volatility give higher exhaust enthalpy and lower CO and UHC emissions, leading to improved catalyst-heating operation.

Finally, Figure I.13.4 shows a picture of the heat-flux micro-sensors fabricated in this project (left), a schematic of the sensor structure (middle), and experimental measurements of the sensor temperature response (right). Sensors incorporate two layers of platinum, a resistance temperature detector (RTD) material that provides a measurable and consistent electrical resistance change to a change in temperature. A layer of insulation material between the two layers of RTD creates a temperature gradient within the sensor that is

proportional to the heat flux. Experiments in a well-controlled environment show that the two RTD layers have remarkable linearity, demonstrating a reliable response of the sensor and providing a direct measurement of heat flux.

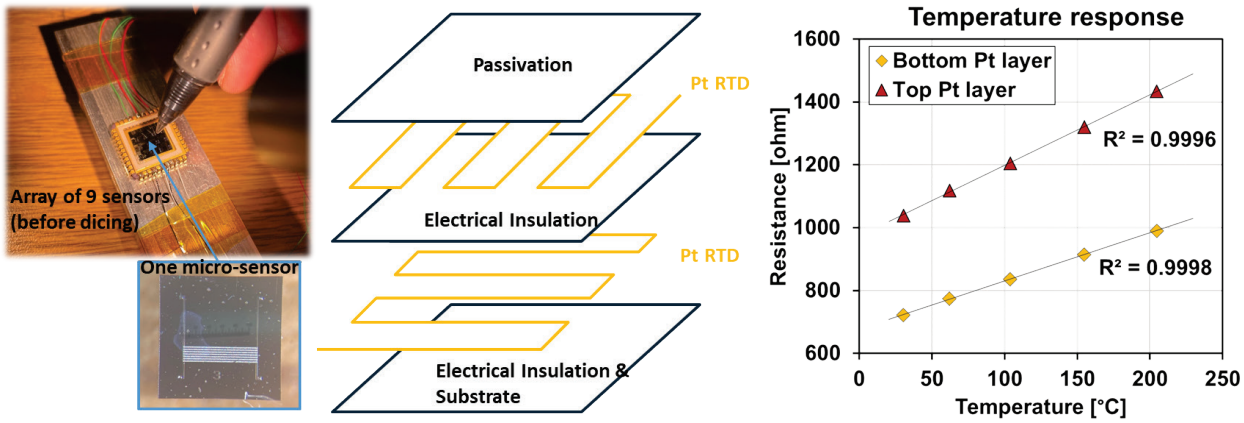

Figure I.13.4 Heat-flux micro-sensors (left), sensor structure (middle), and sensor temperature response (right)

Conclusions

- Vortex enhancement has been demonstrated to be a very effective mechanism to reduce soot emissions, owing to better air utilization and soot oxidation. Compared to a production SL piston, the improved DSL piston reduces smoke emissions by 45% at early injection timings at both low and part engine loads.
- Vortex enhancement may not necessarily lead to improved thermal efficiency, as it can cause increased wall heat transfer losses due to higher convection in the squish region and cylinder head, which counteracts the positive effects of vorticity on efficiency due to faster mixing-controlled heat release rate.
- UHC and formaldehyde emissions under catalyst-heating operation are formed by two main sources: by overly mixed regions from the post injections that do not burn efficiently, and by the interactions between partially oxidized hydrocarbons from the pilot injections and the main injection.
- Improving ignitability of the post injections while keeping their timing as retarded as possible is the silver bullet to simultaneously improve the exhaust enthalpy and UHC and formaldehyde emissions. A novel operation strategy aimed to improve post-injection ignitability provided 3.5% higher efficiency, 4.0% higher exhaust enthalpy, 32.1% less UHCs, 14.8% less CO, and 17.3% less NO_x than an optimized five-injection strategy representative of those used in diesel engines under catalyst-heating operation.
- Catalyst-heating operation benefits from fuels with higher cetane number and/or lower volatility, which lead to higher exhaust enthalpies and lower CO and UHC emissions.
- A novel heat-flux micro-sensor has demonstrated reliable response for temperatures up to 200°C and can be combined with an existing wireless telemetry system for heat-flux engine characterization.

Key Publications

1. Wu, A., S. Cho, D. Lopez Pintor, S. Busch, F. Perini, and R. D. Reitz. 2022. “Effects of a CFD-Improved Dimple Stepped-Lip Piston on Thermal Efficiency and Emissions in a Medium-Duty Diesel Engine.” *International Journal of Engine Research*, 14680874221117869. https://doi.org/10.1177/14680874221117869.

2. Cho, S., S. Busch, A. Wu, and D. Lopez Pintor. 2022. "Effect of Fuel Cetane Number on the Performance of Catalyst-Heating Operation in a Medium-Duty Diesel Engine." SAE Technical Paper 2022-01-0483. https://doi.org/10.4271/2022-01-0483.

3. Lopez Pintor, D., and J. Dec. 2022. "Development and Validation of an EHN Mechanism for Fundamental and Applied Chemistry Studies." SAE Technical Paper 2022-01-0455. https://doi.org/10.4271/2022-01-0455.

4. Wu, A., S. Busch, F. Perini, S. Cho, D. Lopez Pintor, and R. Reitz. 2022. "Numerical and Experimental Studies of a Novel Dimpled Stepped-Lip Piston Design on Turbulent Flow Development in a Medium-Duty Diesel Engine." SAE Technical Paper 2022-01-0400. https://doi.org/10.4271/2022-01-0400.

5. Lopez Pintor, D., and S. Cho. 2022. "Effects of the Stability of 2-Methyl Furan and 2, 5 Dimethyl Furan on the Autoignition and Combustion Characteristics of a Gasoline-Like Fuel." *Fuel* 312: 122990. https://doi.org/10.1016/j.fuel.2021.122990.

6. Perini, F., A. Wu, S. Busch, and R. Reitz. 2022. "Non-Equilibrium Law-of-the-Wall Modeling for Improved Heat Transfer Predictions: Model Development and Validation." SAE Technical Paper 2022-01-0405. https://doi.org/10.4271/2022-01-0405.

References

1. Wu, A., S. Busch, F. Perini, S. Cho, D. Lopez Pintor, and R. Reitz. 2022. "Numerical and Experimental Studies of a Novel Dimpled Stepped-Lip Piston Design on Turbulent Flow Development in a Medium-Duty Diesel Engine." SAE Technical Paper 2022-01-0400. https://doi.org/10.4271/2022-01-0400.

2. Kurtz, E., and C. Polonowski. 2017. "The Influence of Fuel Cetane Number on Catalyst Light-Off Operation in a Modern Diesel Engine." *SAE International Journal of Fuels and Lubricants* 10 (3). https://doi.org/10.4271/2017-01-9378.

3. Gingrich, E., M. Tess, V. Korivi, P. Schihl, J. Saputo, G. M. Smith, S. Sampath, and J. Ghandhi. 2021. "The Impact of Piston Thermal Barrier Coating Roughness on High-Load Diesel Operation." *International Journal of Engine Research* 22 (4): 1239–1254. https://doi.org/10.1177/1468087419893487.

4. Busch, S., A. Wu, and S. Cho. 2021. "Catalyst-Heating Operation in a Medium-Duty Diesel Engine: Operating Strategy Calibration, Fuel Reactivity, and Fuel Oxygen Effects." SAE Technical Paper 2021-01-1182. https://doi.org/10.4271/2021-01-1182.

5. Fitzgerald, R., A. Dempsey, R. Barlow, C. Nilsen, B. F. Yraguen, and C. J. Mueller. 2023. "Fast Exhaust-Runner Soot Measurements in a Diesel Optical Engine." *SAE International Journal of Engines* 16 (4). https://doi.org/10.4271/03-16-04-0032.

6. Musculus, M., D. Splitter, C. Zhang, K. Kelly, K. Walkowicz, P. Miles, R. Wagner, G. Singh, and M. Weismiller. 2019. "Analysis of In-Use Heat-Maps across MD/HD Applications: Where Are Opportunities for BTE Improvement Relative to SuperTruck/Line-Haul?" Advanced Engine Crosscut Meeting, July 18.

Acknowledgements

Sandia National Laboratories is a multi-mission laboratory managed and operated by National Technology and Engineering Solutions of Sandia, LLC., a wholly owned subsidiary of Honeywell International, Inc., for the U.S. Department of Energy's National Nuclear Security Administration under contract DE-NA-0003525.

I.14 Direct Numerical Simulation/Large Eddy Simulation and Modeling of Sustainable Aviation Fuel Flame Stabilization (Sandia National Laboratories)

Jacqueline H. Chen, Principal Investigator
Sandia National Laboratories
7011 East Avenue
Livermore, CA 94550
Email: jhchen@sandia.gov

Gurpreet Singh, DOE Program Manager
U.S. Department of Energy
Email: Gurpreet.Singh@ee.doe.gov

Start Date: October 1, 2021 End Date: September 30, 2022
Project Funding: $150,000 DOE share: $150,000 Non-DOE share: $0

Project Introduction

Concern for emission reduction and energy security have motivated the development of new cost-effective alternative sustainable aviation fuels (SAFs). Drop-in SAFs are beneficial because they are made from renewable biomass and waste resources and may not require engine modifications for use in current aviation engines. However, any new fuel must characteristically match commercial Jet-A (or A2) in order to meet the criteria for drop-in SAFs. Fuel chemistry effects and liquid evaporation characteristics are of particular concern when comparing a new fuel with Jet-A since they have a direct impact on flame stabilization. Fuel propensity to ignition, also defined as derived cetane number, is the most important feature impacting lean blow-off (LBO) in gas turbines [1]. The National Jet Fuels Combustion Program (NJFCP) proposed an alcohol-to-jet (C1) fuel with lower derived cetane number and liquid properties compared to Jet-A as a possible sustainable drop-in fuel. Large eddy simulation (LES) has been performed to study the flame dynamics in a lab-scale combustor at pressures close to atmospheric and inlet temperature below aero-combustor conditions [2]. However, mixture reactivity and low-temperature chemistry effects increase at pressures and temperatures relevant to aero-combustor conditions. A greater dependency of LBO on fuel chemistry (derived cetane number) was observed at relatively high temperatures and pressures [3]. Therefore, further investigation is required to identify the effects of turbulence-chemistry interactions on flame stabilization dynamics under those high pressures and temperatures.

The project uses high-fidelity simulation to glean fundamental understanding of the impacts of SAFs on flame stabilization combustion dynamics as well as providing benchmarks for combustion model testing and development. The proposed configuration closely follows laboratory experiments performed at Sandia National Laboratories Combustion Research Facility.

Objectives

Overall Objectives

- Glean fundamental understanding of the impacts of SAFs on flame stabilization combustion dynamics using high-fidelity simulations.
- Perform statistical analysis of the data to evaluate, develop, and improve combustion models.

Fiscal Year 2022 Objectives

- Perform high-fidelity simulations of spray flames under gas turbine operating conditions.
- Verify spray injection modeling strategy using experimental data.

- Identify chemical mechanisms capable of predicting flame stabilization at high pressures and moderate temperatures.
- Identify mixing and mixture reactivity effects on flame stabilization dynamics.

Approach

While there are many different designs and operating principles for aero-pilot combustors, key features for flame holding or flame stabilization are employed in all designs. Colket et al. [4] describe the technologies for swirl-stabilized combustors used in the NJFCP as containing a central recirculation zone (CRZ) or outer recirculation zone (ORZ). At the top of Figure I.14.1, we depict these zones in a schematic specifically adopted for the Air Force Research Laboratory (AFRL) referee rig, based upon computational fluid dynamics simulations performed by Esclapez et al. [2]. Several streamlines from the simulations at a near LBO condition are depicted, which show the CRZ and ORZ nestled between the predicted evaporating liquid boundaries. Temperature predictions from Esclapez et al. [2] show that hotter gas temperatures advance further upstream in the CRZ compared to the ORZ in this case. Also, Figure 1 shows that the layer of fresh air tends to be in contact with the liquid region at the top for a longer distance near the ORZ compared to the CRZ, while the CRZ is in direct contact with the liquid region. Sandia is performing experiments of spray flames with the goal to replicate inlet and CRZ gas conditions within a constant-volume pre-burn vessel also referred to as the single-hole atomizer.

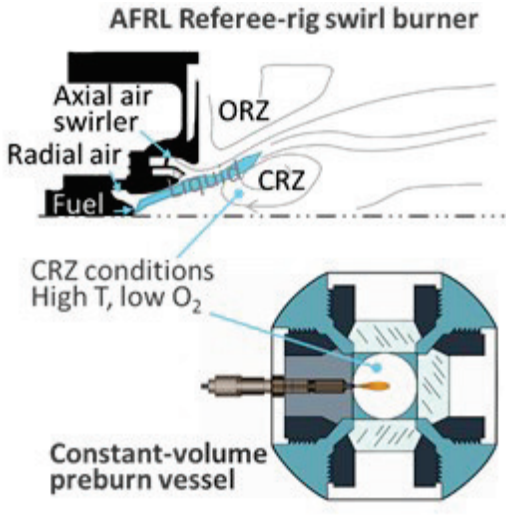

Figure I.14.1 Schematic of AFRL swirl burner (top) and Sandia constant-volume pre-burn vessel (bottom) creating ambient gas to mimic the CRZ conditions

The numerical investigation replicates the experiments covering take-off and cruise conditions relevant to modern aero-combustors, respectively 900 K and 60 bar (take-off) and 1,200 K and 20 bar (cruise). The take-off temperature value corresponds to the conditions at the combustor inlet, whereas the cruise conditions are related to the CRZ region that yields a higher temperature and lower oxygen concentration of 15% in mole. The simulations are performed using two different codes: the commercial software CONVERGE and the low-Mach solver of the Pele Suite, PeleLMeX, developed under the Exascale Computing Project. CONVERGE is used to perform LES simulations of the liquid fuel breakup process in order to provide the boundary conditions for PeleLMeX, and test detailed chemical mechanisms at more stringent conditions (high ambient pressure, 60 bar). PeleLMeX uses Lagrangian multi-phase modeling to capture the liquid spray injection and adaptive mesh refinement to enable a cost-efficient simulation with a more refined solution. Only the cruise ambient conditions are simulated with PeleLMeX due to lower grid resolution requirements, compared to higher pressure take-off conditions. The inlet boundary condition for PeleLMeX uses both the liquid quantities (Sauter mean diameter, liquid temperature, and velocity) and the gas-phase thermochemical state and velocity

components obtained 5 mm downstream from the injector nozzle, where a dilute spray can be assumed. The C1 fuel with low derived cetane is compared to the reference Jet-A fuel. Reaction rates are computed with the reduced University of Illinois at Urbana-Champaign (UIUC) mechanisms [5], [6] for the cruise conditions where high-temperature chemistry is dominant. On the other hand, the take-off condition is in the negative temperature coefficient regime where reduced chemical mechanisms may not accurately predict ignition. For instance, the well-stablished chemical mechanism package HyChem [7] and the recent mechanism developed by UIUC [5] are still under development to accurately account for low-temperature chemistry in SAFs. In this case, a new chemical mechanism for C1 developed at Sandia with 443 species was tested in the context of LES in CONVERGE. The new mechanism uses two surrogate components to describe the liquid properties and chemical behavior of the C1 fuel: 0.135 isocetane; 0.865 isododecane by volume. It was reduced from the Lawrence Livermore National Laboratory detailed model targeting experimental results of ignition delay time in a shock-tube and rapid compression machine for C1, as well as pure mixtures of isododecane and isocetane.

Results

Take-off conditions

Figure I.14.2 presents the comparison between the LES results and the experimental measurements in terms of liquid penetration evolution for the C1 fuel. Despite small differences, the combined Kelvin-Helmholtz and Rayleigh-Taylor breakup model provides good agreement for the liquid length.

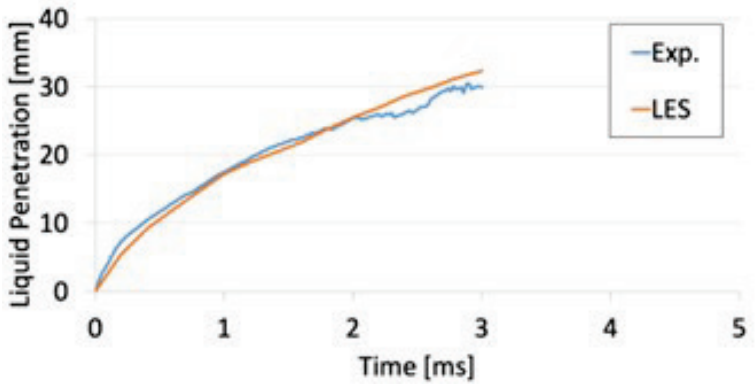

Figure I.14.2 Comparison between LES and experiment in terms of liquid length as a function of time for C1 at 900 K and 60 bar

One of the key difficulties in simulating SAFs in regimes where low-temperature chemistry (LTC) applies, i.e., 60 bar and 900 K (take-off conditions), is due to the lack of a reduced chemical mechanism that correctly captures low-temperature ignition. Figure I.14.3 presents the comparison with the experiments for the single-hole atomizer case at take-off conditions in terms of ignition delay time (IDT) and lift-off length (LOL) using the newly developed Sandia chemical mechanism for C1. Comparisons with simulations using reduced mechanisms were also performed but, due to the poor description of LTC, such mechanisms could not capture ignition at a similar time compared to the experiment, and therefore were not included in this report. The IDT using the Sandia chemical mechanism exhibits very good agreement with the experiment. Despite the good prediction of liquid length, ignition delay time, and the detailed chemical mechanism, flame lift-off length is under-predicted by the LES. This observation highlights the complexity involved in predicting stabilization of spray flames using SAFs under relevant aero-combustor conditions. Further investigation is required to identify the shortcomings of the LES models used to simulate this flame. Nonetheless, the Sandia mechanism development efforts of Fiscal Year (FY) 2022 resulted in a simulation set-up that has a closer agreement with experiments at take-off conditions.

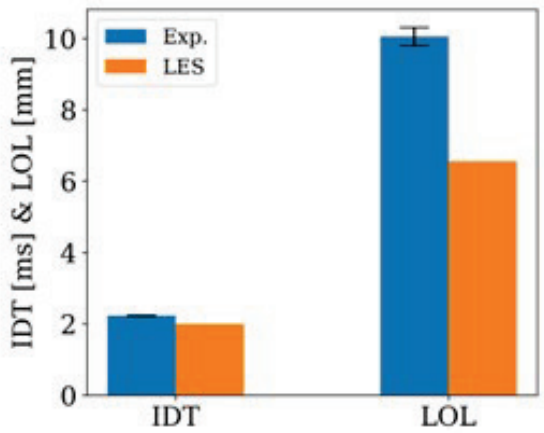

Figure I.14.3 Comparison between experimental results and LES simulation in terms of IDT and LOL for the C1 fuel

Cruise conditions

The two simulations performed with PeleLMeX at cruise conditions compare the flame stabilization dynamics using Jet-A as reference and C1 as the sustainable fuel. The configuration reproduces in full-scale the constant volume vessel experiment from Sandia. The validated set up in CONVERGE (Figure I.14.2) is used to compute the early mixture formation and serve as a virtual boundary condition for the PeleLMeX runs. Information for both liquid and gas phases are used.

The instantaneous temperature iso-contours for both fuels, presented in Figure I.14.4, show a lifted and highly turbulent flame with ignition pockets present near the stabilization point. C1 (on the left) exhibits a slightly higher lift-off height compared to Jet-A for the same ambient conditions and fuel mass flow rate. The first appearance of high temperature gas is observed to occur upstream of the stoichiometric mixture fraction iso-line (dashed white line) indicating that the flame is stabilized at fuel-lean conditions. Ignition delay times obtained with homogeneous reactor calculations, shown by the solid lines in Figure I.14.5a, predict the most reactive mixture fraction ξ_{MR} (mixture fraction with the shortest ignition delay time denoted by the vertical dashed lines) [8] to occur at lean mixtures for the conditions used here. The stoichiometric mixture fraction is 0.045 for both fuels.

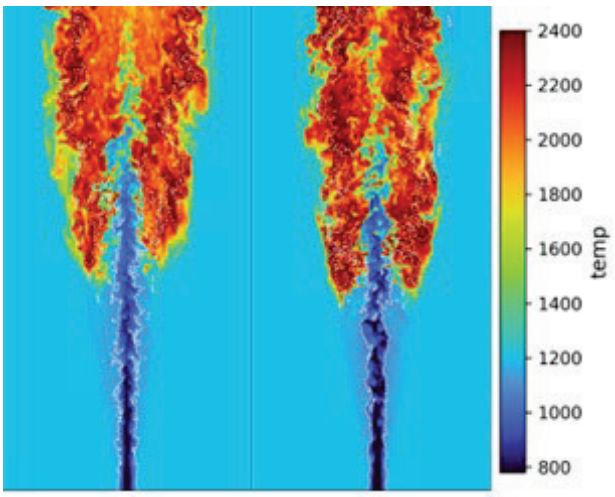

Figure I.14.4 Instantaneous temperature iso-contours in a cross-sectional plane at the domain center for C1 (left) and Jet-A (right). The dashed white line corresponds to the stoichiometric mixture fraction.

The mixture fraction and scalar dissipation rate (χ_ξ) at the stabilization point, as well as LOL, were sampled for different snapshots in time and different sectors in the azimuthal positions of the jet in order to compute a probability density functions (PDF). The dashed-dotted lines in Figure I.14.5a show that both fuels have the same maximum mixture fraction probability at the stabilization point which occurs at even learner mixtures compared to ξ_{MR} (vertical dashed lines). The PDF shapes indicate a narrower range of mixture fraction for flame stabilization for C1 which may be related to the flame response to χ_ξ. Regions closer to the stoichiometric mixture fraction often experience higher χ_ξ compared to the fuel-lean mixtures due to its proximity to the fuel injection region. However, Figure I.14.5b shows that the stabilization points of both flames experience similar scalar dissipation rates. It is important to note that the ignition delay time for Jet-A is longer than for C1 for the most probable mixture fraction at the stabilization point. Nonetheless, the lift-off height PDF in Figure I.14.5c shows Jet-A stabilizing closer to the injector.

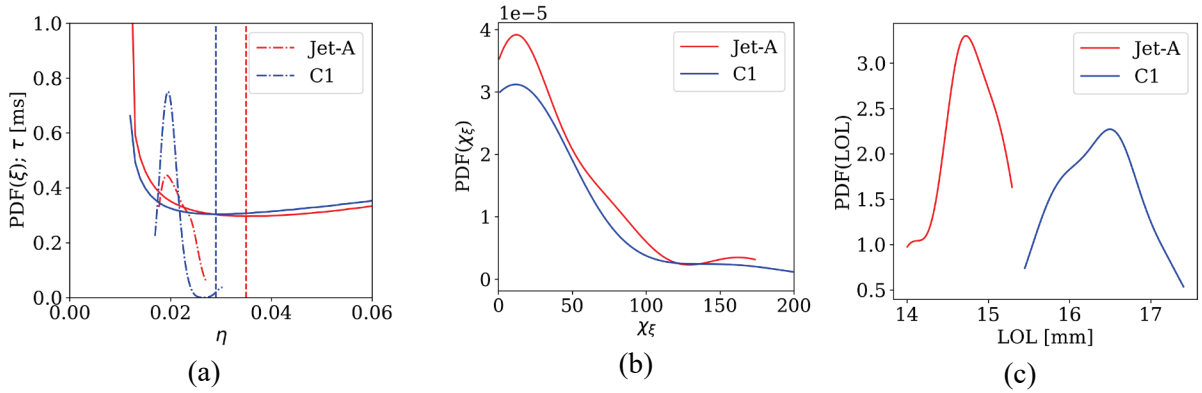

Figure I.14.5 PDFs for (a) mixture fraction at the stabilization point (dashed-dotted lines), (b) mixture fraction scalar dissipation rate at the stabilization point, and (c) lift-off length. In (a), solid lines correspond to ignition delay time in a homogeneous reactor and dashed lines correspond to the most reactive mixture fraction.

Key scalars are doubly conditioned on mixture fraction and scalar dissipation rate to investigate the mixing effects on flame structure. Figure I.14.6 presents doubly conditional means for OH mass fraction (Figure I.14.6a) as a marker for the high-temperature chemistry and HO_2 mass fraction (Figure I.14.6b) as a marker for mixture reactivity prior to ignition. Conditional means use the data for the entire domain. Both fuels present a similar distribution for OH mass fraction, with the intermediate scalar dissipation rate promoting OH production as also observed in other studies for different heavy hydrocarbons [9]. The conditional means for HO_2 mass fraction show a different response of mixture reactivity with respect to scalar dissipation rate. It is evident that Jet-A is insensitive to scalar dissipation rate at mixture fractions corresponding to the flame stabilization values presented in Figure I.14.5a. At scalar dissipation rates of the order of 25 s^{-1} (as reported in Figure I.14.5b), intermediate species provide chemical support for flame stabilization of Jet-A. However, C1 presents a small production of intermediate species at similar scalar dissipation rates (χ_ξ < 100 s^{-1}) and mixture fractions which could explain the narrower distribution for the mixture fraction PDF at the stabilization point for C1 (Figure I.14.5a). The analysis also shows an increase of intermediate species production at high scalar dissipation rate. Similar behavior is observed for conditional formaldehyde (not shown here).

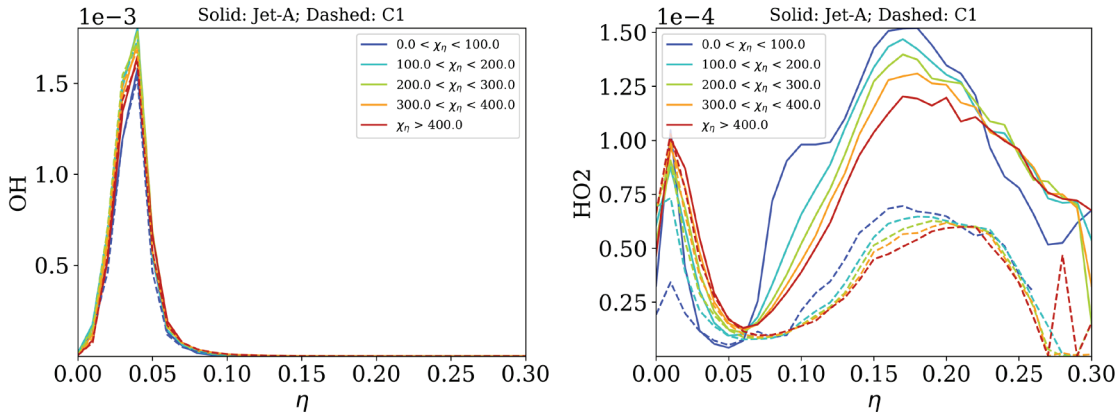

(a) OH mass fraction **(b) HO_2 mass fraction**

Figure I.14.6 Doubly conditional means of OH and HO_2 mass fraction on mixture fraction and scalar dissipation rate

Conclusions

The activities in FY 2022 focused primarily on the study of the flame stabilization of sustainable aviation fuels at aero-combustor relevant conditions. The simulations performed closely followed the Sandia experiments of a single-hole atomizer.

The simulations at take-off conditions were identified to be the most challenging in terms of correctly predicting ignition delay time and flame stabilization due to low-temperature chemistry effects.

- The liquid spray modeling correctly reproduced the liquid penetration measurements.
- A more detailed mechanism for C1 developed at Sandia demonstrated good agreement with experiments for ignition delay time.
- Despite the improved prediction compared to other chemical mechanisms, lift-off height is still under-predicted when compared to experiments.

The simulations at cruise conditions resulted in the following conclusions:

- Flame stabilization does not occur at the most reactive mixture fraction, and flame lift-off height is shorter for Jet-A compared to C1 despite stabilization occurring at the same mixture fraction.
- C1 presented a narrower range of mixture fractions for the stabilization point, indicating a narrower range of operation.
- High temperature chemistry is observed to respond similarly to scalar dissipation rate.
- Mixture chemical reactivity upstream of the stabilization point could be an important contribution to differences in flame stabilization dynamics. The chemical reactivity for Jet-A, denoted by HO_2 mass fraction, is higher than for C1 and insensitive to scalar dissipation rate for mixture fractions close to the stabilization point. The C1 flame presents similar levels of chemical reactivity only at high scalar dissipation rate.

References

1. Heyne, J., E. Peiffer, M. Colket, A. Jardines, C. Shaw, J. Moder, W. Roquemore, T.J. James, C. Li, M. Rumizen, and M. Gupta. 2018. “Year 3 of the National Jet Fuels Combustion Program: Practical and Scientific Impacts of Alternative Jet Fuel Research.” AIAA 2018-1667. AIAA Aerospace Sciences Meeting.

2. Esclapez, L., P.C. Ma, E. Mayhew, R. Xu, S. Stouffer, T. Lee, H. Wang, and M. Ihme. 2017. “Fuel Effects on Lean Blow-Out in a Realistic Gas Turbine Combustor.” *Combustion and Flame*, 181, 82–99.

3. Stouffer, S., T. Hendershott, J. Monfort, J. Diemer, E. Corporan, P. Wrzesinski, A. Caswell. 2017. “Lean Blowout and Ignition Characteristics of Conventional and Surrogate Fuels Measured in a Swirl Stabilized Combustor." 55th AIAA Aerospace Sciences Meeting.

4. Colket, M., J. Heyne, M. Rumizen, M. Gupta, T. Edwards, W.M. Roquemore, G. Andac, R. Boehm, J. Lovett, R. Williams, and J. Condevaux. 2017. “Overview of the National Jet Fuels Combustion Program.” *AIAA Journal* 55(4), 1087–1104.

5. Keunsoo, Kim, Je Ir Ryu, Brendan McGann, Kyungwook Min, Jacob Temme, Chol-Bum Kweon and Tonghun Lee. 2021. “Data-Driven Combustion Kinetic Modeling Concept of Alternative Alcohol-to-Jet (ATJ) Fuel.” AIAA 2021-1245. AIAA Scitech 2021 Forum. January.

6. Ryu, Je Ir and Kim Keunsoo, Min Kyungwook, Riccardo Scarcelli, Sibendu Som, Kenneth S. Kim, Jacob E. Temme, Chol-Bum M. Kweon, and Tonghun Lee. 2021 “Data-Driven Chemical Kinetic Reaction Mechanism for F-24 Jet Fuel Ignition.” *Fuel* (290): 119508.

7. Xu, R., K. Wang, S. Banerjee, J. Shao, T. Parise, Y. Zhu, S. Wang, A. Movaghar, D.J. Lee, R. Zhao, X. Han, Y. Gao, T. Lu, K. Brezinsky, F.N. Egolfopoulos, D.F. Davidson, R.K. Hanson, C.T. Bowman, and H. Wang. 2018. “A Physics-Based Approach to Modeling Real-Fuel Combustion Chemistry - II. Reaction Kinetic Models of Jet and Rocket Fuels.” *Combustion and Flame*, 193, 520–537.

8. Mastorakos, E. 2009. “Ignition of Turbulent Non-Premixed Flames.” *Progress in Energy and Combustion Science.*

9. Borghesi, Giulio, Alexander Krisman, Tianfeng Lu, Jacqueline H. Chen. 2018. “Direct Numerical Simulation of a Temporally Evolving Air/n-dodecane Jet at Low-Temperature Diesel-Relevant Conditions.” *Combustion and Flame* 195, 183–202.

Acknowledgements

- Spray Combustion Laboratory, Sandia National Laboratories
- National Energy Research Scientific Computing Center, Lawrence Berkeley National Laboratory

I.15 Ducted Fuel Injection (Sandia National Laboratories)

Charles J. Mueller, Principal Investigator
Sandia National Laboratories
7011 East Avenue, MS 9053
Livermore, CA 94550-9517
Email: cjmuell@sandia.gov

Gurpreet Singh, DOE Program Manager
U.S. Department of Energy
Email: Gurpreet.Singh@ee.doe.gov

Start Date: October 1, 2021 End Date: September 30, 2022
Project Funding: $500,000 DOE share: $500,000 Non-DOE share: $0

Project Introduction

Certain heavy-duty applications are difficult to decarbonize via electrification and/or carbon-free fuels. Challenges include lack of required infrastructure, limited available time for recharging, severe ambient conditions, demanding duty cycles, the need for maximum work capacity per unit powertrain mass and volume, and cost. These hard-to-decarbonize sectors historically have relied on diesel engines burning petroleum-based fuels. A pragmatic approach for reducing the pollutant and net-carbon emissions from these sectors is needed. Ducted fuel injection (DFI) with low-net-carbon fuels is such an approach.

DFI involves injecting fuel along the axis of a small cylindrical duct within the combustion chamber of a diesel engine to achieve more complete local premixing at or near the end of the duct where autoignition occurs (see Figure I.15.1). DFI is capable of curtailing engine-out soot emissions dramatically, even when relatively high levels of intake charge-gas dilution (i.e., exhaust gas recirculation) are used to cost-effectively mitigate emissions of nitrogen oxides (NO_x). Furthermore, the soot reductions possible with DFI are larger when commercially available low-net-carbon fuels, such as biodiesel and renewable diesel, are used. Hence, DFI with low-net-carbon fuels and dilution can enable simultaneous, order-of-magnitude reductions in engine-out emissions of net carbon, soot, and NO_x in the near term [1], [2].

Despite these benefits, industry has been slow to adopt the technology because of uncertainties about efficacy under high-load operating conditions (e.g., see Svensson, et al. [3]). This project is aimed at overcoming uncertainties such that the beneficial impacts of DFI can be realized without delay.

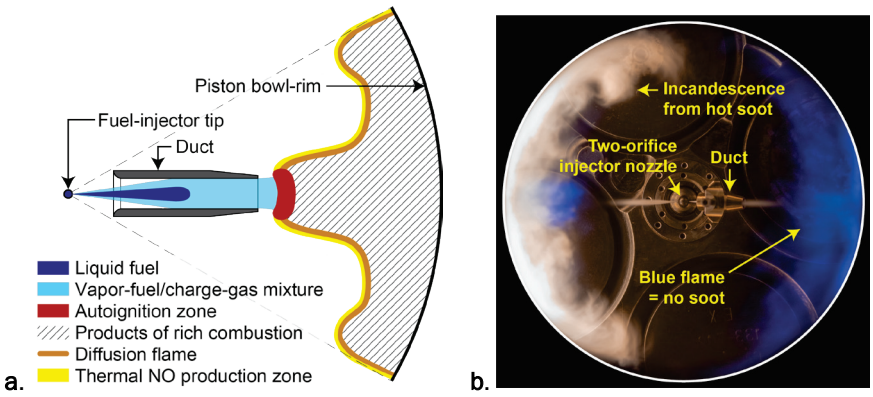

Figure I.15.1 (a) Schematic of DFI as applied to a single fuel spray in a diesel engine. (b) Image acquired through a window in the piston of an optical engine, showing a conventional diesel combustion spray on the left, producing a cloud of incandescent soot particles, and DFI on the right, producing no soot. The DFI configuration on the right corresponds to the schematic shown in (a).

Objectives

Overall Objective

Enhance the fundamental and practical understanding of DFI to facilitate its successful and rapid commercial implementation to reduce net-carbon and criteria pollutant emissions from difficult-to-decarbonize, heavy-duty applications.

Fiscal Year 2022 Objectives

- Determine whether DFI can be used to curtail soot emissions at full-load conditions with a low-net-carbon fuel.
- Continue advancing the fundamental understanding of key physical processes governing DFI performance.
- Assemble a consortium of industry stakeholders to assist in further developing DFI for successful commercial application.

Approach

The approach to achieving the above Fiscal Year (FY) 2022 objectives took three main paths. The first was to upgrade the peak cylinder pressure capability of the optical engine to enable DFI experiments at conditions representative of full-power conditions in a heavy-duty, all-metal engine. The second was to conduct fundamental and applied experiments—teaming with other stakeholders wherever possible—to continue learning about key factors influencing DFI performance and implementation. The third was to participate in technology commercialization training and conduct outreach to industry stakeholders to form a consortium focused on testing DFI for the first time in a multi-cylinder engine with low-net-carbon fuels.

Results

The following are key results from this project in FY 2022:

- Upgraded the peak cylinder pressure capability of the optical engine to 200 bar to enable detailed experimental investigations to full-power metal-engine operating conditions.
- Tested the upgraded optical engine to full-load conditions with a low-net-carbon fuel and measured 45% lower engine-out soot emissions for DFI vs. conventional diesel combustion.
- Completed the Energy I-Corps Program on technology commercialization and assembled a consortium to de-risk DFI for widespread deployment. Consortium members are John Deere, Clean Fuels Alliance America, Coordinating Research Council, Cummins Inc., and Sandia National Laboratories.

Optical Engine Upgrades

To determine whether DFI can provide substantial engine-out soot emissions reductions at full-load conditions, researchers increased the optical engine's peak cylinder pressure capability from 120 bar to 200 bar. This is an uncommonly high peak-cylinder-pressure capability for an optical engine. Achieving it required the design, fabrication, and construction of two major new component assemblies: a DFI-equipped cylinder head and an optical piston. The new head was made from a strong, ductile cast iron, was finish-machined, and was equipped with a new zero-leakage common-rail fuel-injection system capable of operating to rail pressures >250 MPa. The new piston consists of a single-piece titanium alloy body with options for either a single-piece titanium alloy piston top or an optical piston-top assembly featuring a sapphire window. While the engine hardware was being upgraded, the experimental data acquisition hardware also was upgraded, including a new programmable engine controller and a 12-channel, 225 kHz system to enable engine time-series data to be acquired with 0.1 crank angle degree (CAD) resolution at 1,800 rpm. The new cylinder head and optical piston-top assembly are shown in Figure I.15.2.

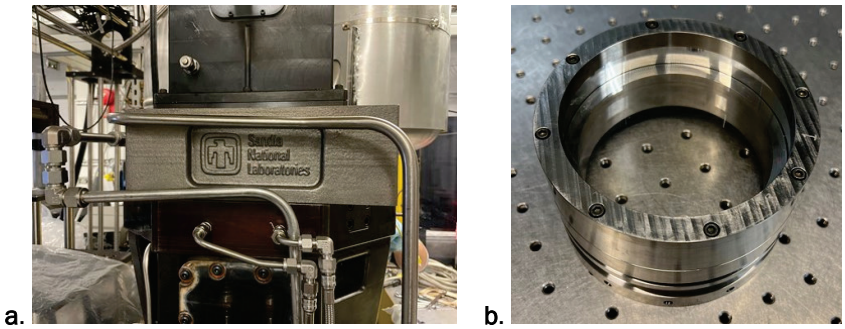

Figure I.15.2 New 200-bar-capable engine components: (a) cylinder head (with Sandia logo) and (b) optical piston-top assembly.

Optical Engine Testing

Once the optical engine and data acquisition hardware upgrades were completed, the system was tested. After some initial design iterations related to piston-bowl geometry, spray included angle, and injector-tip protrusion, acceptable operation was achieved. The engine was then fired at 1,200 rpm and 17 mol% intake oxygen from 6 bar (27% load) to 22 bar (100% load) gross indicated mean effective pressure ($IMEP_g$) under both conventional diesel combustion and DFI conditions. Peak cylinder pressures reached 165 bar. These peak loads and cylinder pressures are extremely high for an optical engine of this bore size (125 mm). The fuel used was a low-net-carbon blend of 80 vol% renewable diesel with 20 vol% biodiesel, denoted R80B20. Pressure and apparent heat-release rate (AHRR) data from these experiments are shown in Figure I.15.3.

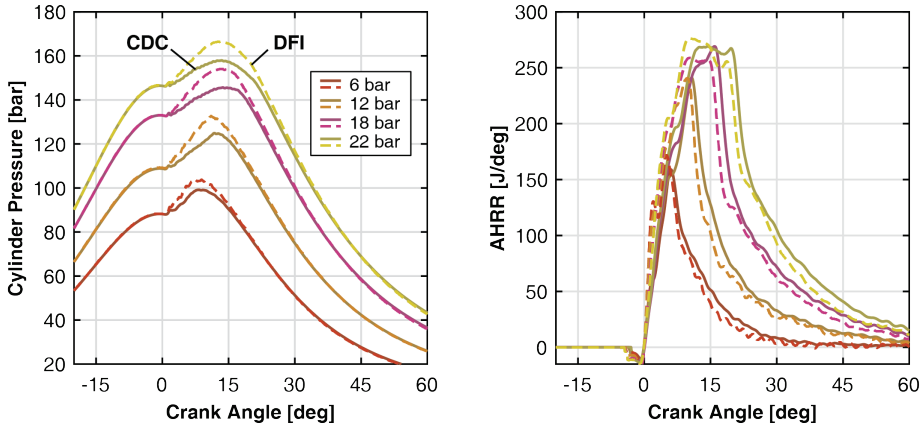

Figure I.15.3 Timeseries data, 1,200 rpm, 17 mol% intake oxygen, R80B20 fuel, load sweep from 6–22 bar IMEPg.

The emissions and efficiency data from this set of experiments are shown in Figure I.15.4. The engine-out soot emissions for DFI are 40%–60% lower than for conventional diesel combustion across the load range, including 45% lower at full load. The fuel conversion efficiency (η_f) is also higher for DFI at the two higher loads. While the NO_x emissions are higher for DFI, it is believed that they can be brought to parity with a small increase in dilution without substantially affecting soot emissions, as has been shown in past work [4]. It is worth noting that these are initial results from a highly non-optimized combustion system. This is evidenced by the rather high absolute soot levels and the fact that DFI soot reductions are only ~60% at 6 bar $IMEP_g$, whereas in past experiments at this load, DFI soot reductions were ~90% [4]. Hence, it is believed that additional substantial soot reductions can be achieved across the load range with further refinement of the DFI combustion system.

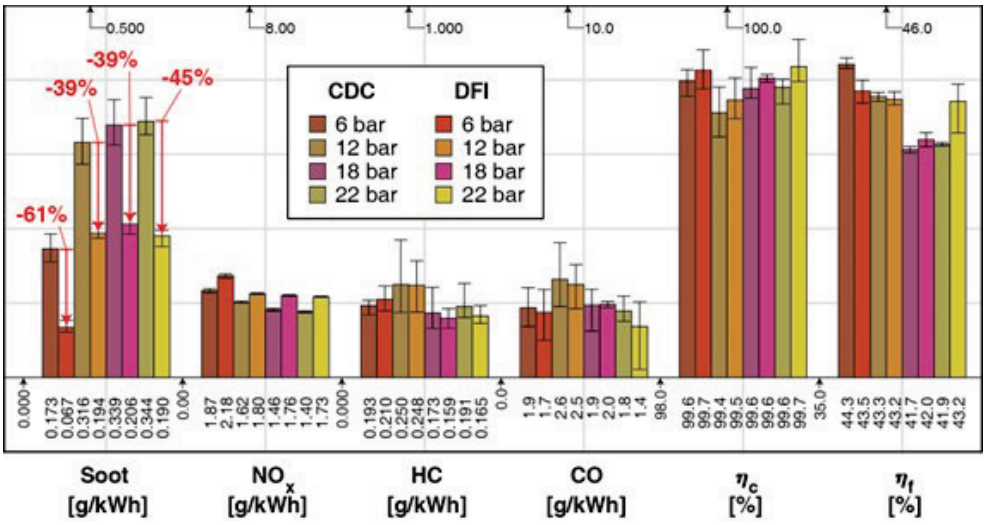

Figure I.15.4 Indicated specific emissions of soot, NO_x, hydrocarbons (HC), and carbon monoxide (CO), and combustion and fuel conversion efficiency data for the load sweep from 6–22 bar IMEPg.

Technology Commercialization Efforts

To facilitate the achievement of the U.S. Department of Energy (DOE) goal of successfully bringing improved technologies to market as quickly as possible, the principal investigator and two colleagues from John Deere participated in the Energy I-Corps program (Cohort 13, Team 148). During the program, the team conducted 77 interviews with stakeholders in the heavy-duty equipment and fuels ecosystem, with each interview approximately 30 minutes in duration. This helped the team identify the most promising paths to DFI commercialization and the stakeholders best able to move the technology into commercial applications quickly. The outcome was the above-noted consortium's developing a joint proposal and securing federal and industry funding for a cooperative research and development agreement (CRADA) to test DFI in a multi-cylinder John Deere engine with low-net-carbon fuels. The ultimate objective of the three-year CRADA is to achieve simultaneous reductions in engine-out soot, NO_x, and net carbon emissions of >70% each, relative to the current production engine operated on conventional petroleum diesel fuel.

Conclusions

This project made substantial progress toward achieving DOE objectives during FY 2022. The main conclusions from this performance period are as follows:

- DFI was shown to reduce soot by 45% while increasing fuel conversion efficiency at full-load conditions, without severe degradations in other emissions. This addresses concerns raised by Svensson, et al. [3], indicating that the DFI implementation in that study was not optimal and that the results therefrom may not be typical.
- DFI was shown to reduce soot by ~60% at 6 bar IMEPg in the current dataset, whereas the technology achieved ~90% lower soot in past testing in similar conditions [4]. This indicates that the current DFI implementation also is not optimal and further improvement is likely possible.
- Stakeholders from the engines and fuels industries and a DOE national laboratory have formed a consortium focused on successfully moving DFI with low-net-carbon fuels into commercial applications without delay. This indicates that DFI shows promise for providing pragmatic, clean, low-net-carbon power for difficult-to-decarbonize, heavy-duty applications.

Invention Disclosure

1. Sandia Invention Disclosure SD-16000: Mueller, C. J. and C.W. Nilsen. 2021. "Techniques for Further Mixing Enhancement with Ducted Fuel Injection." Sandia National Laboratories.

Key Publications

1. Nyrenstedt, G., C.W. Nilsen, D.E. Biles, and C.J. Mueller. 2023. "Ducted Fuel Injection with Low-Net-Carbon Fuels as a Solution for Meeting Future Emissions Regulations." *Fuel* 338: 127167. https://doi.org/10.1016/j.fuel.2022.127167.

2. Sener, R., C.W. Nilsen, D.E. Biles, and C.J. Mueller. 2023. "A Computational Investigation of Engine Heat Transfer with Ducted Fuel Injection." *International Journal of Engine Research*. https://doi.org/10.1177/14680874221149321.

3. Yraguen, B.F., A.M. Steinberg, C.W. Nilsen, D.E. Biles, and C.J. Mueller. 2022. "Parametric Evaluation of Ducted Fuel Injection in an Optically Accessible Mixing-Controlled Compression-Ignition Engine with Two- and Four-Duct Assemblies." Presented at the THIESEL 2022 Conference on Thermo- and Fluid Dynamics of Clean Propulsion Powerplants, Valencia, Spain, September 13–16.

4. Fitzgerald, R.P., A.B. Dempsey, R.S. Barlow, C.W. Nilsen, B.F. Yraguen, and C.J. Mueller. 2022. "Fast Exhaust-Runner Soot Measurements in a Diesel Optical Engine." *SAE International Journal of Engines* 16, no. 4. https://doi.org/10.4271/03-16-04-0032.

References

1. Nyrenstedt, G., C.W. Nilsen, D.E. Biles, and C.J. Mueller. 2023. "Ducted Fuel Injection with Low-Net-Carbon Fuels as a Solution for Meeting Future Emissions Regulations." *Fuel* 338: 127167. https://doi.org/10.1016/j.fuel.2022.127167.

2. C.J. Mueller, C.W. Nilsen, D.E. Biles, and B.F. Yraguen. 2021. "Effects of Fuel Oxygenation and Ducted Fuel Injection on the Performance of a Mixing-Controlled Compression-Ignition Optical Engine with a Two-Orifice Fuel Injector." *Applications in Energy and Combustion Science* 6: 100024. https://doi.org/10.1016/j.jaecs.2021.100024.

3. Svensson, K., C. Kim, P. Seiler, G. Martin, and C. Koci. 2021. "Performance and Emission Results from a Heavy-Duty Diesel Engine with Ducted Fuel Injection." SAE Technical Paper 2021-01-0503. https://doi.org/10.4271/2021-01-0503.

4. Nilsen, C.W., D.E. Biles, B.F. Yraguen, and C.J. Mueller. 2020. "Ducted Fuel Injection vs. Conventional Diesel Combustion: An Operating-Parameter Sensitivity Study Conducted in an Optical Engine with a Four-Orifice Fuel Injector." *SAE International Journal of Engines* 13, no. 3: 345–62. https://doi.org/10.4271/03-13-03-0023.

Acknowledgements

The excellent progress made during FY 2022 would not have been possible without major contributions from the following: post-doctoral appointees Gustav Nyrenstedt and Christopher Nilsen; technologists Nathan Harry, Keith Penney, and Tim Gilbertson; contractor Kirby Baumgard; and I-Corps industry mentor Danan Dou of John Deere. The project team is grateful to the DOE Vehicle Technologies Office for supporting this research. The research was conducted at the Combustion Research Facility, Sandia National Laboratories, Livermore, California.

Sandia National Laboratories is a multi-mission laboratory managed and operated by National Technology and Engineering Solutions of Sandia, LLC, a wholly owned subsidiary of Honeywell International, Inc., for DOE's National Nuclear Security Administration under contract DE-NA-0003525.

I.16 Sprays and Spray Combustion (Sandia National Laboratories)

Lyle Pickett, Principal Investigator
Sandia National Laboratories
P.O. Box 969, MS 9053
Livermore, CA 94551-9053
Email: LMPicke@sandia.gov

Gurpreet Singh, DOE Program Manager
U.S. Department of Energy
Email: Gurpreet.Singh@ee.doe.gov

Start Date: October 1, 2021 End Date: September 30, 2022
Project Funding: $400,000 DOE share: $400,000 Non-DOE share: $0

Project Introduction

Off-road engines must tolerate a range of various renewable fuels. Intentionally creating better fuels and better injectors requires an understanding of how specific fuel properties affect the spray mixing and evaporation processes. Renewable fuels with a lower carbon footprint, such as renewable diesel, methanol, and oxymethylene ethers (OME), have demonstrated successful engine operation with low particulate emissions, but lack of accurate fuel spray computational fluid dynamics (CFD) models using these fuels limits further engine and injector improvement. One key research area is understanding the combustion interaction between neighboring plumes, which may change with different degrees of fuel oxygenation and different low-temperature combustion.

Objectives

This project utilized a research diesel injector of special design to understand the interaction between separate plumes, with diagnostics performed within optically accessible spray chambers. The research injector is based upon a stock 10-hole injector but has only four plumes. One plume is in complete isolation, with a triplet of regularly spaced plumes opposite (180°) this plume, resembling a “chicken-foot” hole pattern. Sets of these chicken-foot injectors have been provided by Cummins Inc. and Bosch to the Engine Combustion Network for research within multiple organizations [1].

Specific objectives for project activities during Fiscal Year (FY) 2022 are summarized below:

- Characterize spray, combustion, and sooting behavior of the four-hole Engine Combustion Network diesel injector.
- Measure the limits of soot-free diesel combustion using OME, including detailed mixture fraction, upstream formaldehyde, and high-temperature combustion [2].
- Assess liquid penetration, ignition, and combustion for methanol diesel sprays.
- Lead a multi-institution, international research effort on engine spray combustion called the Engine Combustion Network [1].

Approach

Optically accessible spray chambers and advanced diagnostics are utilized for this research. The chicken-foot injector is mounted in a heated continuous-flow pressure vessel, as depicted in y Figure I.16.1. Pressure- and temperature-controlled gases flow from the bottom of the chamber to the top. Fuel vapor or combustion products are scavenged by this flow after injection, presenting fresh gas of controlled composition before the next injection and facilitating multiple injections. The temperature of the fuel injector is controlled with liquid cooling and an insulating jacket. With precise boundary condition control, the datasets are especially useful for

CFD model development. Experiments using OME fuel were performed using single-plume injectors, as described in [2].

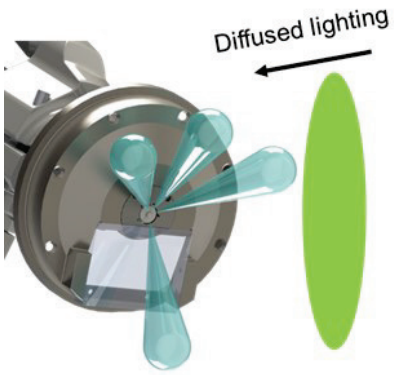

Figure I.16.1 Schematic of chicken-foot injector (with plume rendering) mounted in continuous-flow pressure vessel. The bottom isolated plume has a reflective prism installed behind it.

A range of optical diagnostics were applied for the chicken-foot spray experiments. Diffused backlighting using a light-emitting diode (LED) and engineered diffuser was employed to measure extinction from liquid in the vaporizing environment. As depicted in Figure I.16.1, the backlighting experiences extinction from one isolated plume at the bottom, or three plumes along the line of sight at the top. Simultaneous to the backlight imaging, Mie scatter imaging was collected from the front view (Figure I.16.1) to characterize the liquid position from a different view. In reacting experiments, high-speed OH chemiluminescence imaging at 310 nm, rather than Mie scatter imaging, was performed. Time-resolved OH chemiluminescence was used to detect ignition and flame lift-off length.

Results

Example imaging results for non-reacting but vaporizing chicken-foot experiments are shown in Figure I.16.2. The ensemble average shows the extent of axial and radial liquid penetration at a particular time after start of injection (aSOI). The isolated plume at the bottom penetrates past 20 mm, as confirmed by both the side view light extinction and front view Mie scatter imaging. Extinction from the top plumes is more difficult to interpret from the side view because light extinction is caused by all three plumes along the line of sight. Nevertheless, each plume is distinct in the front view, although precise quantification of liquid is more difficult from the Mie scatter.

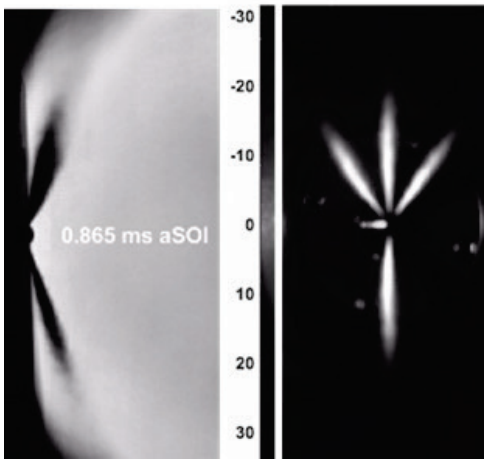

Figure I.16.2 Diffused backlight imaging (left) and Mie scatter imaging (right) under non-reacting conditions. Ensemble-averaged images at 0.865 ms aSOI. Injector conditions: 0.213 mm nozzles, 1,500 bar, n dodecane, 363 K. Ambient conditions: 900 K, 60 bar, 0% volume oxygen (100% nitrogen). Scale in millimeters.

In contrast to the non-reacting results, experiments with combustion are shown in Figure I.16.3. Results for extinction imaging and OH chemiluminescence are shown here for an instant in the same injection, rather than an ensemble average. A timing of 0.43 ms aSOI at the far left corresponds to the onset of high-temperature ignition, with distributed kernels of chemiluminescence first appearing. By 0.67 ms, distinct lifted flames are visible in each plume. The flames are clearly closer to the injector axis for the trio of plumes at the top compared to the isolated plume at the bottom, demonstrating that the flame lift-off length is shorter for the plume trio. The liquid extinction imaging at this same time shows a new, bright signal at the top, which is collected natural luminosity in addition to the diffused backlighting intensity. This bright signal is caused by the collective luminosity of three plumes along the line of sight, but the brightness also suggests soot incandescence, rather than weaker chemiluminescence, is a major contributor. The bottom extinction image also shows some growing background luminosity, evidence of a schlieren effect suggesting high gradients in temperature from the reacting flame, and shorter liquid penetration because of mixing by high-temperature combustion products into the spray. A decrease in liquid penetration because of reaction has been noted before for large-nozzle diesel injectors in Maes, et al. [3].

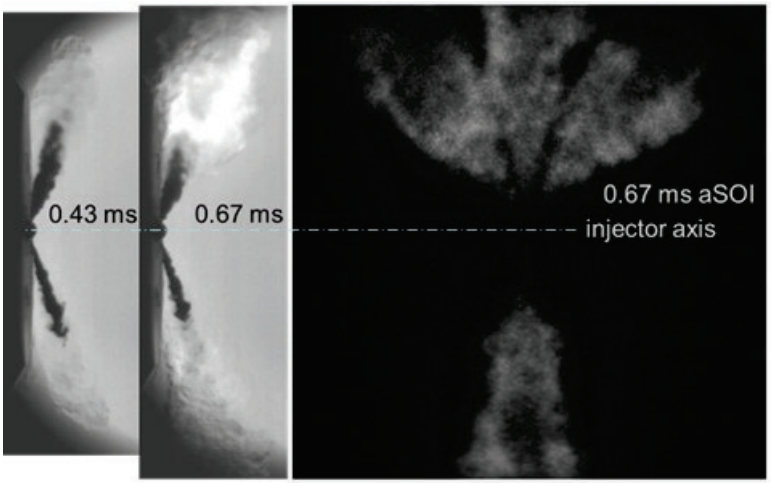

Figure I.16.3 Diffused backlight imaging (left) and OH chemiluminescence imaging (right) under reacting conditions. Conditions are the same as in Figure I.16.2, except the gas is air (21% oxygen).

The intensity of the background soot incandescence continues to increase with increasing time. Figure I.16.4 shows the same event from Figure I.16.3 at approximately 0.79 ms. The growing soot incandescence signal is confirmed in the diffused backlighting experiment, where the LED used for backlighting was disabled on every other frame. The frame with the LED off (displayed with brightness adjustment) shows a faint signal where liquid is present, for the isolated plume as well as the plume triplet. This signal is the result of flame luminosity reflected from the liquid. Figure I.16.2 clearly shows that liquid is present in these regions during injection, although there was no intentional illumination of the liquid under reacting conditions. The faint signal from reflected liquid is also present at 310 nm, which needs to be understood and distinguished from actual OH chemiluminescence to have certainty about the real flame lift-off length. While the flame clearly looks closer to the nozzle for the plume triplet, the scatter from liquid does obscure or soften the gradient to the flame itself.

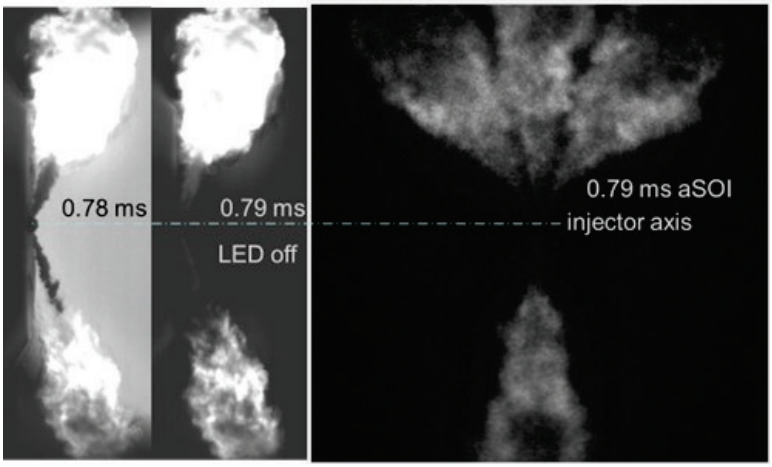

Figure I.16.4 Imaging for the conditions of Figure I.16.3 at a later timing.

One way to address the influence of the liquid scatter is to focus on timings immediately after the end of injection. Shown in Figure I.16.5 is the ensemble-averaged 310 nm emission at two timings that span the end of injection, which occurs at approximately 0.85 ms aSOI for the reacting dataset. Data at 0.79 ms are therefore potentially affected by liquid scatter, but data at 0.93 ms are not because this timing is after the end of injection and after liquid has vaporized. The chemiluminescence at 0.93 ms is unambiguously closer to the injector for the plume triplet compared to the isolated plume, confirming that flame lift-off length is indeed shorter for the plume triplet. Moreover, a careful examination of time sequences at the end of injection shows that the typical response of the flame is to recede closer to the injector after the end of injection, rather than lifting away from the injector. Consequently, the flame positions after the end of injection support the indication that the flame lift-off length is less for the plume triplet.

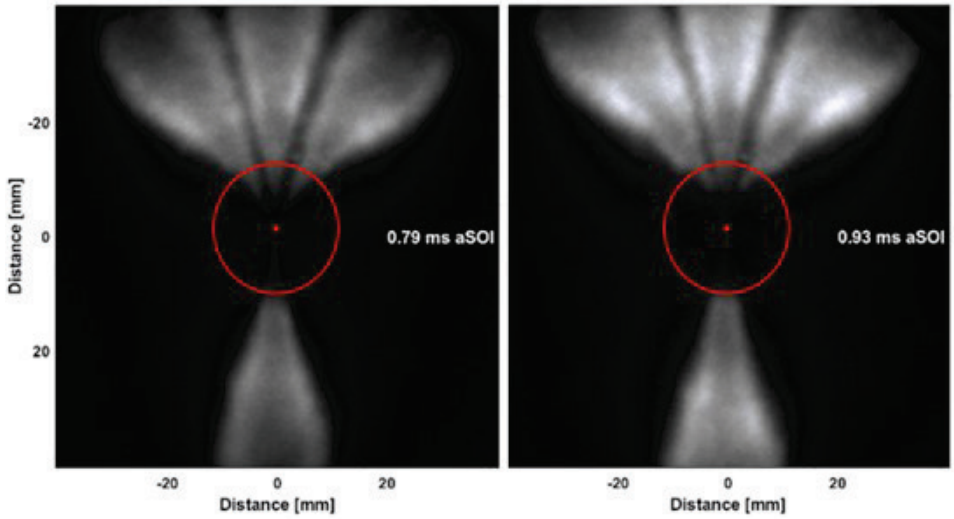

Figure I.16.5 Ensemble-averaged OH chemiluminescence imaging at two timings near the end of injection. Conditions are the same as in Figure I.16.2. The red circle is provided for reference.

This study conclusively demonstrates how plume interactions from practical fuel injectors may shorten lift-off length and increase soot formation. A potential reason for the shorter lift-off length is a stronger upstream air motion between closely spaced plumes [4], which can pull high-temperature products toward the injector tip. Further work to support this hypothesis will focus on the jet width and the dynamics of product motion between plumes. In addition, measurements of soot concentration within the plumes will be performed using the reflecting prism and light collection to the front view, as depicted in Figure I.16.1.

Conclusions

The project has generated a large dataset documenting the liquid spray penetration, vaporization, ignition, lift-off length stabilization and soot formation for a novel four-hole, chicken-foot injector. The new data support the notion that plume-to-plume interactions play an important role in practical diesel combustion systems. This project is increasing our understanding of the degree of interaction when using various renewable fuels with different levels of oxygenation. This understanding is needed to predict the response and to exercise CFD models that will guide design of the injectors and engine.

Major research efforts were also conducted using oxygenated fuels OME and methanol during FY 2022. While there was not sufficient space to review these results in this report, an initial summary of results is provided in the key publication and papers, as well as in the list below.

Overall, the major findings and accomplishments for FY 2022 in sprays and spray combustion include:

- Development of operation in a heated flow pressure vessel for optical diagnostics from multiple viewing angles to assess combustion from practical fuel injectors.
- Quantification of liquid and vapor radial and axial penetration from individual plumes of a novel four-hole chicken-foot injector under non-reacting, vaporizing conditions, as a baseline for understanding combustion.
- Plume-to-plume interaction produces lift-off lengths that are shorter than those of isolated plumes, thereby increasing soot formation.
- Soot-free combustion occurs when using OME and methanol at ambient temperatures as high as 1,200 K, where lift-off lengths are short and fuel-rich combustion occurs.

The experimental data are widely available to improve CFD models used to optimize future off-road engines that utilize sustainable/renewable fuels.

Key Publications

1. Tagliante, F., T.M. Nguyen, M.P. Dhanji, H.S. Sim, L.M. Pickett, J. Manin, G. Kukkadapu, R. Whitesides, and K. Wan. 2022. “The Role of Cool-Flame Fluctuations in High-Pressure Spray Flames, Studied Using High-Speed Optical Diagnostics and Large-Eddy Simulations.” *Proceedings of the Combustion Institute*. https://doi.org/10.1016/j.proci.2022.07.242.

2. Nguyen, T.M., R.N. Dahms, L.M. Pickett, and F. Tagliante. 2022. “The Corrected Distortion Model for Lagrangian Spray Simulation of Transcritical Fuel Injection.” *International Journal of Multiphase Flow* 148: 103927 (March). https://doi.org/10.1016/j.ijmultiphaseflow.2021.103927.

3. Oh, H., J. Hwang, L. White, L.M. Pickett, and D. Han. 2022. “Spray Collapse Characteristics of Practical GDI Spray for Lateral-Mounted GDI Engines.” *International Journal of Heat and Mass Transfer* 190: 122743 (July). https://doi.org/10.1016/j.ijheatmasstransfer.2022.122743.

References

1. Sandia National Laboratories. Engine Combustion Network data archive. Accessed 2022. https://ecn.sandia.gov/.

2. Wiesmann, F., L. Strauß, S. Rieß, J. Manin, K. Wan, and T. Lauer. 2022. “Numerical and Experimental Investigations on the Ignition Behavior of OME.” *Energies* 15, no. 18: 6855. https://www.mdpi.com/1996-1073/15/18/6855.

3. Maes, N., S.A. Skeen, M.B. Russell, P. Fitzgerald, L-M Malbec, G. Bruneaux, L.M. Pickett, K. Yasutomi, and G. Martine. 2020. "Spray Penetration, Combustion, and Soot Formation Characteristics of the ECN Spray C and Spray D Injectors in Multiple Combustion Facilities." *Applied Thermal Engineering* 172: 115136 (May). https://doi.org/10.1016/j.applthermaleng.2020.115136.

4. Malbec, L., and G. Bruneaux. 2010. "Study of Air Entrainment of Multi-Hole Diesel Injection by Particle Image Velocimetry – Effect of Neighboring Jets Interaction and Transient Behavior after End of Injection." *SAE International Journal of Engines* 3, no. 1: 107–123. https://doi.org/10.4271/2010-01-0342.

Acknowledgements

The author would like to thank Julien Manin, Zach Buen, Tyler Strickland, Kevin Wan, Logan White, Meghna Dhanji, Fabien Tagliante, Tuan Nguyen, Nathan Harry, and Aaron Czeszynski for their contribution to this research and/or their technical support. We thank Cummins Inc. for providing the research diesel injector to the entire Engine Combustion Network. The experiments and analyses were performed at the Combustion Research Facility of Sandia National Laboratories, California.

Sandia National Laboratories is a multi-mission laboratory managed and operated by National Technology and Engineering Solutions for Sandia LLC, a wholly owned subsidiary of Honeywell International, Inc., for the U.S. Department of Energy's National Nuclear Security Administration under contract DE-NA0003525.

I.17 Low-Life-Cycle Carbon Fuel Combustion and Emission Models (Lawrence Livermore National Laboratory)

Scott W. Wagnon, Principal Investigator
Lawrence Livermore National Laboratory
P.O. Box 808, L-372
Livermore, CA 94550
Email: Wagnon1@llnl.gov

Gurpreet Singh, DOE Program Manager
U.S. Department of Energy
Email: Gurpreet.Singh@ee.doe.gov

Start Date: October 1, 2021 End Date: September 30, 2022
Project Funding: $450,000 DOE share: $450,000 Non-DOE share: $0

Project Introduction

Transportation is the largest source of greenhouse gas emissions from any economic sector. Transportation also accounts for 50% of the U.S. energy expenditures and contributes to local pollution issues with combustion products such as soot and nitrogen oxides (NO_x). While light-duty passenger vehicles may readily take advantage of renewable electricity, difficult-to-decarbonize markets such as off-road, rail, marine, and aviation need lowlife-cycle carbon fuels (LLCFs) to reach zero net greenhouse gas emissions. Literature studies indicate the available biomass may sustain the future fuel needs for off-road, rail, marine, and aviation markets. However, major advances are still necessary to reduce the cost and carbon intensity of the conversion processes to create market-driven paths to decarbonization. Given the uncertainties surrounding full-scale adoption of LLCFs in the hard-to-electrify markets, there is a need to develop accurate fuel chemistry models for use by industry designers. Accuracy is particularly important for predicting the expected NO_x and sooting tendencies of an LLCF, as these emissions can have severe impacts on local air quality, contributing to the inherent environmental injustice plaguing our current transportation systems.

Objectives

The objectives of this investigation are as follows:

- Develop predictive kinetic models for the combustion of LLCF components and mixtures with LLCF components that span near-term to long-term decarbonization goals.
- Develop predictive kinetic models for emissions, such as soot and NO_x, from the combustion of LLCFs.

Approach

Typically, diesel and Jet A/A-1 are the fuels currently utilized in the U.S. transportation markets of off-road, rail, marine, and aviation. These fuels are complex mixtures containing several hundred components, the majority of which are relatively large hydrocarbons with more than eight carbon atoms. In the long term, these markets may adopt LLCFs, such as hydrogen and ammonia, that comprise smaller components and no carbon content. However, relatively more mature production pathways exist at scale for LLCFs such as renewable diesel and sustainable aviation fuels. In the near term, it is also likely that conventional fuels will be blended with LLCFs. The components of conventional fuels and LLCFs can be grouped into chemical classes including n-alkanes, iso-alkanes, cyclo-alkanes, and aromatics. Then, detailed chemical kinetic models can be developed for these selected components. These component models are subsequently merged to produce a surrogate fuel model that can simulate important fuel properties and emissions. This approach creates realistic surrogate fuels that can reproduce experimental behavior of the practical real fuels that they represent. Detailed kinetic models

for surrogate fuels and their emissions can then be simplified as needed for inclusion in multidimensional computational fluid dynamics simulations of engine combustion.

Results

Kinetic Modeling of LLCF Components and Mixtures

Normal and branched alkanes are often used as surrogate fuel components for conventional fuels and LLCFs [1], [2], [3], [4]. The kinetic models for normal alkane components were most recently updated in [1]. However, LLCFs such as renewable diesel and synthetic paraffinic kerosene for the aviation market also feature significant amounts of lightly branched alkanes. For Fiscal Year 2022, the development of kinetic models for LLCF components and mixtures has focused on improving kinetic models for 2-methyl alkanes as potential surrogate fuel components. In previous work at Lawrence Livermore National Laboratory (LLNL), researchers developed kinetic models for 2-methyl alkanes containing seven to 20 carbon atoms [2]. Since the kinetic model of Sarathy, et al. [2] was published, additional experimental and theoretical studies have significantly advanced our understanding of the combustion chemistry of lightly branched alkanes. Work in this fiscal year was devoted to updating kinetic rate constants, thermochemical properties, and transport properties of the 2-methyl alkanes.

Over 6,500 species from Wang, et al. and Sarathy were merged into a single detailed kinetic model containing over 11,000 species and 40,000 reactions [1], [2]. Of these species, approximately 4,500 species were unique to the 2-methyl alkane components. The 2-methyl alkane components required updated thermodynamic and transport properties to be self-consistent with the n-alkanes from Wang [1]. Given the nature of the kinetic model's size, publicly available and in-house automated codes were employed to estimate new parameters for thermodynamic and transport properties of the species in the 2-methylalkane kinetic models. The codes were used to estimate new properties after updating critical information such as group additivity values used for thermodynamic property estimates to LLNL's established values. Reaction rate constant rules consistent with Wang's findings were also adopted for 21 reaction classes for the surrogate fuel components 2-methylheptane and 2-methyloctane [1]. Updates to the rate constant rules for the 2-methylalkanes with 10–20 carbon atoms will be completed in the next fiscal year, with the understanding that future research is subject to change based on funding levels.

When available, measurements from fundamental experimental facilities such as shock tubes, burners, and jet-stirred reactors were used to validate the updated kinetic models. For example, autoignition and laminar flame speed measurements are available for the surrogate component 2-methylheptane [2]. Ignition delay time measurements provide valuable insights into the autoignition timing and heat release rates associated with fuel–air mixtures. Figure I.17.1 shows validation comparisons of the 2-methylheptane kinetic model against ignition delay time measurements from Sarathy's work [2]. The updated kinetic model is typically within a factor of two of the measurements, which is considered acceptable agreement. Further improvements to the kinetic model may be achieved by further optimizing the rate constant rules for 2-methyl alkanes and improving kinetic models for intermediate species such as olefins. Modeling flame initiation, stabilization, and propagation are also critical aspects of simulating combustion processes well in engines and turbines. Therefore, it is also desirable to validate the chemical kinetic models for diesel fuel and jet fuel components against flame measurements such as laminar flame speeds. Presented in Figure I.17.2 are measured laminar flame speeds of 2-methylheptane in air reported by Sarathy at 353 K and 1 atm with simulations using the detailed kinetic model updated by LLNL this fiscal year [2]. The updated kinetic model is typically within 10% of the measurements up to an equivalence ratio of 1.1, which is considered acceptable agreement. The simulations for richer mixtures are typically faster than the measurements by up to 20%. It is anticipated the simulations would be slower, and in better agreement with the reported measurements, if multicomponent diffusion coefficients and radiation heat transfer effects were considered. However, these refinements are computationally expensive even for 1D simulations, prohibitive when using the full detailed kinetic model, and were not included at this time.

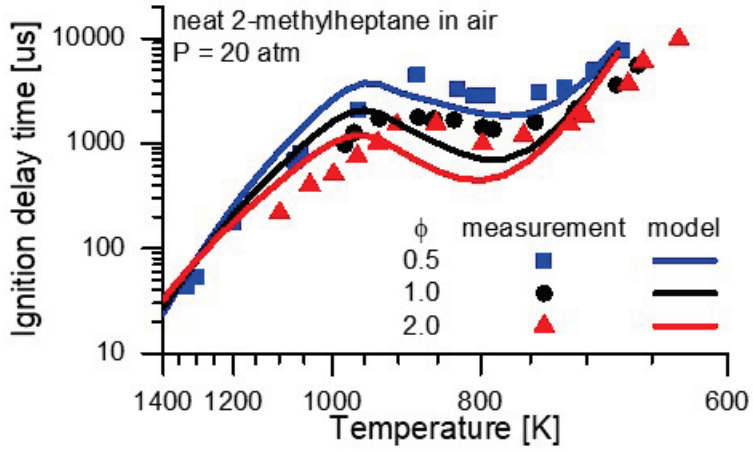

Figure I.17.1 Autoignition measurements [2] and simulations of 2-methylheptane. Simulated ignition delay times for neat 2-methylheptane in air use a detailed kinetic model from LLNL, containing 11,183 species and 41,078 reactions, over equivalence ratios of 0.5–2.0 at 20 atm.

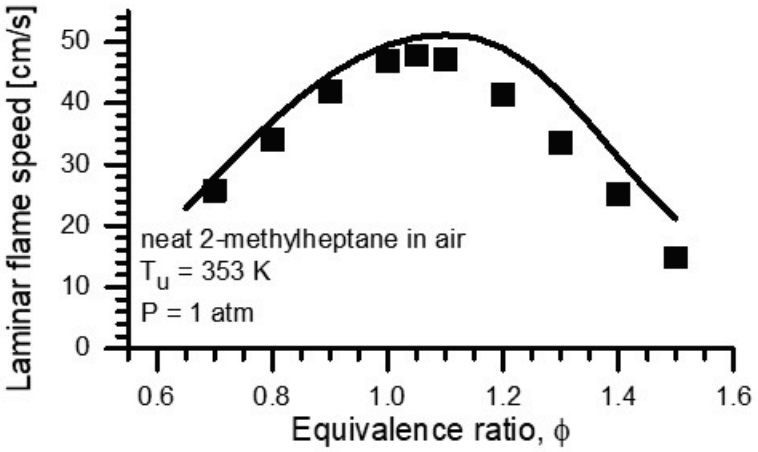

T_u – unburnt gas temperature; P – pressure

Figure I.17.2 Laminar flame speed measurements [2] and simulations of 2-methylheptane. Simulated laminar flame speeds for neat 2-methylheptane in air use a detailed kinetic model from LLNL, containing 11,183 species and 41,078 reactions, over equivalence ratios of 0.65–1.5 at 1 atm.

Kinetic Modeling for LLCF Emissions

For Fiscal Year 2022, project researchers selected two surrogate fuel components, n-dodecane and iso-dodecane, to improve the polycyclic aromatic hydrocarbon (PAH) and soot kinetic modeling efforts. The combustion chemistry of n-dodecane and iso-dodecane has been previously studied in the literature. However, soot formation of these two surrogate components has not been significantly explored. In collaboration with Professor Sung's group at the University of Connecticut, LLNL researchers developed and validated a predictive soot model for dodecane flames this fiscal year. A detailed kinetic model developed at LLNL for the formation of PAH [5] was extended to predict soot formation and growth. The developed soot model is based on the discrete sectional method. Following a similar methodology to that outlined in Saggese et al. [6], heavy PAHs and soot particles were discretized into 20 sections of lumped species labeled BINn, where n varies from one to 20. There are 20 carbon atoms in BIN1 and 10 million in BIN20. Currently, a single hydrogen-to-carbon ratio for the BINn species has been implemented, which greatly reduces the number of species and reactions in the model. Kinetic parameters for important reaction classes such as H-atom abstraction and acetylene addition, PAH addition to BIN surfaces, BIN coalescence, and aggregation were taken from

literature studies. The developed soot model was validated with experimental data obtained in a counterflow burner facility at the University of Connecticut under atmospheric pressure conditions using a laser-induced incandescence technique combined with a light extinction method to measure the soot volume fraction (SVF). The soot model has also been validated against lighter fuel components such as ethylene, n-heptane, and iso-octane, indicating that the current kinetic model is applicable to other fuel components. To study the effect of alkane branching on soot formation in non-premixed counterflow flames, n-dodecane and iso-dodecane were studied as neat components and as binary dodecane isomer blends with an iso-dodecane liquid volume fraction ranging from 0.25 to 0.95 (balance n-dodecane). For all measurements, a stoichiometric mixture fraction was maintained below 0.5, i.e., soot formation flames were studied. The use of these mixtures maintains conditions such that the influence of soot particle oxidation processes is considered minor, unlike in soot formation oxidation flames. Figure I.17.3 shows examples of the measurements and simulations of the peak SVF for three dodecane fuel–air mixtures. In Figure I.17.3, the developed soot model underpredicts the measurements by a factor of three or less, which is typical of other cases studied and is considered acceptable. Using the detailed kinetic model, it is possible to explain trends in the peak SVF as a function of the blending ratio between n-dodecane and iso-dodecane. Intermediate species formed during the high-temperature decomposition of n-dodecane primarily lead to high concentrations of ethylene, while iso-butene is produced at significantly higher levels from iso-dodecane. Both ethylene and iso-butene can react further to form propargyl radicals, which quickly self-react to form benzene. Benzene is considered a foundational aromatic ring that leads to soot in combustion processes. However, the rate of propargyl radical formation from iso-butene is faster than that of ethylene. Therefore, the concentration of propargyl radicals is significantly higher in mixtures with more iso-dodecane than n-dodecane. The influence of iso-dodecane on propargyl radical formation directly leads to the increased formation of benzene and higher levels of peak SVF.

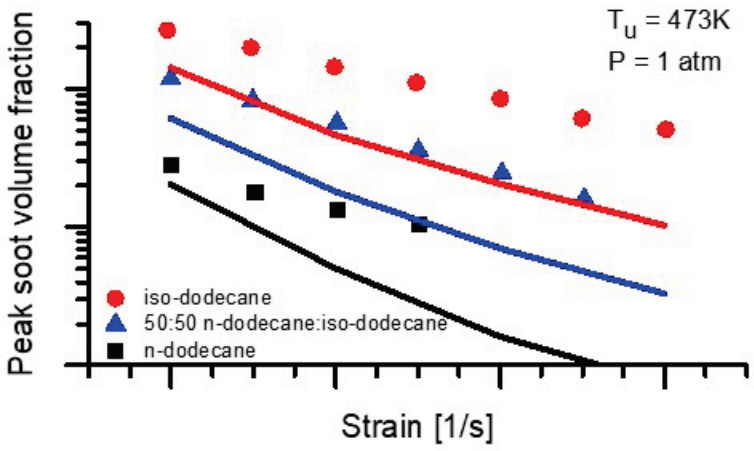

Figure I.17.3 Peak SVF measurements by the University of Connecticut and simulations using the LLNL detailed PAH and soot kinetic model for counterflow flames of neat n-dodecane, neat iso-dodecane, and a 50:50 mixture of the two isomers. Horizontal and vertical axis values are unlabeled, as the measurements are currently unpublished.

Conclusions

- A detailed kinetic model for large 2-methyl alkanes was merged, updated, and validated against targets such as ignition delay times and laminar flame speeds to extend the palette of surrogate fuel components available for modeling complex renewable diesel and sustainable aviation fuels.

- A kinetic model for soot formation was improved and validated against fundamental measurements of SVF from counterflow flame experiments with neat mixtures and binary blends of n-dodecane and iso-dodecane.

Key Publications

1. Richter, Sandra, Goutham Kukkadapu, Charles K. Westbrook, Marina Braun-Unkhoff, Clemens Naumann, Markus Köhler, and Uwe Riedel. 2022. "A Combined Experimental and Modeling Study of Combustion Properties of an Isoparaffinic Alcohol-to-Jet Fuel." *Combustion and Flame* 240: 111994. https://doi.org/10.1016/j.combustflame.2022.111994.

References

1. Wang, Mengyuan, Goutham Kukkadapu, Kuiwen Zhang, Scott W. Wagnon, Marco Mehl, William J. Pitz, Charles K. Westbrook, and Chih-Jen Sung. 2020. "Autoignition of CRC Diesel Surrogates at Low Temperature Combustion Conditions: Rapid Compression Machine Experiments and Modeling." *Combustion and Flame* 219: 178–197. https://doi.org/10.1016/j.combustflame.2020.05.017

2. Sarathy, S. Mani, Charles K. Westbrook, Marco Mehl, William J. Pitz, Casimir Togbe, Philippe Dagaut, Hai Wang, et al. 2011. "Comprehensive Chemical Kinetic Modeling of the Oxidation of 2-Methylalkanes from C7 to C20." *Combustion and Flame* 158, no. 12: 2338–2357. https://doi.org/10.1016/j.combustflame.2011.05.007.

3. Cowart, Jim, Michael Raynes, Len Hamilton, Dianne Luning Prak, Marco Mehl, and William Pitz. 2014. "An Experimental and Modeling Study into Using Normal and Isocetane Fuel Blends as a Surrogate for a Hydroprocessed Renewable Diesel Fuel." *Journal of Energy Resources Technology* 136, no. 3. https://doi.org/10.1115/1.4027408.

4. Richter, Sandra, Goutham Kukkadapu, Charles K. Westbrook, Marina Braun-Unkhoff, Clemens Naumann, Markus Köhler, and Uwe Riedel. 2022. "A Combined Experimental and Modeling Study of Combustion Properties of an Isoparaffinic Alcohol-to-Jet Fuel." *Combustion and Flame* 240: 111994. https://doi.org/10.1016/j.combustflame.2022.111994.

5. Kukkadapu, G., S.W. Wagnon, W.J. Pitz, and N. Hansen. 2021. "Identification of the Molecular-Weight Growth Reaction Network in Counterflow Flames of the C_3H_4 Isomers Allene and Propyne." *Proceedings of the Combustion Institute* 38, no. 1: 1477–1485. https://doi.org/10.1016/j.proci.2020.07.130.

6. Saggese, Chiara, Sara Ferrario, Joaquin Camacho, Alberto Cuoci, Alessio Frassoldati, Eliseo Ranzi, Hai Wang, and Tiziano Faravelli. 2015. "Kinetic Modeling of Particle Size Distribution of Soot in a Premixed Burner-Stabilized Stagnation Ethylene Flame." *Combustion and Flame* 162, no. 9: 3356–3369. https://doi.org/10.1016/j.combustflame.2015.06.002.

Acknowledgements

LLNL performed this work under the auspices of the U.S. Department of Energy under Contract DE-AC52-07NA27344.

Contributors from LLNL include the following: Tanusree Chatterjee, Goutham Kukkadapu, Simon Lapointe, Matthew J. McNenly, Chiara Saggese, and Russell Whitesides.

I.18 Advanced and Low-Temperature Emissions Control – Low-Temperature Oxidation (Pacific Northwest National Laboratory)

Yong Wang, Principal Investigator
Pacific Northwest National Laboratory
902 Battelle Boulevard
Richland, WA 99354
Email: Yong.Wang@pnnl.gov

Siddiq Khan, DOE Technology Manager
U.S. Department of Energy
Email: Siddiq.Khan@ee.doe.gov

Start Date: October 1, 2021 End Date: September 30, 2022
Project Funding: $150,000 DOE share: $150,000 Non-DOE share: $0

Project Introduction

Advanced engine control, fuel injection, and combustion strategies have significantly lowered engine-out exhaust emission levels of internal combustion engines. However, persistent particulate matter and nitrogen oxides emissions, coupled with carbon monoxide and hydrocarbon emissions specific to advanced combustion, require improved catalytic emission control systems. These emission control systems are necessary to enable advanced, high-efficiency combustion strategies while minimizing the vehicle-level energy penalty associated with attaining applicable emissions standards.

Objectives

The overarching goal of this project is to help advance aftertreatment catalyst technology with high durability and low-temperature activity applicable to internal combustion engine exhaust systems deployed throughout the United States. Project support will take the form of providing the fundamental knowledge and understanding essential to advancing this technology. Specifically, this project is focused on developing the fundamental information that clarifies current barriers to aftertreatment materials and enables the pursuit of pathways to mitigate or circumvent those barriers through materials design. The desired outcomes of these efforts are to (1) understand the function of aftertreatment devices at the atomic, nano, and micro scales and (2) predict the integrated performance of system designs considered. Findings will enhance the ability of industry (across multiple markets, including off-road vehicles and equipment, rail, and marine) to offer the highest possible fuel efficiencies while meeting applicable mandated and upcoming emissions standards. Collectively, these efforts will protect the global climate, reduce U.S. dependence on foreign oil, and maintain U.S. competitiveness.

Specific objectives include:

- Developing new classes of thermally stable single-atom catalysts to reduce the use of platinum group metals for low-temperature oxidation.
- Improving the performance and stability of next-generation oxidation catalysts so that engines with dramatically enhanced fuel efficiencies can be implemented while still meeting future U.S. Environmental Protection Agency emissions regulations.

Approach

This project builds off Pacific Northwest National Laboratory's strong base in fundamental sciences by effectively leveraging capabilities from the Institute for Integrated Catalysis and the Environmental Molecular Sciences Laboratory. The Institute for Integrated Catalysis is the largest non-industrial catalysis organization in the United States, and the Environmental Molecular Sciences Laboratory is a U.S. Department of Energy

(DOE) scientific user facility located at Pacific Northwest National Laboratory. The project team collaborates closely with industry partners (BASF, John Deere, Caterpillar, and Kymanetics, Inc.) to address the important science questions of broad interest to industry. The project is strongly oriented toward working closely with industry to address fundamental issues with broad impacts on applications and commercialization.

Results

- Thermally stable Cu single-atom catalysts are active for CO oxidation and have the potential to replace or reduce the usage of platinum group metals for low-temperature oxidation.
- The enhanced activity of single-atom Cu catalysts is due to the facile modulation of the Cu charge state through facile charge transfer between active site and support.

Requiring catalysts to be both active and stable over long periods of time under variable reaction conditions, including high and low temperatures, is a daunting challenge due to the almost mutual exclusivity of these constraints. Using CO oxidation as a probe reaction, we demonstrate that thermally stable single-atom Cu catalysts prepared by high-temperature synthesis (atom trapping [1]) on ceria can achieve this feat by allowing modulation of the Cu charge state through facile charge transfer between active site and support.

Here, polyhedral CeO_2 support was prepared by thermal decomposition of Cerium(III) nitrate hexahydrate ($Ce(NO)_3 \cdot 6H_2O$ 99% purity from Sigma-Aldrich) in air at 350°C for 2 hours. The particle size was maintained between 0.149–0.125 mm with the use of 100 and 120 mesh number sieves. The Cu/CeO_2 catalysts of 0.37, 1, 2, 3, 6, and 10 wt% of Cu content were prepared by incipient wetness impregnation of Copper(II) nitrate trihydrate ($Ce(NO)_3 \cdot 6H_2O$ from Sigma-Aldrich) on the polyhedral ceria. After impregnation, the catalysts were dried in air at 150°C for 1 hour and, in the cases of 6 and 10 wt% Cu content, cooled down to room temperature for a second impregnation. Subsequently, the project performed calcination at 350°C, 600°C, 700°C, and 800°C (calcination at 800°C is referred to also as atom trapping [1]) for 10 hours at a heating rate of 10°C/min.

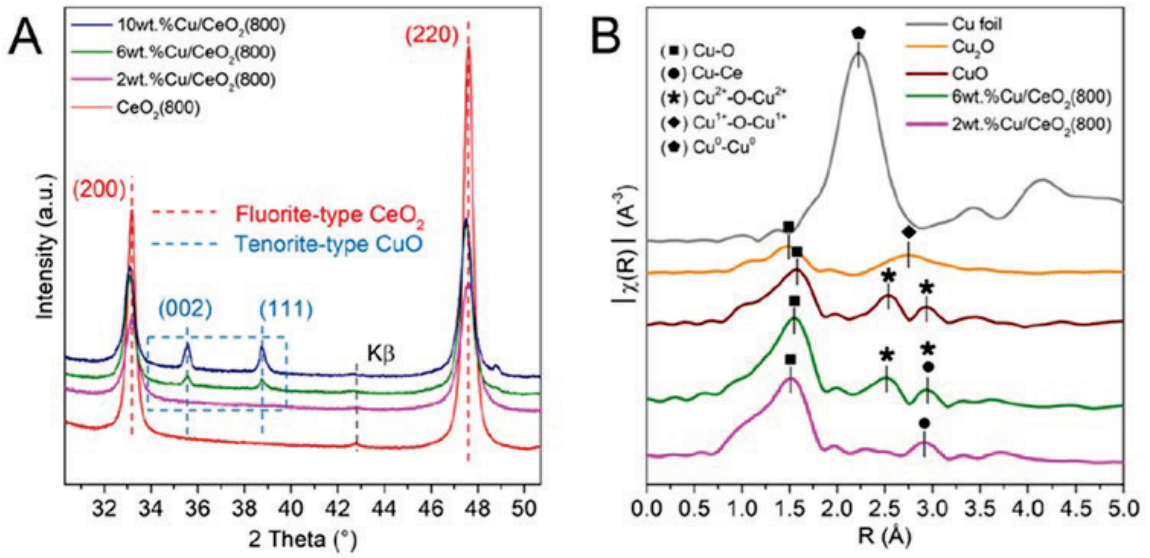

Figure I.18.1 (a) XRD patterns of Cu/CeO_2 prepared via high-temperature calcination (800°C) at different loadings, along with CeO_2 reference calcined at the same temperature (800°C). (b) EXAFS of the Cu/CeO catalyst with 0.37–6 wt% calcined at 800°C and Cu references.

As shown in Figure I.18.1., at a loading of 2 wt% Cu on ceria, there are no x-ray diffraction (XRD) peaks corresponding to the CuO phase. At 6 wt% Cu, the CuO peaks start to show up in the XRD pattern (Figure I.18.1a), and the extended x-ray absorption fine structure (EXAFS) data also show that a Cu-O-Cu bond is

detected (Figure I.18.1b). The nature of the second shell atoms is critical for tuning the reactivity of the Cu atoms. The Cu single-atom catalyst shows the highest reactivity for CO oxidation, while the phase-segregated CuO is much less active. Atom trapping enhances the CO oxidation reactivity of $Cu_1@CeO_2$ because of the improved total and dynamic oxygen storage capacity (OSC) at low temperatures (150°C), measured by U.S. DRIVE protocol [2] or using a dynamic OSC procedure reported in the literature [3] (see Table I.18.1).

Our density functional theory calculations further suggest that the modulation of the Cu charge state through facile charge transfer between active site and support provides the catalysts with the ability to activate either lattice or adatom oxygen atoms, accessing additional reaction channels as the catalyst environment changes. Such adaptability allows dynamic response of such catalysts, enabling them to remain active under variable reaction conditions. The inherent stability of the catalyst arises from the enhanced strength of the Cu-O interactions established by high-temperature synthesis, i.e., atom trapping, and the catalyst remains stable even as the Cu oxidation state varies, effectively halting sintering and deactivation. As shown here, one can circumvent the dilemma of designing catalysts that are simultaneously active and stable by matching the redox properties of the active site and support and establishing an environmental adaptability in the active sites.

Table I.18.1 OSC in 2 wt% $Cu@CeO_2$ Measured by Both U.S. DRIVE Protocol and Dynamic OSC Method (in Parentheses)

Catalysts	Surface area (m^2/g)	OSC at 550°C (μmol/g)	OSC at 350°C (μmol/g)	OSC at 150°C (μmol/g)
CeO_2 (800)	26.3	211	135	0
2wt% $Cu@CeO_2$	39.2	744	483 (149)	249 (98)

Conclusions

- Low-temperature CO oxidation over Cu_1/CeO_2 proceeds via Cu single-atom active sites trapped at step defects, with Cu-O-Ce being the primary active oxygen species, in the form of both lattice oxygen and oxygen adatoms.
- Cu cycles between 2+ and 1+ oxidation states during its primary catalytic cycle (the "Cu-Dioxygen" cycle) with mostly CO-Cu^{2+} making up the putative most abundant surface intermediate.
- The remarkable robustness of this catalyst results from strong anchoring of Cu to step defects and its ability to adapt to changes in thermodynamic conditions while always manifesting a viable low-temperature route for CO oxidation.

Key Publications

1. Xiong, X., D. Kunwar, D. Jiang, C.E. García-Vargas, H. Li, C. Du, G. Canning, X.I.P. Hernández, Q. Wan, S. Lin, S.C. Purdy, J.T. Miller, K. Leung, S.S. Chou, H.H. Brongersma, R. ter Veen, J. Huang, H. Guo, Y. Wang, and A.K. Datye. 2021. "Engineering Catalyst Supports to Stabilize Pd/PdO Two-Dimensional Rafts for Water-Tolerant Methane Oxidation." *Nature Catalysis* 4: 830–839.

2. Lin, F., K. Rappé, L. Kovarik, M. Song, X.S. Li, M. Engelhard, and Y. Wang. 2022. "Effects of High-Temperature CeO_2 Calcination on the Activity of Pt/CeO_2 Catalysts for Oxidation of Unburned Hydrocarbon Fuels." *Catalysis Science & Technology* 12: 2462–2470.

3. Jiang, D., Y. Yao, T. Li, G. Wan, X.I. Pereira-Hernández, Y. Lu, J. Tian, K. Khivantsev, M.H. Engelhard, C. Sun, C.E. García-Vargas, A.S. Hoffman, S.R. Bare, A.K. Datye, L. Hu, and Y. Wang. 2021. "Tailoring the Local Environment of Platinum in Single-Atom $Pt1/CeO_2$ Catalysts for Robust Low-Temperature CO Oxidation." *Angewandte Chemie International Edition* 60: 26054–26062.

4. Khivantsev, K., N.R. Jaegers, H.A. Aleksandrov, L. Kovarik, M.A. Derewinski, Y. Wang, G.N. Vayssilov, and J. Szanyi. 2021. "Biomimetic CO Oxidation below -100°C by a Nitrate-Containing Metal-Free Microporous System." *Nature Communications* 12: 6033. https://doi.org/10.1038/s41467-021-26157-3.

References

1. Jones, J., H.F. Xiong, A.T. Delariva, E.J. Peterson, H. Pham, S.R. Challa, G.S. Qi, S. Oh, M.H. Wiebenga, X.I.P. Hernandez, Y. Wang, and A.K. Datye. 2016. "Thermally Stable Single-Atom Platinum-on-Ceria Catalysts via Atom Trapping." *Science* 353, no. 6295: 150–154.

2. Rappe, K., Craig DiMaggio, Josh A. Pihl, Joseph R. Theis, Se H. Oh, Galen B. Fisher, Jim Parks, Vencon G. Easterling, Ming Yang, Mark L. Stewart, and Kenneth C. Howden. 2019. "Aftertreatment Protocols for Catalyst Characterization and Performance Evaluation: Low-Temperature Oxidation, Storage, Three-Way, and NH_3-SCR Catalyst Test Protocols." *Emission Control Science and Technology* 5: 183–214.

3. Theis, J.R. 1996. "An Engine Test to Measure the Oxygen Storage Capacity of a Catalyst." *SAE Transactions* 105: 1226–1235.

Acknowledgements

We acknowledge continuous support and advice from DOE program managers Gurpreet Singh and Siddiq Khan.

I.19 Advanced and Low-Temperature Emissions Control – NO_x Reduction (Pacific Northwest National Laboratory)

Yong Wang, Principal Investigator
Pacific Northwest National Laboratory (PNNL)
902 Battelle Boulevard
Richland, WA 99354
Email: yong.wang@pnnl.gov

Siddiq Khan, DOE Technology Manager
U.S. Department of Energy
Email: Siddiq.Khan@ee.doe.gov

Start Date: October 1, 2021 End Date: September 30, 2022
Project Funding: $200,000 DOE share: $200,000 Non-DOE share: $0

Project Introduction

Advanced engine control, fuel injection, and combustion strategies have significantly lowered engine-out exhaust emission levels of internal combustion engines. However, persistent particulate matter (PM) and nitrogen oxides (NO_x) emissions, coupled with the unique CO and hydrocarbon (HC) emissions challenge of advanced combustion, require improved catalytic emission control systems. These emission control systems are necessary to enable advanced, high-efficiency combustion strategies while minimizing the vehicle-level energy penalty associated with attaining applicable emissions standards.

Objectives

The overarching goal of this project is to provide the fundamental knowledge and understanding that is essential in advancing aftertreatment catalyst technology with high durability and low-temperature activity applicable to internal combustion engine exhaust systems deployed throughout the United States.

This project is focused on developing the fundamental information that clarifies current barriers to aftertreatment materials and enables the pursuit of pathways to mitigate or circumvent those barriers through materials design. The desired outcomes of these efforts are to (1) understand the function of aftertreatment devices at the atomic-, nano-, and micro-scales, and (2) predict the integrated performance of system designs considered. This will enhance the ability of industry (across multiple markets, including off-road vehicles and equipment, rail, and marine) to offer the highest possible fuel efficiencies while meeting applicable mandated and upcoming emissions standards. Collectively, these efforts will protect global climate, reduce U.S. dependence on foreign oil, and maintain U.S. competitiveness. Specific objectives include:

- Demonstrating and establishing the structure-function relation of next generation selective catalytic reduction (SCR) catalyst technologies with superior SCR performance and hydrothermal stability.
- Developing the necessary fundamental and applied understanding of barriers faced by current generation SCR materials so that their function can be accurately predicted through full useful life.

Approach

This project builds on PNNL's strong foundation in fundamental sciences by effectively leveraging capabilities from the Institute for Integrated Catalysis and the Environmental Molecular Sciences Laboratory. The Institute for Integrated Catalysis is the largest non-industrial catalysis organization in the United States, and the Environmental Molecular Sciences Laboratory is a U.S. Department of Energy scientific user facility located at PNNL. The project team closely collaborates with industries (BASF; John Deere; Caterpillar; Kymanetics, Inc.) to address the important scientific questions of broad interest to industries. The project is strongly

oriented towards addressing fundamental issues of broad impact to applications and commercialization by closely working with industries.

Results

- A series of seven Cu/SSZ-13 catalysts with Si/Al = 6.7 are used to elucidate key rate-controlling factors during low-temperature standard ammonia selective catalytic reduction (NH_3-SCR), via a combination of SCR kinetics and operando electron paramagnetic resonance (EPR) spectroscopy.

- Strong Cu-loading-dependent kinetics, with Cu atomic efficiency increasing nearly an order of magnitude, is found when per hexagonal unit cell occupancy for Cu-ion increases from ~0.1 to ~1.0. This is due mainly to the release of intercage Cu transfer constrains that facilitates the redox chemistry, as evidenced from detailed Arrhenius analysis.

- Operando EPR spectroscopy studies reveal strong connectivity between Cu-ion dynamics and SCR kinetics, which leads to the conclusion that under low-temperature steady-state SCR, the kinetically most-relevant Cu species are those with the highest intercage mobility. Transient binuclear Cu species are mechanistically relevant species, but their splitting and cohabitation are indispensable for low-temperature kinetics.

Seven Cu/SSZ-13 catalysts (Si/Al = 6.7), denoted as Cu-1 to Cu-7 in a Cu-loading increasing manner, were synthesized via solution ion exchange. Table I.19.1 presents Cu quantification results, i.e., total Cu loading by ICP-AES and isolated Cu^{II}-ion content by EPR and hydrogen temperature programmed reduction (H_2-TPR). Based on the total Cu contents by inductively coupled plasma-atomic emission spectrometer (ICP-AES), Cu^{II}-ions per chabazite (CHA) cage ($T_{12}O_{24}$) were calculated, and the results are also tabulated in Table I.19.1.

Table I.19.1 Cu Quantification Results for the Cu/SSZ-13 Catalysts

Sample	Total Cu content by ICP (wt%)	Isolated Cu-ion by H2-TPR (wt%)	Isolated Cu-ion by EPR (wt%)	Cu-ion per chabazite cage
Cu-1	0.16	0.20	0.17	0.02
Cu-2	0.35	0.39	0.36	0.04
Cu-3	0.64	0.66	0.64	0.07
Cu-4	0.87	0.91	0.90	0.10
Cu-5	1.28	1.29	1.15	0.14
Cu-6	2.43	2.26	2.27	0.26
Cu-7	2.75	2.72	2.58	0.30

Figure I.19.1a presents standard SCR steady-state light-off curves for the seven catalysts, measured at a gas hourly space velocity (GHSV) of ~2×10^5 h^{-1}. From Cu-1 to Cu-6, low-temperature (< 250°C) NO_x conversion gradually increases with increasing Cu loading. Cu-7 displays very similar NO_x conversions as Cu-6. Above ~400°C, all samples show NO_x conversions ≥90%. Such a high SCR selectivity is consistent with the lack of CuO cluster in these samples; CuO cluster is known to catalyze NH_3 oxidation by O_2 ($4NH_3 + 3O_2 = 2N_2 + 6H_2O$), which lowers high-temperature SCR selectivity [1]. Low-temperature NO_x conversion data in Figure I.19.1a are further analyzed using a first-order kinetic equation $r = \frac{F}{W}(-\ln(1-x))$, where F is the NO_x flow rate (moles of NO per second), W is the mass of the catalyst (g), and x is the NO_x conversion. The Arrhenius equation, $k = \frac{r}{[NOx]_0} = Ae^{\frac{-E_a}{RT}}$, is used for calculating rate constants k, pre-exponential factor (A) and apparent activation energy (E_a), where $[NO_x]_0$ is the molar concentration of NO_x in the feed [2], [3], [4]. Figure I.19.1b depicts the corresponding k vs. 1/T Arrhenius plots; based on which A and E_a values are derived.

Figure I.19.1c presents A values as a function of Cu loading. With increasing Cu^{II}-ion occupancy per CHA cage, A values rapidly increase and then plateau. Such a trend reflects rapid catalytic efficiency improvement as Cu loading increases (Figure I.19.1a). From the E_a versus Cu loading plots shown in Figure I.19.1d, E_a values also increase with increasing Cu loading, from ~40 kJ/mol at the lowest Cu occupancy, to ~80 kJ/mol as Cu occupancy approaches ~1/3 per CHA cage. Such Cu loading-dependent kinetic results are highly consistent with literature reports [4], [5].

Low-temperature catalytic efficiency is further compared among the seven samples at a temperature of 200°C. We chose this temperature for its technical importance; commercial Cu/zeolite SCR catalysts are required to display high efficiency at this temperature [6], [7]. From the light-off plots shown in Figure I.19.1a, however, NO_x conversions over most catalysts are already far beyond differential (<20%) at 200°C. To derive rates that are free from reactant mass transfer limitations, temperatures at which a 20% NO_x conversion is achieved on the various catalysts (i.e., T_{20}) are used for a simple rate extrapolation. This is based on a reasonable assumption that at 20% NO_x conversion, SCR over all catalysts is still free from reactant transfer limitations. By measuring such T_{20} from Figure I.19.1a and by applying E_a values derived from Figure I.19.1b, Arrhenius equation $\ln(\frac{r_1}{r_2}) = \frac{E_a}{R}(\frac{1}{T_2} - \frac{1}{T_1})$ is then used to calculate "kinetically controlled" rates at 200°C. EPR active Cu^{II}-ion contents from Table I.19.1 are used for the calculations. Atomic efficiency of the isolated Cu^{II} active sites displays three stages: a low efficiency stage at the lowest Cu loadings (<0.04 Cu per CHA cage), a high efficiency stage at the highest Cu loadings (>0.26 Cu per CHA cage), and a transition stage in between where turnover rate increases almost linearly with increasing Cu loading.

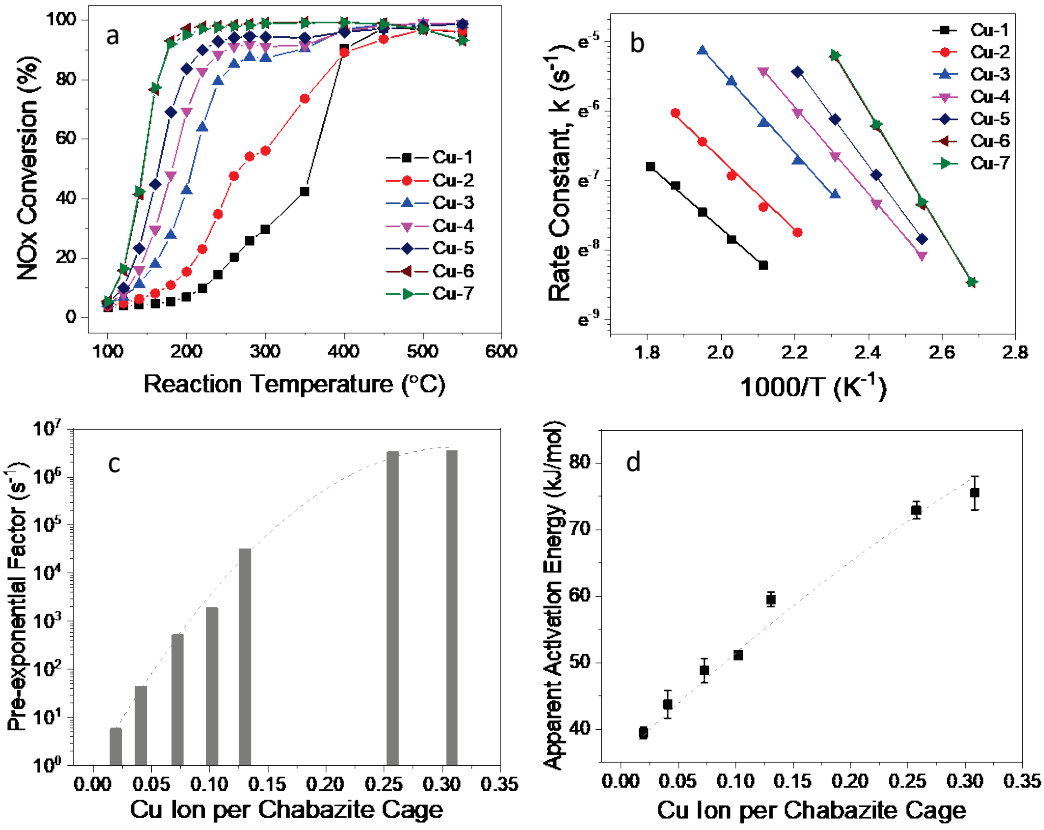

Figure I.19.1 (a) NO_x conversion as a function of reaction temperature for standard SCR on the seven Cu/SSZ-13 catalysts. The reactant feed contains 350 ppm NO_x (including ~10 ppm NO_2), 350 ppm NH_3, 2.5% H_2O, 10% O_2, and balanced N_2 at a GHSV of ~2×105 h-1. (b) Arrhenius plots derived using low-temperature NO_x conversion data shown in (a), corrected using first-order rate expression. (c) The corresponding pre-exponential factors derived from Arrhenius analysis. (d) The corresponding apparent activation energies derived from Arrhenius analysis. Dashed lines in (c) and (d) are a guide to the eye.

Operando EPR spectra were acquired under steady-state standard SCR conditions from 100°C to 350°C at a GHSV of ~4×10^5 h^{-1}. The operando EPR studies clearly demonstrate Cu loading and temperature dependences on the evolution of hyperfine and super-hyperfine spectra. Particularly, well-resolved fine structurers only appear on Cu^{II} species with low mobility, i.e., resolution of fine structures increases with increasing Cu-zeolite interactions but decreases with increasing Cu-Cu interactions (e.g., spin-spin coupling).

From the detailed kinetics and spectroscopic discussions above, rapid Cu^{II} dynamics, characterized by the lack of well-defined hyperfine or super-hyperfine structures, positively links to enhanced low-temperature (≤250°C) SCR rates. Regarding dynamics of isolated Cu^{I} species during low-temperature SCR, we note that EPR is "blind" to Cu^{I} species. Therefore, operando EPR here cannot provide direct information on their dynamics. However, it has been demonstrated previously via ab initio molecular dynamics [8] and in situ impedance spectroscopy measurements [9] that $Cu^{I}(NH_3)_2$ has higher mobility than any coexisting Cu^{II} species. Moreover, $Cu^{I}(NH_3)_2$ mobility appears to decrease in the presence of vicinal ZNH_4 [8], but increase with increasing Cu loading [9]. Based on these considerations, we postulate here that isolated Cu^{I} follows the same trend as isolated Cu^{II}, i.e., its mobility increases with increasing Cu density. Overall, increasing Cu occupancy (up to 1/3 Cu per CHA cage studied here) favor the formation of key reaction intermediates for both reduction half cycle and oxidation half cycle. As reflected in SCR kinetics, atomic efficiency of the Cu active centers increases almost an order of magnitude as Cu loading increases up to 1/3 Cu per CHA cage (Figure I.19.1b). Such a Cu mobility and atomic efficiency correlation leads to two important conclusions for low-temperature standard SCR: (1) when more mobile, e.g., $Cu^{II}(OH)(NH_3)_3$, and less mobile, e.g., $Cu^{II}(O_L)(NH_3)_3$, Cu^{II} species coexist, the more mobile ones must have stronger kinetic contribution; (2) any operation that leads to Cu mobility decrease, e.g., lowering Cu loading, hydrothermal aging of the catalyst, destabilizing $Cu^{II}(NH_3)_4$ or $Cu^{II}(OH)(NH_3)_3$, will decrease intercage transfer of Cu-ions, leading to decrease in SCR rate.

Standard SCR displays interesting kinetic behavior between ~250°C and ~350°C where reaction rate decreases with increasing temperature [4]. Based on the EPR, this is due at least partially to decreased Cu mobility as evidenced from the gradually loss of NH_3 ligands from the Cu active sites as temperature rises, causing more difficult Cu intercage transfer. Note also that we have shown in the past that adding alkali cations to low Cu-loaded Cu/SSZ-13 catalysts effectively boost low-temperature SCR rate. At least two reasons can be used to understand this effect. First, the presence of alkali cations weakens coulombic attractions between Cu-ions and zeolite support; second, alkali cations promote conversion of less mobile Z_2Cu^{II} to more mobile $ZCu^{II}OH$ by partially occupying paired Al exchange sites that Z_2Cu^{II} must need.

By assigning the most active Cu species to the most mobile Cu species capable of intercage transfer for low-temperature SCR, it is also important to realize that such species very likely are no longer present when gas phase NH_3 supply is cut off. Particularly, in the frequently applied titration measurements carried out on samples pre-dosed with NH_3, or transient titrations in the absence of gas phase NH_3, reactive Cu^{II} species are not necessarily the same as those under steady-state measurements. Therefore, one must be cautious in attempting to apply conclusions derived under transient titration conditions to steady-state measurements. For example, the "NH_3 inhibition effect" identified in Zhang, et al., and Marberger, et al., discovered from transient titration measurements is not extrapolatable to steady-state SCR [10], [11]. Low-temperature steady-state SCR typically displays a zero-order dependence on NH_3 pressure [5], [12] rather than a negative order anticipated from NH_3 inhibition, consistent with the kinetically relevant Cu^{II} sites under steady state being saturated with NH_3 ligands.

Conclusions

- Standard NH_3-SCR has a strong dependence on Cu loading in low-temperature (<250°C) kinetics. With increasing Cu loading from ~0.03 to ~0.3 Cu site per CHA cage, catalytic efficiency increases by nearly an order of magnitude. Based on detailed Arrhenius analysis, this is due primarily to the release of rate constrains from intercage transfer of SCR active Cu-ions.

- Operando EPR during steady-state standard NH_3-SCR reveal strong correlations between dynamics of NH_3-solvated Cu^{II} species and the resolution of hyperfine and super-hyperfine EPR features, where highly mobile status corresponds to poorly resolved fine structures. Mobility of NH_3-solvated Cu^{II} species increases with increasing Cu loading but decreases when such species lose NH_3 ligands.

- Such characteristics correlate nicely with SCR kinetics, demonstrating strong connectivity between atomic efficiency and intercage mobility of Cu active sites.

Key Publications

1. Wu, Y., Y. Ma, Y. Wang, K.G. Rappé, N.M. Washton, Y. Wang, E.D. Walter, and F. Gao. 2022. "Rate Controlling in Low-Temperature Standard NH_3-SCR: Implications from *Operando* EPR Spectroscopy and Reaction Kinetics." *Journal of the American Chemical Society* 144: 9734–9746.

2. Lin, F., T. Andana, Y.Q. Wu, J. Szanyi, Y. Wang, and F. Gao. 2021. "Catalytic Site Requirements for N_2O Decomposition on Cu-, Co-, and Fe-SSZ-13 Zeolites." *Journal of Catalysis* 401: 70–80.

3. Andana, T., K.G. Rappe, F. Gao, J. Szanyi, X. Pereira-Hernandez, and Y. Wang. 2021. "Recent Advances in Hybrid Metal Oxide–Zeolite Catalysts for Low-Temperature Selective Catalytic Reduction of NO_x by Ammonia." *Applied Catalysis B: Environmental* 291: 120054.

References

1. Gao, F., N.M. Washton, Y.L. Wang, M. Kollar, J. Szanyi, and C.H.F. Peden. 2015. "Effects of Si/Al Ratio on Cu/SSZ-13 NH_3-SCR Catalysts: Implications for the Active Cu Species and the Roles of Bronsted Acidity." *Journal of Catalysis* 331: 25–38.

2. Long, R.Q., and R.T. Yang. 2001. "Fe-ZSM-5 for Selective Catalytic Reduction of NO with NH_3: A Comparative Study of Different Preparation Techniques." *Catalysis Letters* 74: 201–205.

3. Huang, H.Y., R.Q. Long, and R.T. Yang. 2002, "Kinetics of Selective Catalytic Reduction of NO with NH_3 on Fe-ZSM-5 Catalyst." *Applied Catalysis A: General* 235 (1–2): 241–251.

4. Gao, F., E.D. Walter, M. Kollar, Y.L. Wang, J. Szanyi, and C.H.F. Peden. 2014. "Understanding Ammonia Selective Catalytic Reduction Kinetics over Cu/SSZ-13 from Motion of the Cu Ions." *Journal of Catalysis* 319: 1–14.

5. Bates, S.A., A.A. Verma, C. Paolucci, A.A. Parekh, T. Anggara, A. Yezerets, W.F. Schneider, J.T. Miller, W.N. Delgass, and F.H. Ribeiro. 2014. "Identification of the Active Cu Site in Standard Selective Catalytic Reduction with Ammonia on Cu-SSZ-13." *Journal of Catalysis* 312: 87–97.

6. Lambert, C.K. 2019. "Current State of the Art and Future Needs for Automotive Exhaust Catalysis." *Nature Catalysis* 2: 554–557.

7. Beale, A.M., F. Gao, I. Lezcano-Gonzalez, C.H.F. Peden, and J. Szanyi. 2015. "Recent Advances in Automotive Catalysis for NO_x Emission Control by Small-Pore Microporous Materials." *Chemical Society Reviews* 44: 7371–7405.

8. Paolucci, C., A.A. Parekh, I. Khurana, J.R. Di Iorio, H. Li, J.D.A. Caballero, A.J. Shih, T. Anggara, W.N. Delgass, J.T. Miller, F.H. Ribeiro, R. Gounder, and W.F. Schneider. 2016. "Catalysis in a Cage: Condition-Dependent Speciation and Dynamics of Exchanged Cu Cations in SSZ-13 Zeolites." *Journal of the American Chemical Society* 138: 6028–6048.

9. Chen, P.R., A. Khetan, M. Jablonska, J. Simbock, M. Muhler, R. Palkovits, H. Pitsch, and U. Simon. 2018. "Local Dynamics of Copper Active Sites in Zeolite Catalysts for Selective Catalytic Reduction of NO_x with NH_3." *Applied Catalysis B: Environmental* 237: 263–272.

10. Zhang,Y.N., Y. Peng, K.Z. Li, S. Liu, J.J. Chen, J.H. Li, F. Gao, and C.H.F. Peden. 2019. "Using Transient FTIR Spectroscopy to Probe Active Sites and Reaction Intermediates for Selective Catalytic Reduction of NO on Cu/SSZ-13 Catalysts." *ACS Catalysis* 9: 6137–6145.

11. Marberger, A., A.W. Petrov, P. Steiger, M. Elsener, O. Krocher, M. Nachtegaal, and D. Ferri. 2018. "Time-Resolved Copper Speciation during Selective Catalytic Reduction of NO on Cu-SSZ-13." *Nature Catalysis* 1: 221–227.

12. Gao, F., E.D. Walter, E.M. Karp, J.Y. Luo, R.G. Tonkyn, J.H. Kwak, J. Szanyi, and C.H.F. Peden. 2013. "Structure-Activity Relationships in NH_3-SCR over Cu-SSZ-13 as Probed by Reaction Kinetics and EPR Studies." *Journal of Catalysis* 300: 20–29.

Acknowledgements

We acknowledge continuous support and advise from DOE program managers Gurpreet Singh and Siddiq Khan.

I.20 Cummins-Pacific Northwest National Laboratory Cooperative Research and Development Agreement (CRADA): Fundamental Understanding of Cu-Zeolite SCR Catalyst Aging Mechanism (Pacific Northwest National Laboratory)

Feng Gao, Principal Investigator
Pacific Northwest National Laboratory (PNNL)
902 Battelle Boulevard
Richland, WA 99354
Email: feng.gao@pnnl.gov

Siddiq Khan, DOE Technology Manager
U.S. Department of Energy
Email: Siddiq.Khan@ee.doe.gov

Start Date: March 1, 2020 End Date: February 28, 2023
Project Funding: $600,000 DOE share: $300,000 Non-DOE share: $300,000

Project Introduction

The selective catalytic reduction (SCR) technology leads to effective reduction of nitrogen oxides (NO_x) from diesel engine exhausts in off-road, rail, and marine applications. Cu-zeolite is one of the most active catalysts achieving the required NO_x reductions. The recent rise in the emissions enforcement activities by regulators pointed out potential Cu-SCR catalyst durability concerns, especially under in-use conditions. Furthermore, the future regulations will be needing the SCR catalysts to maintain their high activity for significantly prolonged useful life.

Fundamental understanding of the Cu-zeolite catalyst material and performance degradation mechanisms are imperative to design and develop more durable Cu-SCR aftertreatment architectures and new formulations to meet current and future NO_x regulations. In the last decade, both academia and industry efforts were heavily focused on identification of active sites in Cu-zeolite SCR catalysts, reaction mechanisms, and kinetics. The critical information such as the dynamic response of the catalyst active sites and material to various long-term operating conditions and their degradation (typically termed as aging) is relatively less researched. Furthermore, the simplistic approaches used for degradation studies were inadequate to address the real-world catalyst changes and failures and the resulting emission deterioration.

PNNL and Cummins have been collaborating for more than 16 years in addressing the critical issues to meet the future standards. PNNL and Cummins will build on this long-term collaboration in jointly tackling the fundamental issues related to Cu-zeolite SCR catalyst aging.

Objectives

Overall Objectives

- Characterize high-mileage field-aged catalysts from Cummins to provide guidance in developing complex aging protocols.
- Develop characterization tools to monitor the dynamic changes upon progressive aging.
- Identify the cause of degradation and develop procedures to simulate real-world aging of SCR catalysts.

Fiscal Year 2022 Objectives

- Reveal gaps between real-world and laboratory accelerated aging via detailed kinetics studies of standard SCR and NH_3/NO oxidation, and NH_3+NO, NO_2, CO titrations of the catalysts.
- Use in situ X-ray photoelectron (XPS) and electron paramagnetic resonance (EPR) spectroscopies to reveal the nature of sulfur poisoning and elucidate possible mechanisms.
- Use operando EPR spectroscopy to elucidate transformations of SCR active Cu during real-world and laboratory accelerated aging.
- Develop real-world sulfur aging models that accurately describe the aging behavior of catalysts.

Approach

Typical Cu-zeolite SCR degradation research studies were carried out by taking simple approaches: for example, simulating the degradation by accelerated hydrothermal aging using high temperatures followed by the characterization of catalyst material and performance. Such approaches addressed gross deactivation trends, yet these are perceived to be inadequate to represent the dynamic changes that occur in real-world operation. Furthermore, a large portion of the research studies (advanced synthesis, spectroscopic characterization, newly developed titration methods, kinetics, density functional theory [DFT] simulation, etc.) were focused on probing the active sites and reaction mechanisms typically found in fresh or extremely aged catalysts with the intent of quickly reaching an understanding of the major underlying processes such as those needed for optimized and improved Cu-zeolite catalysts preparation. There was limited emphasis on the fundamental understanding of the dynamic processes responsible for active site degradation and the active sites in gracefully aged catalysts that are representative of real-world conditions, i.e., exposure to complex aging conditions. The above understanding is critical in developing more robust aftertreatment systems through design of controls, engineering solutions, and discovery of new formulations.

This project proposes to significantly expand the scope of the previous work done at PNNL and Cummins, to emphasize the aged Cu-zeolite SCR catalysts and characterize them using advanced characterization tools to demystify the dynamic processes and reactions responsible for active site and performance degradation. The various work streams and research tasks include the development of complex but more representative simulated and accelerated aging procedures. To this end, six Cu-chabazite catalyst cores—including a laboratory degreened (DG); a laboratory hydrothermally aged (HTA); a laboratory hydrothermally aged in the presence of SO_x (HTA+SO_x); and three field-aged, high-mileage healthy (HM1, HM2, HM3) catalysts provided by Cummins to PNNL—were used as key catalyst specimens for Fiscal Year 2022 research. The latter four samples are sulfur-poisoned.

Results

We applied a wide range of catalyst characterization methods to gain atomic-level knowledge on Cu transformation under different aging protocols, including surface area/porosity analysis, X-ray diffraction, H_2-temperature programmed reduction (TPR), NH_3-temperature programmed desorption, solid-state nuclear magnetic resonance (NMR), in situ XPS, and EPR spectroscopies. We then correlated such knowledge to SCR, NH_3/NO oxidation kinetic behavior of the catalysts.

Low-temperature NO_x conversion data in standard SCR were processed using a first-order kinetic equation $r = \frac{F}{W}(-\ln(1-x))$, where F is the NO_x flow rate (moles of NO per s), W the mass of the catalyst (g), and x the NO_x conversion. The Arrhenius equation, $k = \frac{r}{[NOx]_0} = Ae^{\frac{-E_a}{RT}}$, is used for calculating rate constants (k), pre-exponential factor (A), and apparent activation energy (E_a), where $[NO_x]_0$ is the molar concentration of NO_x in the feed [1], [2], [3].

Figure I.20.1a depicts the corresponding k versus 1/T Arrhenius plots. The DG sample displays the highest catalytic efficacy, the HTA sample shows minor decrease, and the S-containing samples show additional

decrease. Based on these Arrhenius plots, A and E_a values are derived; these are presented in Figure I.20.1b and Figure I.20.1c, respectively. To better understand the trends, we reiterate here that standard SCR is a redox reaction, and both the reduction half cycle ([RHC], $Cu^{II} \rightarrow Cu^{I}$) and the oxidation half cycle ([OHC], $Cu^{I} \rightarrow Cu^{II}$) play important rate-controlling roles. Literature has clearly demonstrated that low-temperature OHC involves a pair of $Cu^{I}(NH_3)_2$ intermediates, which requires diffusion of two distant $Cu^{I}(NH_3)_2$ species to the same cage of the SSZ-13 support [4], [5]. As such, OHC rate controlling lowers atomic efficiency of Cu active sites. Reflected in Arrhenius analysis, OHC rate controlling leads to a decrease in A and E_a values, whereas RHC rate controlling leads to an increase in A and E_a values. From the A and E_a values shown in Figure I.20.1b and Figure I.20.1c and quantification results of isolated Cu^{II}-ions and S shown in Table I.20.1, hydrothermal aging appears to be less influential than sulfur aging in promoting OHC rate controlling. This notion is clearly reflected by the calculated turnover rates at 160°C, shown in Figure I.20.1d. As compared to the DG sample, the HTA displays a ~30% loss in atomic efficiency. Since these two catalysts have the same density of active Cu sites, this loss may be caused by Cu mobility decrease resulting from hydrothermal aging [6] or ammonia storage capacity drop from the minor support dealumination [7]. The S-containing catalysts show similar Cu atomic efficiency, ~50% of the DG sample efficiency. Atomic efficiency loss for these latter samples was due to combined hydrothermal and sulfur aging effects.

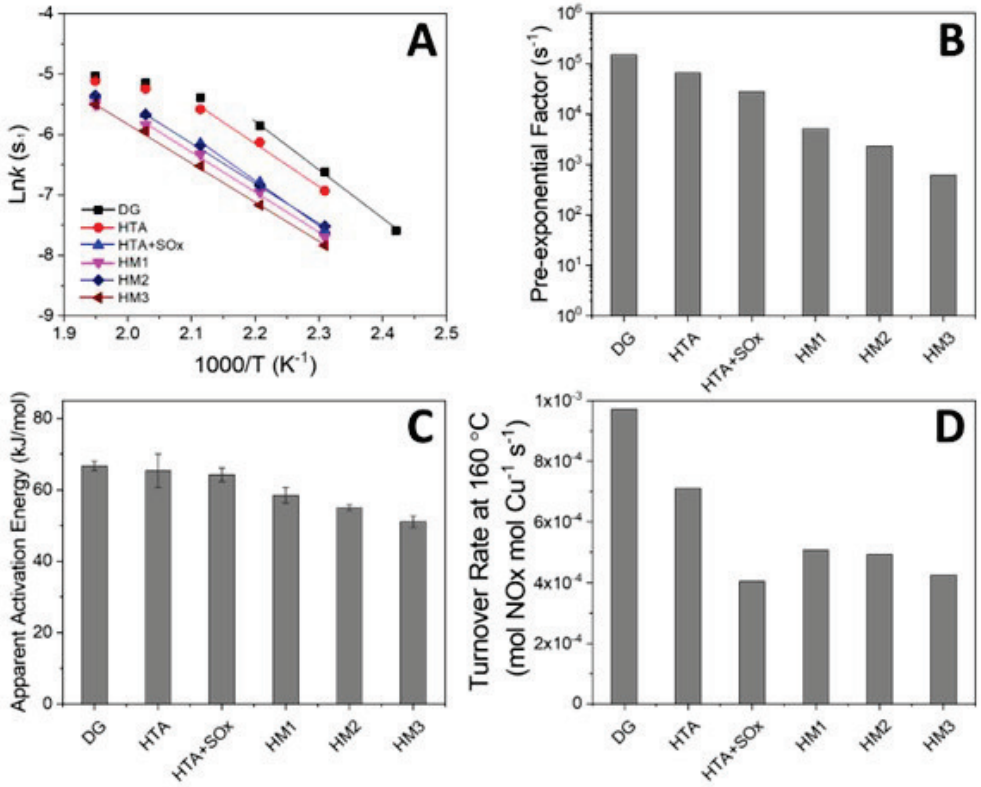

Figure I.20.1 (a) Arrhenius plots derived using low-temperature NO_x conversion data corrected using first-order rate expression. (b) The corresponding pre-exponential factors derived from Arrhenius analysis. (c) The corresponding apparent activation energies derived from Arrhenius analysis. (d) SCR turnover rates at a reaction temperature of 160°C, calculated using normalized rates based on first-order rate expression, and reducible Cu contents from NO+NH_3 titration.

To better reveal the nature of sulfur contamination, in situ XPS spectra were collected after reducing the HM3 sample to 300°C, 400°C, and 500°C, respectively, with H_2. This sample was chosen here because of its high S content, allowing both Cu and S reduction to be readily probed. As shown in Figure I.20.2a, the ambient sample (after evacuation) showed strong satellite peaks, suggesting that the majority of Cu species stayed at a +2-oxidation state. This followed since Cu with +1 or 0 oxidation states barely display satellites [8]. In the Cu $2p_{3/2}$ regime, two features were observed with binding energies of 933.7 eV and 935.3 eV, respectively. Based on literature, the 933.7 eV feature is readily assigned as CuO-like species [9], [10], i.e., Z_2Cu^{II}, $ZCu^{II}OH$, and

CuO species. The 935.3 eV peak has been attributed to Cu in $CuSO_4$ [11]. As shown in Table I.20.1 from S 2p XPS analysis, the nature of sulfur species in HM3 was indeed sulfate. In addition to $CuSO_4$, $CuSO_4$-like moieties—e.g., Z-Cu^{II}-HSO_4 and Z[Cu^{II}-SO_4-Cu^{II}]Z—may also give rise to the 935.3 eV peak.

Table I.20.1 Cu and S Content Determined Via Inductively Coupled Plasma (ICP) and XPS, Isolated Cu(II) Ion Content Determined Via EPR, and Reducible Cu Content Determined Via NO+NH_3 Titration

Catalyst	Total Cu content ICP (wt%)	S content ICP (wt%)	Isolated Cu(II) EPR (wt%)*	Reducible Cu NO+NH3 titration (wt%)
DG	2.31	-	2.32	2.27
HTA	2.42	-	2.35	2.27
HTA+SO_x	2.38	0.14	1.83	2.09
HM1	2.42	0.22	1.45	1.48
HM2	2.50	0.31	1.67	1.82
HM3	2.50	0.58	1.65	1.54

** = normalized by excluding cordierite contamination*

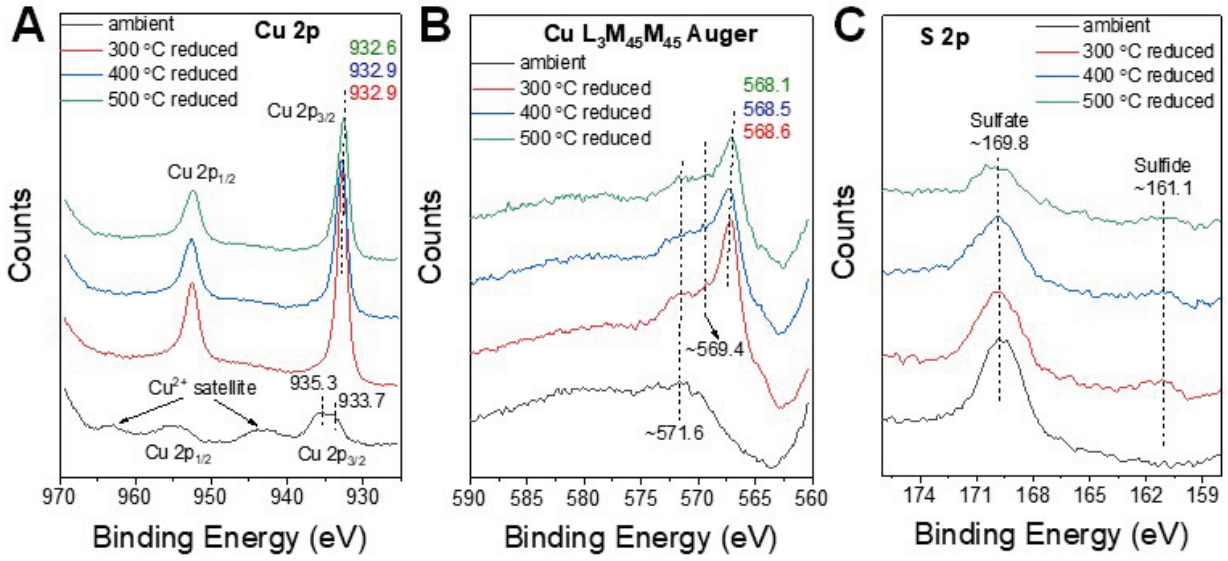

Figure I.20.2 In situ XPS for the HM3 sample in (a) Cu 2*p* region, (b) Cu $L_3M_{45}M_{45}$ Auger region, and (c) S 2*p* region

Upon H_2 reduction of HM3 at 300°C, the Cu^{II} satellites largely diminished due to ZCu^{II}OH and CuO reduction. The Cu $2p_{3/2}$ binding energy of 932.9 eV indicates that some Cu species (Z_2Cu^{II} and $CuSO_4$) remained at a +2 oxidation state. When the reduction temperature increases to 500°C, the Cu $2p_{3/2}$ binding energy reached 932.6 eV, almost identical to that of metallic Cu. Still, isolated ZCu^{I} should remain intact at this reduction temperature as indicated by H_2-TPR; however, Cu^{I} and Cu^{0} 2p binding energies were hardly distinguishable. Figure I.20.2b presents the corresponding Cu $L_3M_{45}M_{45}$ Auger transitions. The evacuated ambient sample displayed a few poorly resolved bands with binding energies at 571.6 eV, corresponding to a kinetic energy of 915.1 eV by Al Kα irradiation that is readily assigned to fully oxidized Cu. Upon reduction by H_2, strong transitions occurred on HM3 at 568.6–568.1 eV binding energy, corresponding to kinetic energies of 918.1–918.6 eV that can be readily assigned to Cu^0. In comparison to the metallic Cu $L_3M_{45}M_{45}$ reference spectrum, the weak and broad features that persisted on the reduced HM3 sample around 571.6 eV

may be attributed to Cu^0; however, the new band at ~569.4 eV (kinetic energy ~917.3 eV) can be assigned to Cu^I species. Thus, the Cu $L_3M_{45}M_{45}$ Auger transition appeared more sensitive than Cu 2p XPS in distinguishing Cu^I and Cu^0 species. The S 2p regime spectra are depicted in Figure 2c. The evacuated ambient sample displays a feature at ~169.8 eV, which is readily attributed to sulfate [11], [12], [13]. This reinforced our assignment of the Cu $2p_{3/2}$ peak at 935.3 eV to $CuSO_4$ and $CuSO_4$-like species. However, this does not suggest that all sulfur in the sample was associated with Cu; the presence of $Al_2(SO_4)_3$ cannot be excluded. Upon H_2 reduction at 300°C and 400°C, the somewhat decreased intensity of the ~169.8 eV sulfate band, and the appearance of a weak sulfide band at ~161.1 eV [12], [14] pointed to sulfur reduction at these temperatures. This reduction becomes more significant at 500°C.

Figure I.20.3a presents the ^{27}Al NMR results. For each sample, at least five resonances were observed, at approximately 58, 45, 40, 27, and 10 ppm, respectively. In comparison to spectra acquired previously on pure SSZ-13 [7] and cordierite [15], the 58, 27, and 10 ppm resonances can be attributed to tetrahedral, pentahedral, and octahedral Al of SSZ-13, and the 45 and 40 ppm signals are attributed to (tetrahedral) Al of the cordierite support. Again, because of the presence of cordierite, it is difficult to quantify dealumination levels of the catalysts. However, the similar spectrum line shapes across the samples do not indicate significant differences in dealumination. Figure I.20.3b displays the NH_3-TPR results. All samples showed three NH_3 desorption states, a shoulder peak at ~220°C to desorption from weak Lewis acid sites (e.g., extra framework Al), a main peak at ~300°C to desorption from Cu, and another (shoulder) peak above ~400°C to desorption from Brønsted acid sites. A comparison between the DG and HTA samples immediately revealed that desorption from Brønsted acid sites greatly declines for the HTA sample. Whereas SSZ-13 support dealumination is clearly a possible cause for this decline, previous studies revealed that $ZCu^{II}OH$ conversion to Z_2Cu^{II} (i.e., $ZCu^{II}OH + ZH \rightarrow Z_2Cu^{II} + H_2O$) is also an important contributor.

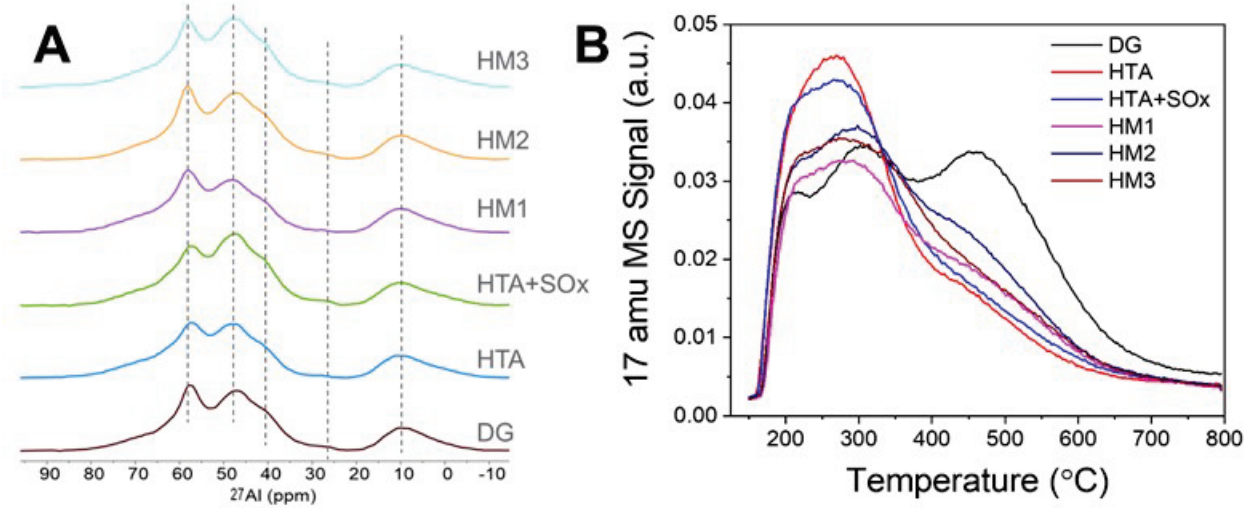

MS – mass spectroscopy

Figure I.20.3 (a) ^{27}Al NMR spectra and (b) NH_3-TPR results for the Cu/SSZ-13 catalysts

Because the ^{27}Al NMR measurements failed to provide quantitative dealumination information, NH_3 desorption yields from NH_3-TPR were used to provide indirect evidence. The HTA sample had an ~16% decrease in NH_3 storage compared to the DG sample, suggesting mild dealumination during aging. However, this level of dealumination is not severe enough to cause isolated Cu^{II}-ions in the HTA sample to agglomerate to CuO. Interestingly, the HTA+SO_x, HM2, and HM3 samples showed NH_3 storage almost identical to that of the HTA sample (the slight variations of the desorption curves can be largely attributed to different extents of the $ZCu^{II}OH + ZH \rightarrow Z_2Cu^{II} + H_2O$ reaction); the HM1 sample displayed the lowest NH_3 storage but was still ~90% that of the HTA sample. As such, the presence of SO_x during sulfur aging mildly aggravates

dealumination and promotes CuO formation. Sulfur-aging-induced catalyst degradation may be attributed to two mechanisms.

It is important to note that sulfur aging leads to (1) conversion of isolated Cu(II) ions to CuO clusters and (2) dealumination of the chabazite support. Since hydrothermal aging alone also leads to such changes, it can be argued that the presence of sulfur may lead to more severe hydrothermal aging effects. Based on detailed EPR spectra analysis of the g and A tensor values of the residual Z_2Cu^{II} sites, however, the real-world high mileage catalysts clearly underwent hydrothermal aging less severe than the laboratory aged samples. As such, the additional CuO formation and support dealumination during sulfur aging was due to the formation of $CuSO_4$-like species and the subsequent chemistries related to such species. CuO cluster formation was likely due to agglomeration of $CuSO_4$-like species to multinuclear $CuSO_4$ clusters, and decomposition of such clusters during desulfation lead to CuO formation (i.e., $CuSO_4 \rightarrow CuO + SO_3$). On the other hand, $CuSO_4$-like species can also interact with framework Al, forming CuO and causing support dealumination (i.e., $O\text{-}Al\text{-}O\text{-}CuHSO_4 \rightarrow CuO + Al_2(SO_4)_3$).

Conclusions

- SCR kinetics studies demonstrate that SCR active site concentration decrease for field-aged catalysts triggers stronger involvement of the CuI oxidation to CuII step in rate limiting, thus decreasing low-temperature NO_x-reduction efficiency.
- XPS and EPR studies demonstrate that the real-world catalysts undergo less severe hydrothermal aging relative to lab-aged catalysts; however, they suffer from more severe CuO formation and catalyst support dealumination.
- Such additional CuO formation and support dealumination is likely due to formation of $CuSO_4$-like species and the subsequent chemistries related to such species. Possible reaction pathways are suggested.

Key Publications

1. Wu, Y., T. Andana, Y. Wang, Y. Chen, E.D. Walter, M.H. Engelhard, K.G. Rappé, Y. Wang, F. Gao, U. Menon, R. Daya, D. Trandal, H. An, Y. Zha, and K. Kamasamudram. 2022. "A Comparative Study between Real-World and Laboratory Accelerated Aging of Cu/SSZ-13 SCR Catalysts." *Applied Catalysis B: Environmental* 318, 121807.

References

1. Long, R.Q., and R.T. Yang. 2001. "Fe-ZSM-5 for Selective Catalytic Reduction of NO with NH_3: a Comparative Study of Different Preparation Techniques." *Catalysis Letters* 74: 201–205.
2. Huang, H.Y., R.Q. Long, and R.T. Yang. 2002. "Kinetics of Selective Catalytic Reduction of NO with NH_3 on Fe-ZSM-5 Catalyst." *Applied Catalysis A: General* 235: 241–251.
3. Gao, F., E.D. Walter, M. Kollar, Y. Wang, J. Szanyi, and C.H.F. Peden. 2014. "Understanding Ammonia Selective Catalytic Reduction Kinetics over Cu/SSZ-13 from Motion of the Cu Ions." *Journal of Catalysis* 319: 1–14.
4. Gao, F., D. Mei, Y. Wang, J. Szanyi, and C.H.F. Peden. 2017. "Selective Catalytic Reduction over Cu/SSZ-13: Linking Homo- and Heterogeneous Catalysis." *Journal of the American Chemical Society* 139: 4935–4942.
5. Paolucci, C., I. Khurana, A.A. Parekh, S. Li, A.J. Shih, H. Li, J.R.D. Iorio, J.D. Albarracin-Caballero, A. Yezerets, J.T. Miller, W.N. Delgass, F.H. Ribeiro, W.F. Schneider, and R. Gounder. 2017. "Dynamic Multinuclear Sites Formed by Mobilized Copper Ions in NO_x Selective Catalytic Reduction." *Science* 357: 898–903.

6. Zhang, Y.N., Y. Peng, J.H. Li, K. Groden, J.S. Mcewen, E.D. Walter, Y. Chen, Y. Wang, and F. Gao. 2020. "Probing Active-Site Relocation in Cu/SSZ-13 SCR Catalysts during Hydrothermal Aging by In Situ EPR Spectroscopy, Kinetics Studies, and DFT Calculations." *ACS Catalysis* 10: 9410–9419.

7. Gao, F., N.M. Washton, Y.L. Wang, M. Kollar, J. Szanyi, and C.H.F. Peden. "Effects of Si/Al Ratio on Cu/SSZ-13 NH3-SCR Catalysts: Implications for the Active Cu Species and the Roles of Bronsted Acidity." *Journal of Catalysi*s 331: 25–38.

8. Chusuei, C.C., M.A. Brookshier, and D.W. Goodman. 1999. "Correlation of Relative X-ray Photoelectron Spectroscopy Shake-Up Intensity with CuO Particle Size." *Langmuir* 15: 2806–2808.

9. Vasquez, R. 1998. "CuO by XPS." *Surface Science Spectra* 5: 262–266.

10. Zhang, R., Y. Li, and T. Zhen. 2014. "Ammonia Selective Catalytic Reduction of NO over Fe/Cu-SSZ-13." *RSC Advances* 4: 52130–52139.

11. Vasquez, R. 1998. "CuSO4 by XPS." *Surface Science Spectra* 5: 279–284.

12. Wijayanti, K., K. Xie, A. Kumar, K. Kamasamudram, and L. Olsson. 2017. "Effect of Gas Compositions on SO_2 Poisoning over Cu/SSZ-13 used for NH3-SCR." *Applied Catalysis B: Environmental* 219: 142–154.

13. Walton, R.A. 1980. "The X-Ray Photoelectron-Spectra of Metal-Complexes of Sulfur-Containing Ligands - Sulfur 2p Binding-Energies." *Coordination Chemistry Reviews* 31: 183–220.

14. Laajalehto, K., I. Kartio, and P. Nowak. 1994. "XPS Study of Clean Metal Sulfide Surfaces." *Applied Surface Science* 81: 11–15.

15. Ma, L., Y.S. Cheng, G. Cavataio, R.W. McCabe, L.X. Fu, and J.H. Li. 2013. "Characterization of Commercial Cu-SSZ-13 and Cu-SAPO-34 Catalysts with Hydrothermal Treatment for NH_3-SCR of NO_x in Diesel Exhaust." *Chemical Engineering* J 225: 323–330.

Acknowledgements

The principal investigator thanks Yiqing Wu, Tahrizi Andana, Kenneth G. Rappe, and Yong Wang from PNNL, and Unmesh Menon, Dylan Trandal, Rohil Daya, Mi-Young Kim, Yuhui Zha, Hongmei An, and Krishna Kamasamudram from Cummins, Inc. for their contributions to this project and report. We also acknowledge continuous support and advice from DOE program managers Gurpreet Singh and Siddiq Khan.

I.21 LLCF Effects on Emissions Control Catalyst Performance and Durability (Oak Ridge National Laboratory)

Sreshtha Sinha Majumdar, Principal Investigator
Oak Ridge National Laboratory
2360 Cherahala Boulevard
Knoxville, TN 37932
Email: sinhamajumds@ornl.gov

Siddiq Khan, DOE Technology Manager
U.S. Department of Energy
Email: Siddiq.Khan@ee.doe.gov

Start Date: October 1, 2021 End Date: September 30, 2022
Project Funding: $400,000 DOE share: $400,000 Non-DOE share: $0

Project Introduction

Achieving decarbonization of the hard-to-electrify rail, marine, and off-road sectors will require a combination of both powertrain electrification and low lifecycle carbon fuels (LLCFs). These transportation sectors are challenging to electrify due to application characteristics such as large travel distances, heavy load requirements, longer uptime needs, and operations in remote locations that may not have the infrastructure needed to support electrified vehicles. Nearly all the powertrains in the rail, marine, and off-road sectors rely on diesel engines. While renewable diesel and biodiesel provide lower-carbon, nearly drop-in alternatives to petroleum-derived diesel fuel, it is unlikely they will be able to meet all the fuel demands for these sectors. Therefore, other LLCFs such as methanol, ethanol, ammonia, and hydrogen will play a crucial role in the decarbonization of these hard-to-electrify transportation sectors. Modifying diesel engine powertrains to run on promising LLCFs is a challenge that industry has started to address only recently. One of the key end-use challenges for any LLCF/engine combination is compliance with U.S. Environmental Protection Agency emissions regulations.

The focus of this project is on measuring the catalytic reactivity of alcohol LLCFs and their aldehyde partial oxidation products over commercially relevant emissions control catalysts. The results of these measurements will determine if there are any challenges that need to be addressed through improved catalyst formulations or other aftertreatment strategies.

Objectives

Overall Objective

The objective for this project is to address any emissions control challenges associated with running rail, marine, and off-road engines on LLCFs.

- Measure the fuel chemistry effects of LLCFs and their partial oxidation products on a commercial emissions control catalyst under relevant synthetic exhaust conditions.
- Identify and evaluate potential alternative emissions control solutions to handle the unique emissions from promising LLCFs.

Fiscal Year 2022 Objectives

- Measure the catalytic reactivity of alcohol LLCFs and their aldehyde partial oxidation products over a commercially relevant, aged diesel oxidation catalyst (DOC).
- Publish results from prior investigations of Co-Optima blendstock fuel reactivity on emissions control catalysts.

Approach

This project utilizes targeted synthetic exhaust flow-reactor studies to (1) evaluate the reactivity of LLCFs on commercial emissions control catalysts to identify fuels and operating conditions that could lead to emissions challenges and (2) to develop potential alternative emissions control solutions to handle the unique emissions from promising LLCFs. The synthetic exhaust gas flow reactor systems are designed to offer maximum flexibility to mimic the exhaust conditions expected in transportation applications and further allow the exploration of the boundary conditions associated with the candidate emissions control systems. Great care has been taken to ensure the results from the flow reactors will correlate well with engine-based studies.

Results

Fiscal Year 2022 Accomplishments

- Measured the catalyst light-off and light-down temperatures for 13 LLCFs (Table I.21.1) and a baseline C10 (molecule with 10 carbon atoms) equivalent of a surrogate diesel blend (49% n-decane, 24% decalin, 27% tetralin).
- Demonstrated that promising LLCFs such as alcohols and polyoxymethylene ethers (POME) start reacting at low temperatures over the DOC but can generate less reactive and potentially toxic aldehyde intermediates.
- Investigated the impact of LLCFs on other criteria pollutants and found that CO oxidation is not typically inhibited by the LLCFs.

Table I.21.1 LLCFs Evaluated on a Commercial DOC under Exhaust-Relevant Lean Conditions

Functional Group	alcohols	aldehydes (partial combustion products)	POME	esters	alkanes		aromatics
					linear	cyclic	
LLCFs	methanol ethanol isobutanol	formaldehyde acetaldehyde isobutyraldehyde	dibutoxy-methane	methyl octanoate pentyl pentanoate	n-decane	decalin	tetralin n-propyl benzene

Prior work by Oak Ridge National Laboratory (ORNL) researchers on fuel chemistry effects on emissions control catalysts has shown that changes in fuel composition can introduce new emissions control challenges and opportunities. The fuel reactivity on an emissions control catalyst was reported to be sensitive to its chemical structure and to the exhaust composition [1], [2], [3]. As vehicles powered by combustion engines running on LLCFs will still need to meet the stringent pollutant emissions regulations, understanding the emissions control catalyst efficiency in handling LLCFs and their products of incomplete combustion is essential.

To quantify the impacts of LLCFs on emissions control catalyst performance, synthetic exhaust flow reactor experiments were conducted according to industry-developed protocols [4]. A commercial DOC was used to measure the reactivity of the LLCFs. Prior to the light-off/light-down experiments on the automated synthetic exhaust flow reactor system, the DOC was aged for 50 h at 800ºC under lean conditions. The light-off/light-down temperatures of the LLCFs on the aged commercial DOC were measured under the full synthetic exhaust composition shown in Table I.21.2. The LLCFs investigated in this study include a wide range of chemical structures including alcohols and their partial combustion products (aldehydes), ethers, esters, alkanes, and aromatics (details in Table I.21.1). In addition to the LLCFs, a surrogate diesel blend containing 49% n-decane, 24% decalin, and 27% tetralin was used as a baseline for comparison. This surrogate mix consists of the C_{10} (10 carbon atoms) equivalents of the chemical structures found in a surrogate developed elsewhere [5].

Table I.21.2 Synthetic Exhaust Compositions

Component	Pretreatment	Lean (LTC-D)
O_2	12%	12%
CO_2	6%	6%
H_2O	6%	6%
CO	--	0.2%
H_2	--	0.04%
NO	--	0.01%
HC (C_1 basis)	--	0.3%
SV	30,000 h^{-1}	30,000 h^{-1}

LTC-D – low-temperature combustion (diesel), SV – space velocity, h – hour

The light-off curves for methanol (purple), ethanol (red), and isobutanol (orange) in Figure I.21.1a showed that the alcohols start oxidizing over the DOC at lower temperatures than the surrogate diesel baseline (grey). Interestingly, they exhibit distinctly different light-off behaviors. The light-off curve for methanol is very steep, and it lights off the earliest among the alcohols investigated. Ethanol, on the other hand, reacts over a wide range of temperatures (>120ºC), likely due to the formation of intermediates, which are harder to oxidize.

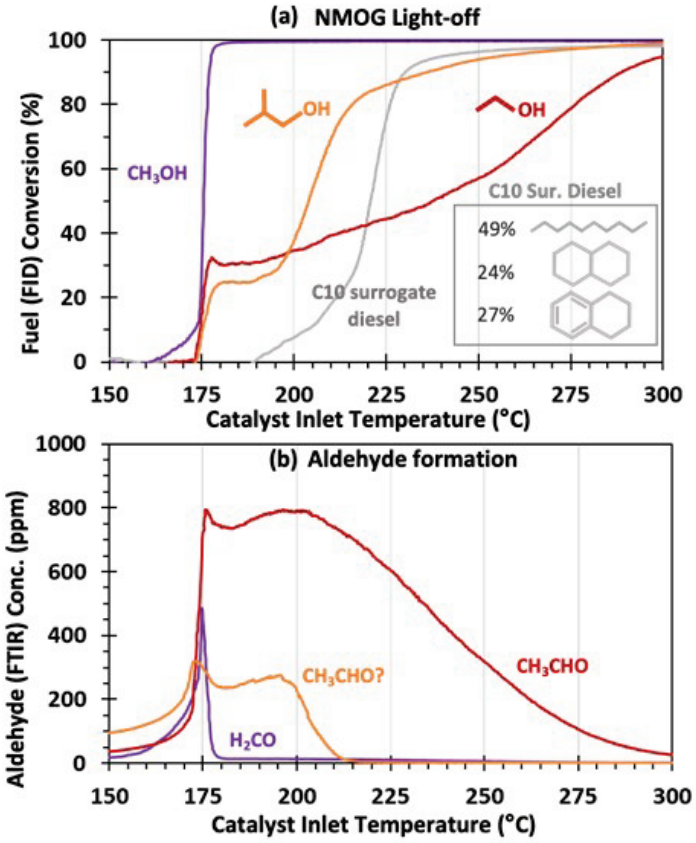

FID – flame ionization detector

Figure I.21.1 (a) Non-methane organic gases (NMOG) conversion of a C_{10} diesel surrogate and LLCF alcohols such as methanol (purple), ethanol (red), and isobutanol (orange) with (b) corresponding FTIR aldehyde traces over an aged commercial DOC under lean conditions. Source: Sreshtha Sinha Majumdar, ORNL.

Prior work has shown that alcohol oxidation via the dehydrogenation pathway leads to the formation of aldehydes as an intermediate product [1]. The aldehyde traces in Figure I.21.1b from the Fourier Transform Infrared (FTIR) spectrometer—which allows differentiation of the organic species in the outlet gas of the flow reactor—provide qualitative insights into the aldehyde intermediates formed during oxidation of alcohols. Aldehydes were formed starting at very low temperatures for all three alcohols. In the case of ethanol, significant levels of acetaldehyde formation occurred, and much higher temperatures were required to fully oxidize the acetaldehyde. The acetaldehyde observed in the FTIR trace during isobutanol oxidation was likely isobutyraldehyde (an isobutyraldehyde FTIR method was not available).

To better understand the aldehydes' catalytic reactivity, formaldehyde, acetaldehyde, and isobutyraldehyde were introduced as part of the synthetic exhaust feed. Figure I.21.2 summarizes the temperatures at which 10% (T_{10}, bottom of vertical bar), 50% (T_{50}, "X" symbols), and 90% (T_{90}, top of vertical bar) of the alcohols and aldehydes were converted over the DOC. Stable formaldehyde delivery is extremely difficult to achieve and not widely reported in the literature. ORNL researchers were able to attain a stable concentration of 1,000 ppm formaldehyde (as compared to 3,000 ppm C_1 [molecule with one carbon atom] for the other alcohols and aldehydes) in the synthetic exhaust mixture. Methanol and formaldehyde were the most reactive of all the organic species investigated in this study. Acetaldehyde had a higher T_{10}, T_{50}, and T_{90} than ethanol and underwent complete oxidation only above 300ºC. Similarly, isobutyraldehyde also oxidized at temperatures higher than isobutanol, indicating that both acetaldehyde and isobutyraldehyde are less reactive than their corresponding alcohols. Aldehydes were also observed (results not shown) with other oxygenated LLCFs containing a methoxy group (-OCH_3). Aldehyde formation in-cylinder in an engine and over the oxidation catalyst could be an issue when exhaust temperatures are low, such as during cold-start or at idle. Future work will focus on new oxidation catalyst formulations that may be better at handling some of these unique emissions from LLCFs.

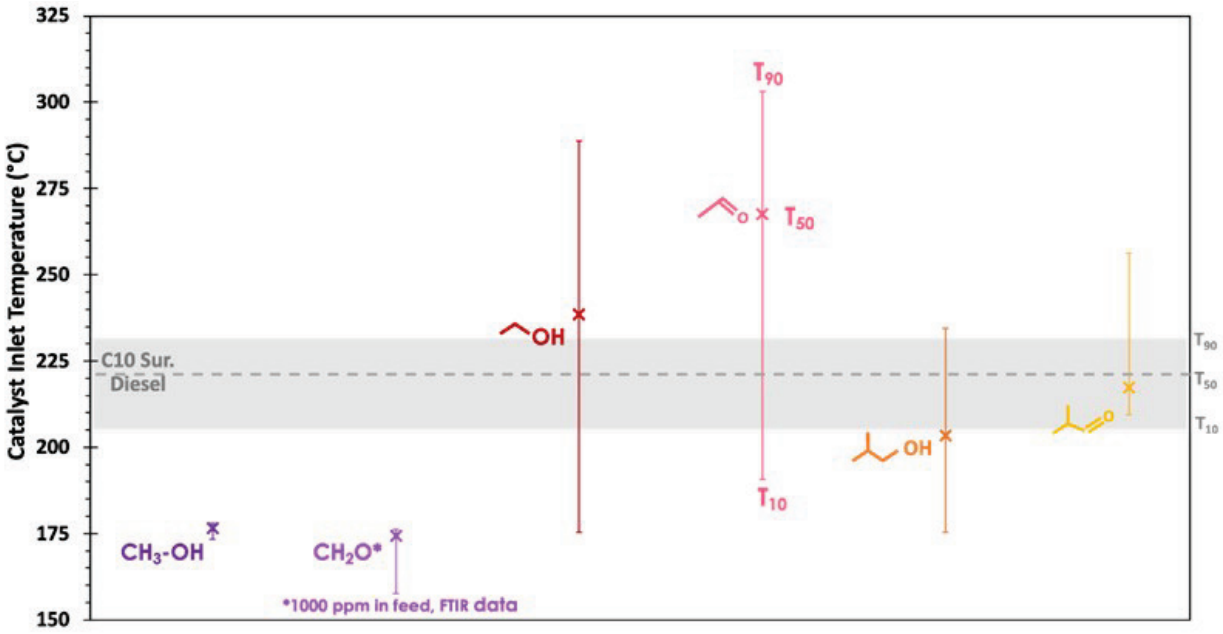

Figure I.21.2 NMOG light-off temperatures of methanol (dark purple), ethanol (dark red), isobutanol (orange), and their partial oxidation products formaldehyde (light purple), acetaldehyde (light red), and isobutyraldehyde (gold) over an aged DOC under lean conditions. The gray rectangle and dashed line indicate the light-off temperatures of the surrogate diesel mixture. Source: Sreshtha Sinha Majumdar, ORNL.

The impact of LLCF reactivity on other criteria pollutants such as CO and nitrogen oxides (NO_x) was also investigated (not shown). Overall, the LLCFs studied did not inhibit CO oxidation on the DOC. Additionally,

appreciable levels of N_2O formation from NO_x reduction were not observed with the LLCFs examined in this study.

Conclusions

- LLCFs can create both challenges and opportunities for emissions control.
- DOC reactivity depends on the chemical structure of LLCFs.
- Alcohols start reacting at low temperatures on the DOC.
- Methanol is the most reactive among the LLCFs investigated.
- Significant levels of acetaldehyde are formed as ethanol lights off.
- Acetaldehyde and isobutyraldehydes are less reactive than ethanol and isobutanol.
- LLCFs with methoxy groups form aldehyde intermediates during oxidation.
- LLCFs do not typically inhibit CO oxidation or form appreciable levels of N_2O.

Key Publications

1. Ladshaw, A.P., S. Sinha Majumdar, and J.A. Pihl. 2023. "Experiments and Modeling to Evaluate Global Reaction Kinetics of Three-Way Catalyst Light Off for Net-Zero Carbon Fuels and Selected Fuel Blends." *Applied Catalysis B: Environmental* 324 (May 5). https://doi.org/10.1016/j.apcatb.2022.122281.

2. Dagle, V.L., M. Affandy, J.S. Lopez, L. Cosimbescu, D.J. Gaspar, S. Scott Goldsborough, T. Rockstroh, S. Cheng, T. Han, C.P. Kolodziej, A. Hoth, S. Sinha Majumdar, J.A. Pihl, T.L. Alleman, C. Hays, C.S. McEnally, J. Zhu, and L.D. Pfefferle. 2022. "Production, Fuel Properties and Combustion Testing of an Iso-Olefins Blendstock for Modern Vehicles." *Fuel* 310, Part A (February 15). https://doi.org/10.1016/j.fuel.2021.122314.

References

1. Majumdar, S. Sinha, J.A. Pihl, and T.J. Toops. 2019. "Reactivity of Novel High-Performance Fuels on Commercial Three-Way Catalysts for Control of Emissions from Spark-Ignition Engines." Applied Energy 255 (December 1): 113640. https://doi.org/10.1016/j.apenergy.2019.113640.

2. Majumdar, S. Sinha, and J.A. Pihl. 2020. "Impact of Selected High-Performance Fuel Blends on Three-Way Catalyst Light Off under Synthetic Spark-Ignition Engine-Exhaust Conditions." Energy and Fuels 34 (10): 12900–12910. https://doi.org/10.1021/acs.energyfuels.0c02102.

3. Dagle, V.L., M. Affandy, J.S. Lopez, L. Cosimbescu, D.J. Gaspar, S. Scott Goldsborough, T. Rockstroh, S. Cheng, T. Han, C.P. Kolodziej, A. Hoth, S. Sinha Majumdar, J.A. Pihl, T.L. Alleman, C. Hays, C.S. McEnally, J. Zhu, and L.D. Pfefferle. 2022. "Production, Fuel Properties and Combustion Testing of an Iso-Olefins Blendstock for Modern Vehicles." Fuel 310, Part A (February 15). https://doi.org/10.1016/j.fuel.2021.122314.

4. Rappé, K.G., C. DiMaggio, J.A. Pihl, J.R. Theis, S.H. Oh, G.B. Fisher, J. Parks, V.G. Easterling, M. Yang, M.L. Stewart, and K.C. Howden. 2019. "Aftertreatment Protocols for Catalyst Characterization and Performance Evaluation: Low-Temperature Oxidation, Storage, Three-Way, and NH3-SCR Catalyst Test Protocols." Emission Control Science & Technology 5 (2): 183–214. https://doi.org/10.1007/s40825-019-00120-7.

5. Fioroni, G.M., L.A. Fouts, J.H. Luecke, D.R. Vardon, N.A. Huq, E.D. Christensen, X. Huo, T. Alleman, R.L. McCormick, M. Kass, E. Polikarpov, G. Kukkadapu, and R.A. Whitesides. 2019. "Screening of Potential Biomass-Derived Streams as Fuel Blendstocks for Mixing Controlled Compression Ignition Combustion." SAE International Journal of Advances and Current Practices in Mobility 1 (3):1117–1138. https://doi.org/10.4271/2019-01-0570.

Acknowledgements

The Principal Investigator gratefully acknowledges coauthor Josh Pihl of ORNL. The authors gratefully acknowledge the support and direction of Siddiq Khan, Kevin Stork, Gurpreet Singh, and Mike Weismiller at the Vehicle Technologies Office.

I.22 Hardware-in-the-Loop Toolkit for Off-Road and Marine (Argonne National Laboratory)

Muni Biruduganti, Principal Investigator
Argonne National Laboratory
9700 South Cass Avenue
Lemont, IL 60439
Email: MBiruduganti@anl.gov

Gurpreet Singh, DOE Program Manager
U.S. Department of Energy
Email: Gurpreet.Singh@ee.doe.gov

Start Date: October 1, 2021 End Date: September 30, 2022
Project Funding: $550,000 DOE share: $550,000 Non-DOE share: $0

Project Introduction

Testing powertrains with innumerable combinations of hardware components and real-life conditions is a cumbersome, time-consuming, and expensive process [1], [2]. These limitations to actual testing create the need for alternate means; one solution is to use hardware-in-the-loop (HIL) simulation. HIL simulation refers to the methodology of testing a subsystem that co-exists in a simulation environment and mimics actual real-life conditions. This methodology is especially useful when it is not possible to model the subsystem in question. HIL minimizes, or in some cases eliminates, the hazards involved in actual testing and ensures system and personnel safety while system responses to extreme procedures are evaluated. HIL testing is hence being increasingly adopted in the industry and in research for fine-tuning new technology.

The Powertrain Research Facility (PRF) at Argonne National Laboratory is being set up with HIL capability for system-level and drive-cycle technology evaluation for off-road (mining) and marine applications. This work will be crucial to fulfilling the mission of the Decarbonization of Off-Road, Rail, Marine, and Aviation (DORMA) program. Integration and optimization at a vehicle and system level, regardless of power source (e.g., internal combustion engines [ICEs], fuel cells, or batteries), is important to decarbonize these non-road machines with very distinctly different duty cycles. The upgraded PRF will provide unique research capabilities at a U.S. national laboratory.

Objectives

There has been an increasing focus on decarbonizing ICEs for on-road applications to reduce greenhouse gas emissions (thereby keeping global warming well below 2°C), and this interest is now reaching many applications in off-road sectors as well. The transition of ICEs from fossil fuels to alternate fuel sources such as hydrogen and renewables, with the goal of becoming CO_2-neutral or CO_2-free, is becoming increasingly apparent. This change will bring challenges associated not only with the fueling infrastructure but also with engine and emission control technologies, which must be developed and deployed if we are to replace conventional fossil-fueled ICEs.

Overall Objective

The objective of this project is to enable net-zero-carbon, fuel-efficient design for hydrogen ICEs for off-road (mining) and marine applications using HIL PRF for system-level and drive-cycle-appropriate technology development.

Fiscal Year 2022 Objectives

- Commission a new Vieletech test cell control system:
    - Install the Vieletech test cell control system and software.

  - Enable operation of engines coupled to the dynamometer (dyno) with the Vieletech control system.
  - Actuate test cell ancillaries.
  - Stream and capture all test cell data.
  - Commission a National Instruments (NI) indication system (the Combustion Analysis System).
  - Establish an interface between the Vieletech LabVIEW system and Navistar engine control unit.
- Commission an HIL powertrain test cell control system.
- Develop a LabVIEW interface with Autonomie/RoadRunner (d-Space only currently).

Approach

The HIL capability demonstration will be conducted in two parts:

1. New Vieletech control system
   a. Install PXIe (PCI [Peripheral Component Interconnect] eXtensions for instrumentation) and new personal computer (PC) hardware.
   b. Install Vieletech control system hardware.
   c. Install the power supply box.
   d. Implement Vieletech software.
   e. Attain steady-state operation of a Navistar engine.
2. HIL integration
   a. Develop a LabVIEW plug-in for Autonomie.
   b. Commission the interface.
   c. Run a driving cycle using HIL.

Results

In Fiscal Year (FY) 2022, the Argonne research team moved the Vieletech control system from a light-duty automotive test cell to realign research objectives to off-road, heavy-duty ICEs. Effort went into decommissioning the newly installed hardware for light-duty work and reconfiguring a heavy-duty, high-horsepower test cell. This test cell was controlled using a dated Wineman and proprietary software from an original equipment manufacturer; the software was uninstalled and the Wineman was decommissioned after the project end date. Subsequently, the new Vieletech hardware and software were installed, and ancillary equipment was upgraded to support HIL testing. The schematic and layout of the HIL test cell are shown in Figure I.22.1 and Figure I.22.2 below, respectively. The Vieletech system uses NI hardware and LabVIEW to control the 623 hp alternating current (AC) dyno and other supporting equipment.

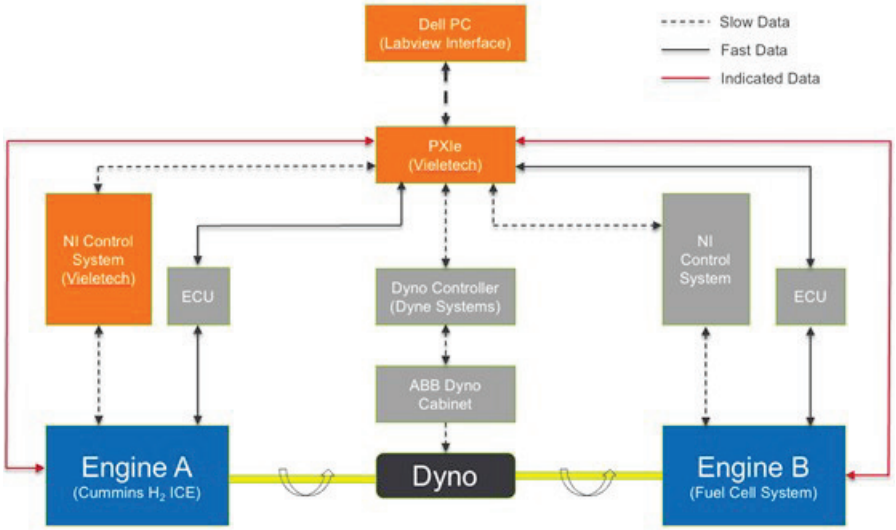

Figure I.22.1 Schematic of powertrain research facility

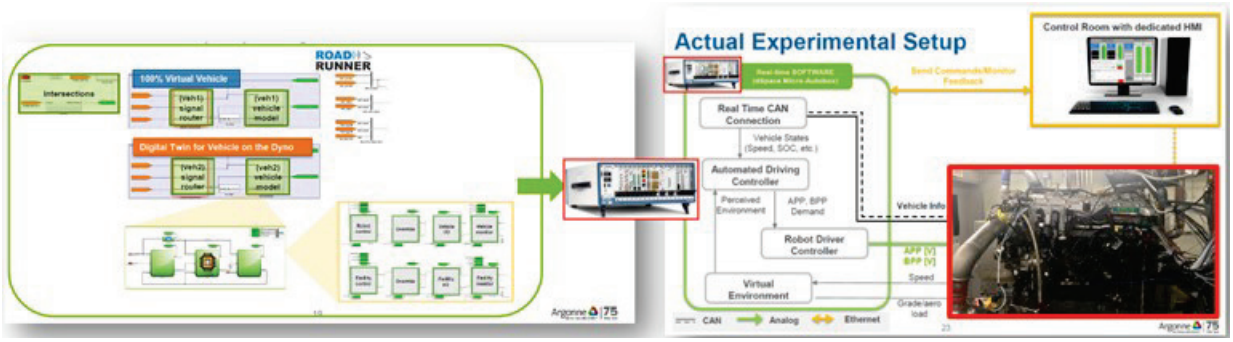

SOC – state of charge; APP – accelerator pedal position; BPP – brake pedal position; CAN – controller area network; I/O – input/output

Figure I.22.2 Conceptual rendering of HIL capability

A dyno-ready Navistar engine was borrowed from Navistar to replace the SuperTruck 2 engine and used as a mule platform with a production engine control unit (ECU). The engine was mounted on the bedplate and coupled to the AC dyno and is ready for testing.

Conclusions

The Vieletech controller has been installed and checked for functionality. Building ancillaries are functioning as intended. The commissioning of the PRF is pending the support of the original equipment manufacturer to interface between the ECU and the Vieletech controller. In FY 2023, new hardware will be procured to demonstrate drive-cycle capability. This hardware includes a dSpace microAutoBox that can run Autonomie models and control device under test. HIL capability will be demonstrated by integrating Autonomie software for heavy-duty off-road drive cycles. Additionally, the project team will initiate provisions for increased-capacity hydrogen fuel storage and delivery to the engine and install a hydrogen-ready production Cummins 6.7 L engine.

References

1. Isermann, R., J. Schaffnit, and S. Sinsel. 1999. “Hardware-in-the-Loop Simulation for the Design and Testing of Engine-Control Systems.” *Control Engineering Practice* 7, no. 5: 643–653. https://doi.org/10.1016/S0967-0661(98)00205-6.

2. Riccio, Antonio, Felice Di Iorio, Fabio Siccardi, Daniele Severi, Gabriele Lucchetti, Alexander Karlon, and Plamen Valchev. 2019. “Heavy Duty Diesel Engine and EAS Modelling and Validation for a Hardware-in-the-Loop Simulation System.” SAE Technical Paper 2019-24-0082. https://doi.org/10.4271/2019-24-0082.

Acknowledgements

The author gratefully acknowledges the support of our U.S. Department of Energy program manager Gurpreet Singh and technology manager Siddiq Khan. The author is also grateful to the Navistar team for their support through provision of the 13 L Class 8 truck engine and hardware for commissioning of the test cell.

II Rail

II.1 Ducted Fuel Injection and Cooled Spray Technologies for Particulate Control in Heavy-Duty Diesel Engines (Westinghouse Air Brake Technologies Corporation)

Adam Klingbeil, Principal Investigator
Westinghouse Air Brake Technologies Corporation
30 Isabella Street
Pittsburgh, PA 15212-5862
Email: Adam.Klingbeil@Wabtec.com

Siddiq Khan, DOE Technology Manager
U.S. Department of Energy
Email: Siddiq.Khan@ee.doe.gov

Start Date: October 1, 2020 End Date: February 29, 2024
Project Funding: $3,114,481 DOE share: $2,472,668 Non-DOE share: $641,813

Project Introduction

Heavy-duty diesel engine manufacturers are continuously in pursuit of simple and low-cost technologies that can reduce emissions. Ducted fuel injection (DFI) and cooled spray (CS) technologies are two technologies that continue to show promise for significant particulate emissions reductions [1], [2]. These technologies represent a breakthrough in diesel engine combustion with the potential for nearly sootless diesel combustion. This can provide a significant decrease in harmful particulate matter emissions and may enable further system optimization for reduced NO_x emissions and increased efficiency. Combustion vessel experiments and engine demonstrations at Sandia National Laboratories, together with the large bore engine tests performed by Wabtec Corporation, show that this technology may be applicable to heavy-duty diesel engines across a wide range of engine sizes and speeds representing the majority of off-road diesel engines. However, very little is known about the ideal geometry, scaling properties, or effectiveness of these technologies over the engine operating map. This project addresses those uncertainties through a series of experiments performed in an optical and a metal single-cylinder engine.

The second year of this program has focused on evaluating some CS configurations in the Wabtec metal engine and commissioning the new engine hardware for the optical engine. Four CS inserts were tested in the metal Wabtec engine. Some inserts were tested with more than one alignment and nozzle flow, and tests were performed at many different operating conditions. The team has learned important details about the impact of alignment and geometry on the soot reduction potential of the components. Performance benefits have been observed at some conditions, and continuous progress is being made in terms of improved performance at other operating conditions. The optically accessible engine has been commissioned with updated hardware, and a sample image taken with a high-speed camera is included in this report. DFI has been tested in the optical engine, and future studies will focus on testing DFI and CS for the injector geometries and thermodynamic conditions of interest in this study.

Objectives

Overall Objectives

- Provide critical dimensional scaling guidance for DFI and CS technologies.
- Demonstrate more than 75% particulate matter reduction over a range of operating conditions using CS technology.

Fiscal Year 2022 Objectives

- Evaluate at least three CS configurations in a Wabtec metal engine.
- Quantify the performance impacts of CS components over the engine operating map.
- Demonstrate at least 50% soot reduction for some operating conditions using CS.
- Compare conventional diesel combustion to DFI in the optical engine at higher loads with larger injector orifices than previously demonstrated.

Approach

The optical engine at Sandia National Laboratories is a scientific tool that will enable detailed investigation of the combustion behavior of DFI and CS components. This is an ideal apparatus for exploring dimensional scaling studies. The engine is being upgraded as part of this project to enable operation at high speed and load (up to 24 bar gross indicated mean effective pressure [$IMEP_g$], 1,800 RPM). Optical access and state-of-the-art imaging diagnostics will enable the team to visualize the effect of geometric changes in both the hardware design (e.g., length and/or diameter of the ducts in DFI) and also changes to the injector (nozzle hole size) that are representative of larger or smaller engines. This data will be used to develop scaling correlations and also correlate performance between DFI and CS.

The metal single-cylinder engine installed at Southwest Research Institute will be used to explore the performance of CS hardware over the engine operating map. This engine is equipped with full-sized hardware from a Wabtec diesel engine, but the one-cylinder research engine enables faster and lower-cost testing of prototype hardware. Evaluations will be performed to identify a CS candidate for this engine, and then the performance will be studied over the operating map to determine how well the technology performs. Iterations are planned so that improved geometries can be explored over the operating map. Many CS design variants are being generated in parallel, and ongoing testing will evaluate a subset of those designs. Additionally, a series of experiments will be performed where the metal and optical engines operate under similar thermodynamic conditions with similar injector orifice sizes. Test results from the metal engine will be used to validate performance on real engine hardware at real engine conditions.

Results

Key accomplishments for Fiscal Year (FY) 2022 are listed below:

- Acquired baseline performance data for the supplemental engine test (SET) for exhaust gas recirculation (EGR) and non-EGR conditions in the Wabtec metal engine.
- Tested four CS inserts and showed filter smoke number (FSN) reductions of up to 75% at some conditions.
- Built and tested a new cylinder head for the optical engine with increased firing pressure capability and a rotational stage for mounting DFI and CS components.
- Built a new optical piston with 200 bar cylinder pressure capability; tested to 165 bar firing pressure.
- Tested DFI in the optical engine from 6 bar to 22 bar IMEPg, showing 40%–60% soot reduction. This is the first time DFI has successfully demonstrated significant soot reduction at this high of a load.

Metal Engine Testing

To demonstrate the performance impact of the CS inserts, baseline non-CS data is needed at all the operating conditions of interest. Hence, the first engine tests on the Wabtec metal engine were baseline performance tests for EGR and non-EGR conditions. The baseline data were recorded for the 13 operating conditions described in the SET [3]. Results for non-EGR operation are shown in Figure II.1.1. The weighted NO_x emissions scale

primarily with power and weighting factor of the SET, where the middle speed has higher weighting and the power scales up in proportion to torque. The soot emissions show a different trend, such that a significant amount of soot is generated at low torque and high engine speed. This suggests that the CS hardware should be particularly effective at the low-load, moderate- and high-speed conditions for non-EGR operation.

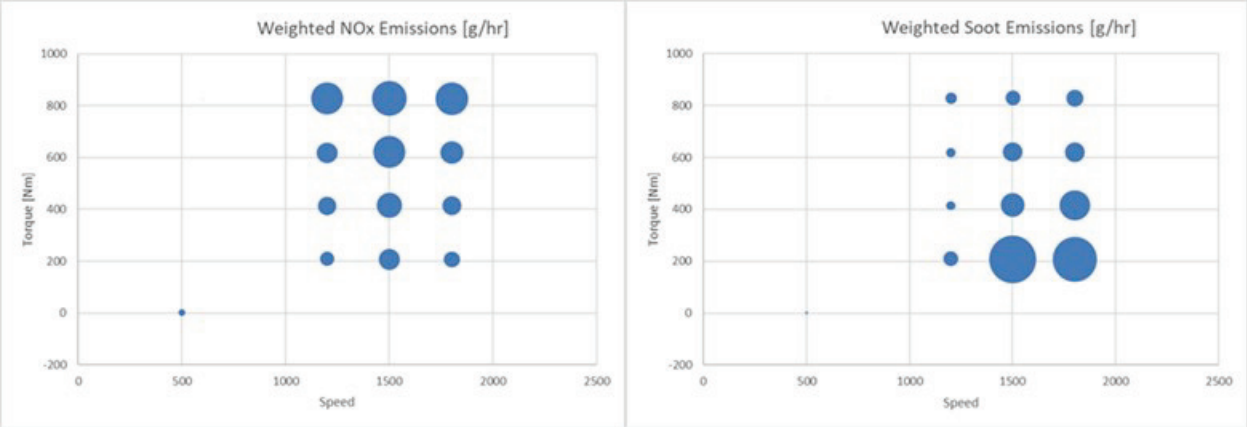

Figure II.1.1 NO_x and soot performance data for non-EGR operation in the Wabtec metal engine

Similar performance data are shown in Figure II.1.2 for EGR operation. In these tests, the EGR level was maintained at ~25%–30% for all conditions except idle, which did not use EGR. The EGR results show a different trend compared to the non-EGR results. The NO_x emissions are more evenly spread over the operating conditions without strong correlation between emissions and power. The moderate-speed, medium-load cases have the highest soot emissions; however, the soot emissions are also more evenly spread over the operating conditions. Thus, for EGR operation, the CS inserts will need to be fairly effective at all operating conditions to provide the most benefit. It is interesting to note that the lowest-speed conditions generally have the lowest NO_x and soot emissions.

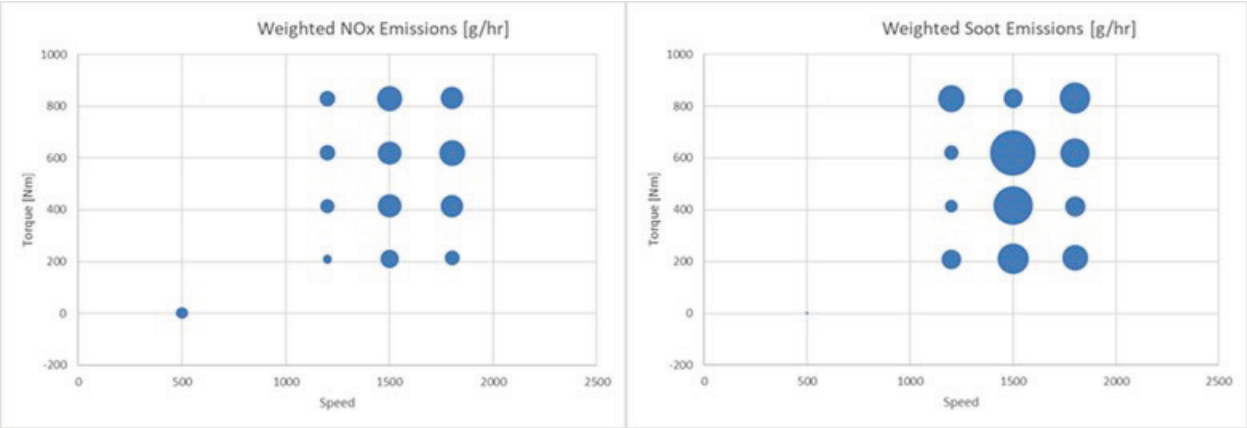

Figure II.1.2 NO_x and soot performance data for EGR operation in the Wabtec metal engine

After the baseline tests were completed, various CS insert designs were tested on the engine, and the geometry differences are summarized in Table II.1.1. The inserts have multiple air and fuel passages, but the fuel passage geometry is of primary importance for these studies. The first two inserts had drilled fuel passages with either a 2 mm or 1 mm diameter. Initial test results showed that Insert 2 (1 mm fuel passage) had poor overall performance while Insert 1 (2 mm drilled passages) had performance improvement at some conditions and degradation at other conditions. The second two inserts had fuel passages that were printed rather than drilled. Due to the rough surface finish of printing internal passages, the inserts were printed with undersized fuel passages that were hydro-eroded to the final dimensions. Insert 3 was printed with a converging inlet

section followed by a straight section while Insert 4 was printed with a cylindrical fuel passage. Both inserts with the printed passages had a nominal fuel passage diameter of 2.7 mm at the exit. However, with the hydro-grinding process, the inlet and outlet section developed a diverging opening. Comparing the drilled and printed fuel passages, the authors expect that the printed passages will be more precisely aligned in the insert, but with more variability in fuel passage diameter compared to the drilled passages. Measurements being made in FY 2023 will allow comparison of characteristics of the fuel passages for the two manufacturing methods.

Table II.1.1 Summary of Cooled Spray Geometries Tested

Configuration	Fuel Passage Inlet D [mm]	Fuel Passage Outlet D [mm]	Fuel Passage Manufacturing Method	Nozzle Orifice D [mm]	Misalignment Tested [mm]
Insert 1	2	2	Drill	0.32, 0.29	0.06, 0.37, 0.22, 0.08
Insert 2	1	1	Drill	0.32	0.14
Insert 3	3.2	2.7	Printed/Honed	0.29	0.18
Insert 4	2.7	2.7	Printed/Honed	0.29	0.1

The inlet and outlet diameters refer to the diameters of the fuel passages at the inlet where the fuel enters the passage and the outlet where the fuel leaves the passage.

Sample results from Insert 1 (2 mm drilled fuel passages) are shown in Figure II.1.3. The three conditions shown here are the full torque conditions at 1,200, 1,500, and 1,800 RPM. For the baseline measurements, an injection timing swing was performed to illustrate the NO_x/FSN tradeoff for the baseline engine. Any data that falls below or to the left of the baseline tradeoff represents an emissions improvement, while data that falls to the right or above the baseline tradeoff points represents an emissions degradation.

Two sets of CS data are plotted in Figure II.1.3. One data set, which contains only one data point, had a misalignment of approximately 0.37 mm (as estimated using a borescope). For this condition, there was approximately an eightfold increase in FSN compared to the baseline. There are multiple data points plotted in the Mode 2, 8, and 10 plots showing the performance data of the 0.22 mm misalignment case. These data show some interesting trends. First, comparing the 0.22 mm and 0.37 mm misalignment data at Mode 8, it is clear that a small amount of misalignment leads to a significant increase in emissions. Thus, it is likely that alignment sensitivity will be important when comparing designs.

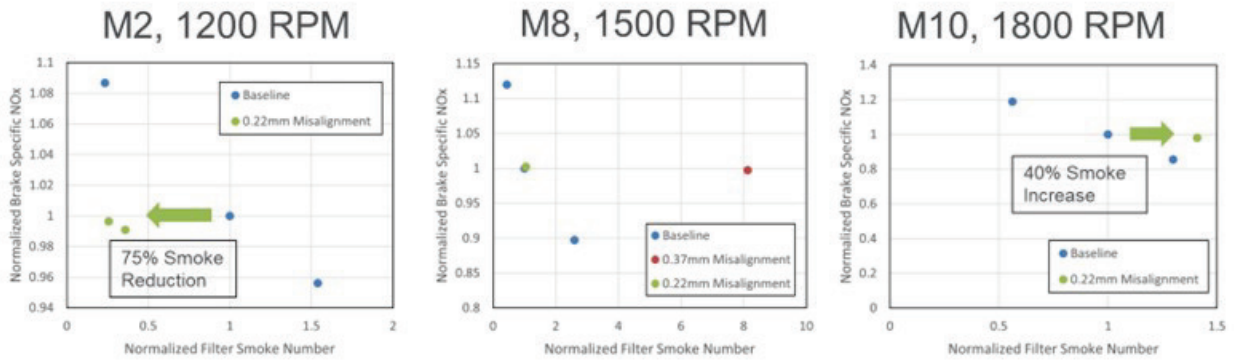

Figure II.1.3 NO_x versus FSN for three operating conditions comparing cooled spray Insert 1 to baseline non-cooled spray operation

The other key observation from Figure II.1.3 is that the CS insert is showing a 75% FSN reduction at Mode 2 (100% torque, 1,200 RPM). This is a significant achievement, illustrating the soot-reduction potential of the technology. However, at Mode 8 the emissions are similar between CS and the baseline, and at Mode 10 the

FSN increases 40%. Hence, more work is required to demonstrate performance improvements over all the operating conditions.

Figure II.1.4 summarizes the performance change of some of the CS configurations compared to the baseline. The first hardware configuration, 0.22 mm misalignment, is the same hardware configuration evaluated in Figure II.1.3. Note that this hardware configuration shows a performance penalty at most conditions. Given the improvement in performance that was observed from 0.37 mm to 0.22 mm misalignment, an additional series of tests were performed with even better alignment (0.076 mm misalignment) that resulted in operating conditions for EGR and non-EGR operation where the performance improved. However, performance degradation was also observed at many operating conditions. The last hardware configuration compared here is for the converging insert (Insert 3). For the alignment used (~0.18 mm misalignment), this hardware showed performance improvement at many conditions for both EGR and non-EGR operation, illustrating that—as the design is refined and alignment improves—the overall performance of the CS hardware is improving.

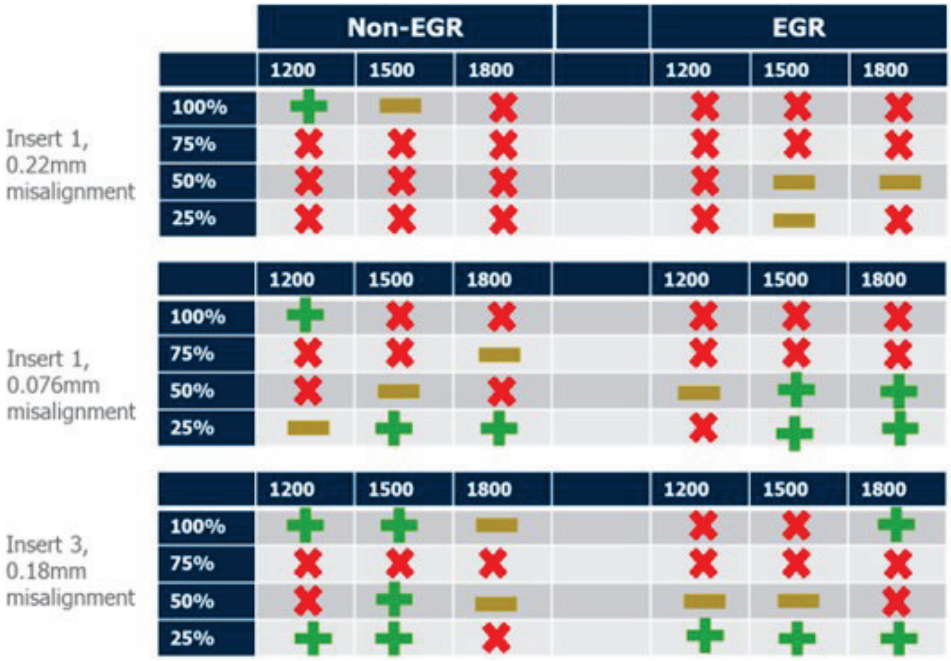

Figure II.1.4 Summary of performance change of cooled spray inserts compared to baseline. Green crosses indicate improvement, yellow dashes indicate performance parity, and red Xs indicate performance degradation.

Optical Engine Modification and Testing

Most of the effort at Sandia during this reporting period was focused on upgrading the optical engine for operation at higher firing pressures and higher loads, preparing for the two-duct DFI and CS experiments, and assisting the team with DFI combustion-system design and alignment details. A new cylinder head was designed with a novel mechanism for mounting DFI and CS hardware to facilitate fast, precision alignment. A new optical piston was fabricated to withstand the higher peak cylinder pressures of interest in this project (Figure II.1.5). The optical engine was operated to peak cylinder pressures of 165 bar with both conventional diesel combustion and DFI combustion (a significant achievement for an optical engine of this bore diameter), setting the stage for two-duct DFI and CS experiments early in FY 2023. Two-duct DFI modules were designed and submitted for finish-machining, and two-duct CS module design was initiated. DFI was tested with the new optical piston from 6 bar to 22 bar $IMEP_g$, and 40%–60% lower soot was observed versus conventional diesel combustion. To this team's knowledge, this is the first time DFI has demonstrated significant soot reduction above 20 bar $IMEP_g$. The project team believes that, through continued design improvements, additional and significant DFI and CS performance benefits will be possible.

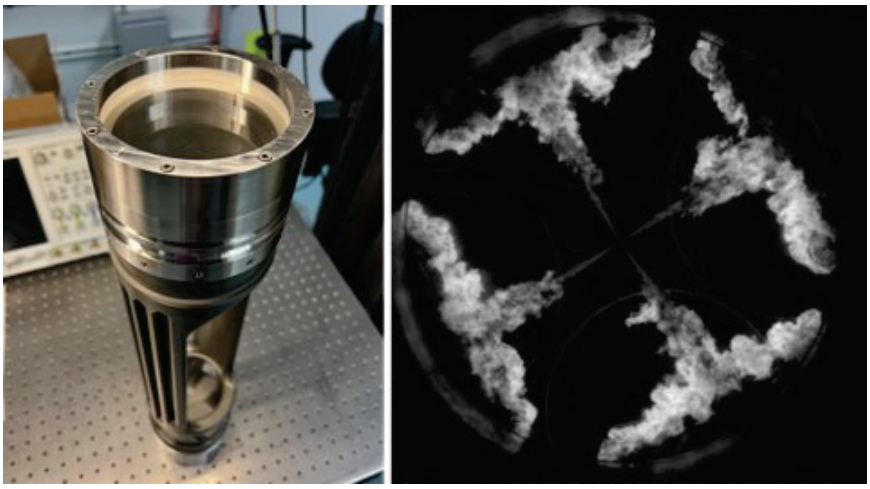

Figure II.1.5 Image of the new high-pressure optical piston (left). Combustion image for a four-hole injector using the new high-pressure optical piston (right).

Conclusions

Conclusions for FY 2022 are as follows:

- Multiple CS configurations were tested on the metal engine, showing up to 75% soot reduction at some conditions but soot increases at other conditions.
- The new optical engine hardware was commissioned for both conventional diesel combustion and DFI at higher load conditions.
- Metal and optical engine results are showing promising soot reduction for DFI and CS.

Key Publications

1. Klingbeil, A., B. Heher, M. Flores, A. Triana Padilla, T. Lavertu, T. Tinar, and S. Ellis. 2022. "Cooled Spray Technology for Particulate Reduction in a Heavy-Duty Engine." Proceedings of the ASME 2022 ICE Forward Conference, Indianapolis, IN, October 16–19. https://doi.org/10.1115/ICEF2022-90604.

References

1. Mueller, Charles J., Christopher W. Nilsen, Daniel J. Ruth, Ryan K. Gehmlich, Lyle M. Pickett, and Scott A. Skeen. 2017. "Ducted Fuel Injection: A New Approach for Lowering Soot Emissions from Direct-Injection Engines." *Applied Energy* 204: 206–220. https://doi.org/10.1016/j.apenergy.2017.07.001.

2. Nilsen, Christopher W., Drummond E. Biles, and Charles J. Mueller. 2019. "Using Ducted Fuel Injection to Attenuate Soot Formation in a Mixing-Controlled Compression Ignition Engine." *SAE International Journal of Engines* 12 (3): 309–322. https://www.jstor.org/stable/26840429.

3. DieselNet. 2016. "Heavy-Duty Supplemental Emissions Test (SET)." Last modified December 2016. https://dieselnet.com/standards/cycles/set.php.

Acknowledgements

The project team gratefully acknowledges David Ollett (National Energy Technology Laboratory); Chuck Mueller, Gustav Nyrenstedt, Christopher Nilsen, Nathan Harry, and Drummond Biles (Sandia National Laboratories); and Tristen Tinar, Scott Ellis, Travis Shaw, and Taylor Burns (Southwest Research Institute) for the support of this project.

II.2 Methanol Compression Ignition, Dual Fuel (Argonne National Laboratory)

Essam Elhannouny, Principal Investigator
Argonne National Laboratory
9700 South Cass Avenue
Lemont, IL 60439
Email: eel-hannouny@anl.gov

Siddiq Khan, DOE Technology Manager
U.S. Department of Energy
Email: Siddiq.Khan@ee.doe.gov

Start Date: October 1, 2021 End Date: September 30, 2022
Project Funding: $350,000 DOE share: $350,000 Non-DOE share: $0

Project Introduction

Millions of miles are covered on railroads every day to transport goods and people very efficiently. According to the Association of American Railroads, railroads are 3–4 times more efficient at moving freight than trucks [1]. Rail consumes around four billion gallons of diesel per year in North America [2], which translates to about 90 billion pounds of CO_2 emissions annually. The increasing focus on decarbonization of the internal combustion engine (ICE) for on-road applications—with the goal to reduce the greenhouse gas emissions to keep global warming well below 2°C—has also reached many applications in the off-road sectors, including rail. Essentially, the use of pure fossil-fueled engines must be reduced drastically, and with that, the deployment of ICE must become CO_2-neutral or CO_2-free. This change will bring challenges not only to the fueling infrastructure but also to engine and emission-control technologies that must be developed and deployed in order to replace conventional fossil-fueled ICEs.

Argonne National Laboratory entered in an advanced rail/marine research partnership with industry and is actively working toward enabling zero-carbon/low-carbon fuel-efficient engine designs for compression ignition in a dual-fuel mode to decarbonize the rail sector. Among the potential solutions that can achieve decarbonization of the rail sector is the use of methanol fuel. Methanol can be sustainably produced as a biofuel, as it can be made from cellulose (which does not compete with food sources). It can also be synthesized from CO_2 and hydrogen. The proposed work will focus on lowering the carbon impact of ICEs by using environmentally sustainable fuels such as methanol and dimethyl ether (DME) in a dual-fuel mode.

Objectives

Overall Objective

The objective of this new project is to develop and evaluate the performance of a dual-fuel technology in the Progress Rail 1010J single-cylinder, four-stroke locomotive engine (1010J-SCE) using methanol and DME fuels. The experimental work will focus on making modifications to the 1010J-SCE engine and the facility where the engine is housed to enable the use of the dual-fuel technology. Direct-injected methanol will be used as the main fuel, while DME will act as an ignition source. This work will have several stages as identified in the following bullets:

1. Initiate provisions for methanol fuel storage and delivery to the engine, working with Progress Rail to adapt the engine to a direct-injection fuel technology for the four-stroke 1010J-SCE.

2. Install a DME fuel system (including storage, measurement, and control) for DME pilot ignition of direct-injected methanol.

3. Evaluate initial engine performance using the 1010J-SCE fueled with methanol and compared to the baseline diesel tests.

4. Modify the 1010J-SCE engine with variable valve actuation for future combustion optimization.

Fiscal Year 2022 Objectives

- Recommission the Progress Rail 1010J-SCE four-stroke locomotive engine.
- Prepare facility and recommission all the 1010J-SCE subsystems.
- Perform engine shakedown tests to assess the engine condition.

Approach

Argonne National Laboratory and Progress Rail, with more than 25 years of advanced research partnership, will initially focus on the technical challenges of adapting locomotive ICEs to methanol fuel in a compression-ignition dual-fuel-mode technology. The dual-fuel technology will be developed toward a fuel-flexible engine capable of burning multiple environmentally sustainable fuels (liquid and gas fuels). Flexibility would be valuable in a commercial engine, enabling rail operators to choose from the most viable zero-carbon/low-carbon fuel depending on price and availability. Challenges with pilot ignition, direct fuel injection, and mixing are initially targeted to be addressed using the following approaches:

1. High-fidelity ICE modeling capabilities that leverage advanced physics-based sub-models for fuel injection, mixing, and combustion using high-performance computing.

2. Advanced X-ray diagnostics of fuel injection carried out at the Advanced Photon Source for characterizing injector geometries and near-nozzle sprays.

3. Advanced engine combustion research performed using dedicated single-cylinder locomotive engines.

Results

In Fiscal Year 2022, the Argonne National Laboratory research team moved the 1010J-SCE engine from storage and reinstalled it on the test platform as shown in Figure II.2.1. It is also noted that nearly half of this year's funds are destined for the computational modeling effort. On the other hand, this activity has not yet started, as the Argonne and Progress Rail teams are working toward establishing a Cooperative Research and Development Agreement (CRADA). As a result, all single-cylinder engine subsystems were commissioned/tested, and the following were executed in Fiscal Year 2022:

- Recommissioned the 1010J-SCE Progress Rail locomotive engine.
- Recommissioned the 1010J-SCE subsystems and performed all the required calibration.
- Executed engine shakedown and exercised the engine's capability to reach high throttle notch (TN1–TN8).
- Part of this year's effort was spent to establish a CRADA between Argonne National Laboratory and Progress Rail.

Figure II.2.1 Locomotive facility (left) and 1010J four-stroke single-cylinder engine (right) at Argonne National Laboratory

Conclusions

The commissioning of the 1010J single-cylinder locomotive engine has been completed. It incorporates various subsystem components. Engine shakedown was completed and showed the engine's capability to reach various throttle notches (load and speed). A CRADA agreement with Progress Rail is in progress.

References

1. Association of American Railroads. 2023. https://www.aar.org/climate-change. Accessed February 2023.

2. Davis, Stacy C., and Robert G. Boundy. 2019. *Transportation Energy Data Book: Edition 37*. Prepared by Oak Ridge National Laboratory, Oak Ridge, TN. Washington, DC: DOE Office of Energy Efficiency and Renewable Energy Vehicle Technologies Office.

Acknowledgements

The author gratefully acknowledges the support of our DOE Program Managers Gurpreet Singh and Siddiq Khan. The author is also grateful to the Progress Rail team for their support through provision of the 1010J engine, injectors, and all the required Tier 4 hardware.

II.3 Hydrogen Combustion Research – Cooperative Research and Development Agreement with Wabtec (Argonne National Laboratory)

Muhsin Ameen, Principal Investigator
Argonne National Laboratory
9700 South Cass Avenue
Lemont, IL 60439
Email: mameen@anl.gov

Siddiq Khan, DOE Technology Manager
U.S. Department of Energy
Email: Siddiq.Khan@ee.doe.gov

Start Date: May 12, 2022 End Date: Project continuation evaluated annually
Project Funding: $200,000 DOE share: $150,000 Non-DOE share: $50,000

Project Introduction

The U.S. Department of Energy (DOE) has identified rail transport as a hard-to-electrify sector. Rail is one of the most energy-efficient transportation modes, especially from a tonne-mile perspective. However, rail accounts for 2% of the U.S. transportation sector's GHG emissions, according to the EPA [1]—hence the need for decarbonization and emissions reduction. DOE identifies three key technologies to achieve rail decarbonization: battery/electric, hydrogen, and sustainable liquid fuels [2]. While hydrogen can be used in fuel cells to generate electricity, it can also be burned in internal combustion engines as a sustainable fuel. Hydrogen substitution in diesel engines offers a short-term emissions reduction solution for rail, on track to full hydrogen operation. For each diesel-powered locomotive converted to alternative energy sources, up to 5.6 million pounds of CO_2 per year can be eliminated. However, before tackling hydrogen, computational fluid dynamics (CFD) techniques for locomotive engines need to be investigated further. The current project is focused on developing CFD best practices and accurate submodels that can be used to assess different technologies that can enable up to 100% operation of hydrogen combustion in large-bore locomotive engines. This project is part of a cooperative research and development agreement (CRADA) that includes Wabtec Corporation and Convergent Science, Inc., and will also leverage strong collaborations with a parallel experimental effort at Oak Ridge National Laboratory (ORNL).

The project officially kicked off in May 2022. The first year of the project was focused on developing a baseline CFD framework that will be used for modeling hydrogen–diesel dual-fuel combustion in locomotive engines. The commercial CFD code, CONVERGE [3], was used for performing the simulations and developing best practices. A preexisting experimental dataset for a Wabtec engine on a dual-fuel natural gas (NG)–diesel operation was used for validation in the current year. This dataset provides a good starting point for validating the simulations before the hydrogen measurements become available from ORNL in Fiscal Year (FY) 2023. This setup shares several key features, including the injection system and combustion chamber, with the hydrogen engine. The project team analyzed the effect of several numerical parameters, including turbulence models, combustion models, numerical grid setup, etc., on the accuracy and cost of the simulations. Techniques to improve the speed of the simulations without sacrificing accuracy were assessed. Initial simulations on hydrogen port-injection were also performed. The simulations were used to evaluate the effect of the NG substitution rate on combustion, emissions, and stability.

Objectives

This project focuses on developing and validating computational tools for combustion of low-carbon fuels, with a focus on hydrogen, in heavy-duty rail engines. We intend to then use these simulations to assist in

evaluating different technologies and fuel injection options to enable up to 100% operation on hydrogen and low-carbon fuels for rail engines.

Overall Objectives

- Develop a CFD modeling framework for hydrogen combustion in locomotive engines.
- Evaluate the effect of hydrogen substitution rates on combustion performance and stability.
- Optimize the injection and combustion system for improving combustion performance and minimizing emissions.

Fiscal Year 2022 Objectives

- Develop an accurate CFD tool for modeling dual-fuel combustion in locomotive engines.
- Quantify accuracy of tool through comprehensive validation studies.
- Evaluate the effect of turbulence and combustion models on model accuracy.

Approach

The current project is aimed at using CFD simulations to enable up to 100% operation of hydrogen for large-bore rail engines. The commercial CFD code, CONVERGE [3], is being used to perform the simulations. The engine considered in this work is a single-cylinder 15 L Wabtec locomotive research engine. Experimental data for validation are available from Wabtec Corporation for NG–diesel operation and will be available in FY 2023 from ORNL for hydrogen–diesel operation. The engine has two intake valves/ports and two exhaust valves/ports. The engine is equipped with an eight-hole diesel injector located at the center of the cylinder and an NG injector in the intake port. Figure II.3.1 shows the engine without the intake and exhaust plenums, which are not part of the computational domain.

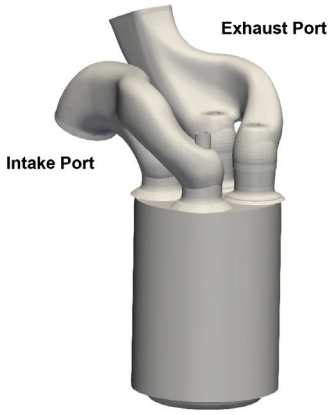

Figure II.3.1 Engine geometry, with intake and exhaust ports marked

This project is taking a two-stage approach. Phase 1 of the project will focus on port fuel injection of hydrogen with direct injection of diesel. For low substitution rates of diesel with hydrogen, a port-fuel injection strategy will allow up to a 50% substitution rate of hydrogen and can be used for retrofitting currently existing engines. Simulation efforts will involve determining the maximum substitution rates that can allow stable combustion and low emissions. For higher substitution rates, direct injection of hydrogen will be utilized. This will involve improvements in the currently existing submodels for injection, wall heat transfer, and flame–wall interaction. Thus, Phase 2 will involve model development and evaluation for direct injection of hydrogen in locomotive engines. Both low-pressure and high-pressure injection systems will be evaluated.

Results

The key accomplishments for FY 2022 were in performing CFD simulations of NG–diesel dual-fuel combustion in the Wabtec single-cylinder 15 L research engine (Figure II.3.1). These simulations are aimed at baselining the CFD setup and identifying scopes for improvement. The computational grid setup is shown in Figure II.3.2 and detailed in Table II.3.1. Four different cases were simulated with increasing levels of NG substitution rates: Case 1 is pure diesel, while Cases 2, 3, and 4 corresponded to NG substitution rates of 53.6%, 64.1%, and 79.5% respectively. All the simulations were validated with available experimental measurements from Wabtec. The major findings are discussed in the next section.

Figure II.3.2 In-cylinder computational grid used for the simulations. The figure shows the refinements used near the injector and combustion zones.

Table II.3.1 Details of the Different Computational Grids Used in This Work

Grid Sizes (mm)	Grid 0	Grid 1	Grid 2	Grid 3	Grid 4	Grid 5
Base Size	6	6	4	4	3	3
Cylinder Embedding	3	1.5	1	1	0.75	0.75
Valve Embedding	0.375	0.375	0.25	0.25	0.1875	-
Injector Embedding	0.375	0.375	0.25	0.25	0.1875	0.09375
Piston Wall Embedding	0.75	0.375	0.25	0.25	0.1875	0.09375
Intake Adaptive Mesh Refinement (AMR)	0.75	0.75	0.5	0.25	0.375	-
Cylinder AMR	0.75	0.75	0.5	0.25	0.1875	0.09375

Effect of Turbulence Model

Prior work [4] has shown that, for large-bore engines, the traditional k-ε turbulence models do not perform well because of the strong anisotropy that is observed. In the current study, two different turbulence models were used: the RNG k-ε model and the Reynolds Stress Model (RSM). Figure II.3.3 shows the effect of the turbulence model for Case 1. The results are normalized against the maximum value. Figure II.3.3 shows that the in-cylinder pressure predicted by the different setups is identical till around 5° crank angle (CA) at top dead center (aTDC), after which the pressure traces diverge with the RSM results (in red) providing the best agreement with the experimental average (in black). The k-ε model underpredicts the in-cylinder pressure, especially as the grid is refined from Grid 0 to Grid 1. This behavior is also observed in the apparent heat release rate (AHRR) plots, where k-ε underpredicts the heat release rate compared to RSM, which then carries over to combustion phasing, especially at CA90. Hence, it can be concluded here that, in line with the literature, RSM provides better results than k-ε for large-bore engines. As a result, RSM is implemented as the standard turbulence model for all results going forward.

Grid Convergence Studies

Refining the grid in premixed combustion can sometimes reduce the burn rate and in-cylinder pressure. Here, Case 2 with a mixed-mode combustion operation (diesel non-premixed and NG premixed) is simulated using four grid sizes (Grid 1–4) and the RSM turbulence model. The results are shown in Figure II.3.4 and, as in Figure II.3.3, include the in-cylinder pressure, AHRR, and combustion phasing. The results are normalized against the same maximum value. Figure II.3.4 shows that, as expected for premixed combustion, the in-cylinder pressure decreases when refining from Grid 1 to Grid 2 and to Grid 3. However, when refining to Grid 4 (AMR < 0.25 mm), the in-cylinder pressure increases compared to Grid 3, which is an indication of grid convergence. In addition, the combustion phasing shows improvements when refining the grid from Grid 1 to 3, especially at CA90.

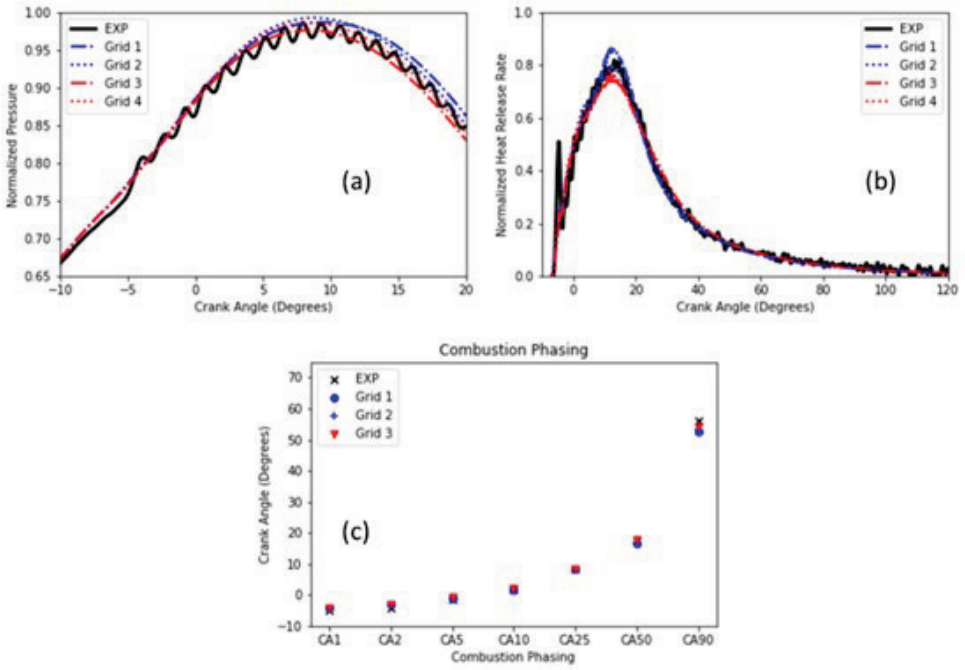

EXP – experimental

Figure II.3.3 Normalized pressure, normalized heat release rate, and combustion phasing comparing results from Grids 1–4 for Case 2 using the RSM turbulence model

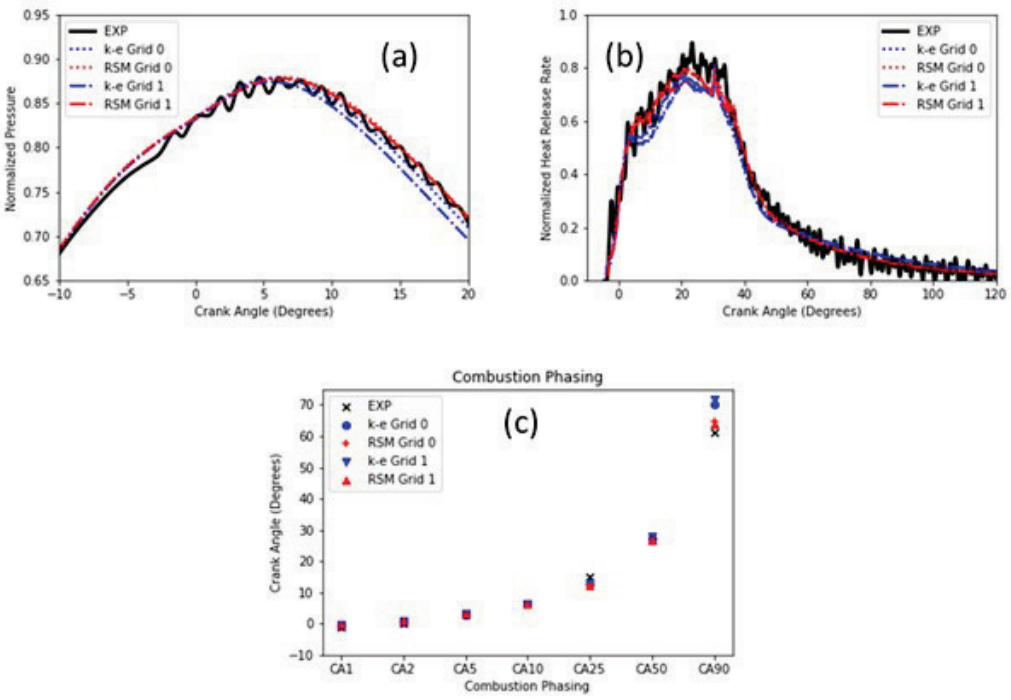

Figure II.3.4 Normalized pressure, normalized heat release rate, and combustion phasing comparing RSM and k-ε turbulence models for Case 1 using Grids 0 and 1

Effect of Combustion Model

The well-stirred reactor multizone (WSR MZ) model allows multidimensional zoning strategies to group computational cells with similar properties into zones (or bins) and speed up the simulation. The bin size can be decreased to improve accuracy and increase computational cost. For dual-fuel operation, three-dimensional zoning is recommended. The default bins are temperature and progress equivalence ratio. The third bin used here is that of n-heptane (C_7H_{16}). Figure II.3.5 shows the normalized in-cylinder pressure, heat release rate, and combustion phasing of Case 3 using Grid 1 with WSR MZ (two bins), WSR MZ (three bins), and WSR without MZ. WSR without MZ will produce the most accurate results with a higher computational cost. The results show that, while the difference between the results of two and three bins is not significant, MZ with three bins produces better results and matches the results produced without MZ. Using three bins produces the same accuracy as WSR without MZ, with reduced computational cost.

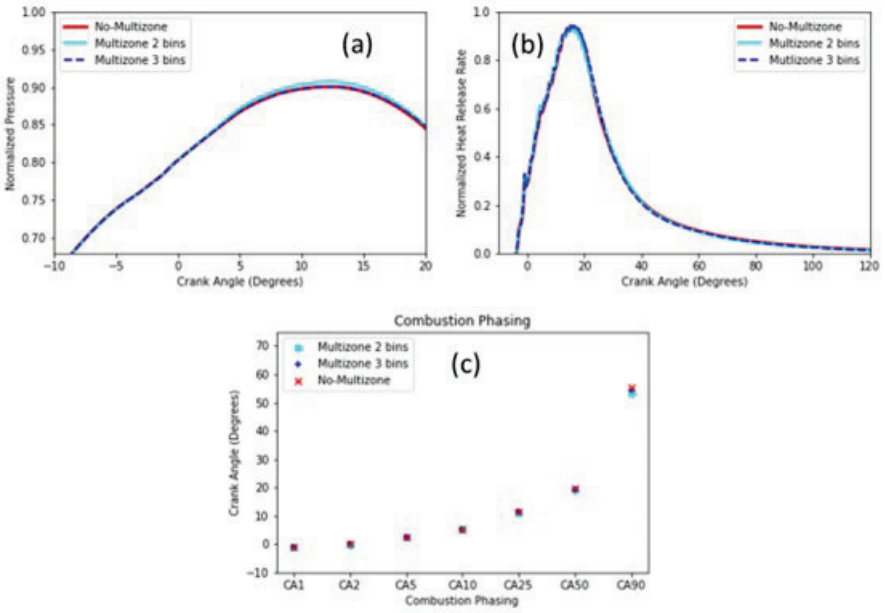

Figure II.3.5 Normalized pressure, normalized heat release rate, and combustion phasing comparing the different bin options of the multizone WSR solver using Grid 1 for Case 3

Conclusions

The major conclusions from the work conducted this year are as follows:

- Accurate CFD simulations of the Wabtec locomotive engine operating on diesel–NG dual-fuel were performed, and simulations were validated using experimental data.
- The RSM turbulence model provided better results than Reynolds-averaged Navier–Stokes (RANS) k-ε, and the computational cost associated with RSM was 6%–7% higher.
- Grid convergence is achievable with grid sizes <0.2 mm, and the in-cylinder pressure does not keep decreasing with grid refinement.
- Three zones (or bins) are required when using the WSR MZ combustion model.
- As the substitution rate increases, a finer grid is required to account for the increase in mixed-mode (premixed and non-premixed) combustion within the cylinder.

Key Publications

1. Kazmouz, S., A. Klingbeil, T. Lavertu, V. Jayakar, P. Sheth, S. Wijeyakulasuriya, and M. Ameen. 2023. "Simulations of Dual-Fuel Natural Gas/Diesel Operation in Large-Bore Locomotive Engines." 13th US National Combustion Meeting, College Station, TX.

References

1. Environmental Protection Agency. n.d. Fast Facts on Transportation Greenhouse Gas Emissions (2022) EPA. Accessed January 14, 2023. https://www.epa.gov/greenvehicles/fast-facts-transportation-greenhouse-gas-emissions.

2. DOE Office of Energy Efficiency and Renewable Energy. 2023. The U.S. National Blueprint for Transportation Decarbonization: A Joint Strategy to Transform Transportation. DOE/EE-2674. https://www.energy.gov/eere/us-national-blueprint-transportation-decarbonization-joint-strategy-transform-transportation.

3. Richards, K.J., P.K. Senecal, and E. Pomraning. 2021. CONVERGE 3.0. Convergent Science, Madison, WI.

4. Addepalli, S.K., G.M. Magnotti, S. Som, P. Sheth, V. Jayakar, A. Klingbeil, and T.A Lavertu. 2022. "CFD Study on Mixture Preparation and Combustion in a Heavy-Duty Locomotive Diesel Engine at High Load Condition." Proceedings of the ASME 2022 ICE Forward Conference, Indianapolis, IN, October 16–19.

Acknowledgements

The work was performed jointly by Samuel Kazmousz and Muhsin Ameen from Argonne National Laboratory. The technical support from Tom Lavertu, Adam Klingbeil, Pushkar Sheth, and Vijayaselvan Jayakar from Wabtec Corporation is acknowledged. We also acknowledge Sameera Wijeyakulasuriya from Convergent Science for his guidance. Computing resources were provided by the Argonne Laboratory Computing Resources Center.

II.4 Experimental Biodiesel Blends and Renewable Diesel (Argonne National Laboratory)

Chao Xu, Principal Investigator
Argonne National Laboratory
9700 South Cass Avenue
Lemont, IL 60439
Email: chaoxu@anl.gov

Siddiq Khan, DOE Technology Manager
U.S. Department of Energy
Email: Siddiq.Khan@ee.doe.gov

Start Date: October 1, 2021 End Date: September 30, 2022
Project Funding: $100,000 DOE share: $100,000 Non-DOE share: $0

Project Introduction

Given the increased focus on global warming and reduced greenhouse gas emissions, the off-road and rail markets must be equally vigilant about the decarbonization of their internal combustion engines as has been the case for on-road applications. Biodiesel blends and renewable diesel are promising alternative fuels to conventional diesel fuel to reduce the carbon footprint of locomotive operations for the rail sector. This project focuses on evaluating impacts of biodiesel blends and renewable diesel on engine operation, performance, and emissions using the Progress Rail 1010J single-cylinder four-stroke locomotive engine (1010J-SCE) at Argonne National Laboratory. Computational fluid dynamics (CFD) simulations will be used to improve the knowledge of the fuel's behavior in terms of internal injector flow, spray, fuel–air mixing, combustion, and emission formation. This knowledge can in turn enable targeted injection strategies for internal combustion engines in rail applications, which aim to unlock higher combustion efficiency, lower fuel consumption, and minimized tailpipe emissions while accounting for differences in the physical and chemical properties between biodiesel/renewable diesel and conventional diesel fuels.

Objectives

This work is a coordinated experimental and numerical effort that aims to enable efficient engine operation in rail applications via the use of low-life-cycle carbon fuels such as biodiesel and renewable diesel. The goal is to identify the necessary modifications to be made to the 1010J-SCE engine and injection system that will allow use of these fuels while ensuring the engine's compliance with Tier 4 emission regulations. It is envisioned that this goal will be achieved through CFD-guided optimization of the injection and combustion system operation, which will be used to inform the engine experiments.

Overall Objectives

- Develop CFD models and best practices for 1010J-SCE's injector and engine.
- Quantify the fuel effects on internal injector flow, spray formation, and combustion and emissions performances of the 1010J-SCE engine for a wide range of biodiesel blends and renewable diesel.

Fiscal Year 2022 Objectives

- Recommission the 1010J-SCE engine test facility.
- Develop baseline models for high-fidelity nozzle flow simulations.

Approach

The scope of the internal injector flow simulation effort is to build a high-fidelity CFD model of the injector, formulate best practices for describing the internal flow and the ensuing spray of the fuels of interest (baseline diesel, biodiesel, renewable diesel, and their blends), and extract spatio-temporally resolved maps of the internal flow at the exit of the injector's orifices. Particular focus will be placed on identifying the injector propensity for cavitation when alternative fuels such as biodiesel and renewable diesel are used. Injector design modifications will be proposed to suppress or mitigate such occurrences, which could otherwise be detrimental to the correct functioning and durability of the injector units. The extracted maps will then be used in the engine simulations to ensure accurate initialization of the fuel spray via a static-coupling approach, as documented in previous work by the Argonne team [1]. The impact of different fuel properties on spray morphology, atomization, and evaporation characteristics will be quantified. All simulations will rely on physics-based models and all calculations will be conducted using the CONVERGE CFD software.

Results

The major accomplishments of Fiscal Year 2022 are summarized as follows:

- Preparation and setup of a CFD model of the Tier 4 common rail injector used in the Progress Rail 1010J engine.
- Preliminary evaluation of the internal flow's injector behavior.

CFD Model Setup of Tier 4 Common Rail Injector

The drawings of the injector model (Figure II.4.1) were provided by the project collaborators at Progress Rail. These drawings were used to generate a CFD-ready geometry of the injector's internal passages, specifically the injector tip where the injector needle tip, sac, and orifices are located. A methodology first introduced and described in previous work by the Argonne team [2] was employed to achieve easy modification of the injector geometry via a MATLAB script that allows the user to modify in an automated way the injector's K-factor, the sac-to-orifice fillet's radius of curvature, the orifice's inlet ellipticity, and the orifice outlet diameter.

Figure II.4.1 View of entire domain (left), injector tip (center), and detail of injector sac and orifices (right)

Preliminary Evaluation of the Internal Flow's Injector Behavior

The injector geometry model introduced in the previous section was used to assess the opportunity to extend typical heavy-duty injector best practices [3] to much larger injectors, such as the Tier 4 rail injector used in this work. A typical Notch 8 operating condition was targeted, which is represented by an injection pressure of ~2,300 bar, ambient pressure of ~180 bar, and injection duration of slightly more than 6.0 ms. The preliminary results showed that no cavitation is expected when the nominal design of the injector and diesel fuel are used (Figure II.4.2). The peak mass flow rate is currently underestimated by 5%–7%, which could be ascribed to the use of a computer-aided-design-based geometry that does not account for the effect of manufacturing processes such as injector hydrogrinding. A new simulation campaign is currently ongoing to assess the effect of hydrogrinding via modifications of the outlet diameter and the shape of the orifice inlet.

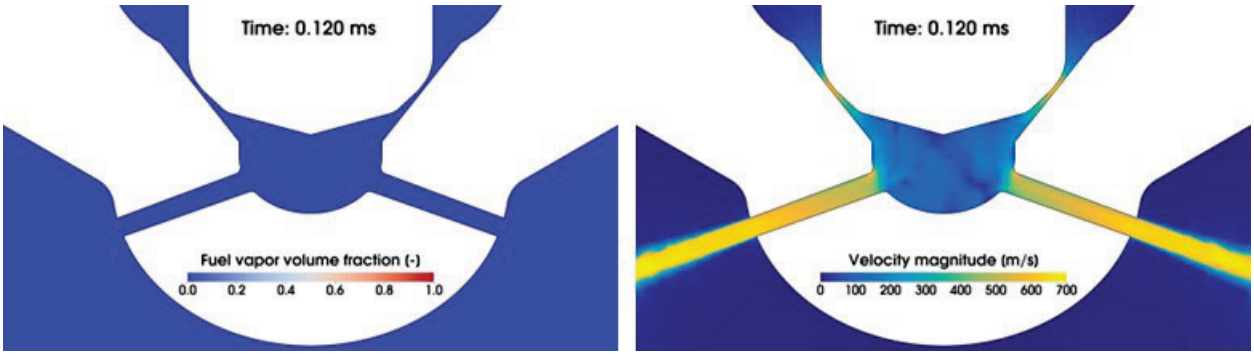

Figure II.4.2 Fuel vapor volume fraction and corresponding velocity magnitude flow fields at 0.120 ms after the start of injection

Conclusions

- A CFD model of the Tier 4 injector geometry was successfully generated and set up to perform simulations of the injector's internal flow. The ability to modify the injector geometry was added to the model in order to evaluate the effect of injector design features on the cavitation and performance of the injector.

- Preliminary simulations have been performed to baseline the injector model using conventional diesel fuel. This activity is ongoing and will be completed in Fiscal Year 2023.

References

1. Torelli, R., Y. Pei, Y. Zhang, and S. Som. 2022. "End-to-End Modeling of Fuel Injection via Static Coupling of Internal Flow and Ensuing Spray." Communications Engineering 1 (42). https://doi.org/10.1038/s44172-022-00038-z.

2. Torelli, R., G.M. Magnotti, S. Som, Y. Pei, and M.L. Traver. 2019. "Exploration of Cavitation-Suppressing Orifice Designs for a Heavy-Duty Diesel Injector Operating with Straight-Run Gasoline." SAE Technical Paper 2019-24-0126. https://doi.org/10.4271/2019-24-0126.

3. Torelli, R., K.E. Matusik, K.C. Nelli, A.L. Kastengren, K. Fezzaa, C.F. Powell, S. Som, Y. Pei, T. Tzanetakis, Y. Zhang, M.L. Traver, and D.J. Cleary. 2018. "Evaluation of Shot-to-Shot In-Nozzle Flow Variations in a Heavy-Duty Diesel Injector using Real Nozzle Geometry." SAE International Journal of Fuels and Lubricants 11 (4): 379–396. https://doi.org/10.4271/2018-01-0303.

Acknowledgements

This research was funded by DOE's Office of Vehicle Technologies and Office of Energy Efficiency and Renewable Energy under Contract No. DE-AC02-06CH11357.

The Principal Investigators gratefully acknowledge the contributions of Dr. Fu Xiao from Progress Rail for sharing injector and engine geometries.

The authors wish to thank Gurpreet Singh and Siddiq Khan, Program Managers at DOE's Office of Energy Efficiency and Renewable Energy Vehicle Technologies Office, for their support.

The authors would also like to acknowledge the Laboratory Computing Resource Center at Argonne National Laboratory for computing time on the Bebop cluster, which was used in this research.

II.5 Implementing Low Life Cycle Carbon Fuels on Locomotive Engines–Cooperative Research and Development Agreement with Wabtec (Oak Ridge National Laboratory)

K. Dean Edwards, Principal Investigator
Oak Ridge National Laboratory
P.O. Box 2008, MS 6472
Oak Ridge, TN 37831
Email: EdwardsKD@ornl.gov

Siddiq Kahn, DOE Technology Manager
U.S. Department of Energy
Email: Siddiq.Khan@ee.doe.gov

Start Date: July 18, 2022	End Date: July 17, 2026	
Project Funding: $1,250,000	DOE share: $1,000,000	Non-DOE share: $250,000 + $2,100,000 in-kind

Project Introduction

With increasing efforts to decarbonize the transportation sector, focus is now being placed on heavy-duty sectors including rail, marine, off-road, and aviation, which present difficult challenges for electrification and decarbonization. Decarbonization of the rail freight industry has significant challenges due to many factors including high power demands, operating duty cycle, long service lifetime of locomotives (30+ years), and prohibitive cost of electrifying the extensive existing railway system. However, the potential benefits are significant, with each decarbonized locomotive reducing greenhouse gas emissions by an estimated 5.6 million pounds of CO_2 per year. The use of alternative low life cycle carbon fuels (LLCFs) into existing engine technologies is an attractive pathway for near-term impact through retrofit solutions and for longer-term benefits as the LLCF infrastructure is developed.

This project supports a cooperative research and development agreement (CRADA) between Oak Ridge National Laboratory (ORNL) and Westinghouse Air Brake Technologies Corporation (Wabtec), the leading U.S. manufacturer of freight locomotives, to develop solutions for use of LLCFs and low-emissions technologies for locomotive engines. Together, ORNL and Wabtec will work to identify hardware configurations and operating strategies required for dual-fuel operation of locomotive engines to achieve at least 50% fuel substitution in retrofit applications and near 100% substitution in new locomotive applications while still meeting requirements for engine performance and pollutant emissions.

Objectives

Overall Objectives

- Install and commission a Wabtec single-cylinder research locomotive engine at ORNL with infrastructure to support LLCF studies.
- Develop port-fuel-injection retrofit hardware configurations and operating strategies for dual-fuel operation with LLCFs and identify maximum fuel substitution rates while maintaining engine performance and emissions compliance.
- Develop direct injection hardware configurations and operating strategies for near-complete fuel substitution with LLCFs while maintaining engine performance and emissions compliance.

Fiscal Year 2022 Objectives

- Execute the CRADA agreement between ORNL and Wabtec.

- Begin installation of the Wabtec single-cylinder research engine, subsystems, and LLCF infrastructure at ORNL.

Approach

Once the single-cylinder engine is installed and commissioned at ORNL, the project team will begin experimental studies to fully explore dual-fuel retrofit approaches with port injection of hydrogen. These studies will initially focus on exploring the operating space to understand the boundaries for avoiding engine knock, backfire, and high nitrogen oxides (NO_x) emissions. We will then focus on maximizing diesel displacement with hydrogen within those boundaries. The next phase of the study will repeat this process for direct injection strategies targeting near-complete displacement of diesel with hydrogen. The project will also conduct studies with other LLCFs, such as methanol, ammonia, and renewable and bio-derived diesel fuels.

Experimental data from these studies will be shared with Argonne National Laboratory researchers, who, under a related CRADA with Wabtec and Convergent Science, will develop and validate computational fluid dynamics models of the engine to further explore and optimize LLCF operating strategies. Guidance from those simulations will, in turn, be brought back to ORNL for experimental evaluation on the research engine.

Results

During the first year of this project, efforts focused on finalizing the legal terms of the CRADA and planning infrastructure upgrades to research facilities at ORNL to support installation and operation of the Wabtec single-cylinder research engine with LLCFs.

- Fully executed the CRADA between ORNL and Wabtec on July 18, 2022, allowing work to officially commence.
- Began upgrades to the ORNL research laboratory to support operation of the single-cylinder locomotive engine: additional electrical and chilled water capacity, upgraded fueling infrastructure for diesel and LLCFs, and hoisting capabilities to enable hardware swaps and engine maintenance.
- Received Wabtec single-cylinder engine and dynamometer at ORNL in August 2022, and performed an engine rebuild to install the new Tier 3 power assembly, instrumented head, and dual-fuel injection system (see Figure II.5.1).
- Completed the initial phase of third-party assessment and planning for safe operation with hydrogen in the research facility at the ORNL National Transportation Research Center.

Figure II.5.1 Wabtec single-cylinder locomotive research engine and dynamometer at the ORNL National Transportation Research Center

Conclusions

This project is just commencing, with installation of the single-cylinder engine at ORNL underway.

III Marine

III.1 Enabling Hydrogen and Methanol Combustion (Argonne National Laboratory)

Riccardo Scarcelli, Principal Investigator
Argonne National Laboratory
9700 South Cass Avenue
Lemont, IL 60439
Email: rscarcelli@anl.gov

Kevin Stork, DOE Technology Manager
U.S. Department of Energy
Email: Kevin.Stork@ee.doe.gov

Start Date: Expected April 2023 End Date: Expected March 2027
Project Funding: $600,000 DOE share: $600,000 Non-DOE share: $0

Project Introduction

This project embodies a Cooperative Research and Development Agreement (CRADA) between Argonne National Laboratory (Argonne), Caterpillar Inc. (Caterpillar), and Convergent Science Inc. (CSI). The goal of this collaboration is to develop advanced engine technologies for low-carbon fuels and the corresponding computational models and tools. Argonne is a national laboratory with expertise in multi-physics computations, internal combustion engine modeling, and high-performance computing. Caterpillar is a U.S. company and worldwide leader in developing and manufacturing internal combustion engines for off-road applications. CSI is the owner and developer of the computational fluid dynamics (CFD) commercial software CONVERGE.

Objectives

This collaborative effort aims to develop predictive computational capabilities for the analysis and design of advanced internal combustion engines for off-road applications. The focus of this project is on engine combustion utilizing zero-carbon (hydrogen) or low-carbon (methanol) fuels. CFD will be used to analyze and predict in detail all the physical processes that characterize the engine operation, from the fuel injection to the combustion and emission-formation processes.

Overall Objectives

- Develop predictive models for the simulation of low-carbon-fuel off-road internal combustion engines.
- Define modeling best practices to efficiently design off-road engines using low-carbon fuels.

Fiscal Year 2022 Objectives

- Finalize the scope of work to address DOE/industry priorities for off-road sector decarbonization.
- Define the technical scope and legal terms of the CRADA and submit CRADA documents for approval.

Approach

The entire CRADA is planned over a duration of 48 months (four years) and divided into two main tasks that will each last 24 months (two years) and be performed sequentially:

- Task 1: Predictive CFD Models for Hydrogen Combustion in Off-Road Engines (M1–24)
  This task aims at developing predictive CFD models and best practices for the simulation of hydrogen internal combustion engines for off-road applications. The final deliverables to Caterpillar will be made through the optimization of the CFD setup for hydrogen internal combustion engine (ICE) simulations and the implementation of improved and/or newly developed models into the commercial solver CONVERGE. Argonne will leverage high-fidelity simulations using the exascale-ready code Nek5000 together with high-performance computing resources to guide the development of new models and the optimization of existing models in CONVERGE. Engine data for model validation will be provided by Caterpillar.

- Task 2: Predictive CFD Models for Methanol Combustion in Off-Road Engines (M25–48)
  This task aims to develop and enhance predictive models for simulating injector wear, injection, spray-wall interaction, and combustion for methanol in off-road engines. Argonne will leverage X-ray measurements from Argonne's Advanced Photon Source to guide the development of new models and the enhancement of existing ones within CONVERGE. Injector hardware, durability testing, spray vessel data, and engine data will be provided by Caterpillar.

Throughout the project duration, CSI will provide the CONVERGE software license and technical expertise as their in-kind cost-share contributions.

Results

In Fiscal Year (FY) 2022, we defined the scope of work and the CRADA legal terms. CRADA documents have been submitted and are currently under revision. The expectation is to have the CRADA approved and started in FY 2023. The project has not started yet. Accordingly, funds received in FY 2022 are considered a forward-funding DOE contribution towards FY 2023 activities.

Conclusions

- The CRADA scope of work was finalized in FY 2022.
- The CRADA documentation package is currently under review for approval.

Acknowledgements

The project principal investigator (PI) would like to thank Argonne's co-PIs Chao Xu, Roberto Torelli, and Chris Powell. The PI would also like to thank the PIs at Caterpillar (Jon Anders and Robert McDavid) and CSI (Peter Kelly Senecal).

III.2 Renewable Methanol-Fueled Engines for Marine and Off-Road Applications (Oak Ridge National Laboratory)

James Szybist, Principal Investigator
Oak Ridge National Laboratory
2360 Cherahala Boulevard
Knoxville, TN 37932
Email: szybistjp@ornl.gov

Kevin Stork, DOE Technology Manager
U.S. Department of Energy
Email: Kevin.Stork@ee.doe.gov

Start Date: October 1, 2021 End Date: December 8, 2026
Project Funding: $500,000 DOE share: $500,000 Non-DOE share: $0

Project Introduction

The world has seen a dramatic shift toward an emphasis on greenhouse gases (GHGs) over the past several years, with a focus on reducing carbon dioxide (CO_2) and other GHG emissions, such as nitrous oxide and methane. Companies across the globe are announcing dramatic decarbonization plans to stem climate change. The marine market segment is similarly evaluating strategies for significant GHG reductions.

Alternative fuels with low life-cycle GHG emissions offer an attractive solution for marine applications, as they have the potential to provide the energy needed using existing engine technology while fitting into an acceptable footprint on marine vessels. Multiple low-life-cycle-carbon fuels are being considered for future use in the marine industry. Methanol is attracting particular interest because it offers a desirable set of fuel properties. Methanol is a liquid at ambient temperature and pressure and is not highly toxic unless ingested, making it easy to store on board marine vessels. While methanol does contain carbon (resulting in CO_2 emissions when it is burned in an engine), low life-cycle carbon emissions can be achieved using a renewable methanol feedstock, such as bio-methanol (through gasification/reforming of biomass or reforming of renewable natural gas) and e-methanol (through electrolysis using renewable electricity and CO_2 captured from the air). These pathways are currently being scaled up to meet the anticipated demand for green methanol.

While the marine industry has significant interest in methanol as a future low-life-cycle-carbon fuel, additional work is required to increase methanol utilization while demonstrating the required engine performance, emissions, and durability. Furthermore, marine vessels have extremely long service lifetimes that can exceed 30 years. Retrofit solutions will be essential to achieving significant near-term reductions in GHG emissions within the marine industry. New engine technologies that allow flexibility for end users to transition from the currently dominant petroleum-derived diesel fuel to a low life-cycle carbon fuel, such as methanol, will also be needed.

Existing four-stroke marine engines are not optimized for running on methanol, but careful design of retrofit hardware and operating strategies have demonstrated more than 50% diesel substitution with methanol in dual-fuel four-stroke marine engines, resulting in significant reductions in life-cycle CO_2 emissions. Achieving near 100% substitution with methanol in four-stroke marine engines requires additional research, development, and demonstration. Nearly all commercial marine applications currently utilize compression-ignition engines that operate on diesel fuel. By comparison, methanol has significantly reduced reactivity and is difficult to ignite and consume in compression-ignition applications. Shifting to a spark-ignited combustion strategy provides a way to directly ignite methanol but increases the complexity of retrofits and may present other tradeoffs, such as lower engine efficiency.

Objectives

Overall Objectives

- Develop engine technologies to displace the maximum amount of diesel fuel with methanol (up to 100%), in collaboration with a major marine engine manufacturer.
- Maintain or improve engine performance, efficiency, durability, and emissions relative to the current diesel baseline.

Fiscal Year 2022 Objectives

- Establish support for a multi-year cooperative research and development agreement (CRADA) with a major marine engine original equipment manufacturer to pursue marine engine decarbonization with methanol, develop a scope of work, and submit the CRADA document for approvals.
- Solicit project input and support from the U.S. Department of Transportation (DOT) Maritime Administration (MARAD) for the CRADA project.

Approach

In order to have the largest impact on marine sector decarbonization, a CRADA project with a major marine engine manufacturer was pursued. The project focuses on using methanol to displace diesel fuel. Methanol can be produced renewably and with a very low life-cycle carbon footprint, and marine engine manufacturers are already moving towards making commercial products. Oak Ridge National Laboratory (ORNL) activities will focus on developing the next-generation methanol combustion systems in the CRADA project. Simultaneously, additional support for this activity was identified through discussions with DOT MARAD, including a need to expand the scope of work for some tasks.

ORNL will perform experimental engine work using both single- and multi-cylinder variants of the major marine engine manufacturer's engine design, representative of inland and coastal marine applications. ORNL will also perform experiments using a spark-ignited active prechamber system on a different heavy-duty engine, currently installed at ORNL, with the prechamber combustion strategy offering one possibility for achieving 100% diesel displacement. Lastly, the project will also investigate on-board reforming of methanol to dimethyl ether through catalytic dehydration, which will be critical in developing a different pathway to 100% diesel displacement. Activities at ORNL will use flow reactors to develop a better understanding of process-conditions effects on product distribution (dimethyl ether, water, and methanol) and the need for product purification before it can be used in the engine.

Results

The CRADA statement of work has been agreed upon by all parties and submitted for approvals. Experimental work on the project will begin after all approvals have been granted, so there are no results from the project this year.

Conclusions

- A project was developed to decarbonize the inland and coastal marine sectors by displacing diesel fuel with methanol. In addition to DOE support, the project is a CRADA involving a major marine engine manufacturer and also has support from DOT MARAD.
- A CRADA statement of work was agreed upon by all parties and submitted for approvals.

Acknowledgements

The project team would like to thank Vasileios Tzelepis at DOT MARAD for his interest and support in this project.

IV Aviation

IV.1 Accelerating Adoption of Sustainable Aviation Fuels (SAFs) with End-Use Research (Argonne National Laboratory)

Sibendu Som, Principal Investigator
Argonne National Laboratory
9700 South Cass Avenue
Lemont, IL 60439
Email: ssom@anl.gov

Kevin Stork, DOE Technology Manager
U.S. Department of Energy
Email: Kevin.Stork@ee.doe.gov

Start Date: October 1, 2021 End Date: September 30, 2025
Project Funding: $550,000 DOE share: $550,000 Non-DOE share: $0

Project Introduction

A fundamental grasp of internal atomizer flows and spray atomization is of critical importance to understanding fuel property effects, as the fuel injector exit profile has important consequences on downstream processes such as mixing, evaporation, ignition, combustion, and heat transfer. In simulating internal combustion engines, we have demonstrated the importance of linking injector and spray simulations to allow for differences in fuel properties and injector performance to be linked to combustion and emissions. Our long-term vision is to develop an end-to-end simulation tool for a reference combustor to screen candidate sustainable aviation fuels (SAFs) and gain improved fundamental understanding of fuel property effects on combustor performance. Argonne National Laboratory also has prior expertise in gas turbine modeling with SAFs and has developed best practices for performing high-fidelity simulations to predict lean blow-out. A validated two-phase flow model based on X-ray data—together with appropriate combustion, turbulence, chemical kinetics models, and best practices—will be leveraged for assessing fuel behavior. In coordination with the U.S. Department of Energy's Bioenergy Technologies Office, the fuels and fuel properties of interest will be determined and subsequently evaluated both experimentally and computationally. Data, knowledge, and improved simulation tools for SAFs will be transferred to industry.

Objectives

Argonne's research is mainly performed under four major tasks, the objectives of which are as follows:

X-ray Measurement

The X-ray measurements collected in this project will typify available validation measurements for model development.

- Existing hardware and geometries were utilized for examining fuel property effects on fuel injection and atomization. Industry-relevant hardware was obtained, designed, and procured for demonstration testing.
- Characterization of relevant hardware will be performed for the purpose of complementary computational fluid dynamics (CFD) boundary conditions. Internal geometry characterization measurements will highlight realistic hardware influences on spray development, which is critical in removing unknown variables in the prediction of fuel effects.
- Preliminary imaging of real fuels was performed, including sprays of SAFs, to examine fuel property effects. High-speed X-ray imaging of early fuel introduction will provide unique insight to

preliminary multiphase phenomena (where fuel physical properties can impact the atomization processes) and confirm if simulations capture these effects.

CFD Simulations and Validation

Fuel behavior assessment is critical prior to utilization in gas turbine combustors. A CFD model of a gas turbine combustor was developed to assess the behavior of SAFs in a combustor.

- A validated Air Force Research Laboratory Referee Rig was utilized to simulate the A-2 fuel that served as the baseline condition for the study.
- Sensitivity of fuel properties, such as fuel viscosity, density, and heat of vaporization, were assessed by perturbing the liquid properties of A-2 to understand their impacts on the combustion characteristics under stable operating conditions.
- The analyses will be further expanded to understand the fuel property response to key figures of merit such as lean blow-out, high altitude relight, and cold start.

Accelerating Rapid Compression Machine (RCM) Adaptation for SAF Fuels and Operating Conditions

The ability to accurately model the compositionally dependent auto-ignition and combustion behavior of SAFs and SAF-blended fuels is critical to enabling rapid advances in SAF utilization and next-generation gas turbine engine design. For this work, Argonne's RCM facility is upgraded to handle these less-volatile fuels while achieving measurement fidelity similar to previous work with gasoline fuels, where ignition time and heat-release-rate behavior could be quantified with excellent repeatability and very low measurement uncertainties [1]. Combustor-relevant temperatures, pressures, and fuel loadings will be targeted to quantify fuel behavior, covering conventional jet fuel, SAFs, SAF-blended fuels, and fuel surrogates in collaboration with chemical modeling groups.

High-Fidelity Simulations of Combustor toward Direct Numerical Simulation Capability

Development of a numerically accurate simulation framework to capture the flow and flame dynamics in the midsize Army Research Combustor (ARC-M1) [2] using Nek5000 software [3] is ongoing. These simulations will help develop a detailed understanding of the impact of fuel properties on flame dynamics using a combination of wall-resolved large-eddy simulations (LES) and direct numerical simulation, with a specific focus on SAFs.

Approach

Arrangements were made to use existing flow rig equipment [4] and industry-relevant geometry hardware. The liquid spray nozzle used in this demonstration campaign was borrowed from the Air Force Research Laboratory Referee Rig as an industry-accepted and experimentally characterized test hardware. Confinement swirling air flow was provided by a modified design of the non-proprietary Aero-spray atomizer geometry, configured to fit the Referee Rig nozzle body. This swirler body was 3-D printed to capture the complex internal geometry. A schematic of the rig configuration, including the Referee Rig nozzle and modified swirler, is depicted in Figure IV.1.1, with the diagnostic region of interest highlighted to study the produced fuel spray. Assembly of hardware, operability,

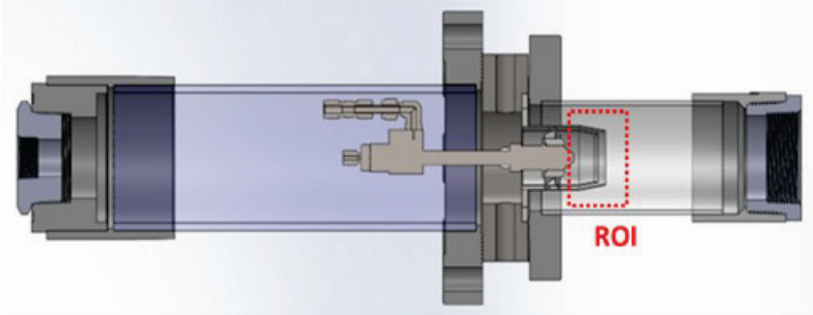

ROI – region of interest

Figure IV.1.1 Schematic of the rig configuration

and safety checks were performed prior to shakedown and the diagnostic campaign. High-speed X-ray imaging of near-nozzle flow was performed for several fuels of interest, namely, Jet-A, R-8 (hydroprocessed esters and fatty acids [HEFA]), and a diesel/Viscor blend, designed to replicate the viscosity of the National Jet Fuels Combustion Program C-3 fuel [5] at cold temperatures. The fuels were injected at 25°C and 12.5°C. These fuels and temperatures were chosen to observe fuel physical property effects. Separately, hard X-ray nozzle tomography was conducted to characterize the internal geometry of the Referee Rig with the required analysis for delivering insights to the modeling team.

The Referee Rig modeling was performed using CONVERGE 3.0 [2] with all the geometric details including the swirler, effusion holes, and diffusion holes. A schematic of the computational model with the flow paths is shown in Figure IV.1.2. The temperature-dependent liquid properties for A-2 are utilized for the baseline study. The density and lower heating value of the fuel are perturbed by -8% and +3%, respectively. These are the expected bounds for different drop-in SAFs. Reacting flow simulations for these perturbed quantities, at a stable equivalence ratio of 0.095, are performed for a preliminary assessment of fuel property behavior. High-fidelity simulations were also performed to resolve the flow fields in the ARC-M1 gas turbine using Nek5000, an open source high-order spectral element method code that accurately models the fluid, thermal, and combustion processes with high parallel efficiency on supercomputer platforms and is highly scalable up to a million processors.

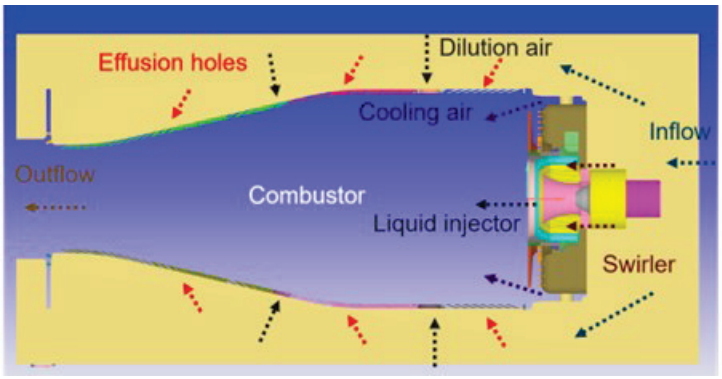

Figure IV.1.2 CFD geometry with the flow paths for the Referee Rig

The reaction chamber of the RCM can create and maintain well-controlled, elevated temperature and pressure environments (e.g., temperatures from 600 K to 1,100 K and pressures from 5 bar to 80 bar), absent of complicated mixing and fluid dynamics interactions, where the chemically active period preceding autoignition can be monitored and probed via advanced in situ and ex situ diagnostics. Fuel autoignition affects lean blow-out behavior in combustors as well as flame dynamics under autoignition-assisted conditions, which are common in gas turbine combustors.

Results

The Referee Rig hardware was successfully scanned and reconstructed using hard X-ray computed tomography. Established methods were used to segment the reconstruction volume and produce a CFD-ready geometric model of the internal flow passages and external surfaces. The details of this geometry are rendered in Figure IV.1.3. The pilot circuit was the focus of the experiments and will be the focus of near-term simulations. The high-resolution internal geometry details will be influential to the internal flowfield when simulated. Specifically, feed passages to the spin chamber of the injector have a rough surface finish that may induce turbulence, and a ridge exists on the spin chamber wall, which can influence the swirling liquid flow prior to exiting the nozzle.

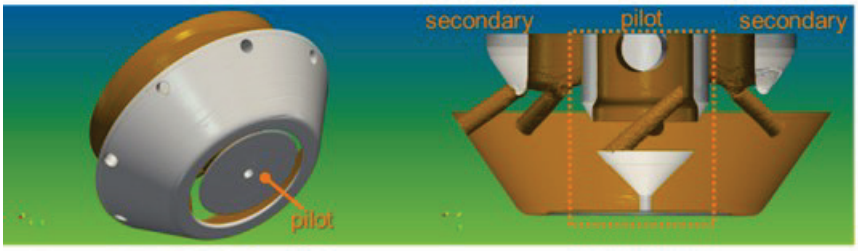

Figure IV.1.3 Renderings of the external surface and internal passages of the Referee Rig nozzle, as measured through hard X-ray computed tomography. The pilot fuel circuit was used during spray experiments.

Demonstration spray experiments were successfully carried out using X-ray imaging diagnostics to observe the pilot spray within the confinement of the 3-D printed nylon swirler. Time-resolved image sequences were collected and representative images for each fuel at the two supply temperature conditions are depicted in Figure IV.1.4. The original experimental matrix included imagery in other regions of interest, including the filming region and the shear breakup at the trailing edge of the prefilming geometry. However, for these demonstration experiments, representative swirling co-flow was not achieved and therefore the focus was solely on the pilot spray. As seen in the images, the contrast of the sheet and thickness of the sheet are increased at the colder temperatures. Additionally, initial dynamic analysis of the HEFA fuel indicates differences in the periodic behavior of the spray. The high viscosity fuel exhibited the highest degree of morphological differences from the other two fuels. At the room temperature condition, the diesel blend hollow cone spray had a thicker sheet with a much longer disintegration distance. Additionally, the dynamic behavior of the sheet and spray were considerably different from the other two fuels. Furthermore, at cold temperatures, the pilot spray changed operational modes completely, having a continuous liquid jet exiting the nozzle with no air core extending into the injector. The variety of behavioral differences seen through this conditions space will provide valuable validation to complementary high-fidelity simulations and modeling efforts. Additional analysis of the detailed experimental data is ongoing.

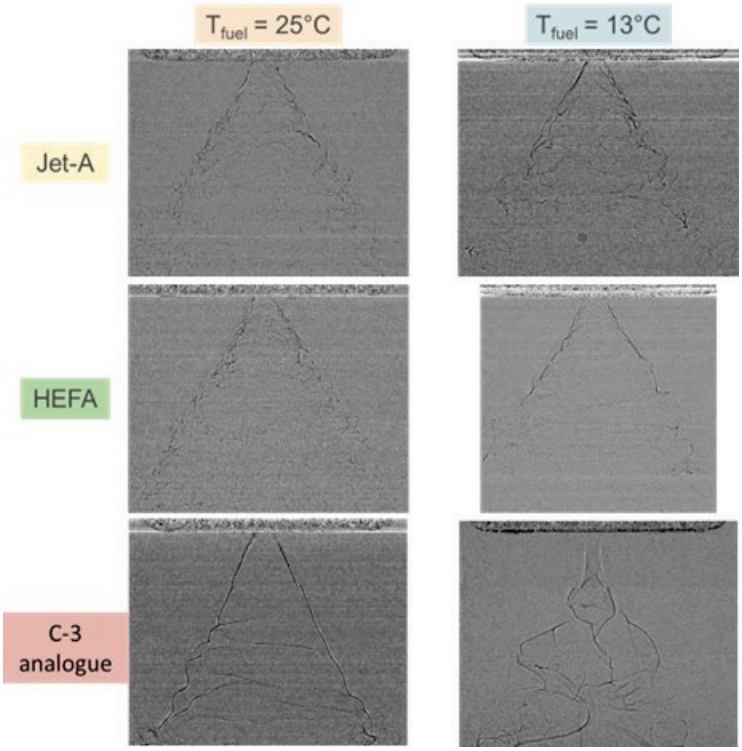

Figure IV.1.4 Instantaneous x-ray images of the pilot spray for each test fuel (at two supply temperatures)

The Referee Rig was modeled using CONVERGE 3.0 [6]. The model was validated, and the results were compared with experimental data and earlier results for A-2 [7] using an older version of CONVERGE. For the liquid properties, baseline A-2 properties as a function of temperature are used. These quantities include density, viscosity, heat of vaporization, specific heat, conductivity, and surface tension. For density perturbation, the density (expressed as ρ in Figure IV.1.5) of A-2 at 16ºC is reduced by 8%. For the energy content perturbation, the lower heating value (LHV) is increased by 3%. The results for the three simulations are shown in Figure IV.1.5, with the temperature and OH mass fraction contours (expressed as Y_{OH} in Figure IV.1.5) on the center plane. The instantaneous (time = 65 ms) contours show differences in the flame shape and stabilization with a perturbation of the liquid properties. For the baseline A-2, the flame stabilizes near the nozzle and the temperature distribution remains connected as the flame expands outwards downstream of the nozzle. The connected high-temperature regions can be seen with the OH mass fraction contours as well, which show the same behavior. With a decrease in density, the flame stabilization remains the same, but a disconnect in the high-temperature regions can be noted. With a decrease in density and an increase in energy content, the flame stabilization changes, stabilizing further downstream. The higher temperatures and higher OH mass fractions are seen further downstream. The results clearly show that small perturbations in the liquid properties can lead to notable changes in the flame shape. Additional simulations with perturbation of viscosity and combined perturbations of density, viscosity, and energy content are ongoing. Furthermore, detailed analyses of the current simulations and ongoing simulations will be performed.

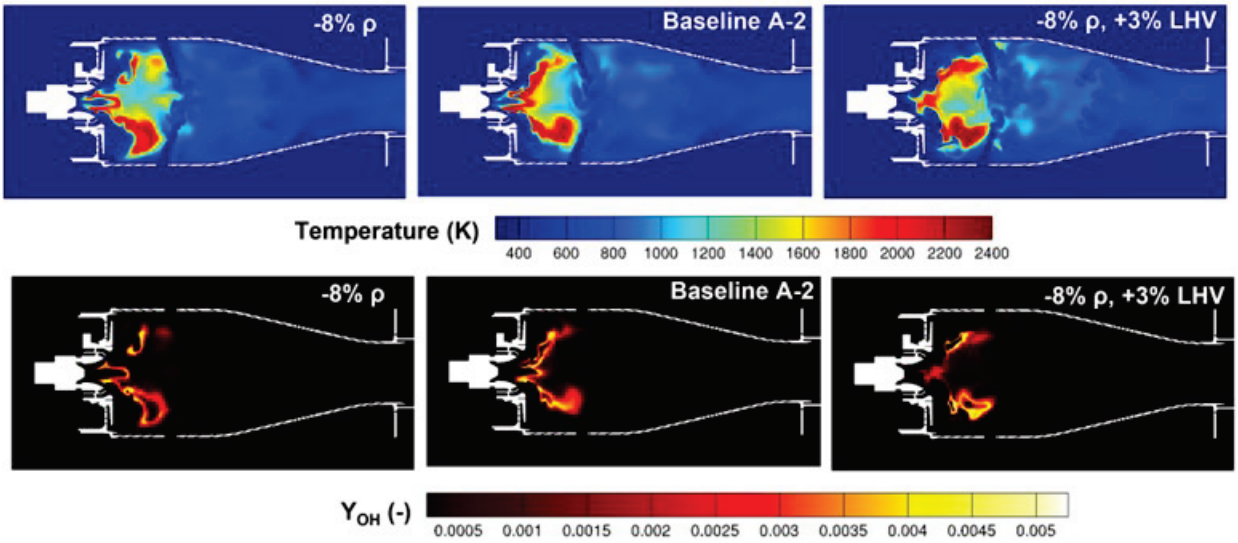

Figure IV.1.5 Temperature contours (top) and OH mass fraction contours (bottom) on the center plane for different fuel property perturbations

A new fuel mixing and delivery system was designed for the RCM facility capable of achieving temperatures near 150°C (necessary to prevent fuel condensation/fractional loss of heavier components), along with integration of high-resolution transducers and automated valving. A new heating system was implemented to achieve uniformity for these very high temperatures. Many of the components of the ancillary systems had very long lead times (4–8 months), and some critical pieces are still not expected until the second quarter of Fiscal Year (FY) 2023. The LabView control system was also upgraded. Shakedown testing is underway where possible. Collaborations were initiated with chemical modeling groups at Lawrence Livermore National Laboratory and Politecnico di Milano, which have expertise and prior experience developing kinetic models for transportation/jet fuels and SAFs, as well as the National Renewable Energy Laboratory, which will be conducting analogous testing using SAFs.

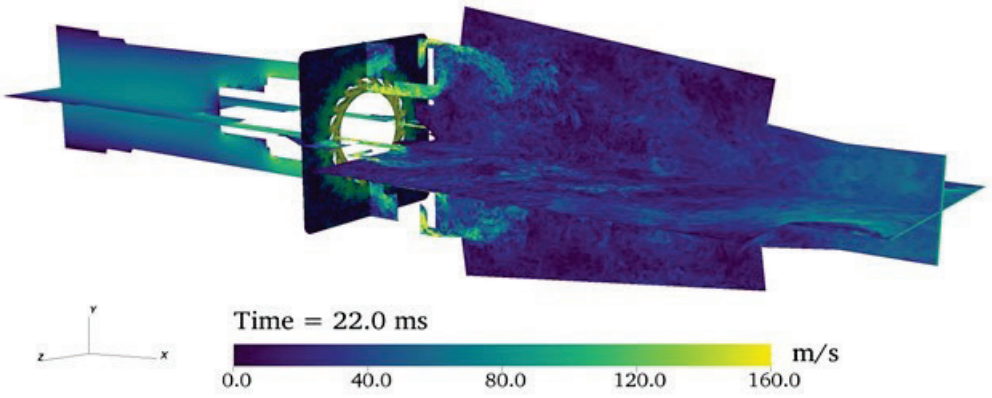

Figure IV.1.6 Perspective view of instantaneous velocity magnitude within the ARC-M1

The high-fidelity data obtained from the wall-resolved LES of the ARC-M1 provide the opportunity to investigate flow characteristics and structural development in a realistic gas turbine setup that embodies a relatively complex geometry. The perspective view of the instantaneous velocity magnitude in the combustor is shown in Figure IV.1.6 at time = 22 ms, which is about 28.9 flow-through times based on the combustor length and characteristic velocity scale in the combustor. At this time instant, the flow within the combustor has reached a statistically fully developed state, as the time-integrated mean flow is statistically converged

with no significant variations in time. This flow is currently being compared with experimental data [8] and previous simulations [2].

Conclusions

Spray experiments were carried out successfully with real fuels of interest and examined with X-ray diagnostics, demonstrating the diagnostic capabilities to differentiate fuel property effects. The X-ray diagnostics can reveal multiphase flow behavior within the confinement of relevant atomizer geometries and provide valuable datasets for the development and validation of computational models of fuel flows and sprays. The hardware is also characterized to a degree of detail that allows for geometric influences to be resolved through complementary modeling efforts and for accurate validation to experiments with common geometry. Appropriate validation and high-fidelity qualitative and quantitative experimental data, provided through these X-ray diagnostics, will strengthen these modeling methods. Improvements to these models will speed the verification of SAF behavior in existing systems as well as accelerate the development of future propulsion systems.

Reacting flow simulations of the Referee Rig were performed to understand the impact of liquid properties on the stable combustion behavior. The changes in the liquid properties from A-2 were estimated based on typical drop-in fuel properties. The simulations reveal changes in the stable flame behavior with a reduction of 8% in density and an increase of 3% in the fuel's energy content. These changes in the flame behavior change the heat-release-rate behavior within the combustor and will subsequently impact the behavior of the fuel for lean blow-out, a key figure of merit for fuel certification. The ongoing work will be expanded to other properties, and their impact individually and combined on the stable flame behavior and lean blow-out will be explored.

Progress was made toward upgrading Argonne's RCM facilities to enable investigations of SAFs and SAF-blended fuels at combustor-relevant temperatures, pressures, and fuel loadings. Fuel autoignition affects lean-blow-out behavior as well as flame dynamics under autoignition-assisted conditions, which are common in advanced gas turbine combustors, and therefore it is critical to properly model this in design-relevant, CFD simulations. Shakedown of the equipment will continue in FY 2023 as the delayed components are integrated into the RCM's ancillary systems, with validation tests to be conducted in collaboration with chemical modeling groups at Lawrence Livermore National Laboratory and Politecnico di Milano.

A high-fidelity CFD model for a realistic gas turbine has been developed using Nek5000. As a precursor to performing reacting simulations, work in FY 2022 demonstrated the use of wall-resolved LES to study the small- and large-scale flow dynamics in the ARC-M1 combustor under non-reacting conditions. In FY 2023, the work will be extended to perform reacting flow computations. The instantaneous and time-averaged liquid and vaporized fuel distribution, flame shape, and flame anchoring location will be analyzed. These simulations will shed light on how and why varying fuel properties lead to a change in the vaporization resulting in a change in flame shape and dynamics.

Key Publications

1. Wu, Sicong, Debolina Dasgupta, Muhsin Ameen, and Saumil Patel. 2022. "LES Modeling of Gas Turbine Combustor Using Nek5000." Bulletin of the American Physical Society.

References

1. Cheng, S., S.S. Goldsborough, S.W. Wagnon, R. Whitesides, M. McNenly, W.J. Pitz, D. Lopez-Pintor, and J.E. Dec. 2022. "Replicating HCCI-Like Autoignition Behavior: What Gasoline Surrogate Fidelity Is Needed?" *Applications in Energy and Combustion Science* 12 (December): 100091. https://doi.org/10.1016/j.jaecs.2022.100091.

2. Dasgupta, D., S. Som, E.J. Wood, T. Lee, E. Mayhew, J. Temme, and C.-B. Kweon. 2022. "X-ray Data Enabled Improved Near Nozzle Spray Validation for ARC-M1 Combustor." *AIAA SCITECH 2022 Forum*, 2059.

3. Fischer, P.F., J.W. Lottes, and S.G. Kerkemeier. 2019. Nek5000 (Version 19.0) [software]. Available through Argonne National Laboratory, Lemont, IL. https://nek5000.mcs.anl.gov.

4. Sforzo, B.A., A.L. Kastengren, K.E. Matusik, F. Gomez del Campo, and C.F. Powell. 2019. "X-Ray Phase Contrast Imaging of Liquid Film and Spray Development Inside an Aircraft Engine Swirler." ASME. *Journal of Engineering for Gas Turbines and Power* 141, no. 12 (December): 121003. https://doi.org/10.1115/1.4045217.

5. Edwards, James T. 2017. "Reference Jet Fuels for Combustion Testing." 55th AIAA Aerospace Sciences Meeting, Grapevine, TX, January 9–13. https://doi.org/10.2514/6.2017-0146.

6. Richards, K.J., P.K. Senecal, and E. Pomraning. 2021. "CONVERGE 3.0 Manual." Madison, WI: Convergent Science. https://convergecfd.com/about/user-resources.

7. Hasti, V.R., P. Kundu, G. Kumar, S.A. Drennan, S. Som, S.H. Won, F.L. Dryer, and J.P. Gore. 2018. "Lean Blow-Out (LBO) Computations in a Gas Turbine Combustor." AIAA Propulsion and Energy Forum and Exposition, Cincinnati, OH, July 9–11. https://doi.org/10.2514/6.2018-4958.

8. Wood, E.J., B. McGann, A. Motily, K. Min, K. Kim, T. Lee, E. Mayhew, C.M. Mitsingas, J. Temme, C.-B. Kweon, and A. Kastengren. 2020. "Impact of Fuel Properties on Combusting Jet Fuel Spray Breakup, Analyzed using High-Speed Phase Contrast Imaging." AIAA SciTech 2020 Forum, Orlando, FL, January 6–10. https://doi.org/10.2514/6.2020-0522.

Acknowledgements

The principal investigator gratefully acknowledges the contributions of colleagues Brandon Sforzo, Debolina Dasgupta, Muhsin Ameen, and Scott Goldsborough of Argonne National Laboratory.

Measurements were performed at the 7-BM beamline of the Advanced Photon Source at Argonne National Laboratory. Use of the Advanced Photon Source is supported by the U.S. Department of Energy under Contract No. DEAC0206CH11357.

The CONVERGE simulations were run on Bebop at Argonne's Laboratory Computing Resource Center and Eagle at the National Renewable Energy Laboratory's Computing Facilities. The Nek5000 simulations were run on Theta at the Argonne Leadership Computing Facility. We would also like to acknowledge Convergent Science for providing us with licenses for performing the simulations.

IV.2 Sustainable Aviation Fuel Combustion, Soot, and Contrail Formation (Sandia National Laboratories)

Julien Manin, Principal Investigator
Sandia National Laboratories
P.O. Box 969, MS 9053
Livermore, CA 94551-9053
Email: jmanin@sandia.gov

Kevin Stork, DOE Technology Manager
U.S. Department of Energy
Email: Kevin.Stork@ee.doe.gov

Start Date: October 1, 2021 End Date: September 30, 2022
Project Funding: $500,000 DOE share: $500,000 Non-DOE share: $0

Project Introduction

Emission characteristics of aero-engine combustors need to be improved to reduce harmful effects that the aviation sector has on human health and the environment. Stringent emission regulations are being implemented by government agencies across the world, putting pressure on engine manufacturers to produce cleaner engines. As such, it is of extreme importance to investigate combustion and emissions from aero-engines to support the development of next-generation engines. While key aspects of aero-engine combustion have improved, soot predictions remain a significant challenge to researchers. Highly turbulent swirl flows coupled with unsteady fuel atomization and vaporization, fuel air mixing, recirculation zones, and possible acoustic instabilities make the analysis of soot properties very complicated. In addition, it is also hypothesized that non-volatile particulate matter (nvPM) or soot is responsible for the formation of aircraft-made contrails—identified as major climate forcers—by acting as inception particles that can enable the heterogenous nucleation of water to form droplets, which later turn into ice crystals. Sustainable aviation fuels (SAFs) are a great way to reduce the impact of aviation on both human health and climate forcing. Beyond the obvious decarbonization benefit of SAFs, well-engineered fuel formulations may also reduce soot emissions. However, it is acknowledged that nvPM emission numbers are only part of the problem with respect to contrails, and that specific properties of soot may bear as much importance as the total soot mass emitted by the engine.

To be better understood, these aspects demand advanced testing, combined with diagnostic capabilities that are extremely challenging to apply in ground-based aero-engine combustor testing facilities. We therefore proposed a novel approach to study the combustion and soot formation processes in spray flames generated by different types of jet fuels, including SAFs. A non-continuous injection system based on a solenoid-actuated injector unit called the single-hole atomizer (SHA) is used to inject jet fuels in a constant-volume pre-burn vessel with highly controlled ambient conditions set to represent thermodynamic conditions inside real aero-engine combustors.

The research reported in this document was an essential piece of the aviation effort undertaken at Sandia National Laboratories (SNL) for Fiscal Year (FY) 2022, as it was leveraged to support research projects funded by NASA or the SNL Laboratory Directed Research & Development (LDRD) office to obtain a more complete dataset for spray injection, mixing, combustion, and emissions, including contrail formation, with the SHA approach. Specifically, the project funded by NASA, which started in FY 2022 but is set to continue into at least FY 2023, aims at investigating the evaporation regime of fuel droplets, which can be transcritical at relevant aero-engine conditions. The project funded by the Energy and Homeland Security investment area under the LDRD program delved into detailed soot properties of particulates sampled directly in the combustion zone of the SHA-generated spray flame, to link soot morphology and surface chemistry properties to contrail formation. Together with the LDRD-funded work, the current project also supported the development of a new altitude chamber facility at SNL to investigate the nucleation process of water on soot

particles or other aerosols. Nucleation has been identified as a key weakness in current sub-scale models implemented in weather- and climate-oriented large eddy simulations.

Objectives

This project aims at investigating the combustion characteristics of spray combustion at conditions relevant to modern aero-engines across the main yet challenging operating points. The custom injection system based on the SHA was used to inject different types of liquid jet fuels, including SAFs, in a constant-volume pre-burn chamber where ambient conditions were set to mimic representative thermodynamic conditions that can be found in real aero-engine combustors. This configuration allows the decoupling of soot formation from the other complex phenomena evolving in combustors.

In this work, flame stabilization (the process that leads to a stable flame) and associated fundamental mechanisms under conditions relevant to aero-engine combustion were investigated, using formaldehyde (CH_2O) planar laser-induced fluorescence (PLIF) and excited hydroxyl radical (OH*) chemiluminescence. The data acquired with these two diagnostic techniques were combined with diffuse back-illumination extinction imaging (DBI-EI) measurements to investigate differences in soot formation between the fuels. The experimental results this approach can provide are highly valuable in the context of better understanding the combustion processes from a variety of fuels, including sustainable fuels, without the need to operate complex and expensive facilities such as ground-based combustors at conditions relevant to modern and next-generation aero-engines. The optical soot experiments were also elemental to the LDRD-funded project (mentioned earlier) that studied fundamental soot properties in the context of contrail formation.

Approach

The measurements were performed in a constant-volume pre-burn combustion chamber (c.f. Figure IV.2.1) using the SHA concept. Unlike the continuous injection mechanism used in aero-engines, the SHA is a direct-acting, solenoid-actuated unit, allowing injections of defined durations. While non-continuous injections are not strictly representative of the process in aero-engines or gas turbines, the injection duration can be sufficiently long to allow the processes to be steady over a finite time period, as discussed in the Results section. The injector is equipped with a custom single-hole nozzle with a nominal diameter of 135 µm. The SHA can operate over a wide range of injection pressure conditions, from atmospheric up to 35 MPa.

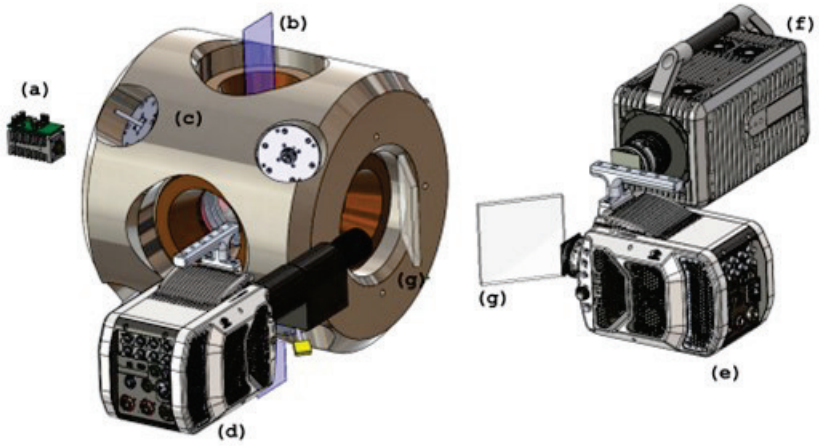

Figure IV.2.1 Schematic of the experimental setup, consisting of (a) 520 nm light-emitting diode (LED), (b) 355 nm laser sheet, (c) optically accessible constant-volume combustion vessel, (d) OH* chemiluminescence imaging camera with intensifier, (e) DBI-EI imaging camera, (f) CH_2O PLIF camera, and (g) dichroic beam splitters

The ambient conditions inside the chamber were carefully selected to be representative of injection and combustion conditions in modern and next-generation aero-engines. Concretely speaking, the conditions were

set based on the assumption that the overall pressure ratio across the compressor was on the order of 60. Two ambient pressures were selected, one corresponding to combustor pressures representative of take-off conditions (6.0 MPa) and another more characteristic of cruise conditions (2.0 MPa). The ambient temperature was adjusted to closely match the expected air temperature entering the combustor at the respective conditions. As such, the take-off temperature was set to 900 K, while the cruise temperature was 800 K, as a result of the lower engine inlet temperature at altitude. The results collected at this condition are not reported here because C-1 and C-4 fuels did not ignite, making it an incomplete dataset. The way the results are plotted next and the trends can be confusing to the reader, which is why the results for this condition were not plotted. A higher ambient temperature was also tested, aiming at representing the combustion process in the inner recirculation zone, where the mixing of the freshly injected fuel with combustion products is expected to feature higher temperatures, as well as reduced oxygen concentration. The experimental conditions analyzed in this work are summarized in Table IV.2.1.

Table IV.2.1 Summary of the Operating Conditions

Conditions	Pressure [MPa]	Temperature [K]	% O_2
Take-off combustor inlet	6.0	900	21
Take-off inner recirculation zone	6.0	1,200	15
Cruise combustor inlet*	2.0	800	21
Cruise inner recirculation zone	2.0	1,200	15

** Results omitted from the present report due to incomplete dataset*

Several fuels were used for this study. The project tested three samples from the National Jet Fuel Combustion Program fuel matrix [1]: a nominal reference Jet A fuel (A-2), an alcohol-to-jet fuel containing highly branched dodecane and hexadecane type components (C-1), and a blend made of 40% C-1 and 60% iso-paraffins ranging from 9 to 12 carbon atoms (C-4). We also studied an advanced bio-derived cyclo-alkane fuel (BCH), representative of a next-generation type of fuel, both reducing emissions and presenting a high degree of compatibility with the engine system (drop-in). The project also tested n-dodecane (nC12) since it has been a logical surrogate choice for jet fuel, and detailed/reliable kinetic mechanisms are available. The injection duration was set to around 10 ms to stabilize the flame for a relatively long period of time and establish a quasi-steady state.

An array of advanced laser and optical diagnostics was used to study the various processes of spray combustion. Namely, we applied PLIF to monitor CH_2O formation and consumption, OH* chemiluminescence, and DBI-EI to investigate low- and high-temperature combustion processes, as well as aromatic growth and soot formation. The optical arrangement used to perform the different laser and optical diagnostics in a quasi-simultaneous manner is shown schematically in Figure IV.2.1.

Results

Figure IV.2.2 shows the time evolution of OH* chemiluminescence emissions for A-2 at take-off combustor inlet conditions. The images are all normalized according to their respective intensity ranges. First and foremost, because these results may be misleading, we note the presence of a strong signal coming from soot (most of the yellow and red regions). However, the main flame stabilization and propagation features can still be quantified. The OH* chemiluminescence images show that the flame propagates mainly downstream in these conditions. One important aspect of these tests, given the non-continuous injection scheme, is that the stabilization distance of the flame, or lift-off length (LOL)—the distance between the base of the flame and the injector tip—was relatively constant over time for both conditions, as well as for all the other fuels and operating conditions tested in this work. This observation supports that the approach based on the SHA and the relatively long injection duration could be used to investigate flame stabilization mechanisms, as well as combustion and emission characteristics of these fuels, under a mode of operation relevant to aero-engines.

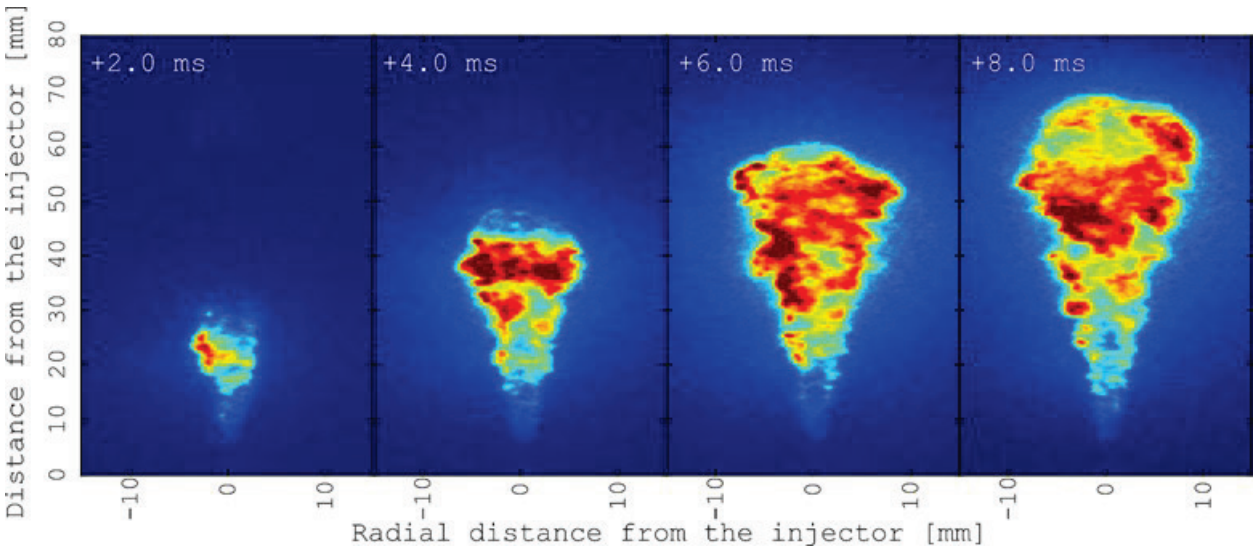

Figure IV.2.2 Example of OH* chemiluminescence images at select timings for A-2 fuel at 60 bar and 900 K ambient conditions

Similar behavior was observed for the other fuels and take-off conditions (not depicted in Figure IV.2.2). At cruise conditions, we observe that the flame propagates both longitudinally, away from the injector, and radially around the liquid jet, up to 4 ms after start of injection (aSOI). After 4 ms aSOI, the flame continued propagating axially and maintained a constant LOL. It is worth noting that the spray characteristics measured under both cruise conditions were very peculiar, with liquid droplets penetrating all the way to the back wall of the chamber as a result of the narrow spray dispersion.

The ignition delay time (IDT) and LOL can be evaluated by analyzing the high-speed OH* chemiluminescence recordings. These two parameters are depicted in Figure IV.2.3. In evaluating IDT and LOL, the project team followed the procedures recommended by the Engine Combustion Network [2]. The cetane number measurements are also reported as grey bars in these figures to provide a comparison point to both the IDT and LOL across conditions and for all fuels.

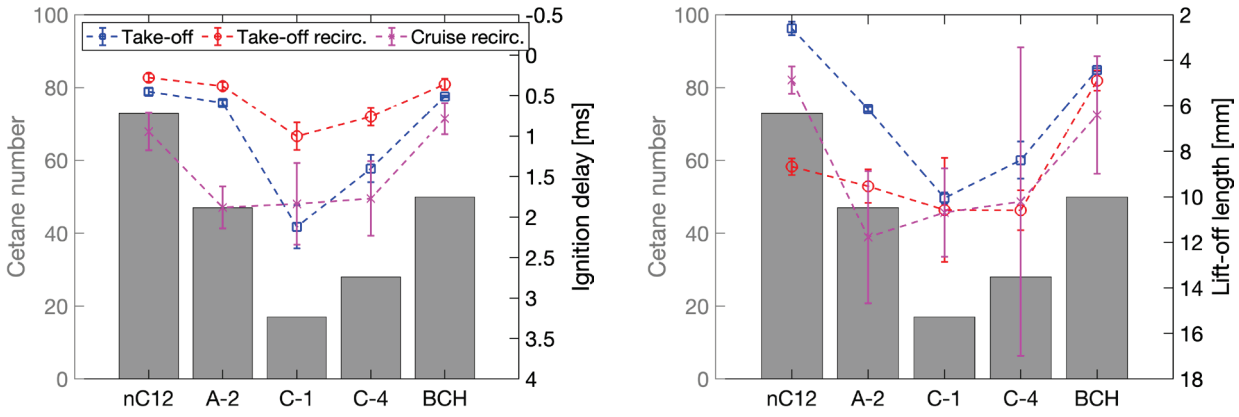

Figure IV.2.3 Measured IDTs (left) and LOLs (right) for all fuels, under the selected target conditions. The results are compared to the derived cetane number measured for the fuels.

A large variation in ignition delays between the different fuels tested can be observed in Figure IV.2.3 (left) at take-off, compared to cruise conditions. As expected, based on their lower cetane numbers, C-1 (cetane number = 17) and (to a lesser extent) C-4 (cetane number = 28) exhibited significantly longer ignition delays at

take-off conditions compared to the other fuels, whose cetane numbers range from 47 to 73. This was not the case at cruise conditions, but peculiar liquid spray behavior may affect autoignition and combustion.

A similar spread in LOLs was observed for different fuels under all target conditions except the one corresponding to the combustor inlet temperature at cruise altitude, as shown in the right plot of Figure IV.2.3. As described earlier, neither C-1 nor C-4 ignited at this condition, which is the reason why the results were omitted from the present report. It is expected that shorter flame stabilization distance coincides with richer combustion because of less mixing with ambient O_2, which leads to higher soot production. However, this behavior may be countered by other aspects such as the sooting propensity of each fuel, as will be discussed later.

The 355 nm excitation PLIF measurements were used in this case to probe both CH_2O and polycyclic aromatic hydrocarbons (PAHs). The onset timing corresponding to the time when 3- to 4-ring PAHs (main contributors to the laser-induced fluorescence signal when excited at 355 nm) first appeared was measured. Figure IV.2.4 shows the onset timing for PAHs for conditions at which there is sufficient temporal separation between PAHs and soot formation, namely take-off combustor inlet and the recirculation zone at cruise altitude.

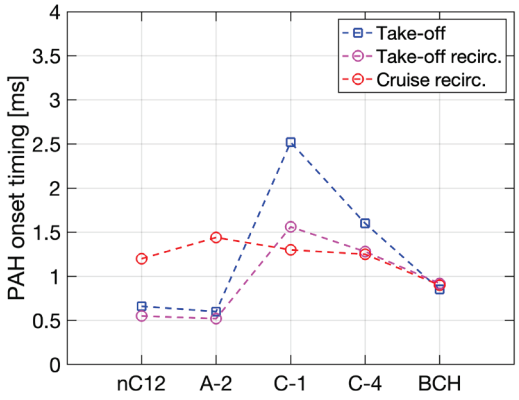

Figure IV.2.4 PAH onset timings for all fuels under the selected target conditions

The trend of PAH onset time resembled what was measured with OH* chemiluminescence for high-temperature IDT (see left plot of Figure IV.2.3). In agreement with their low reactivity, PAH formation was delayed for C-1 and C-4 at the take-off combustor inlet condition compared to the other fuels. Delayed ignition and PAH formation (assuming the growth of PAH and the signal recorded by the diagnostic scales with the actual onset, or formation of the first aromatic ring) have been associated with not only delayed but also lower soot production.

Images collected using DBI-EI were processed to evaluate the soot optical thickness, KL, according to the Engine Combustion Network convention [2]. An example of time evolution of the two-dimensional KL fields is shown in Figure IV.2.5 for C-1 at take-off recirculation zone conditions.

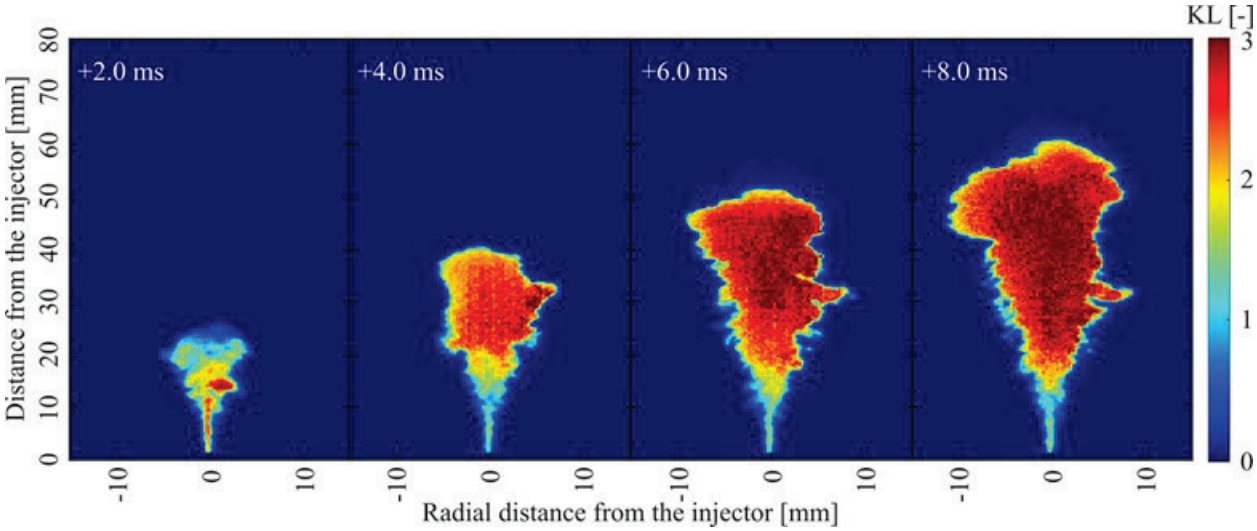

Figure IV.2.5 Example of KL images at select timings for C-1 fuel at 60 bar and 1,200 K ambient conditions

The DBI-EI data show that strong soot emissions appear shortly after injection, highlighting the significant sooting propensity of A-2 at this operating point, with measured extinction levels, i.e., KL, well above 3. Similar results were obtained for the other fuels. Note that 2-D extinction will also be sensitive to the liquid region and that most of the signal between 0 and 10 mm shall be attributed to the liquid portion of the spray, rather than soot. The determination regarding extinction in the near-field being caused by liquid droplets or soot was supported by the absence of high-temperature reactions (no OH* chemiluminescence signal) or soot incandescence in that region. The minimal separation between the extinction signal produced by the liquid extent of the spray and the soot field renders the interpretation of the data more challenging.

Detailed analysis of the information gathered by the different diagnostics is needed to provide a more complete and accurate representation of the injection and combustion processes. In any event, the high-speed image sequences indicated that soot formed shortly after 10 mm under these conditions and that the soot field extended all the way to the end of the visualization window, corresponding to the back wall of the constant volume chamber, more than 80 mm away from the injector exit. We made similar observations regarding the development of the soot field in a way analogous to what was observed with the OH* chemiluminescence high-speed images, where the field propagated axially from the nozzle tip.

The soot onset timing and the peak soot mass, defined as the maximum soot mass produced within the observable field of view at any given point in time, can be evaluated from the time evolution of the soot/KL field. These quantities are reported in Figure IV.2.6 for all fuels and operating conditions. Note that C-1 and C-4 did not ignite at cruise combustor inlet conditions, so no results are available.

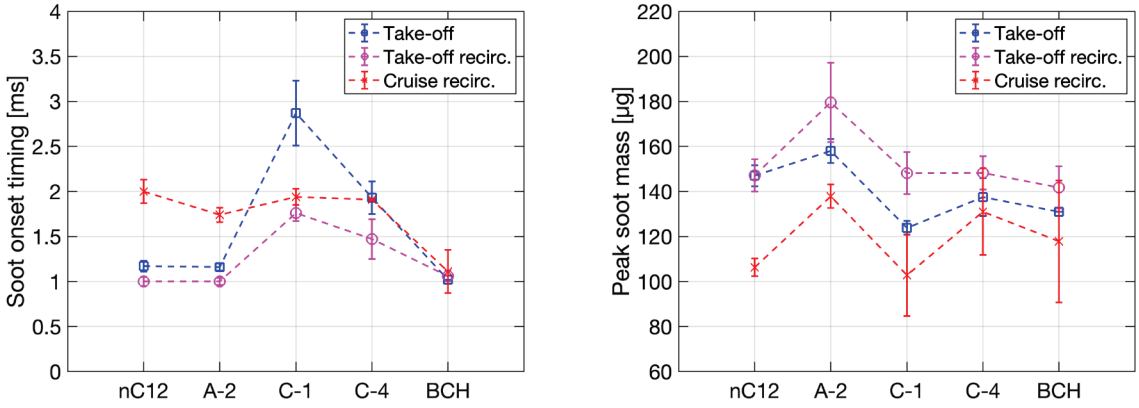

Figure IV.2.6 Measured onset timing (left) and peak soot mass (right) for all conditions and fuels

The trends of soot onset timings agree with the IDT and PAH onset timing results. Specifically, C-1 and C-4, because of their lower reactivity, feature a delayed soot onset compared to the other fuels at take-off conditions. All fuels produce copious amounts of soot under the investigated operating conditions, as the relatively low injection velocities lead to rich mixtures in the reaction region, as demonstrated by the short LOLs. With that said, we observe that peak soot mass responds well to differences in operating conditions. The mean values (averaged from three to five repetitions) indicate the following ranking of conditions in terms of soot level production (ranked from low to high, according to the soot production metric): cruise recirculation zone, take-off, and take-off recirculation. While not reported here, it can be noted that the experimental data indicate that the cruise combustor inlet operating point produced the lowest amount of soot of all target conditions. This ranking highlights the effect of both ambient pressure and temperature, with peak soot mass tending to increase both with increasing pressure and increasing temperature. Over the range applied in this work, the variation associated with pressure dominated over that of temperature. Both cruise conditions (2 MPa, 800 and 1,200 K) produced less soot than either of the take-off conditions (6 MPa, 900 and 1,200 K).

Looking into the specifics and the potential benefit SAFs can bring to aero-engine combustion, the results showed that C-1, C-4, and BCH featured a lower peak soot mass compared to A-2 at all conditions. Given the results, this difference in soot production could certainly be attributed to the aromatic content of A-2 compared to the other fuels.

Conclusions

This effort began with the introduction of a new concept to investigate aero-engine combustion, relying on a non-continuous injection strategy that uses a single-hole nozzle (called the single-hole atomizer, or SHA) to inject jet fuels into quiescent environments at well-controlled thermodynamic conditions relevant to modern or next-generation aero-engines. Five fuels and a range of operating conditions relevant to modern and future aero-engines were tested. We applied quasi-simultaneous time-resolved optical diagnostics—OH* chemiluminescence images and PAH PLIF—to monitor the presence of PAHs and DBI-EI to quantify soot production. The main findings of this work are the following:

- The SHA approach relying on non-continuous and non-premixed injections proved successful, as it led to stabilized flames over a relevant time period.
- The trend of ignition delays at take-off conditions matched what the anticipated delays would be, based on cetane numbers, across the different fuels considered in this study.
- The onset of PAHs and, consequently, the formation of soot was delayed for certain fuels, as a result of their lower reactivity.
- Rather than follow the PAH and soot onset trends, fuels that are free of aromatics produced less soot across most conditions.
- Substantially longer liquid penetration was observed at cruise condition, which potentially affected combustion, leading to even more challenging data interpretation.

It should be noted that while aromatic-free fuels appear to produce less soot, more information (in addition to raw nvPM emissions) must be considered before drawing any conclusions regarding the performance of different fuels with respect to contrail formation.

This project not only produced the valuable data presented herein but also supported companion projects, specifically, the NASA-funded project studying the effect of transcritical evaporation on fuel–air mixing in aero-engines and the LDRD project doing detailed characterization of soot properties in the context of contrail formation. Funds were also directed toward the development of a new altitude chamber facility, with the aim of investigating contrail formation at conditions relevant to aircrafts by obtaining critical information regarding the heterogenous nucleation process of water from soot particles or other aerosols.

The results presented herein constitute valuable information regarding combustion properties and soot formation for different types of jet fuels relevant to aviation in the context of moving toward sustainable fuels. Furthermore, these experiments, along with the companion studies, provide a comprehensive dataset that can be used to benchmark a multitude of models and kinetic mechanisms developed for aero-engine applications.

Key Publications

1. Pickett, L.M., et al. AIAA SciTech 2023.
2. Di Sabatino, F., et al. AIAA SciTech 2023.
3. Manin, J., et al. SAND2022-12926R, 2022.
4. Di Sabatino, F., et al. ASME Turbo Expo 2023.

References

1. Colket, M., et al. AIAA SciTech 2016.

2. Sandia National Laboratories. n.d. Engine Combustion Network data archive. Accessed 2022. https://ecn.sandia.gov/.

Acknowledgements

The author would like to thank Lyle Pickett, Kevin Wan, Francesco Di Sabatino, and Kyra Schmidt for their contributions to this research and/or their technical support. The experiments and analyses were performed at the Combustion Research Facility of SNL, California, while the numerical work was performed at both SNL and Lawrence Livermore National Laboratory. SNL is a multi-mission laboratory managed and operated by National Technology and Engineering Solutions for Sandia LLC, a wholly owned subsidiary of Honeywell International, Inc., for the U.S. Department of Energy's National Nuclear Security Administration under contract DE-NA0003525.

IV.3 Contrail Chemistry for Sustainable Aviation Fuels (Lawrence Livermore National Laboratory)

Scott Wagnon, Principal Investigator
Lawrence Livermore National Laboratory
7000 East Avenue, L-372
Livermore, CA 94550
Email: Wagnon1@llnl.gov

Matthew J. McNenly, Principal Investigator
Lawrence Livermore National Laboratory
7000 East Avenue, L-792
Livermore, CA 94550
Email: McNenly1@llnl.gov

Kevin Stork, DOE Technology Manager
U.S. Department of Energy
Email: Kevin.Stork@ee.doe.gov

Start Date: May 1, 2022 End Date: September 30, 2022
Project Funding: $500,000 DOE share: $500,000 Non-DOE share: $0

Project Introduction

Global aviation contributes over 1 Gt of CO_2 emissions each year, an amount that is expected to continue to grow through 2050. Aviation is also anticipated to become a larger contributor (by percentage) to anthropogenic climate change as other areas of the economy decarbonize quicker. Because aviation is one of the hardest transportation sectors to decarbonize, several government agencies worked together to launch the Sustainable Aviation Fuel Grand Challenge to reduce cost, enhance sustainability, and expand production for sustainable aviation fuel (SAF) to 35 billion gallons annually by 2050, enough to replace petroleum-derived jet fuel in its entirety. This initiative directly addresses the contribution of CO_2 emissions; however, recent studies estimate that non-CO_2 effects contribute nearly two-thirds of the total climate impact of aviation [1]. The engine exhaust produces condensation trails, or contrails, and the resultant aircraft-induced cloudiness is the largest contributor to the climate forcing, with roughly double the impact of CO_2.

Despite contrails' significance in overall climate impacts, it has been difficult to estimate the contribution of contrails relative to the other aviation emission sources. It has also been difficult to understand to design combustor operation and SAF composition (beyond the removal of high-soot-producing molecules such as aromatics) to reduce the impact of contrails. The challenge is due to the complex interactions between soot particle formation and oxidation in the jet engine combustor, the turbulent cooling and mixing with local atmospheric conditions, and the longer-term microphysics governing the evolution of the contrail cirrus. These conflating factors can lead to conditions in which the contrail dissipates in a matter of minutes with little climate impact; alternately, the contrail can persist for hours, interact with natural clouds, and ultimately increase the net effective radiative forcing. The modified clouds trap outgoing long-wave infrared radiation more effectively than they reflect incoming solar short-wave radiation. The aim of this project is to improve the understanding of the earliest contributors to contrail formation, including the soot formation mechanism for SAFs, and its coupling with ice nucleation models and other cloud microphysics models.

Objectives

Overall Objectives

- Develop a chemistry model that captures significant trends in particle size and number of the formation and destruction of water–ice particles.

- Create a method to couple soot and ice formation models with existing cloud microphysics models to predict the initial evolution of SAF contrails.
- Release updates onto the combustion solver software library Zero-RK (Zero-order Reaction Kinetics) (https://github.com/LLNL/zero-rk) [4] so the larger community can take advantage of the combustion and contrail modeling tools.

Fiscal Year 2022 Objectives

- Establish access to atmospheric thermodynamic data at flight conditions (temperature, pressure, relative humidity, etc.) relevant to the contrail formation and evolution processes.
- Verify that the current SAF chemistry and soot formation model will produce stable simulations of jet engine exhaust cooling and mixing processes with ambient conditions at cruising altitudes.
- Identify additions to expand the SAF combustion model to include atmospheric chemistry, ice nucleation, and other cloud microphysics models.

Approach

The project builds from the surrogate mechanism developed for the Co-Optima program at Lawrence Livermore National Laboratory (LLNL) [2]. This fuel model contains over 4,200 reacting species to accurately resolve combustion phenomena, including more than two dozen hydrocarbon blendstocks commonly found in gasoline, jet fuel, and diesel. The model also contains more than two dozen oxygenates and bio-derived blendstocks, including all those identified in the blending study by McCormick et al. [3] as promising candidates to lower the life cycle carbon contribution of transportation fuels. Pathways for soot formation have recently been included to predict the impact of fuel composition and operating conditions on the growth and oxidation of soot particles. Predicting the size and number distributions of soot in jet engine exhaust is necessary for modeling contrail formation mechanisms, as the particles play a major role in the ice nucleation process.

The team is also building on other LLNL resources to understand the role of SAF composition in the propensity for contrail formation, persistence, and impact on the climate. The team is working with atmospheric scientists at the National Atmospheric Release Advisory Center (NARAC) to get the latest cloud microphysics models and support in assessing how changes to SAF design and utilization impact contrail formation. NARAC provides real-time computer predictions of the atmospheric transport of material from radioactive releases and of the downwind effects on health and safety. The team is also working with the Advanced Combustion Numerics group, who developed Zero-RK, which is used by computational fluid dynamics software vendors and combustion system designers in industry. The Zero-RK developers can rapidly create new capabilities to couple the latest in atmospheric microphysics models with the SAF and soot chemistry models.

Results

There are three main results during Fiscal Year (FY) 2022 for the project launch:

- Established access to the atmospheric thermodynamic data maintained by NASA's Global Modeling and Assimilation Office and obtained seasonal and diurnal variations for altitudes ranging from 9 km to 12 km (typical of aviation cruise).
- Verified that LLNL's current sustainable aviation fuel mechanism with soot formation will have stable simulation performance at temperatures as low as 190 K when the cooling and mixing processes of the engine exhaust plume are modeled.

- Identified chemistry additions and code advancements for LLNL's Zero-RK combustion solver for FY 2023 to include ice nucleation and more general atmospheric microphysics needed to simulate contrail formation.

The core SAF and soot mechanism was initially developed to accurately predict ignition and other combustion phenomena above 600 K. As the soot and water vapor cool when the engine exhaust mixes with the ambient atmospheric conditions, the chemistry model will need to transition from combustion temperatures to ice nucleation temperatures. It is important to understand the range of atmospheric conditions encountered in aviation as the persistence of contrails (and their subsequent climate impacts) is highly sensitive to local pressure, temperature, relative humidity, and particle density. The Modern-Era Retrospective Analysis for Research and Applications, Version 2 (MERRA-2) dataset [5] is used to sample the diurnal and seasonal variation in the atmospheric data to quantify the range of conditions in which the new coupled soot, ice nucleation, and cloud microphysics model must simulate. The temperature as a function of altitude is sampled across the globe for 24 full days (1st and 15th of each month in 2021) at three-hour intervals each day, and the annual extrema, mean, and inner 95% is plotted in Figure IV.3.1. The lower bound of the inner 95% range extends as low as 190 K at the range of altitudes typically used for aviation cruise (9 km to 12 km).

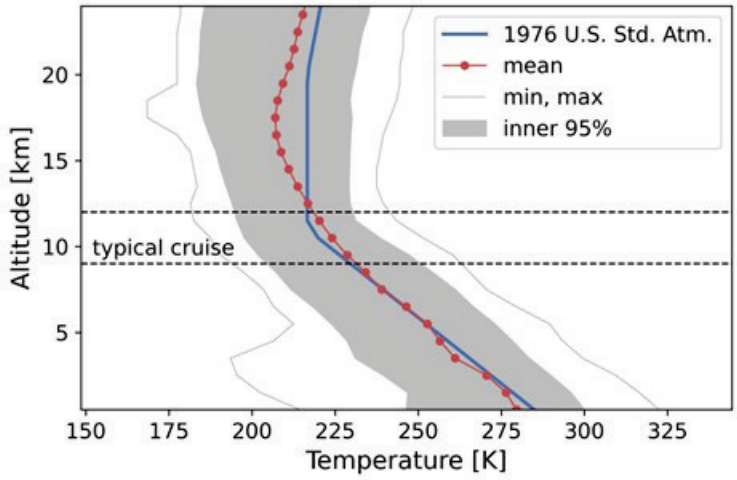

Figure IV.3.1 Atmospheric temperature variations across the globe as a function of altitude from the MERRA-2 dataset: mean temperature (red circles), inner 95% range (shaded gray), and the annual extrema (dots) for 2021. The 1976 U.S. Standard Atmosphere (U.S. Std. Atm.) is plotted in a solid blue line for reference.

To assess the suitability of the core SAF and soot formation mechanism for modeling the initial contrail formation processes, the Mech Checker tool (https://combustiontools.llnl.gov/) developed by Killingsworth et al. [6] is used to verify the expected performance of the thermodynamics and chemistry models. Less than 11% of the 4,200 species have thermodynamic functions defined below 250 K. If the specific heat or related thermodynamic properties are held fixed at their low temperature limit, a discontinuity in the first derivative of the governing ordinary differential equations will exist. These discontinuities can negatively affect the performance of the combustion solver and can lead to larger computational costs and even numerical instabilities that cause the simulation to crash. To avoid the discontinuities, the polynomial functions approximating the thermodynamic properties may be used to extrapolate beyond the temperature limits, but the functions are not guaranteed to produce physically valid results and must be verified. The extrapolation of the thermodynamic functions down to 190 K revealed that only 14 species in the core mechanism had any unphysical, non-monotonic specific heat functions. Further, the relative non-monotonic variation is less than 7%, with no species going below the theoretical minimum specific heat for an atomic species, which indicates the extrapolated thermodynamic functions should not introduce any instabilities when used in low-temperature simulations encountered for modeling contrails.

The Mech Checker tool is also used to evaluate the reaction rates in the core SAF and soot mechanism to temperatures as low as 190 K. The original model was initially designed to make predictions in the combustion regime and was validated only to temperatures as low as 600 K. Not surprisingly, a subset of the binary reactions is found to have artificially fast reaction rates in the reverse direction at these lower temperatures, as shown in Figure IV.3.2. The binary reaction rate is considered artificially (or unphysically) fast if its estimated collision probability exceeds 1. That is, the species react faster than they can collide to create the products. While non-physical, the large reaction rates may not necessarily cause numerical instabilities like the thermodynamic discontinuities. However, these rates do indicate that the low-temperature approximation of the enthalpy and entropy of formation needs to be reevaluated to have a more accurate low-temperature simulation and will be corrected in FY 2023.

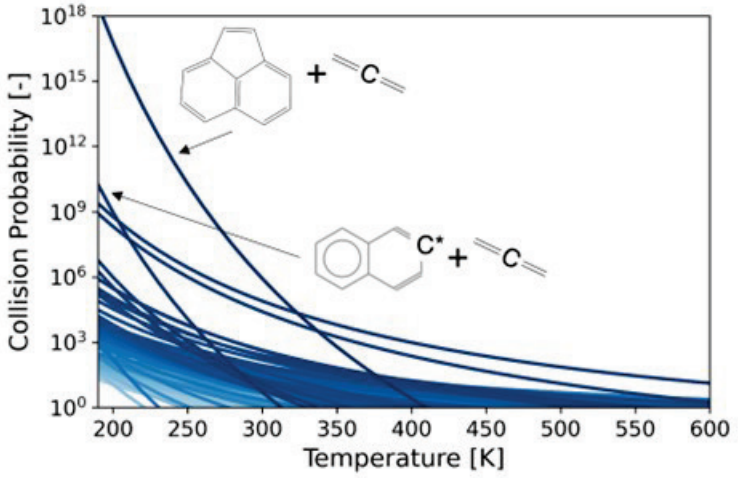

Figure IV.3.2 The largest 150 binary collision probabilities in the core SAF and soot mechanism. Values >1 indicate a binary reaction that is reacting faster than is physically possible.

Atmospheric "microphysics" refers to the micron-scale physical phenomena that affect the evolution of clouds and their precipitation particles. Near-field contrail formation models are highly sensitive to the linkage between the soot formation mechanisms, sulfur and volatile organic chemistry interactions with soot particles, and the microphysics models. Recent reviews of challenges facing predictive microphysics models [7], [8], [9] include numerous references that allow an assessment of the current atmospheric models needed for contrail prediction. The project team is reviewing these literature models to determine their suitability to be coupled with the state-of-the-art SAF and soot model developed at LLNL and then categorizing the models into three main categories: (A) may be added directly to the existing model, (B) require a new reaction class to be added to LLNL's Zero-RK software, and (C) are best coupled via a user-defined function to Zero-RK.

The atmospheric chemistry kinetic mechanisms for nitrogen oxides, sulfur oxides, and sulfuric acid [10], [11] are Category A, as they are represented by traditional mass-action formulas with modified Arrhenius parameters defining the reaction rate coefficients. Similarly, the bin sectional methods for resolving the size distribution of ice nucleating particles using a fixed discretization has the same formulation as the current LLNL soot model and thus falls into Category A. More complex formulations of the bin sectional methods that include surface activation rates based on the local concentration of sulfur compounds [12], unburned or partially burned fuel, and other organics would be best handled by adding a new reaction class to Zero-RK to provide a formulation that represents the surface kinetics; these formulations and are in Category B. Some global reaction models for the decomposition of an arbitrary hydrocarbon or bioderived fuel [13] include function terms that are not currently available in standard kinetic models. These non-standard functions may be approximated using one or a series of the currently available reactions in Zero-RK, making them Category A, or may fall into Category B if accuracy demands that the formulation be implemented exactly. Finally, some

microphysics models that couple with an instantaneous equilibrium approximation for the vapor pressure [14] are sufficiently complex that they are best implemented as independent code, Category C. This code could then be callable via a standardized user-defined function in Zero-RK to be integrated simultaneously with the chemical kinetic model. Many other models defined in the references from the reviews [7], [8], [9] fall in Category C because they have custom governing ordinary differential equations that are not sufficiently reused to warrant new functional forms in Zero-RK. Overall, a clear path exists to couple the most relevant microphysics models from the atmospheric simulation community with LLNL's state-of-the-art SAF soot model in FY 2023.

Conclusions

The project completed the initial verification of the base SAF and soot mechanisms and identified a clear path to continue coupling the latest ice nucleation and other cloud microphysics models. The success of the project will improve the understanding of the earliest contributors to contrail formation and provide engine and fuel engineers in industry with tools to limit the climate impact of persistent contrails and contrail-induced cloudiness for future SAF utilization. Three objectives were completed in FY 2022 to launch the new research project at LLNL:

- Established access to atmospheric thermodynamic data at flight conditions (temperature, pressure, relative humidity, etc.) relevant to the contrail formation and evolution processes.
- Verified that the current SAF chemistry and soot formation model will produce stable simulations of the jet engine exhaust cooling and mixing processes with the ambient conditions at cruising altitudes.
- Identified additions to expand the SAF combustion model to include atmospheric chemistry, ice nucleation, and other cloud microphysics models.

Key Publications

1. McNenly, M. J., S. W. Wagnon, C. Saggese, T. Chatterjee, S. Lapointe, and R. A. Whitesides. 2022. "Advanced Soot Models and the Path to SAF Contrail Prediction." Presented at the International Energy Agency, Clean and Efficient Combustion Technology Collaboration Program, Sendai, Japan, August 1–4.

References

1. Lee, D.S, D.W. Fahey, A. Skowron, M.R. Allen, U. Burkhardt, Q. Chen, S.J. Doherty, et. al. 2021. "The Contribution of Global Aviation to Anthropogenic Climate Forcing for 2000 to 2018." *Atmospheric Environment* 244: 117834.

2. Mehl, M., S. Wagnon, K. Zhang, G. Kukkadapu, W. Pitz, C. Westbrook, Y. Zhang, et al. 2017. "A Comprehensive Detailed Kinetic Mechanism for the Simulation of Transportation Fuels." 10th U.S. National Combustion Meeting, paper 1A17, College Park, MD, April 23–26.

3. McCormick, R., G. Fioroni, L. Fouts, E. Christensen, J. Yanowitz, E. Polikarpov, K. Albrecht, D. Gaspar, J. Gladden, and A. George. 2017. "Selection Criteria and Screening of Potential Biomass-Derived Streams as Fuel Blendstocks for Advanced Spark-Ignition Engines." *SAE International Journal of Fuels and Lubricants* 10, 2: 442–460. https://doi.org/10.4271/2017-01-0868.

4. McNenly, M.J., R.A. Whitesides, and D.L. Flowers. 2015. "Faster Solvers for Large Kinetic Mechanisms using Adaptive Preconditioners." *Proceedings of the Combustion Institute*. 35: 581–587.

5. Gelaro, R., W. McCarty, M.J. Suarez, R. Todling, A. Molod, L. Takacs, C.A. Randles, et al. 2017. "The Modern-Era Retrospective Analysis for Research and Applications, Version 2 (MERRA-2)." *Journal of Climate* 30, 14: 5419–5454.

6. Killingsworth, N.J., M.J. McNenly, R.A. Whitesides, and S. Wagnon. 2020. "Cloud Based Tool for Analysis of Chemical Kinetic Mechanisms." *Combustion and Flame* 221: 170–179.

7. Burrows, S.M., C.S. McCluskey, G. Cornwell, I. Steinke, K. Zhang, B. Zhao, M. Zawadowicz, et al. 2022. "Ice-Nucleating Particles That Impact Clouds and Climate: Observational and Modeling Research Needs." *Reviews of Geophysics* 60: e2021RG000745.

8. Morrison, H., M. van Lier-Walqui, A.M. Fridland, W.W. Grabowski, J.Y. Harrington, C. Hoose, A. Korolev, et al. 2019. "Confronting the Challenge of Modeling Cloud and Precipitation Microphysics." *Journal of Advances in Modeling Earth Systems* 12: e2019MS001689.

9. Paoli, R. and K. Shariff. 2016. "Contrail Modeling and Simulation." *Annual Review of Fluid Mechanics* 48: 393–427.

10. Mueller, M.A., R.A. Yetter, and F.L. Dryer. 2000. "Kinetic Modeling of the $CO/H_2O/O_2/NO/SO_2$ System: Implications for High-Pressure Fall-Off in the $SO_2 + O (+ M) = SO_3 (+ M)$ Reaction." *International Journal of Chemical Kinetics* 32: 317–339.

11. Brown, R.C., R.C. Miake-Lye, M.R. Anderson, C.E. Kolb, and T.J. Resch. 1996. "Aerosol Dynamics in Near-Field Aircraft Plumes." *Journal of Geophysical Research* 101 (D17): 22939–22953.

12. Wong, H.-W., and R.C. Miake-Lye. 2010. "Parametric Studies of Contrail Ice Particle Formation in Jet Regime Using Microphysical Parcel Modeling." *Atmospheric Chemistry and Physics* 10: 3261–3272.

13. Varatharajan, B., M. Petrova, F.A. Williams, and V. Tangirala. 2005. "Two-Step Chemical-Kinetic Descriptions for Hydrocarbon-Oxygen-Diluent Ignition and Detonation Applications." *Proceedings of the Combustion Institute* 30, 2: 1869–1877.

14. Yu, F., and R.P. Turco. 1998. "Contrail Formation and Impacts on Aerosol Properties in Aircraft Plumes: Effects of Fuel Sulfur Content." *Geophysical Research Letters* 25, 3: 313–316.

V Crosscutting

V.1 Zero-RK Acceleration of Low-Lifecycle-Carbon Fuel (LLCF) Simulations (Lawrence Livermore National Laboratory)

Russell Whitesides, Principal Investigator
Lawrence Livermore National Laboratory
7000 East Avenue, L-792
Livermore, CA 94550
Email: whitesides1@llnl.gov

Kevin Stork, DOE Technology Manager
U.S. Department of Energy
Email: Kevin.Stork@ee.doe.gov

Start Date: October 1, 2021 End Date: September 30, 2022
Project Funding: $250,000 DOE share: $250,000 Non-DOE share: $0

Project Introduction

Designing modern combustion systems now relies on computer models that predict how changes in design will affect performance. These models have replaced older methods that relied on the designer's intuition or costly and time-consuming physical testing. By using improved models, design cycles can be shortened, and cleaner and more efficient combustion devices can be created. This project aims to improve computer simulations of low-lifecycle-carbon fuels (LLCFs) with the goal of making these simulations faster and more accurate for predicting combustion in vehicles.

Objectives

Overall Objectives

- Advance state-of-the-art in LLCF combustion simulation through the development of fast and accurate models.
- Work with industry partners to prove capability and impact of combustion software.

Fiscal Year 2022 Objectives

- Create fuel surrogate and reduced kinetic models for LLCF combustion research in support of Lawrence Livermore National Laboratory (LLNL) kinetic modeling team.
- Develop neural-network species prediction models (NNSPMs) that accelerate computational fluid dynamics (CFD) simulations containing detailed reaction models by reducing the number of kinetic species that need to be resolved.

Approach

The computational models are critical for the transition of U.S. transportation markets for off-road, rail, marine, and aviation away from carbon-intensive fuels (e.g., diesel and Jet-A/A1) and towards LLCFs. These models rely on detailed kinetic/reaction models as developed in the sibling project and described in the associated report [1]. The LLCF models are designed to capture as much real combustion behavior for as many fuel components as possible. The level of detail in these models makes them exquisite tools for investigating impacts of fuel interactions and fuel/emissions coupling in canonical combustion devices (e.g., shock-tubes, laminar flames) but also makes them intractable for use in CFD due to the extreme cost of such simulations. The current effort in this project bridges the simulation gap by (1) creating matched fuel surrogate mixtures and reduced kinetic models, (2) reducing the cost of transport equation solution in CFD with NNSPMs.

Results

Surrogate Mixture and Reduced Reaction Models

Although previous work in this project and elsewhere has accelerated solutions for detailed kinetic models, it is still not possible to use models with thousands of species in practical combustion devices using CFD. Relatedly, practical market fuels in wide use in transportation (e.g., diesel and jet fuels) contain thousands of components which vary from region to region and seasonally. This project has previously advanced the state of the art in these areas by creating new tools for reaction model reduction and tuning as well as surrogate fuel mixture creation. The prior focus of application for these tools was applied to fuels with an on-road focus (e.g., gasoline, diesel, and related bio-fuel analogs). The current effort aims to apply these tools to fuels relevant to off-road, rail, marine, and aviation markets, including existing market fuels, nascent LLCF candidates, and related blends.

Reaction model reduction and tuning keeps the most important features of a fully detailed kinetic model at a limited set of environmental conditions (e.g., temperature and pressure) and fuel components. Using the Global Pathway Selection methodology [2], coupled to the Zero-RK fast chemistry solvers [3], LLNL can quickly create customized models suited to fuel and model conditions. This capability allows reduced models to closely follow development of the detailed models, and to quickly adjust to changing CFD model requirements (either in reacting conditions or reaction model size). While this tool can make highly reduced reaction models (i.e., with very low species/reaction counts), the fidelity of the reduced models can be significantly degraded. LLNL has developed a reaction model tuning toolkit to minimize the discrepancy between full and reduced model predictions. The combination of the reduction and tuning process creates kinetic models that are practical to use in device-scale CFD while maintaining excellent predictions for ignition and emissions.

For combustion modeling, the reality of complex and varying market fuels necessitates the use of fuel surrogates that can match the physical and chemical qualities of a target fuel with a limited mixture of well-characterized fuel components. Historically, modelers have employed single or binary component surrogate fuels, largely due to the lack of practical reaction models for more complex mixtures. In the last decade, surrogates with ten or more components have been proposed in the literature for a wide range of liquid transportation fuels. The increasing availability of detailed fuel models and the goal of transitioning to LLCF have motivated the need for a tool that can design a surrogate fuel for existing market fuels, LLCF candidate fuels, as well as blends of the two. LLNL has created a tool that can evaluate fuel surrogates based on a range of targeted physical and chemical characteristics. Given a set of surrogate components, this tool can find mixtures that optimally fit the targeted characteristics. The flexibility and speed of the surrogate generation tool enables combustion researchers to fully leverage detailed reaction models to investigate practical fuel and fuel blending effects on combustion device performance.

In Fiscal Year 2022, the reduction, tuning, and surrogate generation tools have been employed across a range of transportation fuel studies [4], [5], [6], [7]. Figure V.1.1 and Figure V.1.2 show examples of the impact of the tools with (Figure I.1.1) the improvement in predictions of first stage ignition of a reduced n-dodecane fuel model as a result of parameter tuning (more details in Tagliante, et al. [4]) and (Figure V.1.2) a comparison of the measured and predicted distillation curves for diesel surrogates developed using the surrogate generation tools [6]. The tools are maintained and updated in response to the needs of the kinetic modeling team and will continue to be applied to LLCF combustion research.

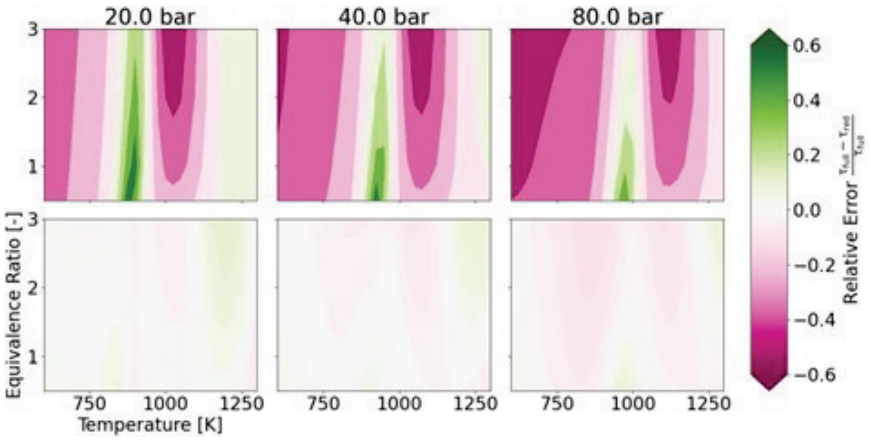

Figure V.1.1 Relative error in prediction of first stage ignition for a reduced n-dodecane model before (top) and after (bottom) reaction rate parameter tuning [4]. Lighter colors indicate predictions that are in better agreement with the detailed model.

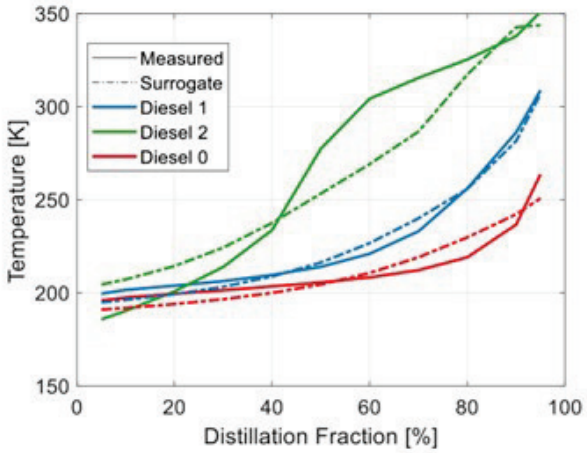

Figure V.1.2 Comparison of distillation curves measured for three diesel fuels and the corresponding surrogates as predicted by the LLNL surrogate generation tool [6]

Acceleration of CFD with Detailed Kinetics with Neural-network Species Prediction Models

Even with the new capabilities discussed above, the inclusion of kinetic models with ~100 species or more in CFD of combustion devices remains computationally expensive. One of the impacts of the large species counts is the number of equations that must be solved to track the transport of species within the flow domains. The cost of transport equation solution scales linearly with the number of species included in the reaction model, and in some cases this cost can become the bulk of the computational cost of a CFD analysis. LLNL is developing a methodology to substantially lower the cost of transport equation solution through the use of NNSPMs. The NNSPMs are designed such that only a fraction of the species included in the chemical model need to be resolved in the transport. The concentrations of the "missing" species are predicted by a neural network model that has been trained on a large dataset of reaction states (all species, temperature, and pressure) from zero- and one-dimensional reacting systems. The initial and boundary conditions for the training datasets are designed such that the resulting states cover all the conditions that will be seen during practical CFD simulations. The cost of generating the training dataset and training the neural network is amortized over all future CFD simulations using the NNSPM through the reduction in transport equation cost. LLNL has shown that >50% of species can be accurately predicted by properly trained NNSPMs for a reaction model containing >200 species, and future work will focus on connecting the models to CFD through a plug-in architecture.

Conclusions

- LLNL tools for practical application of detailed reaction models in CFD, including model reduction, model tuning, and surrogate generation were applied across a range of vehicle combustion problems and continue to be developed and supported for future LLCF research.

- NNSPMs have been shown to accurately predict >50% of the chemical species, with the promise to cut transport equation solution time in half. Developments to integrate the NNSPM into CFD are ongoing.

Key Publications

1. Tagliante, F., T.M. Nguyen, M.P. Dhanji, H.S. Sim, L.M. Pickett, J. Manin, G. Kukkadapu, R. Whitesides, and K. Wan. 2022. "The Role of Cool-Flame Fluctuations in High-Pressure Spray Flames, Studied Using High-Speed Optical Diagnostics and Large-Eddy Simulations." *Proceedings of the Combustion Institute*. https://doi.org/10.1016/j.proci.2022.07.242.

2. Kalvakala, K.C., P. Pal, J.P. Gonzalez, C.P. Kolodziej, H.J. Seong, G. Kukkadapu, M. McNenly, S. Wagnon, R. Whitesides, N. Hansen, and S.K. Aggarwal. 2022. "Numerical Analysis of Soot Emissions from Gasoline-Ethanol and Gasoline-Butanol Blends under Gasoline Compression Ignition Conditions." *Fuel* 319: 123740. https://doi.org/10.1016/j.fuel.2022.123740.

3. Chuahy, F.D.F, C.S. Sluder, S.J. Curran, G. Kukkadapu, S.W. Wagnon, and R. Whitesides. 2022. "Numerical Assessment of Fuel Physical Properties on High-Dilution Diesel Advanced Compression Ignition Combustion." *Applications in Energy and Combustion Science* 100102. https://doi.org/10.1016/j.jaecs.2022.100102.

4. Cheng, S., S.S. Goldsborough, S.W. Wagnon, R. Whitesides, M. McNenly, W.J. Pitz, D. Lopez-Pintor, and J.E. Dec. 2022. "Replicating HCCI-Like Autoignition Behavior: What Gasoline Surrogate Fidelity is Needed?" *Applications in Energy and Combustion Science* 100091. https://doi.org/10.1016/j.jaecs.2022.100091.

References

1. Wagnon, S.W. 2022. "LLCF Combustion and Emissions Models" in *Decarbonization of Off-Road, Rail, Marine, and Aviation Program: 2022 Annual Progress Report*. U.S. Department of Energy, Washington, D.C.

2. Gao, X., S. Yang, and W. Sun. 2016. "A Global Pathway Selection Algorithm for the Reduction of Detailed Chemical Kinetic Mechanisms." *Combustion and Flame* 167: 238–247. https://doi.org/10.1016/j.combustflame.2016.02.007.

3. McNenly, M.J., R.A. Whitesides, and D.L. Flowers. 2015. "Faster Solvers for Large Kinetic Mechanisms Using Adaptive Preconditioners." *Proceedings of the Combustion Institute* 35: 581–587. https://doi.org/10.1016/j.proci.2014.05.113.

4. Tagliante, F., T.M. Nguyen, M.P. Dhanji, H.S. Sim, L.M. Pickett, J. Manin, G. Kukkadapu, R. Whitesides, and K. Wan. 2022. "The Role of Cool-Flame Fluctuations in High-Pressure Spray Flames, Studied Using High-Speed Optical Diagnostics and Large-Eddy Simulations." *Proceedings of the Combustion Institute*. https://doi.org/10.1016/j.proci.2022.07.242.

5. Kalvakala, K.C., P. Pal, J.P. Gonzalez, C.P. Kolodziej, H.J. Seong, G. Kukkadapu, M. McNenly, S. Wagnon, R. Whitesides, N. Hansen, and S.K. Aggarwal. 2022. "Numerical Analysis of Soot Emissions from Gasoline-Ethanol and Gasoline-Butanol Blends under Gasoline Compression Ignition Conditions." *Fuel* 319: 123740. https://doi.org/10.1016/j.fuel.2022.123740.

6. Chuahy, F.D.F, C.S. Sluder, S.J. Curran, G. Kukkadapu, S.W. Wagnon, and R. Whitesides. 2022. "Numerical Assessment of Fuel Physical Properties on High-Dilution Diesel Advanced Compression Ignition Combustion." *Applications in Energy and Combustion Science* 100102. https://doi.org/10.1016/j.jaecs.2022.100102.

7. Cheng, S., S.S. Goldsborough, S.W. Wagnon, R. Whitesides, M. McNenly, W.J. Pitz, D. Lopez-Pintor, and J.E. Dec. 2022. "Replicating HCCI-Like Autoignition Behavior: What Gasoline Surrogate Fidelity is Needed?" *Applications in Energy and Combustion Science* 100091. https://doi.org/10.1016/j.jaecs.2022.100091.

Acknowledgements

This work was performed under the auspices of DOE by LLNL under Contract DE-AC52-07NA27344.

Contributors include Matthew McNenly, Simon Lapointe, Scott Wagnon, and Nick Killingsworth.

LLNL Document Number: LLNL-TR- 844484

V.2 ASTM Standards Development and Ignition Studies of 100% Biofuels (National Renewable Energy Laboratory)

Robert McCormick, Principal Investigator
National Renewable Energy Laboratory
15013 Denver West Parkway
Golden, CO 80401
Email: Robert.McCormick@nrel.gov

Kevin Stork, DOE Technology Manager
U.S. Department of Energy
Email: Kevin.Stork@ee.doe.gov

Start Date: October 1, 2021 End Date: September 30, 2022
Project Funding: $800,000 DOE share: $800,000 Non-DOE share: $0

Project Introduction

Introduction of low-/net-zero-carbon liquid fuels is potentially the lowest-cost pathway for rapid reduction in greenhouse gas emissions from difficult-to-electrify sectors of transportation. Biofuels are low-carbon fuels that can be used to decarbonize these sectors, which include long-haul freight, large off-road equipment, rail, marine shipping, and aviation. Currently available biofuels are used at relatively low blend levels. This research is targeted at increasing blend levels to 100% and accelerating the introduction of new low-carbon biofuels. The primary focus of this project is on synthetic aviation turbine fuel (SATF), which, if shown to be produced with a low carbon intensity, is sometimes called sustainable aviation fuel (SAF).

Low-technology-readiness-level fuel production processes generate small volumes (e.g., 10 mL), while full fuel qualification (especially for aviation) can require tens of thousands of liters—a quantity not available until the process reaches pilot scale. The "valley of death" for new fuel development is the huge risk of investing in multimillion-dollar pilot plants caused by the coupling of scale-up risk with uncertainty as to whether the resulting fuel will meet regulatory and user requirements. Research under this project endeavors to reduce these risks and accelerate SATF introduction by using high-fidelity simulations to predict fuel property effects on turbine combustion. The research leverages improved simulations of combustion in an aviation gas turbine developed under previous research sponsored by the Office of Science [1]. To further improve the fidelity of these simulations, critical fuel properties will be measured at actual turbine operating conditions, and high-quality, reduced-order combustion kinetic models will be developed. Simulation results can provide confidence that a new fuel can meet fuel qualification requirements very early in the development process, thereby reducing risk and accelerating the introduction of low-net-carbon fuels and attainment of the SAF Grand Challenge goal of 35 billion gallons per year [2]. Simulations might also show that fuels outside of the currently allowable property range could provide acceptable performance, which would also accelerate new fuel development.

Objectives

Overall Objectives

- Create unique experimental capabilities for measuring critical properties of conventional jet fuel and SATF over the full range of turbine engine operating conditions (−40°C to 525°C and 0.4 atmosphere [atm] to 70 atm—and as high as 130 atm in the fuel injection nozzle upstream of the combustor). This capability will be developed incrementally over several years; properties of interest include density, viscosity, surface tension, heat capacity, and heat of vaporization (at a minimum).

- Develop an improved ignition delay metric for jet fuels (including SATF) that is more optimized for the conditions of turbine combustion than cetane number (CN) and has a reduced fuel volume requirement.
- Utilize the National Renewable Energy Laboratory's (NREL's) existing flow reactor (up to 1,200 K, 10 atm) and constant volume combustion chamber (up to 973 K, 40 atm) capability to inform development of reduced kinetic models for current and future forms of SAF.
- Simulate the impacts of fuel properties on performance (ignition, extinction, emissions formation, and other aspects) of a single-nozzle flame tube and investigate the impacts of uncertainty in fuel property measurements on the simulation results.

Fiscal Year 2022 Objectives

- Identify and acquire instruments to measure density and viscosity over the full temperature and pressure range. Identify an instrument (to be acquired in Fiscal Year [FY] 2023) to measure surface tension over the full temperature and pressure range.
- Demonstrate that the Advanced Fuel Ignition Delay Analyzer (AFIDA) can measure CNs for jet fuels and SATF that are identical to those measured by other methods.

Approach

The ASTM International methods used to measure fuel properties for new aviation fuel qualification [3] were reviewed to understand their accessible temperature and pressure ranges and principles of operation. Vendor offerings for instruments that could go beyond these conditions—to cover the full turbine engine operating range while providing comparable property measurements—were identified.

CN measured in the AFIDA is called indicated cetane number (ICN)—measured by ASTM D8183 [4]—and is an approved method for measuring the CN of diesel fuels. ASTM D4054 [3], *Standard Practice for Evaluation of New Aviation Turbine Fuels and Additives*, requires measurement of derived cetane number (DCN) using ASTM D6890 [5]. To evaluate the equivalence of these methods, the research team obtained several of the Federal Aviation Administration National Jet Fuel Combustion Program's (NJFCP's) standard fuels, as well as SATFs from three producers (described in more detail in the Results section). CNs of these fuels were measured by NREL using the AFIDA, and, for some fuels, DCN values were also measured using NREL's Ignition Quality Tester (IQT) via ASTM D6890. The AFIDA is a constant-volume combustion chamber that measures ICN using an initial temperature and pressure of 580°C and 17.5 atm. These conditions were chosen to provide an ignition delay metric (CN) that is relevant to combustion in a diesel engine. Notably, ICN requires 40 mL, versus the 150 mL required for DCN measurement—a significant advantage for evaluating fuels at low technology readiness levels.

Temperature and pressure can be easily varied in the AFIDA, and so, in addition to measuring ICN, the team has begun to measure ignition delay over a broad range of conditions with the goal of determining whether different conditions would provide results more predictive of turbine engine performance (e.g., lean blowout).

Results

Accomplishments in FY 2022 in acquiring instruments for measuring properties at actual conditions are as follows:

- Identified, ordered, and installed an Anton Parr DMA 4200 density meter with an operating range of −10°C to 200°C and 1 atm to 500 atm (for aviation fuels, pressures up to 130 atm will be employed).
- Acquired a conventional (ASTM D7042) viscometer (Anton Parr SVM 3001) for the measurement of kinematic viscosity at 1 atm from −60°C to 130°C; this device is also capable of measuring density according to ASTM D4052. Identified and ordered (with installation scheduled for the first quarter of

FY 2023) two Cambridge Viscosity viscometers with a combined operating range of −40°C to 315°C and 1 atm to 1,300 atm (for aviation fuels, pressures up to 130 atm will be employed).

- Worked with KRÜSS Scientific to design a tensiometer for measuring surface tension with an operating range of −35°C to 400°C and 1 atm to 60 atm. The team plans to order this instrument in FY 2023.

For comparison of ICN and DCN, the fuels listed in Table V.2.1 were employed. These include several of the NJFCP fuels, whose properties (including DCN) were reported by Edwards [6]. Commercial SAF samples were obtained from three producers; these were tested in neat form and as 50% blends into sample A-2 (a Jet A fuel). A low-CN reference fuel, methyl cyclohexane, was also evaluated. According to their standard methods, the AFIDA is calibrated for the ICN range of 35 to 85, while the IQT is calibrated for the DCN range of 33 to 64. Initial experiments showed good agreement between these methods in their calibration ranges; however, agreement deteriorated for lower-CN materials, and, in fact, the neat alcohol-to-jet (ATJ) fuels did not even ignite in the AFIDA experiment using the standard method. In collaboration with ASG Analytik-Service AG, the manufacturer of the AFIDA, the team developed a low-ICN calibration for fuels ranging in ICN from 5 to 35 that exhibits a correlation coefficient (r^2) of 0.99 over six primary standard binary mixtures of 1-methylnaphthalene and n-hexadecane.

Table V.2.1 DCN and ICN Measured Values (New Low-ICN Calibration Applied for ICN Values)

Fuel	DCN [6]	DCN (NREL)	ICN (NREL)	Comments
NJFCP Identification				
A-1 (10264)	48.8	--	52.3	JP-8 (Jet Propellant 8)
A-2 (10325)	48.3	--	51.3	Jet A
A-3 (10289)	39.2	--	41.7	JP-5
C-1 (13718)	17.1	--	9.0	ATJ (isobutanol)
C-2 (12223)	50.4	--	51.9	84% C14 iso-paraffins/16% 1,3,5 trimethyl benzene
C-3 (12959)	47.0	--	49.4	64:36 A-3:Amyris farnesane
C-4 (13217)	28.0	--	18.2	60:40 FT-SPK:C-1
Other Fuels				
Commercial HEFA-SPK#1		59.4	60.5	
Commercial HEFA-SPK#2		67.0	64.7	
Commercial ATJ-SPK		15.4	8.4	ATJ (isobutanol)
NREL Blend		54.8	56.9	50:50 A-2:HEFA-SPK#1
NREL Blend		36.3	31.0	50:50 A-2:ATJ-SPK
Low-CN fuel		23.3	22.0	Methylcyclohexane

HEFA – hydroprocessed esters and fatty acids; SPK – synthetic paraffinic kerosene; FT – Fischer–Tropsch

Figure V.2.1 shows the final DCN/ICN comparison results using the newly developed low-ICN calibration for ICN. The r^2 obtained between all measured results is 0.98, but this number rises to 0.99 by removing results obtained outside of the ASTM calibrated range for the IQT. For CNs below ~25, the ICN is typically significantly lower than DCN. There is a large degree of uncertainly in DCN results obtained below 33 since

the IQT is not calibrated in that region. These results demonstrate the equivalence of ICN and DCN for alternative jet fuel qualification.

Pressure traces for ignition delay measurement at 530°C for A-2 and a 50% blend with HEFA-SPK#1 are shown in Figure V.2.2. Both pressure traces show an initial decline in pressure from evaporative cooling followed by two-stage heat release—as expected for these relatively high-CN materials. This reaction temperature is 50°C lower than that used for ICN measurements, yet ICN still serves to describe the materials' relative reactivity. A-2 exhibits an ICN that is almost 6 units lower than the 50% blend with HEFA-SPK and shows measurably longer ignition delay.

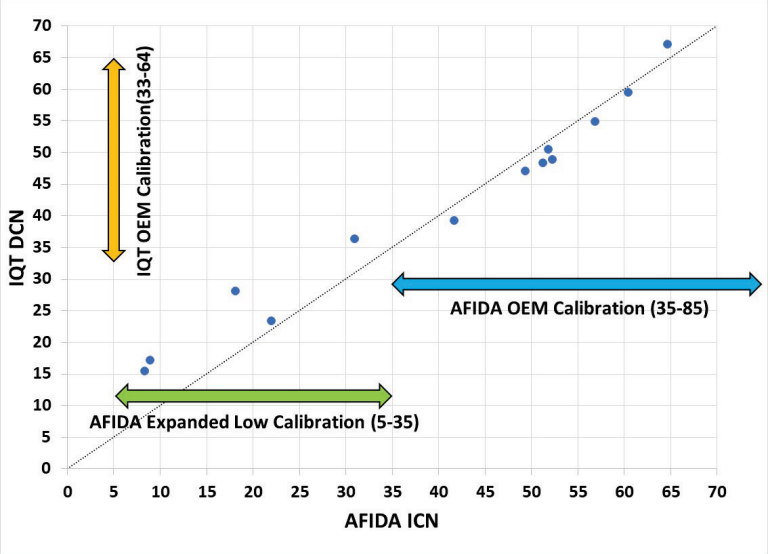

OEM – original equipment manufacturer

Figure V.2.1 Comparison of DCN and ICN results

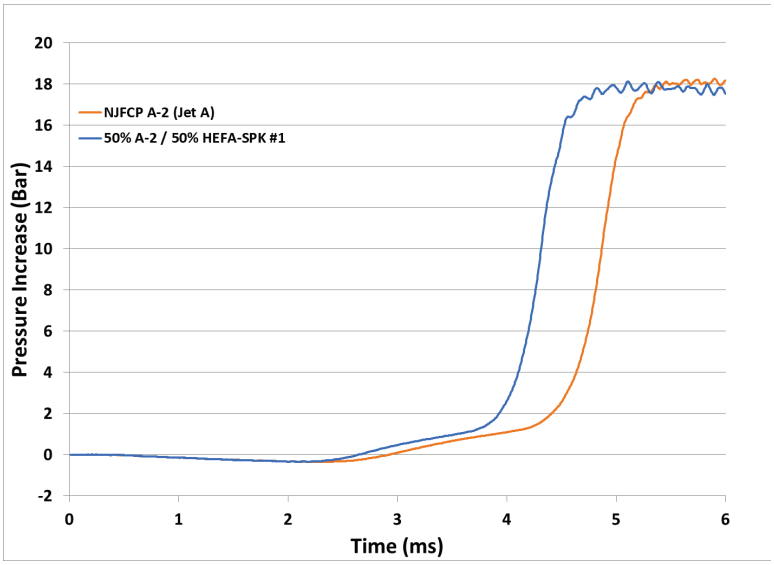

Figure V.2.2 Measured pressure traces during ICN measurement for NJFCP A-2 and a 50% blend of A-2 with HEFA-SPK#1. Initial temperature and pressure of 530°C and 17.5 bar, respectively.

Ignition delay times (IDTs) over a range of temperatures were measured for A-2 and the 50:50 blend of A-2:HEFA-SPK, and results are shown in Figure V.2.3. IDT was defined as the time for the pressure to increase to 0.5 bar above the starting pressure. Comparisons between these fuels show a consistently faster IDT for the blend, which is unsurprising considering the higher ICN value of 56.9 versus 51.3. Differences in the negative temperature coefficient region begin to appear, as neat A-2 shows signs of more prominent negative-temperature-coefficient activity evidenced by flatter IDTs at the highest measured temperatures. Further data collection above 580°C is necessary to understand the true differences here.

Future work (in FY 2023) will investigate density, viscosity, and surface tension over a wide range of temperatures and pressures for conventional and alternative jet fuels. The research team will also initiate simulations of a single-nozzle burner and expand ignition-delay measurements to other conditions.

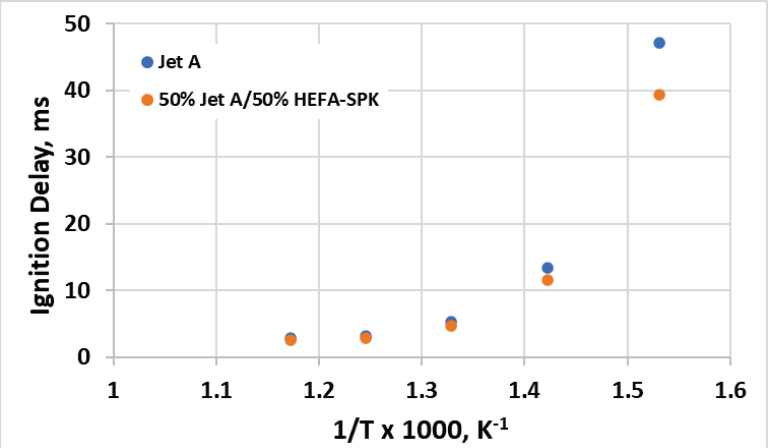

T – temperature

Figure V.2.3 Comparison of IDT results for A-2 vs. 50:50 A-2:HEFA SPK#1

Conclusions

- Identified, ordered, and installed an Anton Parr DMA 4200 density meter with an operating range of −10°C to 200°C and 1 atm to 500 atm.
- Acquired a conventional (ASTM D7042) viscometer (Anton Parr SVM 3001) to measure kinematic viscosity at 1 atm from −60°C to 130°C; this device is also capable of measuring density according to ASTM D4052. Identified and ordered (with installation scheduled for the first quarter of FY 2023) two Cambridge Viscosity viscometers with a combined operating range of −40°C to 315°C and 1 atm to 1,300 atm.
- Worked with KRÜSS Scientific to design a tensiometer for measuring surface tension with an operating range of −35°C to 400°C and 1 atm to 60 atm.
- Demonstrated equivalence of DCN (via ASTM D6890) and ICN (via ASTM D8183) for measurement of jet fuel CN, an advantage for new fuel qualification because of the much lower fuel volume required for ICN measurements.

References

1. Henry de Frahan, M.T., J.S. Rood, M.S. Day, H. Sitaraman, S. Yellapantula, B.A. Perry, R.W. Grout, et al. 2022. “PeleC: An Adaptive Mesh Refinement Solver for Compressible Reacting Flows.” *The International Journal of High Performance Computing Applications*. https://doi.org/10.1177/10943420221121151 (source code available at https://github.com/AMReX-Combustion).

2. U.S. Department of Transportation. 2021. "Memorandum of Understanding: Sustainable Aviation Fuel Grand Challenge." September 8. https://www.energy.gov/sites/default/files/2021-09/S1-Signed-SAF-MOU-9-08-21_0.pdf.

3. ASTM International. 2022. *ASTM D4054 Standard Practice for Evaluation of New Aviation Turbine Fuels and Fuel Additives*. West Conshohocken, PA: ASTM International. https://www.astm.org/d4054-22.html.

4. ASTM International. 2022. *ASTM D8183 Standard Test Method for Determination of Indicated Cetane Number (ICN) of Diesel Fuel Oils using a Constant Volume Combustion Chamber–Reference Fuels Calibration Method*. West Conshohocken, PA: ASTM International. https://www.document-center.com/standards/show/ASTM-D8183.

5. ASTM International. 2021. *ASTM D6890 Standard Test Method for Determination of Ignition Delay and Derived Cetane Number (DCN) of Diesel Fuel Oils by Combustion in a Constant Volume Chamber*. West Conshohocken, PA: ASTM International. https://www.document-center.com/standards/show/ASTM-D6890.

6. Edwards, T. 2017. *Reference Jet Fuels for Combustion Testing*. Reston, VA: American Institute of Aeronautics and Astronautics. https://www.caafi.org/news/pdf/Edwards_AIAA-2017-0146_Reference_Jet_Fuels.pdf.

Acknowledgements

The coauthors for this project are Marc Day, Gina M. Fioroni, Jon Luecke, and Shashank Yellapantula from NREL.

VI Legacy On-Road Projects

VI.A Combustion

VI.A.1 Enabling Low-Temperature Plasma Ignition Technologies for Multimode Engines through the Development of a Validated High-Fidelity Low-Temperature Plasma Model for Predicative Simulation Tools (Auburn University)

Nicholas Tsolas, Principal Investigator
Auburn University
Department of Mechanical Engineering
1418 Wiggins Hall
Auburn, AL 36849
Email: ntsolas@auburn.edu

Fabrizio Bisetti, Principal Investigator
University of Texas at Austin
Department of Aerospace Engineering and Engineering Mechanics
2617 Wichita Street, C0600
Austin, TX 78712
Email: fbisetti@utexas.edu

Isaac Ekoto, Principal Investigator
Sandia National Laboratories
7011 East Avenue
Livermore, CA 94551
Email: iekoto@sandia.gov

Riccardo Scarcelli, Principal Investigator
Argonne National Laboratory
9700 South Cass Avenue
Lemont, IL 60439
Email: rscarcelli@anl.gov

Gurpreet Singh, DOE Program Manager
U.S. Department of Energy
Email: Gurpreet.Singh@ee.doe.gov

Start Date: October 1, 2019 End Date: June 30, 2023
Project Funding: $1,503,342 DOE share: $1,199,978 Non-DOE share: $303,364

Project Introduction

The goal of multimode engine architectures is to extend current lean-burn and exhaust gas recirculation (EGR) dilution limits, which requires spark plugs to deposit high energies (hundreds of millijoules) in order to initiate ignition and complete combustion. At elevated energy deposition rates, spark plugs experience increased electrode erosion and thermal losses, which ultimately shorten the spark plug lifetime and lower ignition efficiency. As such, safeguarding the efficiency gains of multimode concepts will require new and improved ignition technologies. Recently, non-equilibrium low-temperature plasmas (LTPs) have been shown to promote energy-efficient ignition via quenching and transport of electronically excited atoms and molecules, selective radical production, and fast heating of hydrocarbon–air mixtures [1], [2]. Thus, LTP is seen as a

technology that can potentially enable kinetically controlled combustion modes toward fuel-leaner conditions to realize current U.S. Department of Energy (DOE) Vehicle Technologies Office goals of improving fuel economy by 25% to ensure the sustainability of future mobility [3]. Although many previous studies have demonstrated the efficacy of plasma-assisted ignition to enhance combustion, the detailed enhancement mechanisms remain largely unknown, especially at elevated pressures that are most relevant to practical engine conditions. These barriers hinder the development of accurate and comprehensive numerical models that seek to describe LTP-based ignition in existing engine design software tools and methods.

Current state-of-the-art simulation capabilities for LTP ignition systems need improvements as they deliver qualitative results only, owing to important limitations of existing approaches. First, validated kinetic models with elementary steps for plasma discharges in fuel–air mixtures of relevance to the transportation sector are required. Such kinetic models do not exist at present and will be developed and validated within this project. Second, plasma discharges and reactive mixture ignition are multiscale, unsteady processes requiring high-performance numerical methods and software that execute efficiently on DOE supercomputers. Such software does not exist at present and will be developed and applied to practical LTP ignition scenarios as part of this project. Third, experimental databases that are tailored to serve as benchmarks in support of the development of predictive computational models of LTP ignition do not exist and will be part of this project.

Objectives

This multiyear research project seeks to advance the predicative capabilities of LTP ignition sub-models for the optimization of fuels and multimode engines by:

Overall Objectives

- Develop an experimentally validated LTP-specific kinetic mechanism for relevant fuels: iso-octane, ethanol, and EGR blends. (Auburn University)
- Develop a validated and benchmarked massively parallel, exascale, high-fidelity solver for the simulation of LTP discharges/ignition of fuel–air mixtures in complex geometries. (University of Texas at Austin [UT Austin])
- Develop an experimental database of LTP ignitions of blended mixtures with fuel/EGR/air for benchmarking and validating high-fidelity solvers and kinetic models. (Sandia National Laboratories)
- Appraise the performance and accuracy of existing LTP commercial software tools as a benchmark for the development of high-fidelity solvers and plasma/combustion kinetics models, and identification of areas of improvement and directions for future development. (Argonne National Laboratory)

Successful completion of these objectives will support the development of LTP ignition technologies to enable multimode engine concepts and will also contribute to the overarching goal of developing more efficient engines with sustainable future fuels.

Fiscal Year 2022 Objectives

- Develop a plasma-specific kinetic mechanism for ethanol oxidation and pyrolysis.
- Simulate LTP ignition of ethylene–air mixtures using the AMReX library[1] and newly developed high-fidelity models.

[1] AMReX is a numerical library containing the functionality to write massively parallel, block-structured adaptive mesh refinement (AMR) applications.

- Integrate circuit dependence in a discharge model to estimate discharge efficiency and implement fuel dissociation via electron impact in VizGlow.[2]

Approach

Plasma Flow Reactor Studies for LTP Kinetic Mechanism Development

At Auburn University, experimental reaction kinetic studies are performed in a purpose-built variable-temperature and constant-pressure plasma flow reactor (PFR). Studies are focusing on oxidation and pyrolysis kinetics of fuels, with and without the effects of a non-equilibrium plasma, for temperatures ranging from 400 K to 1,250 K at 0.5 atm pressure. Experiments are performed under highly dilute conditions in N_2 to minimize the exothermicity of observed reactions. The plasma is administered to the reactive mixture via dielectric barrier discharge plasma cell, where two copper electrodes are situated in a plane-to-plane orientation around a quartz reactor. The energy deposition by the plasma is kept constant by perturbing the reactive mixtures at 20 kV peak voltage and adjusting the pulse-repetition rate to maintain 120 pulses. Product speciation, as a result of observed reactions, is identified and quantified by simultaneous ex situ gas chromatography and mass spectroscopy. Datasets derived from experiments are used to develop plasma-specific kinetics mechanisms through a 0D numerical model. The mechanisms are developed to consider import subsets of chemistry intrinsic to plasma-assisted combustion, namely electron-impact reactions, collisional-quenching with plasma-excited species (i.e., electronic and vibrational species), and neutral (thermal) reactions.

Exascale Modeling and Skeletal Mechanism Development

At the University of Texas at Austin, researchers assembled a mathematical model for multidimensional LTP discharges in reactive mixtures. The mathematical model features detailed transport models for charges in the presence of an electric field, considers the voltage induced by the space charge, allows for arbitrary finite rate plasma/combustion kinetics parametrized by the local electric field strength (local field approximation), includes photo-ionization, and describes compressible flow effects. The model relies on adaptive mesh refinement (AMR) and embedded boundary (EB). The mathematical model was successfully implemented in the AMReX library, and preliminary three-dimensional simulations of pin-to-pin (P2P) discharges were performed. In parallel, the newly developed plasma-specific extension to the directed relation graph method with error propagation (P-DRGEP) approach was applied to the generation of a skeletal mechanism capable of simulating the plasma-assisted ignition of fuel–air mixtures for lean to stoichiometric conditions at compression ratios suitable for internal combustion engines.

LTP Ignition Studies in Static Cell

At Sandia National Laboratories, P2P nanosecond repetitively pulsed discharge thermal energy deposition and ignition kernel growth rates for fuel–air mixtures were characterized in customized ignition test facilities for lean and exhaust gas diluted ethylene–air mixtures. Initial pressures were varied between 1.1 bar and 2.1 bar, with the initial temperature fixed at 343 K. Both lean and dilute ignition limits were identified during testing. Gap distances and pulse repetition frequency/voltage were adjusted to maintain glow-phase plasma between the electrodes prior to ignition. Total pulse energy deposition into the gas was measured via pressure-rise calorimetry for single-pulse discharges in inert mixtures. Finally, collected datasets benchmarked complementary non-equilibrium plasma simulations conducted at Argonne National Laboratory.

VizGlow Commercial LTP Model

At Argonne, non-equilibrium plasma simulations are carried out using VizGlow. These simulations enable the study of two important problems in discharge modeling: (1) the effect of the circuit on the discharge and (2) the initialization of kernels in computational fluid dynamics (CFD) suites such as CONVERGE for the simulation of ignition (or extinction) processes. The effect of the circuit is developed to account for streamer breakdown, streamer velocity, plasma density evolution, O-radical production, the cathode fall, circuit currents, and the impedance mismatch effects due to transmission lines. For the ignition/extinction simulations, VizGlow runs are

[2] VizGlow™ is an industrial simulation tool for high-fidelity modeling of non-equilibrium plasma discharges.

used to develop an energy deposition model that is implemented as a user-defined function in CONVERGE. The deposited energy accounts for cathode and anode falls and the effect of streamer collision.

Results

Major Accomplishments Fiscal Year 2022

- Plasma-assisted pyrolysis and oxidation of ethanol experiments utilizing the PFR have been performed as a function of reduced electric field and temperature, resulting in the development of a plasma-specific kinetic mechanism for ethanol with sufficient predictive capabilities.
- Simulations of LTP ignition of ethylene–air reactive mixtures following pulsed P2P streamer discharges were performed with the AMReX library.
- A circuit model was demonstrated and validated against observations in literature, while ethylene dissociation via electron impact was added to the commercial software VizGlow.

Development of Plasma-Specific Ethanol Kinetic Mechanism

Non-equilibrium plasma-assisted pyrolysis and oxidation experiments of ethanol (C_2H_5OH) were completed at Auburn University, utilizing the PFR to obtain speciation data as function of temperature and effectively reduced electric field (280 Td < E/N < 660 Td)[3] to develop an LTP-specific kinetic mechanism. Experiments were performed under highly dilute conditions, using nitrogen, to ensure reactions kinetics are studied under isothermal conditions at 0.5 atm pressure. Experiments were performed with 900 ppm ethanol for pyrolysis studies and a stoichiometric mixture with oxygen (2,700 ppm) in oxidation studies. The developed mechanism is an extension of an LTP mechanism developed in prior project years to describe iso-octane kinetics. In this version, ethanol neutral kinetics have been added to the existing mechanism, while existing plasma-specific reaction sets are modified to reconcile the observed experimental enhancements in reactivity. These include electron-impact reactions leading to ionization, dissociation, and electronic excitation of N_2 and O_2, as well as collisional quenching processes between plasma species and ethanol. Ongoing efforts are leveraging developed mechanisms to constructed skeletal mechanisms for use in high-fidelity simulations, in collaboration with the UT Austin group. Figure VI.A.1.1 shows a comparison between the experiments and numerical results from the conclusion of the mechanism development efforts.

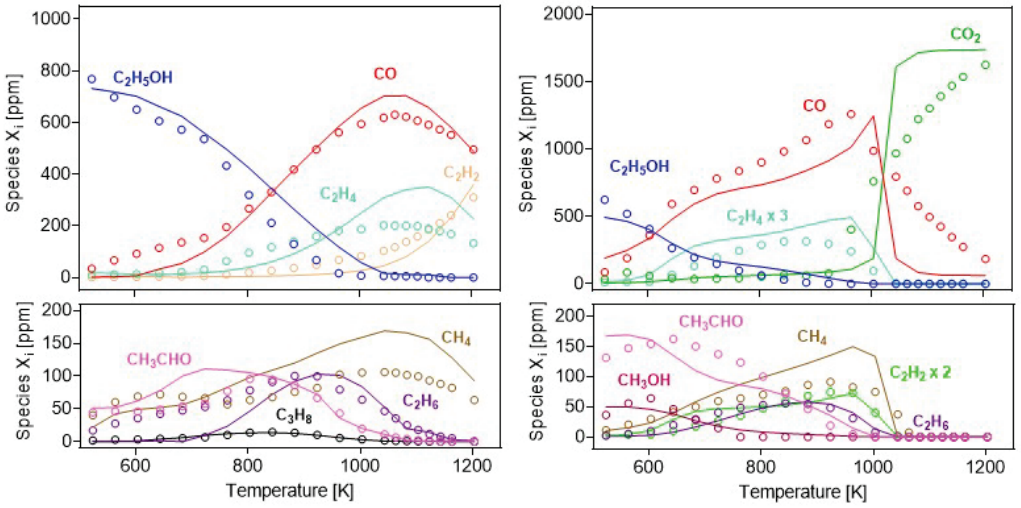

Figure VI.A.1.1 Comparison of experimental (hollow points) and numerical model (solid lines) results of plasma-assisted (a) pyrolysis and (b) oxidation of ethanol.

[3] The townsend (symbol Td) is a physical unit of E/N, where E is electric field and N is concentration of neutral particles.

For plasma-assisted pyrolysis, the experiments demonstrated enhanced reactivity for all temperatures in comparison to thermal pyrolysis. Ethanol consumption begins at temperatures as low 520 K, with full consumption by 963 K, nearly 200 K lower than observed in the pure thermal reaction. For temperatures 523 K to 723 K, ethanol proceeds with a steady linear rate of decomposition and then proceeds at a faster rate for temperatures greater than 723 K. This indicates a transition in the chain reaction sequence leading to fuel consumption. Similar intermediates as seen in the thermal reaction are observed in the plasma-assisted reaction, although their formation is observed at different temperature ranges. At low temperatures (T < 800 K), the major intermediates of ethanol decomposition are CO, acetaldehyde (CH_3CHO), methane (CH_4), and ethane (C_2H_6). By 800 K, ethylene (C_2H_4) becomes a major intermediate formed—interestingly, formation of C_2H_4 does not outcompete CO as seen in the thermal reaction, indicating that CO formation is probably through an accelerated production route dissimilar to the thermal reaction. Unlike the thermal reaction, propane (C_3H_8) was observed at intermediate temperatures between 700 K and 900 K, suggesting plasma polymerization reactions are playing an important role in fuel decomposition because of the enhancement of fuel radicals. By 1,000 K, most of the intermediates are being consumed, and the reaction predominately accelerates the formation of acetylene (C_2H_2). The developed mechanism demonstrates satisfactory agreement with the experimental results. The maximum extent of deviation is less than 20% for all measured species and for all temperatures considered. The numerical model elucidates several competing reaction pathways leading to fuel consumption based on different timescales. Enhanced reactivity is attributed to collisional quenching processes of ethanol with electronically excited $N_2(A)$ generated by the plasma to enhance the initial formation of radical pools (i.e., fuel fragments and H-atoms) at early timescales within the plasma. As such, the enhancement of radicals subsequently leads to driving propagating chain reactions of the neutral chemistry (H-atom and OH-radical attack channels) to sustain reactivity at longer timescales.

For plasma-assisted oxidation, plasma effects are observed to enhance fuel decomposition reactivity for all temperatures compared to plasma pyrolysis. Ethanol consumption is observed to attain another 10% consumption at 523 K in comparison to the pyrolysis reaction at the same temperature; ethanol is also fully consumed nearly 300 K lower compared to the thermal oxidation reaction. Similar to the plasma-pyrolysis reaction, the fuel consumption profile indicates a transition in the rate of fuel consumption, with an initial fast rate of reaction up until 643 K and a slower rate for temperatures greater than 643 K. The major byproduct of ethanol decomposition leads to CO and C_2H_4 formation. Similar to the thermal reaction, the major byproduct of immediate oxidation of ethanol is CH_3CHO at temperatures as low as 523 K, where it reaches its maximum extent of reactivity at 643 K and steadily decreases up until 1,000 K. Unlike the thermal reaction, ethanol oxidation leads to methanol (CH_3OH) formation at relatively low temperatures (below 800 K). At intermediate temperatures (below 1,043 K), considerable enhancement of CH_4, C_2H_2, and C_2H_6 is observed. By 1,050 K, all intermediates are consumed, and the reaction proceeds toward hot ignition converting all the carbon content of the fuel to CO_2. The numerical model performs relatively well at predicting the experimental plasma-assisted oxidation results, with the maximum deviation being less than 15% for all species and all temperatures considered. Similar to plasma-pyrolysis, enhanced reactivity is attributed to collisional quenching of $N_2(A)$ with O_2 to enhance the O-atoms radical pool to instigate fuel-attack. This subsequently drives the neutral chemistry to enhance propagating chain reaction sequences (i.e., $O+C_2H_5OH$ and $OH+C_2H_5OH$) to sustain reactivity with the plasma timescales. The neutral chemistry then controls the reactivity behavior with temperature, where hydrogen peroxide (HO_2) and terminating reactions play a preferential role in the observable variation in rate of reactivity with temperature.

Simulations of LTP Ignition of Ethylene–Air Mixtures Using AMReX Library and High-Fidelity Models

Simulations of LTP ignition of ethylene–air mixtures up to ~3 atm were performed at UT Austin using the high-performance computing library AMReX coupled with a plasma–fluid model, compressible and reactive Navier–Stokes equations, and a detailed plasma/combustion skeletal kinetics mechanism developed for this project. The simulations leveraged high-fidelity models capable of describing all relevant physical processes across relevant temporal and spatial scales: (1) nanosecond pulsed low-temperature plasma discharges (including streamer phase followed by glow-to-spark transition), (2) ultrafast heating and radical production due to the relaxation of electronic states and slow heating due to vibrational relaxation, (3) acoustic phase

associated with the expansion of the discharge channel following rapid isochoric heating, and (4) kernel ignition and outward flame propagation.

The configuration consists of two axisymmetric parabolic pin electrodes with a radius of curvature of 50 um, separated by 2.5 mm. Two high-voltage nanosecond pulses (peak pulse is 12 kV, and pulse duration is ~10 ns) are applied at a frequency of 500 kHz (inter-pulse period of 2 μs). We considered stoichiometric ethylene–air mixtures at 300 K and 1 atm and 400 K and 2.7 atm along an isentropic compression curve. We also considered single-pulse ignitions, which are compared against the two-pulse cases. Simulations were performed using semi-implicit time integration for the electrostatic potential and second-order time integration for drift–diffusion and advective–diffusive fluxes using a method of line. The kinetics mechanism includes 57 species, featuring ions (anions and cations) and neutral species, which consist of both ground state and electronically and vibrationally excited species. Time step sizes ranging from 1 ps to 10 ns were required at various stages of the discharge and pulse interval. Calculations featured O (50–100 M) finite volume cells using up to seven AMR levels with spatial resolution down to O (1 μm). The simulations were executed on O (1,000–5,000) processors with parallel efficiencies above 60% for the least efficient cases.

Figure VI.A.1.2 provides a comprehensive overview of the multi-pulse case at 1 atm (300 K) and 2.7 atm (400 K). At both pressures, the first pulse leads to a streamer discharge with minor energy deposition (~10 μJ), while the second pulse leads to a much higher one (~50 μJ), highlighting that energy coupling is controlled by the thermochemical state of the background mixture, which evolves in response to the first pulse. As shown in Figure VI.A.1.2a, following the formation of electronically and vibrationally excited nitrogen, radicals are formed also. For such thin electrodes, heating is mostly concentrated at the electrode tips, where Joule heating is highest because of the elevated values of the electric field strength. This results in elevated temperatures (up to 1,000 K for the first pulse and 5,000 K for the second) and kernels of hot gases of size comparable to the radius of curvature of the electrode. The region in between the electrodes remains at lower temperatures, although significant amounts of radicals are formed (Figure VI.A.1.2b). Following isochoric heating at the pin tips, strong spherical expansion waves are seen, while weaker cylindrical waves propagate away from the gap region (Figure VI.A.1.2c). When comparing the low (1 atm) and high pressure (2.7 atm) cases (Figure VI.A.1.2d), we find that, when normalized with respect to increased number densities, the 2.7 atm case shows higher energy deposition and a more efficient production of combustion radicals, primarily as a result of faster quenching of electronically excited species.

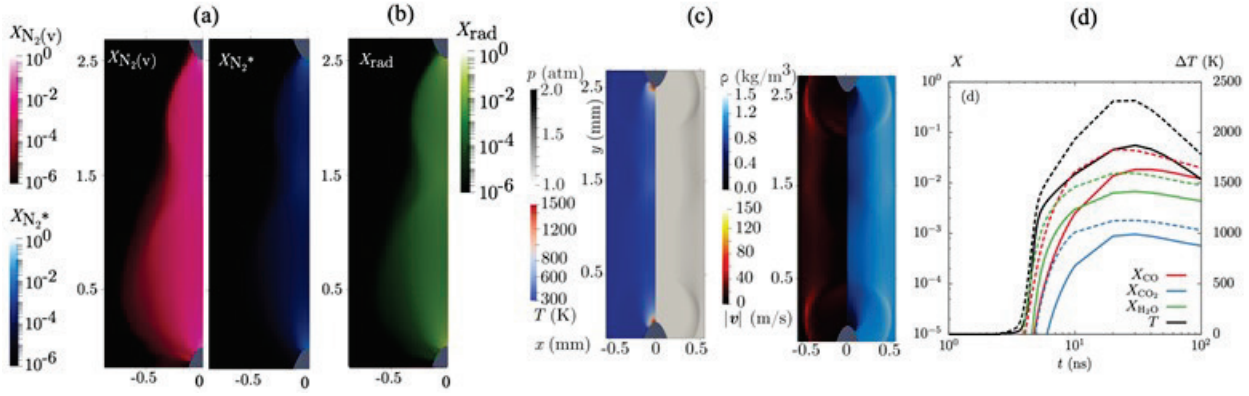

Figure VI.A.1.2 (a) Mole fractions of vibrationally excited and electronically excited nitrogen at 20 ns following the second pulse at 500 kHz; (b) mole fractions of all radicals (O, OH, and H) in the same configuration as (a); (c) pressure, temperature, velocity magnitude, and density at 1 μs following the high-voltage pulse in the same configuration as in (a); (d) mole fractions of select combustion species and temperature sampled near the anode tip (solid lines: 300 K and 1 atm; dashed lines: 400 K and 2.3 atm)

To avoid localized energy deposition at the tips of the electrodes, we are now focusing on LTP ignition with thicker pins (radius of curvature between 250 μm and 500 μm), leading to more homogeneous energy

deposition across the gap and larger energy kernels, which we expect to facilitate the formation of a successful flame kernel.

Development of LTP Model to Predict Plasma–Circuit Coupling and Fuel Dissociation via Electron Impact

The circuit model is able to predict discharge performance at engine-relevant conditions. Figure VI.A.1.3a shows the variation of energy efficiency and energy density delivered to air at 1 atm and 300 K as a function of streamer radius in the presence of a transmission line. It is observed that the energy efficiency decreases with increasing streamer radius, indicating that small discharges are preferred. The model also shows that energy delivery is sensitive to transmission line parameters and that optimal energy loading occurs only at one pressure between atmospheric and maximum when all discharge parameters are kept the same. These results are discussed in greater detail in a recently published paper [4]. Past nano-second pulse discharge modeling using the software VizGlow has been carried out in pure air, therefore neglecting fuel radicals in the coupling of the discharge to the kernel development. To address this approximation, we have recently superimposed ethylene decomposition chemistry, with the help of UT Austin, onto the air–plasma chemical mechanism that we typically use in VizGlow. Figure VI.A.1.3b aligns well with what is understood about such discharges, namely that regions of high electron density and temperature correspond to the highest fuel decomposition. The radical and fast gas heating characteristics were then exported to CONVERGE via a user-defined function to simulate ignition kernel development in the presence of fuels. These results are shown and discussed in a recently published paper [5].

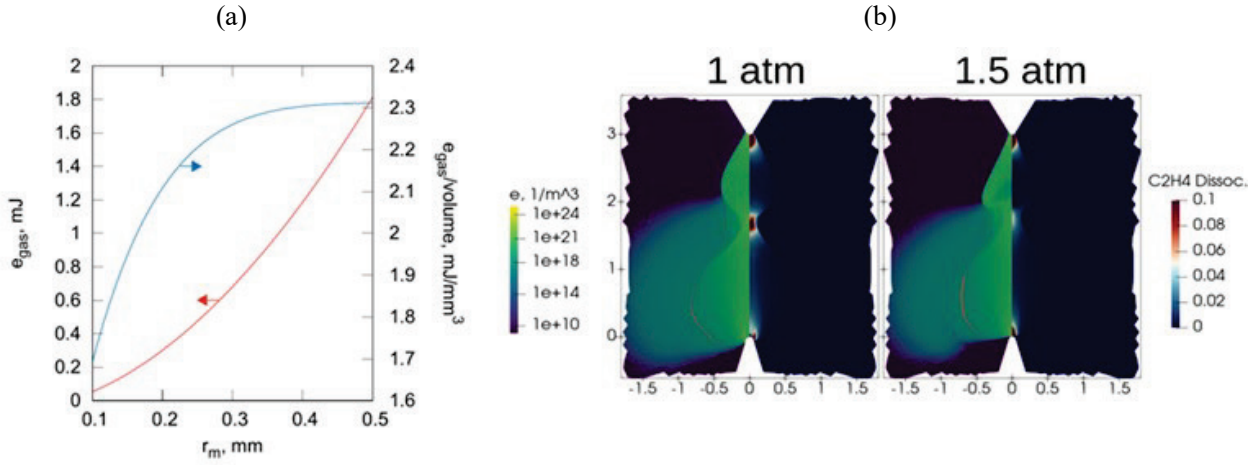

Figure VI.A.1.3 (a) Energy efficiency and energy density deposited for a nanosecond pulsed discharge as a function of streamer radius in the presence of a transmission line; (b) spatiotemporal profiles of electron density and dissociated ethylene (ratio of H radical to C_2H_4) at two different pressures, 30 ns after a pulse

Conclusions

- PFR experiments elucidated the enhanced chemical reactive of ethanol pyrolysis and oxidation kinetics with the effects of an LTP for temperatures ranging from 400 K to 1,200 K in comparison to thermal kinetics.
- Experimental measurements guided the development of a plasma-specific mechanism to describe ethanol kinetics coupled with LTP effects, resulting in a mechanism with relatively good predicative capabilities across all temperatures considered.
- Large-scale simulations of LTP ignition of ethylene–air reactive mixtures following pulsed P2P streamer discharges were performed with the AMReX library leveraging up to 5,000 processing units on DOE supercomputers.

- The simulations feature high-fidelity models for plasma discharges, coupled plasma and combustion kinetics, and compressible reactive flow, leading to the most accurate description of LTP ignition of complex fuels available to date.

- Plasma streamer discharge in air and LTP ignition of an ethylene–air mixture were simulated and successfully validated against experiments from Sandia, using the commercial codes VizGlow and CONVERGE CFD, respectively. These simulations included circuit effects and fuel molecule dissociation through electron impact.

Key Publications

1. Bopaiah, K., and N. Tsolas. n.d. "Non-Equilibrium Plasma Flow Reactor Studies of Iso-Octane Pyrolysis and Oxidation Kinetics." *Combustion and Flame*. Under review.

2. Bopaiah, K., T. Middleton, and N. Tsolas. n.d. "Low-Temperature Plasma Assisted Kinetics Study of Ethanol." Accepted for presentation at AIAA Scitech 2023 Forum, National Harbor, Maryland, January 23–27, 2023.

3. Gomez, A. Duarte, N. Deak, and F. Bisetti. 2022. "One-Dimensional Streamer Simulations Using a Jacobian Free Newton-Krylov Method with Physics Based Preconditioning." AIAA 2022-1620. Presented at AIAA Scitech 2022 Forum, San Diego, CA, January 3–7.

4. Gomez, A. Duarte, N. Deak, and F. Bisetti. n.d. "Jacobian-free Newton–Krylov Method for the Simulation of Non-Thermal Plasma Discharges with High-Order Time Integration and Physics-Based Preconditioning." *Journal of Computational Physics*. Under review.

5. Deak, N., A. Duarte Gomez, M. Day, L. Esclapez, and F. Bisetti. n.d. "Simulations of Streamer Propagation and Cathode Sheath Formation during Nanosecond Glow Discharges." *Computers & Fluids*. Under review.

6. N. Deak, A Duarte Gomez, M. Day, L. Esclapez, and F. Bisetti. n.d. "Towards Massively-Parallel High-Fidelity Simulations of Plasma-Assisted Ignition of Hydrocarbon Fuels using Nanosecond Pulsed Discharges." *Computers & Fluids*. Under review.

7. Gururajan, V., and R. Scarcelli. 2022. "A Nanosecond Pulsed Discharge Circuit Model for Engine Applications." *Journal of Physics D: Applied Physics* 55, 15: 155205.

References

1. Popov, N.A., and S.M. Starikovskaia. 2022. "Relaxation of Electronic Excitation in Nitrogen/Oxygen and Fuel/Air Mixtures: Fast Gas Heating in Plasma-Assisted Ignition and Flame Stabilization." *Progress in Energy and Combustion Science* 91: 100928.

2. Ju, Y., and W. Sun. 2015. "Plasma-assisted Combustion: Dynamics And Chemistry." *Progress in Energy and Combustion Science* 48: 21–83.

3. Biswas, S., I. Ekoto, D. Singleton, K. Mixwell, and P. Ford. 2020. "Assessment of Spark, Corona, and Plasma Ignition Systems for Gasoline Combustion." ICEF2020-3034Presented at ASME 2020 Internal Combustion Engine Division Fall Technical Conference, Virtual, November 4–6.

4. Gururajan, V., and R. Scarcelli. 2022. "A Nanosecond Pulsed Discharge Circuit Model for Engine Applications." *Journal of Physics D: Applied Physics* 55, no. 15: 155205.

5. Gururajan, V., R. Scarcelli, S. Biswas, and I. Ekoto. 2021. "CFD Modeling of Low Temperature Ignition Processes from a Nanosecond Pulsed Discharge at Quiescent Conditions." Proceedings of

ASME Internal Combustion Engine Division Fall Technical Conference, Virtual, October 13-15. V001T06A010. https://doi.org/10.1115/ICEF2021-67902.

Acknowledgements

The UT Austin authors wish to thank the National Renewable Energy Laboratory high-performance computing center for the allocation of computing hours on the “Eagle” and “Swift” systems and the National Science Foundation Texas Advanced Computing Center for the allocation of computing hours on the “Stampede2” system. The Argonne authors also wish to thank the Laboratory Computing Resource Center folks at Argonne for supporting this project with their cluster Bebop.

VI.A.2 Hierarchically Informed Engineering Models for Predictive Modeling of Turbulent Premixed Flame Propagation in Pre-Chamber Turbulent Jet Ignition (Purdue University)

Haifeng Wang, Principal Investigator
Purdue University
701 West Stadium Avenue
West Lafayette, IN 47906
Email: haifeng@purdue.edu

Riccardo Scarcelli, Principal Investigator
Argonne National Laboratory
9700 South Cass Avenue, Building 362
Lemont, IL 60439
Email: rscarcelli@anl.gov

Gurpreet Singh, DOE Program Manager
U.S. Department of Energy
Email: Gurpreet.Singh@ee.doe.gov

Start Date: October 1, 2019 End Date: December 31, 2023
Project Funding: $1,093,781 DOE share: $875,000 Non-DOE share: $218,781

Project Introduction

Developing the capability to predictively simulate combustion of real fuels in complex engine geometries with a comprehensive computational fluid dynamics (CFD) model can greatly accelerate engine optimization efforts. However, current simulation inaccuracies have created a lack of confidence in modeling predictions as engine operating parameters change, and current models require substantial tuning and calibration, which is time-consuming, costly, and ultimately reduces the effectiveness of the model to apply to many situations. This project aims at improving sub-models for engine combustion simulations in terms of ignition and turbulent flame propagation. The target for the model development is pre-chamber turbulent jet ignition (TJI) [1]. TJI is an innovative high-energy source ignition technique, and its use has been quite successful, especially because it applies to a large range of engine platforms and allows multi-mode operation. It enables ultra-lean burning in engines which reduces emissions and increases thermal efficiency. The predictive capability of TJI, once achieved, will enable the co-design/co-optimization of TJI with engines and fuels. The existing CFD models have shown significant challenges in predicting the combustion mechanism in the actual experiments [2], mainly due to the complex combustion regimes observed in TJI. Those complex regimes require a superior combustion model with more general validity with respect to the state of the art.

Objectives

The goal of the project is to radically improve the predictive accuracy and efficiency of turbulent combustion sub-models for TJI. This goal will be achieved through the development of a hierarchically informed engineering model for turbulent combustion in TJI. The model development starts with the highest level of description of turbulent combustion with direct numerical simulation (DNS) from which fundamental characteristics and scaling properties of turbulent premixed flame propagation under TJI-relevant conditions are obtained. The acquired premixed flame characteristics and scaling properties will be used as model constraints to drive the model reduction to the next level based on large-eddy simulations (LES) and probabilistic modeling for TJI. Data-driven modeling and machine learning will then be used to aggressively reduce the model to the final target level based on Reynolds-average Navier-Stokes (RANS) with minimum loss of fidelity. The hierarchically reduced model for TJI will ensure predictive accuracy to be close to high-order models but with a significantly reduced computational cost.

Overall Objectives

- Gain DNS informed characteristics and scaling of turbulent premixed flames relevant to TJI.
- Construct combustion LES model for TJI informed by using the obtained DNS scaling.
- Develop a data-driven engineering RANS combustion model for TJI informed by LES.

Fiscal Year 2022 Objectives

- Develop a high-fidelity predictive LES solver for the entire cycle of TJI combustion.
- Validate the high-fidelity LES combustion solver by using a model TJI rig.
- Simulate the Argonne National Laboratory engine with conventional combustion models to verify the model validation framework.

Approach

The adopted hierarchical approach for the TJI model development considers all three different levels of common model descriptions (i.e., DNS, LES, and RANS) of turbulence and turbulent combustion in a hierarchy to gradually reduce the order of models. The step-by-step approach ensures a minimum loss of model fidelity and predictivity during the decrease of the model description level. In the step-by-step approach, fundamental characteristics and scaling properties of turbulent premixed flame propagation under TJI-relevant conditions are obtained from DNS. The acquired premixed flame characteristics and scaling properties are used to drive the model reduction to LES. Data-driven modeling and machine learning will ultimately be used to aggressively reduce the model to the target RANS level. The hierarchically reduced model for TJI will ensure predictive accuracy to be close to high-order models but with a significantly reduced computational cost. These developed sub-models will be validated in a single-cycle model TJI rig and an Argonne single-cylinder engine equipped with pre-chamber TJI.

The project teams consist of the Purdue University team led by Professor Haifeng Wang and the Argonne National Laboratory team led by Dr. Riccardo Scarcelli. The Purdue team focus on the fundamental development and testing of the proposed TJI model and the Argonne team focus on the development of a validation framework for model testing. The two teams collaborate closely to ensure a highly integrated research program.

Results

Development and validation of a high-fidelity LES solver for TJI combustion (Principal Investigator: H. Wang, Purdue)

- Completed the solver development of a high-fidelity LES simulation model for TJI combustion.
- Finished the case setup, simulations, and validation of the developed solver for the Purdue model TJI rig.
- Achieved the pressure rise prediction accuracy within $\pm 30\%$ when compared with the experimental data in both the pre-chamber and main chamber of the model TJI rig.

The LES simulation framework was developed based on the open-source OpenFOAM (Open-source Field Operation and Manipulation) solver. The flow-field was solved using compressible Navier-Stokes equations discretized using finite volume approach on an unstructured mesh. LES was used to solve for turbulence. The Smagorinsky model [4] was used for sub-filter turbulence. The value of $C_s = 0.16$ was used as the Smagorinsky model constant. The reacting scalars such as the chemical species and enthalpy were solved using transported probability density function (PDF) method [5] which allows for a complete closure of the chemical source terms in their transport equations. An Eulerian Monte-Carlo fields approach [6] was used for solving the PDF transport equations by using stochastic fields to give a reasonable approximation of the resolved reacting scalars in the physical space. Mixing at sub-filter scales was modeled using interaction by

exchange with the mean of all stochastic fields [7]. A machine-learning assisted mixing timescale model developed during this project was adopted for improving the integrated enterprise model. A reduced chemical mechanism DRM-19 containing 19 reacting species and 84 reactions was used to solve for chemical kinetics. A double gaussian energy deposition model was used to model the spark-plug ignition process in pre-chamber [8]. Pressure-velocity coupling in the pressure-based solver was achieved using SIMPLE (Semi-Implicit Method for Pressure-Linked Equations) algorithm combined with PISO (Pressure-Implicit with Splitting of Operators) algorithm to make it compatible for transient problems. Second order numerical schemes were used for discretization of both space and time.

A single-cycle model TJI rig [3] shown in Figure VI.A.2.1 was used for the validation of the developed solver. The experimental setup consisted of a cylindrical pre-chamber and a cuboidal shaped main chamber. The diameter and height of the pre-chamber is 3.81 cm and 8.9 cm respectively. The dimensions of the main chamber are 43.18 cm × 15.24 cm × 15.24 cm, making the volume ratio between the two chambers 1:100. The two chambers are separated by a small cylindrical orifice with a diameter of 4.5 mm and length to diameter ratio of 5:1. CH_4-air was used as fuel-air mixture with the initial temperature of 500 K in both pre-chamber and main-chamber. The mixture in the pre-chamber was at stoichiometry, however the equivalence ratio of the lean mixture in the main chamber was varied. The two mixtures are separated by a thin 25 μm aluminum diaphragm that breaks when the pressure difference between the two chambers goes above 0.21 MPa (2.1 bar) [3].

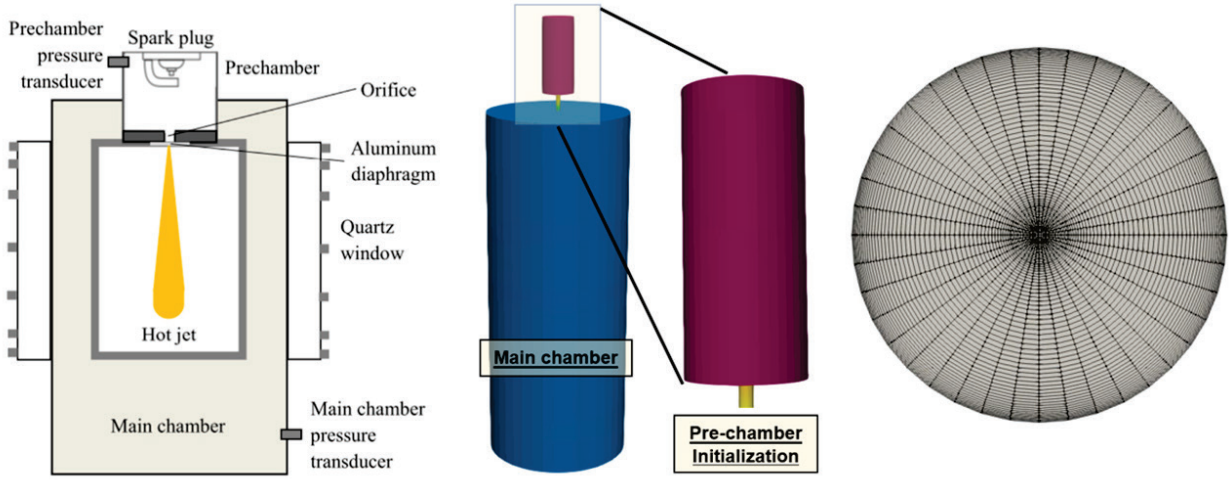

Figure VI.A.2.1 Left: Sketch of the Purdue model TJI rig [3]. Right: the computational domain with a cross-section of the O-grid mesh.

The simulations were divided into two phases since the two chambers are physically separated. Phase 1 included the simulation of pre-chamber until the time when the pressure reached the diaphragm rupture threshhold. The main chamber remained static during Phase 1. The pre-chamber results from Phase 1 were then used as the initial condition for the Phase 2 simulation of a full TJI. An unstructured 3D O-grid type of mesh was generated for both phases of the simulation as shown in Figure VI.A.2.1 with approximately 350,000 grid cells in Phase 1 simulation and 1.2 million grid cells in Phase 2. Mesh refinement was done in the region of spark ignition and orifice inlet where it became important to capture small-scale flow dynamics. Figure VI.A.2.1 also shows the pre-chamber and the main-chamber geometry along with the cross-sectional view of the O-grid unstructured mesh generated for the simulation.

The Phase 1 simulation yielded a smooth laminar flame propagating at low speed as shown in Figure VI.A.2.2 (the upper left) and significantly delayed pressure rise (red line in the right plot). It was found that initial turbulence in the prechamber was critical to yield a correct flame propagation. Spark ignition is a dynamic process that can lead to turbulence generation in the prechamber. This turbulence generation mechanism was not considered in the spark model [8]. Meanwhile, the initial laminar to turbulence flow transition was

generally difficult to capture for the current solver. A forcing scheme was thus employed to provide the needed initial turbulence for the flame propagation in the prechamber. The effectiveness of the turbulence forcing is illustrated in Figure VI.A.2.2 (bottom left and right). The increase in the turbulence forcing significantly increased the pressure rise and the flame propagation. A good match of the pressure rise with the experiment justified the needed forcing level. The correct prechamber ignition is critical since it serves as the initial condition for the Phase 2 main-chamber simulation which is the main point of interest of the study.

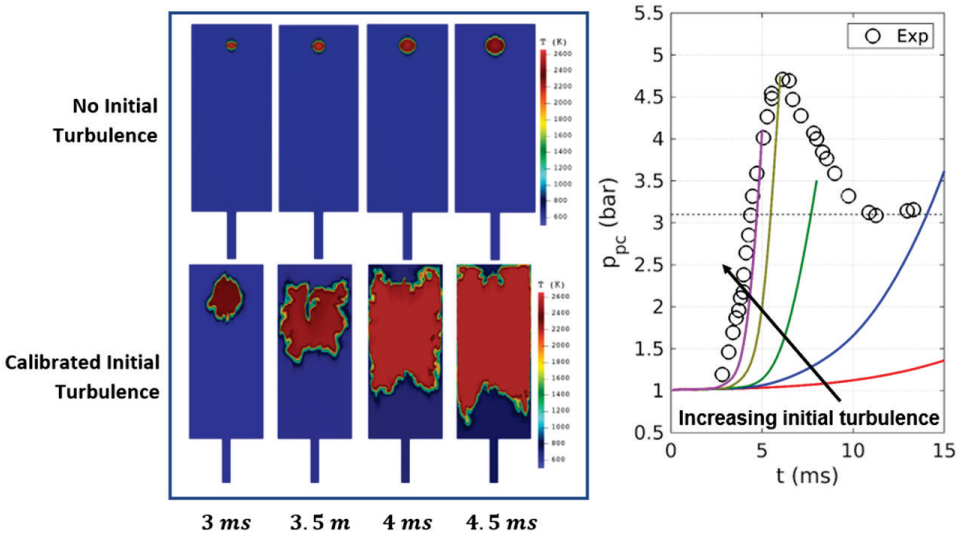

Figure VI.A.2.2 Time series of temperature contour for the case with no initial turbulence (top row) and with a calibrated initial turbulence (bottom row). The right plot shows a quantitative comparison of the effect of forcing constant with experimental data (black symbols) with the arrow to show the increase of forcing (red line: no forcing).

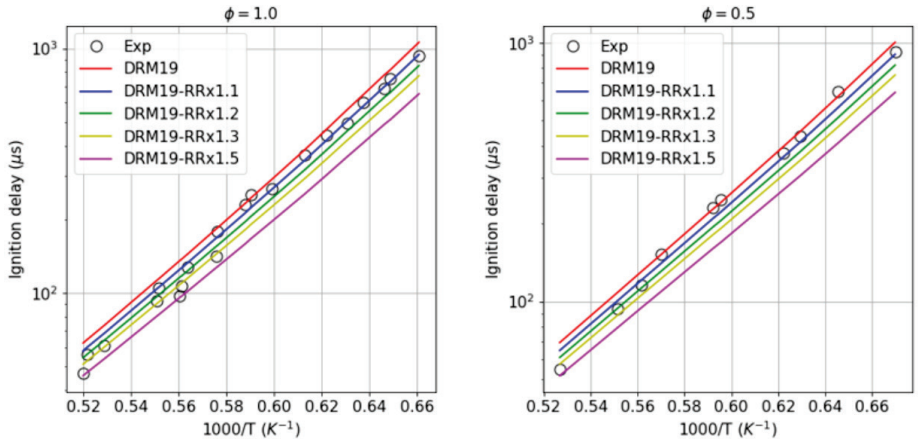

Figure VI.A.2.3 0-D auto-ignition study showing ignition delay vs 1,000/T for CH_4–air mixture for two different equivalence ratios, 0.5 and 1.0. Black symbols represent the experimental data, whereas the different line represents the results of DRM-19 chemical mechanism with different reaction rate multipliers.

In Phase 2 simulation of the full TJI, no ignition was captured initially as shown in Figure VI.A.2.4 (upper plot). It was found that the main-chamber ignition was very sensitive to the chemical reaction rate and the initial turbulence in the main-chamber. A 0-D auto-ignition test of homogeneous mixture of CH_4–air under a similar condition to the TJI showed that a 20% increase of the reaction rate yields the ignition delay well within the margin of the error of the experiment as shown in Figure VI.A.2.3. A turbulence forcing similar to the pre-chamber simulation was also used. This can be readily justified since the rupture of the diaphragm acts as a turbulence generator in the experiments but is not considered in the simulations. The 20% increase of the

reaction rate and the turbulence forcing leads to successful main chamber ignition as shown in Figure VI.A.2.4 (lower plot). A single ignition spot was created at time t = 8 ms which then detached from the main jet leading to a lifted flame front. As the pressure difference between the pre-chamber and main-chamber decreased leading to decrease in jet momentum, more ignition spots were created at the tip of the jet at around t = 11.6 ms. The experiments [3] reported ignition spots near the jet at 12 ms and hence the simulation provided a good qualitative agreement.

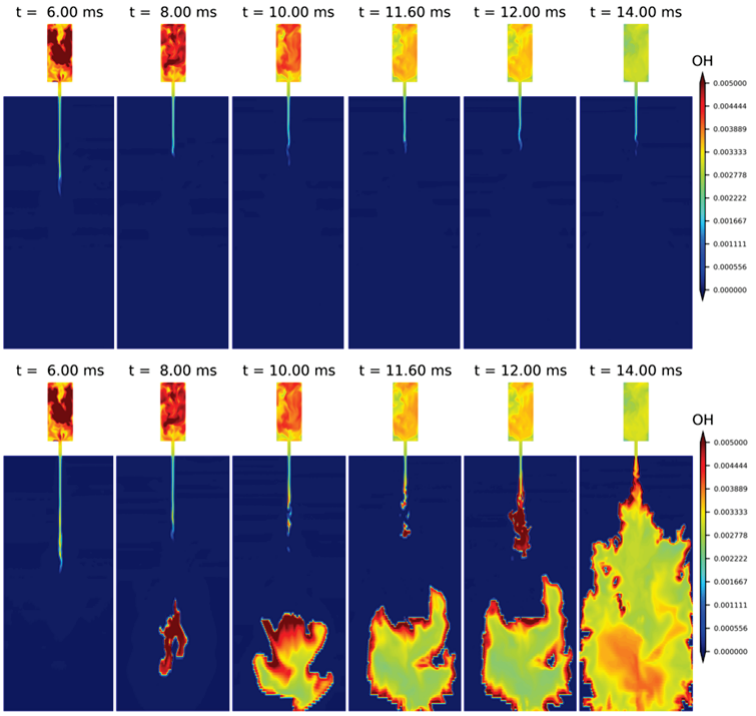

Figure VI.A.2.4 Time series of the OH mass fraction contours with DRM-19 chemical mechanism (top row) and the same with 20% enhancement in reaction rates and initial turbulence forcing (bottom row).

Figure VI.A.2.5 shows a more quantitative comparison of the pressure profiles in both pre-chamber (left) and the main chamber (right). The black symbols indicate the experimental results with ±30% errors bars. The no-ignition case (red line) leads significant under-prediction of the pressure rise. The case with 20% reaction rate increase and a local turbulence forcing (blue line) provides an excellent agreement with the experimental data, within the targeted ±30% accuracy.

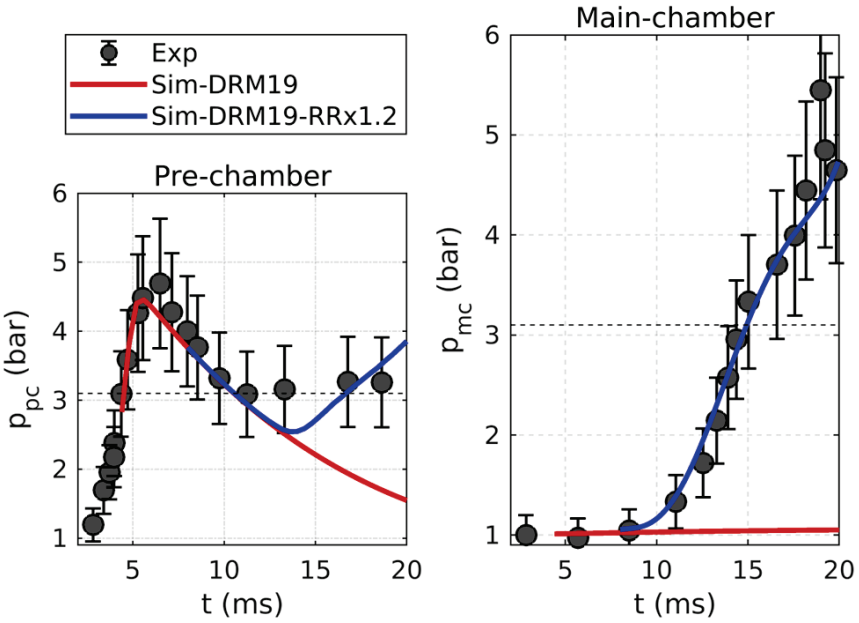

Figure VI.A.2.5 Pre-chamber and main-chamber pressure profiles as a function of time. The black symbols represent the experimental data with ±30% error bars.

Benchmark TJI CFD cases for model validation (Principal Investigator: R. Scarcelli, ANL)

The Argonne team has migrated to the latest release of the CONVERGE CFD software (i.e., version 3.0.x). CFD simulations showed similar results with respect to the previous 2.4.x version (see Figure VI.A.2.1, left) in terms of combustion characteristics, while being more efficient computationally. The comparison showed that version 3.0.x could complete engine simulations faster (by a factor of 4), and with excellent scaling performance up to 720 processors (see Figure VI.A.2.6, right). The structure of the user defined functions was also updated to v3.0. This is the platform that will be used for future TJI model implementation.

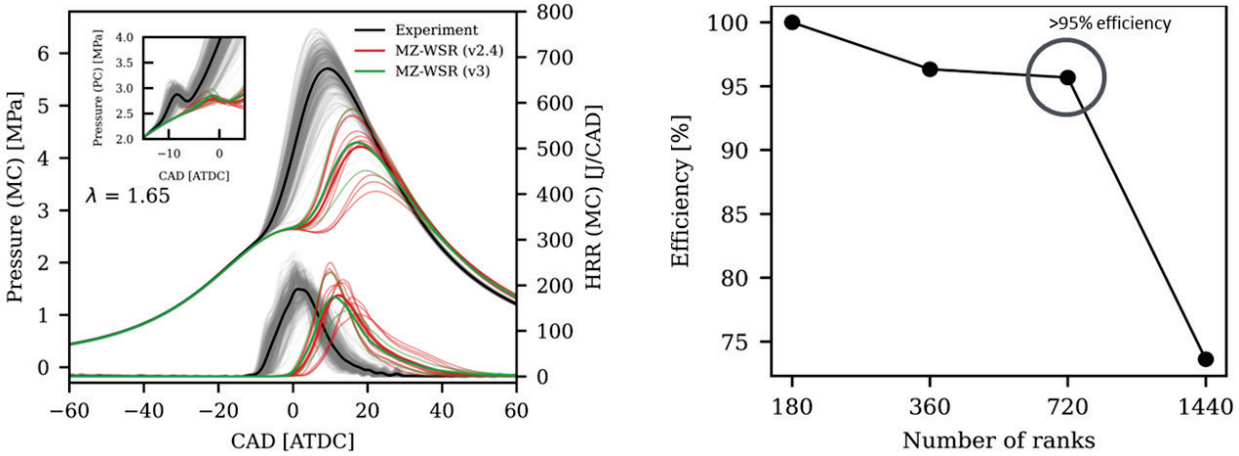

MC – main chamber; HRR – heat release rate; MZ-WSR – multi-zone well-stirred reactor model; CAD – crank angle degrees; ATDC – after top dead center

Figure VI.A.2.6 Left: Baseline Argonne CFD engine simulations results using the previous version (v2.4) and the newest version (v3.0) of CONVERGE, and comparison with engine experiments. Right: Scaling performance versus number of processors for the latest version of CONVERGE (v.3.0).

Conclusions

A high-fidelity LES solver for TJI simulations has been implemented and validated against a model TJI rig. The initial turbulence and the chemical reaction rate were found to affect the ignition significantly. The slightly tuned reaction rate, which still yields excellent results in the ignition delay test and added forcing to account for the missing mechanism of laminar-turbulence transition and turbulence generation in the chambers, yields excellent agreement with the measured pressure rise in both chambers. Argonne completed the migration to the newer version of CONVERGE that will be used for the future implementation of the TJI model developed by Purdue via user defined functions and defined the baseline in terms of scaling performance versus number of processors. The completed work enables our future planned work during the next reporting period.

Key Publications

1. Liu, J., and H. Wang. 2022. "Machine Learning Assisted Modeling of Mixing Timescale for LES/PDF of High-Karlovitz Turbulent Premixed Combustion." *Combustion and Flame* 238: 111895. https://doi.org/10.1016/j.combustflame.2021.111895.

2. Wang, H., P. Zhang, and J. Tao. 2022. "Examination of Probability Distribution of Mixture Fraction in LES/FDF Modeling of a Turbulent Partially Premixed Jet Flame." *Combustion Theory and Modelling*, 26 (2): 320–337. https://doi.org/10.1080/13647830.2021.2016980.

References

1. Toulson, E., H.J. Schock, W.P. Attard. 2010. "A Review of Pre-Chamber Initiated Jet Ignition Combustion Systems." *SAE Technical Paper* 2010-01–2263. doi:10.4271/2010-01-2263.

2. Kim, J., R. Scarcelli, S. Som, A. Shah, M.S. Biruduganti, D.E. Longman. 2019. "Evaluation of Combustion Models for CFD Simulation of Pre-Chamber Ignition in a Natural Gas Engine." 11th U.S. National Combustion Meeting, Pasadena, California.

3. Biswas, S., S. Tanvir, H. Wang, L. Qiao. 2016. "On Ignition Mechanisms of Premixed CH_4/Air and H_2/Air Using a Hot Turbulent Jet Generated by Pre-Chamber Combustion." *Applied Thermal Engineering*, 106: 925–937.

4. Smagorinsky, J. 1963. "General Circulation Experiments with the Primitive Equations: I. the Basic Experiment." *Monthly Weather Review*, 91 (3): 99–164.

5. Pope, S.B. 1985. "PDF Methods for Turbulent Reactive Flows." *Progress in Energy and Combustion Science*, 11 (2): 119–192.

6. Valino, L. 1998. "A Field Monte Carlo Formulation for Calculating the Probability Density Function of a Single Scalar in a Turbulent Flow." *Flow, Turbulence and Combustion*, 60 (2): 157–172.

7. Dopazo, C., E.E. O'Brien. 1974. "An Approach to the Autoignition of a Turbulent Mixture." *Acta Astronautica*, 1 (9–10): 1239–1266.

8. Lacaze, G., E. Richardson, T. Poinsot. 2009. "Large Eddy Simulation of Spark Ignition in a Turbulent Methane Jet." *Combustion and Flame*, 156 (10): 1993–2009.

Acknowledgements

We greatly acknowledge the hard work done by the graduate students and postdocs involved in this project at Purdue and Argonne: Mr. Utsav Jain (Purdue) and Dr. Bulut Tekgul (Argonne).

VI.A.3 Development of High-Fidelity and Efficient Modeling Capabilities for Enabling Co-Optimization of Fuels and Multimode Engines (Stanford University)

Matthias Ihme, Principal Investigator
Stanford University
440 Escondido Mall
Stanford, CA 94305
Email: mihme@stanford.edu

Tianfeng Lu, Principal Investigator
University of Connecticut
191 Auditorium Road U-3139
Storrs, CT 06269
Email: tlu@engr.uconn.edu

Pinaki Pal, Principal Investigator
Argonne National Laboratory
9700 South Cass Avenue
Lemont, IL 60439
Email: pal@anl.gov

Gurpreet Singh, DOE Program Manager
U.S. Department of Energy
Email: Gurpreet.Singh@ee.doe.gov

Start Date: October 1, 2019 End Date: December 31, 2023
Project Funding: $424,172 DOE share: $324,327 Non-DOE share: $99,845

Project Introduction

Advanced engine concepts that utilize lean-burn and low-temperature combustion offer opportunities for delivering higher indicated thermal efficiencies relative to their spark-ignited counterparts. However, extending low-temperature-combustion strategies to low-load operation and enhancing combustion stability are particularly challenging since underlying processes are closely coupled to heat losses and combustion-mode transition. Exhaust gas recirculation with reactivity enhancement, advanced ignition concepts, and mixture stratification are promising strategies for improving lean operation. Homogeneous charge compression ignition (HCCI) has been shown to achieve appreciable extensions of the lean operation. While the low combustion temperature and shorter residence time reduce heat losses, the faster pressure-rise and kinetics-controlled ignition limits the operation to low-load conditions.

Different concepts have been examined as viable strategies for extending the HCCI load range. Spark-assisted compression ignition is a hybrid combustion mode to extend the high load limit of HCCI, as this concept can reduce the high heat release rate effectively while partially maintaining the advantages of high thermal efficiency and low nitrogen oxide emission simultaneously. The reduced burn rate due to mixed-mode combustion reduces the peak heat release at high-load operating conditions, which favorably affects the ringing and stability near engine-misfire limits. These advanced combustion concepts take advantage of multimode combustion regimes to enable intermediate- and high-load extensions while also improving combustion stability. However, the successful implementation, control, and optimization of these multimode combustion regimes over the range of operating conditions, in conjunction with the simultaneous optimization of the fuels, require accurate and reliable high-fidelity modeling tools. Such models are not currently available. Therefore, a

critical need exists to develop high-fidelity modeling capabilities for the accurate prediction of key critical processes that involve multimode combustion, high-energy ignition processes, and wall-heat transfer.

Objectives

The objective of this closely coordinated research project is to develop improved physical submodels and examine multimode combustion regimes to support the Office of Energy Efficiency and Renewable Energy (EERE) Co-Optima program. To this end, this research project addresses the following issues:

- Develop accurate submodels for predicting multimode combustion regimes, wall-heat transfer, non-equilibrium plasma ignition, and combustion-mode transition.
- Validate the computational submodels against experiments and direct numerical simulation (DNS) data in conjunction with sensitivity analysis.
- Support the direct transition of the resulting submodels into other engine simulation tools through the development of self-contained modules. All submodels will be integrated into the open-source exascale engine simulation platform Nek5000.
- Examine complex combustion regimes in multistage ignition and high-pressure spray combustion.

Approach

To achieve the stated objectives, the following research approach is undertaken:

- Task 1: Examine turbulence–chemistry interaction on low-temperature-combustion behavior in rapid-compression machines (RCMs) and high-pressure fuel injection systems.
- Task 2: Develop high-energy ignition models for predicting non-equilibrium plasma ignition and flame-mode transition.
- Task 3: Develop non-equilibrium wall-heat transfer models for integration into Nek5000 and validation against state-of-the-art wall models.
- Task 4: Perform multimode engine simulations on the Nek5000 exascale platform.

Results

Chemistry Effects in Multimode RCM Engines

To evaluate the utility of 3-D large-eddy simulations (LESs) in investigating HCCI flame propagation modes of large hydrocarbon fuels (especially within the low-temperature chemistry), we perform simulations of the experimental RCM configuration of Strozzi et al. [1]. This configuration features a combustion chamber of size $L_x \times L_y \times L_z = 50 \times 50 \times 36.5$ mm^3 (at top dead center) with a square cross-section, a flat piston, and a compression ratio of 12.5. The piston velocity during the compression phase is prescribed on the deforming control volumes (governed by the Arbitrary Lagrangian–Eulerian method [2]) following a sine function fitted to measurements [3]. To examine different flame propagation modes in HCCI combustion, two cases are considered: (i) the short ignition case and (ii) the long ignition case. Both cases share the same initial temperature $T_0 = 294$ K, compression duration $\tau_{comp} = 47.6$ ms, and fuel–air equivalence ratio $\varphi = 0.5$. However, the initial pressures for the short and long ignition cases are $p_0 = 1.00 \pm 0.07$ bar and $p_0 = 0.65 \pm 0.07$ bar, respectively.

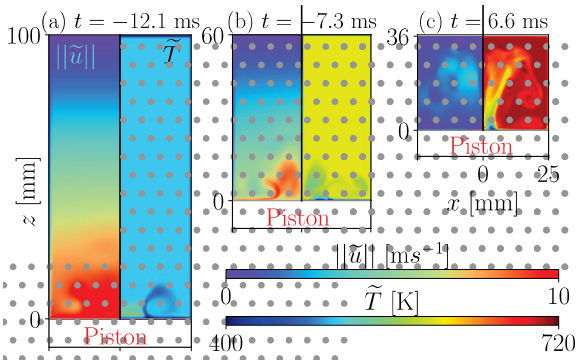

Figure VI.A.3.1 Velocity (left, mirrored) and temperature (right) fields on the deforming RCM quarter domain of the short ignition case at three time instances

Figure VI.A.3.1 presents the velocity (ũ) and temperature ($\tilde{T}$) fields in the deforming domain of the short ignition case for three instances. A quarter domain with two symmetry boundary conditions is employed to reduce the computational expense of simulating turbulent combustion with the Lawrence Livermore National Laboratory (LLNL) 99-species iso-octane mechanism [4]. All other boundary conditions are prescribed as isothermal walls with the initial gas temperature set to $T_w = 294$ K. The minimum cell length at the walls was 0.08 mm corresponding to $y^+ < 10$, and the domain stretches up to a maximum cell length of 0.6 mm, where - y^+ is the normalized distance from the wall based on friction velocity and kinematic viscosity.

To validate the accuracy of the chosen reduced chemistry mechanism, we perform 0-D reactor simulations with a range of mechanisms. Figure VI.A.3.2 compares the pressure evolution of the two RCM cases, with the simulation uncertainty (originating from experimental uncertainty) of the 0-D LLNL simulations shown in gray. For the short ignition case, 0-D non-adiabatic simulations performed with the LLNL 99-species (LLNL-99) reduced mechanism [4] shows slightly greater than 1 ms underprediction from experimental measurements [1], while the LLNL-874 detailed parent mechanism [5] shows less than 1 ms overprediction. The LLNL-99 mechanism demonstrates higher accuracy in ignition delay predictions than the skeletal 203-species mechanism by Jerzembeck et al. [6], which shows an overprediction of 20 ms. In the long ignition case, all simulations demonstrate large discrepancies in both first-stage and second-stage ignition. Since these discrepancies are also present in the 0-D simulations employing the detailed LLNL-874 mechanism, these results indicate a limitation of present capabilities for modeling combustion chemistry in the negative temperature coefficient range at lower pressures of heavy hydrocarbon fuels. This is consistent with the findings from a previous study [7] involving low-temperature combustion of iso-octane.

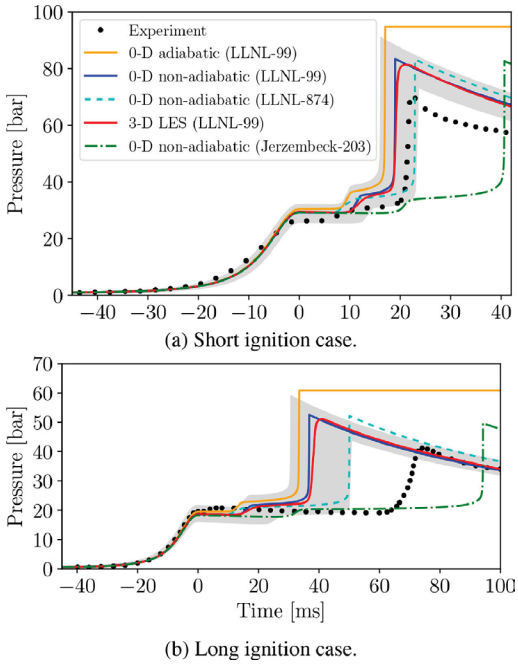

Figure VI.A.3.2 Comparisons of pressure evolution from simulations of two RCM cases, shown with experimental measurements

Plasma-Ignition Model

A phenomenological model of plasma-assisted ignition is implemented for the high-order spectral element computational fluid dynamics solver, Nek5000. This model, described by Castela et al. [8], assumes that the non-equilibrium plasma pulse energy is being deposited through three channels. The first two channels are ultra-fast gas heating and dissociation, which are modeled via a two-step mechanism to account for excitation and relaxation of electronically excited N_2. The third channel is a slower gas heating effect that accounts for vibrational–translational relaxation, which is neglected in the current implementation since it is found to be slower than the other two channels by orders of magnitude. Hence, the ultra-fast deposition channels are incorporated as extra source terms to the species and energy equations.

Nek5000 is then used to perform 2-D simulations of nanosecond repetitively pulsed plasma in a premixed CH_4–air mixture of 0.8 equivalence ratio. A 30-species mechanism of methane combustion reduced from GRI-Mech [9] is utilized. The mixture is initially 300 K at a pressure of 1 atm. Different turbulent Reynolds

numbers (0, 44, and 395) are tested to study the competition between the kinetic effects of plasma and the convection of heat and active radicals. The computational domain is taken as a 2-D plane perpendicular to the axis of the plasma discharge channel. The domain is discretized into 64 × 64 elements with a seventh-order polynomial for each of them. It is initialized with preheated air at a temperature of 1500 K and pressure of 1 atm. Good agreement in O radical concentration and temperature after the end of the pulse was achieved.

However, the characteristic rise time of both temperature and O radical concentration could not be well captured simultaneously. This was also reported by Castella et al. [8], and it is a compromise to be taken for the low cost of such a model, provided that it can adequately predict the thermochemical state after the pulse. It is further found that for the quiescent and lower turbulence case, ignition occurs after the second pulse where both higher temperatures and higher O radical concentration are localized within the pulse channel right after the second pulse ($100\ \mu s + 50\ ns$).

Fundamental Insight of Ducted Fuel Injection from Detailed LES

We utilized 3-D LES to examine ducted fuel injection (DFI). As proposed through an experimental study by Mueller et al. [10], DFI is a diesel spray configuration in which the liquid fuel spray is injected through a coannular duct. Through hypothesized increased mixing and entrainment, the duct modifies the spray structure as a means of attenuating the soot produced (compared to an unconfined free spray). The computational setup involves a finite-volume compressible solver with a reduced 33-species chemical mechanism. The soot is modeled using a two-equation model [11]. The mesh consists of 2.2 million control volumes, with a minimum cell size of 8 μm in the spray core to resolve the ignition kernel and the diffused interface. We examine two cases (one DFI, one free spray) at ambient pressure $p_0 = 6.00$ MPa, ambient temperature $T_0 = 1{,}000$ K, and ambient oxygen mole fraction $X_{O_2} = 0.21$. The fuel is n-dodecane, injected at a temperature of 363 K and a pressure of 150.0 MPa, in accordance with the Engine Combustion Network Spray A setup. Time series plots of the transient temperature behavior for the free spray are shown in Figure VI.A.3.3. Compared with the free spray, the DFI case exhibits a delayed ignition, increased flame lift-off length, and increased liquid penetration.

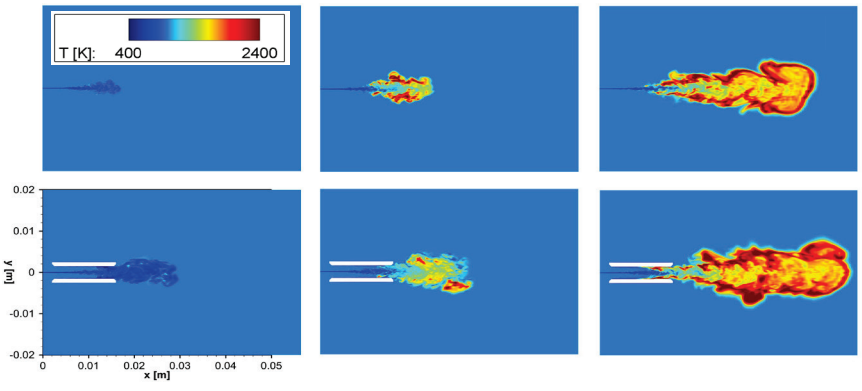

Figure VI.A.3.3 Contours of transient temperature at various times offset by the ignition delay time (IDT), $t - IDT$. From left to right, $t - IDT$ = -0.05 ms, 0.05 ms, 0.5 ms. Plots on the top row are for the free spray (unducted) case, and plots on the bottom row are for the DFI (ducted) case.

Development of Wall Models in Nek5000

The enrichment-based wall model in Nek5000 was further developed for wall-modeled LES. To summarize, the key idea is to add an ansatz enrichment function, ψ, that represents the near-wall behavior, to the solution vector in the wall-adjacent elements, $u = u_0 + \psi = \sum_i \phi_i u_i + \psi$, where u_0 is the polynomial solution. The enrichment function is designed to contain the modeled shear stress to ensure the proper stress is transferred to the bulk flow. The enrichment method allows the solution to accurately represent the large gradients in the boundary layer with large elements without unphysical oscillations while using a no-slip wall boundary condition. Including the modeled profile in the solution maintains a physically relevant solution up to the wall. This technique allows for larger elements to be used without the log–layer mismatch that is seen if only the polynomial modes are used.

The enrichment wall-model (ENWM) was compared to a traditional shear stress wall-model (SSWM) for channel flow cases with a range of Reynolds numbers and grid resolutions. Figure VI.A.3.4 shows the mean velocities compared between standard polynomial spectral element method (SEM), SSWM, and ENWM for wall-modeled LES with higher-order polynomial of order P=7 and for friction Reynolds number Re_t=543, 1,000, and 2,000, with the results shifted upwards as the Reynolds number increases. The results are also compared with the DNS data from Lee and Moser [12]. It was found that the ENWM performs better in matching the DNS mean velocity profile than the SSWM for under-resolved cases. The implementation of the ENWM is currently being extended to curved-wall scenarios, and its performance for flows with separation is currently under investigation using the test case of flow over periodic hills.

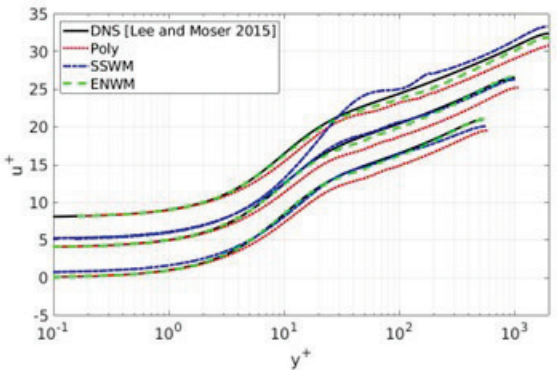

Figure VI.A.3.4 Mean velocity comparison between ENWM, SSWM, and purely polynomial SEM for P=7 and Ret=543, 1,000, and 2,000 (with the results shifted up for visibility)

High-Fidelity Nek5000 Simulations

The finite-rate chemistry model integrated within Nek5000 was validated for a realistic reacting jet-in-crossflow configuration. Specifically, DNS of the reacting jet in crossflow was performed for a nitrogen-diluted hydrogen jet using a detailed hydrogen–air chemical kinetic mechanism. The mixture-averaged molecular transport model was employed to account for the differential diffusion effect that is critical for hydrogen combustion. The operator-splitting scheme was further applied to accelerate the reacting flow simulation with detailed chemistry. An auxiliary non-reacting channel flow DNS was performed to provide fully developed turbulent flow at the crossflow inlet. Simulation results were compared with experimental measurements for jet trajectory and 2-D contours of velocity and reactive scalars, shown in Figure VI.A.3.5. Good agreement on mean jet trajectory was observed between simulation and experiment. The predicted instantaneous, mean, and root-mean-square velocity fields also resembled the experimental observations. Lastly, instantaneous and mean OH contours from the simulation revealed the presence of two flame branches (a thin windward branch and a thick leeward branch) matching the experimental observations well. Currently, tests are under way to verify the coupled implementation of finite-rate chemistry and spray models in Nek5000 for the Engine Combustion Network Spray A configuration. In addition, Argonne's Unsteady Flamelet Progress Variable combustion model is being integrated within Nek5000.

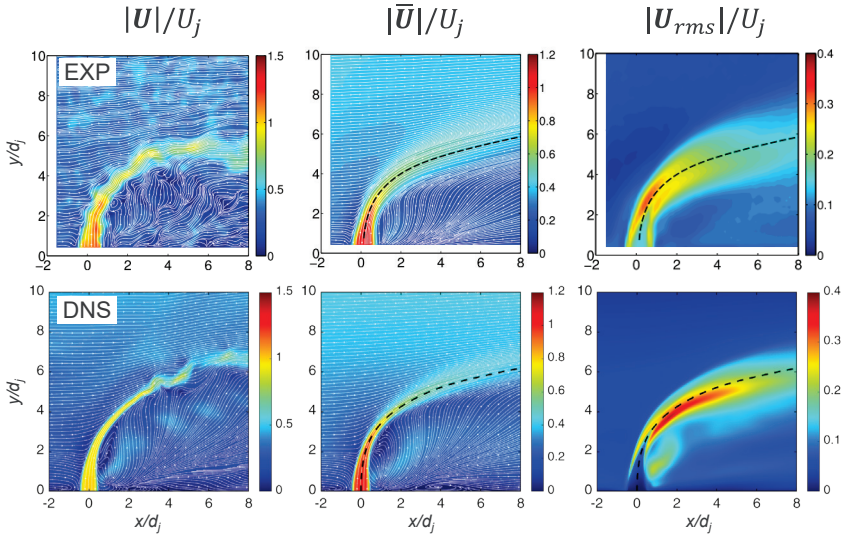

Figure VI.A.3.5 Instantaneous, mean, and root mean square of the velocity magnitude (normalized by jet velocity) from the experiment (top) and simulation (bottom)

Conclusions

The following conclusions can be drawn:

- LES studies of RCMs show qualitative agreement with experimental data, but strong sensitivity to low-temperature chemistry affects the long ignition case. This suggests the need for further improvements in chemical mechanisms.
- Comparative LES calculations of free-spray and ducted-fuel ignition uncover the effects of different ignition delays and soot formation as a result of the enhanced entrainment, mixing, and turbulence generation in the duct.
- Detailed simulation of jet in crossflow using reactive Nek5000 formulation demonstrates agreement in capturing the jet-trajectory and mixing characteristics.

Key Publications

1. Chung, W.T., N. Ly, and M. Ihme. 2023. "LES of HCCI Combustion of Iso-Octane/Air in a Flat-Piston Rapid Compression Machine." Proceedings of the Combustion Institute, in press. https://doi.org/10.1016/j.proci.2022.07.233.
2. Kabil, I., C. Xu, and T. Lu. 2022. "Spectral Element Modeling of Plasma-Assisted Ignition Using a Phenomenological Model." Presented at the 75th Annual Meeting of the American Physical Society's Division of Fluid Dynamics, Indianapolis, IN, November 20–22.
3. Guo, J., W.T. Chung, and M. Ihme. 2022. "Computational Analysis of Ducted Fuel Injection at High-Pressure Transcritical Conditions Using Large-eddy Simulations." THIESEL 2022 Conference, Valencia, Spain.
4. Brill, S.R., P. Pal, M.M. Ameen, C. Xu, and M. Ihme. 2022. "An Enrichment Wall Model for the Spectral Element Method." AIAA SciTech 2022 Forum and Exposition, San Diego, CA (and virtual), January 3–7. http://dx.doi.org/10.2514/6.2022-1206.
5. Brill, S.R., P. Pal, M.M. Ameen, C. Xu, and M. Ihme. 2022. "Solution Enrichment Wall-Modeled LES in the Spectral Element Method Framework." Presented at the 75th Annual Meeting of the American Physical Society's Division of Fluid Dynamics, Indianapolis, IN, November 20–22.
6. Pal, P., M.M. Ameen, and C. Xu. 2022. "Near-Wall Modeling of Turbulent Flow and Heat Transfer Using a Spectral Element CFD Solver." AIAA SciTech 2022 Forum and Exposition, San Diego, CA (and virtual), January 3–7. https://doi.org/10.2514/6.2022-1369.
7. Xu, C., M.M. Ameen, P. Pal, and S. Som. 2022. "Direct Numerical Simulation of a Reacting Hydrogen Jet in Turbulent Vitiated Crossflow Using Spectral Element Method." AIAA SciTech 2022 Forum and Exposition, San Diego, CA (and virtual), January 3–7. https://doi.org/10.2514/6.2022-0823.
8. Xu, C., M.M. Ameen, P. Pal, and S. Som. Forthcoming. "Direct Numerical Simulation of Partial Fuel Stratification Assisted Lean Premixed Combustion for Assessment of Hybrid G-Equation/Well-Stirred Reactor Model." ASME Journal of Engineering for Gas Turbines and Power 145, no. 5 (May 2023). https://doi.org/10.1115/1.4055873.
9. Xu, C., P. Pal, M.M. Ameen, and S. Som. 2022. "DNS of Lean Premixed Combustion Assisted by Partial Fuel Stratification for Assessment of G-Equation Modeling Approach." Presented at the 75th Annual Meeting of the American Physical Society's Division of Fluid Dynamics, Indianapolis, IN, November 20–22.

References

1. Strozzi, C., A. Claverie, V. Prevost, J. Sotton, and M. Bellenoue. 2019. "HCCI and SICI Combustion Modes Analysis with Simultaneous PLIF Imaging of Formaldehyde and High-Speed Chemiluminescence in a Rapid Compression Machine." *Combustion and Flame* 202 (April): 58–77. https://doi.org/10.1016/j.combustflame.2019.01.002.

2. Hirt, C.W., A.A. Amsden, and J.L. Cook. 1974. "An Arbitrary Lagrangian-Eulerian Computing Method for All Flow Speeds." *Journal of Computational Physics* 14, no. 3 (March): 227–253. https://doi.org/10.1016/0021-9991(74)90051-5.

3. Strozzi, C., J. Sotton, A. Mura, and M. Bellenoue. 2008. "Experimental and Numerical Study of the Influence of Temperature Heterogeneities on Self-Ignition Process of Methane-Air Mixtures in a Rapid Compression Machine." *Combustion Science and Technology* 180 (10–11): 1829–1857. https://doi.org/10.1080/00102200802260656.

4. Yoo, C.S., Z. Luo, T. Lu, H. Kim, and J.H. Chen. 2013. "A DNS Study of Ignition Characteristics of a Lean Iso-Octane/Air Mixture under HCCI and SACI Conditions." *Proceedings of the Combustion Institute* 34 (2): 2985–2993. https://doi.org/10.1016/j.proci.2012.05.019.

5. Mehl, M., W.J. Pitz, M. Sjöberg, and J.E. Dec. 2009. "Detailed Kinetic Modeling of Low-Temperature Heat Release for PRF Fuels in an HCCI Engine." SAE Technical Paper 2009-01-1806. https://doi.org/10.4271/2009-01-1806.

6. Jerzembeck, S., N. Peters, P. Pepiot-Desjardins, and H. Pitsch. 2009. "Laminar Burning Velocities at High Pressure for Primary Reference Fuels and Gasoline: Experimental and Numerical Investigation." *Combustion and Flame* 156, no. 2 (February): 292–301. https://doi.org/10.1016/j.combustflame.2008.11.009.

7. Goldsborough, S.S. 2009. "A Chemical Kinetically Based Ignition Delay Correlation for Iso-Octane Covering a Wide Range of Conditions Including the NTC Region." *Combustion and Flame* 156, no. 6 (June): 1248–1262. https://doi.org/10.1016/j.combustflame.2009.01.018.

8. Castela, M., et al. 2016. "Modelling the Impact of Non-Equilibrium Discharges on Reactive Mixtures for Simulations of Plasma-Assisted Ignition in Turbulent Flows." *Combustion and Flame* 166 (April): 133–147. https://doi.org/10.1016/j.combustflame.2016.01.009.

9. Smith, Gregory P., David M. Golden, Michael Frenklach, Nigel W. Moriarty, Boris Eiteneer, Mikhail Goldenberg, C. Thomas Bowman, Ronald K. Hanson, Soonho Song, William C. Gardiner, Jr., Vitali V. Lissianski, and Zhiwei Qin. GRI Mech 3.0. http://www.me.berkeley.edu/gri_mech/.

10. Mueller, C.J., C.W. Nilsen, D.J. Ruth, R.K. Gehmlich, L.M. Pickett, and S.A. Skeen. 2017. "Ducted Fuel Injection: A New Approach for Lowering Soot Emissions from Direct-Injection Engines." *Applied Energy* 204 (October 15): 206–220. https://doi.org/10.1016/j.apenergy.2017.07.001.

11. Brookes, S.J., and J.B. Moss. 1999. "Predictions of Soot and Thermal Radiation Properties in Confined Turbulent Jet Diffusion Flames." *Combustion and Flame* 116, no. 4 (March): 486–503. https://doi.org/10.1016/S0010-2180(98)00056-X.

12. Lee, M., and R.D. Moser. 2015. "Direct Numerical Simulation of Turbulent Channel Flow up to $Re_\tau \approx 5200$." *Journal of Fluid Mechanics* 774: 395–415. https://doi.org/10.1017/jfm.2015.268.

VI.A.4 Co-Optimized Multimode Light-Duty Engine (Hyundai America Technical Center, Inc.)

Shengrong Zhu, PhD, Principal Investigator
Hyundai America Technical Center, Inc.
6800 Geddes Road
Superior Township, MI 48198
Email: SZhu@hatci.com

Jeffrey D. Naber, PhD, Principal Investigator
Michigan Technological University
1400 Townsend Drive
Houghton, MI 49931
Email: JNaber@mtu.edu

Kevin Stork, DOE Technology Manager
U.S. Department of Energy
Email: Kevin.Stork@ee.doe.gov

Start Date: October 1, 2018 End Date: May 31, 2022
Project Funding: $4,950,000 DOE share: $2,170,000 Non-DOE share: $2,780,000

Project Introduction

Hyundai America Technical Center, Inc. (HATCI) and partners have been developing a co-optimized fuel and multimode gasoline compression-ignition (GCI)–spark-ignition (SI) engine capable of achieving 15% improvement in fuel consumption versus a production SI engine over a simulated Federal Test Procedure (FTP)-75 cycle and meeting Low-Emission Vehicle III (LEV III) emission targets. This project aims to overcome challenges and shortcomings of advanced compression-ignition engines, such as mode switching, cold start, and efficient low-load operation. The project also has a high specific power output target of at least 150 hp. The project is using a near-production 2.2 L I4 Hyundai engine with advanced technology, capable of operating in low-temperature combustion (LTC), SI, and GCI modes.

The project is co-optimizing the fuel and production-intent engine with an advanced high-pressure fuel system, advanced engine controls, and variable-inlet compressor turbocharger, as well as a cooled exhaust gas recirculation system. Researchers are developing and testing different fuel formations to determine the optimal fuel for this multimode combustion engine. The engine has production-level dual continuously variable valve duration and dual continuously variable valve timing systems on both intake and exhaust that enable negative valve overlap (NVO) to trap residuals for LTC mode operation up to about 5 bar brake mean effective pressure (BMEP). The SI mode is utilized in both spark-assisted (SA) LTC mode and during cold start to improve ignition and startability.

Objectives

Overall Objectives

This project is co-optimizing a multimode-capable engine with fuel formulation. The project aims to meet the following targets:

- Improve vehicle fuel economy by 15% over the baseline, enabled by operation in SA-LTC mode for part load and mixing-controlled compression-ignition (MCCI) (indicated mean effective pressure [IMEP] >5 bar) over most of the engine operation, as validated by engine dynamometer testing and vehicle simulation.

- Attain a power target of at least 150 hp (15 bar BMEP) with a 2.2 L engine via a variable-inlet-compressor-enabled highly diluted charge system ($\lambda' = 1.8$) over the full load operating range from 1,500 rpm to 4,500 rpm (targeting IMEP = 20 bar from 2,000 rpm to 3,500 rpm and 200 hp at 4,500 rpm).
- Meet or exceed LEV III (ULEV70[1]) emission targets via robust, ultra-low cold-start emissions enabled by port fuel injection combined with direct injection in SI mode for cold start as well as catalyst heating and lean gasoline selective catalytic reduction for LTC mode operation.
- Demonstrate multimode combustion control utilizing a multiple-input, multiple-output controller and cylinder pressure feedback, along with in-cylinder condition estimation.
- Validate computational fluid dynamics (CFD) models incorporating advanced physics-based fuel surrogate models for thermo–physical properties and reaction kinetics.
- Populate a spray and combustion database with a high-pressure direct-injection system with high-reactivity gasoline (60–90 research octane number [RON]) under thermodynamic MCCI and homogeneous-charge compression-ignition (LTC) conditions.
- Produce a CFD mesh and models for spray and engine data, and share them with the Co-Optimization of Fuels and Engines (Co-Optima) team.

Fiscal Year 2022 Objectives

- Refine a multimode rapid prototyping controller for the multimode engine control.
- Develop a combustion strategy for LTC mode.
- Evaluate strategies for rated engine operating conditions.
- Confirm the overall combustion strategy for the multimode engine through engine testing.
- Demonstrate combustion mode switching.
- Complete engine testing for fuel formulation effects and fuel optimization for the multimode engine.
- Validate CFD model for multimode engine and different fuels.
- Confirm fuel economy improvement with the proposed multimode engine.

Approach

A technical specification was developed for the 2.2 L engine. The specification helped establish the overall engine targets for fuel economy and performance, as well as boundary conditions for a set of points that represent the engine's overall operation. These points were used in a 1D air system model to determine the optimal turbocharger specification and to set up the 3D combustion model and optical fuel spray experiments. A matrix of four gasoline blendstocks (RON 60, 70, 80, and 90) was selected for development of a real-fuel chemical mechanism and fuel properties model. The fuel model was validated with experimental data and was used in the 3D combustion code to simulate three discrete modes of SI, SA-LTC, and MCCI combustion.

Meanwhile, a production 2.2 L diesel compression-ignition engine was modified to run multiple modes of combustion. A rapid-prototyping engine controller was developed using Matlab–Simulink model-based code and integrated with the engine. Engine testing was then conducted to explore the operating range of each combustion mode. Finally, a 1D vehicle FTP-75 cycle simulation was conducted using steady-state data from

[1] ULEV70 refers to any light-duty vehicle certified to LEV III ultra-low-emission vehicle 70 standards.

the engine testing above. The project objective of 15% fuel economy improvement will be met with this general approach, which is illustrated in Figure VI.A.4.1.

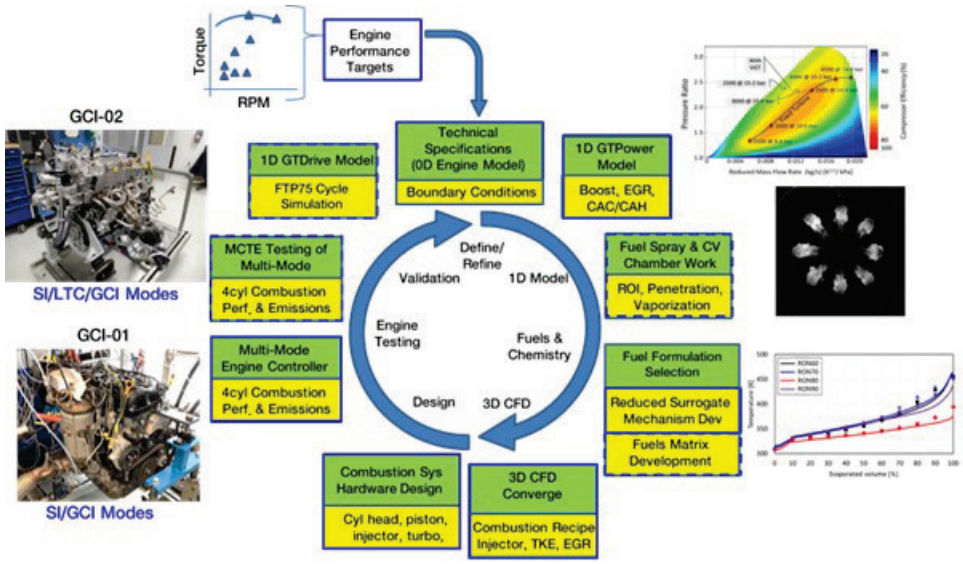

0D, 1D, 3D – zero-, one-, three-dimensional; CAC – charge air cooler; CAH – charge air heater; CV – continuously variable; cyl – cylinder; EGR – exhaust gas recirculation; MCTE – multi-cylinder test engine; ROI – rate of injection; TKE – turbulence kinetic energy

Figure VI.A.4.1 Co-optimized engine development approach

HATCI has been working with Michigan Technological University (MTU) and Phillips 66 for development of a detailed fuel mechanism, validation and engine modeling in CFD, advanced controls algorithm development, and engine testing with nine different fuels, including alcohol blends. Phillips 66 has worked on fuel formulation development, creating gasoline-like fuels with desired physical and chemical properties for multimode combustion. These fuel formulations have been tested at MTU. The MTU team has also been conducting 3D CFD modeling of the SI, SA-LTC, and GCI modes, the latter consisting of both partially premixed compression-ignition (PPCI) and MCCI modes. HATCI is developing the overall engine hardware and multimode steady-state engine testing, as well as 1D vehicle simulation over the FTP-75 cycle. The project will provide the Co-Optima program with validated CFD data, surrogate fuel models, and engine emissions data.

Results

Low- to Medium-Load Operation – LTC

For operation at low to medium loads (BMEP up to ~ 7 bar), LTC was used through NVO without additional intake heating. The amount of NVO was adjusted in real time with respect to the changes in engine loads or operating conditions, thanks to the dual continuously variable valve duration and continuously variable valve timing mechanisms for both intake and exhaust valvetrains, significantly improving LTC phasing control. Spark assist and port fuel injection (PFI) can also be used to further improve combustion stability, along with double injections to create fuel stratification for reduced max pressure rise rate (MPRR) at medium load.

Figure VI.A.4.2 shows the engine test results on LTC combustion phasing control. Figure VI.A.4.2(a) shows the start-of-injection (SOI) timing of direct injection with 250 bar fuel pressure when swept from -380° to -180° after top dead center firing ($ATDC_f$), for different NVO settings (170 to 204 crank angle degrees [CAD]) at 1,500 rpm and approximately 2.6 bar BMEP. The fuel mass flow rate was kept constant, and the throttle was fully open for all cases. The NVO reported here is symmetric NVO, that is, the retard angle during intake valve opening is the same as the advance angle of exhaust valve closing. The NVO was varied while the exhaust

valve opening and intake valve closing were kept constant. Figure VI.A.4.2(b), (c), and (d) show CA50[2] of LTC for different direct-injection (DI) SOI timings with different NVO settings, CA50 against NVO for two SOIs (SOI-360 and SOI-280), and the NVO effect on overall air–fuel ratio (AFR). Clearly, more NVO leads to more trapped high-temperature residuals and less fresh air and, in turn, higher in-cylinder gas temperature and richer mixture, resulting in more advanced CA50. In other words, NVO along with fuel injection can be used to control the combustion phasing of LTC mode.

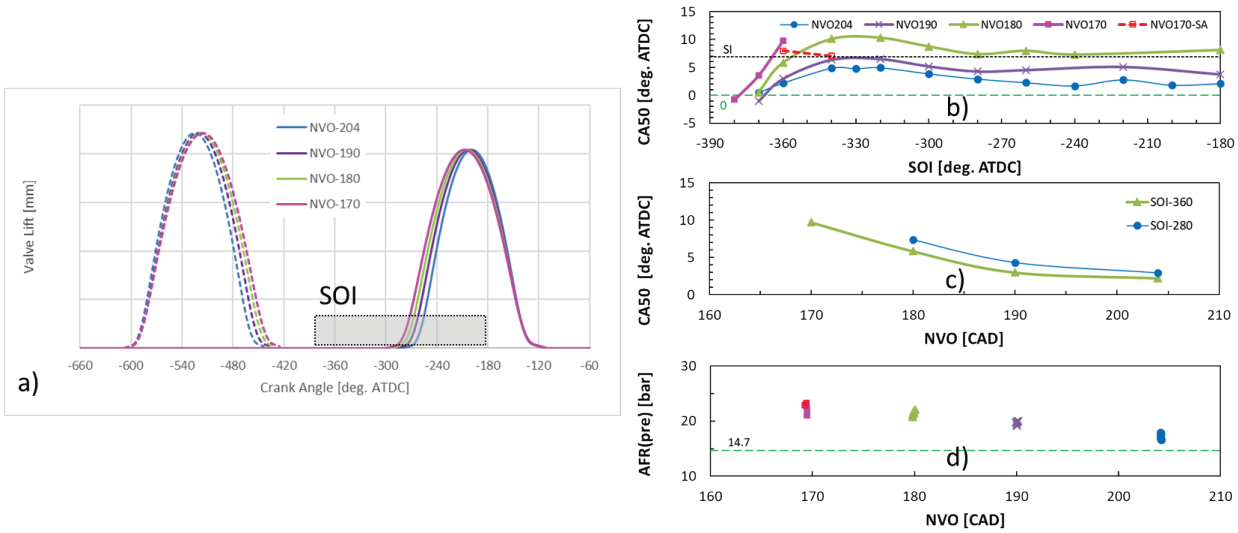

ATDC – after top dead center

Figure VI.A.4.2 LTC combustion phasing control: SOI sweep for LTC with different NVOs at 1,500 rpm/2.6 BMEP (250 bar DI)

Figure VI.A.4.3 shows the engine test results on LTC combustion stability improvement with PFI and spark assist. At the low load of 1,500 rpm and 1.1 BMEP, both PFI and spark assist can reduce the coefficient of variation (COV) of IMEP and stabilize LTC, resulting in extended LTC operating range.

[2] CA50 is the crank angle position where 50% of the heat is released.

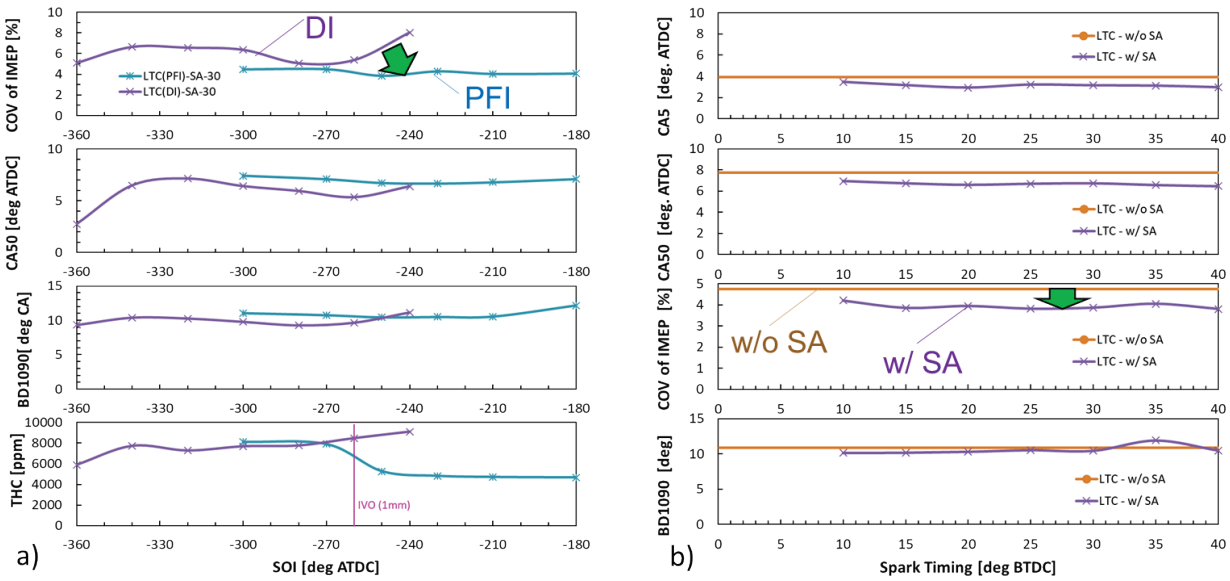

BD1090 – burn duration from mass fraction burned (MFB) 10 to MFB90; THC – total hydrocarbons; BTDC – before top dead center

Figure VI.A.4.3 LTC combustion stability at 1,500 rpm and 1.1 bar BMEP: (a) PFI vs. DI and (b) with and without spark assist

Figure VI.A.4.4 shows the results on the pressure rise rate with LTC. At 3,000 rpm and 3 bar BMEP, introducing a second injection with fuel ratio of about 20% leads to an MPRR reduction from 5.4 bar/deg to 3.9 bar/deg, indicating multiple fuel injection can be used to reduce the pressure rise rate of LTC as engine load increases. This strategy was used in this project since it aligns well with the fueling strategy for GCI at high load operation.

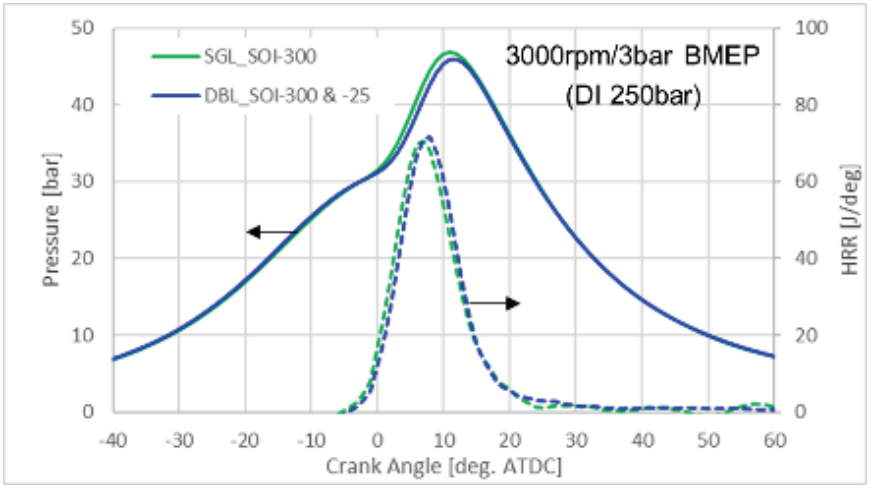

HRR – heat release rate

Figure VI.A.4.4 LTC pressure rise rate of DI single (SGL) vs. double (DBL) injection at 3,000 rpm and 3 bar BMEP

Medium- to High-Load Operation – GCI

For operation at medium to high loads (BMEP greater than 5 bar), GCI was used with two late direct injections near top dead center firing (TDC_f), pilot and main. The SOI timing was around -30° and -5° $ATDC_f$ for pilot and main injections. At medium loads with BMEP around 5 bar, the fuel split ratio between pilot and main can

be around 60/40 to take advantage of high combustion efficiency and low emissions from PPCI. For higher loads with BMEP greater than 15 bar, the fuel split ratio needs to be decreased to around 15/85 for MCCI to reduce the MPRR. More details on the GCI combustion strategy can be found in Zyada et al [1].

Overall Combustion Strategy for Multimode Engine

Figure VI.A.4.5 shows an overall combustion strategy developed for the multimode engine. After the engine is started with SI mode, the combustion mode is switched to LTC by adding NVO and using wide-open throttle, spark assist, and PFI. As engine load increases, spark assist can be turned off. Single and early DI can be used to accommodate the need of increased fuel flow rate if any. As load further increases, double DI with one late DI can be used to suppress the increasing pressure rise rate. NVO is used to regulate the in-cylinder thermodynamic conditions to promote auto-ignition and should be reduced to suppress the unacceptable MPRR at higher loads, where in-cylinder conditions become better suited for auto-ignition. When the boost level reaches about 140 kPa, the combustion mode is then switched to GCI by using minimum NVO and double late DI injections.

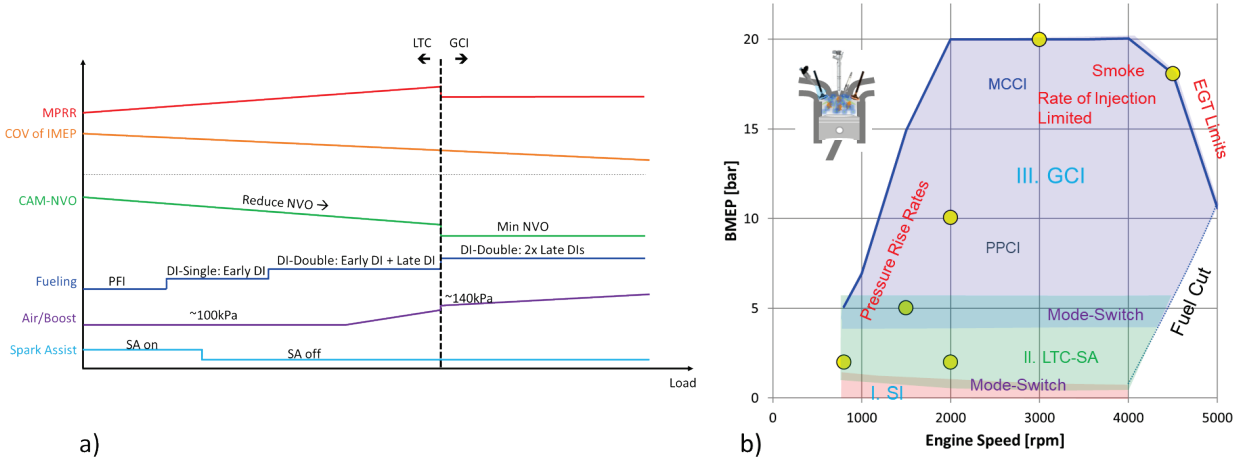

EGT – exhaust gas temperature

Figure VI.A.4.5 Overall combustion strategy (a) and operating map (b) for multimode GCI engine

Evaluation on Rated Condition

To assess high-load and high-speed operation with this multimode engine, CFD evaluation at the rated condition—4,500 rpm and 18.1 bar BMEP (200 hp/150 kW)—was carried out.

As engine results indicated, combustion duration increases as the engine load and speed increase, leading to high exhaust temperature and soot emissions. The exhaust temperature is limited by the allowable turbine inlet temperature of the turbocharger used, which is 860°C. In the evaluation, two other limits were used: maximum cylinder pressure Pmax <180 bar and MPRR <10 bar/deg.

To meet these three criteria, the following three parameters were studied at the rated condition:

- Fuel injection pressure (FUP) (800; 1,000; and 1,600 bar)
- Fueling strategy (timing, single and double injections)
- Boost level (AFR: 20.7 to 22.5).

Table VI.A.4.1 lists the operating conditions for seven cases A to G, along with corresponding combustion performance. As can be seen from these evaluation results, for high-speed and high-load operations, a fuel injection pressure greater than 1,000 bar is needed to allow multiple fuel injections so that the engine hardware

limit requirements can be met and emissions reduction can be achieved. A high-boost turbocharger would also help in lowering exhaust gas temperatures.

Table VI.A.4.1 Summary of CFD Operating Conditions and Results at Rated Condition (4,500 rpm/18.1 bar BMEP)

Case	FUP [bar]	SOI_1 [deg, aTDC]	SOI_2 [deg, aTDC]	CA50 [deg, aTDC]	BD1090 [deg, CA]	AFR [-]	Pmax [bar]	PRR_max [bar/deg]	T_turb_in [C]	Delta soot [%] in g/kWh	Delta Nox [%] in g/kWh	Delta HC [%] in g/kWh	Delta ITE [-]
A	800	-21.5	NA	21.0	67.4	20.7	155	16.6	829	0%	0%	0%	0%
B	1000	-20	NA	16.8	53.1	20.7	166	17.7	780	-49.6%	40.8%	-74.7%	8.3%
C	1600	-19	NA	8.8	39.6	20.7	199	36.7	688	-86.0%	157.5%	-99.7%	13.1%
D	1600	-13	NA	18.3	39.2	20.7	141	9.8	759	-83.4%	32.7%	-98.0%	8.9%
E	1600	-18	-8	18.8	52.0	20.7	157	9.8	752	-49.0%	-19.5%	-85.9%	7.5%
F	1600	-18	-8	17.2	52.4	21.6	165	8.8	730	-68.5%	-4.3%	-99.1%	11.6%
G	1600	-18	-8	17.6	55.7	22.5	170	8.2	706	-45.8%	-16.1%	-90.2%	10.1%

Pmax – maximum pressure; NO_x – nitrogen oxides; HC – hydrocarbons; ITE – indicated thermal efficiency

Mode-Switching Demonstration at Medium Load

For mode switching from SI to LTC right after engine start, engine testing showed a very smooth transition from SI to LTC since both can be operated at similar throttle positions and the NVO can be adjusted in real time.

For mode switching between LTC and GCI at medium load (BMEP around 5 bar), both stationary (with the same speed/load) and transient (with varying load) mode switching were tested for different engine speeds. Figure VI.A.4.6 shows the load sweep from 1 bar to 12 bar BMEP at a ramp rate of 1 bar BMEP/second and engine speed of 2,000 rpm. The combustion mode was switched from LTC to GCI at the recorder time of 9 sec. No IMEP drop was observed across all four cylinders. The combustion phasing of CA50 was about 4° ATDC for low load in LTC mode, then retarded to about 12° ATDC for the higher loading in GCI mode. The MPRR did briefly exceed 10 bar/deg during the transition, at recorder time ~12.5 sec where the CA50 was also advanced, ~ 7° ATDC, but it can be reduced below 10 bar/deg with further engine calibration. At low loads with torque less than 65 Nm (recorder time earlier than 7 sec), only single injection with SOI around 330°–300° BTDC (actual SOI_1) was used. When the torque was greater than 65 Nm (recorder time >7 sec), an additional injection with SOI close to TDC (actual SOI_2) was introduced to suppress the high pressure-rise rate. The exhaust valve closing (EVC) timing was 90° BTDC gas exchange at ~1 bar BMEP, and then retarded as engine load increased. EVC timing was 50° BTDC gas exchange when combustion mode was switched from LTC to GCI at recorder time ~9 sec. Right after that, EVC timing was not immediately set to the most retarded position for the minimum NVO typically used for GCI mode. The reasoning was that turbo lag caused insufficient boost pressure, resulting in longer ignition delay and misfiring cycles. By keeping some NVO before boost pressure reaches the set point, the in-cylinder gas temperature can be increased. This reduces the mixture ignition delay, offsetting the negative impact of insufficient boost pressure on auto-ignition and eliminating misfiring cycles. After the boost pressure is built up and reaches the set level, NVO can be minimized.

In this mode-switching demonstration, the NVO correction for boost deficit was found to be very effective in avoiding misfiring cycles and torque drop.

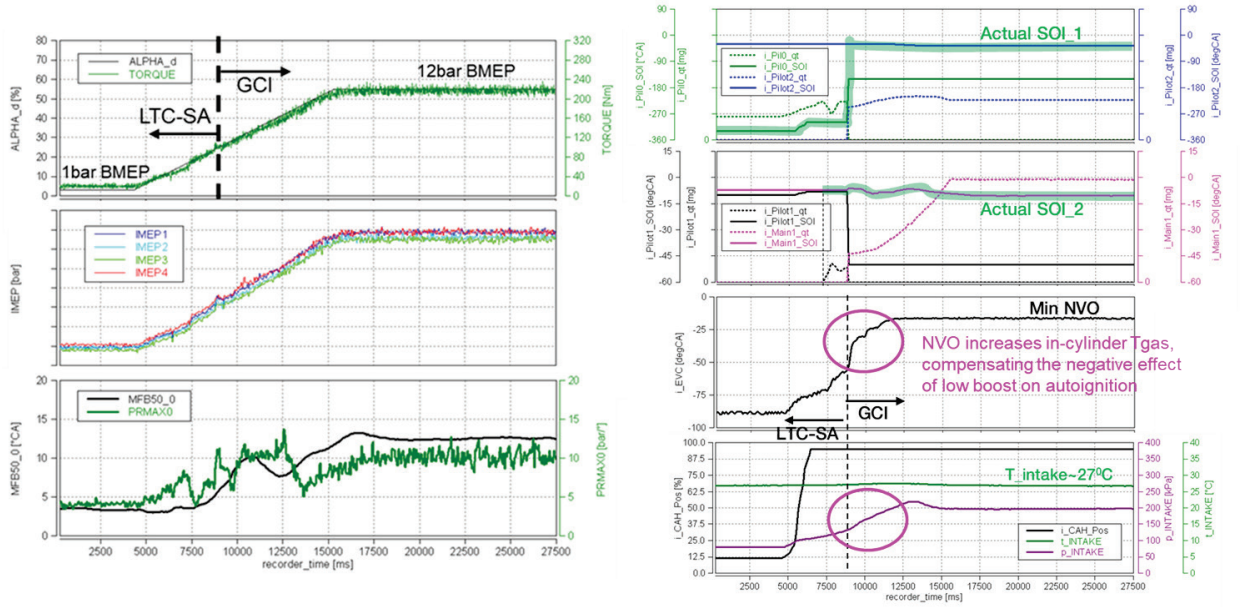

Tgas – gas temperature

Figure VI.A.4.6 Load sweep with ramp rate 1 bar BMEP/sec at 2,000 rpm

Fuel Co-Optimization

To develop new fuels that can boost engine efficiency and reduce emissions when combined with advanced combustion techniques, nine different fuel formulations with RONs ranging from 60 to 90 were blended and tested through collaboration with Phillips 66 and MTU. These fuels were studied with spray and combustion vessel testing, CFD real fuel modeling, and engine testing. Four of these fuels were non-oxygenated gasoline refinery blendstocks, with RONs from 60 to 90, blended by a petroleum refinery at Phillips 66. Additionally, bio-renewable components of ethanol and iso-butanol were added to the base RON 60 gasoline blendstock fuel to increase the overall bio-gasoline fuel to target RONs of 80 and 90. Additionally, for reference, the effect of RON 91 E10 gasoline (standard pump fuel, meeting U.S. specifications, with 10% ethanol) was also included.

Figure VI.A.4.7 shows the fuel test points completed for all nine fuel formations in GCI mode. The lower RON fuels with RON <80 clearly extend the GCI low load limit down to about 1 bar BMEP with COV of IMEP ≤3% due to the improved fuel reactivity.

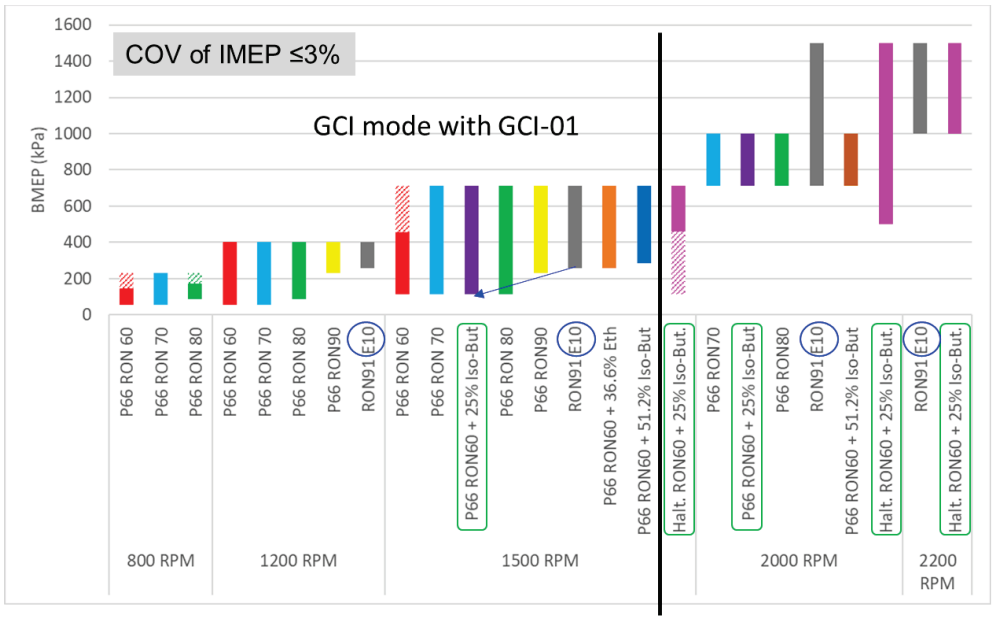

Testing Performed:

- *Solid indicated operation was successful*
- *Hashed indicates operation was assumed*
- *Lowest load tested was 57 kPa BMEP at 800 and 1200rpm, 114kPa at 1500rpm, or at the low load limit*

P66 – Phillips 66

Figure VI.A.4.7 Fuel test points in GCI engines

Figure VI.A.4.8 shows the ignition delay and peak cylinder pressure for nine different fuels at 1,500 rpm and 4.6 bar BMEP. The ignition delay time here is defined as the time duration of mass fraction burnt from 0% to 2%. Each fuel shows consistent ignition delay for different combustion phasing. Higher RON fuels have longer ignition delays. There are two distinct heat release patterns for the fuels with RON >80 and those with RON ≤80 tested: single-stage for RON >80 and two-stage for RON ≤80, as shown in Figure VI.A.4.9.

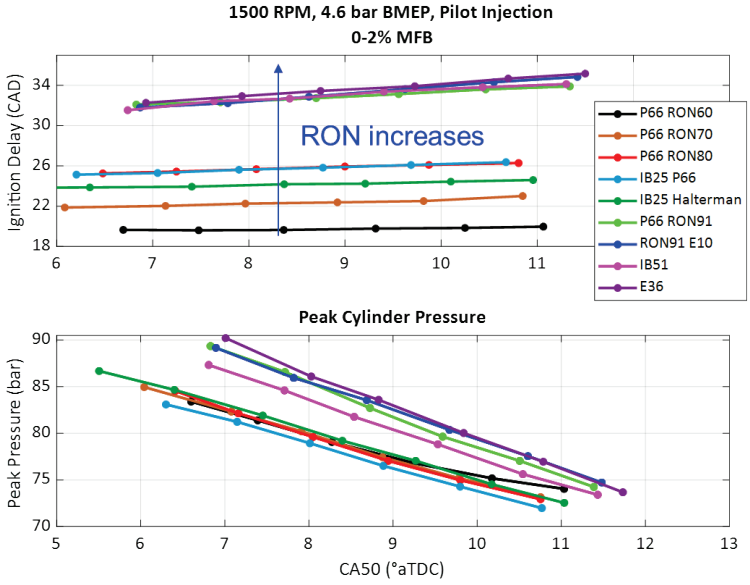

Figure VI.A.4.8 Ignition delay and peak cylinder pressure for different fuels at 1,500 rpm and 4.6 bar

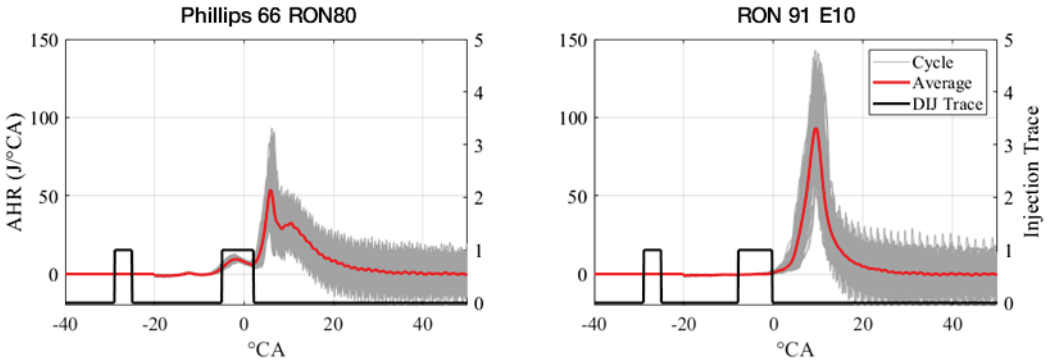

DIJ – direct injection

Figure VI.A.4.9 Apparent heat release (AHR) rate for P66 RON 80 and RON 91 E10 at 1,500 rpm and 4.6 bar BMEP

Among these nine different fuels, iB25 (25% iso-butanol + 75% P66 RON 60) with calculated RON 77.8 appears to be the best candidate in extending GCI low load limit while maintaining good engine startability and having the benefits of reduced greenhouse gas emissions. The iB25 fuel's better combustion performance in thermal efficiency and emissions over E10 was also confirmed at different engine operating conditions, as shown in Table VI.A.4.2. The relatively higher soot with iB25 in GCI mode can be reduced with a higher fuel injection pressure, since the fuel pressure used was relatively low, less than 350 bar, even at 10 bar BMEP.

Table VI.A.4.2 Combustion Performance Comparison Between E10 and iB25 at Three Representative Engine Operating Points

Parameter	1500 RPM, 5 bar BMEP		2000 RPM, 2 bar BMEP		2000 RPM, 10 bar BMEP	
Fuel	RON91 E10	IB25 Halterman	RON91 E10	IB25 Halterman	RON91 E10	IB25 Halterman
ITE Net [%]	40.8	42.5	38.4	38.8	44.4	44.4
NOx [PPM]	503	498	<25	<25	1073	586
FSN[-]	0.19	0.44	<0.01	<0.01	1.05	1.6
FUP [bar]	270	270	270	270	330	337
Mode	LTC	GCI	LTC	LTC	GCI	GCI

FSN – filter smoke number

CFD Model Validation

For the engine CFD validation, the six fuels listed in Table VI.A.4.3 were simulated at 1,500 rpm/IMEP$_{net}$ 7 bar in GCI mode. Table VI.A.4.4 lists the operating conditions. Figure VI.A.4.10 shows corresponding simulation results of combustion pressure and HRR compared to engine test data. Clearly, CFD has good agreement with engine data in capturing the differing fuel effects.

Table VI.A.4.3 Gasoline Surrogates and Oxygenated Fuel Blends

Fuels	Chemical Class (Vol%)				
	n-alkanes	iso-alkanes	cycloalkanes	alkenes	aromatics
P66 RON60	33.4	40.6	18.7	0.0	7.2
P66 RON70	29.8	40.0	16.7	0.0	13.4
P66 RON80	23.7	40.5	16.9	13.5	5.4
P66 RON90	15.0	39.2	12.2	12.0	21.6
P66 RON60+ 51.2% Iso-But.	48.8% P66 RON60 + 51.2% iso-butanol (RON target 90/measured 93.4)				
P66 RON60 + 36.6% Eth.	63.4% P66 RON60 + 36.6% ethanol (RON target 90/measured 94)				

Table VI.A.4.4 Operating Conditions for the Fuel Effect Study at 1,500 rpm/$IMEP_{net}$ 7 bar with GCI Mode

Operating Conditions	
Engine Speed [rpm]	1500
$IMEP_{net}$ [bar]	7.0
Intake Pressure [kPa]	155
Intake Temperature [K]	326
Exhaust Pressure [kPa]	250
Exhaust Temperature [K]	598-600
CA50 [deg., aTDCf]	9
Fueling Injection	
Injection Pressure [bar]	300
SOI_1[deg., aTDCf]	-29.0
SOI_2 [deg., aTDCf]	-8.4 to -5.7
Split Ratio [-]	24/76

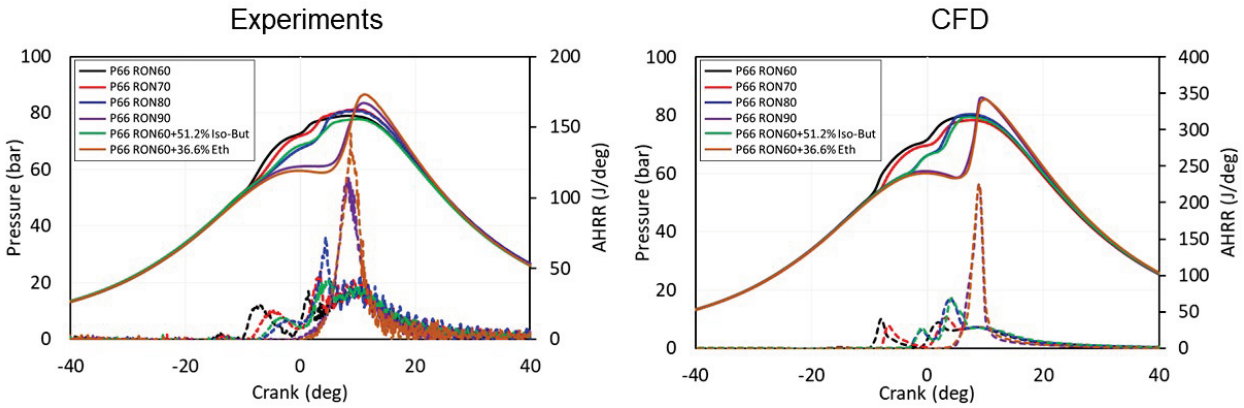

Figure VI.A.4.10 Combustion pressure and apparent heat release rate (AHRR) for engine data and CFD simulations at 1,500 rpm/$IMEP_{net}$ 7 bar with GCI mode

Vehicle Fuel Economy Optimization

To evaluate the fuel economy improvement of the multimode combustion engine, an FTP-75 drive cycle model was built with GT-SUITE (a simulation tool), using engine test data. To make best use of the benefit from this multimode GCI engine, some common state-of-the-art fuel economy applications were studied, including gear schedule optimization, start–stop feature, engine downsizing, and P2 full hybrid.[3] Figure VI.A.4.11(a) and (b) show the FTP-75 residence plots over a brake thermal efficiency (BTE) map before and after the gear shift schedule was optimized. Clearly, with an optimized gear shift schedule, higher BTE points can be utilized. Figure VI.A.4.12 shows progressive fuel consumption reductions for the target 2.2 L multimode GCI engine, GCI + biofuel iB25, a downsized 1.5 L GCI engine, and P2 hybrid cases. The multimode 2.2 L GCI engine can achieve a 16% fuel economy improvement over the baseline SI engine, higher than the improvement target of 15%. By using iB25 biofuel, the fuel economy improvement is increased to 18%. Downsizing the GCI engine to 1.5 L results in about 30% fuel economy improvement over baseline SI engine. With the downsized engine and P2 full hybrid, the fuel economy can then be improved by 76%. The results indicate the significant potential of fuel economy improvement possible with this multimode GCI engine.

[3] In the P2, the electric machine is side-attached (through a belt) or integrated between the internal combustion engine and the transmission.

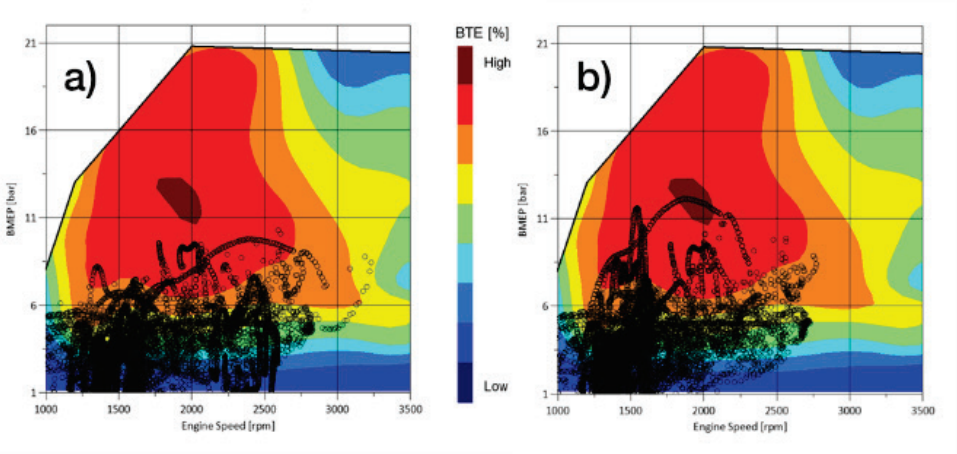

Figure VI.A.4.11 FTP-75 residence plots over BTE contour for (a) a multimode GCI 2.2 L engine and (b) gear optimization

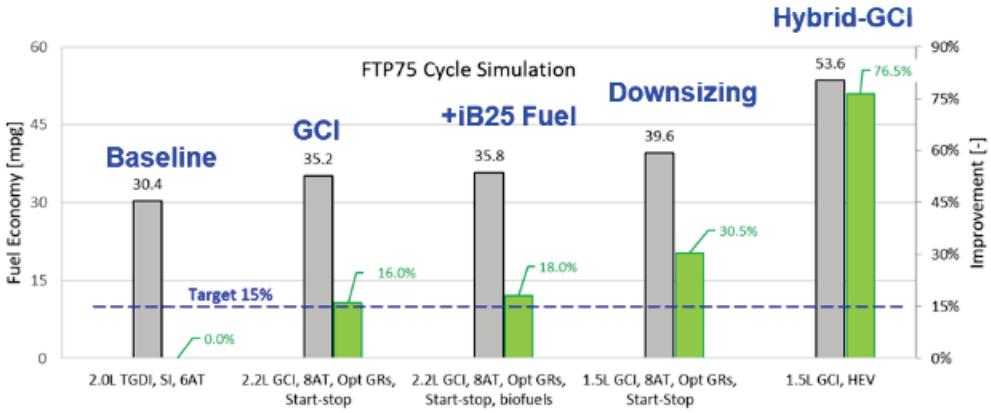

TGDI – turbocharged gasoline direct injection; 6AT – six-speed automatic transmission; 8AT – eight-speed automatic transmission; Opt GRs – optimized gear ratios; HEV – hybrid electric vehicle

Figure VI.A.4.12 FTP-75 fuel consumption improvement with technology progression

Conclusions

The project designed a multimode engine and control system, including model-based combustion controllers and a mode-switching controller. The team developed and tested the proposed multimode GCI engine, which is capable of SI, LTC, and GCI modes. Combustion strategies were determined and successfully used to operate the engine within different modes and to switch between combustion modes. Nine different fuel formulations with RONs ranging from 60 to 90 were blended and tested, including bio-gasoline blends with ethanol and iso-butanol. The fuel blend of 25% iso-butanol and 75% P66 RON 60 (iB25) with calculated RON 77.8 appears to be the best candidate for multimode GCI operation in extending GCI low load limit, maintaining good engine startability and having optimal efficiency–emissions trade-offs. The project team demonstrated that this multimode GCI engine is feasible and capable of achieving a 16% improvement, or 18% with co-optimized fuel iB25, in fuel economy compared to the production SI engine over a simulated FTP-75 cycle while also meeting the ULEV70 standard. Additionally, the team created a spray and combustion database with a high-pressure DI system with high-reactivity gasoline (60–90 RON) and biofuel blends under engine-like operating conditions. The database was used in the CFD spray model. The real fuel model can represent fuel physical properties and chemical kinetics of a real fuel. A physics-based CFD engine model was then built and validated for multimode combustion simulations with different fuels.

Key Publications

1. Zhu, S., N.R. Joo, J. Hollowell, K.Y. Ha, M. Shirley, N. Fantin, and M. Wagh. 2022. "Low Temperature Combustion Exploration with Negative Valve Overlap." SAE Technical Paper 2022-01-0452.

2. Zhu, S., and J. Naber. 2022. "Co-Optimized Mixed-Mode Engine and Fuel Demonstrator for Improved Fuel Economy while Meeting Emissions Requirements." For the U.S. Department of Energy, DOE-HATCI-08478. doi:10.2172/1887341.

References

1. Zyada, A., J. Hollowell, M. Shirley, N. Fantin, S. Zhu, N.R. Joo, and P. Zoldak. 2021. "Demonstration of Better than Diesel Efficiency and Soot Emissions Using Gasoline Compression Ignition in a Light Duty Engine with Fuel Pressure Limitation." SAE Technical Paper 2021-01-0518.

Acknowledgements

The authors would like to recognize the support of National Energy Technology Laboratory officer Michael Ursic, as well as Kevin Stork, Ken Howden, and Gurpreet Singh of the U.S. Department of Energy Vehicle Technologies Office.

Additionally, the authors would like to acknowledge several colleagues at MTU: Professor Youngchul Ra and support staff, in particular Henry Schmidt, Dr. Jeremy Worm, and graduate students Zach Stanchina and Ashwin Purushothaman. We would also like to recognize Dr. Yu Shi and Dr. Brad M. Taylor from Phillips 66 and Dr. Chris Kolodziej from Argonne National Laboratory for providing fuel formulation support, and Dr. Willy de Ojeda and Audrius Brazauskas from WM International Engineering for controls system support.

Finally, we thank all the HATCI team members who supported the project, including (but not limited to) Lisa Philip, Dr. Philip Zoldak, Mark Shirley, Dr. Antowan Zyada, Mark Bourcier, Dr. Nahm Roh Joo, Dr. Kyoung Pyo Ha, Jeff Hollowell, Nick Fantin, Randy Stram, Dave West, Mayuri Wagh, and Frank Lamborghini.

VI.A.5 Co-Optimization of Fuel Physical/Chemical Properties and Combustion System for Mixing Controlled Compression Ignition (MCCI) in a Medium-Duty Engine (Oak Ridge National Laboratory)

Flavio Dal Forno Chuahy, Principal Investigator
Oak Ridge National Laboratory
2360 Cherahala Boulevard
Knoxville, TN 37932
Email: dalfornochuf@ornl.gov

Corey Trobaugh, Co-Principal Investigator
Cummins Inc.
1900 McKinley Avenue
Columbus, IN 47201
Email: corey.trobaugh@cummins.com

Kevin Stork, DOE Technology Manager
U.S. Department of Energy
Email: Kevin.Stork@ee.doe.gov

Start Date: March 29, 2022 End Date: September 30, 2023
Project Funding: $312,500 DOE share: $250,000 Non-DOE share: $62,500

Project Introduction

This program will develop a fundamental understanding of how fuel physical and chemical properties affect mixing-controlled compression ignition (MCCI) combustion in a medium-duty engine through computational fluid dynamic (CFD) simulations. Simulations will be used to study the combined effect of fuel properties, fuel system characteristics (e.g., injector included angle, rail-pressure, nozzle protrusion, injection duration, etc.), and piston bowl geometry to find synergies between them, such that the fuel system/piston bowl design can be co-optimized for a particular fuel composition. This program will fill the knowledge gap about the quantitative effects that fuel physical and chemical properties have on engine performance towards building an MCCI fuel merit function.

The central fuel hypothesis approach of the U.S. Department of Energy Co-Optima (Co-Optimization of Engines and Fuels) program has worked well for spark-ignition fuels; identifying critical fuel properties ranges is sufficient to screen fuel blends that are expected to maximize efficiency and reduce pollutant emissions. However, for MCCI fuels, the information gained from past studies in the literature is not sufficient to build a merit function and perform a similar screening of fuel blends. In this program, Cummins/Oak Ridge National Laboratory will jointly identify and define a range of optimal fuel physical properties and co-optimize fuel properties and injector geometry for two piston bowl geometries through a comprehensive CFD simulation study and the use of machine learning techniques (e.g., Gaussian process regression modeling). Given that simulations allow physical properties to be changed independently of chemical composition, the co-optimization of fuel physical properties, injector geometry and piston geometry will be conducted for two different fuel chemical compositions: (1) a high aromatic paraffinic fuel representative of an ASTM D975 diesel fuel, (2) a low aromatic paraffinic fuel representative of renewable diesel (i.e., EN15940). This program directly addresses the current lack of knowledge regarding fuel properties for MCCI engines and an industry-identified knowledge gap. Through CFD simulations, the proposed plan is set to gather information on the sensitivity of MCCI combustion to a variety of key fuel physical properties for three relevant chemical compositions, as well as the combined effects of fuel properties, fuel system design, and bowl geometry. The

combined fuel/fuel system/piston bowl geometry effect addresses the possible synergy that the injection system geometry can have on the quantitative impacts of fuel properties in MCCI combustion.

Objectives

Overall Objective

- Co-optimize the combustion chamber geometry, injector geometry, and fuel physical properties for two diesel fuel chemistries, conventional diesel and hydrotreated vegetable oil (HVO), subject to emissions and mechanical limit constraints for improved engine thermal efficiency.

Fiscal Year 2022 Objectives

- Define fuel property ranges of interest for conventional diesel and HVO.
- Couple and test optimizer with CAESES and CONVERGE CFD engine model to establish workflow.
- Define operating condition of interest for optimization.
- Discretize piston bowl shape geometry for automatic geometry generation.

Approach

This project combines an advanced global optimizer (DAKOTA), a CFD geometry and case management software (CAESES), and detailed combustion CFD (CONVERGE) to co-optimize the engine geometry, injector geometry and fuel properties (Figure VI.A.5.1). DAKOTA uses an efficient global optimizer to search the design space for the optimal solution. The algorithm uses a Gaussian process regression model as a global surrogate for the response surface such that it can use special functions to intelligently select conditions for further investigation in the design space. DAKOTA does this by defining an expected improvement function that is used to define the location of the new training points that need to be run in CFD to maximize the improvement of the objective function. The goal of the optimization will be to optimize engine gross thermal efficiency. CAESES uses the information generated by DAKOTA to automatically generate new geometries and change CFD input files. CAESES runs the CONVERGE CFD cases that DAKOTA selected and post processes the outputs of the combustion simulation such that the data can be fed back to DAKOTA for the next round of training points. The result is a surrogate model of the system that becomes more accurate as the optimization continues. The optimization stops when the expected improvement function calculated by DAKOTA is below a certain defined threshold. That is, the optimizer thinks adding more information to the response surface will not generate further response improvements.

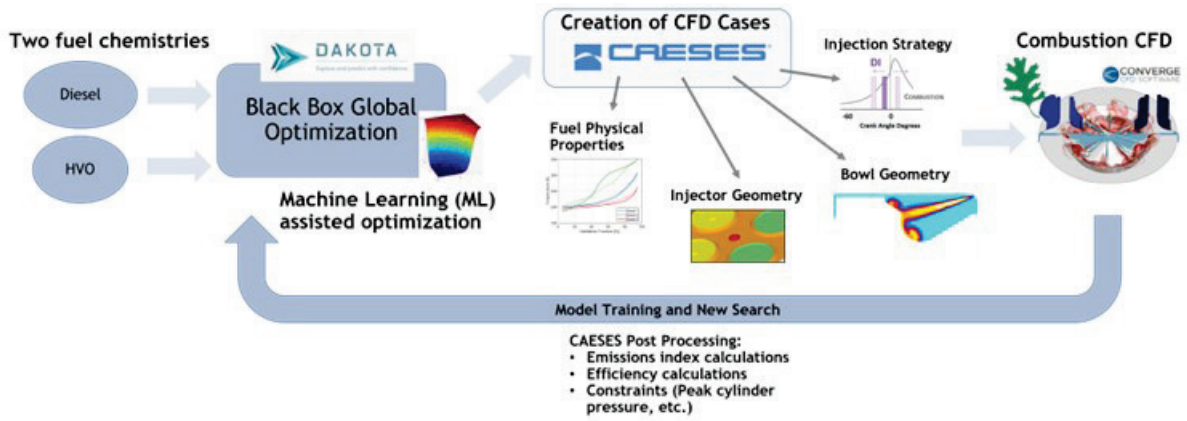

DI – direct injection

Figure VI.A.5.1 Optimization workflow identifying each step and information dependencies

As mentioned previously the objective function will be the engine gross thermal efficiency but emissions indexes like nitrogen oxides, unburned hydrocarbons and soot will also be monitored in addition to other engine mechanical limits such as peak cylinder pressure.

Results

- Established framework to couple CAESES and CONVERGE CFD to generate new geometries and automate the CFD case generation process.
- Defined and tested workflow in DAKOTA to couple advanced global optimizer with CAESES and CONVERGE.
- Defined piston bowl discretization scheme to allow generation of a wide variety of piston bowls. Figure VI.A.5.2 show examples of bowl profiles that can be generated by CAESES and how the bowl shape was discretized. The bowl was discretized into 10 control parameters. Seven of those parameters are used as independent variables for determining the bowl shape. Three parameters Dr, Da and Tm are used to adjust the total bowl volume such that the compression ratio of the combustion chamber can be specified as an independent variable. The variable Dr represents the total bowl diameter, Da represents the inner bowl diameter and Tm represents the distance between the central bowl pip and the cylinder head. With the established discretization scheme any relevant piston geometries can be created.

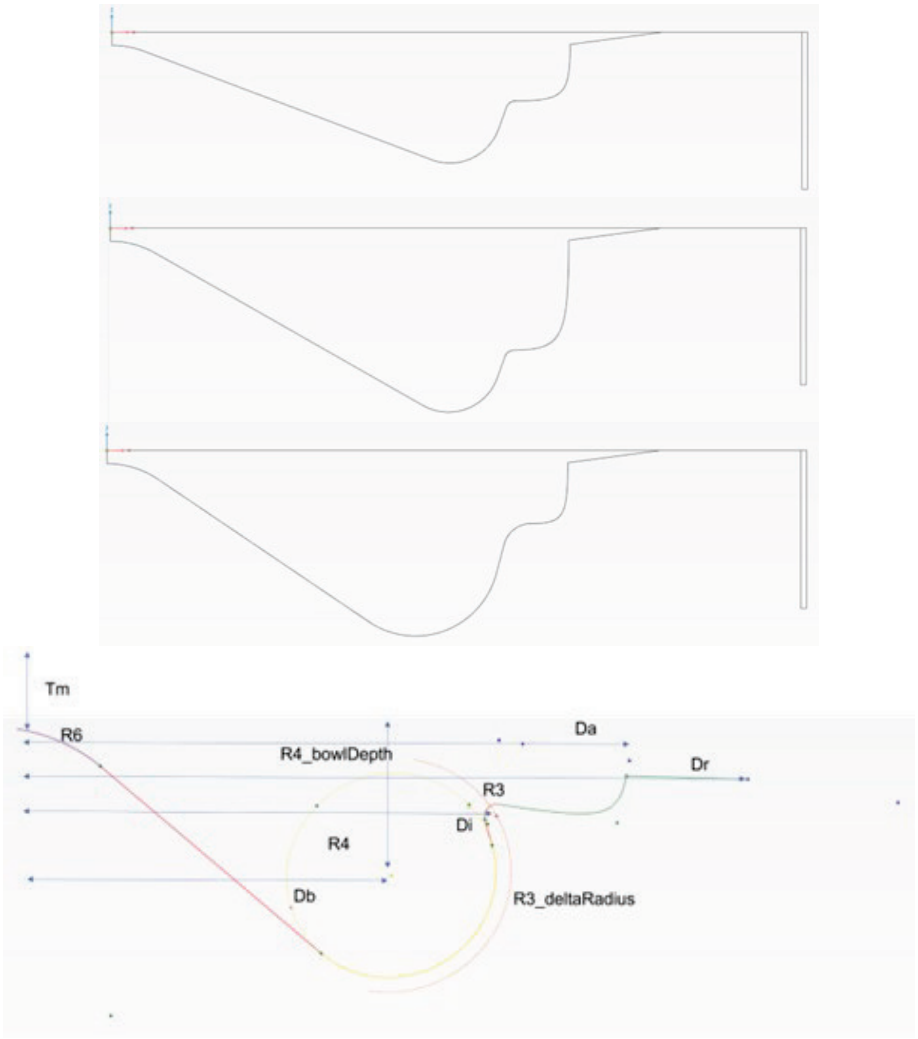

Figure VI.A.5.2 Example of bowl shapes generated by CAESES and bowl discretization scheme

- Defined optimization point of interest of 1,600 rpm engine speed and 400 lb-ft of torque based on duty-cycle analysis.
- Gathered validation data for optimization point of interest.
- Defined HVO composition and relevant fuel properties for surrogate definition shown in Figure VI.A.5.3. The carbon composition and distillation curves will be used to determine appropriate chemical surrogate compositions for the simulation effort. As expected, the HVO fuel is composed mostly of long chain branched paraffins and contains very little of other components. Figure VI.A.5. 4 shows the comparison between the *distillation* curves of HVO and conventional diesel. The highly paraffinic composition of HVO makes its distillation curve flat and overall less volatile than conventional diesel at boiling fractions below 50%. However, the final boiling point of conventional diesel is approximately 100°F higher than HVO, influenced by the large high boiling point species present in conventional diesel fuel. These differences in boiling characteristics are expected to play a role in the optimization of the combustion chamber and result in different optimal bowl shapes.

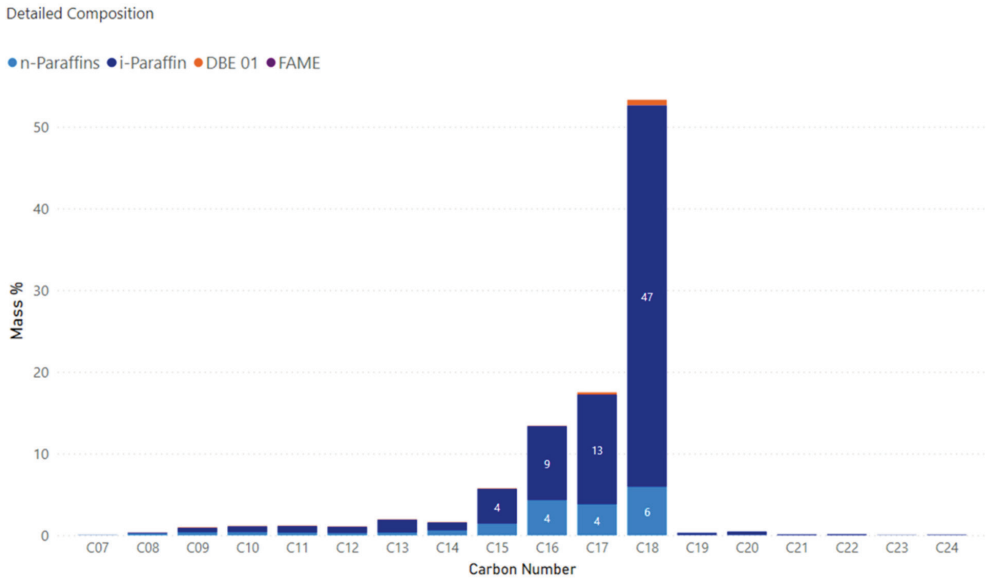

Figure VI.A.5.3 Paraffin, isoparaffin, olefin, naphthene and aromatic hydrocarbon composition of commercial HVO fuel

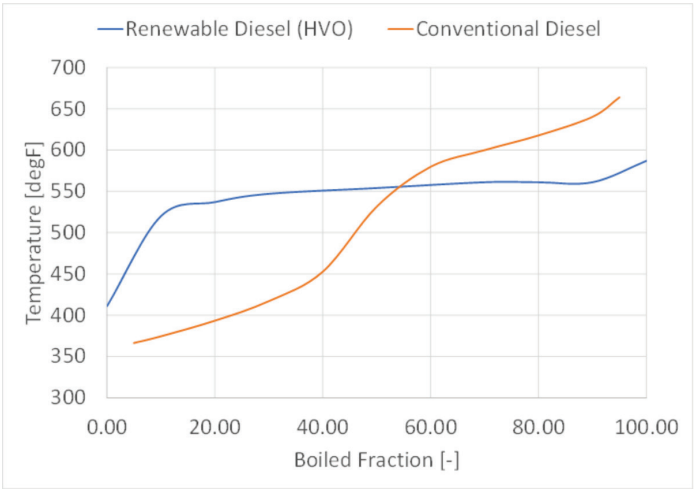

Figure VI.A.5. 4 Comparison between distillation curves of conventional diesel and renewable diesel (HVO)

Conclusions

- Optimization operating condition has been defined based on duty-cycle analysis of Cummins in-use data.
- Optimization workflow has been established and is in final stages of testing for the start of the first optimization set using conventional diesel fuel. Three software packagess are being coupled to achieve the desired results. DAKOTA is using an advanced optimizer to drive CAESES the CFD management software to generate new CONVERGE cases and post process the data.
- Ranges of independent variables have been established for the optimization effort based on experimental measurements of available fuels in the marketplace.
- Fuel properties for conventional diesel and HVO have mostly been gathered. Surrogate development for HVO will begin soon.

Key Publications

1. Chuahy, F.D.F., C. Trobaugh. 2022. “Co-Optimization of Fuel Physical/Chemical Properties and Combustion System for Mixing Controlled Compression Ignition (MCCI) in a Medium-Duty Engine.” U.S. Department of Energy Vehicle Technologies Office Annual Merit Review meeting, June.

VI.A.6 Independent Fuel Property Effects of Fuel Volatility on Low Temperature Heat Release and Fuel Autoignition (Argonne National Laboratory)

Sibendu Som, Principal Investigator
Argonne National Laboratory
9700 South Cass Avenue
Lemont, IL 60439
Email: ssom@anl.gov

James Szybist, Principal Investigator
Oak Ridge National Laboratory
Email: szybistjp@ornl.gov

Allen Aradi, Principal Investigator
Shell Global Solutions
Email: allen.aradi@shell.com

Chao Xu, Principal Investigator
Argonne National Laboratory
Email: cxu@anl.gov

Kevin Stork, DOE Technology Manager
U.S. Department of Energy
Email: Kevin.Stork@ee.doe.gov

Start Date: April 8, 2022 End Date: October 8, 2023
Project Funding: $315,000 DOE share: $250,000 Non-DOE share: $65,000

Project Introduction

In prior studies, Shell Global Solutions (Shell) researchers observed that volatile fuels suppress low-temperature heat release (LTHR) more than expected based on the conventional gasoline autoignition metrics research octane number (RON) and motor octane number (MON). The role of LTHR contributes to autoignition phenomena for both boosted spark ignition (BSI) and advanced compression ignition (ACI) combustion modes. ACI combustion modes are applicable to larger, hard-to-electrify engine applications such as off-road, rail, and marine. Thus, having a reliable understanding of autoignition phenomena, including being able to accurately account for the effects of fuel volatility, is particularly important as new synthetic and bio-fuel compositions are considered.

This Cooperative Research and Development Agreement (CRADA) project between Argonne National Laboratory (ANL), Oak Ridge National Laboratory (ORNL), and Shell will develop a foundational understanding of this phenomenon with the aim of volatility being developed as an independent property to optimize fuel blends for higher efficiency with increased biofuel content for BSI and ACI engines. We hypothesize the decreased LTHR is due to preferential evaporation of multicomponent fuels when using direct injection (DI) fueling technology, creating composition and reactivity stratification. This project brings together fuel blending expertise at Shell, unique experimental measurements of LTHR in engines at ORNL, and high-fidelity engine simulations at ANL. Together, this team will fill this knowledge gap, prove or disprove our hypothesis, and determine the extent to which this phenomenon could be leveraged to optimize future fuels and engine designs.

Objectives

Overall Objectives

- Quantify the effects of fuel volatility as an independent fuel property on LTHR both experimentally and numerically.
- Prove or disprove the hypothesis that preferential evaporation of volatile components in DI engines produces reactivity stratification such that the less reactive volatile components govern the overall reactivity.

Fiscal Year 2022 Objectives

- Finalize the CRADA document and kick off the project.
- Develop and blend a set of fuels designed to test the hypothesis that preferential evaporation of volatile fuel components in DI engines produces reactivity stratification such that the less reactive volatile components govern the overall reactivity.
- Conduct a series of a priori computational fluid dynamics (CFD) simulations to test the differences between single- and multi-component evaporation models on LTHR.

Approach

This project takes a combined experimental and modeling approach to test the hypothesis that preferential evaporation of volatile fuel components in DI engines produces reactivity stratification such that the less reactive volatile components govern the overall reactivity. This approach has three major components: (1) a custom fuel set designed collaboratively among the project partners and blended by Shell, (2) single-cylinder engine experiments conducted at ORNL to directly measure LTHR, and (3) CFD simulations at ANL.

The fuel matrix consists of six matched-pair fuel blends that have nearly identical fuel compositions but have different volatility, as measured by Reid Vapor Pressure (RVP), with a high-volatility (HV) blend and a low-volatility (LV) blend. The matched-pair fuels contain blending components identified during the Co-Optima initiative as promising biofuel components with favorable fuel properties: aromatics, ethanol, prenol, diisobutylene (DIB), and cyclopentane (CPT). The fuels were blended by Shell in the facility located at Hamburg, Germany, using full boiling curve, and shipped to ORNL for experimental studies.

The fuels will be investigated experimentally in a single-cylinder BSI research engine at ORNL using a methodology developed during the Co-Optima initiative that can temporally separate the LTHR event from the main deflagration heat release event [1]. Each fuel will be investigated using both DI fueling as well as port fuel injection upstream of the engine. Port fuel injection should produce a more homogeneous mixture to minimize the effect of preferential evaporation, whereas the DI fueling will maximize this effect. Also, the fuels will be tested under both stoichiometric and fuel-lean conditions to have relevance to both BSI and ACI operating conditions.

A previously developed and validated CFD model [2] for the ORNL engine developed under Co-Optima has been improved to account for preferential evaporation effects. In this CFD model, a hybrid approach that incorporates the G-equation model for tracking the turbulent flame front, and the well-stirred reactor model with detailed chemistry for predicting low-temperature reactions in the unburnt gas, was employed to predict the outcome of the turbulent combustion in the engine cylinder. A multi-component evaporation model is used, where lighter liquid fuel components evaporate into corresponding gaseous molecules first, in contrast to the single-component evaporation model used in the previous CFD model assuming all fuel components evaporate together. As an a priori study to understand volatility effects, multi-cycle simulations were conducted using the Co-Optima alkylate fuel at an operating condition from the Co-Optima program. Effects of differential evaporation on liquid fuel properties such as viscosity, heat of vaporization, vapor pressure, surface tension, density, and specific heat, as well as on gaseous mixture compositions, are quantified by comparing simulation

results from the single-component and multi-component evaporation models. The dynamics of LTHR were further analyzed in detail, investigating the in-cylinder pressure and heat release rate traces.

Results

Shell blended six matched-pair fuels (6 LV fuels + 6 HV fuels) and shipped them to ORNL. HV fuels were prepared by blending light ends (butanes/butenes) into the respective LV fuel to give a 2 psi increase in RVP. Shell provided key fuel properties, as well as detailed hydrocarbon analysis data to assist engine testing and CFD modeling. Key fuel properties and fuel composition differences are shown in Table VI.A.6.1 with the blue and red highlighting the low- and high-volatility blends, respectively, and the green highlighting the major blend component.

Table VI.A.6.1 Matrix of Custom Fuel Blends Produced by Shell Global Solutions and Sent to ORNL

	Aromatic		Ethanol		Prenol		Diisobutylene		Cyclopentane		Carbonate	
	LV	HV	LV	HV	LV	HV	LV	HV	LV	HV	LV	HV
RON (-)	98.2	97.8	99.8	99.8	97.9	98	97.7	97.6	97.5	97.7	96.8	96.8
MON (-)	89.4	90	89.6	89.7	87.4	87.5	88.5	88.5	88.3	88.8	89.5	89.7
RVP (kPa)	51.6	78	55.3	75.5	49.8	75.8	52.4	76.3	59.2	75.5	51	76.5
Aromatic (vol%)	20	20	10	10	10	10	10	10	10	10	10	10
Ethanol (vol%)	0	0	10	10	0	0	0	0	0	0	0	0
Prenol (vol%)	0	0	0	0	10	10	0	0	0	0	0	0
DIB (vol%)	0	0	0	0	0	0	10	10	0	0	0	0
CPT (vol%)	0	0	0	0	0	0	0	0	10	10	0	0
Carbonate (vol%)	0	0	0	0	0	0	0	0	0	0	10	10

The fuel blends have been delivered to ORNL and are shown in Figure VI.A.6. 1. Experiments will commence during the first quarter of 2023.

Figure VI.A.6. 1 Custom fuel blends from Shell Global Solutions delivered to ORNL

Figure VI.A.6.2 shows the in-cylinder pressure and apparent heat release rate obtained from multi-cycle CFD simulations for the alkylate fuel from the Co-Optima initiative for an LTHR engine operating condition with strong pre-spark heat release. Results from two evaporation models, namely the single-component evaporation model and multi-component evaporation model, are compared. It is shown that, using the multi-component evaporation model, the intensity of predicted LTHR is higher than that from the single-component evaporation model. This a priori LTHR study on a non-Shell fuel suggests that the preferential evaporation effects play a non-negligible role in predicting LTHR.

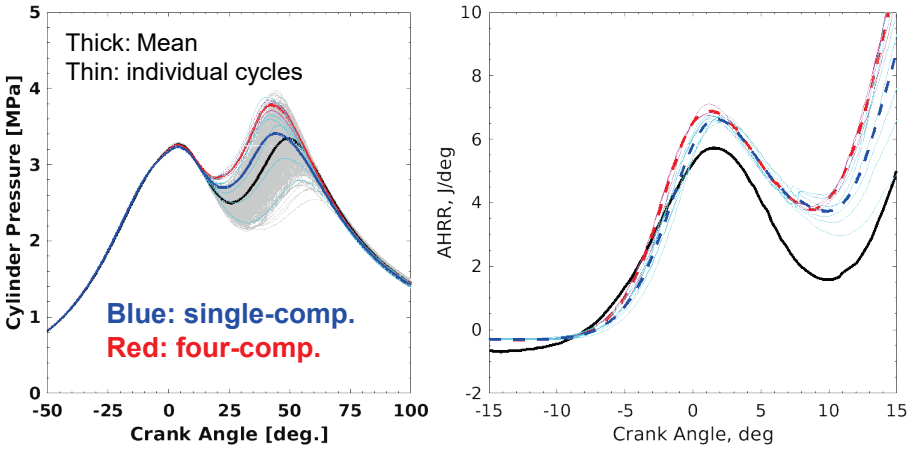

Figure VI.A.6.2 In-cylinder pressure and heat release rate predicted by CFD using single-component and multi-component evaporation models, respectively

Conclusions

- A CRADA project was started among Shell, ANL, and ORNL to investigate the independent role of fuel volatility, as measured by RVP, on LTHR and autoignition processes. The hypothesis is that preferential evaporation causes the most volatile components to dominate the autoignition process in both BSI and ACI engines with DI fueling.
- A set of custom fuels to investigate this phenomenon was designed, blended by Shell, and delivered to ORNL. Experiments will begin in early 2023.
- An improved CFD model accounting for multi-component evaporation was developed in this study, allowing better prediction of pre-spark heat release under LTHR engine operating conditions.

References

1. Szybist, J.P., and D.A. Splitter. 2017. “Pressure and Temperature Effects on Fuels with Varying Octane Sensitivity at High Load in SI Engines.” *Combustion and Flame* 177: 49–66. doi:10.1016/j.combustflame.2016.12.002.

2. Guo, H., R. Torelli, J.P. Szybist, and S. Som. 2021. “CFD Modeling of Pre-Spark Heat Release in a Boosted Direct-Injection Spark-Ignition Engine.” *International Journal of Engine Research*. doi:10.1177/14680874211044110.

Acknowledgements

This research was conducted as part of the Co-Optimization of Fuels & Engines (Co-Optima) project sponsored by the DOE Office of Energy Efficiency and Renewable Energy, Bioenergy Technologies, and Vehicle Technologies Offices. The authors wish to thank Gurpreet Singh, Kevin Stork, Michael Weismiller, and Alicia Lindauer, technical managers at DOE, for their support.

This research was funded by DOE’s Office of Vehicle Technologies and Office of Energy Efficiency and Renewable Energy under Contract No. DE-AC02-06CH11357.

The principal investigators gratefully acknowledge the contributions of Dr. Hengjie Guo for the CFD simulation work on the ORNL engine.

The authors would also like to acknowledge the Laboratory Computing Resource Center at ANL for computing time on the Bebop cluster, which was used in this research.

VI.B Alternative Fuel Engines

VI.B.1 Dynamic Skip Fire (DSF) on a Heavy-Duty Natural Gas Engine (Cummins Inc.)

Jay Shah, Principal Investigator
Cummins Inc.
P.O. Box 3005
Columbus, IN 47201
Email: jay.shah@cummins.com

Kevin Stork, DOE Technology Manager
U.S. Department of Energy
Email: Kevin.Stork@ee.doe.gov

Start Date: May 5, 2021 End Date: February 28, 2025
Project Funding: $5,982,508 DOE share: $3,750,000 Non-DOE share: $2,232,508

Project Introduction

Spark-ignited engines inherently suffer efficiency losses at part load because of throttling to maintain stoichiometric operation. A significant fraction of the drive cycle and real-world usage of medium- to heavy-duty engines is in the low load region during which the engine is relatively inefficient. The current state-of-the-art heavy-duty natural gas engines have a sharp rise in brake-specific carbon dioxide (CO_2) emissions as the average power of the duty cycle decreases. Standard cylinder deactivation (CDA) solutions can partly improve low load efficiencies by deactivating a fixed number of cylinders, but for several reasons, these techniques are severely limited in their applicability over a wide speed/load range. This project will develop Dynamic Skip Fire (DSF®) on a heavy-duty (HD) natural gas (NG) engine. DSF enables the engine to dynamically deactivate any of the cylinders to minimize the amount of pumping losses during the gas exchange in and out of the cylinders while producing the required torque, and without compromising on noise, vibration, and harshness (NVH) vehicle-driving targets. This NG engine will significantly improve engine operating efficiency while delivering diesel-like performance. This work will enhance the commercial viability of NG engines as a low-carbon-emitting bridge technology as the transportation sector transitions to zero-emission vehicles.

Objectives

The objective of the project is to develop and demonstrate a DSF-enabled, HD NG engine capable of diesel-like performance and efficiency, as identified in the following bullets:

- Ramped Modal Cycle Supplemental Emissions Testing (RMCSET) (tractor) certification cycle average brake thermal efficiency of greater than 40%.
- Heavy-duty federal test procedure (HD-FTP vocational) certification cycle average brake thermal efficiency of greater than 38.5%.
- High average power or heavy heavy-duty diesel truck (HHDDT) cycle average brake thermal efficiency of greater than 39%.
- Urban dynamometer driving schedule cycle average brake thermal efficiency of greater than 38%.
- Light loaded drive cycle or port drayage cycle average brake thermal efficiency of greater than 30%.
- All of the above while maintaining the capability to meet 0.02 g/hp-hr nitrogen oxides (NO_x) emissions.

Fiscal Year 2022 Objectives

In Fiscal Year 2022, the project team is on track to complete the requirements of Budget Period 1. Key objectives were to develop the engine overhead layout; design overhead and CDA components; and design, analyze, and simulate engine models to define control system requirements and drive cycle simulation. The focus was on hardware design of the overhead components (the cylinder head, advanced valvetrain, CDA actuators, etc.), development of the control system requirements and interfaces, and engine model development for simulation. The engine model was used to simulate engine operation with DSF to assess the impact of DSF on base engine controls, as well as to develop algorithms. Baseline engine data for the HD NG engine was used to develop the initial DSF firing frequency map.

Approach

- The Cummins-Tula team is to build on the Cummins next-generation HD NG engine being developed by Cummins. Development of this engine is jointly funded by the Natural Gas Vehicles Consortium under Subcontract #NHQ-9-82305-03, administered by the National Renewable Energy Laboratory.
- Analysis and limited component testing will be conducted to establish the detailed component design and fractional firing strategies for the engine.
- Engine and aftertreatment controls will be developed to ensure proper integration of DSF algorithms.
- Selected hardware and software will be validated on a rig.
- A multicylinder engine with DSF will be built for engine and aftertreatment testing, calibration, and certification.
- Finally, the calibrated engine and controller will be installed in a vehicle for NVH and real-world fuel economy, performance, and emissions evaluation.

Results

Engine cylinder head and overhead components design was completed to accommodate an advanced valvetrain that includes all the required components for CDA, variable valve timing, and compression release engine brakes functionality. The design uses a Type III valvetrain system with dual overhead camshafts and independent cam phasing. The complete valvetrain system is shown in Figure VI.B.1.1.

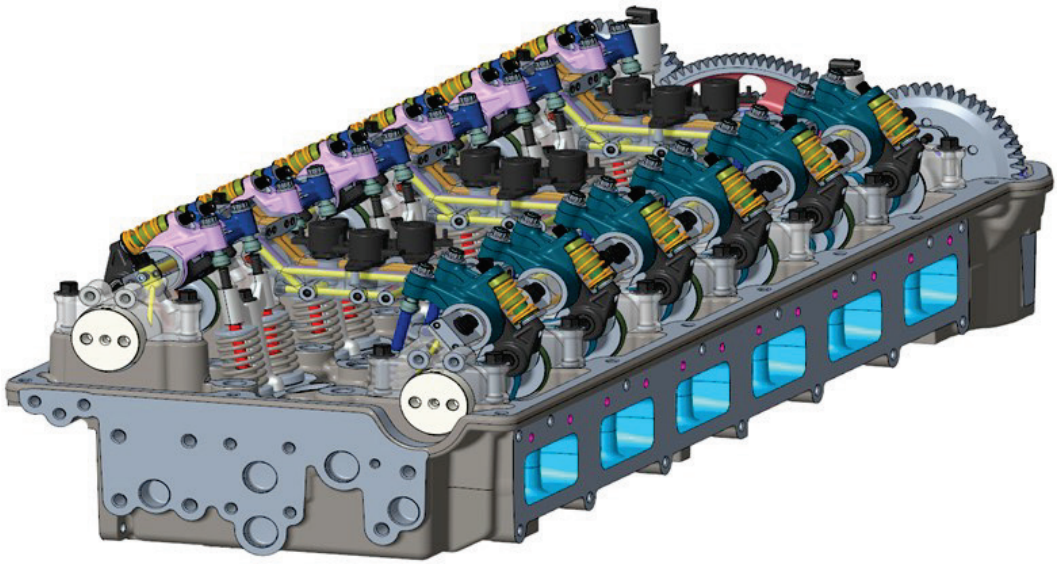

Figure VI.B.1.1 Head and overhead assembly

This valvetrain architecture utilizes a collapsing rocker technology to achieve CDA and 1.5 stroke brake (SB) operation modes as shown in Figure VI.B.1.2. The lost motion of the collapsing rocker is achieved through the "Wedgelock" capsule. Standard, CDA, and braking modes are switched hydraulically with oil control valves. The 1.5 SB is an engine brake technology that retains the normal intake valve lifts but deactivates the main exhaust valve lifts and adds multiple valve lift events on the exhaust side to increase braking power over traditional compression release brakes. Analysis results from a benchmarked product predict that 1.5 SB technology can enable diesel-like power targets.

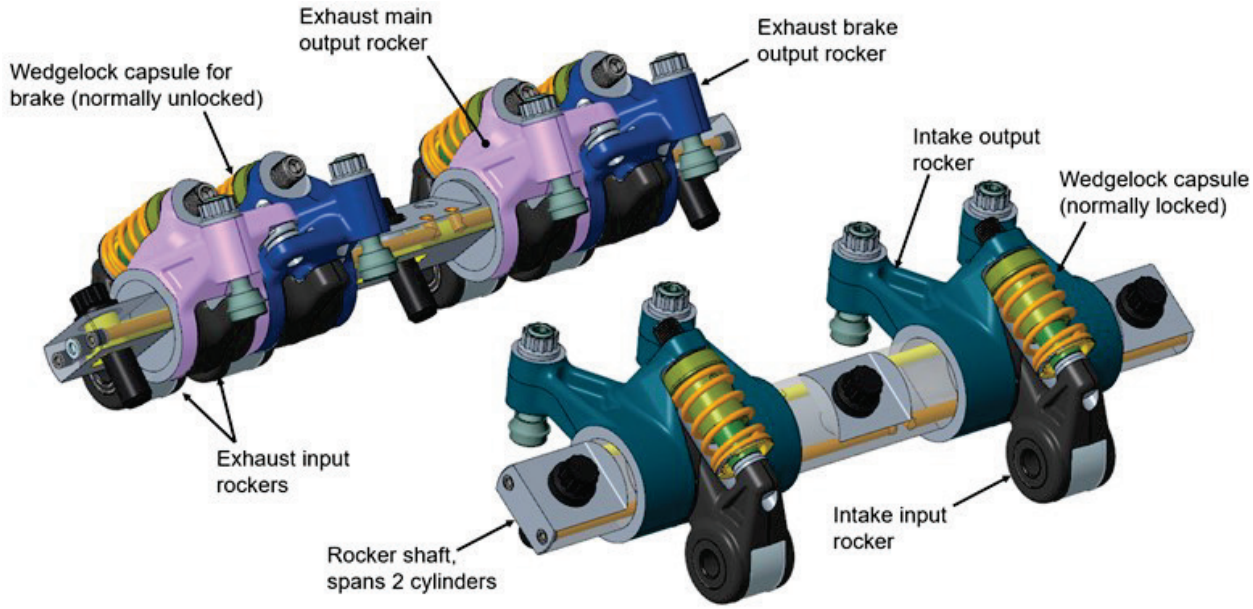

Figure VI.B.1.2 Valvetrain architecture

Figure VI.B.1.3 shows the operating modes of the exhaust rocker assembly during each mode of operation. Both input rocker arms are kept in constant contact with the cam lobe and therefore are either articulating in normal operation or in lost motion. When the Wedgelock capsule is unlocked, it experiences lost motion and therefore will not transfer any motion to the corresponding output rocker.

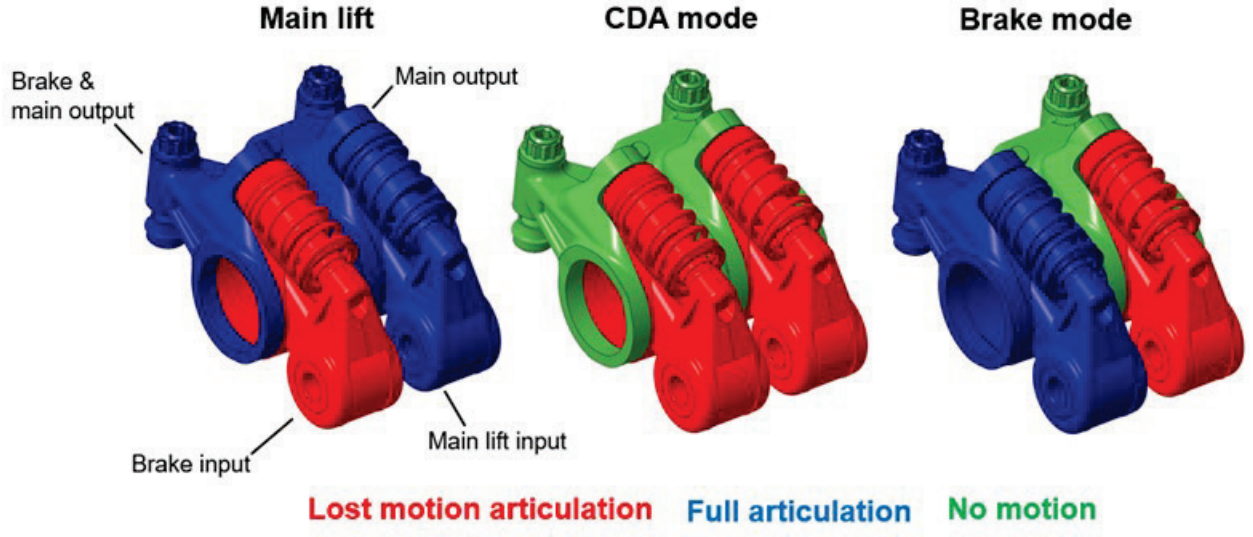

Figure VI.B.1.3 Exhaust rocker modes of operation

Simulation studies show DSF operation to about 5 bar brake mean effective pressure (BMEP) with up to 40% fuel benefit as shown in Figure VI.B.1.4. Simulations were also run to predict CO_2 benefits with deceleration cylinder cut-off (DCCO) upside up to 10% on the HD-FTP and RMCSET cycles as well as the chassis low load cycle and drayage cycles as shown in Table VI.B.1.1.

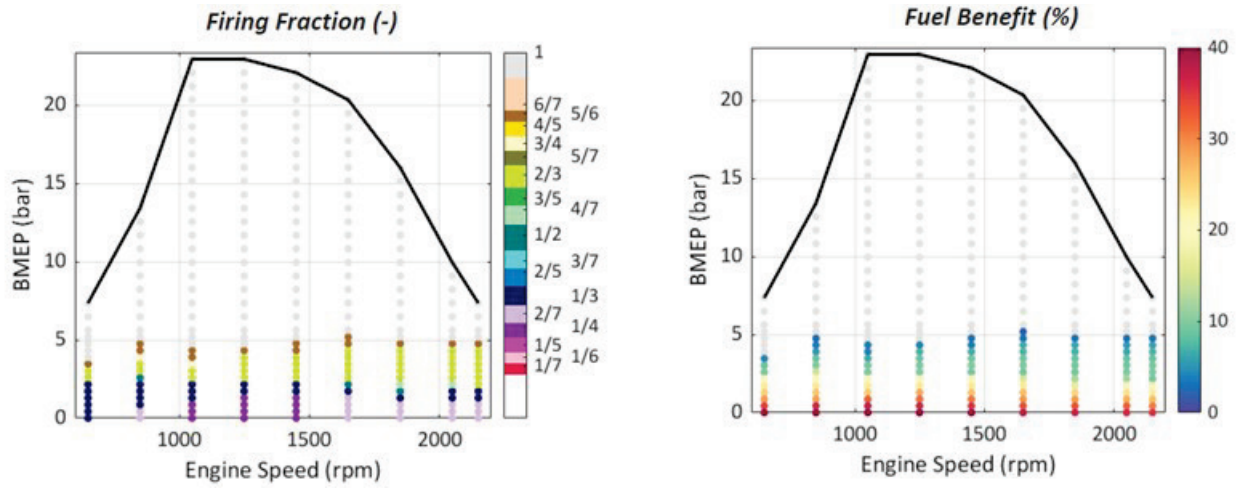

Figure VI.B.1.4 Firing fraction and fuel benefit maps

Table VI.B.1.1 Cycle CO_2 benefits with DSF

ΔCO_2 vs Baseline	DSF, with NVH limits and DCCO potential upside (%)
HD-FTP	-4.0
HD RMCSET	-0.7
POLA Drayage	-10.3
UDDS	-5.1
HHDDT	-4.6

POLA – Port of Los Angeles; UDDS – Urban Dynamometer Driving Schedule

The team completed identification of all the control changes needed for implementation prior to engine testing and development. Air flow estimation and control, exhaust gas recirculation (EGR) control, and spark timing control are the key affected functions identified as shown in Figure VI.B.1.5.

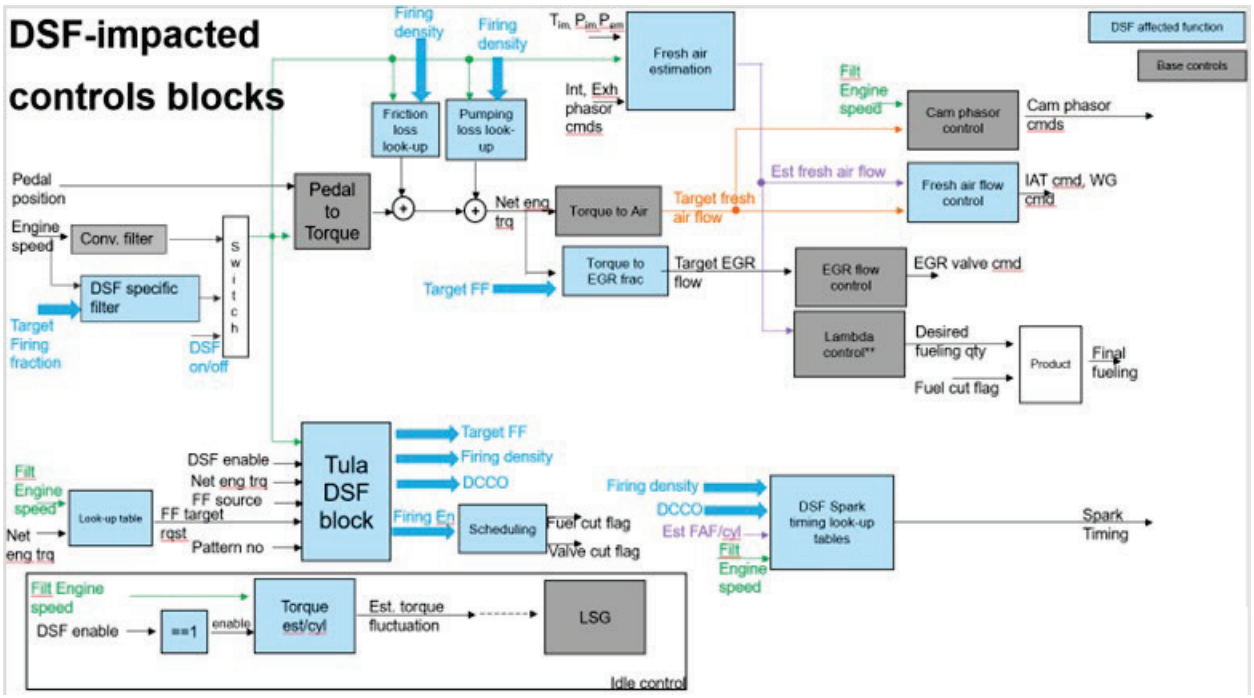

FF – feedforward; IAT – intake air throttle; WG – wastegate; FAF – fresh air flow

Figure VI.B.1.5 Controls architecture layout with DSF (DOE quarterly progress report, Q2 – July 2022)

The co-simulation environment with Simulink+ fast running model in GTPower has been set up to simulate DSF. The model can carry out steady-state and transient simulations with no observed inherent instabilities or lack of robustness. Speed-load sweeps, firing fraction sweeps, and DSF transition tests were run to observe model behavior during DSF.

Electronic hardware interfaces were defined and bench test setup is complete as shown in Figure VI.B.1.6 and Figure VI.B.1.7. Base controls logic (non-DSF) is planned to reside in the Cummins electric control module (ECM). It will drive the air handling actuators. DSF code and interactions with base controls logic will reside in the Speedgoat (SG) hardware. There will be continuous exchange of measurements and overrides between ECM and SG via XCP protocol[1] (indicated by the VX1134 box). The large engine control modules (LECMs) will drive the 12 port fuel injectors while being synchronous with the crank/cam with ECM. The cRIO hardware box will be used to drive the CDA solenoids. This box will also be synchronous with crank/cam with ECM and other scheduling functions (when to turn a particular cylinder ON/OFF) via SG. The development computer (PC) shall be used for measurement, data logging, and analysis.

[1] XCP Protocol is a Universal Measurement and Calibration protocol used for calibration and data acquisition in electronic control units, the successor of CAN calibration protocol.

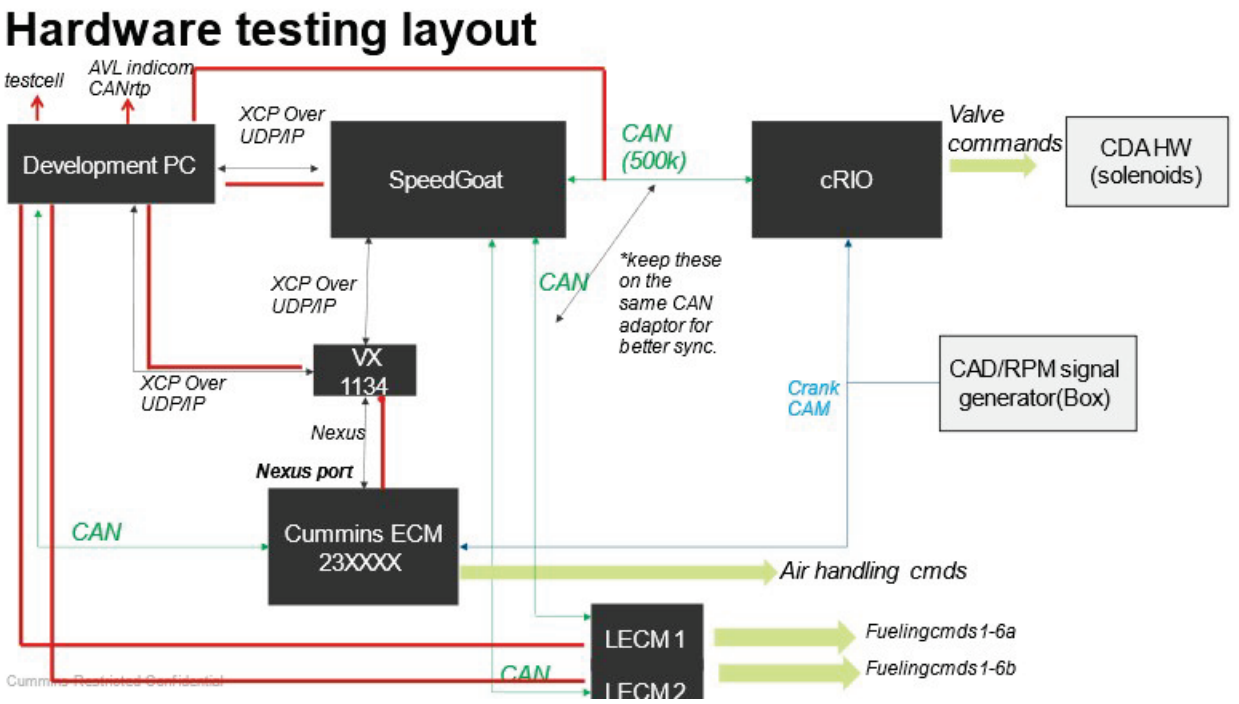

rtp – real-time transport protocol; UDP/IP – user data protocol/internet protocol; HW – hardware; CAD – crank angle degrees; RPM – revolutions per minute

Figure VI.B.1.6 Electronic hardware interfaces (DOE quarterly progress report, Q2 – July 2022)

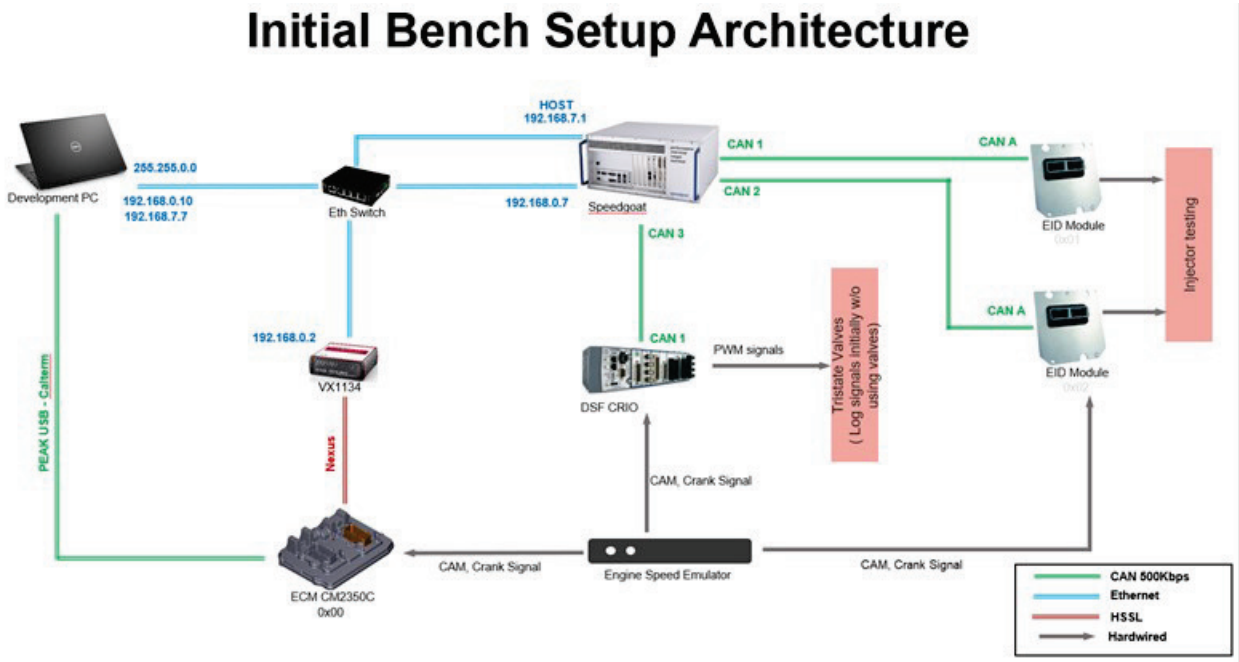

EID – electronic injector definition; PWM – pulse width modulation; HSSL – high speed serial link

Figure VI.B.1.7 Bench test setup (DOE quarterly progress report, Q2 – July 2022)

Conclusions

- The overhead architecture layout is finalized and the valvetrain design is complete.
- Simulation mapping results were generated for steady-state conditions as well as engine dynamometer and chassis dynamometer cycles.
- Control system requirements analysis and development are completed.
- Advanced valvetrain concept selection for CDA utilizing Jacobs Vehicle Systems technologies has been completed.
- Electronic hardware interfaces were defined and bench test setup is complete.

Key Publications

1. DOE quarterly progress report, Q4 – January 2022
2. DOE quarterly progress report, Q1 – April 2022
3. DOE quarterly progress report, Q2 – July 2022
4. DOE quarterly progress report, Q3 – Oct 2022

VI.B.2 Development of Advanced Combustion Strategies for Direct Injection Heavy Duty Liquefied Petroleum Gas Engines to Achieve Near-Diesel Engine Efficiency (Colorado State University)

Daniel B. Olsen, Principal Investigator
Colorado State University
Mechanical Engineering Department
Fort Collins, CO 80523-1374
Email: daniel.olsen@colostate.edu

Bret Windom, Co-Principal Investigator
Colorado State University
Mechanical Engineering Department
Fort Collins, CO 80523-1374
Email: bret.windom@colostate.edu

Hui Xu, Principal Investigator
Cummins Inc.
1900 McKinley Avenue
Columbus, IN 47201
Email: hui.xu@cummins.com

Sibendu Som, Principal Investigator
Argonne National Laboratory
9700 South Cass Avenue
Lemont, IL 60439
Email: ssom@anl.gov

Lorenzo Nocivelli, Co-Principal Investigator
Argonne National Laboratory
9700 South Cass Avenue
Lemont, IL 60439
Email: lnocivelli@anl.gov

Kevin Stork, DOE Technology Manager
U.S. Department of Energy
Email: Kevin.Stork@ee.doe.gov

Start Date: October 1, 2020 End Date: December 31, 2023
Project Funding: $4,020,092 DOE share: $3,450,085 Non-DOE share: $570,007

Project Introduction

The Vehicle Technologies Office funds research, development, demonstration, and deployment (RDD&D) of new, efficient, and clean mobility options that are affordable for all Americans. This work focuses on diversified fuel options through the development of advanced liquefied petroleum gas (LPG) engine technology. The United States maintains a substantial surplus of LPG and it is approximately 40% less expensive than gasoline and diesel. The primary goal of this research is to address fundamental limitations to achieving near-diesel efficiencies in heavy-duty on-road LPG engines. Engine knock and misfire are barriers to pathways leading to higher efficiency engines. This project explores a series of advanced combustion strategies aimed at eliminating these barriers.

Overall, the project team is making excellent progress on technical milestones. Activities include bench testing of gasoline direct injection (GDI) and modified/prototype injectors on LPG, development of computational fluid dynamics (CFD) simulation models, imaging of LPG direct injector spray patterns, and LPG testing on a Cummins 2.5-liter single cylinder engine.

Objectives

The focus of the proposed research is to address fundamental limitations to achieving near-diesel efficiencies in heavy-duty on-road LPG engines. The focus is on the Cummins 15-liter heavy-duty-engine platform, which has a baseline diesel efficiency of 44% at peak torque. The main project goal is to increase the peak torque efficiency of a 15-liter LPG engine to 44%.

Overall Objective

- Characterize flame propagation and end-gas autoignition phenomena for LPG–air–exhaust gas recirculation (EGR) mixtures of varying reactivity under engine-like conditions.
- Develop LPG direct injection (DI) strategies in parallel with a detailed LPG DI spray model for incorporation into engine simulation models.
- Validate, refine, and utilize tools for closed cycle engine combustion design with detailed chemical kinetics (CHEMKIN), three-dimensional computational fluid dynamics (CONVERGE), and cycle simulation (GT-Power).
- Develop advanced real-time control algorithms for the Cummins 2.5-liter X15 single cylinder engine (SCE) to implement LPG DI strategies and controlled end-gas autoignition (C-EGAI).

Fiscal Year (FY) 2022 Objectives

- Fabrication and delivery of Cummins X15 custom cylinder head for LPG direct injection.
- Production and spray imaging of prototype LPG direct injectors.
- Incorporation of LPG spray model into Converge CFD model and generation of initial simulation results.
- Perform LPG port fuel injection (PFI) baseline testing on Cummins X15 single cylinder engine.

Approach

This research is conducted with a combined experimental and computational approach with fundamental experiments utilizing (1) a one-of-a-kind rapid compression machine and laser ignition system that facilitates measurement of flame speed and end gas autoignition at engine like conditions; (2) a constant-volume high pressure spray chamber (HPSC) to study direct LPG fuel injection penetration, vaporization and mixing; (3) a variable compression ratio Cooperative Fuel Research engine to examine knock propensity, EGR limits, emissions tradeoffs, and C-EGAI control algorithms; and (4) a Cummins X15 single cylinder 2.5-liter heavy-duty research engine to demonstrate near-diesel engine efficiencies utilizing the final combustion/control recipe. The rapid compression machine, HPSC, and Cooperative Fuel Research experiments conducted at Colorado State University (CSU), are used to systematically validate computational modeling tools with detailed chemical kinetics, which facilitate the development of a fully validated and predictive model of the 2.5-liter Cummins platform to inform the advanced control and combustion strategies via a better understanding of the underlying in-cylinder phenomena. Development of the LPG DI model, performed at Argonne National Laboratory, is a key component of the engine simulation model. A custom cylinder head for the X15 SCE, designed and fabricated at Cummins, enables LPG direct injection.

Results

LPG DI Injector Design and Bench Testing

Engineering service contractor Czero in collaboration with the CSU and Cummins is developing modified/protype LPG DI injectors and an LPG bench test fuel supply system. Five modified five-hole injectors were fabricated for testing purposes, with additional designs for 1–4 holes (Figure VI.B.2.1). The modified injector was able to deliver a 20% increase in flow rate compared to the stock Delphi GDI injector. Leak testing of the modified injector at CSU prompted a redesign and fabrication of a second generation five-hole injector with pre-load settings doubled from 0.0005 in to 0.001 in. Durability testing of ~8 million cycles was successfully performed with the first generation five-hole injector and GDI pump; durability testing will continue into FY 2023. CSU provided details of an optimized design of a three-hole injector which was the best performing configuration in 3-D CFD spray simulations (discussed later) for mixture homogeneity and swirl. Mechanical design and fabrication of the three-hole injector is planned for FY 2023.

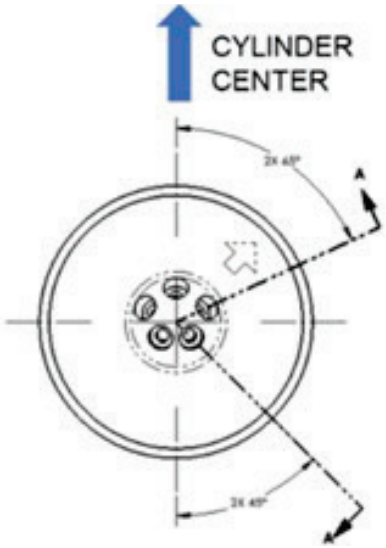

Figure VI.B.2.1 Five-hole nozzle orientation

LPG Injector Spray Imaging

The HPSC is fully functional and can replicate engine-like conditions by changing chamber pressures (ambient), fuel pressures, and temperatures. High-speed Schlieren and planar Mie scattering imaging was carried out for the Delphi five-hole injector. The defined test conditions include a range of engine conditions from low-pressure conditions (i.e., naturally aspirated, injection during intake stroke) to replicate a homogenous, full-load, early injection event observed in direct injection engines, to high-pressure cases that correspond to late injections or boosted engines. Testing was carried out at various engine-relevant temperatures for iso-octane and propane (a surrogate for LPG). Four injectors, including Bosch BMW 325i EU5, Delphi seven-hole stock injector, Engine Combustion Network Spray-G injector, and modified five-hole Delphi injectors, have been tested at various engine-like conditions and high-speed Schlieren and planar Mie scattering for propane and iso-octane fuels. The data was processed and sent to Argonne National Lab for model tuning and validation. More injector nozzle designs will be tested in FY 2023. High-speed Schlieren images are recorded at 30,000 frames per second to obtain high-speed videos with a 33 µs difference between frames. At atmospheric and sub-atmospheric chamber pressure, propane is subjected to spray collapse and flashes, in contrast with iso-octane that propagates through the spray chamber in a conventional spray break-up pattern and exhibits moderate flash-boiling. Measurements such as vapor penetration length, width, and speed are used to characterize the spray structure. Spray development of propane is sensitive to chamber pressures and fuel and chamber temperatures. However, the liquid-vapor boundary is unclear in Schlieren. Schlieren is a 2D projection of a 3D phenomenon that makes it difficult to parse out individual plume behavior to develop high-fidelity spray models. Hence, a sophisticated imaging technique like the planar Mie scattering imaging is needed to define the difference within these structures. The planar Mie scattering imaging setup was modified to capture images of liquid spray at smaller time increments of 33 µseconds for the entire injection duration. These recorded images correspond with the timestamps recorded in high-speed Schlieren imaging; hence, reliable comparison in the vapor and liquid phase can be made when the images from both these imaging techniques are overlapped. Figure VI.B.2.2 shows sample Schlieren and Mie scattering images for LPG injection from the five-hole injector.

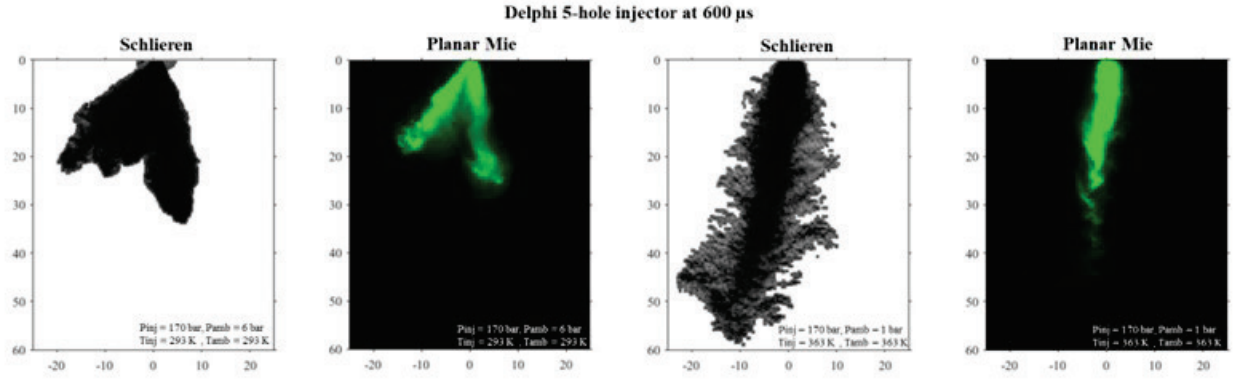

Figure VI.B.2.2 LPG experimental imaging results for Delphi five-hole injector

LPG DI Injector Spray Model

A two-tier approach based on 3-D CFD simulation has been defined to design a numerical model for LPG injection for engine-like domain and conditions. First, high-fidelity simulations of the injector nozzle-flow are carried out to determine the spray characteristics entering the chamber. Then, the obtained thermo-kinematic properties (e.g., jet momentum and angle) of the spray is introduced into the Lagrangian-Eulerian framework, which is a well-established approach for automotive sprays. The simulation effort focused on two GDI multi-hole injectors, the research-grade eight-hole Engine Combustion Network Spray-G injector and the optimized five-hole injector developed within this project. The high-fidelity nozzle flow simulations captured the response of vaporizing LPG spray to the ambient conditions (e.g., P_{amb}, T_{amb}, and super-heat degree) and its behavior has been translated to the Lagrangian injection model. In absence of accurate and reliable flash-boiling vaporization models for Lagrangian sprays, the enhanced atomization and vaporization are obtained by modifying the aerodynamic breakup constants to replicate the phenomena measured experimentally in the HPSC. The simulations have been compared to the HPSC measurements in terms of liquid and vapor morphology through consistent replication of Schlieren and Mie scattering data, obtaining reasonable agreement across a wide range of operating conditions. Full collapse of the plumes is obtained for flashing sprays and a more conventional spray behavior is reported when P_{amb} is higher. The influence of the injector geometry is captured in the injection dynamics and Lagrangian spray models for the CFD software CONVERGE 3.0, to be incorporated in engine simulations. Figure VI.B.2.3 reports the behavior of the liquid and vapor phase for the five-hole injector at different ambient conditions. Alongside its testing in the engine, the model is undergoing refinement in the definition of a correlation between the injector operating conditions and the spray model parameters, to provide a flexible modeling tool able to adapt the spray behavior to the injection timing in the actual operation of the engine.

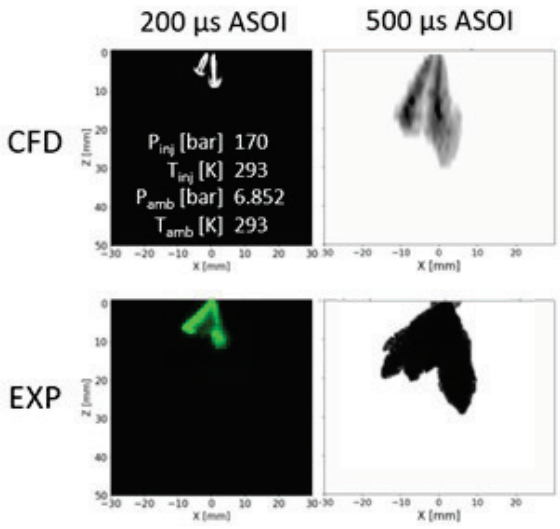

ASOI – after start of injection

Figure VI.B.2.3 Propane spray model of the five-hole injector compared with experiments in HPSC. Mie-scattering for liquid phase (left) and Schlieren for spray morphology (right).

Converge CFD Modeling of X15 SCE

In the second half of 2022, the combustion CFD calibration was carried out for a medium load operation point of the SCE fitted with a liquid propane PFI system. The calibrated condition has about 10.4 bar nominal gross indicated mean effective pressure at 1,200 rpm. With the low compression ratio (9.3), medium load level around 10.4 bar, and propane fuel, the operation is expected to be slightly (if at all) knock limited. At this condition, the intake pressure and exhaust pressure are close to atmospheric pressure. The charge enters the intake manifold at 318.5 K, a temperature easy to achieve with a typical charge air cooler. The model assumes a homogenous propane–air mixture at the gas inlet. The calibrated model includes multiple consecutive cycles and a timing sweep. As shown in Figure VI.B.2.4, the predicted cylinder pressure matches with the individual cycle pressure traces taken from test cell. The apparent heat release rate and knock behavior also agree with the experimental results.

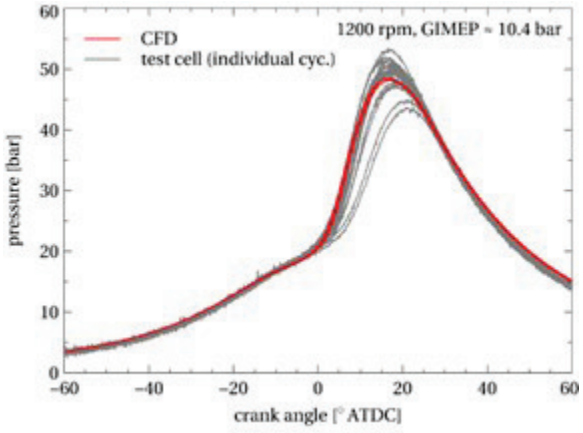

ATDC – after top dead center

Figure VI.B.2.4 Cylinder pressure and apparent heat release rate prediction (three consecutive cycles) compared with experiment (20 consecutive cycles).

Non-combustion CFD simulation is used for the optimization of the spray pattern. The optimization targets low standard deviation of local equivalence ratio at top dead center, a metric of the inhomogeneity of the fuel/air mixture. With a trial of one- to five-hole spray pattern designs, three-hole designs are found to strike a good balance between fuel spreading and jet penetration. With more than three holes, the spray momentum of a single jet is not strong enough to deliver fuel to places far away from the injector. With less than three holes, the fuel spread is inadequate. Around twenty designs with three holes are generated and tested. The top four three-hole designs are selected for additional study. Seven additional operating conditions and model configurations are added to make the final selection such that the final spray pattern is robust against variations of load, injector flow rate, liquid temperature, and flash breakup model parameters. As shown in Figure VI.B.2.5, Revision 15 (r15) of the three-hole design results in the lowest overall standard deviation of local equivalence ratio across the eight cases, which covers wide range of operating conditions and achieves the best overall mixing. The three-hole r15 design was submitted to the injector vender for further review and prototyping.

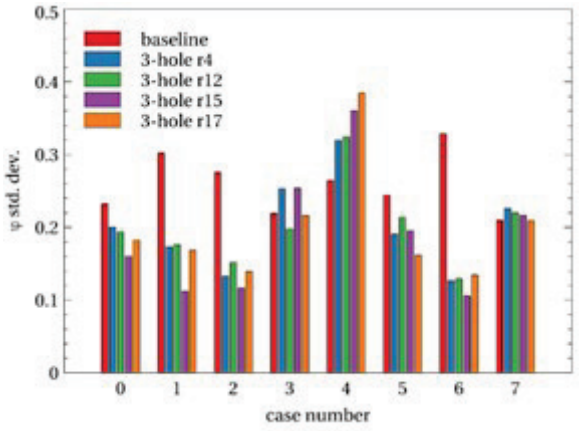

Figure VI.B.2.5 Local equivalence ratio standard deviation of the baseline and four design candidates

Engine Testing: Cummins X15 SCE Baseline Testing

A baseline evaluation was conducted on the 2.5 L Cummins SCE to replicate the performance of current LPG engines in the market and create a benchmark by which further improvements in performance, with the use of direct injection, EGR, increased compression ratio, etc., would be quantified. The baseline tests were performed at an engine speed of 1,200 rpm, at a mixture temperature of 38°C, at a compression ratio of 9.3:1, and with LPG port fuel injected at 1,600 kPa. Parametric sweeps of start of injection (SOI) timings, ignition timing, intake manifold air pressure (IMAP), and equivalence ratio were performed to determine the optimal SOI, combustion phasing, and knock limits on the engine. Open (120°, 150° before top dead center [bTDC])

and closed (330°, 360° bTDC) intake valve timings were considered for the liquid LPG injection, and the tests indicated similar emissions, performance, and combustion behavior between all timings. However, SOI 120° bTDC performed slightly better overall, and was selected for the remainder of the tests. Ignition timing was then varied from 6° bTDC to 18° bTDC as shown in Figure VI.B.2.6a, and the maximum brake torque timing occurred at an ignition timing of 16° bTDC, or a 50% burned location (CA50) between 9° and 11°. This optimal combustion phasing produced a brake thermal efficiency of ~34%. Engine load was then increased by varying the IMAP from naturally aspirated conditions, which produced a BMEP of 9 bar, until the onset of incipient knock. With an SOI of 120° bTDC and combustion phasing of CA50 10° aTDC, the engine experienced knocking combustion at an IMAP of 140 kPa which produced a 13 bar BMEP. The pressure trace and oscillations at knocking and non-knocking conditions are shown in Figure VI.B.2.6b. There was a ~2% improvement in brake thermal efficiency as the load was increased from 9 bar to 13 bar BMEP. Finally, the equivalence ratio (φ) was swept from 0.83 to 1.25. The lean φ = 0.83 condition produced significantly lower brake torque but was 6% more efficient than the rich operation φ = 1.25. A stoichiometric mixture φ = 1 provided a reasonable tradeoff between all the quantified engine-out emissions.

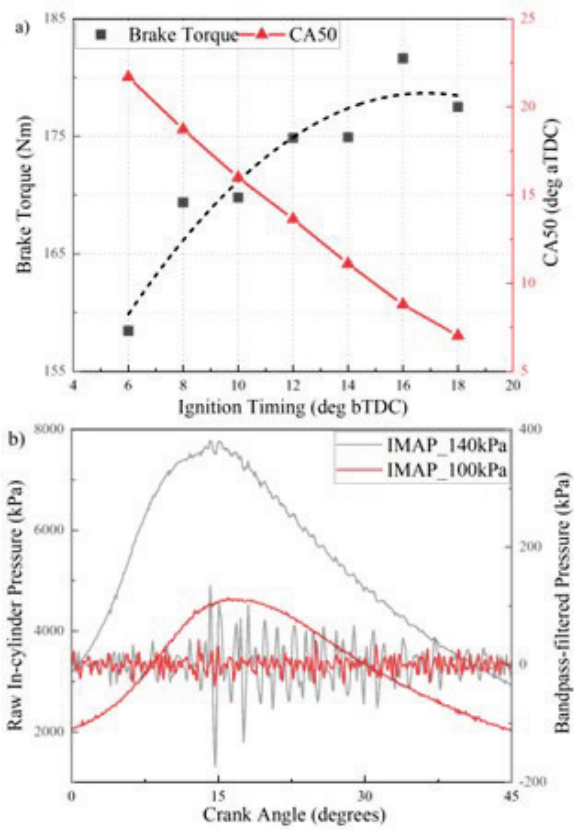

Figure VI.B.2.6 Baseline test results showing (a) brake torque and CA50 versus ignition timing and (b) pressure trace and oscillations for two different engine loads.

A new engine cylinder head machined to accommodate the modified five-hole LPG injector, which was designed for direct injected liquid LPG testing, was installed on the Cummins X15 SCE. An experimental fuel supply system, which can deliver liquid LPG at pressures up to 200 bar, was designed for use in the DI tests. The DI tests will be compared to the baseline PFI results for improvements in performance, combustion, and engine-out emissions.

Conclusions

- CFD modeling of LPG direct injection captures the vaporization-driven full collapse of the plumes and the axial penetration trends observed in Schlieren fuel jet imaging in the HPSC.
- A multi-cycle combustion CFD model is calibrated for a part-load PFI operation point of the X15 SCE. The calibrated model captures the combustion duration and knock behavior of the test engine.
- Through non-combustion CFD simulations and optimization, three-hole spray pattern Revision 15 is identified as the overall best spray pattern for propane DI operation.

Key Publications

1. Tanmay Kar, Toluwalase Fosudo, Anthony Marchese, Bret Windom, and Daniel Olsen. 2022. “Effect of Fuel Composition and EGR on Spark-Ignited Engine Combustion with LPG Fueling: Experimental and Numerical Investigation.” *Fuel* 327.

2. Windell, B., M. Sharma, L. Nocivelli, K. Asztalos, A. Zdanowicz, T. Kar, D. Olsen, A. Marchese, and B. Windom. 2022. “Bulk Spray and Individual Plume Characterization of LPG and Iso-Octane Sprays at Engine-Like Conditions.” SAE Technical Paper 2022-01-0497, doi:10.4271/2022-01-0497.

3. Kar, T., T. Fosudo, C. Slunecka, A. Marchese, B. Windom, and D. Olsen. 2022. “A Study of Propane Combustion in a Spark-Ignited Cooperative Fuel Research (CFR) Engine.” SAE Technical Paper 2022-01-0404, doi:10.4271/2022-01-0404.

4. Fosudo, T., T. Kar, A. Marchese, B. Windom, and D. Olsen. 2022. “The Impact of LPG Composition on Performance, Emissions, and Combustion Characteristics of a Pre-mixed Spark-Ignited CFR Engine.” SAE Technical Paper 2022-01-0476, doi:10.4271/2022-01-0476.

5. Kar, Tanmay, Toluwalase Fosudo, Bret Windom, Jensen Hoke, Jeff Rogers, and Daniel Olsen. 2022. “Development of a Liquid-Phase Lpg Delivery System for Direct Injection Spark-Ignited Engines.” ASME Internal Combustion Engine Division Fall Technical Conference, Paper ICEF2022-91081, October 16–19.

VI.B.3 Propane Long Stroke Engine (Oak Ridge National Laboratory)

Derek Splitter, Principal Investigator
Oak Ridge National Laboratory
2360 Cherahala Boulevard
Knoxville, TN 37922
Email: splitterda@ornl.gov

Flavio Dal Forno Chuahy, Principal Investigator
Oak Ridge National Laboratory
2360 Cherahala Boulevard
Knoxville, TN 37922
Email: dalfornochuf@ornl.gov

Kevin Stork, DOE Technology Manager
U.S. Department of Energy
Email: Kevin.Stork@ee.doe.gov

Start Date: October 1, 2021 End Date: September 30, 2022
Project Funding: $500,000 DOE share: $500,000 Non-DOE share: $0

Project Introduction

This project will develop and demonstrate direct-injected liquified petroleum gas (LPG) stoichiometric spark-ignition engine technologies, including exhaust gas recirculation (EGR) and variable valve actuation to achieve fuel efficiency and torque parity (~20 bar) with current medium-duty diesel engines. The objective is to provide experimental data that demonstrates technologies and approaches to achieve a cycle efficiency of 41% in the supplemental emissions test steady-state cycle while meeting all applicable 2027 criteria emissions regulations. Achieving the target cycle efficiency with LPG will result in cycle CO_2 emissions of 430 g CO_2/hp·hr, a 6% reduction from 2027 Phase 2 greenhouse gas (GHG) regulations. Achieving this goal will require a combination of computational and experimental efforts to optimize engine design and simultaneously provide key fundamental understanding of the limiting factors in highly diluted spark-ignition combustion. Recent single-cylinder experiments at Oak Ridge National Laboratory will be extended to show the potential of high-compression-ratio, highly diluted, and highly turbulent combustion systems for enabling diesel-like efficiencies with LPG. A dedicated single-cylinder engine incorporating these design changes will be built for efficiency and emissions compliance proof of concept.

Objectives

- Optimize a long-stroke stoichiometric propane (LPG) spark-ignition engine platform using advanced simulation tools.
- Develop a fundamental understanding of the particular fuel properties of LPG that promote its stability under exhaust dilution using direct numerical simulations and high-fidelity engine simulations.

Approach

The project combines experiments and simulations to demonstrate and develop fundamental understanding of the opportunity and sources of efficiency with LPG-fueled, high-efficiency engines. The overall project framework that will achieve this goal is represented in Figure VI.B.3.1.

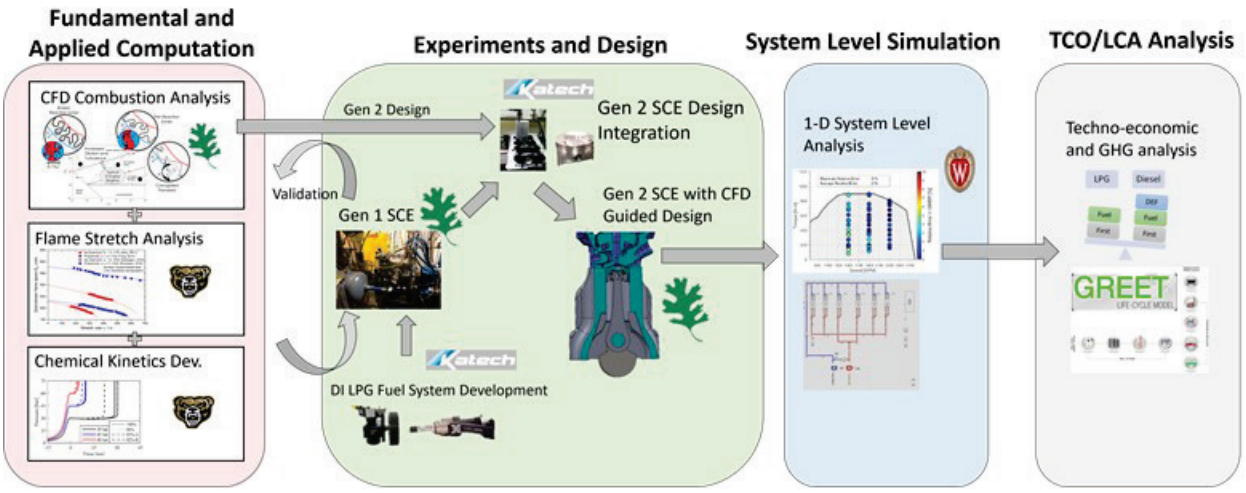

SCE – single-cylinder engine; TCO – total cost of ownership; LCA – lifecycle analysis; CFD – computational fluid dynamics; Gen – Generation; GREET – Greenhouse Gases, Regulated Emissions, and Energy Use in Transportation (model)

Figure VI.B.3.1 Overall project structure, partnerships, and organizational responsibilities

Experiments

An existing long-stroke engine platform at Oak Ridge National Laboratory is being used in initial experiments and analysis. This platform is a custom platform based on the General Motors Ecotec LNF family of engines and was developed to operate under a wide variety of modes and engine operating conditions. The engine's stroke was increased by 50% using a custom-built billet block, crankshaft, and connecting rods, which are paired with the stock cylinder head and piston assemblies. The stock valve actuation system was replaced by a fully flexible Sturman variable valve actuation system. Although proven functional, this system lacks robustness in the valvetrain and cannot replicate true camshaft actuated valve motion; moreover, the LNF engine was never designed to use EGR dilution in its production form. A major part of this project is an updated long-stroke engine design offering significantly increased EGR dilution tolerance and optimization potential. This updated engine will be based on the Stellantis 2.0 L hurricane engine, which will have a displacement increase of up to 50% through this project (i.e., up to a 6 L engine in a V-8 configuration relevant to medium-duty applications).

Figure VI.B.3.2 Production Stellantis 2.0 L hurricane engine used as a second-generation long-stroke engine platform

Targeted experiments will use this updated platform once it has been completed. The fabrication of the updated engine platform has been delayed because of the COVID-19 supply chain and personnel shortages occurring at partner organizations. However, the contracting is in place, and progress will be reported in Fiscal Year (FY) 2023. In the meantime, data from the first-generation engine has been used to guide simulation efforts in designing the second-generation engine.

Simulations

To develop a model framework capable of capturing the key phenomena that limit spark-ignition engine efficiency, a number of new sub-models have to be implemented into a general framework. To make an extensive geometry and parametric optimization modeling effort feasible, advanced numerics related to the

combustion modeling approach have to be implemented and improved. The G-Equation approach has been used pervasively to model the premixed and partially premixed combustion processes [1], [2], [3], [4] and has recently been paired with more complex kernel formation and propagation models [5], [6], [7], forming a comprehensive modeling framework for predicting flame propagation in internal combustion engine environments. This will use a combination of more industry-friendly Reynolds-averaged Navier–Stokes (RANS) simulations and targeted high-fidelity and direct numerical simulation (DNS).

The overall objective of the simulations in the current project is to accurately predict combustion of highly dilute mixtures of LPG (simulated as neat propane) with air. Thus, the effects of G-Equation numerics in the RANS approach must be decoupled as much as possible from potential sub-model adjustment constants. Level set approaches like the G-Equation need high-order accuracy, and the role of finite volume operations on the accuracy of the surface tracking is not well understood. Therefore, the project team is developing more accurate source terms for the G-Equation approach and testing them in the FRESCO computational fluid dynamics (CFD) solver.

- The team will introduce a new signed distance function-based kernel-handling method that is suitable for spark channel modeling via mesh-independent properties and locally fine-grained property evaluations.
- The team will introduce an accurate formulation for the compressible G-Equation source terms and demonstrate its importance in capturing the correct flame propagation.
- The improved numerics will be shown to achieve high fidelity even under coarse meshes, speeding up turnaround times and allowing more complex optimization procedures.

The project developed a framework in the DNS software S3D to study more fundamental flame aspects of LPG that allow it to have a stronger resistance (compared to gasoline) to dilution-driven instabilities. The team is exploring the effect of turbulence and dilution on the developing kernel of an LPG flame (compared to an isooctane flame), and to that end, researchers selected three levels of turbulence intensity based on the turbulent velocity intensity in a corresponding engine simulation. A reduced chemical mechanism by Pachler et al. [8] that has been validated using rapid-compression-machine data was used for the current baseline for DNS simulations. A quasi-steady-state approximation mechanism reduction step was required to allow simulation time steps to fall within a reasonable range and allow the simulation to be completed in a significantly shorter time. A Lewis number model was used to simulate mixture-averaged diffusion and improve numerical stability, resulting in an average time step of $1e^{-9}$ sec for all simulations.

Results

Results in FY 2022 have been focused on simulation efforts guiding the second-generation long-stroke engine platform. Primary focuses have been on understanding experimental observations on improved dilution tolerance of propane and accurately predicting knock of propane. To explore the fundamental processes of dilution tolerance, researchers used two-dimensional DNS simulations to understand the flame structures and diffusion mechanisms present with LPG relative to isooctane.

In the DNS simulation, three levels of turbulence were selected based on data from averages in experimentally validated RANS simulation in FY 2021. For each level of turbulence, simulations with 0% and 25% EGR were conducted. The turbulence levels were chosen to keep the same eddy turnover time. Cases were run for both isooctane and LPG to identify which key differences observed in the simulations may be responsible for propane's increased stability under dilution.

Figure VI.B.3.3 shows preliminary results of the DNS simulations using LPG fuel (orange) and isooctane (green) at a medium turbulence level at the 30% mass fraction burned (MFB) time step in the respective simulation. The contribution of propane flame speed is split into diffusion and tangential aspects, and interestingly, results show no difference between isooctane and propane with 0% EGR (left column). However,

with 25% EGR, diffusion becomes increasingly important, where the curvature becomes more dominant. This is especially important as the high negative curvature observed with isooctane results in flame annihilation and instability, corroborating the findings in experiments from previous fiscal years. The implications of this finding are that, with EGR, isooctane becomes diffusional-rate-limited sooner and experiences increased negative curvature, causing a fundamental source of flame instability, reduced flame speeds, and EGR tolerance.

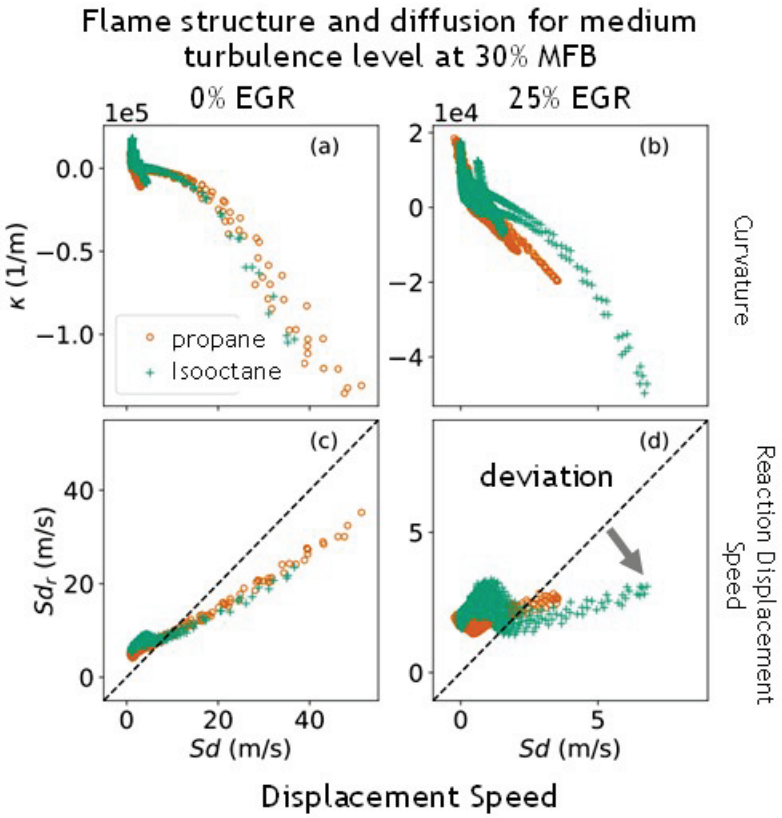

Figure VI.B.3.3 Reaction displacement speed (bottom row) and flame curvature (top row) 2D DNS results for isooctane (green) and propane (orange) at 0% EGR (left column) and 25% EGR (right column)

To leverage the fuel properties of propane's increased dilution tolerance, further simulations were conducted to explore in-cylinder geometry and quenching effects. First, a non-constant Péclet number approach was implemented into multi-dimensional CFD results in the FRESCO and CONVERGE codes. The approach uses direct chemistry integration to calculate true wall quenching, reducing hydrocarbon errors and near-wall combustion instabilities. The results in Figure VI.B.3.4 highlight that the non-constant Péclet number approach does not differ significantly from variable Péclet number approaches. However, when using level-set methods, any wall model implementation is critical to appropriately account for quenching effects near the wall. The results are improved prediction of emissions such as unburned hydrocarbons. These effects are magnified with EGR, so the proper prediction of near-wall combustion for design optimization is critical to achieving this project's goals.

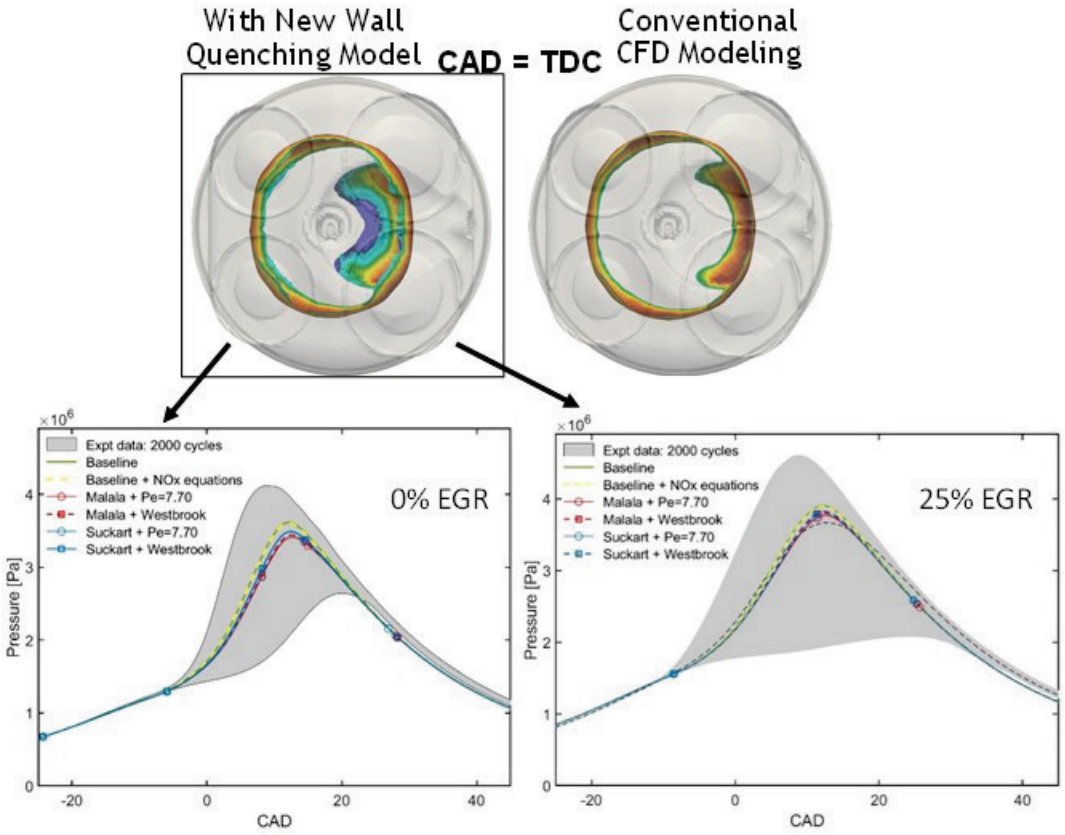

CAD – crank angle degree; TDC – top dead center; NO_x – nitrogen oxides

Figure VI.B.3.4 Non-constant Péclet number 3D CFD results at TDC showing extended flame surface at near engine surfaces, simulation results compared to experimental data (grey) with 0% EGR (left bottom) and 25% EGR (right bottom)

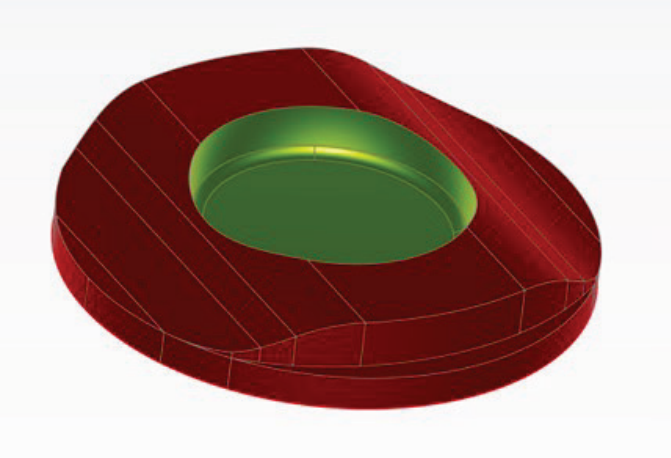

Figure VI.B.3.5 High-efficiency piston bowl concept for propane combustion

Because of propane's high octane number and thus knock resistance, compression ratios higher than 15:1 can be employed without knock. Additionally, propane is injected in a supercritical state under most conditions and evaporates extremely quickly. Therefore, it is not relying on the piston shape to promote fuel–air mixing. These considerations significantly affect the possible piston design shapes that are expected to generate high engine efficiency. Based on these considerations and previous experimental work in the LNF platform with high-compression-ratio pistons, the project team developed a new base piston design for optimization purposes. Figure VI.B.3.5 shows the piston concept. The domed shape of the piston is necessary to achieve the high compression ratios desired for this project. The bowl in the middle is designed to allow the initially spherically propagating flame to expand unencumbered by the interference of cold piston walls. The piston was parameterized to allow the optimization of the geometry. The parameters for optimization are the height of the dome, the angle of the dome slope, the length of the

dome flat, and the diameter of the center bowl. The stroke-to-bore ratio is also being included as a variable to allow optimization of the stroke length in conjunction with the piston geometry. With these parameters, it is expected that an optimum piston can be devised for high-stroke-to-bore and high-turbulence operation while avoiding knock. Tasmanian, a deterministic smart sampler, is being used to probe the piston design space and generate a response surface design that will then be used to optimize the bowl shape. The most promising designs will be evaluated in a spark and EGR sweep to analyze the robustness of the design. The best designs will be manufactured and explored in the second-generation experimental metal engine.

To complete the set of tools necessary to optimize a piston geometry for high-efficiency spark-ignition engines, the project team conducted analysis of previously obtained knock data and zero-dimensional simulations. Results showed that the existing literature mechanisms over-predicted knock onset for all conditions. Chemkin simulations were performed to understand knock onset and critical reactions for knock prediction. A key finding was the importance of low-temperature chemistry reactions in predicting knock for propane when boosted operation and high compression ratio are used. This finding is critical, as these conditions are not common in conventional fuels. The finding highlights that adjusting only 6 reactions in a 352-reaction mechanism with 70 species from the literature [8] enables exceptionally good knock prediction with propane. Figure VI.B.3.6 provides results of a sensitivity analysis of those reactions and prediction with experiential data. The results show that the ignition delay under the conditions of interest is dictated mostly by the low-temperature chemistry of the fuel. A genetic algorithm was used to adjust 6 reaction rates (i.e., only reactions critical to the low-temperature heat release), which resulted in over 50% improvement in knock onset predictions.

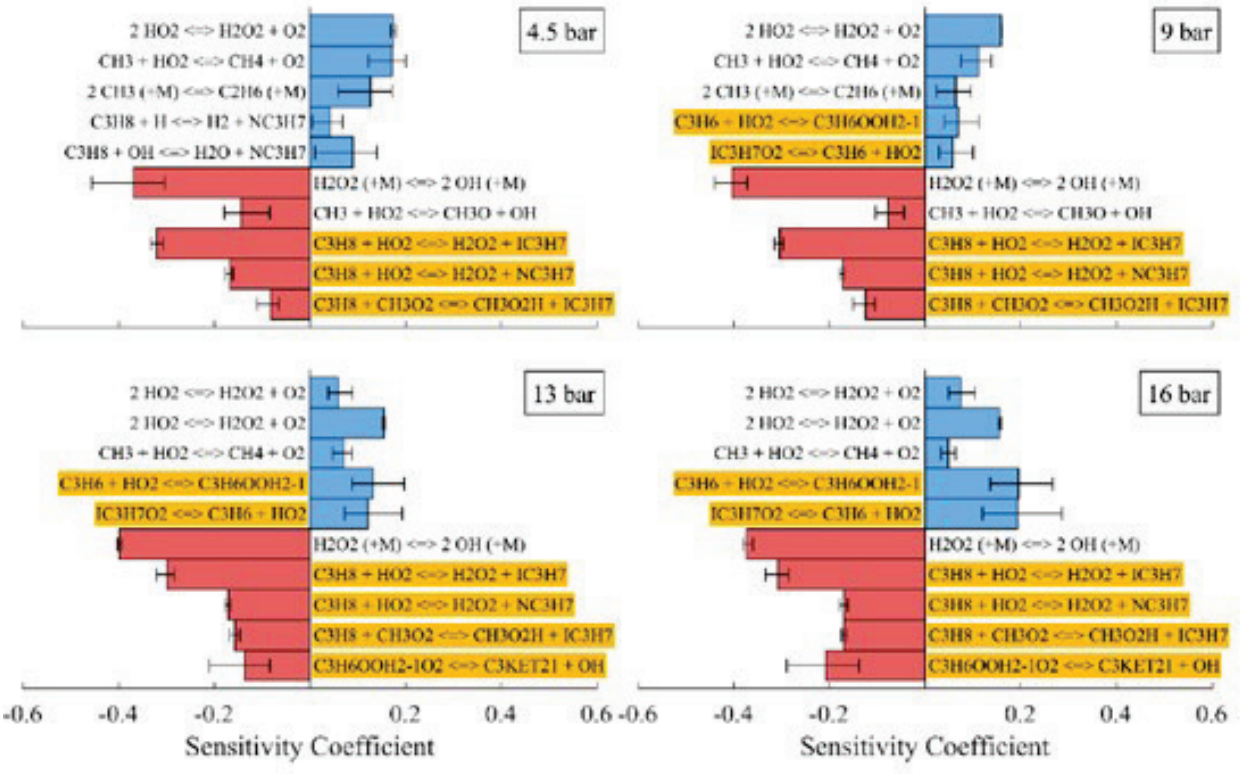

Figure VI.B.3.6 Top five positive and negative average sensitivity coefficients of kinetic mechanism analysis used in genetic algorithm optimization for 4.5 bar (top left), 9 bar (top right), 13 bar (bottom left), and 16 bar (bottom right) operating condition trajectories. Error bars denote range of values.

The fundamental and applied findings of the simulation efforts have been used in this fiscal year to define the second-generation experimental engine configuration. The base engine design is under way and is anticipated to be completed in FY 2023.

Conclusions

Experiments on the first-generation long-stroke engine have shown that LPG offers significantly increased EGR dilution tolerance. Simulation results using detailed 2D DNS highlighted that the sources of the previously observed experimental phenomena are attributable to fundamental flame quenching and curvature effects in propane. Specifically, increased diffusional processes in propane afford improved EGR dilution tolerance. The DNS findings provide significant insights into the importance of near-wall boundary layer reactions; therefore, further simulations were performed to ascertain whether varying the Péclet number improved simulation predictions. Results from that work in the FRESCO and CONVERGE codes clearly highlighted that the high diffusional rates, especially with EGR, were not only present but necessary with propane to accurately predict unburned hydrocarbon emissions and combustion stability in 3D CFD engine simulations. Simulation results were not confined to flow field and diffusional effects. Chemical kinetic optimization was also performed, as existing literature mechanisms were unable to accurately predict knock in our acquired experimental data. Kinetic mechanism results found that improved low-temperature reaction rates were needed to properly predict knock in the high-compression-ratio, long-stroke-to-bore-ratio engine platforms being investigated in the project. Tuning 6 key reactions identified through genetic algorithm optimization resulted in a >50% improvement in knock, offering very good knock prediction agreement with experiments. Lastly, in FY 2022, contracting for the second-generation engine was completed, and work on the second-generation engine will be under way in 2023, with experiments occurring once commissioned.

Key Publications

1. Ge, W., F.D.F. Chuahy, P. Zhang, R. Sankaran, D. Splitter, D. DelVescovo, T. Lu, and P. Zhao. 2022. "A Direct Numerical Simulation Study of the Dilution Tolerance of Propane Combustion under Spark-Ignition Engine Conditions." *Combustion and Flame* 247: 112495.

2. Perini, F., F.D.F. Chuahy, A. Sircar, D. Splitter, and R. Reitz. 2022. "Advanced Finite-Volume Numerics and Source Term Assumptions for Kernel and G-Equation Modelling of Propane/Air Flames." SAE Technical Paper 2022-01-0406.

3. Chuahy, F.D.F., G. Wenjun, P. Zhang, R. Sankaran, T. Lu, D. DelVescovo, and D. Splitter. 2022. "A DNS Study of Highly Diluted Propane Flames under Spark Ignition Engine Conditions." Presentation at Advanced Engine Combustion meeting, February.

4. Perini, F., F.D.F. Chuahy, A. Sircar, D. Splitter, and R. Reitz. 2022. "Advanced Finite-Volume Numerics and Source Term Assumptions for Kernel and G-Equation Modelling of Propane/Air Flames." SAE Technical Paper 2022-03-29. Presented at SAE World Congress Experience, April.

5. Splitter, D., and F.D.F. Chuahy. 2022. "Propane Long-Stroke Engine." U.S. Department of Energy's Vehicle Technologies Office Annual Merit Review, June.

References

1. Peters, N. 2000. Turbulent Combustion. Cambridge, United Kingdom: Cambridge University Press.

2. Fan, L., and R.D. Reitz. 2000. "Development of an Ignition and Combustion Model for Spark-Ignition Engines." SAE Transactions 109: 1977–1989.

3. Ewald, J., and N. Peters. 2006. "A Level Set Based Flamelet Model for the Prediction of Combustion in Homogeneous Charge and Direct Injection Spark Ignition Engines." PhD dissertation.

4. Liang, L., and R.D. Reitz. 2006. “Spark Ignition Engine Combustion Modeling Using a Level Set Method with Detailed Chemistry.” SAE Technical Paper 2006-04-03.

5. Dahms, R.N., M.C. Drake, T.D. Fansler, T.W. Kuo, and N. Peters. 2011. “Understanding Ignition Processes in Spray-Guided Gasoline Engines Using High-Speed Imaging and the Extended Spark-Ignition Model SparkCIMM: Part B: Importance of Molecular Fuel Properties in Early Flame Front Propagation.” Combustion and Flame 158: 2245–2260.

6. Sforza, L., T. Lucchini, A. Onorati, X. Zhu, and S.-Y. Lee. 2017. “Modeling Ignition and Premixed Combustion Including Flame Stretch Effects.” SAE Technical Paper 2017-01-0553.

7. Scarcelli, R., A. Zhang, T. Wallner, S. Som, J. Huang, S. Wijeyakulasuriya, et al. 2019. “Development of a Hybrid Lagrangian–Eulerian Model to Describe Spark-Ignition Processes at Engine-Like Turbulent Flow Conditions.” Journal of Engineering for Gas Turbines and Power 141, no. 9: 091009.

8. Pachler, R.F., A.K. Ramalingam, K.A. Heufer, and F. Winter. 2016. “Reduction and Validation of a Chemical Kinetic Mechanism Including Necessity Analysis and Investigation of CH4/C3H8 Oxidation at Pressures up to 120 bar Using a Rapid Compression Machine.” Fuel 172: 139–145.

VI.B.4 High-Pressure Fast-Response Direct Injection System for Liquified Gas Fuels Use in Light-Duty Engines (WM International Engineering LLC)

William de Ojeda, PhD, PE, Principal Investigator
WM International Engineering LLC
7800 Cass Avenue
Darien, IL 60561
Email: wdeojeda@wminternational-engineering.com

Carrie Hall, Principal Investigator
Illinois Institute of Technology
10 West 35th Street
Chicago, IL 60616
Email: chall9@iit.edu

Sreenath Gupta, Principal Investigator
Argonne National Laboratory
9700 South Cass Avenue
Lemont, IL 60439
Email: sgupta@anl.gov

Kevin Stork, DOE Technology Manager
U.S. Department of Energy
Email: Kevin.Stork@ee.doe.gov

Start Date: March 31, 2022 End Date: March 31, 2023
Project Funding: $749,813 DOE share: $597,615 Non-DOE share: $152,198

Project Introduction

This project seeks to help build a clean energy economy and contribute to a carbon pollution-free environment by means of the development and demonstration of a fuel injection system technology that will improve the efficiency of direct injection engines using dimethyl ether (DME) and propane. Because of its non-sooting nature of combustion, DME has long been considered a clean diesel substitute [2] for compression ignition (CI) engines. In addition to its production from natural gas, DME can be synthesized from biomass. Renewable DME can result in significant CO_2 emission reductions. California Air Resources Board (CARB) estimates the carbon intensity of renewable DME made from dairy biogas is −278 g/MJ. DME can also be blended into propane due to their similar fluid characteristics. With a 5% blend of renewable DME, propane's baseline carbon intensity value decreases from 83 to 65 g CO_2/MJ. Further reductions are possible with renewable propane (i.e., bio propane carbon intensity of 30 g CO_2/MJ) [1], making this a viable pathway for greenhouse gas (GHG) reductions for spark ignition engines.

The present project aims to develop a state-of-art fuel injection system that operates with mixtures of propane and DME to improve the efficiency of a light-duty engine while significantly reducing engine emissions. The novel injection system used with propane–DME mixtures will target Environmental Protection Agency (EPA) Tier 3 Bin 20 emission standards and GHG emission of 126 g CO_2/km when implemented on a 2.2 L CI engine (a reduction of 49.7% with respect to Hyundai's 2021 2.0 L gasoline spark-ignited engine at 251 g CO_2/km). This performance target will merit it being brought into production by original equipment manufacturers as the propane–DME engine would exceed the 2025 fleet average fuel economy [2]. Furthermore, the proposed technology shows a lifetime cost reduction up to $3,600 per engine.

Objectives

The project aims to develop a state-of-the-art fuel system that operates with mixtures of propane and DME to improve the efficiency of a light-duty engine while providing significant emission reductions.

Overall Objectives

- The proposed technology is a fast-response, high-pressure direct injection fuel system for propane–DME mixtures. Injection pressure capability of 2,000 bar is sought with five injections at rated speed, with a maximum dwell between injections of 0.5 ms, fueling resolution of 1 mg/stroke, max deviation below 20 mg at ±0.2 mg/stroke, and max deviation above 20 mg of ±0.5 mg/stroke.

- Provide a design and pathway for a sustained introduction in commercial applications. Durability targets with propane–DME mixtures include an 8-hr cycle as follows: 30 min idle; 6.5 hr cruise (2,000 rpm, 1,500 bar); 1 hr peak power (3,000 rpm, 2,000 bar). This will be repeated five times (5 x 8 = 40 hr total) operation, at which point the injector calibration maps will be examined and parts inspected. This will be repeated five times (200 hr total).

- The fuel system will target Tier 3 Bin 20 emission standards and 2026 GHG outlined by EPA (126 g CO_2/km) and CARB (111 g CO_2/km) on the Hyundai 2.2 L CI engine.

- The work will aim to attain the cleaner 2026 EPA and CARB targets at a lower overall cost to the user; in the best-case scenario, the cost may be reduced by $3,600 per vehicle.

Fiscal Year 2022 Objectives

- Complete fuel system modeling. Activity includes modeling of the electro-hydraulic fuel system, including the low-pressure fuel supply, high-pressure fuel pump (HPFP), metering valve, rail accumulator with regulator valve, and injector. Calibration maps of the first interim design are developed for operation with diesel and the propane–DME mixture.

- Complete design and build of performance fuel bench. The test will be validated with diesel and will be followed by a functional validation with propane–DME, using the base hardware. The performance bench will be used to document the injector calibration and HPFP performance.

- Complete design and build of durability fuel bench. Testing will take place directly with propane–DME. The system will be installed at Argonne National Laboratory for spray visualization experiments with the base hardware. Results from the durability runs will be documented.

- Complete the advanced fuel system design and issue manufacturing drawings for machining. The effort will extend the base system performance, expected to operate within the range of 600–800 bar to 2,000 bar.

- Complete engine performance modeling to demonstrate that the use of a propane–DME mixture supports the efficiency and CO_2 targets of the project (42.9% peak efficiency and 126 g CO_2/km on the federal test procedure [FTP] cycle). Modeling will use diesel and gasoline reference fuels at first and then transition to propane–DME mixtures.

Approach

The project seeks to design and test a fuel system for propane–DME fuel mixtures that can operate at diesel-like pressures and at multiple injections per cycle. The approach begins by defining the engine power, emissions, and GHG targets. The project platform is described in Figure VI.B.4.1 and compared to the base production engines, a model year (MY) 2021 spark ignition (SI) gasoline direct injection (GDI) engine and a CI engine. The approach is captured in Figure VI.B.4.2. The ability of possible engine cycles to attain the project cycles, ranging from SI to spark-assisted compression ignition to CI, is considered, utilizing engine

simulation tools comprised of computational fluid dynamics (CFD) combustion modeling and a one-dimensional (1-D) engine cycle simulator.

The optimum cycle will lead to the definition of the fuel system requirements. The team will then use a zero-dimensional model to do a preliminary sizing of the pump and injectors. The work will then continue to a 1-D time-dependent detailed hydraulic model. Validated performance at the 1-D stage will lead to procurement of parts. Parts will be tested and validated in a dedicated rate-of-injection bench. The bench will incorporate the system that will later be installed on the demonstration engine. The bench will yield a full calibration of the fuel injector and pump. Testing will help tune the modeling and controls. Following a successful verification of the injection equipment on the injection bench, fuel injection parts will then be installed on the engine. Engine tests are scheduled to take place at the Illinois Institute of Technology.

Engine	MY 2021 GDI	MY 2021 CI	Project Platform
Cyl Displ (L)	2.0	2.2	2.2
CR	12	16	16
Peak TQ Nm (rpm)	203	438.75	440
Peak kW (rpm)	115	141	140
Fuel	Gasoline	Diesel	propane-DME
Engine Hardware	CVVT-exh CVVD-Intake	Turbo VNT EGR	Turbo VNT EGR
Inj Press (bar)	200	1800	2000
Aftertreatment	TWC	SCR DOC PM Filter	SCR
EMISSIONS	Tier 3 Bin 70	WLTP g/km	Tier 3 Bin 20
GHG - gCO2/km	251	191	126

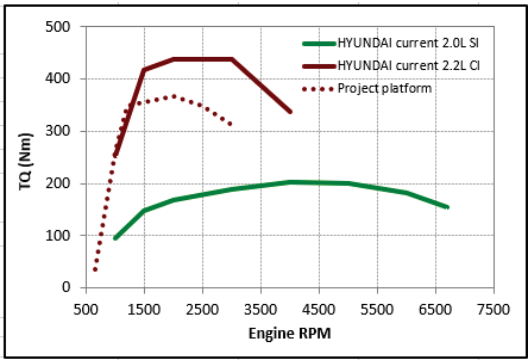

TQ – torque; CR – compression ratio; rpm – revolutions per minute; CVVT – continuously variable valve timing; CVVD – continuously variable valve duration; TWC – three-way catalyst; VNT – variable nozzle turbine; EGR – exhaust gas recirculation; SCR – selective catalytic reduction; DOC – diesel oxidation catalyst; PM – particulate matter; WLTP – Worldwide Harmonised Light Vehicle Test Procedure

Figure VI.B.4.1 Program engine platform and performance targets

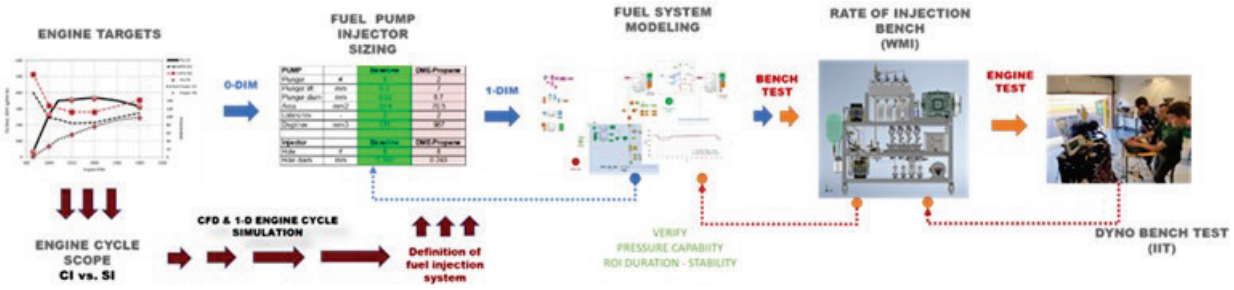

ROI – rate of injection

Figure VI.B.4.2 Program development approach

Results

Fuel System Modeling

The engine fuel injection system and supporting equipment were modeled in MATLAB Simulink and exercised with both diesel and mixtures of propane and DME. The model was used to attain the geometric sizing of both the pump and the injector to meet the targets of the project with the new fuel mixtures.

Fuel System Bench Testing

The performance test bench (Figure VI.B.4.3) construction was completed, and to date, the following milestones were attained using the base hardware.

- Functional validation with diesel and attainment of calibration maps and ROI traces across pressure and times of injection.
- Validation with propane–DME fuel mixtures, and completion of calibration maps and documentation of ROI traces.
- Completion of pressure control by use of the pump inlet metering valve. Tests show the metering valve is effective for pressure control, limiting the excess flow through the system, with optimum results on reducing pump parasitics.

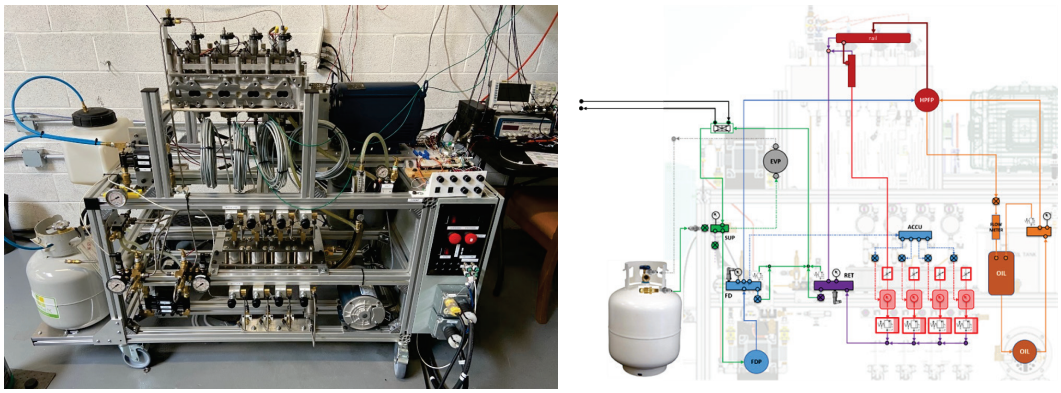

Figure VI.B.4.3 Performance bench for ROI studies

Figure VI.B.4.4 compares the ROI for diesel and DME. Pumping events are similar for diesel and DME, with DME requiring more pumping stroke (~30%), as expected. The greater compressibility of DME is noted on the pressure rise and drop rates, which are longer than those for diesel. For the same injection command, the volume flow of DME is slightly larger than that of diesel, as expected due to its lower viscosity.

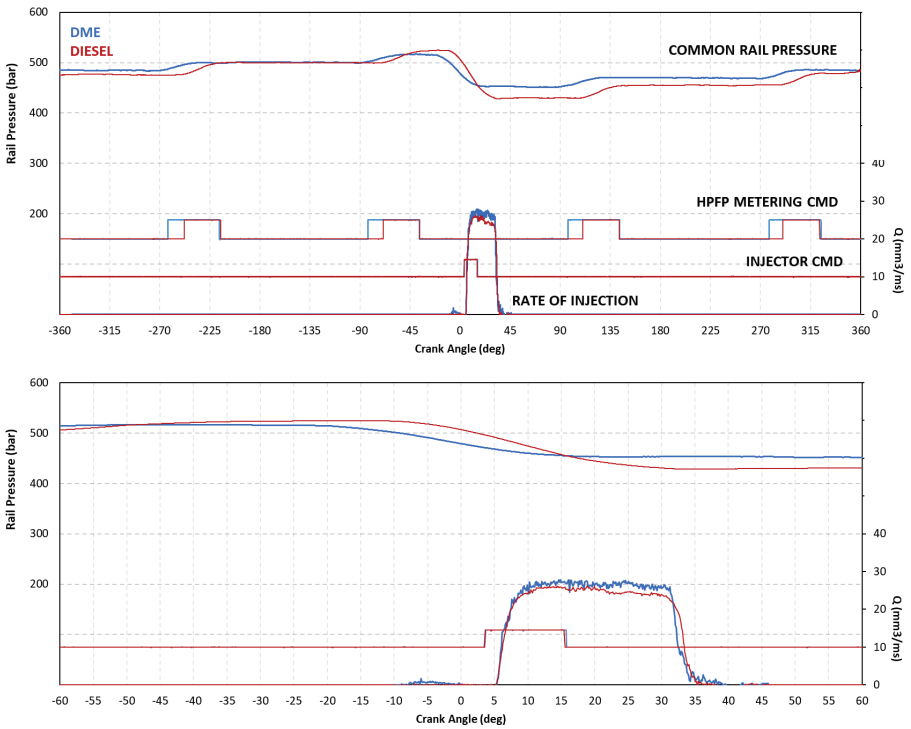

Figure VI.B.4.4 Comparison between diesel and DME rates of injection

Pressure control via the pump inlet metering valve has been successful in steady and near-steady operation. The project will continue to develop the controls while applying various transient conditions. Figure VI.B.4.5 shows the mapping of the HPFP metering valve command across injections from 0.50 to 2.00 ms while holding the pressure constant at 600 bar.

Bench test results closely follow the modeled results, as noted in Figure VI.B.4.6. The modeling captures the flow through the injector across the pressures and pulse widths tested. Particularly notable is the capture of the low-flow quantity pulse width command and the minimum opening times. This provides confidence as the project continues to develop the system for higher pressures.

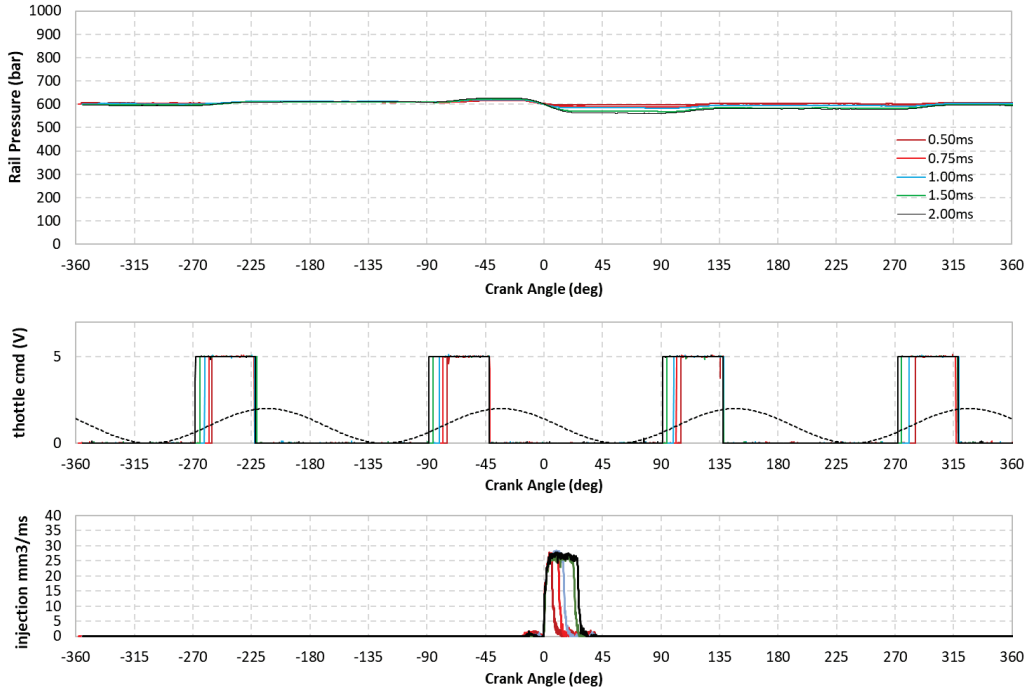

Figure VI.B.4.5 Correlation between HPFP metering valve command and injected fuel amount with DME fuel

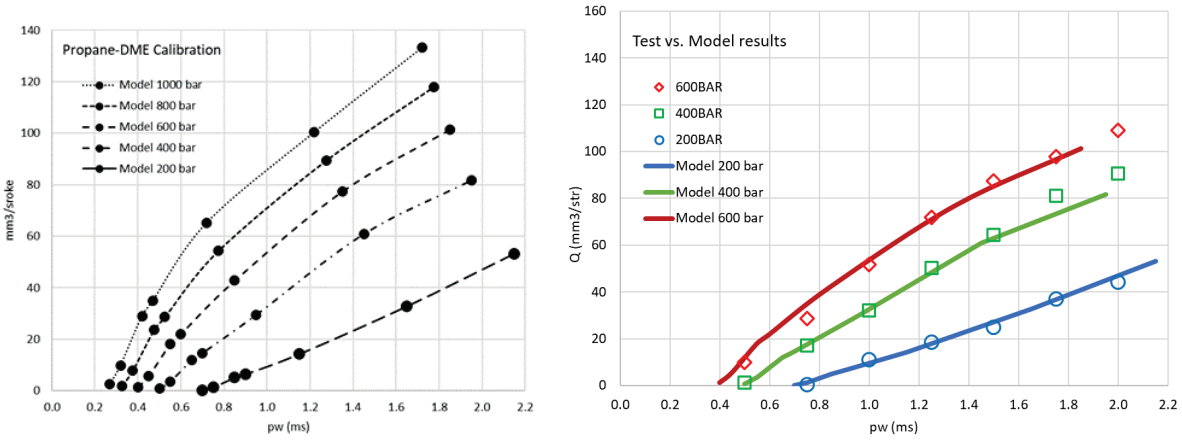

Figure VI.B.4.6 Injector model calibration vs. performance test bench data

Engine Performance Modeling Predictions

The emissions for the Hyundai Santa Fe vehicle are indicated in Figure VI.B.4.7 for the 2.0 L SI and 2.2 L CI powertrain options (251 g CO_2/km and 191 g CO_2/km, respectively). The project utilizes a set of six mini-points to discretize the FTP cycle and will use these points to estimate the FTP cycle performance. MINI-MAP 1 data are weight-averaged to cover over 80% of the FTP points. The MINI-MAP 1 representation of the transient cycle is indicated in Figure VI.B.4.7. The modeling reports 255 g CO_2/km and 192 g CO_2/km for the SI and CI powerplants, closely resembling the drive-dyno results. The MINI-MAP 2 data are an alternative set of points preferred by Hyundai; this set responds to customer feedback for CI powertrain applications. The selection of the mini-points was reviewed by the team members, and the team decided to follow the latter mini-map for modeling and testing optimization moving forward.

Figure VI.B.4.7 also shows program projection for the SI and CI platforms, 126–111 g CO_2/km. The CO_2 numbers reported are associated with engine efficiencies and fuel mixtures. For the efficiencies noted here, the SI powertrain application will need to utilize at least 10% renewable DME (with a negative carbon intensity, –278 g CO_2/MJ) to attain the CO_2 targets. The CI application is expected to attain the targets with the base DME and propane carbon intensity numbers (66.6 g CO_2/MJ and 65 g CO_2/MJ, respectively).

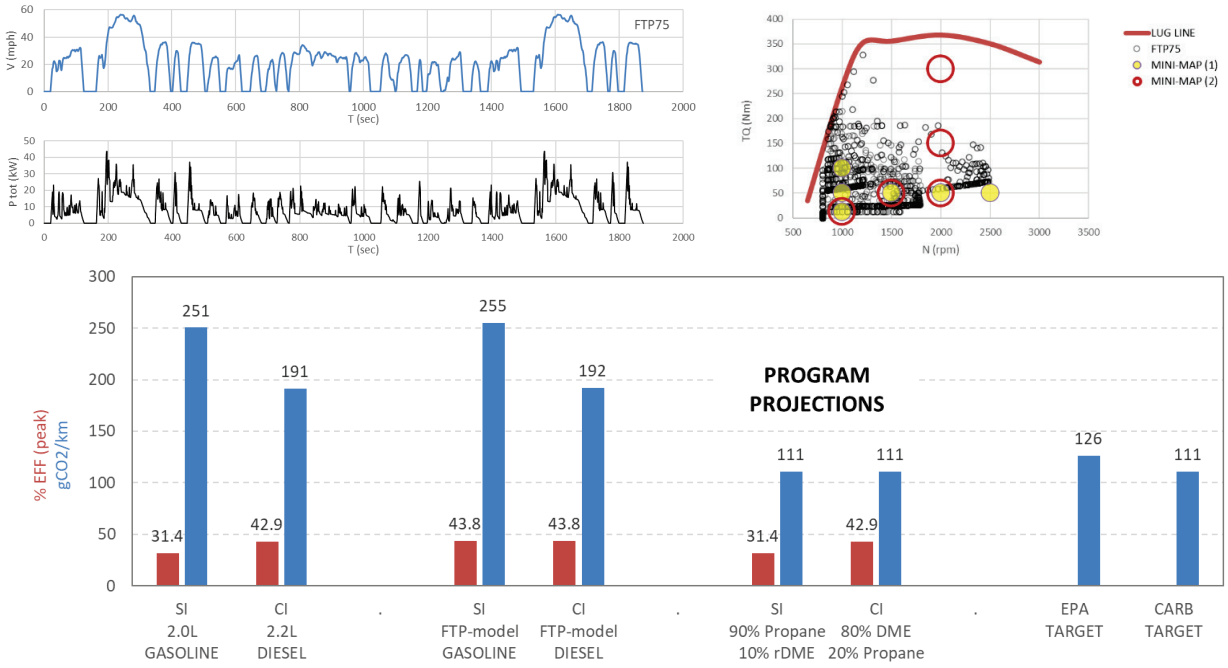

Figure VI.B.4.7 FTP cycle simulation predictions for CI and SI cases

Conclusions

The project is on track on its Budget Period 1 deliverables. The project has completed the design and modeling of the base fuel system and moved to model the advanced system capable of expanding the pressure range from 600 bar to 2,000 bar. The base system was extensively benchmarked with propane–DME mixtures. The pressure and flow control system was completed, demonstrating it can rely on the inlet metering valve windowing alone to control pressure in most cases, with the pressure regulator used to tune pressure during strong transients. The engine performance modeling effort completed its FTP simulator based on a discrete mini-map set of points. Estimates based on the mini-points provide a close approximation to the full cycle results, allowing the project to focus on discrete points for optimization of the engine and fuel system equipment.

References

1. Anselmo, Antonio. 2018. “Pathway to Market for a Superior Fuel.” 8th International DME Conference, San Diego.

2. EPA-NHTSA final fuel economy and GHG standards for light-duty vehicles. Projected 2021–2026 Fleet-Wide CO_2 and Fuel Economy Standards.

3. Makos, Patrycja, Edyta Słupek, Joanna Sobczak, Dawid Zabrocki, Jan Hupka, and Andrzej Rogala. 2019. “Dimethyl Ether (DME) as Potential Environmentally Friendly Fuel.” E3S Web of Conferences 116: 00048. https://doi.org/10.1051/e3sconf/201911600048.

Acknowledgements

The authors would like to recognize the support of Michael Ursic of National Energy Technology Laboratory as well as Kevin Stork and Gurpreet Singh of the U.S. Department of Energy Vehicle Technologies Office.

Additionally, we thank the following contributors from WM International Engineering: Herbert Gosewisch, project manager; Simon Wu, lead engineer on the fuel system controls; Audrius Brazauskas, lead engineer on the engine build; Jorge Pulpeiro, engine controls; and Anthony Galan Barreto, lead designer for the performance and durability test benches. From the Illinois Institute of Technology, we thank King Ankobeaansah, Hafiz Ahmad Hassan, Laura Pereira, and Kelvin Alvarado for their contributions. We also extend our gratitude to Dr. Dave Wickman of WERC, who supported the engine modeling, and to Bill Frauenheim and Sunil Akuluru from DCPC International for their contribution to the scope and for providing the fuel formulations used in the testing.

VI.B.5 High-Efficiency Mixing Controlled Compression Ignition Combustion of Propane Dimethyl Ether (DME) Blends (University of Wisconsin–Madison)

Sage Kokjohn, Principal Investigator
University of Wisconsin System
21 North Park Street Suite 6401
Madison, WI 53715
Email: kokjohn@wisc.edu

Kevin Stork, DOE Technology Manager
U.S. Department of Energy
Email: Kevin.Stork@ee.doe.gov

Start Date: April 1, 2022 End Date: March 31, 2025
Project Funding: $2,973,813 DOE share: $2,373,453 Non-DOE share: $600,360

Project Introduction

Medium-duty greenhouse gas (GHG) emission standards will require a 10% reduction by 2027, necessitating substantial changes in technology to significantly increase engine efficiency. Utilizing propane and dimethyl ether (DME) in these applications has the potential to substantially reduce the GHG or CO_2 emissions compared to conventional diesel operation due to the lower carbon content of the fuel. However, current propane-fueled engines rely on spark-ignited combustion and have efficiencies substantially below those of modern diesel engines, limiting the CO_2 benefits. The present program will develop a medium-duty, mixing-controlled compression ignition (MCCI) combustion system with propane as the fuel. The program will develop a medium-duty engine capable of >37.1% efficiency and >5% reduction in total cost of ownership. The targeted level of performance for the engine is a brake thermal efficiency improvement of >15% over the baseline spark-ignited liquid petroleum gas engine and well-to-wheels GHG emissions less than 450 g/bhp-hr.

Objectives

The overall goal of this project is to enable a 15% reduction in CO_2 emissions compared to current diesel engines by developing an MCCI combustion strategy capable of operating on blends of propane and DME. To achieve this goal, the program will develop and demonstrate a high efficiency mixing controlled combustion engine suitable for operation on propane and propane–DME blends. The use of mixing controlled combustion allows the engine to maintain the low-speed torque needed for many medium- and heavy-duty applications while allowing a high compression ratio to enable high efficiency.

Overall Objectives

- Development and assessment of a fuel system suitable for propane and propane–DME blends.
- Computation-led optimization of the combustion system capable of achieving stable, robust combustion over a range of propane and DME blends.
- Engine-level experiments to demonstrate engine efficiency and emissions of the optimized hardware configuration.
- Quantification of overall system performance, benefits, and drawbacks through comparisons with existing combustion systems. System-level comparison to existing combustion modes using cycle simulation tools.

Fiscal Year (FY) 2022 Objectives

- Design and adapt a propane–DME fuel system to the target medium-duty test engine.

- Set up test cell to enable combustion system development.
- Evaluate predictive ability of propane–DME reaction mechanisms.

Approach

Achieving stable MCCI operation with propane and propane–DME blends comes with two primary challenges. The first challenge is the development of a high-pressure direct-injection fuel system suitable for propane–DME. The second challenge is achieving stable ignition with a low cetane fuel such as propane. The project will address the fuel system challenges with pump designs that minimize wear and erosion from the low lubricity propane and DME at high pressures, and fuel injector designs that will contain the compressibility and tendency of cavitation. The ignition/combustion challenges will be addressed by building on the team's extensive research into achieving stable combustion of low cetane fuels (e.g., gasoline). Approaches that will be considered include use of a glow-plug, exhaust re-breathing to trap hot residuals, and injection into the negative valve overlap region. The overall effort will include fuel system development, fundamental ignition measurements, optical engine and spray measurements, computational fluid dynamics-based optimization, and engine level testing/demonstration.

Results

The following key technical achievements were made in FY 2022:

- Completion of a preliminary propane–DME fuel system design, build, and engine laboratory implementation.
- Evaluation of existing reaction mechanisms for propane–DME blends.
- Collection of baseline engine data for comparison.

A propane–DME fuel system capable of injection pressures up to 500 bar has been designed and fabricated. Figure VI.B.5.1 shows the schematic and final fabricated fuel system. The system includes an improved oil system and a simplified fuel circuit. A bench procedure was developed and automated to simplify the usage of the bench.

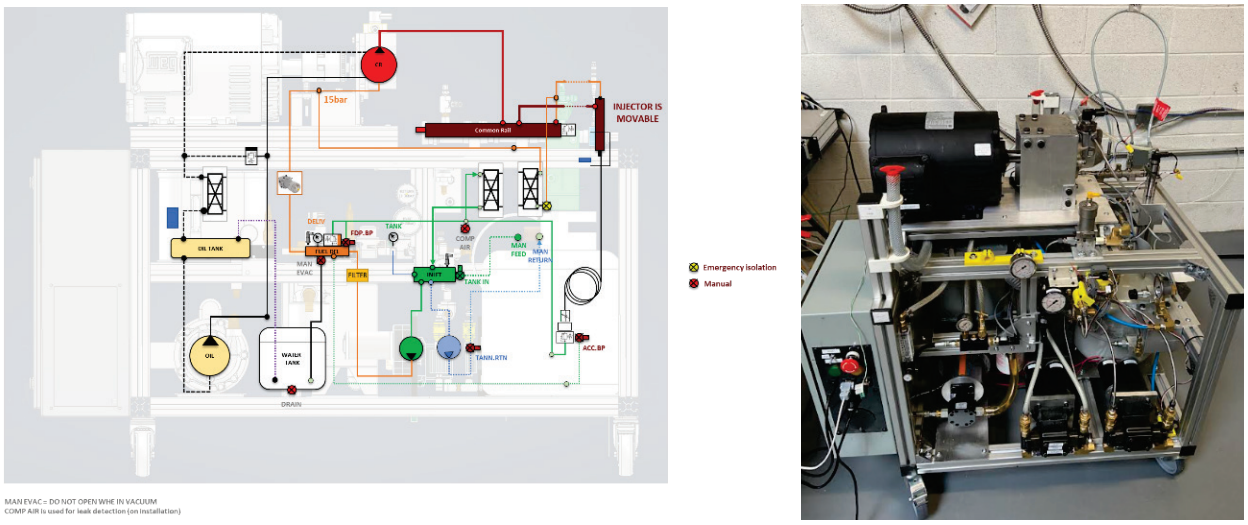

Figure VI.B.5.1 Fuel bench schematic and build

Testing was performed to verify operability of the system and develop flow maps for use in the engine lab. The results are shown in Figure VI.B.5.2. The injector flow is nearly linear with respect to the pulse width of the injection commands. The trends are consistent across the pressure setpoints and engine speeds. At higher

pressure and longer pulse widths, a slight tapering of the fuel amount is noted. This is expected as the rail pressure drops when more fuel is consumed by the injector.

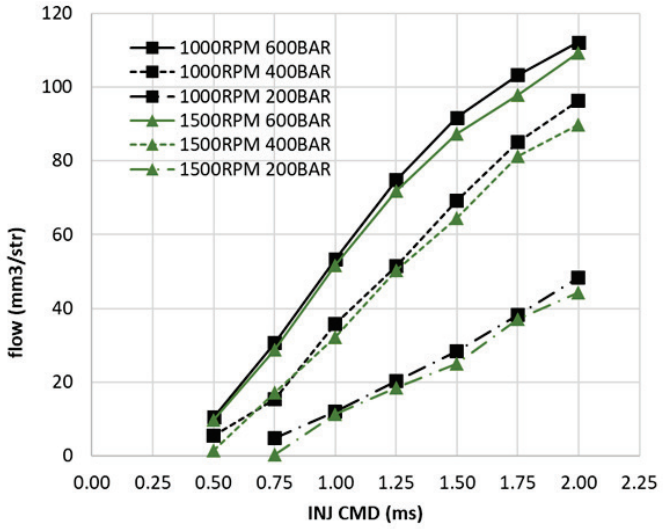

Figure VI.B.5.2 Injection calibration data at 1,000 rev/min and 1,500 rev/min, ranging from 200 to 600 bar

A bench-level model was developed and compared to measured data as shown in Figure VI.B.5.3. The results closely follow the modeled results performed on the pump-injection hardware deployed in the bench. The modeling captures the flow through the injector across the pressures and pulse widths tested. This provides confidence as the project continues to develop the system to higher pressures.

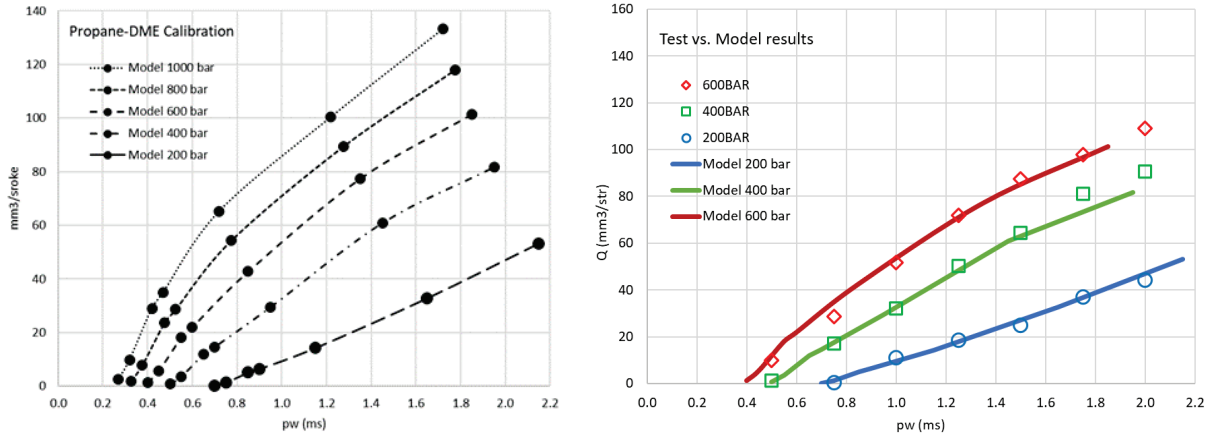

Figure VI.B.5.3 Propane–DME injector calibration

Experiments and simulations were performed to evaluate the performance of existing propane–DME reaction mechanisms that will be used in the computational fluid dynamics effort. This study is being conducted at the University of Central Florida's High-Pressure Extended Range Shock Tube for Advanced Research facility. This facility is capable of high-pressure experiments reaching up to 1,000 atm. The ignition delay times were captured using OH* (310 nm) and CH* radical chemiluminescent emission detection via window ports at the test location. Experiments were performed for neat DME, neat propane, and blends of propane and DME over a pressure range of 60–80 bar and a temperature range of 800 K–1,200 K. The results from the neat oxidation of propane are shown in Figure VI.B.5.4. The general trend of quickly expediting ignition with increased

temperature is observed in agreement with the model. No negative temperature coefficient behavior is observed in the measured temperature range (880 K–1,129 K) for propane oxidation.

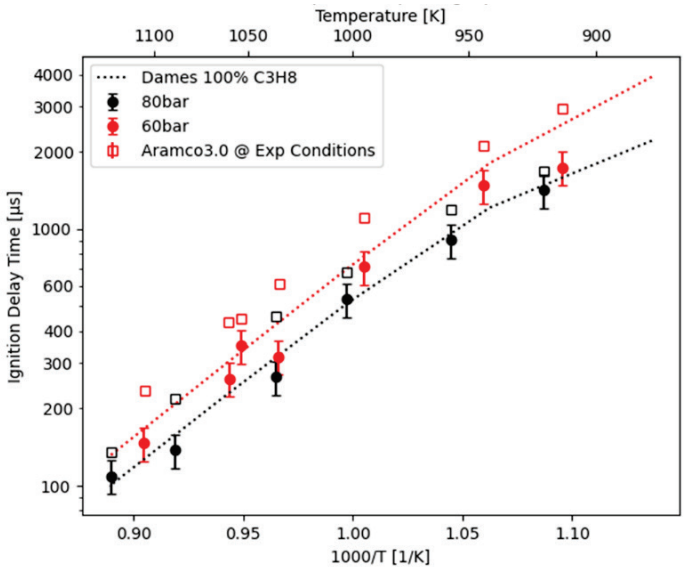

Figure VI.B.5.4 Ignition delay times for neat propane at 60 bar and 80 bar compared with Aramco 3.0 and Dames models

The results are provided in Figure VI.B.5.5 for the 60:40 DME–propane blend. Below 1,000 K, with a reduction in temperature, ignition delay time increases until it attains a peak value. Beyond this peak value, further reduction in temperature shortens ignition delay time. This increase and decrease in ignition delay time are captured by the Aramco 3.0 model qualitatively. Quantitative prediction by the model needs further improvement, which will be pursued in the later stage of this project which involves chemical kinetic model improvement.

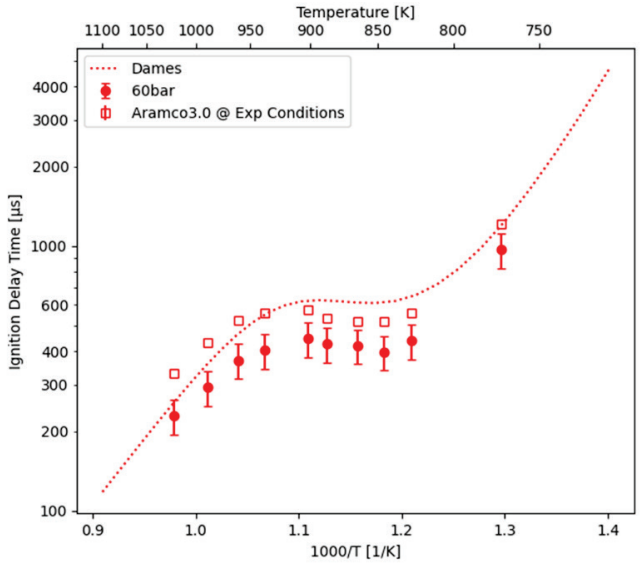

Figure VI.B.5.5 Ignition delay time for DME–propane 60:40 blend at 60 bar compared with Aramco 3.0 and Dames models

Laboratory setup was performed in both the metal and optical engines for the testing campaign to begin in FY 2023. Baseline data, which will be used for system-level model validation, were gathered. Three operating points (B25,

B50, B75) were chosen to cover a reasonable portion of the engine operating map and are typical of medium-duty engine operation, as shown in Figure VI.B.5.6 (left). At these three operating conditions, the engine was run with diesel fuel and used similar boundary conditions as the production calibration. At these loads, sweeps of the operating conditions were performed (intake pressure, exhaust gas recirculation rate, main start of injection (SOI) timing and air–fuel ratio). The engines indicated specific carbon dioxide ($ISCO_2$) emissions and gross thermal efficiency (GTE) from the main SOI timing sweep are shown in Figure 6 (right). From this and all the other different test points, the engine out $ISCO_2$ ranged from ~560 to 600 g/kWh and the GTE was seen to range from about 44% to 48%. These will be the target values to improve on when running on DME–propane fuels.

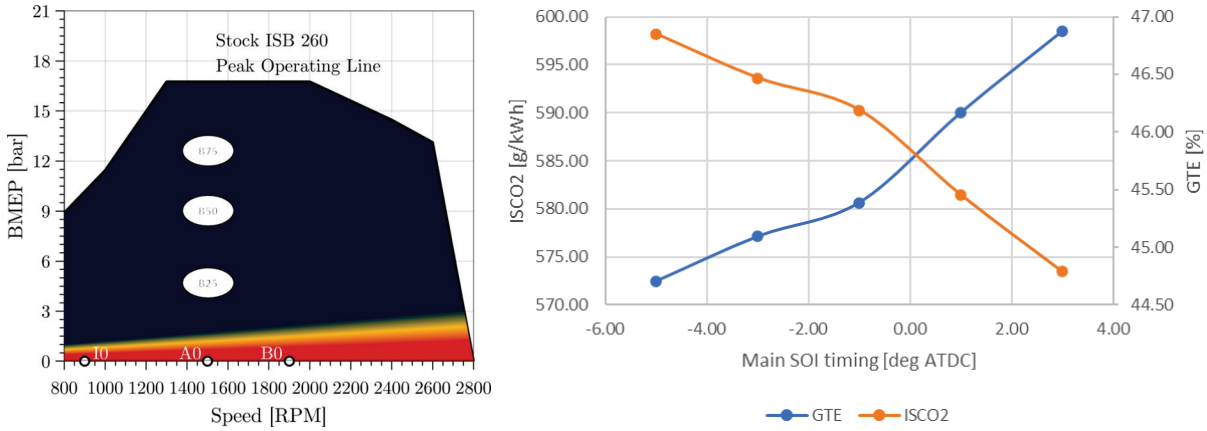

BMEP – brake mean effective pressure; atdc – above top dead center

Figure VI.B.5.6 (left) ISB engine operating map with three chosen operating points for the baseline engine testing. (right) Example $ISCO_2$ and GTE over a main SOI timing sweep.

The optical engine setup and test plan was developed in FY 2022. Experiments are scheduled to be completed in FY 2023. High-speed Schlieren images of a single fuel jet will be taken at three different SOI in-cylinder densities (7.5 kg/m^3, 15 kg/m^3, and 22.5 kg/m^3) under non-reacting conditions. Non-reacting conditions will be created using a liquid nitrogen vaporizer that feeds pure, high-pressure nitrogen gas through a feedback-controlled pressure regulator and an inline intake heater which allows for precise control of in-cylinder densities. Figure VI.B.5.7 shows a schematic detailing the optical engine's construction and the field of view that will be captured using Schlieren imaging.

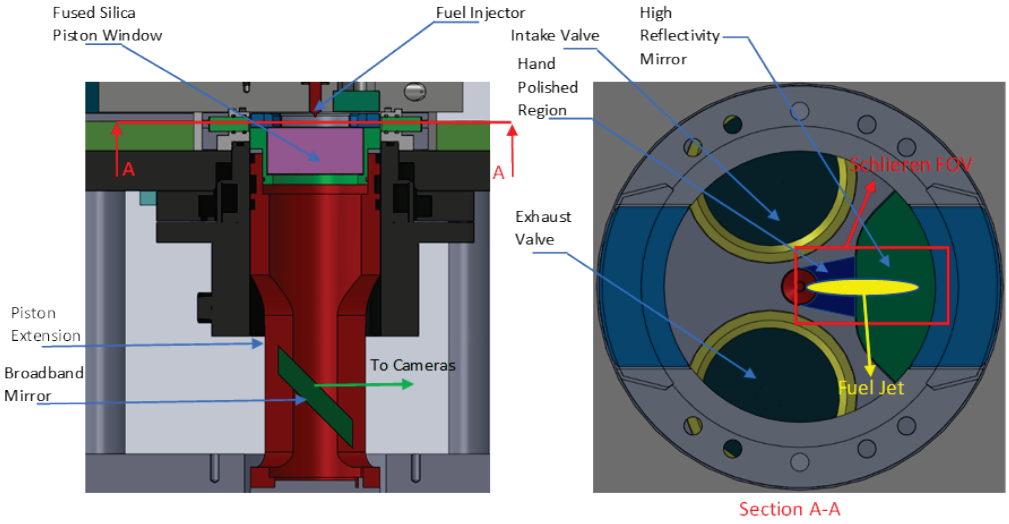

Figure VI.B.5.7 Schematic diagram of optical engine showing important features

Conclusions

- A propane–DME fuel system was designed, fabricated, and tested. The system is shown to be functional for installation in the engine laboratory for proof-of-concept testing.
- Experiments were performed over a range of temperatures, pressures, and blends of propane and DME. The results were compared to existing models. In general, the models show reasonable predictive performance, but several areas of needed improvement were identified.
- Laboratory setup in the optical and metal engines was completed, and baseline metal engine testing using diesel fuel was performed. Data were collected for model validation and technology assessment.

VI.B.6 High Efficiency, Ultra Low Emissions Heavy-Duty 10 Liter Natural Gas Engine Project (Cummins Inc.)

Tim Lutz, Principal Investigator
Cummins Inc.
1900 McKinley Avenue
Columbus, IN 47201
Email: Timothy.P.Lutz@Cummins.com

Kevin Stork, DOE Technology Manager
U.S. Department of Energy
Email: Kevin.Stork@ee.doe.gov

Start Date: February 1, 2022 End Date: April 30, 2025
Project Funding: $6,666,666 DOE share: $4,000,000 Non-DOE share: $2,666,666

Project Introduction

The costs of diesel engine and aftertreatment systems have increased significantly over the past two decades as both on-engine and aftertreatment emission controls have been implemented to meet regulations. The costs for these systems are expected to increase further to meet ultra-low nitrogen oxides (NO_x) emissions. In comparison, spark-ignited natural gas engines meet emissions with a simpler architecture consisting of stoichiometric combustion and a three-way catalyst system to achieve ultra-low NO_x.

Natural gas engines have another potential benefit of lower greenhouse gas emissions due to a favorable hydrogen-to-carbon ratio of fuel composition compared to other liquid petroleum fuels. However, the natural gas engines in the market are still not as efficient as diesel engines used in commercial vehicles or equipment. The impact of this lower efficiency is somewhat offset by a relative advantage in fuel cost per unit of natural gas versus diesel. One additional customer metric of natural gas engine viability is the associated payback period. It is a measure of the time to recover an increase in capital expense from purchasing a new technology through reductions in operating cost or increases in revenue enabled by the technology. Currently, only customers with very high equipment utilization are finding acceptable payback periods for natural gas technology relative to diesel. Therefore, it is essential to have increased efficiency on current natural gas technology to reduce the payback period for broader adoption of the technology.

Objectives

The objective of the project is to research, develop, and validate a next-generation-combustion-system-equipped heavy-duty natural gas engine that utilizes high tumble charge motion building upon a proven high-cylinder-pressure-capable heavy-duty base engine platform in the 10-liter displacement range.

Overall Objective

- Demonstrate a diesel-like torque curve rating of at least 400 bhp and 1,350 lb-ft peak torque.
- Demonstrate peak brake thermal efficiency (BTE) of 42% (>10% improvement over commercially available product).
- Demonstrate cycle-average BTE of 36% on the Heavy Duty Federal Test Procedure cycle and 39% on the Ramped Modal Cycle Supplemental Emissions Test cycle.
- Maintain 0.02 g/bhp-hr brake-specific NO_x capability with a plan to reduce aftertreatment cost while meeting all other criteria pollutant limits for a 2027 U.S. Environmental Protection Agency/California Air Resources Board certification.

Fiscal Year 2022 Objectives

- Create simulation models to predict engine performance based on other models developed for spark-ignition engines.
- Use these models to determine the engine architecture and path to reach program efficiency targets.
- Begin the design of a new cylinder head with pent roof, tumble intake port geometry, and optimized combustion deck cooling. Head design will include double overhead camshafts with camshaft phasers or other variable valve timing technology and hydraulic lash adjusters.
- Begin the design of the port-injected fuel system including injector installation, fuel rail, fuel filter, fuel regulator (if needed), and sensor(s).
- Begin optimization of the combustion system using computational fluid dynamics (CFD) simulation.

Approach

CFD and engine simulation models will be created to design and optimize the cylinder head, valvetrain, intake manifold, pistons, and turbo match. Analysis-led design efforts will confirm the architecture direction to have a non-exhaust gas recirculation (EGR) combustion system. Engine simulation will be used to build confidence in the ability to achieve the BTE and power-density targets while meeting design limits.

Upon completion of the design and analysis tasks, hardware will be ordered and an engine will be built. Initial testing will validate the analysis models and confirm the ability to achieve power and torque targets. Hardware options identified through analysis—such as different camshafts, pistons, or turbos—will be tested for effects on efficiency and emissions. The final hardware will be selected, and engine calibration and tuning will be completed to demonstrate the ability to meet the efficiency targets. Transient emissions testing will be done to demonstrate the ability to achieve ultra-low NO_x emissions along with a reduction in greenhouse gas emissions.

Results

Key Accomplishments and Results in Fiscal Year 2022

- Cylinder Head Design
  - Pent roof design concept with dual overhead camshafts is underway, including port injector installed in the head with an integral fuel rail.
  - Water jacket design for effective cooling around the spark plug and valve bridges is underway.
- GT Power Engine Performance Analysis
  - A preliminary design of experiments (including valve timing, compression ratio, and combustion phasing complete at both rated power and torque peak) is complete. Directionally, this points to the benefits of high compression ratio with late intake valve closing (Miller Cycle) and retarded combustion phasing to limit knock as a preferred strategy on or near the torque curve.
  - Analysis showing the ability to hit the peak efficiency target of 42% BTE is complete. Additional work is needed to reduce the uncertainty in this analysis, but it is an encouraging result.
  - GT Power analysis showing that EGR will be effective in limiting exhaust temperatures is complete. The effect on BTE ranges from negligible to a small positive benefit. The presumptive direction for this project is to have an engine architecture without EGR; however, EGR will be considered as a way to limit exhaust temperatures if other strategies prove to be insufficient.

- Creation of combustion CFD model. Baseline studies of mixing and combustion at rated power and peak torque were completed.

Discussion of Results

Good progress has been made on the cylinder head shown in Figure VI.B.6.1. The pent roof head incorporates intake ports to generate tumble charge motion. Overhead cams with phasers are installed in a cam carrier bolted to the head. Port injectors are incorporated into the head, fed by a fuel rail that is also integrated into the head. Work on the cooling jacket design and other detailed features is underway.

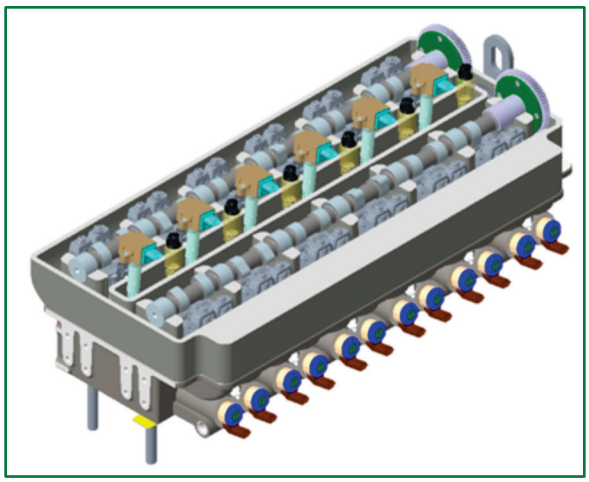

Figure VI.B.6.1 Cylinder head design

A design of experiments run in GT Power engine simulation studied the effects of combustion phasing (controlled by spark timing), compression ratio, and intake valve closing (IVC) on BTE at torque peak. The design of experiments was conducted at constant knock probability, which is a limiting factor in engine performance and efficiency. Increasing compression ratio by itself will increase efficiency but also increases the likelihood of damaging knock. Similarly, advancing combustion phasing will increase efficiency but also increases the likelihood of damaging knock. Late IVC by itself reduces temperatures in the cylinder at top dead center (TDC) by reducing the amount of compression work done on the trapped air in the cylinder, which reduces the likelihood of damaging knock. The tradeoff with late IVC is that it requires more boost to force the same amount of air into the cylinder, which can be a limiting factor.

Figure VI.B.6.2 shows the results of this study where each curve is a different IVC value. What can be seen in these results is that for a given IVC, increasing compression ratio but retarding combustion phasing (to offset the increased knock probability) always results in an increase in BTE. It can also be seen that later IVC also consistently improved BTE. Based solely on these results, the best BTE is achieved with the highest compression ratio, most retarded combustion phasing, and latest IVC possible. However, there are practical considerations that will be studied further in this program. Spark timing that is too retarded risks misfire. Late IVC requires increased boost, which will be limited by turbocharger capability. In addition, the IVC for best BTE at high load may not perform well at low loads or idle. The cam phaser can adjust IVC to a more preferred timing at low loads, but there are limits to how much the phaser can change IVC.

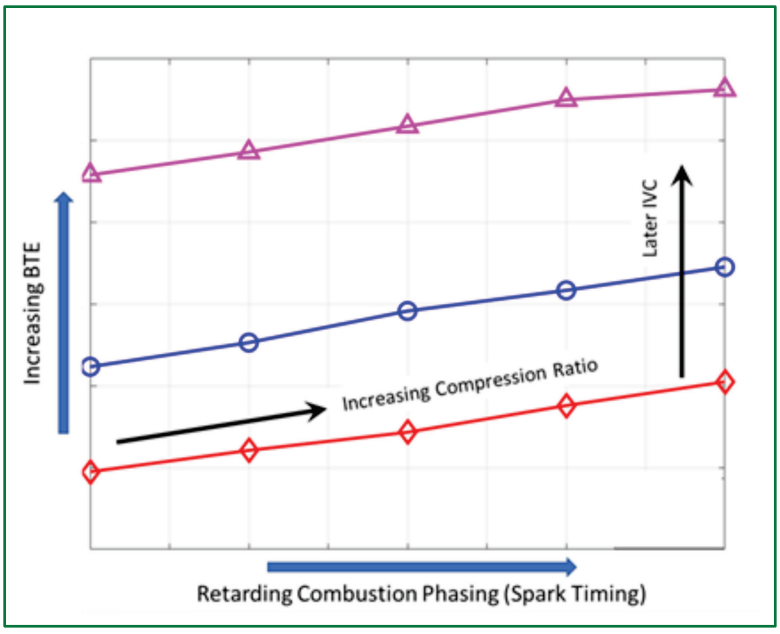

Figure VI.B.6.2 GT Power simulation results at torque peak showing the effects of combustion phasing, compression ratio, and IVC on BTE

Next, a sweep of exhaust valve opening (EVO) was done using values for IVC, combustion phasing, and compression ratio selected from the previous design of experiments. Results at torque peak are shown in Figure VI.B.6.3. Advancing EVO to be earlier in the cycle increased BTE to a point, beyond which BTE started to decrease. In general, earlier EVO reduces the amount of work that can be extracted in the cylinder as the gases expend from combustion, reducing closed-cycle efficiency. However, earlier EVO does provide more energy to the turbocharger, allowing it to generate more boost. The increased boost generates positive work during the intake stroke, which more than offsets the loss in expansion work with a net increase in BTE, up to a point. Beyond that, the loss in expansion work is more than can be recovered by increased open-cycle work.

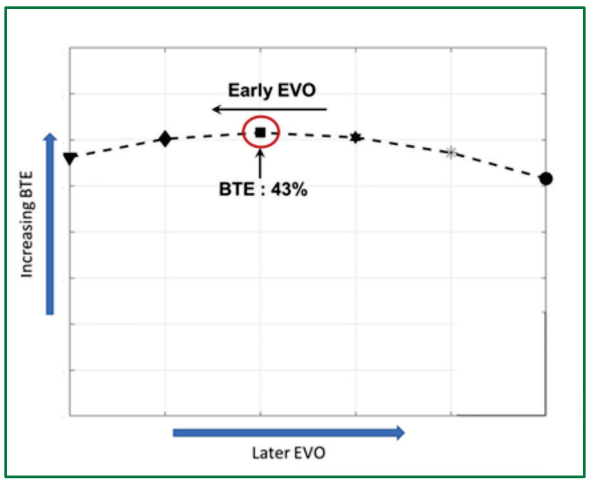

Figure VI.B.6.3 Effect of exhaust valve opening on BTE at torque peak

Note that the peak BTE predicted in this analysis is 43%, which is encouraging relative to the program target of 42%. However, these are uncalibrated models, and there is uncertainty in efficiency predictions as well as the ability to predict knock, which is a key limiting factor. While this is encouraging, work remains to reduce the uncertainty and gain confidence in this result.

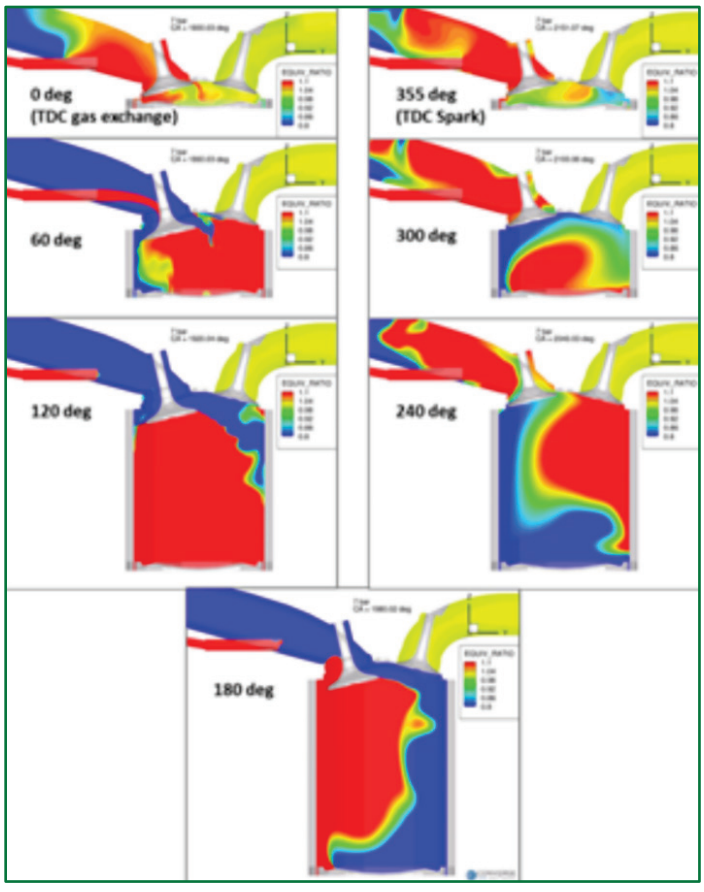

Figure VI.B.6.4 Mixing of air and fuel at rated power

Figure VI.B.6.4 shows mixing of air and fuel driven by the tumble charge motion (with crank angle [CA] indicated). The port injector located near the bottom of the intake port starts injecting fuel shortly after the intake valve opens. The contours of equivalence ratio show fuel-rich zones as red and lean zones as blue. Note that with the late IVC strategy, some amount of fuel is pushed back into the intake port before the intake valve closes. Figure VI.B.6.5 shows the resulting combustion as indicated by temperature contours. This baseline case shows adequate mixing and combustion, but further analysis will be done to optimize these results.

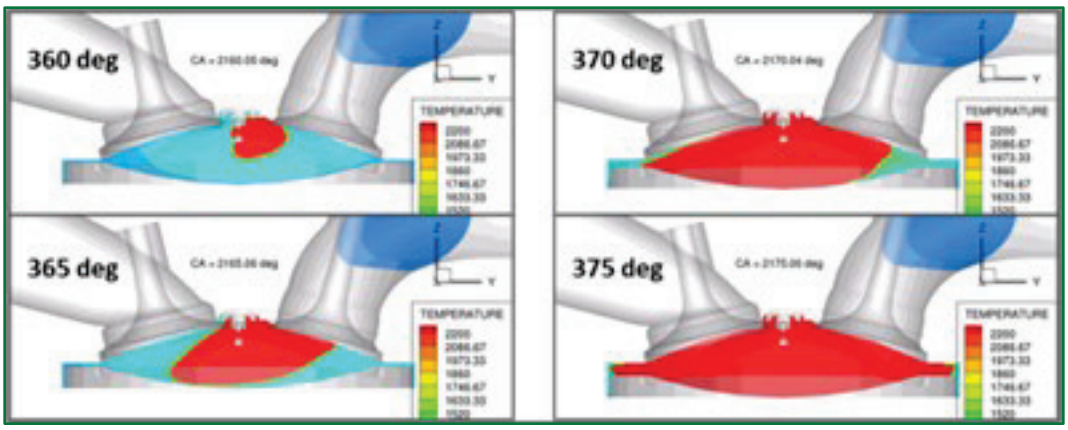

Figure VI.B.6.5 Combustion at rated power

Conclusions

- A design concept for the cylinder head is well underway. This includes dual overhead cams with phasers, pent roof with ports to generate tumble charge motion, and port fuel injectors installed in the head.
- A GT Power model has been created adopting best practices for other spark-ignited models.
- A preliminary design of experiments was completed in GT Power, varying combustion phasing (spark timing), compression ratio, and intake valve closing to optimize BTE. General trends show the best BTE is achieved with the highest compassion ratio, most retarded combustion phasing, and latest IVC. There will be practical limitations for compression ratio, combustion phasing, and IVC that will be assessed in future work.
- A GT Power study of exhaust valve opening was completed. There is a specific value for EVO that provides an optimum balance of closed-cycle work and open-cycle work to produce the best BTE.
- A combustion CFD model has been created. Baseline analysis cases have been completed showing adequate mixing of fuel and air. The combustion is also acceptable. Additional analysis will be conducted to optimize these results.

VI.C Emission Control

VI.C.1 Greatly Reduced Vehicle Platinum Group Metal (PGM) Content Using Engineered, Highly Dispersed Precious Metal Catalysts (Washington State University)

Yong Wang, Principal Investigator
Washington State University
Voiland School of Chemical Engineering and Bioengineering
Wegner Hall, Room 153
P.O. Box 642710
Pullman, WA 99164-2710
Email: wang42@wsu.edu

Siddiq Khan, DOE Technology Manager
U.S. Department of Energy
Email: Siddiq.Khan@ee.doe.gov

Start Date: October 1, 2020 End Date: December 31, 2023
Project Funding: $1,041,666 DOE share: $833,333 Non-DOE share: $208,333

Project Introduction

With the onset of super ultra-low emission vehicle (SULEV) and Tier III emissions standards, automotive PGM demand is driving global industry costs, from $19.1 billion in 2018 to $54.6 billion in 2020, resulting in significant supply deficits of Pd and Rh, which are the most expensive PGMs at present. Growing vehicle weight to meet customer expectations and safety requirements is further driving PGM usage. Given these drivers, along with the fact that greater than 95% of light-duty vehicle fleets employ stoichiometric powertrains with three-way catalyst (TWC) aftertreatment systems, there is an industry-wide call to maximize TWC activity while drastically reducing the PGM content.

The key components of TWCs are PGMs (Pt, Pd, and Rh) for redox reactions (oxidation of CO and hydrocarbons [HC] on Pd and Pt; NO reduction on Rh) and oxygen storage materials (reducible oxides such as CeO_2) that enable the operation of the catalyst under nominally stoichiometric conditions. The operating conditions under which TWCs need to perform effectively are very demanding; they must be active at low temperatures for cold start (The 150°C Challenge [1]) and be able to survive up to ~1,000°C under severe hydrothermal conditions (i.e., at high H_2O concentrations). Additionally, they must be resistant to poisons originating from fuel and engine oil (mostly S and P). Conventional TWCs face two major limitations: (1) Rh or Pd sintering under intermediate aging and (2) further sintering and alloying of Rh and Pd under full useful life aging [2]. Another less critical limitation is the deactivation of Rh due to solid state reactions between Rh and Al_2O_3 at extreme temperatures [3], [4]. Currently, high Pd and Rh loadings are used to offset the activity loss due to sintering and alloying, drastically increasing the catalyst cost. For example, fresh TWCs typically have Pd or Rh particle sizes in a range of 3–5 nm, but towards the end of a vehicle's full useful life, PGM particle sizes in TWCs often reach 50–100 nm, which means less than 2% of the PGM atoms are accessible for catalytic reduction of nitrogen oxides (NO_x) and oxidation of HCs and CO [5]. High Pd and Rh loadings also unavoidably increase the chances of Pd and Rh mobility during catalyst preparation or under aging conditions, leading to Pd/Rh alloy formation with diminished TWC activities.

Objectives

Overall Objective

Our overall objective is to demonstrate vehicle federal test procedure, US06 test performance, and highway fuel economy test performance comparable to a baseline (SULEV30) system with a reduction in PGM content by a factor of 2–4.

Fiscal Year 2022 Objectives

Our Fiscal Year (FY) 2022 objective was to focus on technology transfer and validation by incorporating the powder formulation into a slurry based washcoat and applying it to a suitable ceramic catalyst support. We conducted simulated engine tests (U.S. DRIVE TWC test protocols) and baseline with current BASF TWC catalysts, with the specific goal of meeting or exceeding the BASF baseline catalyst performance (SULEV30) with a factor of 2–4 reduction in PGM content.

Approach

To achieve the overall objective, we proposed to use atom trapping to create thermally durable single-atom catalysts (atSAC) recently reported by us in *Science* [6]. Rh deactivation by rhodate formation was mitigated by the use of modified alumina supports and washcoat preparation procedures by BASF.

- Develop and optimize thermally durable Pd and Rh atSACs using practical BASF modified Al_2O_3 supports with dispersed oxygen storage components (OSC, e.g., ZrO_2 or CeO_2).
- Demonstrate the advantages of the Pd and Rh atSACs in an engineered form (washcoat substrate) over the baseline BASF catalysts.
- Integrate the leading candidate catalyst formulation into a fully functioning light-duty vehicle aftertreatment system.

We anticipated that this would effectively reduce Pd and Rh usage from the current 5–10 g Pd/vehicle and 0.4–1.2 g Rh/vehicle to 1.25–2.5 g Pd/vehicle and 0.1–0.3 g Rh/vehicle, representing cost savings of $360–$820/vehicle and $6.4 billion to $14.3 billion for the light duty sector in North America in 2025. We expect further cost savings in diesel oxidation catalyst applications after leveraging knowledge gained in PGM reduction from the TWC effort.

Results

- We have scaled up the synthesis of a lead catalyst formulation for the preparation of 10 g of catalyst.
- We have demonstrated that the catalyst synthesized at 10-g scale exhibits the similar performance as the baseline BASF catalysts in NO reduction using the U.S. DRIVE protocols, but with five times less Rh content.
- After successfully scaling up the synthesis of a lead catalyst formulation for the preparation of 10 g of catalyst, we have further scaled up the synthesis of the same lead catalyst composition for the preparation of 100 g of catalyst required for the core sample preparation.
- 100 g of catalyst were synthesized and provided to BASF. Three core samples were prepared by BASF including a baseline and two samples with lead composition identified.

We first examined ceria–alumina supports with increasing ceria content (CA08, CA13, CA30, CA50, here “CA” represents ceria–alumina and “08”, “13”, “30”, and “50” represent 8 wt%, 13 wt%, 30 wt%, and 50 wt% ceria content, respectively). These supports were provided by BASF to assess their ability to trap platinum (Pt) atoms compared to pure ceria prepared by decomposition of cerium nitrate (polyhedral ceria). All ceria–alumina supports contained crystalline ceria as well as isolated cerium cations dispersed on alumina, but the two forms of ceria differed remarkably in their ability to trap Pt atoms. The atom-trapped Pt resided primarily

on the ceria crystallites, whereas the atomically dispersed cerium present in the form of Ce^{3+} cations on alumina was not effective in trapping Pt atoms, at least not at 800°C in air.

Using CO oxidation as a probe reaction to evaluate the performance of the Pt catalysts, CA50 was the best catalyst support for achieving very good low temperature reactivity for the Pt catalyst (Figure VI.C.1.1). The ceria–alumina samples retained small crystallite sizes and helped preserve a high surface area compared to pure ceria, which lost almost all its surface area after heating at 800°C in air. However, in terms of atom trapping efficiency, pure crystalline ceria was the most effective, despite having a lower surface area and larger crystallite size. We found that just the presence of Ce^{3+} cations was not sufficient for atom trapping; the extended surface is needed to allow Pt to form the stable four-fold complex. We also found that the smallest ceria crystallites in CA08 provide the greatest thermal stability, since the ceria phase in CA08 sample did not show significant sintering or particle growth after heating to 800°C in air for 10 hr. From the viewpoint of developing sustainable emission control catalysts with the lowest rare-earth loading, we see 50% ceria as the optimal sample since its performance after depositing Pt exceeds that of pure ceria.

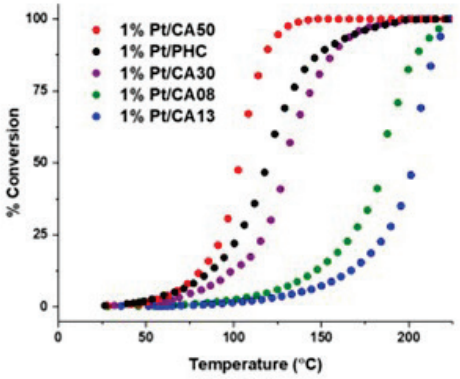

PHC – polyhedral ceria

Figure VI.C.1.1 oxidation on 1 wt% Pt/ceria–alumina and Pt/ceria catalysts after reduction in flowing CO. Data plotted are for the third run. Experimental conditions for CO oxidation: 20 mg sample, He = 75 ml/min, CO = 1.5 ml/min, O_2 = 1 ml/min, ramp rate 2°C/min to 300°C. Reduction treatment: He = 75 ml/min and CO = 5 ml/min at 275°C for 1 hr. The improved performance of Pt/CA50 can be attributed to smaller crystallites of ceria on the alumina, providing a higher surface area and more facile oxygen transfer to the Pt metal crystallites formed during reduction.

Based on the trapping studies using Pt as discussed above, we have selected appropriate ceria–alumina supports to atom trap Rh. Several samples including PNNL3, PNNL5, PNNL6, and PNNL13 were synthesized by atom trapping, all containing 0.1 wt% Rh. The difference of these samples lies in the varied optimization conditions used for selective deposition of Rh on ceria domains. In addition, three baseline catalysts (B1, B2, and B3) with 0.5 wt% Rh were provided by BASF.

These samples were all hydrothermally aged by BASF at 980°C under oscillating lean and rich conditions with 10% steam. Then the light-off measurements were conducted, and results are shown in Figure VI.C.1.2. The lower half panels in Figure VI.C.1.2 (Run 2 input/output [I/O]) indicate that PNNL3 achieves similar activity as baseline B1, B2, and B3 catalysts, as evidenced by similar temperature required to reach 50% conversion of CO (Figure VI.C.1.2a), HC (Figure VI.C.1.2b), and NO (Figure VI.C.1.2c).

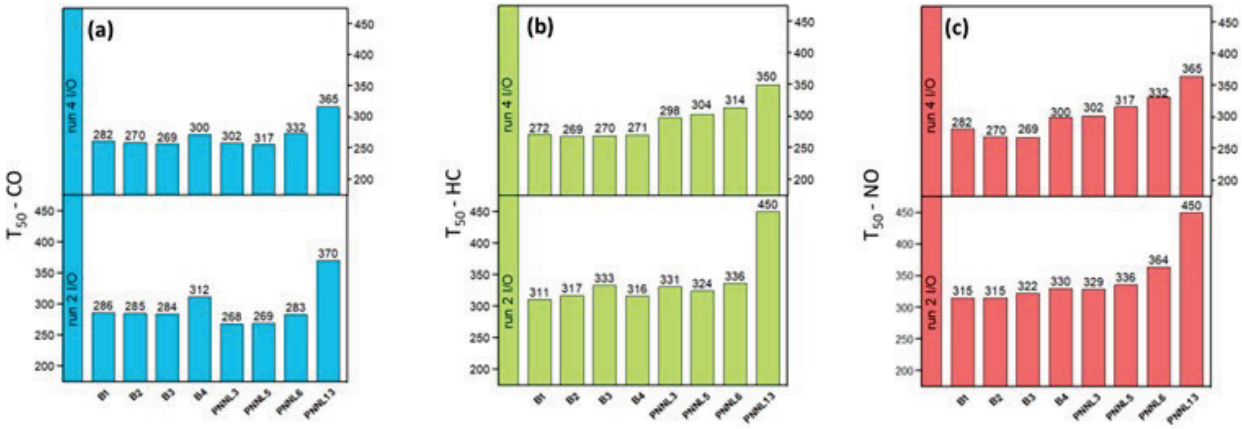

Figure VI.C.1.2 Temperatures required to reach 50% conversion for (a) CO, (b) HC, and (c) NO. Upper panels (Run 4 I/O) were generated after sweeping to rich conditions, lower panels (Run 2 I/O) were generated before sweeping to the rich conditions. Catalyst testing conditions: gas hourly space velocity = 70,000 hr^{-1}, oscillating feed (1 s lean – 1 s rich), feed contains CO, H_2, O_2, HC (C_3, $C_3^=$), NO, CO_2, H_2O.

After sweeping catalysts from lean to rich conditions, another light-off measurement was conducted; results are shown in the upper panel of Figure VI.C.1.2 (Run 4 I/O). Clearly, even after rich treatment, PNNL still exhibited similar activities as B1, B2, and B3, again evidenced by similar temperatures required to reach 50% conversion of CO (Figure VI.C.1.2a), HC (Figure VI.C.1.2b), and NO (Figure VI.C.1.2c).

PNNL3 formulation was thus selected for the scaleup synthesis. Our separate activity testing confirmed that PNNL3 formulation can be replicated at 100-g scale which is required for the synthesis of core samples. After providing 100 g of PNNL3 sample to BASF, BASF developed a protocol to prepare the slurry and washcoat PNN3 on core substrates. A baseline sample with 0.5 wt% Rh was also wash coated on the core substrate. These core substrates will be hydrothermally aged and tested in the first quarter of FY 2023 to confirm that the PNNL3 prepared by atom trapping can achieve similar performance as the baseline catalyst but with five times less Rh.

Conclusions

- Pt was used to probe the atom trapping efficiency of commercial supports containing alumina. It was found that dispersion of Pt is dependent on the ceria content and domain size. Ceria crystallites trap Pt atoms while isolated Ce cations on alumina do not. This discovery enables the design of catalyst support and synthesis protocols to selectively trap Rh on a commercially available ceria–alumina support.
- We identified a lead catalyst formulation based on commercially available supports, which gives similar performance with baseline catalysts but with five times less Rh content.
- Catalyst synthesis was replicated at a 100-g scale, and the core samples were thus prepared and will be used to demonstrate the performance advantages over the baseline catalysts provided by BASF.

Key Publications

1. Pham, H., A. DeLaRiva, E. Peterson, R. Alcala, K. Khivantsev, J. Szanyi, X. Li, D. Jiang, W. Huang, Y. Sun, P. Tran, Q. Do, C. DiMaggio, Y. Wang, and A. Datye. 2022. “Designing Ceria/Alumina for Efficient Trapping of Platinum Single Atoms.” *ACS Sustainable Chemistry and Engineering* 10 (23): 7603–7612. https://doi.org/10.1021/acssuschemeng.2c01380.

References

1. ACEC (Advanced Combustion & Emission Control) Low-Temperature Aftertreatment Group. 2012. “Future Automotive Aftertreatment Solutions: the 150°C Challenge.” U.S. DRIVE Workshop. Southfield, MI.
2. Lambert, C.K. 2019. “Current State of the Art and Future Needs for Automotive Exhaust Catalysis.” *Nature Catalysis* 2 (7): 554–557.
3. Wong, C., and R.W. McCabe. 1989. “Effects of High-Temperature Oxidation and Reduction on the Structure and Activity of Rh/Al_2O_3 and Rh/SiO_2 Catalysts.” *Journal of Catalysis* 119: 47–64.
4. Chen, J.G., et al. 1990. “Thermal Behavior of a Rh/Al_2O_3 Model Catalyst: Disappearance of Surface Rh upon Heating.” *Journal of Physical Chemistry* 94: 5059–5062.
5. Kang, S.B., et al. 2011. “Activity Function for Describing Alteration of Three-Way Catalyst Performance over Palladium-Only Three-Way Catalysts by Catalyst Mileage.” *Industrial & Engineering Chemistry Research* 50 (9): 5499–5509.
6. Jones, J., et al. 2016. “Thermally Stable Single-Atom Platinum-on-Ceria Catalysts via Atom Trapping.” *Science* 353 (6295): 150–154.

Acknowledgements

We greatly acknowledge the continuous discussions and advice from National Energy Technology Laboratory manager Ralph Nine.

VI.C.2 Slashing Platinum Group Metals in Catalytic Converters: An Atoms-to-Autos Approach (General Motors LLC)

Dr. Wei Li, Principal Investigator
General Motors LLC – Research and Development
30470 Harley Earl Boulevard
Warren, MI 48093
Email: wei.1.li@gm.com

Siddiq Khan, DOE Technology Manager
U.S. Department of Energy
Email: Siddiq.Khan@ee.doe.gov

Start Date: October 1, 2020 End Date: December 31, 2023
Project Funding: $967,180 DOE share: $493,262 Non-DOE share: $473,918

Project Introduction

Platinum group metals (PGMs) are used in three-way catalysts (TWCs) for stoichiometric gasoline engine vehicles to simultaneously convert carbon monoxide, hydrocarbons, and nitrogen oxides into nitrogen, carbon dioxide, and water. For U.S. light-duty gasoline vehicles, about 3–8 grams of PGMs are used in each catalytic converter system, and the PGM loading is expected to increase for future vehicles, driven by increasingly stringent emissions standards, potentially lower engine exhaust temperatures, and higher emission control system durability requirements. The technical necessity for the current high PGM loadings is driven largely by (1) poor atomic efficiency (or metal dispersion) of PGMs on catalyst supports with the current synthesis approaches and (2) severe deactivation of unstable PGM nanoparticles in high-temperature engine exhaust. Therefore, the project team will develop catalyst technologies that not only maximize the PGM atom efficiency and intrinsic activity in the fresh state, but also maintain the benefits during aging with extended exposure in engine exhaust.

During the first year of the project, the baseline catalyst technology has been defined and characterized in detail, and this state-of-the-art production catalyst technology will be used as the benchmark for the milestone targets. Practical and representative catalyst aging and testing protocols have been defined for use throughout the project to ensure consistency. Various preparation methods have been attempted to synthesize fresh catalysts with predominantly single-atom Pd and Rh structures, and their three-way catalytic performances have been evaluated after lean–rich cycling aging. Combining these species with engineered support materials led to much-improved, highly efficient Pd and Rh catalysts that have shown the potential for 60% reduction of the PGM loadings while maintaining performance.

Objectives

This project aims to enable new technologies to reduce PGM use in the U.S. gasoline vehicle fleet by 50% while meeting future emission regulations (including super-ultra-low-emission vehicle 30 [SULEV30] standards), thereby reducing TWC cost by 50% with no loss of performance or reliability over the baseline TWC system and enhancing the competitiveness of the U.S. automotive industry.

Overall Objectives

- Design and select optimal Pd and Rh structures in the form of isolated single atoms, coupled ensembles, or alloyed small clusters for high PGM dispersion, excellent intrinsic TWC activity, and promising aging resistance.

- Optimize Pd- and Rh-support interaction through surface defect engineering and local structure design to enhance the stability under realistic aging conditions and maximize the density of targeted PGM species on selected catalyst supports such as alumina and zirconia.

- Design full-size monolithic catalysts, develop manufacturing procedures using the best-performing Pd and Rh formulations, and demonstrate fully formulated TWC technologies in engine or vehicle tests.

Fiscal Year 2022 Objectives

- Optimize Pd and Rh catalyst formulations at the powder level for equivalent performance and improved aging resistance at 60% less PGM loading.
- Optimize Pd and Rh catalyst synthesis techniques at the core-sample level for equivalent performance and simplicity for large-scale production.
- Perform advanced characterization and a reaction kinetics study to gain insights into the deactivation mechanism.

Approach

Our approach uses individual PGM atoms as building blocks—not necessarily as direct catalytic centers—to form highly active catalytic structures with near 100% dispersion. Pd and Rh structures in the form of isolated single atoms, coupled ensembles, or alloyed small clusters will be prepared and evaluated to identify the optimal catalytic sites. Concurrently, surface defects will be generated on the engineered support materials to provide the anchoring sites for these structures.

The project team includes scientists, researchers, and engineers from five different organizations in industry and academia: General Motors LLC (GM), Pacific Northwest National Laboratory (PNNL), University of Virginia (UVA), University of Central Florida (UCF), and BASF. While multiple organizations are involved, each has well-defined tasks that make management of the overall project more efficient. GM and UCF will lead the project activities to develop supported Pd and Rh structures exhibiting near 100% dispersion with optimal interaction with the support materials. UVA and PNNL will carry out kinetic and characterization work to provide feedback for further materials development and optimization. BASF will take the lead on integrating the newly developed materials into full-size, fully formulated TWCs and work together with GM to evaluate/validate the full-size parts on an engine dynamometer and/or a vehicle. Moreover, GM manages all activities and serves as a central point of contact to integrate all the information for this project.

Results

Optimize Pd and Rh catalyst formulations at the powder level for equivalent performance and improved aging resistance at 60% less PGM loading

The team reported spray-dried Rh-Ce/$CeAlO_x$ and Pd-CePr/$CeAlO_x$ concept catalysts at the powder level, showing equivalent light-off performance compared to the baseline technologies with 60% less PGM loading (0.2% Rh and 0.8% Pd by weight, respectively). A series of control samples were also synthesized and tested at the powder level to highlight the uniqueness and novelty of the proposed concepts. Because of multiple steps involved in the synthesis procedure and the complexity (such as PGM and promoter ratio optimization), the team continued to explore opportunities to further simplify the preparation methods for large-scale manufacturing without compromising catalyst light-off performance and aging resistance.

Optimize Pd and Rh catalyst synthesis techniques at the core-sample level for equivalent performance and simplicity for large-scale production

After a series of Pd and Rh catalyst concepts were proposed and proved efficient in PGM thrifting after lean–rich cycling aging at the powder level, the team prepared core samples incorporating the new catalyst concepts while reasonably simplifying the catalysts' synthesis procedure. After the first batch of core sample preparation, one catalyst formulation was ruled out because of unideal slurry properties for wash coating, and the other two were tested after GM lean–rich cycling. The performance of these latter two is reported along with their corresponding powder samples. As shown in Figure VI.C.2.1, we observed comparable—and in some cases even lower—T50s for the two new catalyst technologies at 60% less Pd loading relative to 2% Pd/Al_2O_3 by weight at both the powder- and core-sample levels, regardless of emission type.

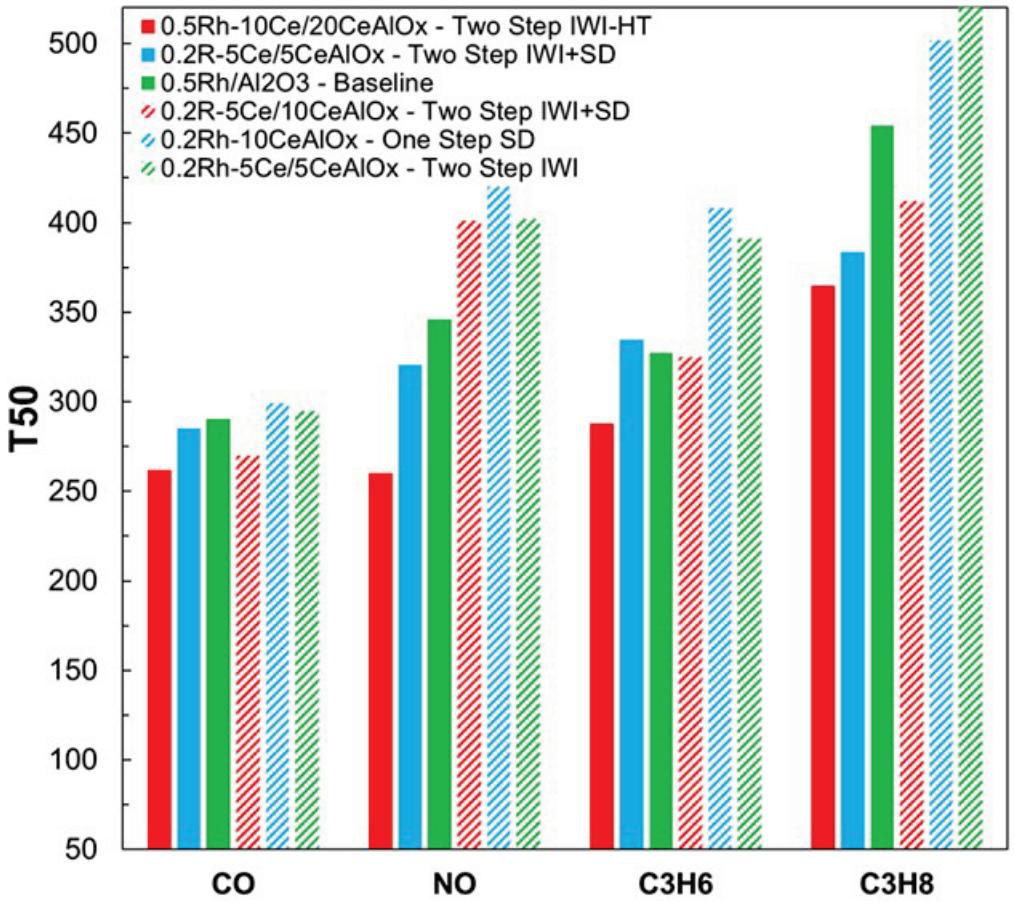

IWI – incipient wetness impregnation; HT – hydrothermal; SD – spray-dried

Figure VI.C.2.1 T50 comparison between newly formulated Pd concept catalysts and Pd baseline catalysts at both the powder-sample and core-sample levels. T50 is the temperature in Celsius where the emission conversion reaches 50%.

Perform advanced characterization and a reaction kinetics study to gain insights into the deactivation mechanism

To understand the potential impacts of supporting PGMs on Ce-containing materials and their response to lean–rich cycling aging, we assessed the redox properties of Pd and Rh as a function of O_2- and H_2-pretreatment temperature and developed a protocol that attempts to isolate the effect of O_2 pretreatment on PGM redox properties and eliminate the effect of H_2 exposure on PGM restructuring. Additionally, to understand the potential impacts of reducing PGM loading, as well as the impacts of aging temperature on catalyst speciation and stability, we investigated a series of Pd/Al_2O_3 catalysts using CO chemisorption and diffuse reflectance infrared Fourier transform spectroscopy (DRIFTS), then combined the characterization results with kinetics experiments to provide mechanistic insights.

Conclusions

Spray-dried Rh-Ce/$CeAlO_x$ and Pd-CePr/$CeAlO_x$ concept catalysts proved to be a viable technical pathway toward a 60% cut in Pd/Rh loadings at the powder level, and the Pd-CePr/$CeAlO_x$ concept also demonstrated consistent performance at the core-sample level. The unique PGM and support interaction appears to be the key to improved aging resistance, and the redispersion of PGM under high-temperature oxidative conditions leads to good dispersion after aging and thus equivalent light-off performance at lower PGM loading.

VI.C.3 Fast Simulation of Real Driving Emissions from Heavy-Duty Vehicle Integrated with Advanced Aftertreatment System (West Virginia University)

Dr. Hailin Li, Principal Investigator
West Virginia University
1306 Evansdale Drive
Morgantown, WV 26505
Email: hailin.li@mail.wvu.edu

Dr. Zhiming Gao, Principal Investigator
Oak Ridge National Laboratory
2360 Cherahala Boulevard
Knoxville, TN 37922
Email: gaoz@ornl.gov

Dr. Pinaki Pal, Principal Investigator
Argonne National Laboratory
9700 South Cass Avenue
Lemont, IL 60439
Email: pal@anl.gov

Dr. Syed Wadhiduzzaman, Principal Investigator
Gamma Technologies
601 Oakmont Lane, Suite 220
Westmont, IL 60559
Email: syed@gtisoft.com

Siddiq Khan, DOE Technology Manager
U.S. Department of Energy
Email: Siddiq.Khan@ee.doe.gov

Start Date: January 18, 2022 End Date: December 31, 2022
Project Funding: $3,392,800 DOE share: $2,500,000 Non-DOE share: $892,800

Project Introduction

Post-2025, further reductions in nitrogen oxides (NO_x) and carbon dioxide (CO_2) emissions from heavy-duty (HD) diesel engines request the development of simulation tools capable of simulating the real driving emissions from HD diesel vehicles integrated with advanced aftertreatment (AT) systems. Supported by Navistar, Gamma Technologies (GT), Convergent Science Inc., Oak Ridge National Laboratory (ORNL), and Argonne National Laboratory (ANL), West Virginia University (WVU) will develop a high-fidelity simulation tool aimed at accurately predicting the fuel economy and exhaust emissions from HD diesel engines and real drive emissions from HD diesel trucks equipped with advanced AT systems, especially during cold- and hot-start processes. The diesel AT system components include a diesel oxidation catalyst (DOC) and selective catalytic reduction (SCR). In this project, the research team will develop a high-fidelity 1D engine simulation model; a pseudo 2D AT system component model, with adaptive channel numbers along the radial direction and computational nodes along the channel axial direction; an optimized reaction chemistry simulating chemical reactions within the AT system components; a urea injection model; an algorithm enabling the adaptive resolution to the AT system component model; and reaction chemistry with changes in engine operating conditions, exhaust temperature, and exhaust gas composition. These models and this algorithm will be developed using high-fidelity computational fluid dynamics (CFD) simulation results as reference,

integrated into the GT-SUITE model platform, and validated against experimental data collected in this project. In the last phase of this project, the research team will apply the simulation tool to simulate advanced diesel engine combustion and AT system packages aimed for near-zero NO_x emissions standards post-2025.

Objectives

This project seeks to:

- Develop and validate the simulation tools that enable virtual coupling of engine combustion with AT systems so that original equipment manufacturers and the research community can use the simulation tools to simulate the real driving emissions from HD diesel trucks, further optimizing HD diesel engines and AT systems for near-zero exhaust emissions.
- Develop the pathways to near-zero NO_x emissions.

Overall Objectives

- Examine engine combustion, emissions, and AT system performance under both steady-state and transient operating conditions.
- Develop a 1D engine combustion model, urea injection model, and 2D and 3D AT system component models necessary for fast and accurate simulation of HD diesel engines and AT systems.
- Integrate the engine and AT system component models into the GT-POWER model for integrated simulation of HD diesel engines and AT systems.
- Develop an algorithm enabling the adaptive simulation of AT system components using 1D, 2D, and 3D models with detailed mesh necessary for accurate and fast simulation.
- Simulate the engine performance, combustion process, and exhaust emissions from HD diesel engines operated under both steady-state and transient operating conditions.
- Simulate the real drive emissions from HD trucks operated on the road.
- Develop the pathway toward near-zero NO_x emissions from HD diesel vehicles.

Fiscal Year 2022 Objectives

- Examine engine combustion, emissions, and AT system performance under steady-state operating conditions.
- Develop a CFD model capable of simulating HD diesel engine combustion and emissions.
- Develop AT system component models.
- Develop a 1D engine simulation model.
- Develop a urea injection model.

Approach

The project combines experiments and simulations to develop and validate a numerical model simulating the real driving emissions from HD diesel vehicles integrated with advanced AT systems. The model will be applied to simulate the exhaust emissions from HD diesel engines and vehicles operated under transient cycles and to develop the pathway toward near-zero NO_x emissions from HD diesel vehicles.

Experiments

In this project, an HD Navistar 15 L A26 engine will be instrumented to measure the cylinder pressure, combustion process, and exhaust emissions. The project team will study the effects of engine speed, load, and exhaust temperature on the engine performance, combustion process, exhaust emissions, and AT system efficiency in converting hydrocarbons, carbon monoxide, and NO_x under both steady-state and transient operating conditions. The fuel economy and exhaust emissions from HD vehicles will be experimentally examined. The data generated will be applied to validate the engine combustion and emissions models developed in this project. WVU will conduct the experimental work. Navistar will provide the engine dynamometer and engine control unit and the technical support that WVU will need to run the A26 engine in the test cell.

Simulations

This project will develop a 1D engine simulation model and AT component models capable of simulating the combustion process and exhaust emissions from an HD diesel engine. A CFD model capable of simulating the combustion and engine-out emissions will be developed and applied to provide high-fidelity data for the development of the 1D engine simulation model. The project team will develop an algorithm to select the most appropriate simulation model—the 1D, 2D, or 3D AT system component model or kinetic model—to enable fast simulation of real drive emissions from HD vehicles. The models developed will be integrated into the GT-SUITE platform and applied to simulate the performance, fuel economy, and exhaust emissions from both HD diesel engines and vehicles. WVU faculty and graduate students will develop the engine model, ANL will develop the engine CFD model, and ORNL and GT will develop the AT system component model.

Results

ANL has developed an engine CFD model for both closed and open engine cycles. The model is able to simulate the engine combustion process and in-cylinder formation of hydrocarbons, carbon monoxide, and NO_x from an HD Navistar A26 diesel engine. The model will be validated against experimental data once the data are made available.

WVU and ORNL have developed an SCR simulation model using both GT-SUITE and CONVERGE CFD models and ORNL chemistry. The model has been validated against the data simulated using in-house software developed by ORNL, which has been validated against experimental results in previous projects. Researchers have used this model to examine the simulation of the SCR system. Figure VI.C.3.1 shows the effect of exhaust gas temperature at inlet on SCR reduction efficiency in converting NO, NO_2, and NO_x. Conversion efficiency over 90% can be achieved at inlet temperatures over 250°C. As expected, longer simulation time is needed for 3D simulation than 1D and 2D simulation, especially at low inlet temperature, as shown in Figure VI.C.3.2. The research team will investigate the algorithm determining the criteria for selecting the resolution of models needed to simulate SCR system operation.

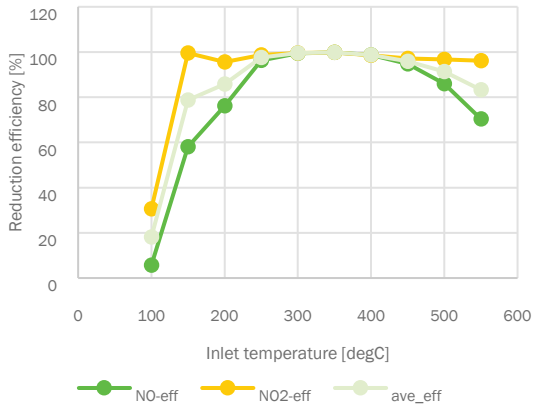

Figure VI.C.3.1 Impact of inlet temperature on SCR efficiency in reducing NO and NO_2

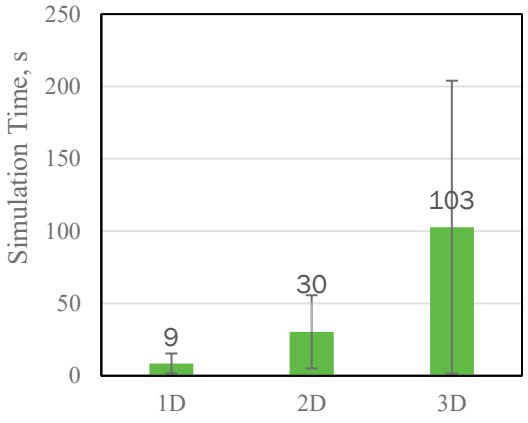

Figure VI.C.3.2 Impact of intake temperature on simulation time using 1D, 2D, and 3D GT-SUITE models

GT developed a phenomenal urea injection simulation model and is currently integrating this model into the GT-SUITE model platform. The droplet size distribution (DSD) of the urea droplets were described using the log-normal distribution shown in Equation (1) and the Rosin-Rammler (RR) distribution expressed in Equation (2). Figure VI.C.3.3 shows the variation of the urea droplet distribution in Rosin-Rammler scale with changes in location. It is evident that the urea droplets become smaller at downstream points because of evaporation of urea droplets. The model developed can be used to simulate the evaporation of water, droplet size change, and urea thermolysis based on droplet radius (area, volume, and user expression).

$$f_X(x) = \frac{1}{\sqrt{2\pi}\sigma_Y} e^{-\frac{1}{2}\left(\frac{\ln(x)-\mu_Y}{\sigma_Y}\right)^2} \quad \text{Equation (1)}$$

$$f_X(x) = \frac{n}{\bar{x}}\left(\frac{x}{\bar{x}}\right)^{n-1} e^{-\left(\frac{x}{\bar{x}}\right)^n} \quad \text{Equation (2)}$$

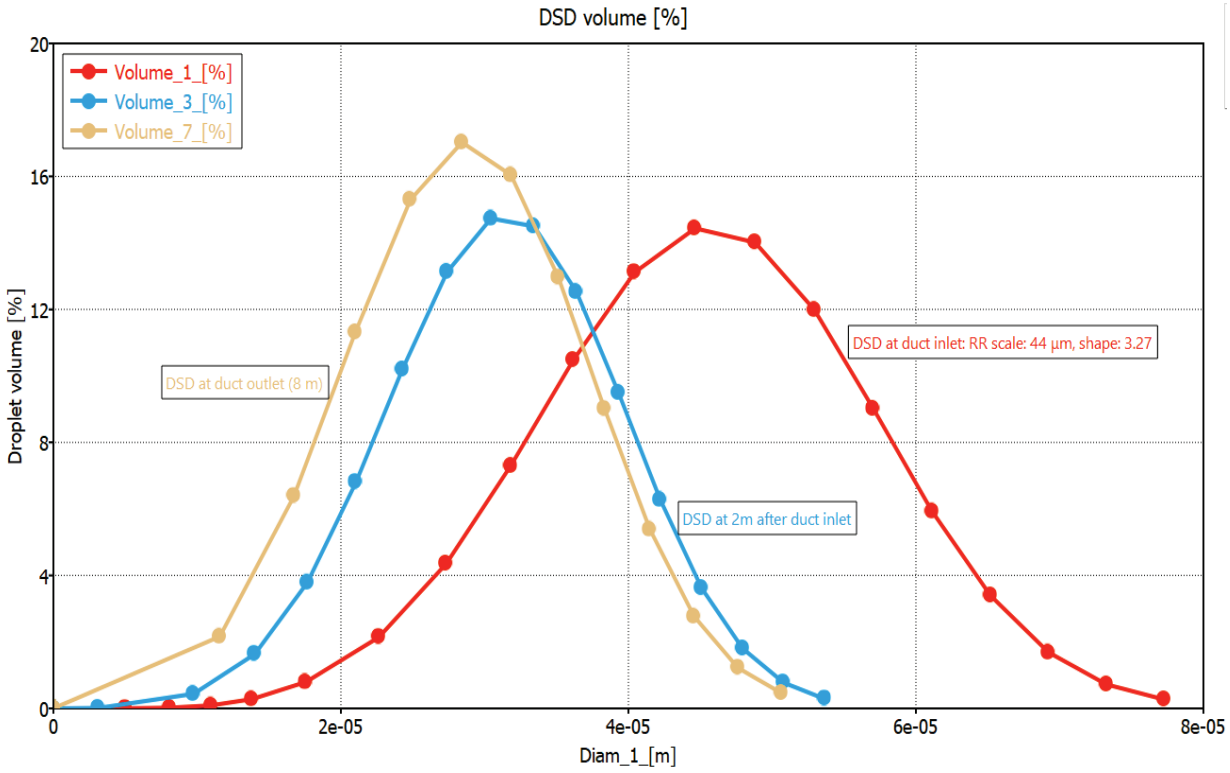

Figure VI.C.3.3 Urea RR droplet size distribution

WVU and ORNL have developed a 5.8 L DOC and a 24 L SCR model in GT-SUITE. The SCR mechanism developed by ORNL has been integrated into GT-SUITE. The model integrated with ORNL chemistry was compared with the AT system model developed by ORNL. The results simulated in GT-SUITE were comparable with those simulated in the ORNL model. The GT-SUITE model was then applied to simulate transient operation of the AT system, as shown in Figure VI.C.3.4. It is evident that the effectiveness of the SCR system in reducing NO_x emissions under transient operation can be simulated.

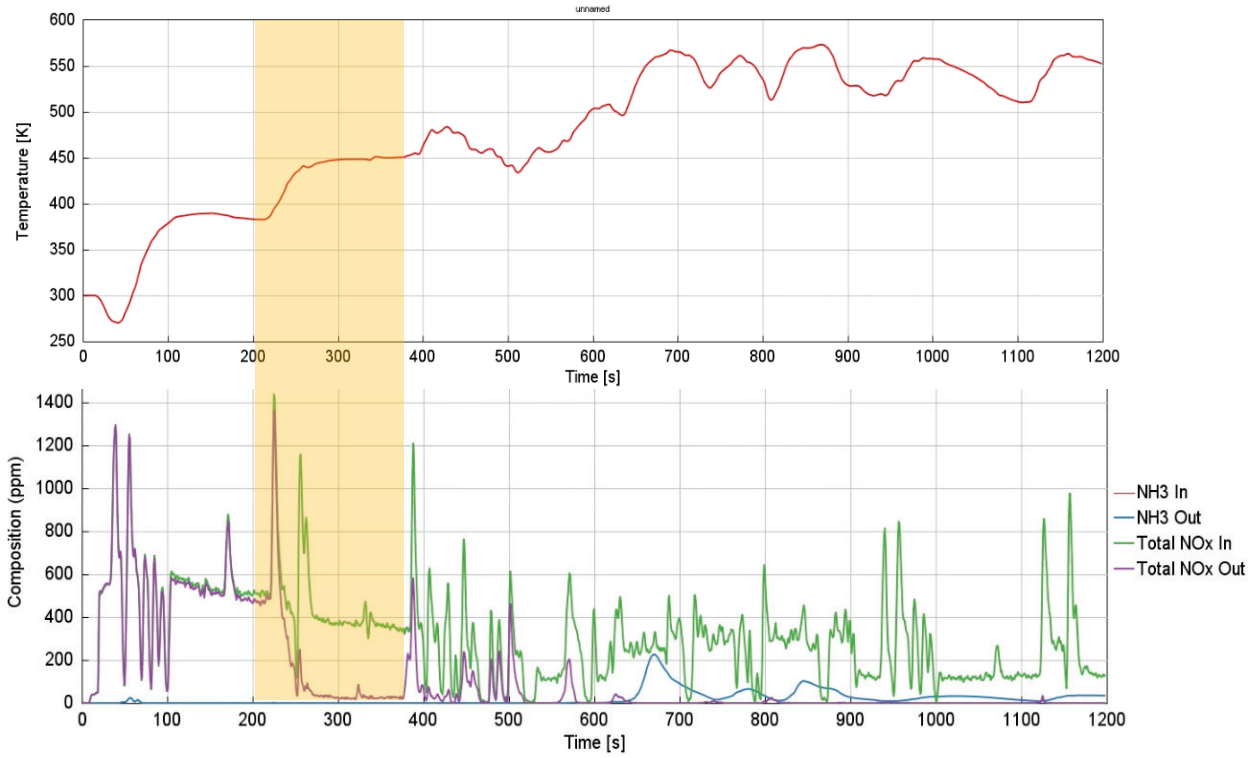

NH_3 – ammonia

Figure VI.C.3.4 GT-SUITE simulation results

Conclusions

The research team has developed the engine CFD model, urea injection model, and AT system model. The urea injection and AT system component models have been integrated into the GT-SUITE platform. The AT system model has been validated against the in-house simulation model developed by ORNL, which has been validated in previous research projects. The validated model can be applied to simulate the operation of SCR and DOC systems operated under transient cycles. The project team will apply this platform to develop the approaches and algorithm enabling the fast simulation of real drive emissions from HD vehicles. Such a tool can be applied to developing engine combustion and AT technologies, further reducing the greenhouse gas emissions and key pollutants such as NO_x from HD diesel engines.

The engine experimental work proposed for the first year has been delayed because of the temporary closure of WVU research. The research team has managed to secure an off-campus research facility for WVU to conduct the engine experimental work proposed in this project.

Key Publications

1. DOE Quarterly progress report, Q1, April 30, 2022
2. DOE Quarterly progress report, Q2, July 31, 2022
3. DOE Quarterly progress report, Q3, October 31, 2022

Acknowledgements

The research team would like to thank the U.S. Department of Energy (DOE) for funding this project. The support and constructive comments from Mr. Michael Ursic and Dr. Siddiq Khan, the DOE project managers, are greatly appreciated.

VI.C.4 Comprehensive Integrated Simulation Methodology for Enabling Near-Zero-Emission Heavy-Duty Vehicles (University of Wisconsin–Madison)

Andrea Strzelec, Principal Investigator
University of Wisconsin–Madison
1500 Engineering Drive
Madison, WI 53706
Email: strzelec@wisc.edu

Siddiq Khan, DOE Technology Manager
U.S. Department of Energy
Email: Siddiq.Khan@ee.doe.gov

Start Date: November 10, 2021 End Date: December 31, 2022
Project Funding: $3,271,376 DOE share: $2,604,870 Non-DOE share: $666,506

Project Introduction

The advent of requirements for low nitrogen oxide (NO_x) emissions, coupled with demand for increased durability, highlights the ever-growing need for tools to predict exhaust system performance, including both impacts of aging throughout useful life and performance at the end of useful life. Regulatory drivers continue to focus on reducing emissions and increasing durability of aftertreatment systems.

Recent decades have brought significant improvements in both fuel economy and emissions through the continued development of both engines and emissions control catalysts—and through their integration as a system. Simulation tools have been substantial enablers of this improvement, as integrated engine and aftertreatment models have allowed for visualization of the dynamic interactions between the system components. For manufacturers, modeling efforts have an important role in product development and calibration.

Both engine and aftertreatment device models have continued to progress, but the onset of new, fast-approaching, challenging emissions regulations, such as for ultra-low NO_x levels, is driving the need for further integration of combustion and aftertreatment systems in simulations. Therefore, there is a targeted need for research and development of modeling tools that would enable virtual optimization and calibration of combustion and aftertreatment to further improve efficiency and reduce emissions—while limiting platinum group metal content.

This will require accurate component models that are able to break through key barriers such as spatially resolving the key factors of species composition and temperature, especially during challenging operation times such as cold start and low-load operations, where a high proportion of the total emissions occur. This project aims to address these barriers.

Objectives

The goal of this work is to develop an integrated simulation of combustion and aftertreatment systems to enable control optimization, thermal management optimization, insulation strategies, etc. while ensuring that conversion efficiencies of the components are improved.

Overall Objectives

- Computationally match the project's Isuzu engine and baseline aftertreatment system performance for combustion and emissions to provide accurate predictions of exhaust temperature and emissions for aftertreatment models.

- Develop kinetic models for the diesel oxidation catalyst (DOC) and selective catalytic reduction (SCR) catalyst that include the effects of hydrothermal aging.
- Implement high-fidelity models for urea spray and thermolysis.
- Integrate all component models (engine, DOC, diesel particulate filter [DPF], and SCR with urea spray model) in GT-SUITE and validate against engine dynamometer testing.
- Exercise the model to demonstrate near-zero emissions concept and real driving emissions performance.

Fiscal Year 2022 Objectives

- Develop the Zero-D Velocity–Composition–Frequency transported Probability Density Function (0D-VCF-tPDF) combustion model and validate it against computational fluid dynamics (CFD) simulations.
- Build and calibrate the baseline engine model, a digital twin of a heavy-duty diesel engine.
- Develop the baseline aftertreatment models for each component device.
- Experimentally evaluate the baseline engine and aftertreatment system for model validation with engine experiments.
- Perform laboratory aging of catalyst samples, and measure properties of the DOC and SCR materials using a synthetic exhaust flow reactor.
- Recalibrate the Oak Ridge National Laboratory SCR model to predict the performance of the SCR material.

Approach

The approach to achieving the goal of this project is to develop an enhanced methodology for the integrated simulation of combustion and aftertreatment systems within the environment of the software tool GT-SUITE. GT-SUITE is a multi-physics system simulation platform and a well-established simulation standard in the industry. It can be used to perform coupled transient simulations of a wide variety of combustion engine and aftertreatment systems with very fast turnaround times. Dedicated libraries of flow, thermal, mechanical, and chemistry components allow any system to be built from the ground up. Typical aftertreatment devices with detailed reaction mechanisms of any catalyst can be easily simulated as a standalone system or as part of an integrated system. Gamma Technologies is performing the GT-SUITE work.

The first part of the development process is to predict the raw in-cylinder emissions, spatial inhomogeneity in temperature, flow and composition in the combustion chamber, effects of turbulence chemistry interaction, and evolution of species via detailed chemical kinetics, which need to be accurately captured. The in-cylinder models capturing the various flow, turbulence, and combustion phenomena will be validated with results from analysis of measurement data (pressure and heat release rate analysis) and 3D-CFD simulations. The raw emission predictions will be compared against steady and transient emission measurements.

The second part of the approach focuses on developing simulation capabilities for an enhanced aftertreatment system—including the DOC, DPF, and SCR—within a reduced dimensionality framework. There is no way to simulate the process other than by reduced dimensionality, because of (1) the required short turnaround time for the simulation predictions and (2) the fact that these multi-physics, multi-scale phenomena are coupled in a complicated fashion. However, validation of these simulation tools is based on synthetic exhaust flow reactor experiments at Oak Ridge National Laboratory, engine experiments at FEV North America Inc. (FEV), and full 3D unsteady methodologies (University of Wisconsin). The full engine and aftertreatment system,

including the DOC, DPF, and SCR, is validated with engine experiments run at FEV. Later in this project, researchers will develop models that account for hydrothermal aging of emissions control components, which can be used to predict the degradation (degradation factor) of catalyst performance with time, as they age. These models are essential to the development of accelerated aging protocols, which are expected to play a crucial role in demonstrating the compliance of aftertreatment systems for the full useful life of a vehicle. Tailpipe emissions from an integrated engine and aftertreatment system model will be validated via steady-state tests and drive cycle tests. To address the need to correctly treat the liquid in the near-spray-nozzle region while simultaneously keeping the computation size to a reasonable level, the proposed strategy combines a Volume of Fluid (VoF) and a Lagrangian–Eulerian (LE) methodology. In the near field, where most of the liquid is not in spherical form, the VoF methodology will be employed. In the remaining part of the spray, where the liquid is essentially all in droplet form, the LE treatment will be used. This proposed treatment is denoted as VoFLE, and it will be used in the CFD validation of the aftertreatment models.

All models developed in this effort—the combustion model, urea-water spray model, and the aftertreatment device models—will be distributed via the Gamma Technologies GT-SUITE software platform so that they can be used to optimize development of the engine and aftertreatment system, enabling original equipment manufacturers to achieve near-zero emissions for their fleets.

Results

Note: Elements of this project have been delayed because of the COVID-19 pandemic and associated supply chain issues. In addition, personnel issues in the Research and Sponsored Projects Office at the University of Wisconsin–Madison have slowed processing of orders and paying of invoices.

The following key accomplishments for Fiscal Year (FY) 2022 are reported:

- Accomplished the development of the 0D-VCF-tPDF combustion model and validation with CFD simulations. Model-predicted indicated mean effective pressure (IMEP) values are within 5% across all operating points, maximum pressure predictions were within 7 bar across all operating points, and the CA50 error was within 2.2 crank angle degrees (CAD).[1]

- Accomplished the development and calibration of the baseline compression ignition engine, combustion chemistry and emissions formation, and aftertreatment models with data provided by Isuzu and calibrated with engine data taken at FEV.

During the first quarter of the project, an aftertreatment system model, including the DOC, DPF, SCR, and ammonia slip catalyst, was calibrated on baseline synthetic flow reactor and engine data provided by Isuzu within a reduced dimensionality framework. Further validation of these simulation tools will require additional synthetic exhaust flow reactor experiments, engine experiments, and full 3D unsteady methodologies. The detailed models of the DOC, SCR, and ammonia slip catalyst aftertreatment system components were developed using synthetic exhaust flow reactor data, and the DOC and DPF performance data were validated with single-cylinder engine experiments.

During the second quarter of the project, researchers further developed the combustion model used to predict the raw in-cylinder emissions, spatial inhomogeneity in temperature, flow and composition in the combustion chamber, effects of turbulence chemistry interaction, and evolution of species via detailed chemical kinetics. For this to be accomplished in a 0D/1D simulation framework, a model derived from the transported probability density function (tPDF) method was introduced. In this method, the gas inside the combustion chamber is considered as an ensemble of notional particles that can mix with each other following a physically accurate mixing model, exchanging mass/energy, and can interact with the walls of the combustion chamber and exchange heat energy. The state of the particles evolves according to various sub-models, such as spray

[1] CA50 is the crank angle at which 50% of the heat from combustion has been released.

dynamics and chemistry. In particular, the new model follows the velocity–composition–frequency (VCF) approach of tPDF method, which provides complete closure for velocity, composition, and turbulence quantities without resorting to further closure models. Within the 0D framework, the VCF tPDF approach (0D-VCF-tPDF), described graphically in Figure VI.C.4.1, is one of the most advanced approaches to modeling combustion inside the cylinder. These kinetic models provide accurate predictions of emission species (such as NO_x, unburned hydrocarbons, and soot) with very fast turnaround times compared to 3D-CFD. The in-cylinder models capturing the various flow, turbulence, and combustion phenomena were validated with results from analysis of measurement data (pressure and heat release rate analysis) and 3D-CFD simulations. The raw emission predictions were then compared against steady and transient emission measurements.

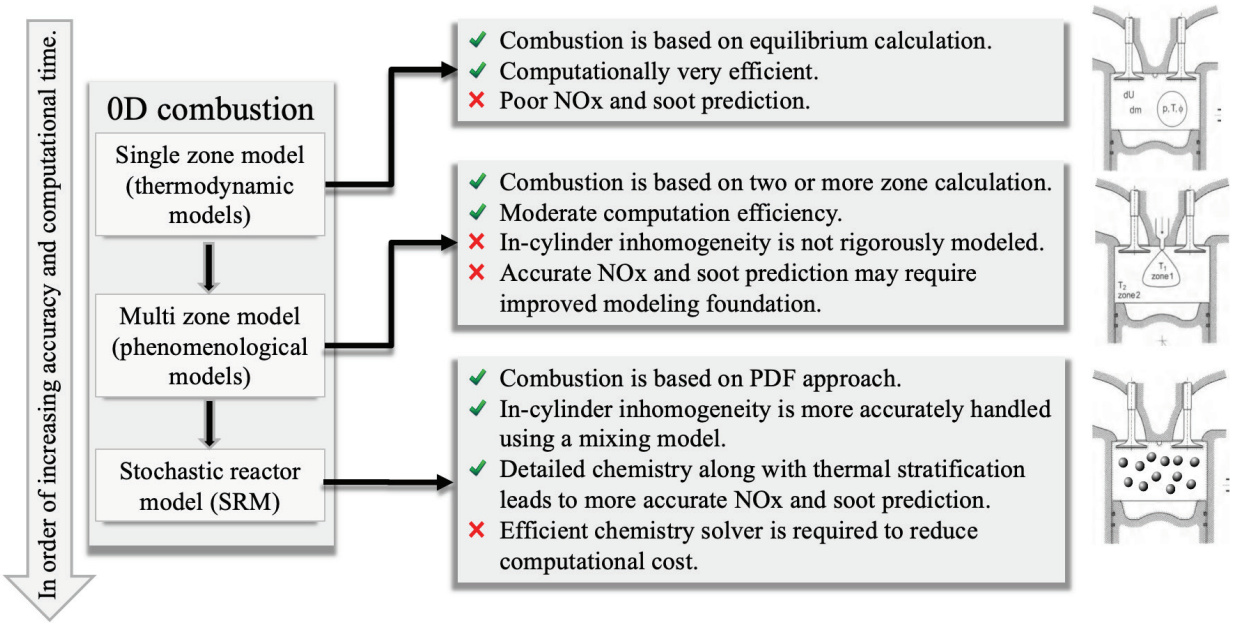

Figure VI.C.4.1 Graphical description of the 0D-VCF-tPDF for diesel combustion

During the third quarter of the project, researchers conducted engine combustion experiments with the Isuzu engine and baseline aftertreatment system installed at FEV with conventional ultra-low sulfur diesel fuel provided by Marathon Petroleum. These data enabled the validation of the combustion model with respect to performance. Model validation was completed against the experimental data and showed excellent agreement. Figure VI.C.4.2 shows the model results plotted against the engine data. Model-predicted IMEP values are within 5% across all operating points, maximum pressure predictions were within 7 bar across all operating points, and the CA50 error was within 2.2 CAD.

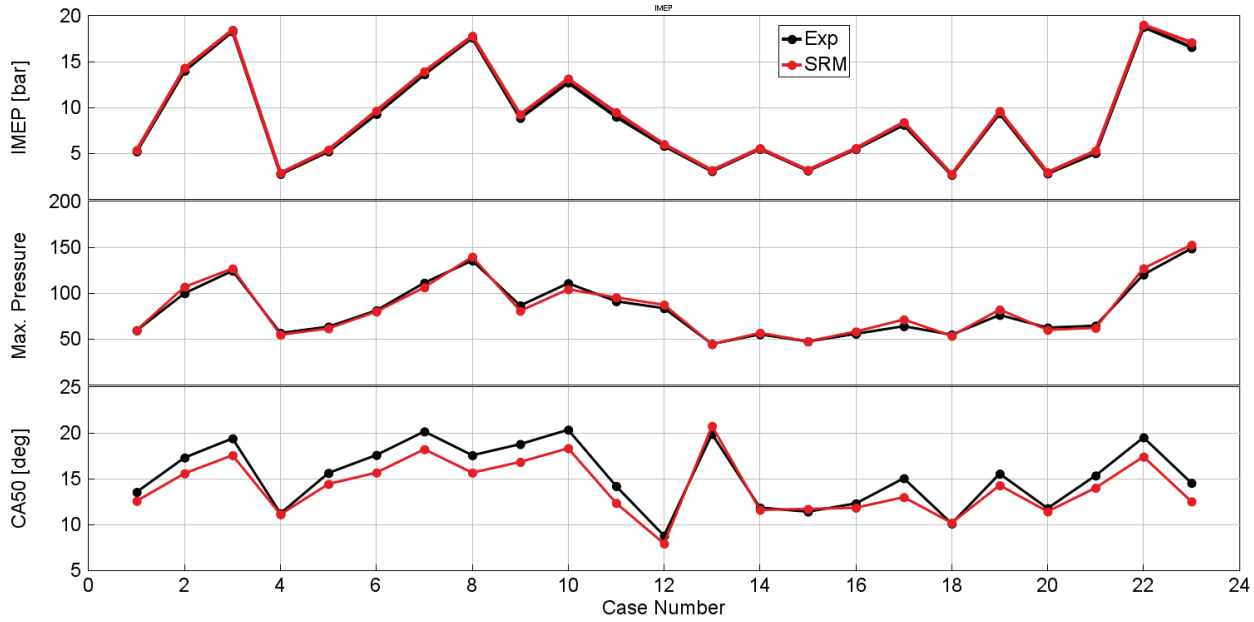

Figure VI.C.4.2 Model-predicted values (black lines) compared against experimental data (red lines). IMEP values are within 5% across all operating points, maximum pressure predictions were within 7 bar across all operating points, and the CA50 error was within 2.2 CAD.

The emissions model generated satisfactory performance for NO_x predictions and poor performance for soot predictions (see Figure VI.C.4.3). This model is undergoing additional improvements.

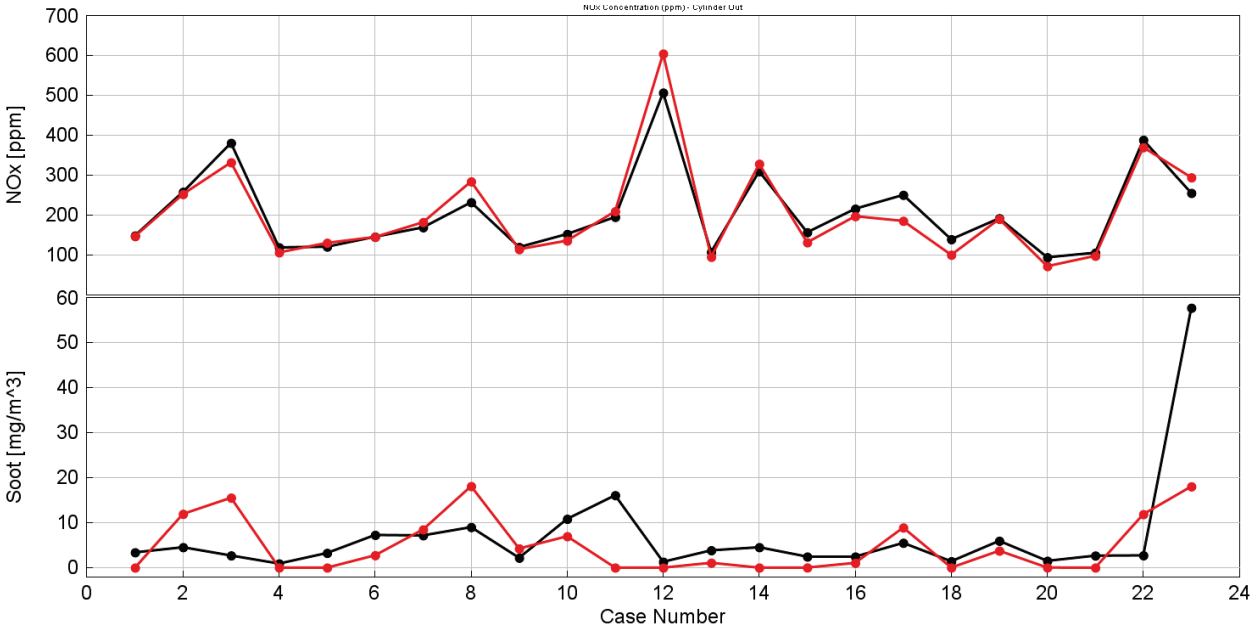

Figure VI.C.4.3 Emissions predictions (black lines) compared to experimental data measured by FEV (red lines). The NO_x model (top) shows satisfactory agreement, but the soot model (bottom) needs improvement.

Conclusions

The conclusions of this year's work are as follows:

- The engine model can accurately predict the Isuzu engine performance. Model-predicted IMEP values are within 5% across all operating points, maximum pressure predictions were within 7 bar across all operating points, and the CA50 error was within 2.2 CAD.
- The baseline engine, combustion, and aftertreatment models have been developed, calibrated, and validated against engine data taken at FEV and are ready for integration into a system model in GT-SUITE, where they will be further improved.
- All project milestones and the go/no-go milestone for FY 2022 have been met, as shown in Table VI.C.4.1.

Table VI.C.4.1 FY 2022 Milestone Table

ID	Milestones	Type	Description
Y1-1	**Baseline aftertreatment system model calibrated**	Technical	The aftertreatment system model was calibrated and verified under the conditions for baseline data provided by Isuzu.
Y1-2	**Baseline combustion model complete**	Technical	The 0D-VCF-tPDF approach was extended to improve accuracy in predicting emission quantities and other transient variables in a compression ignition engine.
Y1-3	**Baseline combustion model validation complete**	Technical	A comprehensively calibrated combustion model was completed with respect to prediction of performance.
Y1-4	**Catalyst aging complete**	Technical	Aging of catalyst samples was completed (Umicore Autocat USA).
GNG1	**Baseline models developed and validated**	Go/No-Go	Baseline engine, combustion, and aftertreatment models have been developed and validated against engine data taken at FEV.

References

1. Wahiduzzaman, S., W. Wang, A. Leonard, and S. Wenzel. 2010. "In Development of Integrated Engine/Catalyst Model for Real-Time Simulations of Control Design Options." FISITA (Fédération Internationale des Sociétés d'Ingénieurs des Techniques de l'Automobile) 2010 World Automotive Congress, Budapest, Hungary.

2. Paul, C., K. Jin, N. Fogla, K. Roggendorf, and S. Wahiduzzaman. 2020. "A Zero-Dimensional Velocity-Composition-Frequency Probability Density Function Model for Compression-Ignition Engine Simulation." SAE Technical Paper 2020-01-0659. https://doi.org/10.4271/2020-01-0659.

Acknowledgements

The project principal investigator gratefully acknowledges the support of National Energy Technology Laboratory Program Manager Ralph Nine and Grants Management Specialist Elizabeth (Liza) Love, University of Wisconsin–Madison Research Administrator Zach Smith, and the entire Research and Sponsored Projects team that administers this award.

In addition, it is imperative to acknowledge the key research team members who are responsible for this work: Drs. Syed Wahiduzzaman and Santhosh Gundlapally of Gamma Technologies, Bruce Vernham of Isuzu Technical Center of North America, Josh Pihl of Oak Ridge National Laboratory, Prof. Mario Trujillo of the University of Wisconsin–Madison, Erik Koehler of FEV North America, Dr. Tom Pauly of Umicore Autocat USA, and Steve McConnell of Marathon Petroleum. This work would not be possible without each of them. This is an exceptional team.

VI.D Advanced Engine Technologies

VI.D.1 Volvo SuperTruck 2: Pathway to Cost-Effective Commercialized Freight Efficiency (Volvo Group North America)

Eric Bond, Principal Investigator
Volvo Group North America
7900 National Service Road
Greensboro, NC 27409
Email: eric.bond@volvo.com

Siddiq Khan, DOE Technology Manager
U.S. Department of Energy
Email: Siddiq.Khan@ee.doe.gov

Start Date: October 1, 2016 End Date: December 30, 2022
Project Funding: $40,000,000 DOE share: $20,000,000 Non-DOE share: $20,000,000

Project Introduction

Volvo's SuperTruck 2 (ST2) builds on the success of the SuperTruck project that demonstrated vehicle freight efficiency (FE) improvements in excess of the program's goals. Many SuperTruck technologies with customer-acceptable payback (e.g., aerodynamics, powertrain components, and tractor lightweighting) are now used in commercial trucks, thereby reducing national energy consumption.

Federal data on truck utilization shows that a majority of Class 8 long-haul trucks operate at or below 65,000 lbs gross combined weight, much lower than the maximum combined vehicle weight of 80,000 lbs. This implies that most trucks are underutilized and overdesigned, i.e., heavier and equipped with more powerful engines than needed to meet their actual operational requirements. Volvo's ST2 will therefore demonstrate an all-new complete vehicle concept designed with an integrated approach to maximize FE.

The project consists of three work packages organized in four sequential phases as illustrated below in Figure VI.D.1.1. During Fiscal Year (FY) 2019, the focus shifted from concept selection to technology development and integration, and then into the concept-truck build phase for FY 2020. During FY 2021, and due to unexpected COVID-19-related delays, the concept-truck build phase was prolonged, and a contract extension was submitted. The overall project timeline was updated, per below.

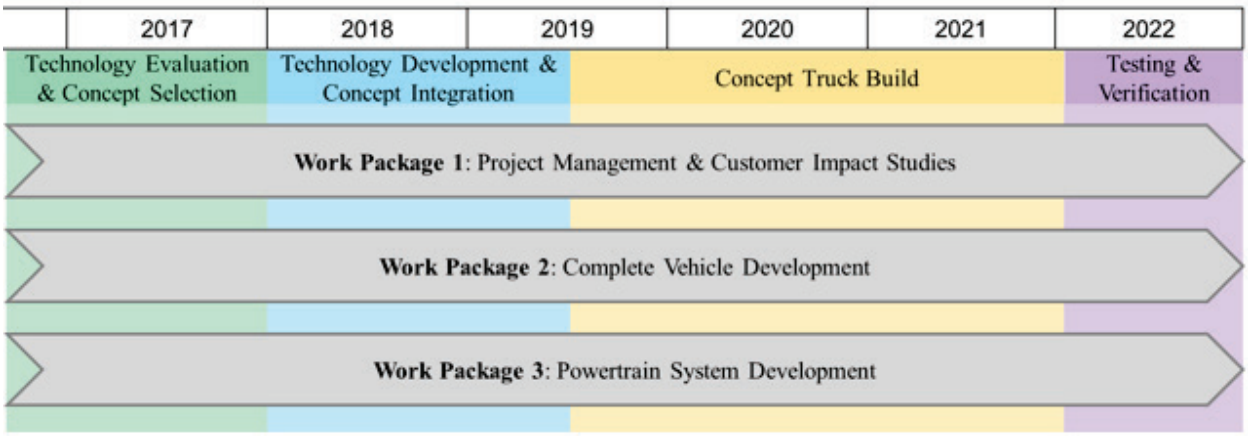

Figure VI.D.1.1 Updated project schedule and phasing. Source: Volvo

Objectives

Overall Objectives

- Demonstrate greater than 100% improvement in vehicle ton-miles per gallon compared with a best in class 2009 truck, with a stretch goal of 120%.
- Demonstrate 55% brake thermal efficiency (BTE) on an engine dynamometer.
- Develop technologies that are commercially cost-effective in terms of a simple payback.

FY 2022 Objectives

- Finalize FE engine installation.
- Complete vehicle demonstrator built and commissioning.
- Demonstrated 55%-BTE engine.
- Field tested demonstrator.

Approach

Volvo's vision is to develop a super-efficient vehicle optimized for 65,000 lbs and designed for the long-haul drivers of the future. The truck has therefore been redesigned from the ground up to ensure that each component contributes to maximizing the payload capacity and fuel economy of the complete vehicle.

The powertrain research in this project is guided by two goals, to demonstrate greater than 100% FE increase in a vehicle and to demonstrate 55% BTE of the engine in a test cell. These goals differ not only in level of efficiency required by the powertrain solution but also in the size of the design space. Consequently, the team is taking a two-pronged approach and will deliver one powertrain shaped as part of a total vehicle optimization toward maximum FE and another focused on demonstrating 55% BTE. Though the dual-path approach may yield two different system-level approaches, significant synergies exist in the fundamental areas of improving internal combustion efficiency.

Results

Powertrain System Development

During FY 2022, the demonstration of the Volvo 13 L 55% BTE base engine was completed. The performance of the 11 L FE demonstrator engine was also verified.

The fuel design study with ExxonMobil was completed at the University of Michigan. ExxonMobil provided a set of fuels with various compositions to the University of Michigan Auto Lab, where researchers explored fuel design impacts on criteria pollutant emissions and performance in a single-cylinder research engine. After extensive data analysis, some of the test fuels show significant promise for enhancing diesel combustion relative to conventional diesel fuel, specifically regarding NO_x and soot emissions when compared at a "cruise" condition for the test engine that simulated the ST2 truck test condition. The decreased engine-out emissions observed with the experimental fuel blends can allow engine operation parameters to be adjusted in pursuit of efficiency targets or other objectives of interest without compromising baseline emissions levels.

The Volvo 11 L high-efficiency engine platform was used as the base for the ST2 50% BTE FE engine. Combustion system improvements include an optimized turbocharger, addition of an exhaust gas recirculation pump, high-compression-ratio wave pistons, and a Miller cycle camshaft. The vehicle's 48 V mild hybrid system, along with the engine-mounted 48 V integrated starter generator, facilitates the removal of the front engine accessory drive, which leads to an improvement in engine efficiency. During this fiscal year, the final system commissioning was completed for the FE engine. The base map tuning and engine calibrations were

completed to optimize performance for the intended duty cycles. The FE engine was installed into the vehicle demonstrator and successfully commissioned.

Simultaneously, the SuperTruck team focused on the 55% BTE base engine commissioning and performance testing based on a Volvo high-efficiency 13 L engine platform in this fiscal year. The objective was to identify an engine hardware specification for maximum fuel efficiency at a single operating point. The technologies verified on the FE-optimized engine were redesigned for adaption to the 13 L engine platform and integrated to the 13 L engine for the final fuel economy demonstration. The high-compression-ratio wave pistons, injector specifications, and a multiple-injection strategy were explored for efficiency improvement. Multiple technologies in gas exchange (high-efficiency turbomachinery, 48 V exhaust gas recirculation pump, Miller cycle camshaft, and divided intake manifold) and friction and auxiliaries (low-viscosity engine oil, 48 V coolant pump, and fuel pump) were also investigated. The final performance demonstration was completed successfully and achieved the peak BTE of 50% on the base engine.

The Rankine waste heat recovery (WHR) system was also commissioned towards the later part of this fiscal year, upgraded with an indirect condenser and a new alternator for performance testing and demonstration. The coolant WHR system was rebuilt with new components and software. The performance testing and final demonstration of both the Rankine WHR system and coolant WHR system are nearing completion.

Aerodynamics

The cab assembly was delivered to the Greensboro Technical Center during FY 2021. Modifications to the cab structure were required before installation onto the chassis. Those modifications were completed, and the cab was decked to the chassis in early FY 2022.

Several steps were required to optimize the complete vehicle aerodynamics. Items included adjustment of the cab fairings, chassis fairings, and ground effects, as well as tuning the suspension to obtain the optimum ride height for aerodynamics.

Advanced Lightweight Concepts

During FY 2019, Metalsa delivered a complete lightweight frame assembly, which was 35% lighter than the standard steel frame assembly of an equivalent wheelbase. During FY 2020, Wabash National delivered the ST2 trailer, weighing in at 12,100 lbs with aerodynamic devices, which is much lighter than a typical, non-aero dry van.

Throughout the fiscal year, some unplanned modifications to the cab and chassis were required to improve performance and robustness. These modifications somewhat offset the original weight reduction achievement, but the team was still able to deliver results that exceeded the 27,000 lbs tractor–trailer weight target. The team achieved a final curb weight of 26,200 lbs.

Low Rolling Resistance Tires

Advanced tires for the tractor and trailer have been installed onto the demonstrator. A test plan has been developed to evaluate the vehicle stopping-distance performance in wet and dry conditions, and preparations are in place to conduct these tests at Michelin's Proving Grounds in South Carolina.

Additionally, testing was initiated earlier in this fiscal year to assess the tire design impact on vehicle fuel consumption and tire longevity. These tests were conducted throughout the year and will yield results in the coming months.

Hotel Mode

Bergstrom provided on-site commissioning support for the heating, ventilation, and air conditioning heat pump. The system was modified to address air bleed issues. There was one component failure in the heating, ventilation, and air conditioning system, which was quickly addressed by Bergstrom.

Complete Vehicle Energy Management

Motivo Engineering provided remote and on-site support for commissioning the battery management unit, door and steps integration, and troubleshooting minor issues with both hardware and software. In collaboration with Bergstrom, Motivo also delivered software updates for the tablet developed to interface with the heating, ventilation, and air conditioning system. Touchscreen programming was updated and operation was verified.

Concept Trailer Development

Wabash completed the engineering, build, and delivery of the ST2 trailer during FY 2020. Due to the lower ride height of the tractor and trailer, Wabash redesigned and delivered a replacement landing gear assembly to provide adequate clearance, which has now been installed.

Demonstrator Vehicle Assembly

System installation, integration, and complete vehicle commissioning was the major focus of the vehicle team throughout FY 2022.

Installation activities included decking the cab to the chassis, completing the new brake system, and installing the 11 L FE engine. Headlamps were installed, and headlamp operation was verified. All cab and chassis aerodynamic devices were installed and adjusted.

Due to the prototype nature of the systems and components used in the demonstrator, a considerable amount of time and effort were required to complete integration and commissioning. Vehicle systems such as braking, suspension, and door/step operation were tuned and verified. Powertrain error codes were investigated and addressed, and operation of the low- and high-temperature coolant pumps was confirmed. Integrated starter generator operation was also tuned and verified.

By the end of this fiscal year, the complete vehicle demonstrator was successfully commissioned, and plans have been established for on-road testing.

Conclusions

The Volvo ST2 project focused on complete vehicle demonstrator build details, system tuning, and final commissioning during FY 2022. In parallel, the 55% BTE base engine and WHR systems were successfully commissioned, and performance testing was initiated. Preparations are underway for on-road testing and final verification of all targets.

Acknowledgements

Ralph Nine (National Energy Technology Laboratory Program Manager) and all partners of the ST2 team: Wabash National, Oak Ridge National Laboratory, Metalsa Roanoke, Johnson Matthey, Michelin Tire, Bergstrom, Motivo Engineering, University of Michigan, Knight Transportation, and Wegman's Food Markets

VI.D.2 Cummins / Peterbilt SuperTruck II (Cummins Inc.)

Jonathan Dickson, Principal Investigator
Cummins Inc.
P.O. Box 3005
Columbus, IN 47201-3005
Email: jon.a.dickson@cummins.com

Siddiq Khan, DOE Technology Manager
U.S. Department of Energy
Email: Siddiq.Khan@ee.doe.gov

Start Date: October 1, 2016 End Date: September 30, 2022
Project Funding: $40,000,000 DOE share: $20,000,000 Non-DOE share: $20,000,000

Project Introduction

The trucking industry is faced with numerous challenges to reduce petroleum consumption while meeting stringent criteria emissions regulations and providing customer value. The United States has approximately 3.5 million Class 8 vehicles on the road today, consuming 4.5 million barrels of petroleum per day. If only half of this fleet implemented half of the benefits proposed, at $3.85/gallon, the nation would see a fuel savings over $30 billion annually and reduce petroleum consumption by over half a million barrels per day. This reduction would have a positive environmental impact by eliminating 200,000 metric tons of CO_2 emissions per day.

The Cummins-led SuperTruck II project goals are to design, develop, and demonstrate a very-high-efficiency engine optimized around the drive cycle that will strongly increase vehicle freight efficiency. The baseline will remain the Model Year 2009 vehicle, and the demonstration vehicle will have similar specifications. The engine will maintain compliance with the current heavy-duty-diesel emissions regulation for line haul vehicles, while the vehicle system will remain compliant with the current greenhouse gas regulatory requirements.

Objectives

- Demonstrate a minimum of 55% brake thermal efficiency (BTE) using 65-mph cruise conditions on an engine dynamometer test.
- Utilize the same engine system demonstrated on the dynamometer in a vehicle operating on real-world drive cycles.
- Achieve a minimum of 125% freight ton efficiency (FTE) improvement over a relevant drive cycle (FTE = [miles per gallon] * [tons of freight]).
- Track, promote, and report on cost-effective solutions, prioritizing those that have an approximately three-year payback period, utilizing a relevant customer counsel for understanding customer acceptance and expectations.

Approach

The approach for meeting the 55% BTE target is via careful dissection of the diesel cycle and reduction of losses via waste heat recovery (WHR). The engine was tuned to take advantage of ideal conditions for the aftertreatment effectiveness, thereby reducing the inefficiency of the exhaust gas recirculation (EGR) and injection timing systems. The closed-cycle efficiency was optimized for high expansion ratio via rapid heat release and insulated surfaces. The open cycle was optimized by using low-pressure EGR, ideal valve events, and a fixed-geometry turbocharger with optimal tip clearance and efficiency. The mechanical efficiency of the engine system was developed to use low-viscosity oil with variable lube and cooling pumps, all while running the engine at a low enough speed to minimize spin and pumping losses. The WHR system was designed as a

two-loop system harvesting both low-quality heat from the coolant and charge cooler and high-quality heat from the EGR coolers and tailpipe boiler. The WHR system was designed to be the primary cooling system for the engine under cruise operating conditions and only requires a small radiator for sustained high-load conditions.

The powertrain has integrated the WHR system and an energy recovery system (motor/generator [M/G]) onto the Eaton automated transmission for compactness and efficiency reasons. During flat-road and uphill operations, this system can input power to the system to reduce fuel consumption. As the vehicle operates downhill, the engine can be decoupled from the powertrain, leaving the controls to apply power from the WHR system as needed and/or recover energy from the system through the M/G, to be stored in an onboard battery.

The vehicle will achieve the high FTE through the combination of low motive resistance and lightweighting. Bridgestone will be supplying tires that can meet customer requirements for longevity yet reduce rolling resistance well beyond the current commercially available tires via compound development and siping design. The vehicle structure will include a new weight-saving composite design that will incorporate a kneeling suspension to aid in the reduction of aerodynamic load. The vehicle design will incorporate aerodynamic features to improve drag in all wind conditions via moving surfaces that react to changing winds detected by the onboard light detection and ranging (LiDAR) system. Finally, the drive axle will incorporate an advanced control system to ensure good low-speed traction with state-of-the-art low-parasitic, high-speed operation.

The technical approach to achieving the freight efficiency improvement of the project has focused on reducing the engine cycle work per mile, improving the system-level BTE via engine and WHR improvements, and reducing the tare weight of the vehicle for an increased payload.

Results

The key accomplishments for Fiscal Year 2022 listed below are fundamental steps required to complete the project objectives. The project team has completed the following milestones:

- The freight efficiency of the demonstration truck exceeded the objective of 125% improvement relative to the 2009 baseline set in the original SuperTruck project.
- The 55% BTE objective was successfully demonstrated in 2021; the generated shaft work was greater than 55% of the fuel energy consumed, a significant improvement to engine efficiency over both the baseline 2009 model year engine as well as current production engines.
- The Cummins powertrain was successfully installed in the Peterbilt demonstrator rolling chassis. This includes the high-efficiency engine, transmission with integral 48 V M/G and WHR, electrification thermal management system, 48 V battery, and aftertreatment with WHR tailpipe boiler.
- Final in-vehicle powertrain calibration was completed for the WHR, axle disconnect, and hybrid powertrain.
- The freight efficiency demonstrator vehicle was successfully completed. This includes the chassis assembly, installation of the powertrain and axle system, cab installation, fairing and hood, and tires.
- The cabin interior trim for the freight efficiency demonstrator was finalized after the installation and validation of the wiring and electrical system. This process was streamlined by using an electrical buck to enable early system testing and validation to reduce the integration time on the final chassis.
- The base Great Dane trailer was completed by Great Dane then shipped to Peterbilt for final installation of the solar panels and aerodynamic fairings prior to the freight efficiency demonstration.

The progress in these key areas supports both the 55% BTE objective and the >125% FTE improvement objective of the project.

Powertrain preparation for the vehicle was performed (Figure VI.D.2.1) and included engine calibration in the test cell; sub-assembly of the powertrain for installation at Peterbilt; final electrical and controls integration; and final in-vehicle calibration of the WHR, 48 V M/G, and disconnect axle.

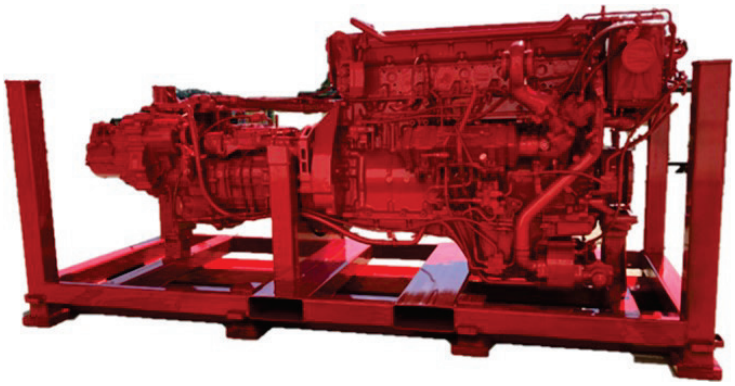

Figure VI.D.2.1 Powertrain prepared for shipment to Peterbilt.

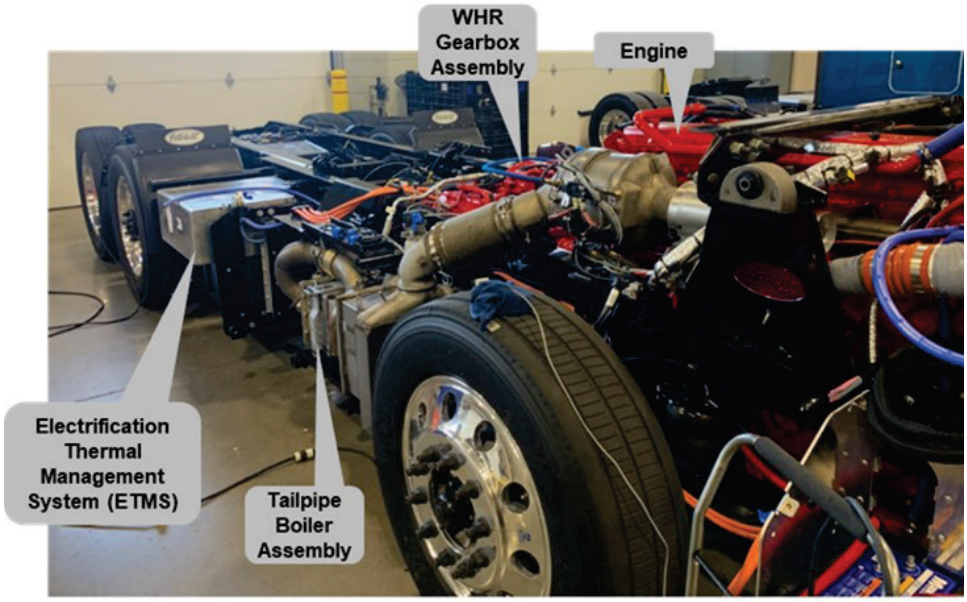

Figure VI.D.2.2 Powertrain installation into rolling chassis.

Key elements of the powertrain (Figure VI.D.2.2) include the WHR, engine and aftertreatment, 48 V mild hybrid system, and battery electrification thermal management system. The integration and build of the freight efficiency demonstrator vehicle was completed this year. Design features include the following:

- A bespoke vehicle shape and new cab with centered driver position and cameras instead of mirrors for aerodynamic improvement (Figure VI.D.2.3).
- A lightweight frame system.
- 48 V accessories, including power steering and cooling fans (Figure VI.D.2.4).
- An adjustable chassis height system for improved aerodynamics.

Testing of the vehicle against the freight efficiency target yielded successful completion of the objective for >125% improvement.

Figure VI.D.2.3 Peterbilt Freight Efficiency Demonstrator.

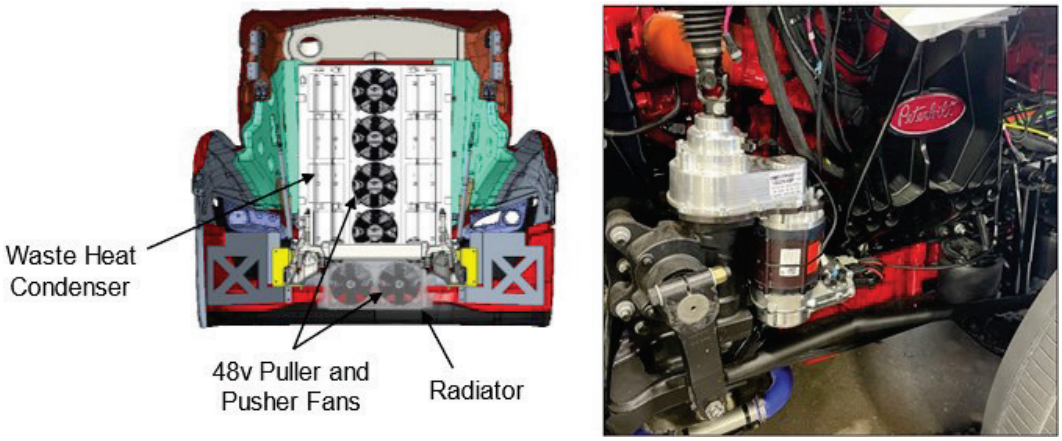

Figure VI.D.2.4 Peterbilt Cooling System and 48V ePS steering.

Conclusions

The Cummins-led SuperTruck II team has completed the sixth year of the planned five-year project. Due to pandemic-related supplier delays, the project was extended an additional year to September 30, 2022. The project team has developed the technology necessary for successfully achieving the freight efficiency objective and has demonstrated this objective. Several technology elements are moving forward into production.

While the project has been successfully completed, with all objectives met, some additional testing at Peterbilt remains to be done on the demonstrator chassis. This final testing will be completed in January 2023.

Key Publications

1. DOE Quarterly progress report, Q17 – January 30, 2022
2. DOE Quarterly progress report, Q17 – April 30, 2022
3. 2021 Annual Merit Review – June 23, 2022
4. DOE Quarterly progress report, Q19 – July 30, 2022
5. DOE Quarterly progress report, Q20 – October 30, 2022

Acknowledgements

The project team acknowledges Ken Damon and David Mielke (Peterbilt), Reubin Close (Bridgestone), and Ralph Nine (National Energy Technology Laboratory Program Manager).

VI.D.3 Development and Demonstration of a Fuel-Efficient Class 8 Tractor and Trailer SuperTruck (Navistar, Inc.)

Russ Zukouski, Principal Investigator
Navistar, Inc.
2701 Navistar Drive
Lisle, IL 60532
Email: Russ.Zukouski@navistar.com

Siddiq Khan, DOE Technology Manager
U.S. Department of Energy
Email: Siddiq.Khan@ee.doe.gov

Start Date: January 1, 2017 End Date: June 30, 2022
Project Funding: $55,595,805 DOE share: $20,000,000 Non-DOE share: $35,595,805

Project Introduction

The objective of the SuperTruck 2 engine project is to research, develop, and demonstrate a heavy-duty engine that can meet 2010 federal emission standards and achieve 55% brake thermal efficiency (BTE) demonstrated in an operational engine at a 65 mph cruise point on a dynamometer. In addition, commercial viability of the technologies applied to this engine should be evaluated.

Objectives

Overall Objectives

- Attain greater than or equal to 55% BTE, demonstrated in an operational engine at a 65 mph cruise point on a dynamometer.
- Develop engine technologies that are commercially cost-effective.
- Contribute to greater than 100% improvement in vehicle freight efficiency relative to a 2009 baseline.

Fiscal Year 2022 Objectives

- Evaluate a newly designed high-flow cylinder head (HFCH) for BTE improvement.
- Optimize an organic Rankine cycle (ORC) waste heat recovery (WHR) system that contributes to achieving 55% BTE.
- Complete technologies assessments for their respective commercial viability.

Approach

The work will include component- and system-level consideration of the base engine architecture, air system, combustion and fuel system, advanced aftertreatment, thermal management, and WHR. The project will involve analysis, development, testing, and down-selection of individual and system-level engine technologies, as well as integration of the final selected technologies into a prototype engine.

Results

HFCH

Engine tests had shown BTE gains due to increased air-to-fuel ratio while minimizing parasitic pumping work. The focus had been on matching turbocharger size and efficiency to engine operating conditions. In addition to the external matching of the turbocharger, a new concept of the cylinder head (detailed in Figure VI.D.3.1) was investigated to improve the gas exchange process for in-cylinder trapped air mass, consequently increasing the

air-to-fuel ratio for combustion. A new cylinder head was proposed, and the shape and size of both intake and exhaust ports were rearranged and optimized (shown in Figure VI.D.3.1b).

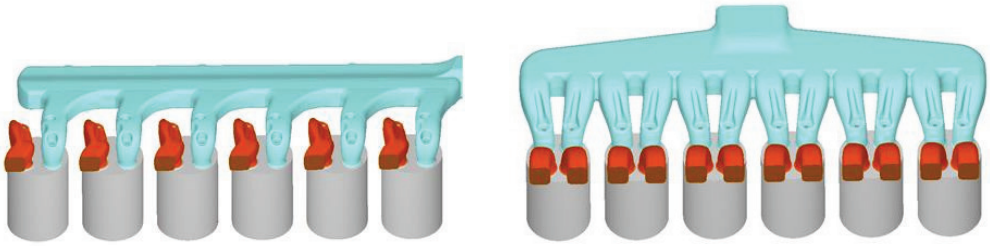

(a) baseline cylinder head *(b) high-flow cylinder head*

Figure VI.D.3.1 The baseline cylinder head versus the newly designed HFCH

Three-dimensional (3D) simulation was employed to quantify the gain in trapped air mass of the new cylinder head. The intake valve profile was also optimized to maximize the gain (Figure VI.D.3.2a). The 3D combustion simulation showed that a gain of 0.3% indicated thermal efficiency (ITE) could be achieved with this new cylinder head (Figure VI.D.3.2b).

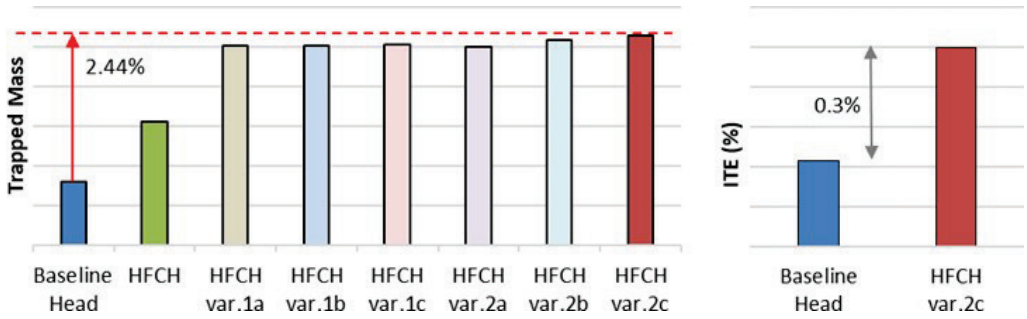

(a) optimization of intake valve profile for trapped mass *(b) improvement on ITE*

Figure VI.D.3.2 3D simulation of HFCH performance

The design of the new cylinder head was initiated. The concept of dual overhead camshafts was selected for the new head (shown in Figure VI.D.3.3). A support frame for the camshafts was designed to reduce the complexity of the head. A coolant inlet manifold was designed to distribute the coolant for the head. The intake manifold was redesigned for the center feed of the air and for the coolant return from the head.

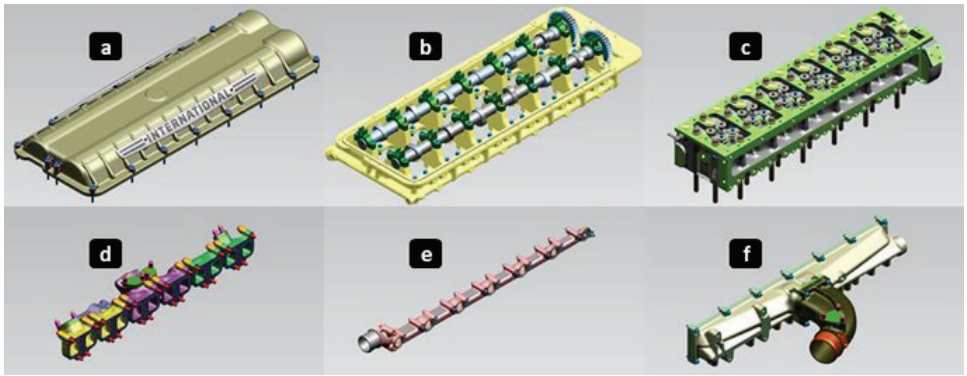

Figure VI.D.3.3 New designs of the HFCH: (a) valve cover, (b) dual overhead camshafts with support frame, (c) HFCH, (d) exhaust manifold, (e) coolant inlet manifold for the head, and (f) intake manifold with coolant return and exhaust-gas-recirculation mixer

Thermal and structural analysis were conducted at AVL. Based on the thermal analysis, the minimum coolant flow rate for the new cylinder head was specified. Two electric water pumps were selected to provide the required coolant flow rate for the cylinder head and the crankcase separately.

The materials for the prototype cylinder head and the camshafts' support frame were recommended based on the structural analysis. The new camshafts and valvetrain were also verified via simulation. The design of each part was completed, and the parts were procured.

The engine was assembled and shipped to Bosch at Farmington Hills, Michigan, for the testing. A design of experiment was employed to map out the BTE surface of this new cylinder head engine. The test results showed an improvement in BTE response surface from the testing (Figure VI.D.3.4a). The further tuning of the confirmation point shows that this engine could achieve greater than 51% BTE (Figure VI.D.3.4b).

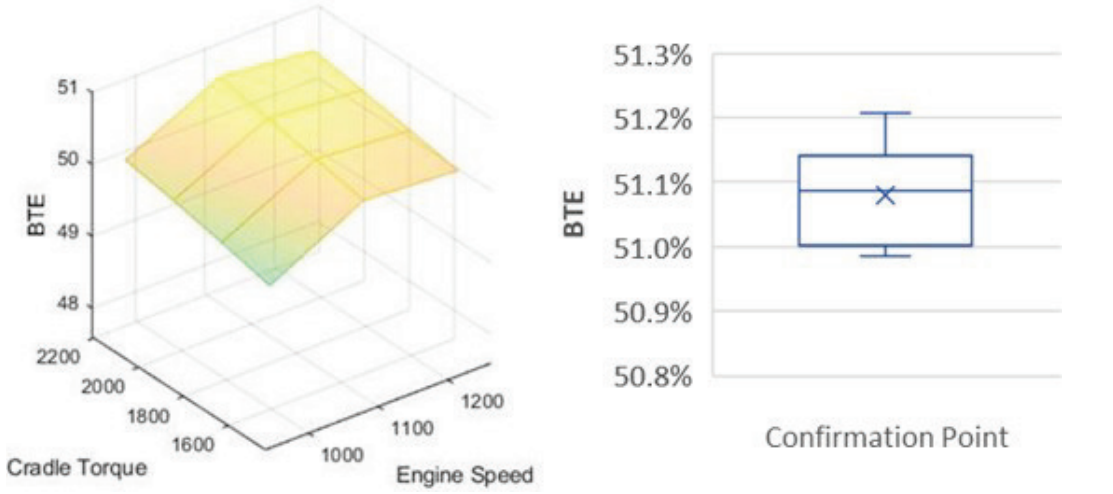

(a) BTE surface from design of experiment *(b) optimized point from design of experiment*

Figure VI.D.3.4 Performance of the HFCH engine

WHT – ORC

To achieve 55% BTE, WHR plays a critical role. Navistar has selected ORC technologies as the prime path for WHR. To maximize ORC system efficiency, energy recovery options from all available waste heat sources were considered. The identified ORC system configuration is being supplied by Borg Warner, with controls provided by AVL and assembly and demonstration performed by Clemson University's International Center for Automotive Research. The final test results at Clemson University met the target BTE of 3.0% with the 55% BTE operational target boundaries achieved using a mule A26 engine. The ORC system, the A26 engine, and the aftertreatment system were disassembled and shipped back to Navistar for confirmation testing. The demonstration at Clemson University was successfully repeated at Navistar.

Based on the initial ORC dynamometer testing results at Navistar, it was identified that the restriction reduction—both intake and exhaust sides—is a challenge to the overall system BTE. Both parallel charged air cooler (CAC) pre-heaters and parallel exhaust boilers were proposed. However, Borg Warner would not recommend the parallel exhaust boilers because of limited time to balance the working fluid flow between two exhaust boilers on the ORC cart.

Simulation predicts a 0.2% overall BTE gain with the implementation of parallel CAC pre-heaters. Owing to limited space, the CAC pre-heaters were stacked vertically. The initial working fluid plumbing was in parallel. The testing results showed that the CAC pre-heaters out air temperature was about 75°C higher than the target. The analysis indicated that the working fluid did not distribute equally through the upper and lower CAC pre-

heaters. The working fluid plumbing was then reconfigured in series for the CAC pre-heaters. The testing was repeated, and the CAC pre-heaters out air temperature came down to around 17°C above the target. Thus, a secondary test cell CAC was added to further reduce the air temperature.

The final ORC setup at Navistar was completed. Insulation was added to minimize the exhaust heat loss. A low-viscosity lube oil, 0W16, was used to minimize the engine friction loss. A design of experiment was carried out to identify the optimal engine operating conditions for the overall BTE with ORC. Finally, a combined BTE of 55.2% was demonstrated (with respective contributions shown in Figure VI.D.3.5).

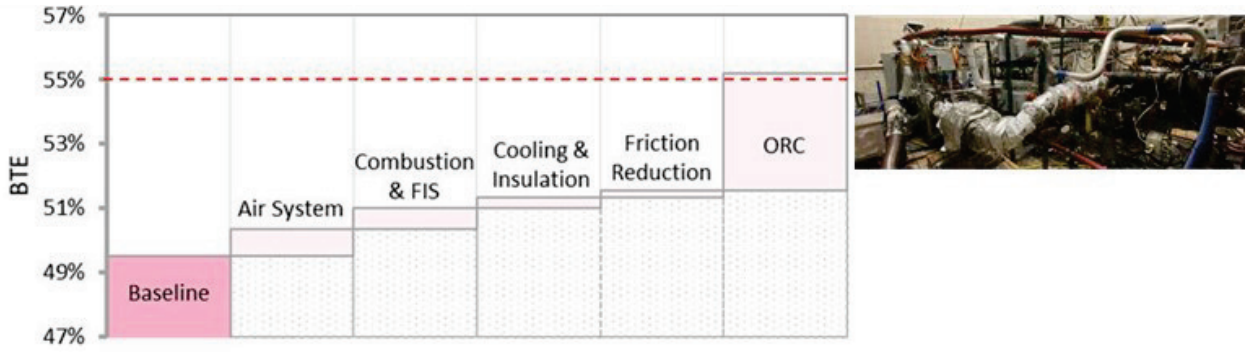

FIS – fuel injection system

Figure VI.D.3.5 Contributions of technologies toward 55% BTE

Technologies Assessments

After achieving the BTE goal, the tasks were to focus on the technologies assessments for their respective commercial viability, including the development time, risk, and cost (shown in Table VI.D.3.1). WHR has been identified as long-lead-time, high-risk, and high-cost development work to become commercially viable for the vehicles. On the other hand, implementation of the advanced aftertreatment system is more feasible and will accommodate the change in engine-out constituents. The assessment of the engine subsystems is also presented. The cylinder deactivation is included in the combustion system.

Table VI.D.3.1 Technologies Assessments for Commercial Viability

	1 to 3 years	4 to 7 years	> 7 years	Risk	Cost
Engine Subsystems					
Air System		X		Medium	$$
Combustion System		X		High	$$$$
Fuel System		X		Medium	$$
Cooling System		X		Medium	$$
Friction Reduction		X		High	$$
Advanced Aftertreatment					
Diesel Exhaust Fluid Dosing System	X			Low	$$
Selective Catalytic Reduction System	X			Low	$
Diesel Particulate Filter System	X			Low	$
Control System	X			Medium	$$

WHR					
Packaging / Weight			X	Very High	$$$$
Boiler			X	High	$$$$
Expander			X	High	$$$$
Condenser			X	Medium	$$$
Control			X	High	$$$$

Conclusions

- An HFCH concept was proposed, simulated, designed, procured, and tested. The dynamometer test results showed that this new cylinder head concept could aid the engine to achieve 51% BTE.
- A dual-loop ORC system was integrated with a prototype engine in a Navistar test cell for the final 55% BTE demonstration on a dynamometer. The test results showed that this combined system could achieve 55.2% BTE.
- The assessment of commercial viability for the engine subsystems, aftertreatment system, and WHR system was completed. The WHR system was identified as long-lead-time, high-risk, and high-cost development work to become commercially viable for the vehicles.

VI.D.4 Improving Transportation Efficiency through Integrated Vehicle, Engine, and Powertrain Research - SuperTruck 2 (Daimler Truck North America)

Darek Villeneuve, Principal Investigator
Daimler Truck North America
4555 North Channel Avenue
Portland, OR 97217
Email: darek.villeneuve@daimlertruck.com

Jeff Murawa, Principal Investigator
Detroit Powertrain
13400 Outer Drive West
Detroit, MI 48239-4001
Email: Jeffrey.Murawa@daimler.com

Siddiq Khan, DOE Technology Manager
U.S. Department of Energy
Email: Siddiq.Khan@ee.doe.gov

Start Date: October 1, 2017 End Date: September 30, 2022
Project Funding: $40,000,000 DOE share: $20,000,000 Non-DOE share: $20,000,000

Project Introduction

Achieving Daimler Truck North America (DTNA) increased targets for SuperTruck 2 (ST2) will require building on SuperTruck 1 (ST1) project's success while considering commercial viability. DTNA will meet or exceed these targets through the development of several advanced vehicle and engine technologies.

The ST2 program finished the last phase of the project in this budget period with the optimization and testing of our final demonstrator vehicle and engine.

Objectives

The objective of the ST2 program is to research, develop and demonstrate a Class 8 long-haul truck that can meet prevailing federal emissions standards, satisfy applicable safety and regulatory requirements, and achieve the following goals.

Overall Objectives

- Demonstrate 115% improvement in vehicle fuel economy (on a ton-mile-per-gallon basis) relative to a 2009 Cascadia baseline (same as ST1). A stretch goal is 125% improvement.
- Demonstrate an engine that meets or exceeds a 55% engine brake thermal efficiency (BTE) demonstrated in an operational engine at a 65-mph cruise point on a dynamometer.
- Develop technologies that are commercially cost effective in terms of a simple payback.

Fiscal Year 2022 Objectives

- Finish building final demonstrator.
- Optimize final vehicle feature integration into final demonstrator.
- Perform dyno testing of engine.
- Complete vehicle tests to demonstrate 115% improvement in fuel economy.

Approach

The basic approach used by DTNA has been to take learnings from ST1 to create further aerodynamic improvements, energy management optimizations, improve tires, light weighting, and practical trailer improvements using a standard 53-foot trailer. The powertrain advancements beyond ST1 include combustion efficiency, along with gearing enhancements, advanced air handling, friction reduction, heat- and energy-loss mitigation, and an improved waste heat recovery system.

We completed interior and exterior installations on the final demonstrator vehicle. Work continued on mechatronic features to gain functionality and reliability up until the test was initiated. Two individual road tests and two stationary tests were completed by the end of the program. The 55% BTE engine final tests were completed on a dynamometer at Oak Ridge National Laboratories (ORNL) with some follow-up testing in Detroit. Final data processing and results will be shared in the final report.

Results

The final demonstrator (Figure VI.D.4.1) accumulated a total of 9,929 miles before testing began with the last 3,000 miles being issue free. Road testing began in August with both the Portland-Pendleton-Portland and the San Antonio-Dallas-San Antonio routes. Stationary tests for both the winter and summer mode were completed in September.

Figure VI.D.4.1 The 2009 baseline and final demonstrator vehicles at start of testing

Overall Weight

The final tare weight of the ST2 model was 30,949 lb compared to the baseline tare weight of 33,546 lb. The increase payload of ST2 was 2,597 lb, thereby increasing ST2's payload by 1.3 tons. Table VI.D.4.1 provides final weight comparisons used in testing.

Table VI.D.4.1 Vehicle Weight Comparison

	Baseline Vehicle Weight (lb)	SuperTruck 2 Weight (lb)
Steer	11,400	11,850
Drive	26,700	24,750
Trailer	26,900	28,400
Total	65,000	65,000
Tare	33,546	30,949
Payload	31,454	34,051

Test Cell Demonstration Engine (55% BTE)

The demonstration engine completed testing at ORNL by the end of 2021. Testing of the thermal barrier coated (TBC) pistons had been completed, but the time allotted for running the engine at ORNL ran out before the TBC cylinder head and valves could be completed. Detroit completed testing of the combustion chamber coating performance.

With the TBC head and valves added to the package, the cumulative BTE of the core engine was 50.6%. Earlier in the ST2 program, development of the ST1 Waste Heat Recovery (WHR) (exhaust and exhaust gas recirculation [EGR] boiling only) continued using a better system based on cyclopentane working fluid. Including the cyclopentane WHR with the complete 50.6%, the core engine demonstrated a combined BTE of 52.9%. The phase change cooling (PCC) WHR system was found to have higher performance through simulation. The PCC WHR engine assembly was completed but testing never started since the budget was depleted and test cell time was not available before the end of ST2 testing. The 55% BTE goal for the test cell demonstration engine would have been met based on the base engine performance, along with using the PCC WHR system simulation results. Figure VI.D.4.2 provides a waterfall view of the incremental improvement to engine BTE.

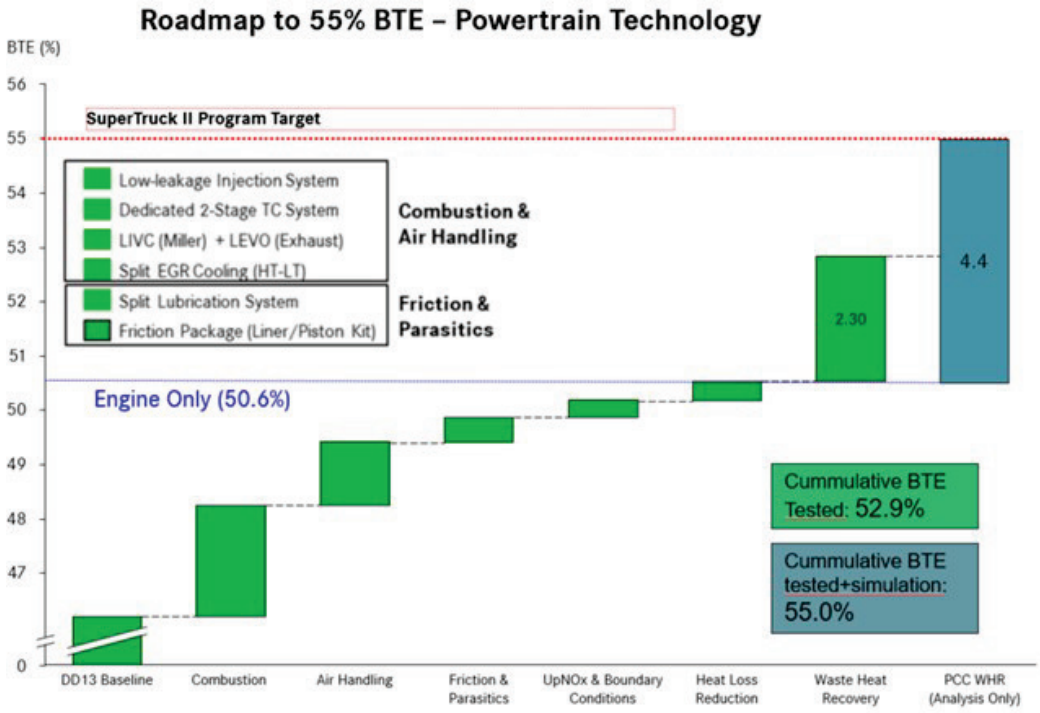

TC – turbocharger; LIVC – late intake valve closing; LEVO – late exhaust valve opening; HT-LT – high temperature–low temperature

Figure VI.D.4.2 55% BTE engine test results

Thermal Barrier Coating

For the final TBC testing in 2022, there was a ~0.3 g brake specific fuel consumption benefit thanks to the coated head alone and a further ~0.7 g from the pistons, giving an overall 1g benefit at best point for the complete coated combustion chamber, as shown Table VI.D.4.2. Worth noting is that the effect of the coatings on efficiency is wide-ranging, with a positive improvement across the entire engine operating range.

During TBC testing, discoloration and loss of coating on the intake valves and seat was noted, which was likely caused by temperature shock from cold intake air interacting with the coated fire deck. (Figure IV.D.4.3)

TBC testing also revealed that coating parameters (material properties, coating thickness, and roughness) has significant influence on actual performance during testing. Slight deviation from optimal values of TBC can make engine freight efficiency worse. Furthermore, TBC measurably impacts the center of combustion, engine out NO_x, and further optimization is needed to re-phase the combustion for same NO_x to contribute to further freight efficiency improvement. Therefore, this investigation in the area of in-cylinder optimization has room for exploration regarding freight efficiency improvement, durability, and coating process variation.

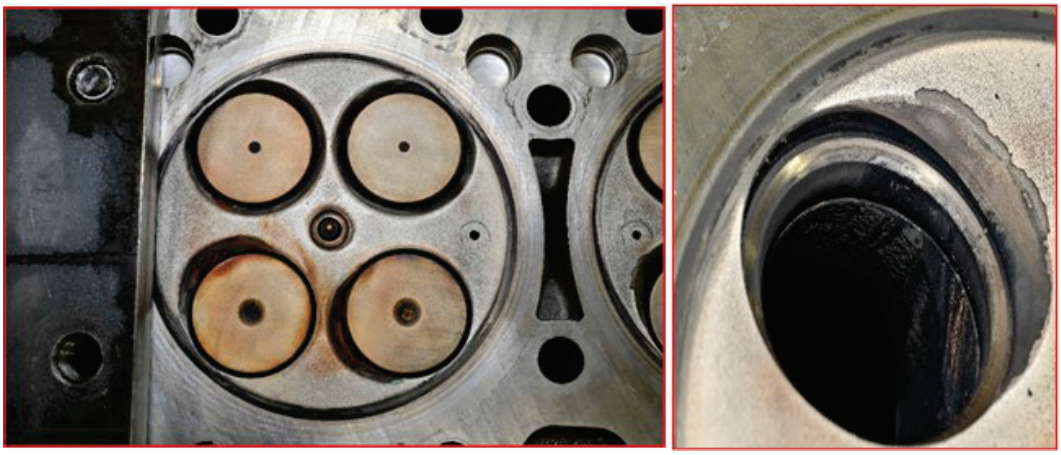

Figure VI.D.4.3 Coated fire-deck (cylinder head and valves) run in Detroit to demonstrate TBC

SuperTruck 2 Road Test Raw Data

The ST2 strategy, from the project's beginning, was to focus on core technologies for the final demonstrator that show the most promising path to production. Core technologies in ST2 included tractor aerodynamics, tire rolling resistance reduction, core engine efficiency, and energy management. Tractor aerodynamics improved by 12% over ST1. The tractor tires also had a 12% reduction in rolling resistance. Lastly, the core engine efficiency improved by 5.7% over ST1 with several features. These changes will raise the industry expectation for significant fuel savings on Class 8 long-haul trucks.

Based on results from our ST1 project, content selection narrowed the focus on ST2. We did not include WHR or high-voltage (HV) hybridization on the final demonstrator tractor nor pursue extreme trailer aerodynamic changes. Although these technologies demonstrated fuel savings on ST1, the feasibility for production was deemed low at the time due to multiple reasons, including unfavorable cost/benefit potential, identification of lower-cost alternative technologies (predictive EcoRoll vs HV hybrid), and adverse impact to other fuel economy measures (particularly WHR vs tractor aerodynamics). Drastic weight reduction using high-cost materials such as carbon fiber or complex chassis redesign has a long path towards production, so few resources were spent on these topics as well. Finally, trailer development was minimized since trailers are not part of DTNA's core business, and extreme trailer aero measures proved to be operationally challenging and unproductive for fleets.

While several technologies did make it to the final demonstrator, issues with software controls and hardware reliability caused some features to not function fully in the final test, resulting in less freight efficiency than expected. Dynamic load shift did not shift as much weight as expected; EcoSail, or predictive cruise, was not functional; boost and recoup hybrid were not functional; and the active aerodynamic panels did not have full deployment during all the individual tests. Lessons from the tests show the importance of reliable sensing, robust wiring, and thorough controls testing for all new features. Ensuring full functionality proved particularly challenging on a proof-of-concept for vehicles relying on prototype systems with low design maturity and high vehicle integration complexity.

One final note on the preliminary results is that the same 2009 baseline truck and trailer that were part of ST1 were retested. The only change to this truck and trailer (other than basic maintenance) was installing new tires. The original tires used were no longer in production or available, so similar rolling resistance tires were selected. The actual rolling resistance of these new tires is currently unknown but is currently being tested. The actual 2009 vehicle performance results were better than anticipated and better than what was reported in ST1. An analysis of the 2009 tires and impact on the data will be provided in the final report.

For the driving portions of the test cycle, the procedure used for measuring the relative fuel consumption between the ST2 and baseline vehicles was a modified version of the TMC Type IV Fuel Economy Test Procedure (RP1109), where the fuel measurement was made using high accuracy on-board flow meters. TMC Type IV is a procedure used to measure the fuel consumption of one vehicle relative to another and provides guidance for running an unbiased test. The procedure calls for a minimum of three valid test runs for each route.

For the driving portions of the test cycle, the drivers are coached to remain on cruise control as much as possible with the goal of reducing non-random error. SuperTruck 2 is a comprehensive tractor/trailer program; as such, the Type IV test procedure was modified to swap only the drivers and flowmeters at the halfway point of each respective test route. Each truck's diesel particulate filter was regenerated prior to each test run such that both trucks started with the same conditions.

By the end of third quarter of 2022, all four freight efficiency tests were completed on time. A thorough analysis of the full results will be provided in the final project report.

Parked Tests

The stationary test duration for ST2 was set to the same five hours for the A/C cycle (summer mode) and five hours for the heating cycle (winter mode) as in ST1. The parked tests were conducted per TMC RP-432 protocol, "Engine Off HVAC Performance Requirements for Truck Cabs with Sleepers." All other test criteria of the TMC protocol were met that included the ability to start the vehicle after the test was completed.

Table VI.D.4.2 Stationary Test Result

	Summer Mode Test	Winter Mode Test
Test Conditions	5 hours 100°F ambient temperature 50% relative humidity 600 w/m^2 solar loading 100	5 hours 0°F ambient temperature
Cab Temperature Target	73°F ± 5°F	73°F ± 5°F
Baseline Fuel Consumption	3.34 gallons	3.00 gallons
ST2 Fuel Consumption	0.49 gallons	0.30 gallons

The baseline 2009 Cascadia tractor consumed 3.0 gal and 3.34 gal of fuel for each of the five-hour winter and summer mode tests, respectively. This was very similar to the ST1 result for the 2009 baseline that consumed 3.0 gal and 3.6 gal for the winter and summer modes. SuperTruck 2 consumed 0.3 gal and 0.49 gal for the winter mode and summer mode, respectively. Savings from the winter mode test stem primarily from the use of a fuel-fired heater for warming the sleeper and better insulation, compared to main engine idling as a heat source for the baseline.

Conclusions

All testing was completed on time, and detailed data analysis will be provided in the final report. Many technologies developed on ST2 have a short path towards production. The final report will provide further insights into production readiness.

- Tractor aerodynamics improved by 12% over SuperTruck 1.
- Tractor tires have a 12% reduction in rolling resistance.
- Core engine efficiency improved by 5.7% over SuperTruck 1 with several features impacted.

Patent and Invention Disclosures

1. Slocum, Jackson, Dinesh Madugundi, and Paolo Zanetti. 2021. "Arrangement of a Side Door on a Cab for a Commercial Vehicle." Owner: Daimler AG (internal ref 2021P01884 GB) GB Patent Application No. 2118962.6 filed December 23.

Key Publications

1. Villeneuve, D., J. Girbach, and M. Bashir. 2022. "Improving Transportation Efficiency through Integrated Vehicle, Engine, and Powertrain Research – SuperTruck 2." Presented at the 2022 Vehicle Technologies Office Annual Merit Review Meeting, Arlington, VA, June 23.

VI.D.5 Development and Demonstration of Advanced Engine and Vehicle Technologies for Class 8 Heavy-Duty Vehicle – SuperTruck II (PACCAR Inc.)

Maarten Meijer, Principal Investigator
PACCAR Inc.
12479 Farm to Market Road
Mount Vernon, WA 98273
Email: maarten.meijer@paccar.com

Siddiq Khan, DOE Technology Manager
U.S. Department of Energy
Email: Siddiq.Khan@ee.doe.gov

Start Date: October 1, 2017 End Date: December 31, 2023
Project Funding: $40,000,000 DOE share: $20,000,000 Non-DOE share: $20,000,000

Project Introduction

PACCAR Inc., through Kenworth Truck Company and PACCAR Technical Center, is collaborating in the design and development of a very high-efficiency engine with advanced combustion, reduced friction, advanced air management, and waste heat recovery. Collaborating partners are the National Renewable Energy Laboratory, Eaton Corporation, AVL North America, and The Ohio State University. A 48 V mild hybrid powertrain, enhanced through accessory electrification and advanced controls, is also under development. The powertrain will be incorporated into a highly aerodynamic and lightweight tractor–trailer combination. The vehicle concept includes advancements in rolling resistance, thermal management, and auxiliary components. Representative customer driving routes have been selected and will be used for development and optimization of the integrated vehicle controls package. Testing of engine, powertrain, and vehicle will demonstrate that project goals have been met.

The combination of technologies is on track to provide greater than 120% improvement in vehicle freight efficiency (with the current prediction at 140%) at an affordable cost and with a short payback time. This level of fuel efficiency improvement, applied over the entire Class 7 and Class 8 vehicle fleet in the United States, will have a tremendous positive impact on the operating efficiency of truck fleets and significantly reduce fossil fuel energy dependency.

Objectives

The objective of this project is to research, develop, and demonstrate a Class 8 long-haul tractor–trailer combination that meets prevailing federal emission standards and applicable safety and regulatory requirements while achieving the objectives listed below.

Overall Objectives

- Greater than 100% improvement in vehicle freight efficiency (on a ton-mile-per-gallon basis), with a stretch goal of 120% relative to a 2009 baseline
- Demonstrated 55% engine brake thermal efficiency (BTE) in an operational point representative of cruise conditions
- Same or improved vehicle performance (acceleration and grade performance) relative to a 2009 baseline

- Cost-effectiveness as expressed in terms of a simple payback to foster rapid market adoption of new technologies

Fiscal Year 2022 Objectives

- Waste heat recovery demonstration (4% BTE)
- SuperTruck II engine build and testing (51% BTE)
- Mild hybrid powertrain validation and integration
- Vehicle design freeze

Approach

The project has been approached in three distinct but related areas: powertrain, vehicle, and engine. For the SuperTruck II vehicle demonstrator, the team is using a systems engineering approach while working with integrated teams, combining areas of technical expertise and leveraging existing development processes and tools.

Although both the engine and vehicle efficiency targets require development and implementation of multiple new technologies, the aim of commercialization is consistently used throughout the selection procedure. As a result, commercialization feasibility of new technologies is evaluated by using a combination of the technology readiness level process, return on investment calculations, and multiple customer councils.

A key element for the SuperTruck II powertrain is the implementation of a 48 V mild hybrid architecture, including the integration of an optimized Li-ion battery system. Primarily and directly because of the SuperTruck II program, 48 V electrification is regarded as a high-potential candidate for accelerated market introduction. This mild hybrid architecture is seamlessly integrated with the high-efficiency PACCAR MX-11 engine, PACCAR transmission, 4x2 axle architecture, and low-rolling-resistance tires. In addition to direct fuel efficiency contributions, mainly due to regenerative braking power capability, the 48 V architecture also supports overnight (predictive) e-hoteling. The overall powertrain component optimization is performed by using extensive vehicle route simulations, including the various developed vehicle-energy-level software control strategies and driver needs.

To find the right balance for the engine between optimum BTE and high future commercialization potential, concepts are categorized into three areas: conventional, modest innovation, and non-conventional. Detailed simulations revealed that implementing only the conventional concepts is not sufficient to achieve the 55% BTE target. Therefore, the team has fully adopted investigating the modest innovation design concepts and is exploring alternative combustion regimes from the non-conventional concepts. Non-conventional concepts that require significant mechanical changes—i.e., basic engine architecture design changes—were excluded. The optimization of highly coupled engine systems requires an integrated simulation and experimental approach. Dedicated test rigs for flow, combustion, and boost are used to validate the simulations, at a component and system level. The detailed insights from the experiments feed additional simulations in order to define the final engine hardware design. For example, the PACCAR SuperTruck II engine, tailored to waste heat recovery (WHR) architecture, is optimized by coupling the detailed engine and WHR Rankine cycle simulations.

The vehicle design includes significant aerodynamic improvements such as tractor wheel well closeouts, camera-based mirrors, optimized windshield curvature and A-pillars, and reduced tractor–trailer gap. The tractor and trailer are undergoing significant lightweighting through the implementation of new designs for modular chassis, rear axle, and cabin. Vehicle energy use will be reduced significantly by applying highly efficient auxiliary electrification and cabin insulation. The overall energy management of the SuperTruck II vehicle demonstrator is supervised by a vehicle-level energy management controller concept.

Results

Powertrain

Mild-hybrid powertrain components, including the 48 V Li-ion battery system, power take-off (PTO) motor, and ultra-low nitrogen oxides (NO_x) system, were installed on the proof-of-concept vehicle in 2022. The team focused on mechanical and electrical integration of the battery system, the 30 kW inverter, the PTO motor (Figure VI.D.5.1), the transmission controller unit, and the 3 kW DC-to-DC converter.[1] Engine off-coast is the only remaining function to validate that will contribute to improved freight efficiency.

Several approaches to optimal charging strategies during propulsion mode have been integrated with the optimal braking strategy. Thus, the controls for the entire driving cycle are completed and tested. Different methods have been tested and compared for energy savings and hoteling management. The methods have been tested on the Akasol battery pack, assuming 1 kW electrical loads for the predictive e-hoteling cycle.

After verifying successful communication from the 48 V mild hybrid system, researchers were able to start the engine using the PTO motor. After a successful engine crank, the battery system was charged using the engine control unit. The team will continue integrating and validating the mild-hybrid system components on the proof-of-concept vehicle, with revisions to controller area network architectures and wiring diagrams as required to achieve desired functionality.

During on-road testing of a high-current inverter in the test vehicle, the Akasol upper current limit was transiently exceeded. The Akasol pack and the MD30 software were modified to disable isolation fault detection via controller area network message to the Akasol battery management module. Once the request to disable isolation fault detection was removed, the Akasol pack functioned normally.

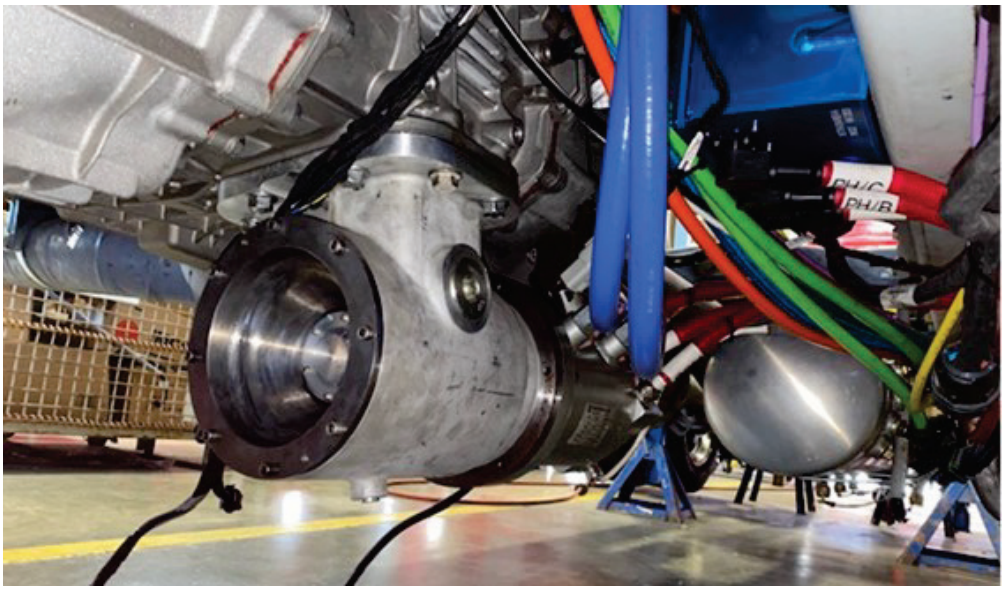

Figure VI.D.5.1 PACCAR SuperTruck II PTO motor

The validated powertrain, including controls and electrical architecture, is ready for integration into the final demonstration vehicle. The mild-hybrid powertrain contributes approximately 40% of our freight efficiency improvement.

[1] A DC-to-DC converter is an electronic circuit or electromechanical device that converts a source of direct current (DC) from one voltage level to another.

Engine

Final proof-of-concept measurements for the engine have been completed. Dedicated test rigs have been utilized throughout the project to isolate the sub-system of interest while operating at the anticipated final engine demonstrator conditions. Activities this year focused mainly on validation of turbocharger efficiencies required to support the late inlet valve closing (Miller) cam timing and long-stroke concepts selected. Experimental activities were supported by detailed simulation activities. A 1D model was used to confirm the best turbocharger match and explore additional options in terms of turbocharger nozzle trims. When the turbocharger hardware was received, it was run on a production multicylinder engine, in combination with the pulsed optimized exhaust manifold, and run in parallel on the 1D model, showing good agreement and proving the anticipated overall turbocharger efficiency.

The demonstration engine build (Figure VI.D.5.2) started this year, as the procurement of components concluded. Engine assembly progressed slowly because of several issues that needed to be addressed. The largest concern was that the crankshaft main bearing bore was undersized and needed to be enlarged before proceeding with the engine assembly. With the crankshaft main bearing bore within specifications, the engine assembly continued to completion of the short block and onto the long block. With the engine build completed, the team is ready for the final step of the project, which is demonstration of 55% BTE in the test cell. Various hardware variants (camshafts, turbochargers, injectors) are available for final engine efficiency optimization in the testbed, if needed. However, with the detailed simulations and sub-system proofs of concept in place, the team is confident about reaching the project goals on time.

Figure VI.D.5.2 Prototype engine build

Testing of the full WHR system at the design point and a wide range of alternate engine operating conditions has been completed. A WHR benefit of >4.0% BTE has been achieved at all operating conditions provided by the engine team, with an above-target result of 4.3% achieved at the design point. Characterization of sensitivity to coolant conditions, as well as flow restriction measurements for engine-side components, has also been completed.

Vehicle

Significant progress has been made on the demonstrator vehicle, with most of the larger tools being completed for the body-in-white (Figure VI.D.5.3). Tools include the roof, cab door assembly, both side outer skins (including the door aperture), rear wall skin, and both floor skins. Tractor architecture comprises approximately 49% of our current freight efficiency goal, with tractor aerodynamic improvements contributing an additional 20% toward our goal.

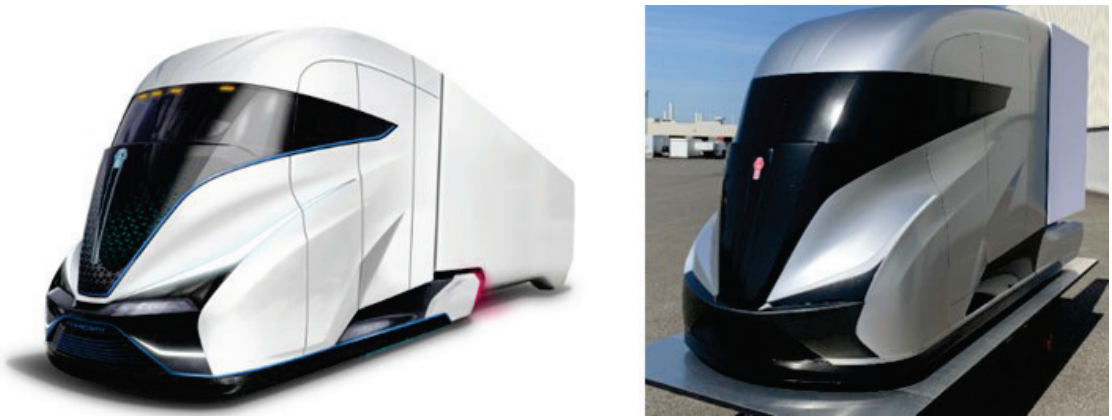

Figure VI.D.5.3 Rendering of PACCAR SuperTruck II cab and trailer (left) and clay model of cab (right)

Interior development continues with a focus on the instrument panel, sleeper compartment, and rear console. Also considered within interior development are project scope and definition, design theme, material selections, and interior layout of center drive with a focus on the instrument panel, two-tier headliner, sleeper compartment, and packaging of electronic controllers on the left side, right side, and rear console (Figure VI.D.5.4). Next steps will include creating A-surfaces, solid modeling, and design for manufacturing and assembly review. The electric heating, ventilation, and air conditioning (e-HVAC) heat pump system was built by MAHLE, our supplier. The e-HVAC system is in the final stages of performance testing at the supplier before being integrated into the demonstrator vehicle.

Figure VI.D.5.4 Rendering of PACCAR SuperTruck II cab interior (left) and e-HVAC system (right)

One focus of the project has been electric power steering solutions to enable engine off-coast operation as a means of supporting fuel economy goals. Several systems were investigated, and an axle-mounted electric power steering system was selected over other alternatives, including electric-over-hydraulic solutions. This concept retains our existing geometry for wheel cut and Ackermann but will allow us to do away with the hydraulic assist pump. The drive-by-wire technology offers some packaging advantages that could be useful in future vehicle platforms to improve aerodynamics and ergonomics, along with other improvements.

Computational fluid dynamics analysis has shown that the skirt and tail concept on the lightweight trailer should provide an estimated 43% increase in drag performance over a standard utility trailer. Stoughton plans to kick off tooling for the components of the lightweight trailer in the fourth quarter (Q4) of 2022. Current activities include developing the auxiliary aero components, and the project is on track to have the aero skirts designed and available by the time the rest of the trailer is complete in Q2 2023.

Conclusions

The PACCAR-led team has integrated the approaches for engine, powertrain, and vehicle into the prototypes for experimental component and system-level validation. Final engine and powertrain hardware components have been fabricated and assembled, and design activities for the final vehicle demonstration have progressed. Based on the proof-of-concept experimental results, it can be concluded that the project is well on track to meet its objectives and to be completed within budget by the contractual deadline of Q4 2023.

The status of the three key project research areas is summarized below.

Powertrain

- Installed and validated 48 V mild hybrid powertrain components on proof-of-concept vehicle.
- Implemented and validated electrical and controls architecture.
- Tested overall powertrain concept and performance on proof-of-concept vehicle.

Engine

- Completed final component/sub-system proof-of-concept measurements.
- Procured engine hardware and completed engine build.
- Started final engine demonstration testing.
- Achieved WHR benefit of >4.0% BTE at all operating conditions provided by the engine team, with 4.3% achieved at the design point.

Vehicle

- Completed majority of tooling for cab structure.
- Making final revisions to interior design, with a center drive position as one of the key features.
- Conducting final performance validation on e-HVAC system.
- Started final vehicle build.

Key Publications

1. DOE quarterly progress report, Q17 – January 30, 2022
2. DOE quarterly progress report, Q18 – April 30, 2022
3. 2021 Annual Merit Review Presentation, June 23, 2022
4. DOE quarterly progress report, Q19 – July 30, 2022
5. DOE quarterly progress report, Q20 – October 30, 2022

Acknowledgements

The project team acknowledges the support from Ralph Nine, National Energy Technology Laboratory Project Manager.

VI.D.6 Low-Mass and High-Efficiency Engine for Medium-Duty Truck Applications (General Motors)

Qigui Wang, Co-Principal Investigator
General Motors
30003 Fisher Brothers Road
Warren, MI 48093
Email: qigui.wang@gm.com

Ed Keating, Co-Principal Investigator
General Motors
28755 Louis Chevrolet Road
Warren, MI 48093
Email: ed.keating@gm.com

Siddiq Khan, DOE Technology Manager
U.S. Department of Energy
Email: Siddiq.Khan@ee.doe.gov

Start Date: October 1, 2019 End Date: December 31, 2023
Project Funding: $10,244,191 DOE share: $7,132,775 Non-DOE share: $3,111,416

Project Introduction

Today's transportation vehicle customers are demanding that manufacturers produce engines with lower weight and improved efficiency to reduce fuel consumption, emissions, and costs associated with vehicle use, while maintaining or even increasing engine performance. Developing the next generation of high-efficiency, very low-emission internal combustion engines thus requires a combination of new combustion strategies, advanced materials, and new materials processing techniques to further increase engine efficiency and reduce weight.

Objectives

The objective of this collaborative project between General Motors (GM), Oak Ridge National Laboratory (ORNL), The Ohio State University (OSU), Michigan Technological University, and ECK Industries Inc. is to develop an advanced medium-duty truck engine. This engine is to be equipped with advanced materials and combustion technologies capable of achieving ≥10% fuel efficiency improvement and ≥15% engine weight reduction when compared to the 2015MY (model year) GM L96 VORTEC 6.0 L V8 engine compliant with applicable U.S. Environmental Protection Agency emission standards, with performance demonstrated via simulation coupled with engine dynamometer testing.

Approach

This project is proposed as a large-scale engine design and demonstration enabled by an advanced materials and manufacturing development program, with a comprehensive plan spanning a period of four years in two phases. The project begins with engine architecture design and analysis activity, advanced materials and manufacturing process development and down-selection. It culminates in an engine test cell evaluation with optimal materials and manufacturing solutions supporting final vehicle simulation. The final engine test is to verify engine weight reduction and performance to the funding opportunity announcement (FOA) objectives [1].

Several advanced combustion technologies are investigated, including stoichiometric combustion, increased compression ratio, aggressive exhaust gas recirculation (EGR) dilution, and load point optimization. High-strength and heat-resistant materials are developed and incorporated with novel metal casting and additive manufacturing (AM) processes to produce highly durable engine structures to maximize performance of the

materials and systems with minimum mass and cost. The opportunity to include advanced materials and manufacturing in conjunction with high-potential combustion system and engine technologies also creates the chance to revisit the most appropriate engine specification to realize the desired efficiencies while reducing engine weight cost-effectively. A point of focus is the most cost-effective solution to promote wide market acceptance using the right materials in the right place and right process for the right parts. Single- and multi-material solutions for key engine components are investigated. Integrated computational materials engineering (ICME) [2], [3] and computer-aided engineering (CAE) tools are fully utilized to accelerate both engine design and material and manufacturing solution development and optimization.

Results

Based on Phase 1 research and development, advanced combustion and materials technologies have been developed and down-selected for the proposed medium-duty truck engine capable of meeting requirements.

Task 3.1 Design and Build Engines to Facilitate Test Cell Evaluation of Proposed Medium-Duty Truck Solution Incorporating Components

Subtask 3.1.1 – Design of Phase 2 engine cylinder head and block was completed, as shown in Figure VI.D.6.1 and Figure VI.D.6.2, incorporating the relevant advanced combustion and materials technologies developed in Phase 1, such as dual ignition, uniform combustion cooling, and charge motion control.

Figure VI.D.6.1 Cylinder head system

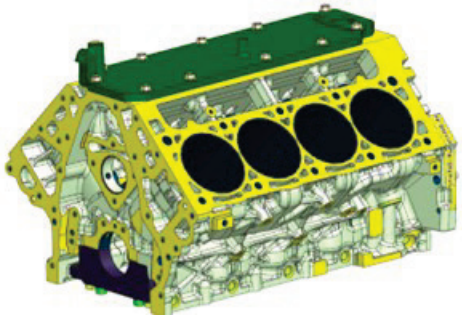

Figure VI.D.6.2 Engine block system

Subtasks 3.1.2–3.1.3 – Figure VI.D.6.3 and Figure VI.D.6.4 show the design completion of valvetrain, induction, and exhaust systems that enable Atkinson cycle strategies, enhanced EGR (E-EGR), and variable induction system strategies.

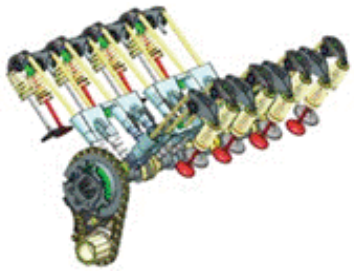

Figure VI.D.6.3 Valvetrain system

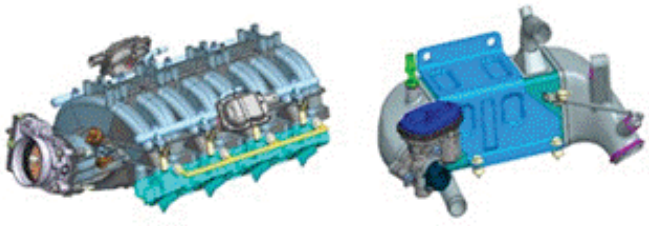

Figure VI.D.6.4 Induction (left) and EGR (right) systems

Subtasks 3.1.4–3.1.8 — Figure VI.D.6.5 shows the design completion of fuel and coolant pump systems capable of ultra-high-pressure (UHP) fuel injection and advanced combustion cooling enhancement. Figure VI.D.6.6 shows the design of the Phase 2 engine completed with integration of all the advanced combustion and materials technologies developed in this project. With the developed material solutions, the Phase 2 engine mass is more than 15% lighter than the baseline engine, while the engine displacement is increased from 6.0 L to 6.6 L. Table VI.D.6.1 compares the Phase 1 engine fuel economy improvement measured from various

advanced combustion technologies with the CAE model predictions. It can be noted that the reported fuel economy improvement of 9.1% is on track to meet or exceed the project target of 10% once the pre-chamber spark plug benefit is added.

Figure VI.D.6.5 Fuel (top) and coolant pump (bottom) systems

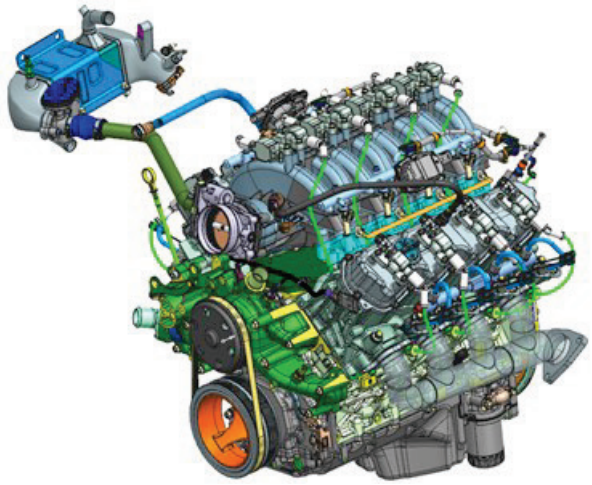

Figure VI.D.6.6 Complete Phase 2 engine system

Table VI.D.6.1 Comparison of Measured and Predicted New Technologies to Baseline L96 Engine at Weighted Average Greenhouse Gas Emissions Model (GEM) Cycle Operating Points

Measured Weighted Fuel Economy Improvement			Predicted Weighted Fuel Economy Improvement from Simulation	
L96 Baseline			L96 Baseline	
PHASE1	0.7%		PHASE1	
Charge Motion Control Valve (CMCV)	2.8%		PHASE1 + Charge Motion Control Valve	4.4%
E-EGR	1.8%		E-EGR	4.3%
Full Authority Cylinder Deactivation	1.3%		Full Authority Cylinder Deactivation	1.3%
UHP Direct Fuel Injection + PFI	2.5%		UHP Direct Fuel Injection	1.8%
Passive Pre-chamber Ignition	TBD		Passive Pre-chamber Ignition	2.8%
TOTAL:	**9.1%**		**TOTAL:**	**14.6%**

PFI – port fuel injection; TBD – to be determined

Task 3.2 Demonstration of the Highest-Payoff Materials and Manufacturing Solutions for Key Engine Components for the Proposed Medium-Duty Truck Engine

Subtasks 3.2.1–3.2.2 – A novel low-pressure precision sand casting (LPPSC) process has been developed for casting high-quality aluminum cylinder head and engine blocks through a comprehensive casting process simulation and multiscale defect and microstructure modeling, gating, and riser system, as well as LPPSC process parameter optimization. The fatigue strength of the LPPSC heads at 250°C has improved by at least 20% compared with baseline heads (Figure VI.D.6.7).

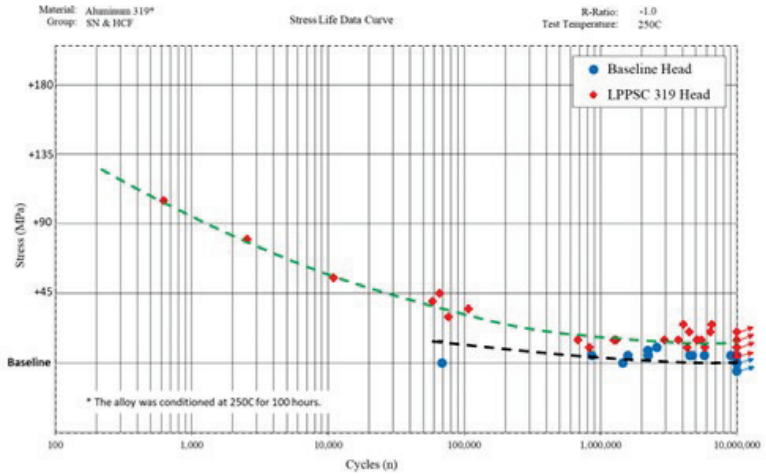

Figure VI.D.6.7 S-N fatigue data of LPPSC and baseline 319 alloy cylinder heads tested at 250 °C

Subtask 3.2.3 – The Phase 2 piston has been designed and printed with ORNL's Al-Ce-based DuAlumin-3D alloy, as shown in Figure VI.D.6.8. The Phase 2 AM piston is ~11 grams lighter than a cast aluminum production piston. CAE durability analysis indicates that the AM piston design exceeds the piston safety factor requirements. Figure VI.D.6.9 shows stress–life (S-N) and staircase fatigue testing of both AM and cast aluminum pistons. The high cycle fatigue (HCF, 10^7 cycles) strength of the AM pistons at 300°C is improved by at least 50% in comparison with the cast aluminum production pistons.

Figure VI.D.6.8 AM-printed Phase 2 pistons

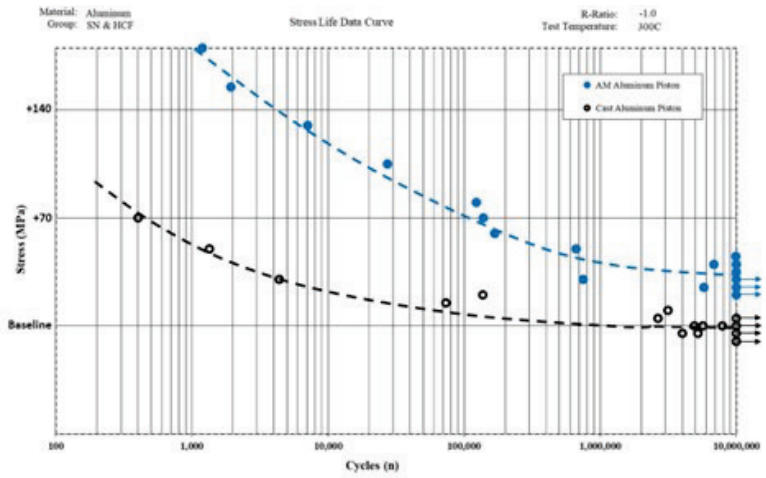

Figure VI.D.6.9 S-N fatigue data of AM-printed and cast aluminum pistons tested at 300 °C

Subtask 3.2.4 – The new design of the chills, gating, and riser system has produced high-quality cast steel cranks with minimum microporosity in Phase 2, as shown in Figure VI.D.6.10. Fatigue performance of the Phase 2 cast steel cranks with the new gating system (called 2nd set cranks) is much improved in comparison with the cranks made in Phase 1 (1st set cranks), particularly in the high cycle fatigue regime (>300,000 cycles) (see Figure VI.D.6.11). The Phase 2 steel cranks have fatigue performance similar to that of the forged steel baseline cranks. After hot isostatic pressing (hipping), the Phase 1 cranks show better fatigue performance than the forged ones. It is believed that the Phase 2 cranks should do the same after hipping, indicating that the cast steel alloy developed in the project has inherent advantages over the baseline forged steels.

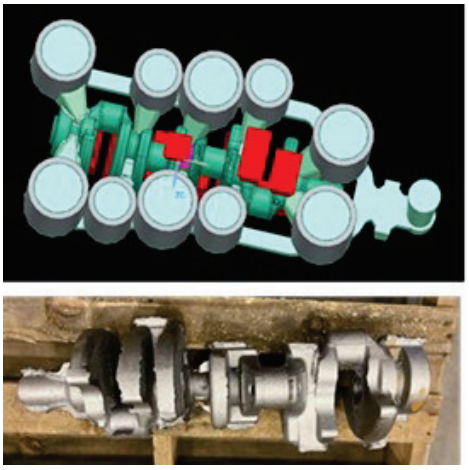

Figure VI.D.6.10 New cast steel crank casting design (top) and a Phase 2 crank made by the project team (bottom)

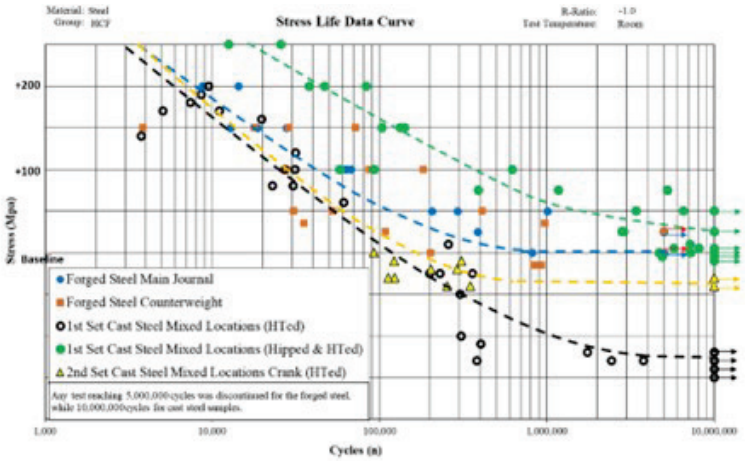

Figure VI.D.6.11 S-N fatigue data of cast tell cranks in various conditions compared with the forged baseline cranks

Subtask 3.2.5 – Through-process modeling and local materials property simulation, following the ICME approach, has been continuously conducted on Phase 2 cast aluminum cylinder head and engine block, cast steel, and nodular iron cranks, as well as cast and AM aluminum pistons, to ensure their designs to meet performance and durability requirements. Figure VI.D.6.12 shows the through process modeling flow for the LPPSC aluminum engine block. After the block casting geometry and gating/riser system is optimized, the comprehensive casting process modeling is carried out to simulate the mold filling and solidification. With the modeling capabilities developed at GM for multiscale defects (e.g., porosity and oxides) and microstructure simulation, nodal-based microstructure (e.g., the secondary dendrite arm spacing) and defect population (e.g., porosity volume fraction and sizes) are predicted throughout the entire block casting. Based on the simulated defects and microstructure from casting process modeling, location-specific material properties (e.g., tensile and fatigue properties) can then be predicted and incorporated in the CAE performance and durability analysis of the block casting. Similarly, the through-process modeling and ICME approach has been applied to other castings, such as cast steel crankshaft. Figure VI.D.6.13 shows an example of using casting process modeling capability in crank casting gating/riser system optimization.

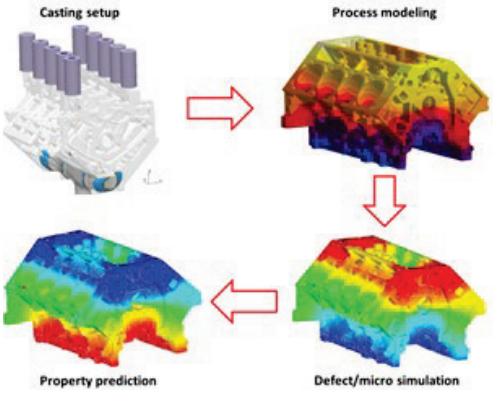

Figure VI.D.6.12 Through process modeling approach flow for cast aluminum block.

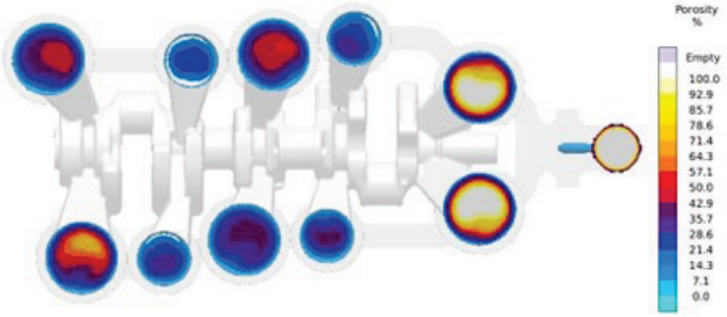

Figure VI.D.6.13 Casting process simulation and casting quality (e.g., porosity) prediction in cast steel crank.

Modeling of AM and cast aluminum microstructure has been continuing at OSU using a cellular automaton technique. In this budget period, cast aluminum microstructure simulation has been focused on columnar to equiaxed transition (CET). Modeling of AM microstructure has been carried out in grain structure simulation. Figure VI.D.6.14 shows an example of the CET simulations of the Al-8.6%Si-0.32%Mg-0.44%Fe-0.22%Mn

alloy during casting solidification. Figure VI.D.6.15 shows an example of AM grain microstructure evolution for a vertical multipass build case.

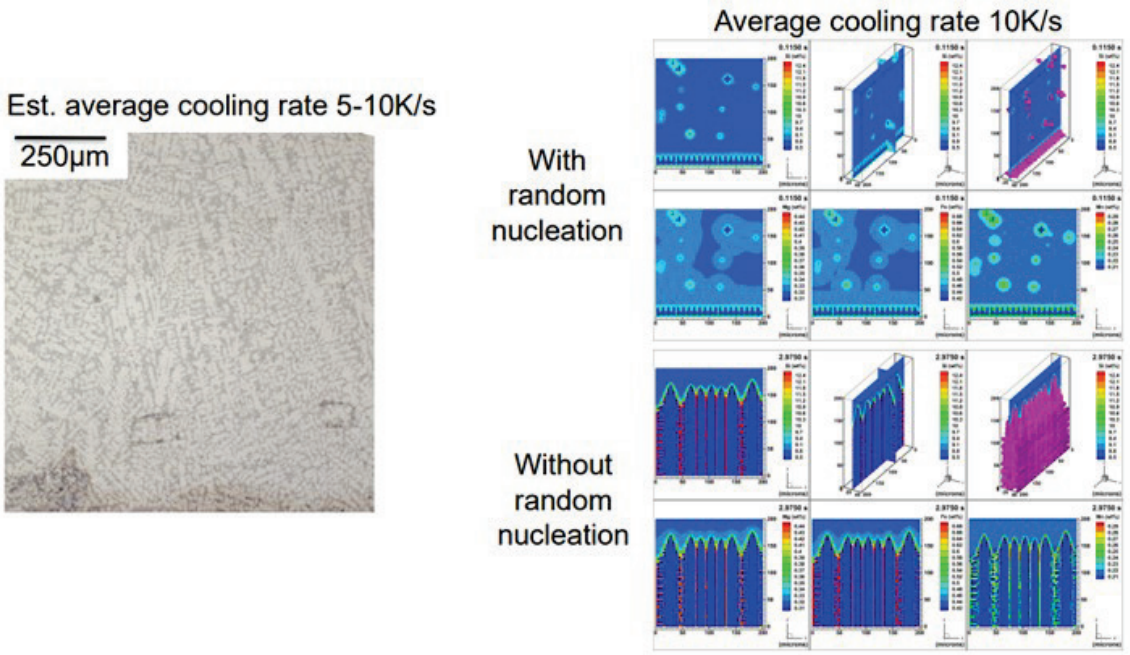

Figure VI.D.6.14 CET simulation for cast aluminum alloy solidified under an average cooling rate of 5-10 K/S, with and without random nucleation

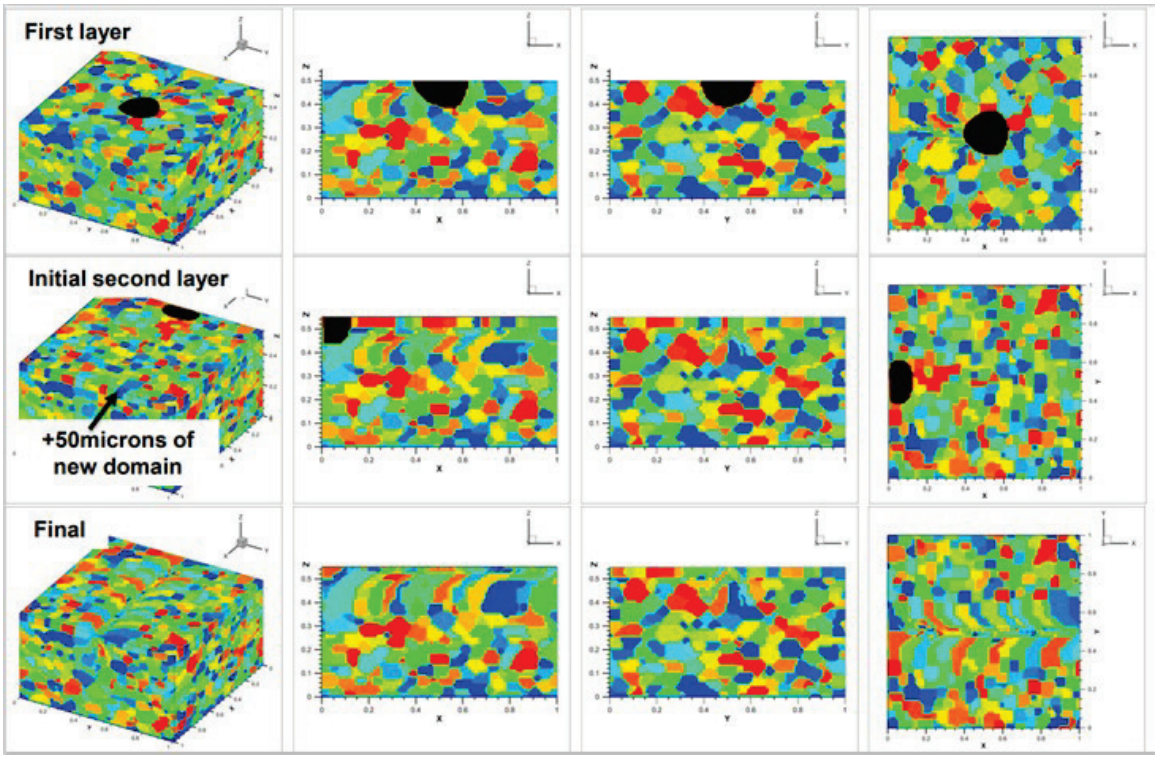

Figure VI.D.6.15 Cellular automaton simulation of AM grain structure. Laser speed of 1.5 M/S and thermal properties of AlSi10 alloy used. Top row shows thermal profile; bottom figures show individual grains.

Conclusions

Phase 2 engine design has been completed with incorporation of advanced combustion and materials technologies developed in Phase 1. Based on the technology development and verification, conducted both computationally and experimentally, the designed Phase 2 engine should be able to achieve the FOA objective of 10% fuel economy improvement and 15% mass reduction. The ICME approach has been used in the project to link materials, manufacturing, and system design into a holistic computational framework to enable the design and manufacturing of key engine parts with location-specific microstructure and material property modeling.

Key Publications

1. Moodispaw, M.P., B. Chen, A.A. Luo, Q. Wang. 2022. "Achieving Metallurgical Bonding in Aluminum/Steel Bimetallic Castings." American Foundry Society Transactions, Paper 22-040. Presented at CastExpo and Metalcasting Congress, Columbus, OH, April 23–26, 2022.

References

1. U.S. Department of Energy, Office of Energy Efficiency and Renewable Energy. 2019. Fiscal Year 2019 Advanced Vehicle Technologies Research Funding Opportunity Announcement, FOA Number DE-FOA-0002014. https://eere-exchange.energy.gov/FileContent.aspx?FileID=25f7a4dd-9874-4aee-9606-2ab52fe9cc18.

2. Pollock, T.M., et al. 2008. *Integrated Computational Materials Engineering: A Transformational Discipline for Improved Competitiveness and National Security*. Washington, DC: National Academies Press.

3. Wang, Q.G., P. Jones, Y. Wang, and D. Gerard. 2011. "Advances in computational tools for virtual casting of aluminum components." In Proceedings of the 1st World Congress on Integrated Computational Materials Engineering (ICME): 217–222.

Acknowledgements

The principal investigators (PIs) would like to thank the U.S. Department of Energy (DOE) Vehicle Technologies Office for the opportunity to work on this important project. We would especially like to thank Dr. Siddiq Khan, Mr. Jerry Gibbs, and Mr. Ralph Nine at DOE for their project oversight. The PIs are also very grateful to Mr. Sean Campbell (contract manager at GM) and the GM project and management team, Dr. Amit Shyam and his team at ORNL, Prof. Alan Luo and his team at OSU, Prof. Paul Sanders and his team at Michigan Technological University, and Mr. David Weiss and his team at ECK Industries Inc. for their extreme support and dedication to the project.

VI.D.7 Next-Generation, High-Efficiency Boosted Engine Development (Ford Motor Company)

Michael Shelby, Principal Investigator
Ford Motor Company
2101 Village Road
Dearborn, MI 48121
Email: mshelby@ford.com

Siddiq Khan, DOE Technology Manager
U.S. Department of Energy
Email: Siddiq.Khan@ee.doe.gov

Start Date: October 1, 2019 End Date: September 30, 2023
Project Funding: $10,000,000 DOE share: $7,566,730 Non-DOE share: $2,433,270

Project Introduction

The next-generation high-efficiency engine development project is a 39-month U.S. Department of Energy Office of Energy Efficiency and Renewable Energy Vehicle Technologies Office-funded research and development effort. As shown in Figure VI.D.7.1, the goal of the project is to combine advanced combustion system technologies, thermal management strategies, and advanced materials to demonstrate a turbocharged gasoline engine with peak efficiency exceeding the best of today's hybrid electric vehicle engines. While the market share of battery electric vehicles is increasing, most light-duty vehicles are projected to contain conventional or hybrid internal combustion engines well beyond 2030. Improvements in engine efficiency and reductions in powertrain weight have strong leverage to reduce vehicle-related carbon dioxide emissions for decades to come. This project develops engine-efficiency and weight-saving technologies that enable competitive, profitable internal combustion engines, targeting the highest-production-volume powertrains.

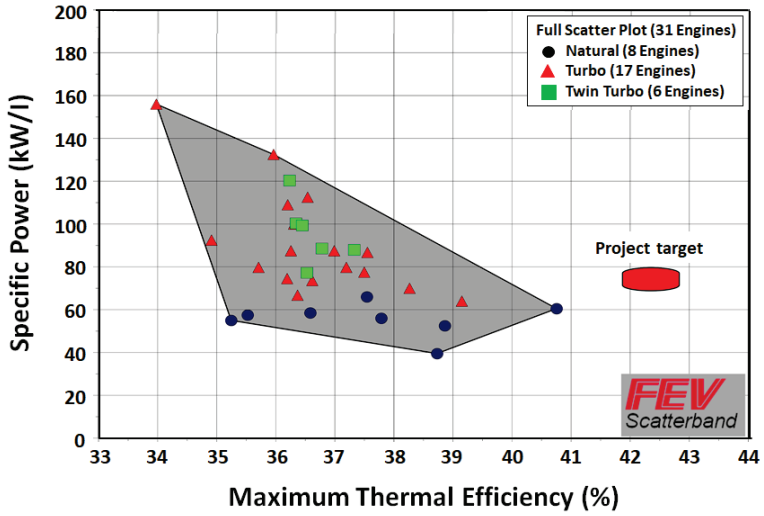

Figure VI.D.7.1 Specific power versus maximum efficiency

The project will achieve more than 20% drive cycle fuel economy improvement through a significant increase in compression ratio, highly dilute stoichiometric combustion, and various actions to reduce friction and weight. Application of advanced materials and additive manufacturing methods will also be investigated to facilitate efficiency improvements and to achieve a 15% weight reduction target.

The project team consists of Ford Motor Company, FEV North America, and Oak Ridge National Laboratory. Each partner brings strengths to this collaboration, and the combined knowledge in powertrain, combustion, component design, analytical development, and manufacturing will ensure a successful project.

Objectives

The objective of this project is to develop an engine with advanced combustion technologies capable of achieving ≥23% fuel efficiency improvement relative to a baseline 2016 model year 3.5 L V6 EcoBoost F150.

The engine will be compliant with applicable U.S. Environmental Protection Agency emissions standards and the fuel economy improvement will be demonstrated via engine dynamometer testing coupled to vehicle drive-cycle simulations. Advanced materials and weight-saving technologies will also be used to demonstrate the capability of ≥15% weight reduction of the baseline engine. These targets are particularly challenging given that the baseline engine is already a lightweight, downsized, boosted engine.

Fiscal Year 2022 objectives are as follows:

- Continue single-cylinder engine (SCE) dynamometer studies supporting calibration optimization.
- Complete fabrication, assembly, and test prep of the first multi-cylinder engine (MCE).
- Complete evaluation of the weight savings and study additional weight-reduction actions.

Approach

To achieve the project goals, work has been divided into several overlapping workstreams, as illustrated in Figure VI.D.7.2. The technology selection process was strongly guided by analytical tools, including three-dimensional flow and combustion modeling as well as structural and thermal analysis. Key items related to engine efficiency, outlined in the blue dotted circles of Figure VI.D.7.2, are being demonstrated and developed using SCEs. The final status of the fuel economy and weight targets will be demonstrated via dynamometer testing of a complete MCE, outlined in yellow, along with regulatory drive-cycle simulations.

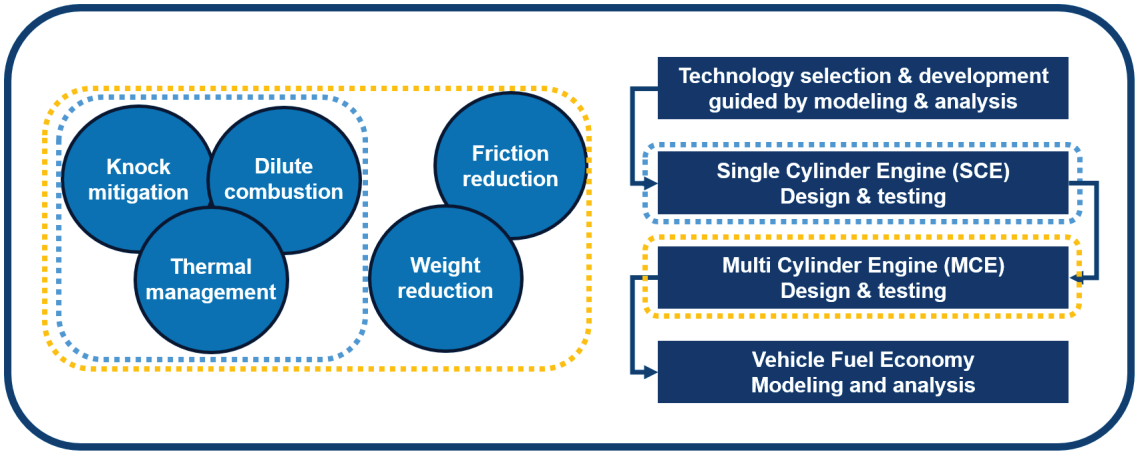

Figure VI.D.7.2 Development approach

This report will emphasize the project's combustion system development, efficiency, and hardware design aspects. A second report, focused on materials and lightweighting, has been prepared for the Materials subprogram's annual report.

Results

High-level engine assumptions were developed to support the project's fuel economy and weight objectives. Analytical assessments led to the selection of a 3.7 L inline six-cylinder engine with a bore-to-stroke ratio of 0.75, a 14:1 compression ratio, and part-load stoichiometric exhaust gas recirculation (EGR) dilution capability in the range of 35%–50%.

Work during this reporting period has been focused in three areas: (1) verifying the dilution tolerance of the combustion system using SCEs; (2) manufacturing, assembling, and preparing to test MCEs; and (3) completing the weight assessment of the engine.

Dilution Tolerance Verification

Analytical tools were leveraged during the design of the combustion system to extend stable combustion to very high concentrations of EGR. Results indicated that the active prechamber combustion system should be stable to 40% EGR. SCE testing was conducted to verify the analytical assessment with example results at 1,500 rpm, 5.6 bar net mean effective pressure (NMEP) shown in Figure VI.D.7.3.

The upper left graph of Figure VI.D.7.3 illustrates how the selected technologies address the knock limit of typical stoichiometric gasoline combustion. Because of the high geometric compression ratio, the engine is significantly knock limited even at 5.6 bar NMEP when operating with a conventional spark plug and valve timing. The continuously variable valvetrain can be leveraged to operate with an early intake valve closing (EIVC) thereby reducing the effective compression ratio and the tendency for knock (arrow A). At 0% EGR, the engine is still somewhat knock limited, but as cooled EGR is added, combustion phasing can be improved to the minimum advance for best torque. Further knock relief is expected from using the pre-chamber ignition system, but at this operating point, minimum advance for best torque is reached with the combination of EIVC and cooled EGR.

The upper right graph of Figure VI.D.7.3 illustrates how, with a typical spark plug ignition system (blue line), the burn duration increases and eventually combustion becomes unstable at high rates of EGR. The active pre-chamber ignition system (green line) dramatically decreases the burn duration (arrow B) and extends the useful dilution limit from 20% EGR to 40% EGR. The lower graph shows the impact of combining EIVC, active prechamber ignition, and cooled EGR on net specific fuel consumption (NSFC). A 14% improvement in NSFC was achieved relative to the 0% EGR, conventional cam timing, spark plug ignition system.

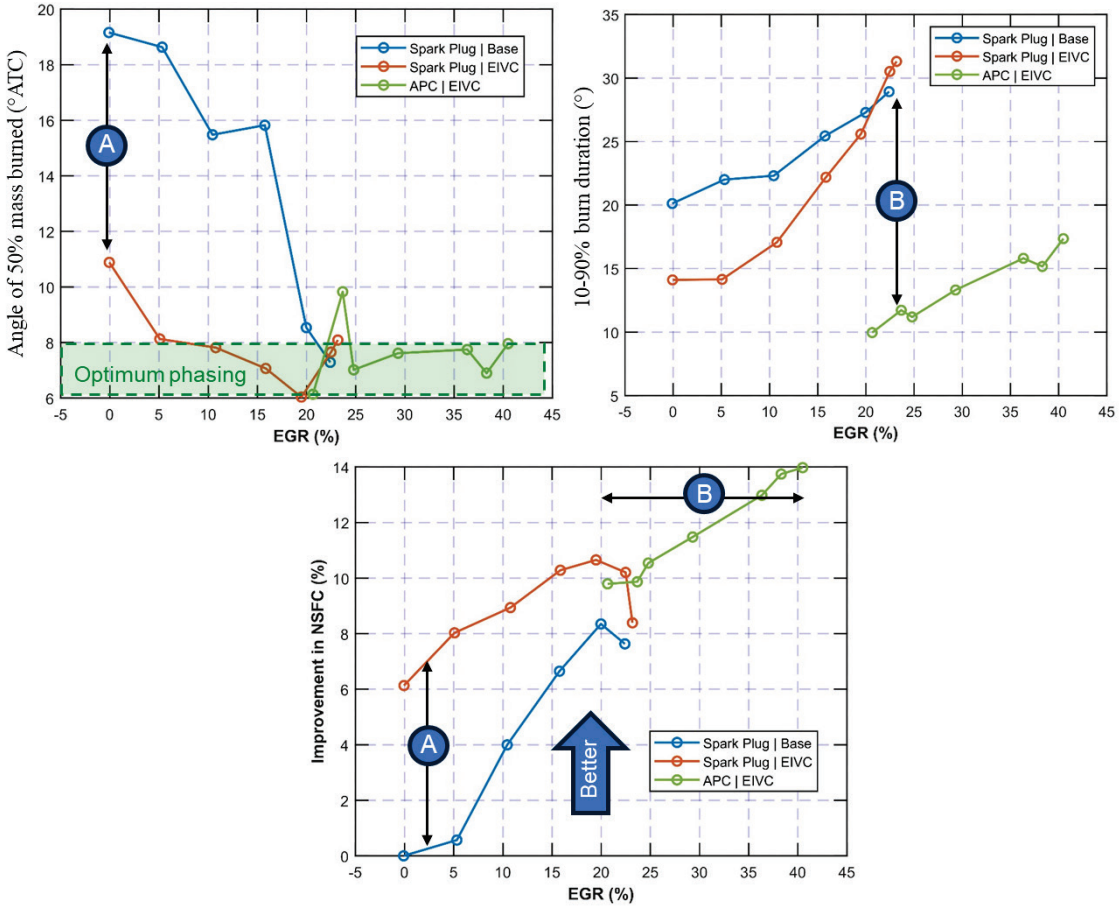

APC = active pre-chamber; °ATC = degrees above top center

Figure VI.D.7.3 Combustion phasing, burn duration, and NSFC improvement for a 1,500 rpm, 5.6 bar NMEP EGR sweep

Manufacture and Assembly of the MCE

One major achievement this year was completing the manufacture of all MCE components. Once the components had been manufactured, engine assembly was carried out in two build phases. The first build phase was conducted with a non-functional block and was used to identify assembly issues and as an assembly buck for the construction of the test pallet and instrumentation. Once the phase-one build was completed, a fully functional engine was assembled and installed on the engine pallet. Once palletized and instrumented, the engine was installed in an engine dynamometer test cell and is expected to begin testing by year-end 2022.

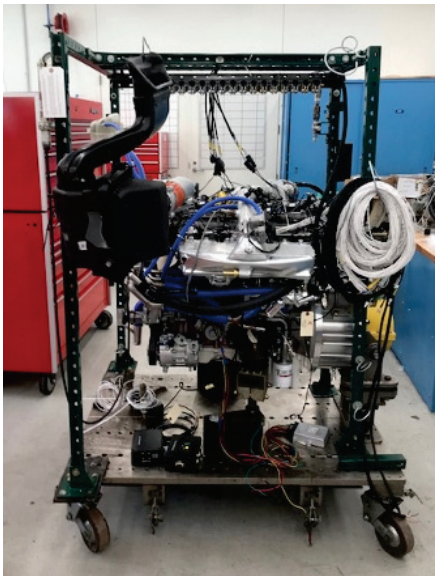

Figure VI.D.7 4 Assembled and palletized prototype engine

A control system to operate the engine has been developed in parallel with the engine hardware. This engine includes many technologies and actuators not present on Ford's production engines. As a result, significant work was required to design and build a control system suitable for completing the required dynamometer testing. The following is a simplified description of the control system hardware. Much of the engine control is managed by two engine control modules, one operating the pre-chamber ignition system, and the other operating most of the typical remaining engine actuators. Additional stand-alone modules were required to interface with the continuously variable valvetrain system, electronic water pump, pre-chamber air injectors, and the EGR valve. Prototype wiring harnesses were designed and built to provide the necessary connections, and a production engine control strategy was modified to accommodate the new actuators. Portions of the control system have been bench tested to validate compatibility and function.

Overall Weight Reduction Status

All MCE components are now available and have been weighed. The total engine weight, assuming a passive pre-chamber (PPC) ignition system, has been calculated based on these individual component measurements. The current prototype 3.7 L engine achieved a 4.3% weight reduction relative to the 2016 model year 3.5 L V6 EcoBoost engine baseline (Figure VI.D.7.5). Therefore, additional weight actions are required to achieve the 15% reduction target. Three items account for a majority of the shortfall to the target. (1) The boost system complexity was increased to facilitate higher boost pressures for more aggressive Miller valve timings. This resulted in a weight penalty for the boost system instead of the expected weight benefit. (2) The engine stroke was increased to improve thermal efficiency. This resulted in a significant increase in the weight of the engine block and crankshaft. (3) The engine architecture shift to an inline engine did not result in the anticipated weight reduction. This can be partially attributed to the long stroke and the required crankshaft structure.

An additional 5.3% weight reduction has been investigated by considering items not included in the project proposal, but in line with other actions demonstrated in the current prototype. These additional actions would maintain the current engine's fuel economy and performance but were not incorporated into the MCE hardware to avoid additional cost. The status of the engine weight reduction, with these items included, is captured in the "3.7 L I6 – Weight Actions" column of Figure VI.D.7.5 and consists of the following items:

- Reduced crankshaft weight (hollow main bearing journals).
- Composite intake manifold.
- Magnesium cam carrier and UniAir bricks.
- Catalyst system inlet and exhaust downpipe optimization (reduced number of bolted connections).

A path to achieve the 15% weight reduction target is possible but requires additional weight actions and some of these actions have the potential to impact the engine fuel efficiency or performance objectives. One way to achieve the 15% weight reduction target would be to utilize a single twin-scroll turbocharger instead of the current dual turbocharger boost system. This action would limit the early intake valve closing knock benefit and could degrade the engine's full load performance. The status of the engine weight reduction with a twin-scroll boost system is shown in the "3.7 L I6 – Further Study" column of Figure VI.D.7.5. The following items are examples of actions that have been studied that improve the weight reduction benefit to the 15% target:

- Single twin-scroll turbocharger boost system (achieves weight target with reduced performance).
- EGR cooler and EGR flow enhancement throttle delete.
- Reduced peak engine speed.
- Reduced engine stroke.

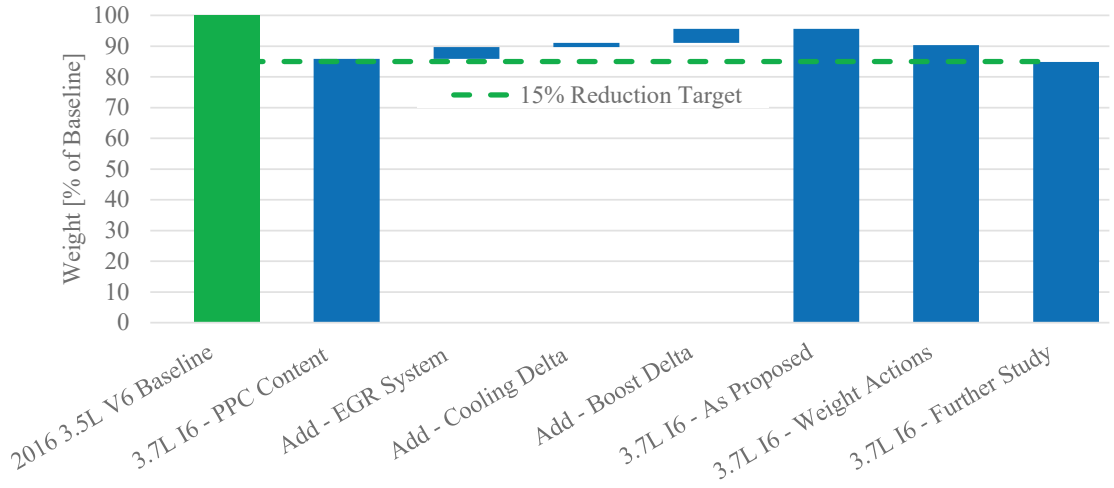

Figure VI.D.7.5 Path to 15% weight reduction

Conclusions

Simultaneously meeting the fuel economy and weight targets of this project presents many challenges. In the third year of this project, SCE testing was conducted confirming the combustion system is capable of stable operation with up to 40% EGR. Manufacturing of the MCE prototype parts was completed as well as the assembly of the first MCE. A control system was designed, and the associated wiring harnesses were fabricated and tested. Finally, weight assessments were completed based on these individual component measurements for several engine configurations. The net impact on engine weight of increasing the engine displacement, adding fuel economy technologies (low-pressure cooled EGR, continuously variable valvetrain, active cooling system, and long stroke), and utilizing lightweighting technologies (composites, additive manufacturing, and changing from a "V" to an "I" architecture) was a 4.3% reduction. Actions achieving an additional 5.3% without compromising fuel economy or performance were identified and analyzed. Several pathways to achieving 15% weight reduction were identified, but each requires some compromise in either performance or fuel economy. These efforts directly support the mass-reduction and efficiency-improvement goals of the project.

Acknowledgements

The author would like to thank our partners at FEV North America and Oak Ridge National Laboratory for their collaboration and support, as well as our National Energy Technology Laboratory Project Manager, Ralph Nine, for his continued guidance.

VI.D.8 New Two-Cylinder Prototype Demonstration and Concept Design of a Next-Generation Class 3-6 Opposed Piston Engine (Achates Power, Inc.)

Fabien Redon, Principal Investigator
Achates Power, Inc.
4060 Sorrento Valley Boulevard
San Diego, CA 92121
Email: redon@achatespower.com

Siddiq Khan, DOE Technology Manager
U.S. Department of Energy
Email: Siddiq.Khan@ee.doe.gov

Start Date: October 1, 2020 End Date: December 31, 2022
Project Funding: $6,250,000 DOE share: $5,000,000 Non-DOE share: $1,250,000

Project Introduction

A healthy economy and environment require reliable, secure, clean, and cost-effective transportation. Commercial vehicle engines are the fastest growing source of transportation emissions, and one most resistant to electric vehicle substitution. Commercial vehicle engines face a wide range of power and torque requirements in different applications, thus multiple engine displacements are typically offered, each with unique engine designs (bore, stroke, block design, etc.) requiring significant development cost.

Opposed-piston (OP) engines have demonstrated potential to reduce carbon dioxide (CO_2) and nitrogen oxides (NO_x) while costing less to manufacture compared to conventional engines of the same power and torque. This cost advantage can be further improved by using a common bore, stroke, block design, etc., to span the range of Class 3 to Class 6 vehicles by adding/subtracting cylinders, thereby minimizing the cost of development and manufacturing of a scalable engine platform. However, the performance and emissions implications of scaling the number of cylinders is not well understood in the OP engine. This research project will advance the cost effectiveness of high-efficiency, low-emissions engines by experimentally validating simulation models of a three-cylinder, six-piston and a novel two-cylinder, four-piston OP engine with electrified air handling components and simulating the performance of a four-cylinder, eight-piston engine.

Objectives

Overall Objective

- Improve the cost-effective development of high-efficiency, low-emissions diesel OP engines for the commercial vehicle sector.
- Optimize engine performance over several cylinder counts of fixed bore and stroke.
- Investigate engine performance opportunities through air and combustion optimization, such as electrified turbochargers, electrified exhaust gas recirculation (EGR) pumps, intake and exhaust chest volume, intake port design, and combustion chamber design.

Fiscal Year 2022 Objectives

- Simulate and optimize two-cylinder OP performance in baseline vehicle drive cycles to verify >10% miles per gallon (MPG) improvement.
- Develop baseline three-cylinder OP engine datasets for model predictive control (MPC) optimization at Clemson University.

- Build, shakedown, and baseline a novel two-cylinder OP engine at Achates Power.
- Validate novel 1D and 3D air handling optimization models and a 3D computational fluid dynamics (CFD) combustion bowl geometry optimization model on a two-cylinder engine with experimental results.

Approach

The approach taken to increase the cost effectiveness of OP engines utilizes a combination of 1D and 3D simulations and engine experiments. Data from a prototype OP engine, built and tested at Achates Power, generates a set of diesel combustion performance and emissions data that is then used to develop and validate 1D GT Power (Clemson University), 3D open cycle (Clemson University), and 3D closed cycle (University of Wisconsin) models. These validated models are then extrapolated and used to guide hardware and control decisions that support a family-of-engines concept, with a fixed bore and stroke but varying cylinder count to cover a range of torque and power requirements. The hardware based on these simulation results is procured and experimentally tested to further validate model prediction. These models are then extrapolated to simulate engine configurations that cannot be readily tested, such as an increase in cylinder count to four compared to the two- and three-cylinder engine variants developed for this program. The results of these simulations will guide a concept engine design that will package into a Class 4 Isuzu vehicle and be modeled over a representative drive cycle that shows >10% MPG improvement over the baseline vehicle.

Results

The key Fiscal Year 2022 accomplishments listed below are fundamental to complete the objectives of the project and to achieve >10% MPG improvement over a baseline Model Year (MY) 2015 commercial vehicle. The prototype three-cylinder OP engine was extensively tested at Clemson University to develop datasets required for model validation and MPC generation. Vehicle simulation at Clemson University predicts >14% MPG improvement compared to the MY 2015 baseline vehicle for a novel two-cylinder OP engine, which was built and shaken down at Achates Power.

Vehicle Drive Cycle Fuel Economy Estimation

- Optimized shift schedule and final drive ratio for a simulated two-cylinder OP engine powered baseline vehicle (Figure VI.D.8.1).
- A net improvement of 12.4% MPG was estimated over five drive cycles, with the largest improvement of 17.78% on an interstate route.

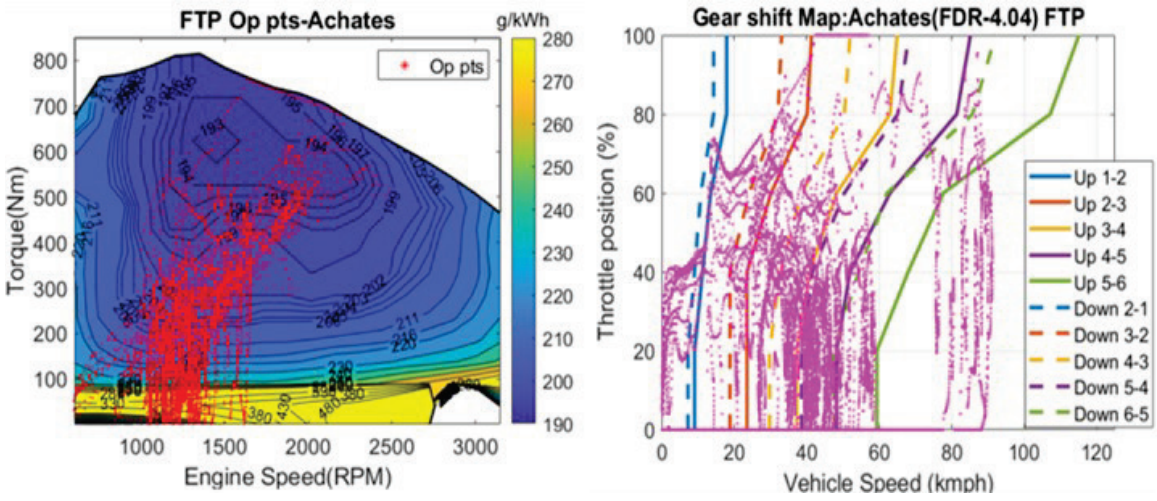

Figure VI.D.8.1 Shift optimization for a two-cylinder OP engine operating in a baseline vehicle over the Federal Test Procedure (FTP) drive cycle

Experimental Results

- Validated Clemson University's experimental facility and extensively tested a three-cylinder OP engine over a wide range of operating points under hot steady-state conditions (Figure VI.D.8.2a) and provided validation data for 1D and 3D simulation models and MPC algorithm calibration (Figure VI.D.8.2b).
- Built and broke in novel two-cylinder OP engine at Achates Power (Figure VI.D.8.3).
- Developed e-turbo controls methodology for supplying required air and boost pressure for relevant operating condition.

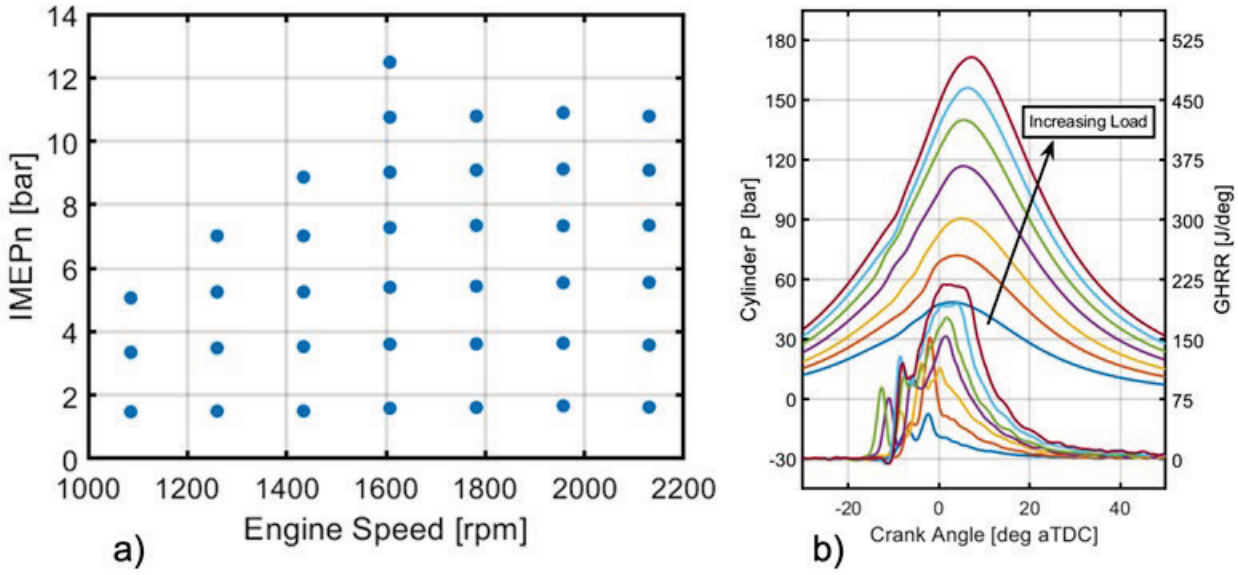

IMEPn – net indicated mean effective pressure; GHRR – gross heat release rate; aTDC – above top dead center

Figure VI.D.8.2 (a) Experimental speed and load map of hot steady state points acquired at Clemson University for model validation and MPC algorithm calibration. (b) Cylinder pressure and heat release plot from Clemson University.

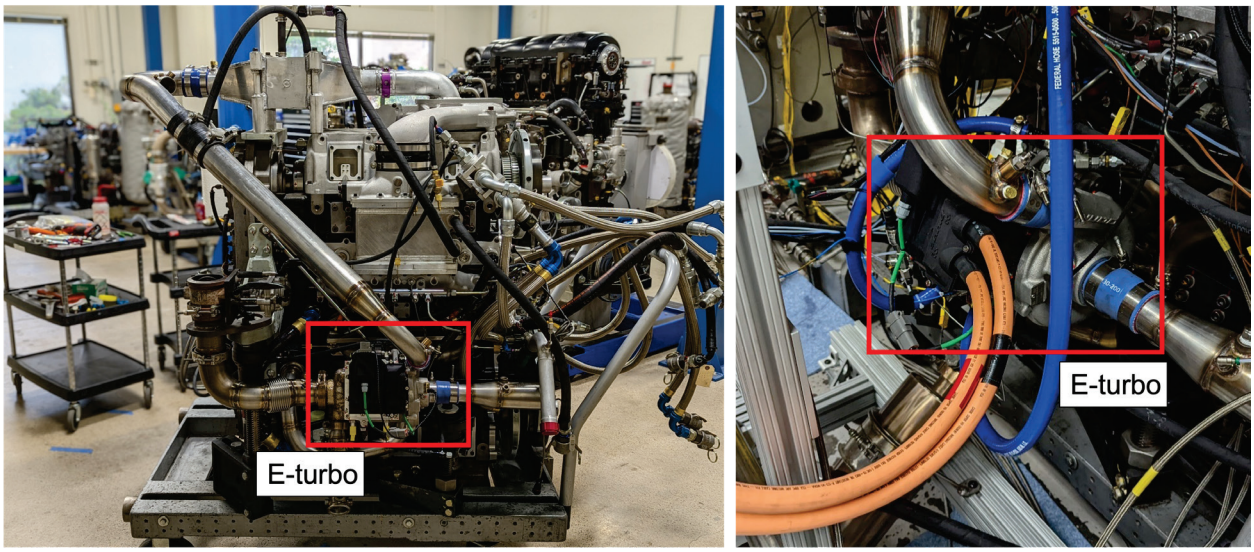

Figure VI.D.8.3 E-turbo installation on novel two-cylinder OP engine

Model Predictive Control Development

- Used experimental data to validate GT Power model and interrogated the GT Power model to provide steady-state training data for artificial neural networks (ANNs).
- ANNs were used to estimate cylinder charge and exhaust temperature using a variety of input conditions (Figure VI.D.8.4a).
- Developed a 0D control-oriented model to optimize control actions with respect to dynamic constraints.
- Estimated EGR transport delay by discretizing the EGR pipeline into multiple control volumes and utilizing 0D filling and emptying dynamics to capture the concentration and temperature change in each volume (Figure VI.D.8.4b).

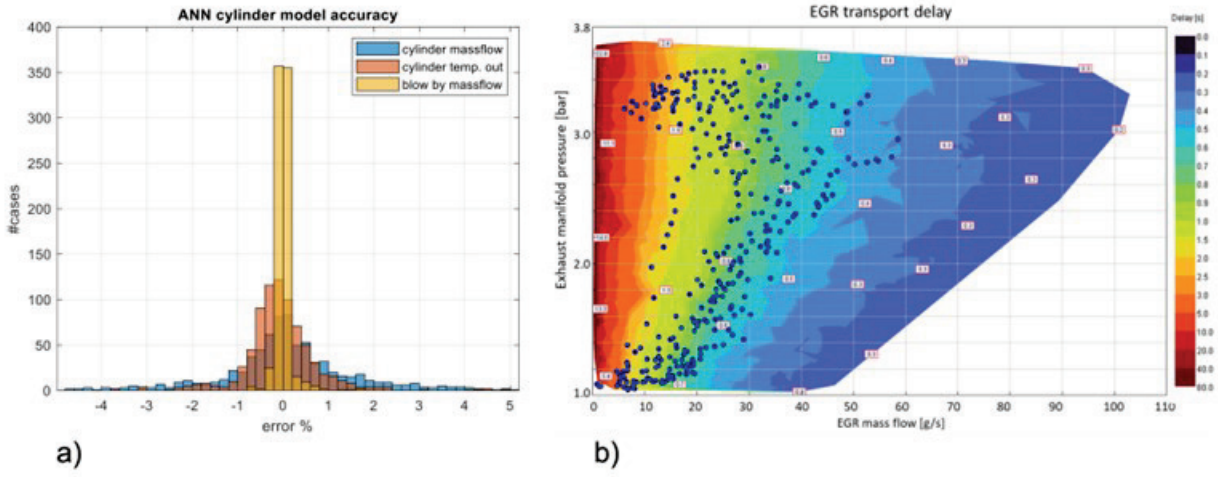

Figure VI.D.8.4 (a) Error distribution of ANN cylinder model. (b) EGR transport delay with electric EGR pump

Combustion Chamber Optimization

- Updated 3D CFD combustion optimization to include various injector and swirl parameters.
- Investigated the impact of the number of injector holes (with constant total effective fuel flow area) and determined that smaller nozzle hole diameters resulted in different spray penetration, liquid-fuel vaporization rates, and Sauter mean diameter (SMD) (Figure VI.D.8.5).
- Combustion bowl geometries depend on the number of fuel injector nozzle holes; even nozzle holes per injector result in more symmetric piston bowls compared to optimal geometries predicted from an odd number of nozzle holes per injector.
- Combustion bowl geometries depend on the level of swirl in cylinder, generally with similar symmetry for varying swirl level but with altered chamber shapes.

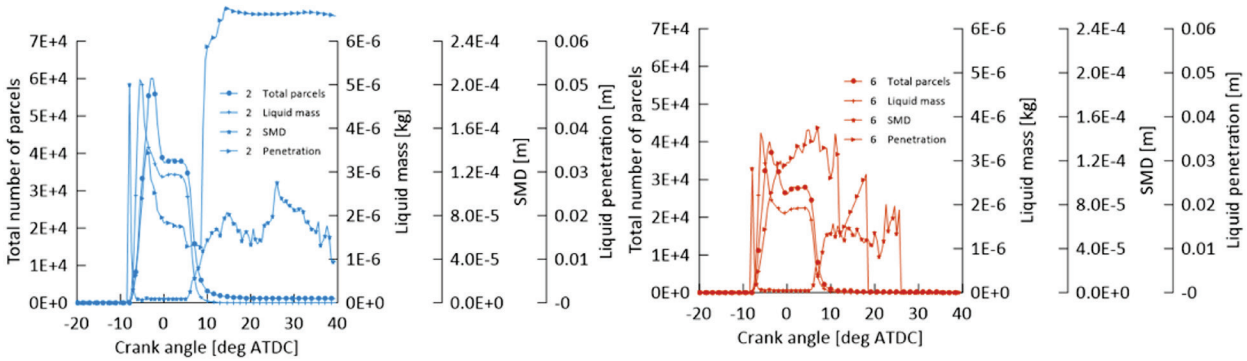

Figure VI.D.8.5 Total number of parcels and liquid-fuel mass in domain, SMD, and spray penetration for 2-hole nozzle (left) and 6-hole nozzle (right) configurations

Conclusions

The following accomplishments were made during Fiscal Year 2022:

- A two-cylinder OP engine equipped with an e-turbo was assembled and broken in at Achates Power.
- The three-cylinder prototype OP engine has been extensively tested at Clemson University, providing validation data for 1D and 3D models.
- Model predictive controls have been developed from validated 1D models and have been used to estimate difficult-to-measure parameters such as trapped cylinder conditions. These capabilities are utilized in transient response characterization and control.
- Vehicle simulations of a two-cylinder OP engine suggest a greater than 12% improvement in MPG compared to a baseline MY 2015 vehicle over a five-drive-cycle average, with an improvement of nearly 18% on an interstate route.
- Combustion volume and chamber CFD optimization by the University of Wisconsin identified that bowl geometries depend on the number of fuel injector nozzle holes, with an even number of holes resulting in more symmetric piston bowls compared to an odd number of nozzle holes per injector.
- University of Wisconsin combustion CFD also identified that combustion bowl geometries depend on the level of swirl in a cylinder, generally with similar symmetry for varying swirl level but with altered chamber shapes.

Key Publications

1. DOE quarterly progress report, Q5 – January 30, 2022.
2. O'Donnell, P., J. Gandolfo, B. Gainey, E. Vorwerk, et al. 2022. "Effects of Port Angle on Scavenging of an Opposed Piston Two-Stroke Engine." SAE Technical Paper 2022-01-0590. https://doi.org/10.4271/2022-01-0590.
3. DOE quarterly progress report, Q6 – April 30, 2022.
4. 2021 Annual Merit Review Presentation, June 23, 2022.
5. DOE quarterly progress report, Q7 – July 30, 2022.

6. O'Donnell, P., B. Gainey, E. Vorwerk, R. Prucka, et al. 2022. "An Investigation into the Effects of Swirl on the Performance and Emissions of an Opposed-Piston Two-Stroke Engine using Large Eddy Simulations." SAE Technical Paper 2022-01-1039. https://doi.org/10.4271/2022-01-1039.

7. DOE quarterly progress report, Q8 – October 30, 2022.

8. Gainey, B., A. Bhatt, P. O'Donnell, et al. 2022. "Experimental Study of the Impact of Scavenging Efficiency on Diesel Combustion in an Opposed-Piston Two-Stroke Engine." International Journal of Engine Research. https://doi.org/10.1177/14680874221135007.

Acknowledgements

The project team would like to thank Ralph Nine, Project Manager, and Angela Bosley, Contract Specialist, at the National Energy Technology Laboratory for their continued project support. The principal investigator would like to thank the entire project team (Clemson University, Isuzu Technical Center of America, and University of Wisconsin–Madison) for their dedicated contributions to this program.

VI.D.9 Opposed-Piston Two-Stroke Hybrid Commercial Vehicle System (Achates Power, Inc.)

Fabien Redon, Principal Investigator
Achates Power, Inc.
4060 Sorrento Valley Boulevard
San Diego, CA 92121
Email: redon@achatespower.com

Siddiq Khan, DOE Technology Manager
U.S. Department of Energy
Email: Siddiq.Khan@ee.doe.gov

Start Date: March 1, 2022 End Date: May 31, 2024
Project Funding: $6,250,000 DOE share: $5,000,000 Non-DOE share: $1,250,000

Project Introduction

Commercial vehicle engines are the fastest-growing source of transportation emissions and the source most resistant to powertrain substitution. Because of the high impact of commercial vehicles, the California Air Resources Board (CARB) has passed the Heavy-Duty Engine and Vehicle Omnibus Regulation, which requires a 90% reduction in nitrogen oxide (NO_x) emissions (to 0.02 g NO_x/bhp-h) by the year 2027, in addition to reducing CO_2 and particulate matter emissions. Furthermore, CARB proposed new low load drive cycles representing the challenges with maintaining aftertreatment temperatures and catalyst activity in real-world driving scenarios, while also implementing longer life warranty periods on aftertreatment systems (from 450,000 miles to 800,000 miles). Hybridization and electrification of powertrains can help resolve new regulation requirements by operating an engine in a more efficient and cleaner range; the architecture, however, adds significant system cost, which hampers commercial adoption. Opposed-piston (OP) engines have demonstrated potential to reduce CO_2 and satisfy CARB emissions regulations while costing less to manufacture compared to conventional engines of the same power and torque. OP engines, however, experience higher relative pumping and frictional losses at low load compared to conventional engines. Therefore, OP engines with hybridization can help mitigate the low-load challenges of the OP engine and the high cost of hybridized conventional powertrains, as well as significantly reducing emissions and increasing efficiency of the commercial vehicle sector. Furthermore, OP engines can virtually eliminate greenhouse gas and criteria emissions and aftertreatment components with the use of alternative and renewable fuels, such as hydrogen, dramatically improving the cost-effectiveness of the technology over conventional engines, conventional hybrid powertrains, battery electric vehicles, and fuel cell vehicles.

Objectives

Overall Objective

The proposed project will demonstrate advanced OP two-stroke technology for heavy-duty commercial vehicles with hybridization that significantly improves energy efficiency and reduces emissions over conventional engines in the 2025–2030 timeframe. This heavy-duty hybrid powertrain project will demonstrate the ability to beat CARB's Clean Truck criteria ***emissions*** standards for NO_x and particulate matter while also reducing CO_2 emissions by 13%–20% compared to a non-hybrid OP baseline, which is already 7% lower CO_2 compared to Model Year 2021 conventional ***engines*** (2021 U.S. Environmental Protection Agency heavy-duty standard). In addition, zero- or near-zero-emissions capability of the OP engine will be investigated through the use of hydrogen fuel.

Fiscal Year 2022 Objectives

- Engine performance, engine-out and tailpipe-out emissions for hybrid powertrain model development

- Hydrogen combustion computational fluid dynamics (CFD) simulation
- Single-cylinder OP engine adaptation for hydrogen combustion

Approach

The approach to performing this project is to leverage the best tools available and expertise from the partners.

Achates Power is using its existing heavy-duty truck engine to collect performance and emissions data for Clemson University to build and correlate the 1D model that will be used as a basis for the hybridization studies.

Achates Power, in collaboration with the University of Wisconsin, is developing a 1D and CFD model to evaluate various strategies and provide the specifications for the single-cylinder engine that will be used to test hydrogen fuel.

The team at Achates Power is using these findings to design and procure components to upgrade one of the single-cylinder OP research engines to operate on hydrogen.

Results

Engine Performance, Engine-Out and Tailpipe-Out Emissions for Hybrid Powertrain Model Development Data Collection

Achates Power collected data on their 10.6 L heavy-duty OP engine and provided it to Clemson University for the hybrid powertrain model development and correlation. The data consisted of engine and aftertreatment system data, including all the necessary engine parameters to correlate the GT-Power models for three different combustion modes. The engine and aftertreatment are shown in the test cell in Figure VI.D.9.1.

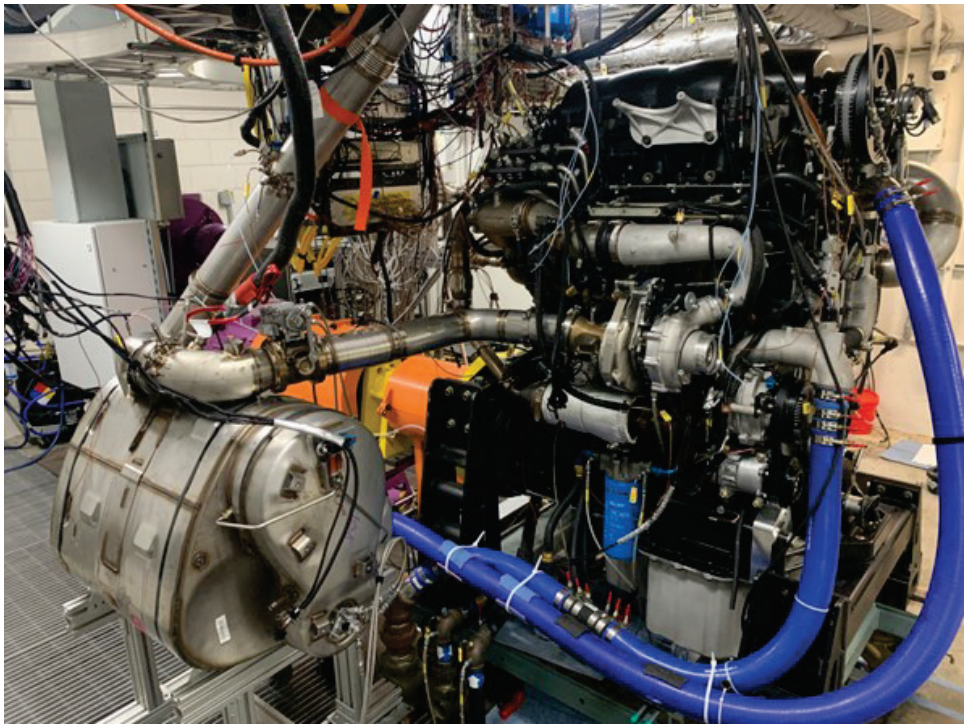

Figure VI.D.9.1 10.6 L heavy-duty Achates Power engine and aftertreatment system in the test cell

Figure VI.D.9.2 illustrates some of the data that were collected from the high-efficiency mode (hybrid with stop-start [HSS]).

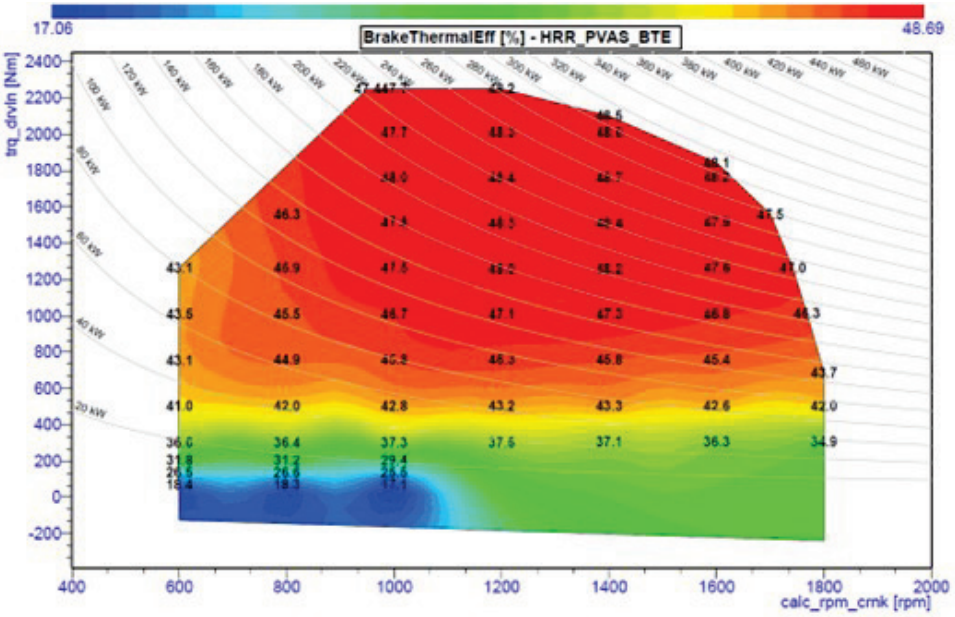

Figure VI.D.9.2 10.6 L heavy-duty Achates Power engine HSS brake thermal efficiency

With these data, engine and aftertreatment models were developed at Clemson University. In addition, various vehicle models were developed for conventional and hybridized vehicle architectures. These included a conventional vehicle model to serve as a reference, a mild parallel hybrid, and a series hybrid.

Hydrogen Combustion Analysis and Single-Cylinder Engine Procurement

The scope of the hydrogen combustion study was to define an initial combustion strategy and system adequate to achieve reliable combustion in the single-cylinder engine.

Minimal modifications to the baseline diesel combustion system were made to accommodate hydrogen combustion. For instance, a spark plug trench was added to the piston crown to provide an uninterrupted path between the spark location and the combustion volume in the center of the cylinder.

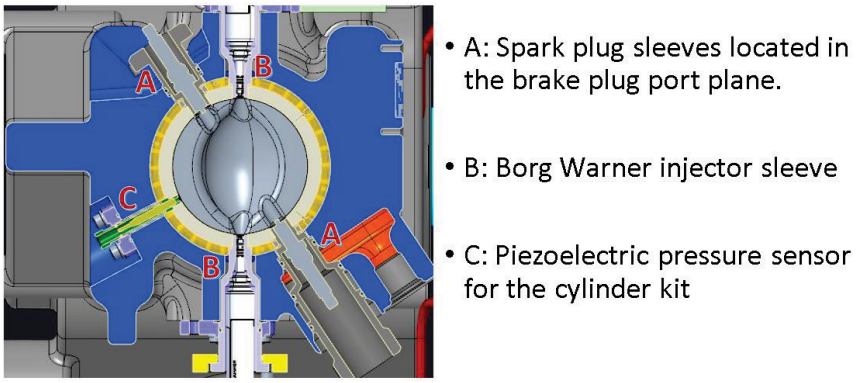

Figure VI.D.9.3 Single-cylinder combustion system layout

BorgWarner provided injectors derived from current production gasoline direct injectors and equipped with a single large-diameter hole suitable for the initial hydrogen testing. The flow rate from this first round of injectors will be somewhat limited but should provide enough to generate representative combustion data that can be used for model correlation.

One-dimensional analysis was performed to generate representative boundary conditions to run the open cycle CFD analysis that determines the flow field, temperature distribution, and constituent distribution in the cylinder at the start of the close cycle simulation. The analysis was also used to verify the intake and exhaust port selection.

Figure VI.D.9.4 BorgWarner injector

The combustion CFD analysis helped define three modes of operation that will be evaluated during testing:

- Low-load point, idle and cold start: Spark ignition combustion; direct injection of hydrogen during compression stroke; ignition from external source. Hardware (i.e., source location) could be optimized in the future.
- Mid- and high load point: Pilot- or spark-assisted compression ignition combustion. Although CFD suggests that the OP engine can operate with hydrogen as the standalone fuel for compression ignition combustion, pilot- or spark-assisted compression ignition will provide much more control over the rate of pressure rise, combustion stability, etc., as well as efficiency improvement.
- High-speed, high-load point: Non-premixed compression ignition combustion. Ignition will rely on free turbulent jet mixing between hydrogen and air; ambient temperature will be sufficiently high to sustain hydrogen auto-ignition.

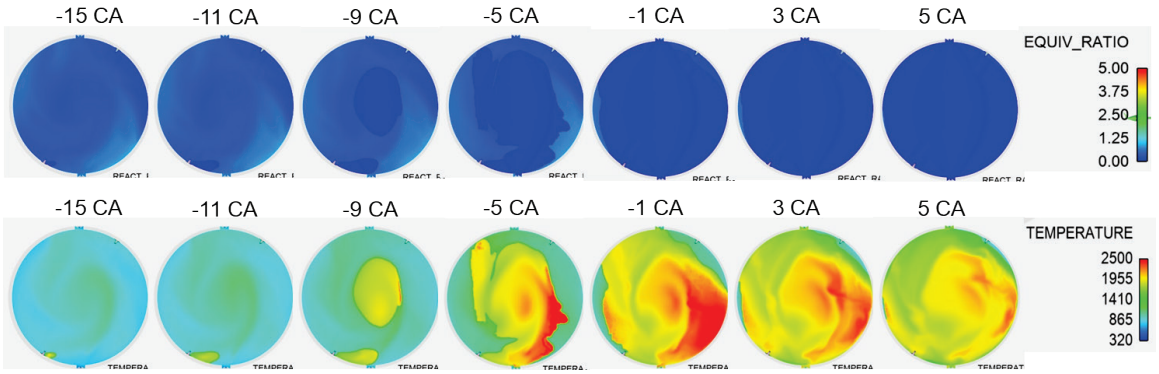

Figure VI.D.9.5 Spark ignition hydrogen combustion

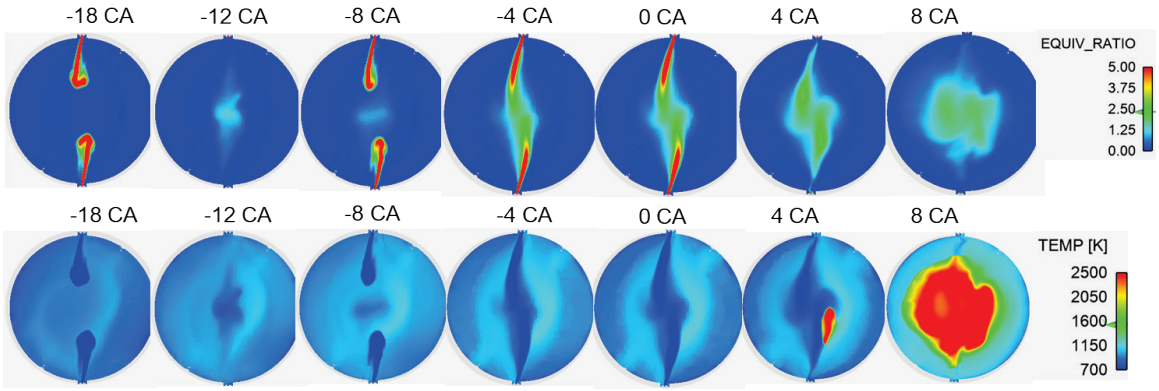

Figure VI.D.9.6 Pilot-assisted compression ignition hydrogen combustion

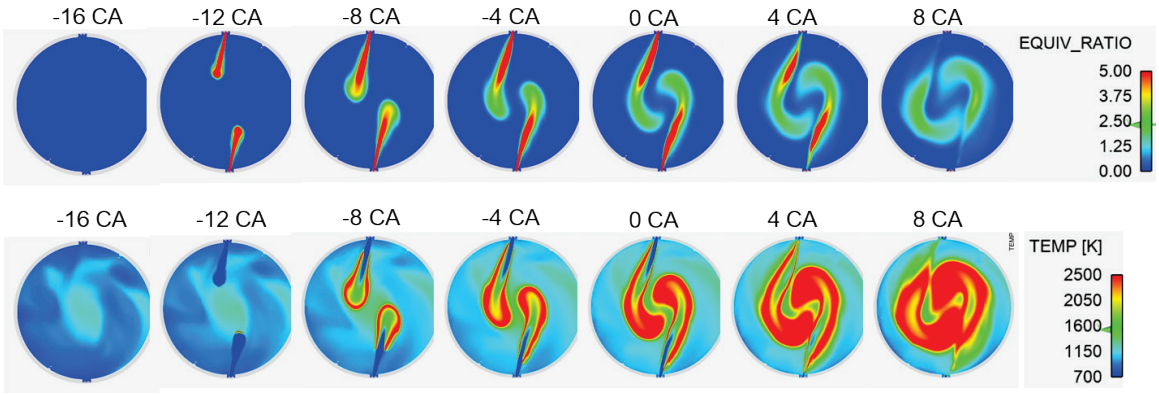

Figure VI.D.9.7 Single-injection compression-ignition hydrogen combustion

The University of Wisconsin–Madison developed a process using gaseous parcels for the hydrogen spray modeling. The process was very successful and will be used for the rest of the project.

Conclusions

The following accomplishments were made during Fiscal Year 2022:

- Data were generated to build and correlate the 1D hybrid powertrain model, and model development was started.
- An initial combustion strategy was defined for hydrogen combustion, and the modeling process was developed.
- A single-cylinder OP engine for hydrogen combustion was designed, procured, and assembled.

Key Publications

1. DOE quarterly progress report, Q1 – April 30, 2022
2. DOE quarterly progress report, Q2 – July 30, 2022
3. 2021 Annual Merit Review Presentation, June 23, 2022
4. DOE quarterly progress report, Q3 – October 30, 2022

Acknowledgements

The project team would like to thank Ralph Nine, the project manager, and Angela Bosley, the contract specialist, at National Energy Technology Laboratory for their continued project support. The principal investigator would like to thank the entire project team (Clemson University, Isuzu Technical Center of America, and University of Wisconsin–Madison) for their dedicated contributions to this project.

(This page intentionally left blank)

U.S. DEPARTMENT OF ENERGY

Office of
ENERGY EFFICIENCY & RENEWABLE ENERGY

For more information, visit:
energy.gov/eere/vehicles

DOE/EE-2728 • August 2023